

Université du Québec  
Institut national de la recherche scientifique  
Centre Énergie Matériaux Télécommunications

# Development of therapeutic bioconjugates for neuroprotection in ischemic stroke

By  
Ahlem Zaghmi

A thesis submitted for the achievement of the degree of Doctor of Philosophy (Ph.D.) in  
Energy and Materials Science

## **Jury Members**

President of the jury and Internal Examiner	Prof. Fiorenzo Vetrono INRS-Centre Énergie Matériaux Télécommunications Varenes, Québec, Canada
External Examiner	Prof. Nicolas Bertrand Faculty of Pharmacy, Université Laval Québec, Québec, Canada
External Examiner	Prof. Xavier Banquy Faculty of Pharmacy, Université de Montréal Montréal, Québec, Canada
Director of Research:	Prof. Marc A. Gauthier INRS-Centre Énergie Matériaux Télécommunications Varenes, Québec, Canada

*This Thesis is dedicated to the memory of my mom, **Aida Dorgham***

*Gone too soon, with whom I would have liked to share this thesis. Although she is not here to give me strength and support, I always feel her presence that used to urge me to strive to achieve my goals in life.*

*“There are footprints on the moon. Those footprints belong to each and every one of you, to all mankind.”*

*Buzz Aldrin*

## ACKNOWLEDGEMENTS

I would like to thank the people who have supported me and who have contributed in some way or another to this project. Without their tremendous amount of inspiration and support, this endeavor would not have been conceivable.

My sincere gratitude goes to my PhD director, **Prof. Marc A Gauthier**, for many reasons that are just uncountable. Thank you for trusting me and welcoming me to your newly opened laboratory to carry out this enriching project. I acknowledge your passion and enthusiasm on supervising every single one of us and I can't thank you enough for always being there for us. Your knowledge and leadership provided us with a priceless model for our own careers. I will always remember your major contributions writing our first paper and your great support during my extremely difficult times. For all this, I thank you!

I would like to thank the examining committee members who agreed to devote the time to read my thesis and for having contributed their respective expertise to the evaluation of my research project. I sincerely thank **Prof. Fiorenzo Vetrone** for accepting to be my internal examiner and the president of jury, as well as for serving on my candidacy and defense committee; **Prof. Xavier Banquy** and **Prof. Nicolas Bertrand** for accepting to be my external examiners and serving on my candidacy and defense committee.

I would like to thank the past and present lab members, **Andrea, Esen, Sharifun, Samira, Tom, Xu, Ahlem, Anees, Hoda, Lei, Sabrine, Julie, and Amir** for creating a friendly atmosphere both in the office and in the laboratory. Thank you for all the fun we had in the last years. I wish to extend my special thanks to **Dr. Andrea A. Greschner** for training me in many lab techniques and for providing me with her assistance in my English communications proof-reading. But above all, I would like to thank her for our long discussions on different subjects, our enjoyment, and her countless support which will always be among the best memories during my PhD. Please keep sending me Arianne pictures, they always make me happy! Thanks to **Dr. Hoda Soleymani Abyaneh** who, in spite of her departure and the distance, always remained attentive. Thank you for being a true friend, for your maturity, your sincerity, and your care. I will keep my promise to come and visit you in Toronto one day!

I would like to thank **Prof. Francisco Campos Perez**, our precious collaborator, for accepting me into his group. A huge thanks to the entire IDIS Group of the University of Santiago de Compostela, for making me feel at home. Thank you, **María, Pablo, Ramón, and Antonio**, for your collaboration in this work. **Clara, Elena, Andres, Paolo, Ana, Esteban, Uxia, Marta, Hector, Manuel, and Adrian**, thank you for the wonderful moments that we had together. I will

always remember the long nights we spent in the streets of Santiago and the many free tapas we had with each drink. I would particularly like to thank **Dr. María Pérez-Mato**, who first was my laboratory colleague and then my friend. Thank you for the great moments we shared, for inviting me to your hometown during the weekends, for showing me your traditional clothes and food, and for always caring about me.

My profound gratitude stands for many organizations: NSERC, CIHR, FRQNT, EuroNanoMed III, INRS/Tunisian Ministry of Education, MITACS, and MEES-INRS. Without their support and funding, this project could not have reached its goal.

I sincerely thank the research members as well as the administrative and technical staff of INRS. They were very kind and helpful, particularly H el ene Tanguay, H el ene Sabourin, Louise Hudon, Sylvain Gingras, and Georges Lamoureux.

I would also like to thank the members of the student association (CEISME) as well as the recruitment committee of INRS with whom I was able to work for two years.

I have an enormous debt to my friends across the Atlantic who were real driving forces for my PhD despite the several miles that separated us. Thank you **Jihen, Hasna, Yosra, Safa, Maroua, Manel, Anabel, Fausta, Cristina, and Noa** for staying the same despite the distance and the time that has passed! I would also like to thank all the people I met in Quebec. Thank you **Azza, Hajer, Hela, Zeyneb, Daniele, Lucas, Mahsa, Esen, Samira, Sharifun, Cybelle, Thiago, Nidhal, Chahinez, Yosra, Arwa, Ines, Nawel, Emile, Artiom, Marija, Maroua, Amel, Soumia, Slimane, Ahmed, Mehdi, Mohamed, Amina, Asma, Amal, and Elissa** (the list would be too long) for your parties, your BBQs, your brunches, and your meals. I would like to recognize the invaluable friendship that you all provided during these last years. I would especially like to thank **Asma and Ahlem** for being such great friends. Your continued love and support are what motivates me to keep aiming higher.

Most importantly, none of this could have happened without my family. These last years have not been easy, strewn with life's trials, but you have always remained strong in your support and kept me motivated. Despite the distance, you lived this thesis daily with me with moments of joy, doubt and stress. I would like to thank my father (**Mhamed**), my sister (**Sahar**), my brothers (**Mongi and Hakim**), my grandparents, my in-laws (especially **tata Halima** and **Sadok**), and the rest of my family members who supported me in my studies.

Finally, a huge thanks to my beloved husband **Mohamed Amin** who has been supporting me, listening to me and soothing me over the last few years. During these six long years you have been the shoulder on which I have been able to rest. Despite the difficulty of distance, you were able to understand and support me in this adventure.

## FOREWORD

This thesis is written based on the INRS Guide-2019, article-based version in order to fulfill the last requirement of the PhD program.

It consists of an abstract (English and French versions), synopsis (required when a thesis or dissertation is written in English), general introduction, general discussion and conclusion, bibliography, and appendix which will be further discussed in below.

Synopsis: Includes the main points discussed in the document and explains the working hypotheses, research objectives, methodology, and results in much more detail than the abstract does.

Chapter 1: Consists of a review of literature about the ischemia, glutamate excitotoxicity, and enzymatic glutamate degradation approaches. This chapter concludes with a contextualization. Of note, some sections of this chapter are published as part of a manuscript accepted for publication in *Biomaterials* (Appendix C).

Chapter 2: Presents concepts related to PEGylation, its benefits and its drawbacks. This chapter ends with a research proposal, the main hypothesis, and objectives. The figures used in Chapter 1 and 2 are either from the literature or made by me (with BioRender) in order to provide further explanation.

Chapter 3: Published as Zaghmi, A.; Mendez-Villuendas, E.; Greschner, A. A.; Liu, J. Y.; de Haan, H. W.; Gauthier, M. A., Mechanisms of activity loss for a multi-PEGylated protein by experiment and simulation. *Mater Today Chem* 2019, 12, 121-131. I was responsible for data collection and analysis as well as the manuscript composition and revision. Andrea A Greschner contributed to manuscript edits and assisted with the PEGylation experiments. Jun Yang Liu was a summer student under my supervision who assisted with some measures of the enzyme activities. Eduardo Mendez-Villuendas performed the simulations with the help and supervision of Hendrick W de Haan. Marc A Gauthier was the supervisory author and was involved with concept formation, manuscript composition and revision. This Chapter starts with a brief contextualization and finishes with a preliminary study introducing the following paper.

Chapter 4: Accepted as Zaghmi, A.; Dopico-López, A.; Pérez-Mato M.; Iglesias-Rey R.; Hervella P.; Greschner A. A.; Bugallo-Casal A.; Da Silva A.; Gutiérrez-Fernández M.; Castillo J.; Campos Pérez F.; Gauthier, M. A., Sustained blood glutamate scavenging enhances protection in ischemic stroke. *Commun Biol* 2020. I participated in the design and conception of the study, carried out most experiments (synthesis, characterisation, and purification of the bioconjugates; *in vivo* experiences including the functional tests). I also wrote and revised the

manuscript. Antonio Dopico-López contributed with the production of the ischemic rat model. María Pérez-Mato contributed with the production of the ischemic rat model and commented on the manuscript at all stages. Ramón Iglesias-Rey and Pablo Hervella helped with technical assistance (mainly for MRI). Francisco Campos Pérez participated to the design and conception of the study, results discussion, and commented on the manuscript at all stages. Marc A. Gauthier was the supervisory author and was involved with concept formation and manuscript composition and revision.

Chapter 5: General discussion, conclusion and perspectives. Summarizes the main elements of the articles and how they are related. This discussion also presents the contribution of this thesis to the field, as well as the limitations of this work. Both are framed with possible future directions that can be explored.

Chapter 6: Appendix. Contains additional information to complement the body of the text and includes elements that are essential to the understanding of the thesis or to support its argumentation. It further presents scientific papers in which I am first author.

- Appendix A: Supplementary information of Paper 1.
- Appendix B: Supplementary information of Paper 2.
- Appendix C: Review paper, accepted as Zaghmi, A.; Drouin-Ouellet J.; Brambilla, D.; and Gauthier, M. A., Treating Brain Diseases using Systemic Parenterally-administered Protein Therapeutics: Dysfunction of the Brain Barriers and Potential Strategies. *Biomaterials* 2020.
- Appendix D: Data in Brief paper, published as Zaghmi, A.; Greschner, A. A.; Mendez-Villuendas, E.; Liu, J. Y.; de Haan, H. W.; Gauthier, M. A., Determination of the degree of PEGylation of protein bioconjugates using data from proton nuclear magnetic resonance spectroscopy. *Data Brief* 2019, 25.
- Appendix E: Book Chapter, published as Zaghmi, A.; Greschner, A. A.; Gauthier, M. A., In vivo properties of therapeutic bioconjugates composed of proteins and architecturally/functionally complex polymers. *Polymer-Protein Conjugates: From PEGylation and Beyond* 2020, 389-406.

Chapter 7: Contains the bibliography used in this thesis. It should be noted that the references used for each scientific paper are included in this chapter (except for Appendix D and E).

# TABLE OF CONTENTS

ACKNOWLEDGEMENTS .....	ii
Foreword .....	iv
Table of contents .....	vi
List of figures and tables .....	ix
List of acronyms and abbreviations .....	xi
English Abstract and keywords .....	xiii
French abstract and keywords .....	xv
Synopsis in French .....	xviii
Chapter 1: Ischemia, Glutamate Excitotoxicity, and Enzymatic Glutamate Degradation Approaches .....	1
Part 1: Literature Review .....	2
1. Physiology of the central nervous system .....	2
1.1. Arterial vascularisation .....	2
1.2. Physical barriers of the central nervous system .....	3
1.2.1. Transport across the blood–brain interfaces .....	5
2. Ischemic stroke: Generalities and prevalence .....	13
2.1. Pathophysiology of ischemic stroke .....	13
2.1.1. Dysfunction of the blood–brain interfaces .....	15
2.1.2. Glutamate excitotoxicity .....	16
2.1.3. Mechanism of glutamate excitotoxicity .....	22
3. Enzymatic glutamate degradation approaches .....	25
3.1. Glutamate dehydrogenase (GDH) .....	25
3.1.1. Structure .....	25
3.1.2. Dynamics .....	25
3.1.3. Activity .....	26
3.1.4. Homotropic and heterotropic regulation .....	27

3.1.5. Exploitation of GDH for treating ischemia .....	29
3.2. Glutamate oxaloacetate transaminase (GOT).....	29
3.2.1. Structure.....	29
3.2.2. Activity.....	30
3.2.3. Exploitation of GOT for treating ischemia .....	30
Part 2: Contextualization .....	33
Chapter 2: PEGylation.....	34
Part 1: Literature Review.....	35
1. Overview .....	35
2. Benefits of PEGylation .....	38
2.1. Influence of PEGylation on protein stability.....	39
2.2. Influence of PEGylation on the kidney clearance of proteins .....	39
2.3. Influence of PEGylation on immunogenicity and antigenicity of proteins .....	40
2.4. Influence of PEGylation on proteolytic degradation of proteins.....	41
3. Potential drawbacks of PEGylation.....	41
Part 2: Research proposal, hypothesis and objectives .....	43
Chapter 3: Article 1 .....	44
1. Preface.....	45
2. Follow-up .....	68
Chapter 4: Article 2.....	70
Chapter 5: General Discussion, Conclusion, and Perspectives .....	93
1. General discussion .....	94
2. Conclusion and perspectives .....	104
Appendix pages.....	106
Appendix A: Supplementary Information of Paper 1 .....	107
Appendix B: Supplementary Information of Paper 2 .....	127
Appendix C: Review Paper .....	139
Appendix D: Data in Brief Paper .....	205

Appendix E: Book Chapter.....	213
Bibliography.....	232

## LIST OF FIGURES AND TABLES

Figure 1: Illustration of cerebrovascular anatomy in rats.....	3
Figure 2: Location of the barriers of the nervous system and structure of the BBB and BCSFB. The five barriers are represented in a longitudinal brain section. (a) Schematic representation of the BCSFB: the capillaries in the choroid plexus permit the facile diffusion of molecules <i>via</i> intracellular fenestrations. Epithelial cells are joined by adherens and tight junctions. The presence of microvilli increases the surface area of the CSF-facing side of the epithelial cells. (b) Schematic representation of the BBB: the BBB is composed of endothelial cells that are surrounded by a basal membrane in close association with astrocyte end feet and pericytes. Neurons and microglia are also important mediators of BBB integrity. Cerebral endothelial cells are sealed together by tight junctions.....	4
Figure 3: Transport mechanisms across brain barriers (a) and the general structure of the transferrin receptor (TfR) (b), insulin receptor (c), and low-density lipoprotein receptor (LDLR) (d). These receptors have been largely explored as brain targeting entities for proteins <i>via</i> a RMT.....	6
Figure 4: Angiopep peptides designs as targeting members of LRP1. (a) The amino acid sequences of tested Angiopep peptides are presented. Changes in the amino acid sequence (when compared to Angiopep-2) are indicated with an asterisk. (b) Volumes of distribution of Angiopep peptides in the brain parenchyma measured by <i>in situ</i> brain perfusion. Reprinted with permission from reference <sup>141</sup> . .....	12
Figure 5: Simplified overview of the pathophysiological mechanisms of ischemic stroke. Energy failure leads to depolarization of neurons, excessive release of glutamate, and failure of ionic pumps. These events lead to an over-activation of specific glutamate receptors, an intracellular accumulation of Na <sup>+</sup> and Ca <sup>2+</sup> , an efflux of potassium, a spreading wave of depolarization, and cell swelling. Increased calcium concentrations cause numerous damages (oxidative stress, inflammation, cell death). .....	14
Figure 6: Illustration of a hypothetical synapse showing glutamatergic receptors. ....	17
Figure 7: Main metabolic and cycling pathways of glutamate in the brain. ....	21
Figure 8: Implication of astrocytes, microglia, and oligodendrocytes in excitotoxicity. Reprinted with permission from reference <sup>259</sup> . .....	23
Figure 9: Structure and main conformational movements of GDH during the oxidative deamination reaction. As glutamate binds, the NAD <sup>+</sup> binding domain rotates and closes the	

catalytic cleft (1), the base of antenna pushes against the pivot helix (2), the antenna becomes distorted (3), and the core of the hexamer compresses (4). .....	26
Figure 10: Mechanism of the scavenging effect. Under physiological conditions, the efflux of glutamate is practically absent. During ischemia, as the concentration of glutamate in the brain increases, the efflux of glutamate into the blood is enhanced. In the presence of a glutamate scavenger (such as GOT), the efflux is much more pronounced. ....	31
Figure 11: Most common potential sites of PEGylation in proteins. ....	37
Figure 12: (a) Visualization of GDH bioconjugates. (b) <i>In vitro</i> enzymatic activity of the bioconjugates. Asterisk denote statistical differences with respect to native enzyme (0 mPEG) (ANOVA, Tukey, $p < 0.05$ ). Data presented as Mean + SD, $n = 3$ . ....	45
Figure 13: GDH activity and glutamate levels in the blood. Saline (a) and unPEGylated GDH (b) were administered to healthy rats. Data presented as Mean + SD, $n = 3$ . Note: No statistical tests are shown here for simplification. ....	68
Figure 14: Overview of the homeostasis of glutamate and/or its metabolites between the different parts of the body following administration of GDH bioconjugates. The size of the arrows indicates the expected respective contribution of each compartment. ....	101
Table 1: Approved PEGylated protein therapeutics. ....	36

## LIST OF ACRONYMS AND ABBREVIATIONS

- ABC:** Adenosine triphosphate binding cassette transporters
- ACA:** Anterior cerebral artery
- Acetyl-CoA:** Acetyl coenzyme
- ADP:** Adenosine diphosphate
- AMPA:**  $\alpha$ -amino-3-hydroxy-5-methyl-4-isoazolepropionic acid
- Apo:** Apolipoprotein
- ATP:** Adenosine triphosphate
- BBB:** Blood-brain barrier
- BCH:** 2-aminobicyclo-(2,2,1)-heptane-2-carboxylic acid
- BCRP:** Breast cancer-resistance proteins
- BCSFB:** Blood-cerebrospinal fluid barrier
- BHE:** Barrière hémato-encéphalique
- cAMP:** Cyclic adenosine monophosphate
- CSF:** Cerebrospinal fluid
- EAAT:** Excitatory amino acid transporter
- GDH:** Glutamate dehydrogenase
- GLUT:** Glucose transporters
- GOT:** Glutamate oxaloacetate transaminase
- GPT:** Glutamate pyruvate transaminase
- GS:** Glutamine synthetase
- GTP:** Guanosine triphosphate
- hrGOT:** Human recombinant glutamate oxaloacetate transaminase
- CI50:** Concentration inhibitrice médiane
- IFN- $\alpha$ :** Interferon- $\alpha$
- Ig:** Immunoglobulins
- LCR:** Liquide céphalorachidien
- LDH:** Lactate dehydrogenase
- LDL:** Low-density lipoprotein
- LDLR:** Low-density lipoprotein receptor
- LRP1:** Low-density lipoprotein receptor-related protein 1
- MCA:** Middle cerebral artery

**MCAo:** MCA occlusion  
**MCT:** Monocarboxylate transporter  
**MDR:** Multidrug-resistance proteins  
**mPEG:** Methoxy-polyethylene glycol  
**MRP:** Multidrug resistance-related proteins  
**MW:** Molecular weight  
**NAD<sup>+</sup>:** Nicotinamide adenine dinucleotide  
**NADP<sup>+</sup>:** Nicotinamide adenine dinucleotide phosphate  
**NMDA:** N-methyl-D-aspartate  
**PEG:** Polyethylene glycol  
**PM:** Poids moléculaire  
**rhGOT:** Glutamate oxaloacétate transaminase recombinante humaine  
**RMN:** Résonance magnétique nucléaire  
**RMT:** Receptor-mediated transcytosis  
**SDS PAGE:** Électrophorèse en gel de polyacrylamide contenant du dodécysulfate de sodium  
**SEC:** Chromatographie d'exclusion stérique  
**TfR:** Transferrin receptor  
**TfRMAb:** Anti-TfR monoclonal antibodies  
**VGLUT:** Vesicular glutamate transporters

## ENGLISH ABSTRACT AND KEYWORDS

Glutamate, the major excitatory neurotransmitter in the brain, is functionally involved in almost all activities of the nervous system but is especially important for learning and memory. Unlike other neurotransmitters, the regulation of extracellular glutamate is unique in that there are no extracellular enzymes for its degradation. Instead, homeostasis of the extracellular glutamate concentration is mainly maintained through cellular uptake by a variety of transporters. This regulation is essential because excess glutamate in the interstitial fluid results in a cascade of harmful processes leading to neuron destruction, a process called excitotoxicity. This pathological process is common to various neurological incidents such as Alzheimer's disease, traumatic brain injury, or stroke, which is the focus of this project. Stroke is the second leading cause of death and the third leading cause of disability in the world. After an ischemic stroke, the rapid increase of glutamate levels in the brain interstitial fluid represents a major gateway for the development and progression of a cascade of events involving a multimodal and multicell series of downstream mechanisms. Consequently, a good deal of effort has been devoted to developing drugs that inhibit glutamate receptors (receptor antagonists). However, although these molecules have shown therapeutic efficacy, they have limited usefulness because of their difficulty in penetrating the blood-brain barrier (BBB). As such, they have low cerebral bioavailability despite large quantities being administered systematically. Furthermore, additional problems arise due to the lack of discrimination between the diverse actions of the receptor; they interfere with both the negative and positive aspects of its signaling.

Because of these shortcomings, an alternative therapeutic strategy is necessary for the efficient reduction of glutamate excitotoxicity. One approach relies on the natural diffusion of cerebral glutamate across the BBB. By using glutamate-degrading enzymes (e.g., glutamate oxaloacetate transaminase (GOT) or glutamate dehydrogenase (GDH)), the depletion of blood glutamate levels occurs and the efflux of cerebral glutamate across the BBB is encouraged. This approach has been explored as a way to lower excessive brain concentrations of glutamate after an ischemic stroke. However, one major shortcoming is that its effect is short-lived, mainly because of the enzymes' rapid elimination from circulation. In this context, frequent re-administration or continuous infusion would be required, creating practical difficulties as well as increasing the risk of developing secondary effects. One approach to increase the therapeutic lifetime of such enzyme is through polymer grafting (creating bioconjugates). Attaching biocompatible polymers, such as methoxy-poly(ethylene glycol) (mPEG), to enzymes of interest has been demonstrated to drastically prolong their circulation lifetime, often from hours to several days. The rationale is that the mPEG corona prevents the tissular uptake and protects the enzyme from proteolytic degradation and immune recognition. Regrettably, these pharmacokinetic ameliorations usually come with the cost of reduced enzymatic activity of PEGylated enzymes, which is most often rationalized as direct modification of the protein's active site or steric hindrance near its surface. While these mechanisms are generally accepted and likely valid, very few studies investigated other possible mechanisms of activity loss.

To explore this question, in the first part of this thesis, we developed several bioconjugates bearing up to 25 chains of mPEG (mPEG-GDH) in order to demystify the mechanisms of activity loss of GDH upon PEGylation. Analysis of the catalytic activity of the bioconjugates

demonstrated that the reduced activity was not associated to the direct modification of the active site of GDH. Moreover, experiments suggested that while the secondary and tertiary structures of GDH were affected by PEGylation, these changes did not necessarily result in a loss of activity. By measuring catalytic activity in the presence of five different allosteric modulators, loss of activity could not be ascribed to an altered local microenvironment at the protein's surface either. As such, coarse-grained simulations were exploited to reveal the effect of PEGylation on protein dynamics, which are long-ranged, cooperative, and essential for GDH catalytic activity. Reduced dynamic motion was observed as a function of mPEG molecular weight (MW) and correlated well with trends observed for the library of bioconjugates tested experimentally. Once the mechanisms of deactivation of GDH were clarified, as a proof of concept, we assessed the *in vivo* effect of native GDH on glutamate levels. Unfortunately, at the tested conditions, no correlation between enzymatic activity and glutamate levels was identified. We suspect (retrospectively at the end of this thesis) that the therapeutic effects of glutamate-degrading enzymes cannot be determined only by measuring the blood/CSF glutamate levels. Therefore, a more advanced study should provide a better discernment of the therapeutic doses and the potential effects of GDH. These results, prompted us to replace GDH with GOT for the next stages of the work, owing to the greater body of literature exploring the latter enzyme.

In the second part of this thesis, we investigated the neuroprotective properties of human recombinant GOT (hrGOT) bioconjugates in an ischemic stroke model. We demonstrated that, following a single administration, PEGylated hrGOT exhibited a significantly prolonged blood residence time (6 days for mPEG-hrGOT *versus* 6 hours for native hrGOT). Substantially greater protection was achieved using the hrGOT bioconjugates compared to the native hrGOT, in terms of infarct size and retention of motor functions using sensorimotor tests, which are important clinical outputs. By measuring the glutamate levels, we concluded that these improvements were likely due to bioconjugates drawing glutamate out of the brain and by displacing homeostasis between the different glutamate pools of the body. Moreover, we hypothesized that while peripheral depletion of glutamate appeared to be well tolerated, the accumulation of hrGOT at the blood side of the BBB (and potentially crossing to the brain parenchyma) could offer better neuroprotection by promoting a more significant glutamate efflux. Therefore, we further modified hrGOT with multiple chains of PEG bearing at their extremity a targeting ligand for the BBB (Angiopep-2). However, targeting the bioconjugates to the BBB did not improve their therapeutic performances. We suggest that brain or near-brain accumulation of the Angiopep-PEG-hrGOT represented only a very minor fraction of the total administered dose and did not contribute significantly to the outcomes.

Overall, our results demonstrated that maintaining high and relatively stable glutamate-degrading enzymatic blood activity over a period of several days had a significant beneficial effect on infarct volume as well as sensorimotor function. Evidently, the protective properties of other enzymes (such as GDH) could be further explored based on the new knowledge acquired in this thesis. The efficacy of this strategy holds great potential as a therapy for stroke, as well as other pathologies associated with excitotoxicity such neurodegenerative diseases.

Keywords: Ischemic stroke, glutamate, excitotoxicity, enzymes, dynamic, structures, PEG, scavenging effects, bioconjugates, therapeutics.

## FRENCH ABSTRACT AND KEYWORDS

Le glutamate, principal neurotransmetteur excitateur du système nerveux, est impliqué dans quasiment toutes les fonctions neuronales, particulièrement celles relatives aux processus d'apprentissage et de mémorisation. Contrairement aux autres neurotransmetteurs, la régulation des niveaux extracellulaires du glutamate est unique: sa recapture est assurée par des transporteurs cellulaires et n'implique pas une dégradation enzymatique extracellulaire. Cette homéostasie est indispensable car l'augmentation des concentrations interstitielles du glutamate conduit à la destruction des neurones par un processus appelé « excitotoxicité ». Ce processus pathologique est commun à diverses maladies neurologiques telles que la maladie d'Alzheimer, la lésion cérébrale traumatique ou encore l'accident vasculaire cérébral, qui fait l'objet de cette thèse. Ce dernier représente la deuxième cause de décès et la troisième cause d'invalidité dans le monde. À la suite d'une ischémie cérébrale, l'élévation rapide des concentrations interstitielles du glutamate et la suractivation des récepteurs glutamatergiques constituent des déterminants initiaux contribuant à promouvoir le stress oxydatif, l'apoptose et l'inflammation, responsables de l'évolution spatio-temporelle de la lésion ischémique. Dans ce contexte, plusieurs molécules thérapeutiques, bloquant les récepteurs glutamatergiques, ont été développées et ont fait leurs preuves dans les modèles expérimentaux. Néanmoins, elles ont abouti systématiquement à un échec dans les applications cliniques. Ceci est dû, en grande partie, à la présence de la barrière hémato-encéphalique (BHE) qui réduit leurs biodisponibilités cérébrales, malgré les grandes quantités ayant été administrées. De plus, ces antagonistes avaient causé des effets secondaires supplémentaires en raison de l'absence de discrimination entre les diverses actions du récepteur: elles interfèrent avec les aspects négatifs et positifs de sa signalisation. De ce fait, d'autres pistes thérapeutiques ont été explorées, notamment celles faisant appel à l'efflux du glutamate du cerveau vers le sang à la suite de la rupture du gradient de concentration entre ces deux compartiments. En effet, il a été suggéré que l'administration intraveineuse d'une enzyme dégradant le glutamate (la glutamate oxaloacétate transaminase (GOT)) avait permis la dégradation du glutamate et la diminution de ses concentrations sanguines, une diminution compensée par la migration du glutamate cérébral « toxique » vers le sang. Cependant, bien que cette enzyme représentât une molécule prometteuse pour la réduction de l'excitotoxicité et le traitement de l'ischémie cérébrale, ses propriétés physico-chimiques et ses profils pharmacocinétiques limitaient considérablement son développement thérapeutique. Dans ce contexte, et dans le but de surmonter ces limitations, plusieurs approches pourraient être envisagées, telles que la modification de la surface de la GOT par des polymères (création de bioconjugués). En effet, le greffage du méthoxy-poly(éthylène glycol) (mPEG) à des protéines avait permis d'améliorer significativement, entre autres, leurs profils pharmacocinétiques.

Dans le cadre de ce projet de thèse, nous avons proposé de développer différents bioconjugués formés par des enzymes de dégradation du glutamate (la forme recombinante humaine de la GOT (rhGOT) dont l'effet a été déjà démontrée et la glutamate déshydrogénase (GDH) pas encore explorée) afin d'étudier leurs effets thérapeutiques pour le traitement de l'ischémie cérébrale. Pour ce faire, nous avons initialement procédé à la PEGylation de nos enzymes d'intérêt, et avons observé que, par rapport à la rhGOT, l'activité enzymatique de la GDH PEGylée avait significativement diminué. Malheureusement, bien que les effets de réduction d'activité soient communs, très peu d'études avaient étudié les mécanismes

potentiels de désactivation des protéines PEGylées.

Par conséquent, dans la première partie de cette thèse, nous avons développé plusieurs bioconjugués portant jusqu'à 25 chaînes de mPEG (mPEG-GDH) afin de démystifier les mécanismes de perte d'activité de la GDH lors de la PEGylation. L'analyse de l'activité catalytique des bioconjugués a démontré que l'activité réduite n'était pas associée à la modification directe du site actif. De plus, les expériences ont suggéré que, même si la structure secondaire/tertiaire de la GDH ait été affectée par la PEGylation, ces modifications n'entraînaient pas nécessairement une perte d'activité. En mesurant l'activité catalytique en présence de cinq différents modulateurs allostériques, la perte d'activité ne pouvait pas, non plus, être attribuée à une modification du microenvironnement local à la surface de la protéine. Ainsi, des simulations ont été effectuées pour révéler l'effet de la PEGylation sur la dynamique moléculaire de la GDH. Une réduction des mouvements dynamiques de la GDH, dépendante du poids moléculaire (PM) du mPEG, a été notée. Cette réduction a parfaitement corrélé avec les tendances expérimentales observées. Dans l'ensemble, nous avons conclu que la perte de l'activité enzymatique était principalement associée à un effet sur la dynamique moléculaire. Une fois que les mécanismes de désactivation ont été clarifiés, nous avons décidé de tester l'effet thérapeutique de certains bioconjugués. Pour cela, nous avons effectué une étude pilote, *in vivo*, dans laquelle l'effet de la GDH sur les niveaux du glutamate a été évalué. Malheureusement, dans les conditions testées, aucune corrélation entre l'activité enzymatique et les niveaux sanguins/cérébraux du glutamate n'a été identifiée. Nous suspectons (rétrospectivement à la fin de cette thèse) que la dose injectée n'était pas adéquate et que les effets thérapeutiques des enzymes dégradant le glutamate ne pouvaient pas être évalués uniquement en mesurant les concentrations du glutamate. À la suite de ces résultats, la rhGOT a été choisie pour les prochaines étapes du travail, étant donné que les effets de cette enzyme étaient relativement beaucoup mieux documentés.

Dans la deuxième partie de cette thèse, nous avons étudié les effets neuroprotecteurs des bioconjugués mPEG-rhGOT dans un modèle animal d'ischémie cérébrale. Nous avons démontré qu'après une seule administration, la rhGOT PEGylée présentait une demi-vie de circulation prolongée (6 jours pour les mPEG-rhGOT *versus* 6 heures pour la rhGOT native). Fait important, les mPEG-rhGOT ont procuré une neuroprotection remarquablement plus importante que celle de la rhGOT non-PEGylée: une réduction significative du volume de l'infarctus cérébral ainsi qu'une préservation des fonctions motrices. En mesurant les niveaux du glutamate, nous avons conclu que ces améliorations thérapeutiques étaient dues à la réduction des niveaux du glutamate au niveau du liquide interstitiel cérébral et au déplacement de l'équilibre du glutamate (ou de ses métabolites) entre les différents compartiments du corps. En outre, nous avons supposé que, même si la déplétion périphérique du glutamate semblait être tolérée, l'accumulation de la rhGOT du côté sanguin de la BHE (et potentiellement son passage vers le parenchyme cérébral) pourrait offrir une meilleure neuroprotection. Nous avons donc modifié la rhGOT avec de multiples chaînes de PEG portant à leurs extrémités un ligand de ciblage de la BHE (Angiopep-2). Nos résultats avaient démontré que le ciblage des bioconjugués n'a pas amélioré les performances thérapeutiques de la rhGOT PEGylée. Nous avons alors suggéré que l'accumulation cérébrale des bioconjugués ne représentait qu'une très faible fraction de la dose totale administrée et ne contribuait pas de manière significative aux effets thérapeutiques.

Dans l'ensemble, nous avons démontré que le maintien d'une activité enzymatique sanguine soutenue de la rhGOT avait un effet bénéfique sur le volume de l'infarctus et sur les fonctions

sensorimotrices. De plus, sur la base des nouvelles connaissances acquises dans le cadre de cette thèse, les effets neuroprotecteurs de la GDH et des bioconjugués produits pourraient être étudiés d'une manière plus approfondie. Finalement, l'efficacité de cette stratégie offre un grand potentiel en tant que thérapie pour l'ischémie cérébrale et pour d'autres pathologies associées à l'excitotoxicité (telles que les maladies neurodégénératives).

Mots-clés: ischémie cérébrale, glutamate, excitotoxicité, enzymes, dynamique, structures, PEG, bioconjugués, thérapeutique.

## SYNOPSIS IN FRENCH

### Développement de bioconjugués thérapeutiques neuroprotecteurs pour traiter l'ischémie cérébrale

#### 1. Introduction

L'accident vasculaire cérébral est un déficit neurologique soudain d'origine vasculaire causé par un infarctus ou une hémorragie au niveau du cerveau. Au Canada, cette pathologie représente la troisième cause de décès et la principale cause d'invalidité chez les adultes <sup>1</sup>. On distingue essentiellement deux types d'accidents vasculaires cérébraux: les hémorragies cérébrales et les ischémies cérébrales (ou infarctus cérébraux). Environ 80 % des accidents vasculaires cérébraux sont ischémiques et résultent le plus souvent de l'occlusion d'une artère cérébrale par un caillot sanguin (thrombus). Au cours d'une ischémie cérébrale, la réduction du débit sanguin restreint profusément l'apport en substrats énergétiques (essentiellement l'oxygène et le glucose). Cette déplétion énergétique altère le fonctionnement des pompes ATPase, ce qui perturbe les gradients ioniques cellulaires. La dépolarisation neuronale, qui en découle, déclenche une libération accrue de neurotransmetteurs, en particulier de glutamate, qui s'accumule au niveau du milieu extracellulaire <sup>2,3</sup>. L'accumulation de ce neurotransmetteur excitateur dans le milieu interstitiel cérébral est néfaste puisqu'elle déclenche une série de processus préjudiciables qui compromettent la viabilité des tissus et qui entraînent l'extension des lésions cérébrales <sup>4-6</sup>. En effet, la présence de concentrations élevées du glutamate au niveau extracellulaire induit la suractivation des récepteurs glutamatergiques, notamment les récepteurs ionotropiques N-méthyl-D-Aspartate (NMDA). Cette suractivation conduit, entre autres, à l'augmentation des niveaux intracellulaires de calcium générant d'autres processus délétères post-ischémiques (stress oxydant, inflammation) et conduisant ultimement à la destruction des cellules neuronales par excitotoxicité <sup>4-10</sup>.

Plusieurs recherches ont démontré que les processus excitotoxiques semblent être des mécanismes au cœur de l'ischémie cérébrale, qui apparaissent assez tôt et qui contribuent au développement de l'ensemble des lésions post-ischémiques. Par conséquent, plusieurs tentatives thérapeutiques ont été entretenues pour réduire l'excitotoxicité. Initialement, la recherche d'agents neuroprotecteurs était concentrée sur le développement des antagonistes des récepteurs NMDA et sur les inhibiteurs des canaux calciques <sup>11</sup>. Cependant, vu que plusieurs problèmes essentiellement relatifs à leurs faibles biodisponibilités cérébrales ont

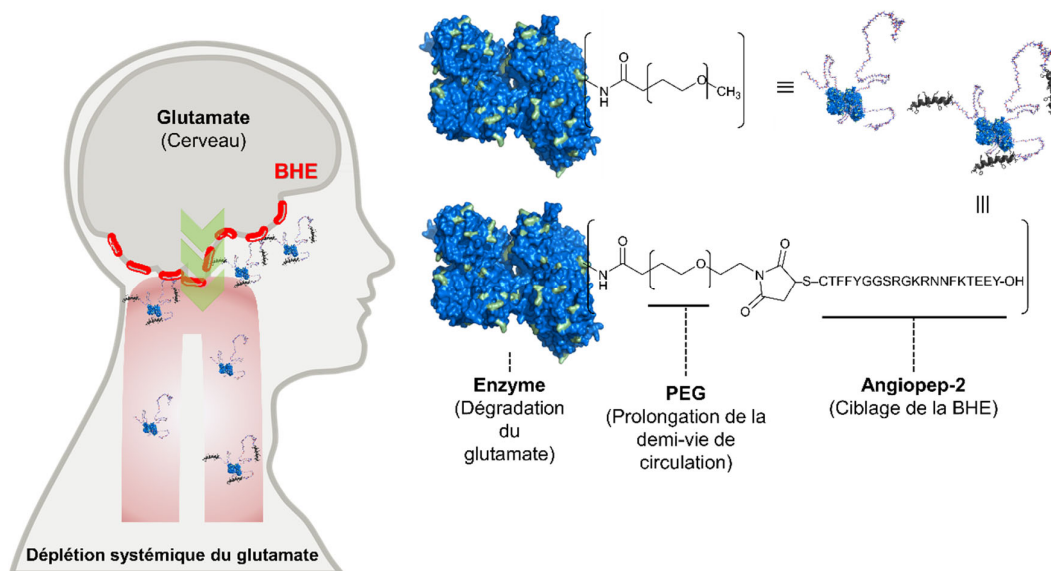
surgi<sup>12-15</sup>, de nouvelles pistes thérapeutiques ont été explorées. Parmi celles-ci, les stratégies visant à réduire les niveaux du glutamate synaptique en utilisant un « piègeur » sanguin. Dans ce sens, la glutamate oxaloacétate transaminase (GOT) a été suggérée comme molécule neuroprotectrice. En effet, son injection intraveineuse avait permis la dégradation du glutamate, la diminution de ses concentrations sanguines, l'activation de l'efflux du glutamate du cerveau vers le sang, et ainsi la réduction de ses concentrations cérébrales extracellulaires. Cette approche diffère considérablement des autres alternatives thérapeutiques étant donné qu'afin d'exercer l'effet souhaité, le passage de la GOT à travers la barrière hémato-encéphalique (BHE) n'est pas nécessaire. De plus, il a été suggéré que le glutamate est éliminé uniquement au niveau des zones cérébrales où il est présent en excès<sup>16</sup>. Le piégeage du glutamate paraît également autolimitant et semble diminuer suite à la réduction du gradient de concentration entre le cerveau et le sang<sup>17</sup>. Malheureusement, ces avantages thérapeutiques sont grandement limités par les propriétés intrinsèques et pharmacocinétiques de la GOT<sup>18-20</sup>. En effet, la GOT possède une demi-vie de circulation assez courte à cause de son internalisation par différents tissus et sa métabolisation rapide<sup>18</sup>. Conséquemment, l'administration répétée ou la perfusion continue de celle-ci pourrait éventuellement prolonger l'effet thérapeutique. Cependant, de telles procédures ne sont pas souhaitables, vu que l'utilisation de quantités élevées de GOT pourrait augmenter le risque de développer des effets secondaires.

Afin d'obtenir une activité efficace et soutenue dans l'organisme, plusieurs stratégies peuvent être envisagées<sup>21-23</sup>, dont la PEGylation. La PEGylation est le processus par lequel des molécules de polyéthylène glycol (PEG) sont attachées aux molécules (l'ensemble PEG-molécule est appelé un « bioconjugué »). La modification des protéines par le PEG offre généralement de nombreux avantages. La PEGylation, d'une part, améliore la stabilité physique et thermique ainsi que la solubilité des protéines et d'autre part, améliore leurs propriétés pharmacocinétiques (en réduisant la clairance rénale, l'immunogénicité, l'antigénicité, la protéolyse, l'absorption tissulaire et la métabolisation des protéines PEGylées). L'ensemble de ces améliorations réduit la fréquence des administrations tout en maintenant les effets pharmacologiques. Malgré ces nombreux avantages, il existe encore quelques inconvénients qui, s'ils sont pris en compte, pourraient encore accroître les bienfaits de la PEGylation. Effectivement, des problèmes liés à l'excrétion par l'organisme ainsi qu'aux réactions immunitaires de certains bioconjugués ont été signalés<sup>24-26</sup>. De plus, étant donné qu'une ou plusieurs molécules de méthoxy-PEG (mPEG) sont généralement liées à la protéine, son activité biologique pourrait diminuer lors de la PEGylation. Toutefois, dans de nombreux cas, cette réduction est compensée dans les systèmes biologiques par une augmentation de la demi-vie.

## 2. Hypothèses et objectifs

En se basant sur les faits présentés ci-dessous, nous avons émis l'hypothèse que la modification des enzymes de dégradation du glutamate par le mPEG pourrait permettre de développer de nouvelles thérapies efficaces pour la réduction des processus excitotoxiques et le traitement de l'ischémie cérébrale. En plus de la forme recombinante humaine de la GOT (rhGOT), nous avons sélectionné la glutamate déshydrogénase (GDH) comme une deuxième enzyme qui pourrait être potentiellement intéressante en tant qu'agent thérapeutique. Notre choix était basé sur des études *in vivo* démontrant que les souris ischémiques, surexprimant la GDH, présentaient des lésions ischémiques et des œdèmes de plus petits volumes par rapport aux souris ayant une expression normale de GDH <sup>27</sup>. De surcroît, des études récentes avaient reporté que l'activation allostérique de la GDH améliorait l'état énergétique intracellulaire, diminuait le volume total de l'infarctus et réduisait la mortalité chez un modèle animal d'ischémie cérébrale temporaire par occlusion de l'artère cérébrale moyenne (MCAo) <sup>28</sup>.

Nos objectifs initiaux étaient de développer des bioconjugués neuroprotecteurs (mPEG-GDH et mPEG-rhGOT) afin d'évaluer leurs effets de « piégeage » du glutamate et leurs efficacités thérapeutiques dans un modèle MCAo. De plus, nous avons suggéré que même si les actions de ces formulations proviendraient essentiellement de leurs actions périphériques, accroître leurs effets centraux (au niveau du cerveau) pourrait offrir une meilleure neuroprotection. Ceci étant possible par le ciblage cérébral et la modification supplémentaire des bioconjugués par des ligands qui reconnaissent des récepteurs à la surface de la BHE <sup>29</sup>. Parmi ces ligands, l'Angiopep-2, une séquence de reconnaissance des récepteurs de lipoprotéine de basse densité (LRP1), a suscité un intérêt considérable pour l'administration de nombreuses molécules à visée cérébrale <sup>30-33</sup>. Les LRP1 sont membres de la famille des récepteurs des lipoprotéines de basse densité (LDL) et sont fortement exprimés au niveau de la BHE <sup>34-36</sup>. De ce fait, notre objectif suivant fut la fonctionnalisation des bioconjugués par l'Angiopep-2 dans le but d'augmenter leurs biodisponibilités (systémiques et cérébrales) ainsi que leurs effets thérapeutiques (Figure S1).



FigureS1: Représentation schématique des objectifs.

### 3. Méthodes, principaux résultats et discussion

Comme première étape, nous avons procédé aux réactions de bioconjugaison entre les enzymes et le mPEG (de poids moléculaire (PM) égal à 5 kDa). Étonnamment, à la suite de la PEGylation, nous avons noté une réduction substantielle de l'activité de la GDH par rapport à celle de la rhGOT. Parallèlement, nous avons remarqué que malgré le grand nombre de littérature sur les protéines multi-PEGylées, les recherches ont rarement exploré les mécanismes potentiels de la perte des activités biologiques de celles-ci. Par conséquent, dans la première partie de ce projet, nous avons entamé une étude fondamentale dans laquelle nous nous sommes intéressés à la conception et au développement rationnel de la GDH multi-PEGylée pour étudier les mécanismes possibles de perte d'activité catalytique.

Treize différents mPEG-GDH (notés 1-13) ont été préparés en ciblant les groupements amines de l'enzyme (Tableau S1). La caractérisation subséquente a révélé que ces bioconjugués possédaient environ 1, 3, 10 ou 25 molécules de 0,5-5 kDa mPEG. Le degré de PEGylation optimal obtenu avec le PM 20 kDa était de 3 mPEG par enzyme et ceci était en accord avec la majorité des travaux PEGylant les protéines avec du mPEG de PM élevé <sup>37,38</sup>. En effet, il a été proposé que lorsque la taille du mPEG augmente (notamment au-delà de 10-20 kDa), celui-ci bloque l'accessibilité aux restes des groupements réactifs par des effets stériques <sup>39</sup>. Ainsi, nos bioconjugués conçus représentaient la plupart des protéines multi-PEGylées.

Tableau S1: Caractéristiques des bioconjugués étudiés.

Bioconjugué	PM du mPEG (kDa)	Degré de PEGylation <sup>1</sup>			Indice de polydispersité
		SDS PAGE <sup>2</sup>	<sup>1</sup> H RMN <sup>3</sup>	SEC <sup>4</sup>	
<b>1</b>	0.5	0 – 1	0	0	1.07
<b>2</b>		0 – 1	2	0	1.07
<b>3</b>		9 – 15	7	18	1.07
<b>4</b>		18 – 24	17	30	1.14
<b>5</b>	2	0 – 1	2	1	1.04
<b>6</b>		0 – 2	3	4	1.03
<b>7</b>		10 – 16	7	6	1.02
<b>8</b>		19 – 23	15	19	1.12
<b>9</b>	5	0 – 1	1	1	1.1
<b>10</b>		1 – 2	3	6	1.1
<b>11</b>		18 – 24	10	14	1.09
<b>12</b>		27 – 35	30	27	1.07
<b>13</b>	20	2 – 3	3	6	1.13

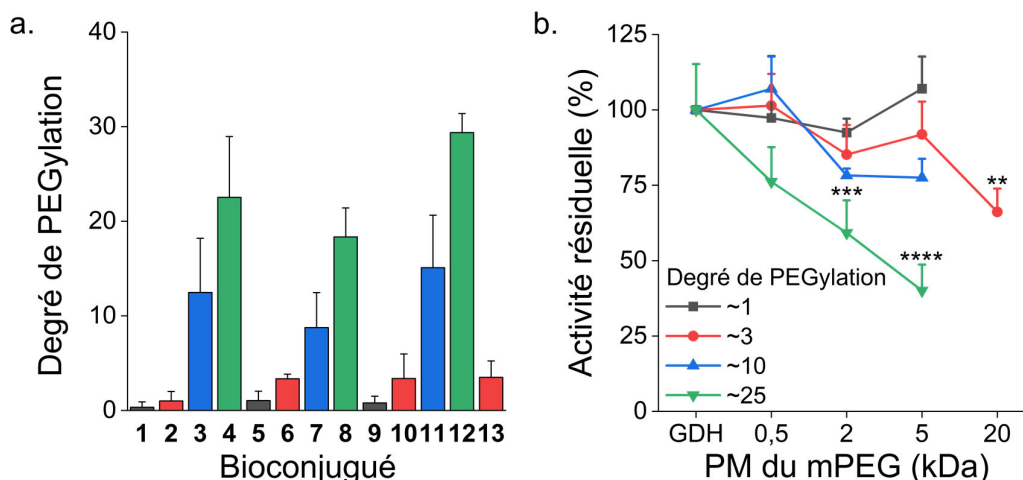
<sup>1</sup>: Nombre de chaînes mPEG par protéine (hexamère)

<sup>2</sup>: Électrophorèse en gel de polyacrylamide contenant du dodécylsulfate de sodium

<sup>3</sup>: Résonance Magnétique Nucléaire de proton

<sup>4</sup>: Chromatographie d'exclusion stérique

La mesure de l'activité enzymatique de ceux-ci a démontré que les bioconjugués présentant un faible degré de PEGylation et de longues chaînes mPEG (~3 × 20 kDa mPEG) ainsi que les bioconjugués présentant un degré de PEGylation plus élevé et des chaînes mPEG plus courtes (~25 × 2 ou 5 kDa mPEG) ont présenté une diminution significative de leurs activités catalytiques. En revanche, l'activité des bioconjugués ayant 25 × 0.5 kDa mPEG n'était pas significativement différente de celle de la protéine native (Figure S2b). Sur la base de ces observations, nous avons exploré chaque cause potentielle de désactivation de la GDH. Évidemment, comme notre objectif ultime serait d'utiliser ces bioconjugués pour des applications thérapeutiques, nous avons anticipé que les bioconjugués portant ~1 et ~3 chaînes de 0,5–5 kDa mPEG seraient moins pertinents que ceux ayant plus de 10 molécules de mPEG par GDH. Par conséquent, dans ce qui a suivi, nous nous sommes intéressés aux bioconjugués portant plus que 10 molécules de 0,5–5 kDa mPEG.

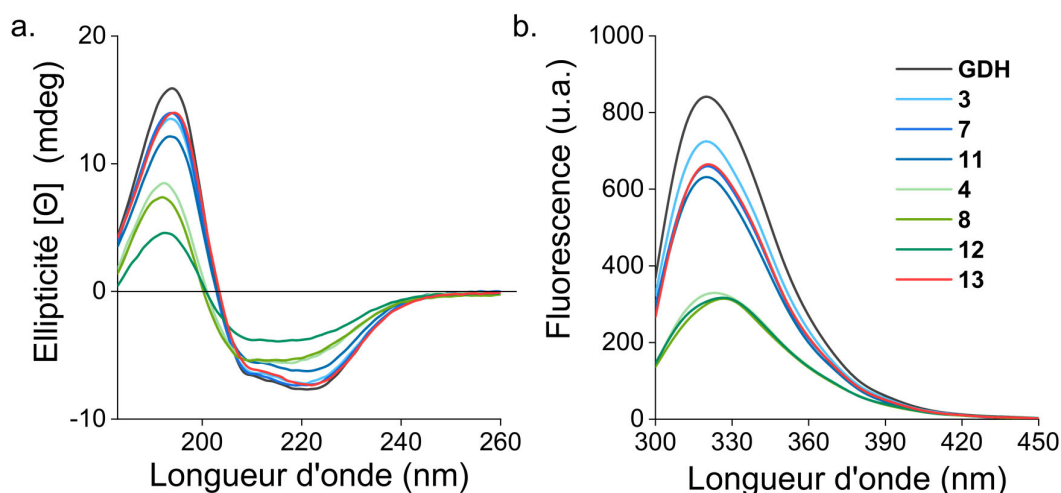


FigureS2: (a) Degré de PEGylation moyen. (b) Activité enzymatique des bioconjugués. (\*) Indique des différences statistiquement significatives par rapport à la GDH native (Tukey,  $p = 0,05$ ). Les résultats sont exprimés en moyennes + SD,  $n=3$ .

Tout d'abord, nous avons évalué si la perte d'activité était due à la modification directe du site actif de la GDH, une hypothèse courante dans la littérature <sup>40-42</sup>. Cependant, l'enzymologie de la GDH révélait certaines particularités permettant d'éviter la désactivation par modification du site actif. D'une part, cette enzyme possède six sites catalytiques identiques qui ne sont pas susceptibles d'être simultanément PEGylés, en raison de la faible accessibilité aux solvants des groupements réactifs présents au niveau de ces régions <sup>43</sup>. D'autre part, des études antérieures ont démontré que chaque monomère de la GDH contribuait au processus catalytique global d'une manière inéquivalente et que l'inhibition d'un seul site catalytique entraînait une perte d'activité de 54% <sup>44-49</sup>. Cela suggérait que les bioconjugués ayant une activité résiduelle supérieure à 46% par rapport à la protéine native possédaient les six sites catalytiques disponibles et non PEGylés. Par conséquent, en considérant l'activité enzymatique de nos bioconjugués, nous avons déduit que la perte d'activité ne pouvait pas être attribuée à la modification du site actif.

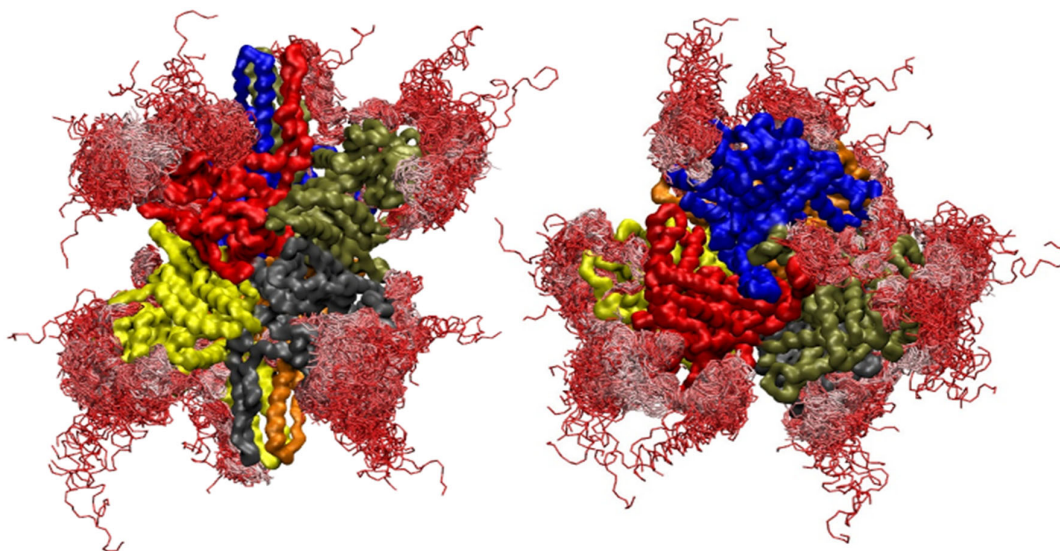
Par la suite, nous avons vérifié la deuxième hypothèse de désactivation correspondante à l'altération des structures secondaires et/ou tertiaires de la GDH (Figure S3). L'étude des altérations structurales des enzymes PEGylées a un intérêt crucial car ces modifications pourraient altérer l'activité enzymatique. La détermination et l'estimation du contenu en structures secondaires de la GDH ont été effectuées par le dichroïsme circulaire (CD) dans l'UV lointain (260–183 nm). Conformément à la littérature, la déconvolution du spectre CD de la GDH avait démontré la richesse de cette protéine en hélices  $\alpha$  <sup>50</sup>. Une diminution du contenu en structures hélicoïdales, proportionnelle à la fois au degré de PEGylation et au PM du mPEG, a été observée. Néanmoins, dans l'ensemble, ces modifications ne corrôlaient pas

avec les résultats de l'activité catalytique. Par exemple, bien que les bioconjugués 3 (~10 × 0,5 kDa mPEG), 7 (~10 × 2 kDa mPEG) et 13 (~3 × 20 kDa mPEG) ont possédé des spectres comparables, leurs activités catalytiques furent différentes. Conséquemment, pour compléter ces expériences, les structures tertiaires des bioconjugués ont été déterminées par spectroscopie de fluorescence du tryptophane. L'altération de ces structures a été dépendante du PM du mPEG notamment pour les faibles degrés de PEGylation. Toutefois, la plupart des données indiquaient que ces modifications n'affectaient pas nécessairement l'activité. Par exemple, les bioconjugués 4 (~25 × 0,5 kDa mPEG) et 12 (~25 × 5 kDa mPEG) possédaient des spectres de fluorescence très similaires mais des activités enzymatiques différentes. Conséquemment, on a suggéré que probablement, en raison de ses propriétés dynamiques, la GDH pouvait accommoder ces modifications de structure avec un impact minimal sur son activité catalytique. Par conséquent, des mécanismes alternatifs seraient responsables de la perte d'activité des bioconjugués.



FigureS3: (a) Spectres du CD dans l'UV lointain (260–183 nm). (b) Spectres de fluorescence du tryptophane.

Nous avons ensuite évalué si la perte d'activité était relative à un phénomène d'encombrement stérique. En effet, la présence des chaînes de mPEG à la surface de la protéine pourrait prévenir l'accès des substrats/cofacteurs/modulateurs à leurs sites potentiels de liaison. Pour ce faire, et vu que la caractérisation expérimentale de ce phénomène fut difficile, nous avons réalisé des simulations dans lesquelles 25 chaînes de 2 kDa mPEG ont été distribuées, d'une manière aléatoire, sur les groupements amines accessibles aux solvants. L'analyse de la distribution de ces chaînes polymériques autour de la GDH a clairement démontré que la surface de cette protéine restait hautement accessible aux solvants (Figure S4). Ainsi, l'hypothèse de l'encombrement stérique était très peu plausible.



FigureS4: Distribution des chaînes du mPEG autour de la GDH.

Nous avons alors suggéré que, même si la surface restait accessible, probablement il y a eu des changements au niveau du microenvironnement des sites de liaison. Pour vérifier ceci, l'activité enzymatique de la GDH a été mesurée en présence de cinq inhibiteurs allostériques différents (Tableau S2). Les sites de liaison de la première série de modulateurs (hexachlorophène et bithionol) sont enfouis dans la profondeur hydrophobe de la GDH <sup>51</sup>. En revanche, les sites de liaison de la seconde série d'inhibiteurs (GTP, ATP et le zinc) sont situés à la surface, au niveau d'une région riche en hélices  $\alpha$  <sup>52-54</sup>.

Nous avons d'abord démontré que, d'une manière collective, les sites de liaison de la première série d'inhibiteurs n'étaient pas affectés par les effets stériques ou micro-environnementaux résultant de la PEGylation. Étonnamment, la liaison de ces modulateurs a été affectée par la présence de  $\sim 25$  chaînes de 0,5 kDa mPEG, ce qui suggérait que la PEGylation utilisant ce court mPEG a probablement modifié les groupements amines profonds et a donc partiellement affecté les sites de liaison de ces modulateurs. D'autre part, on avait noté que les profils de liaison de la deuxième série de modulateurs (en particulier le GTP) corrélaient avec les tendances des changements de structures. Par conséquent, considérant l'altération des structures hélicoïdales de la GDH, les effets observés pourraient être reliés aux changements structuraux plutôt qu'aux changements micro-environnementaux. Ceci a été, encore, confirmé par l'action inhibitrice du dernier modulateur (zinc) qui n'a pas été affectée. En effet, contrairement au GTP/ATP, le zinc possède un second site de liaison distinct de ces deux inhibiteurs, une région qui n'a pas été potentiellement altérée par la PEGylation <sup>55</sup>. Dans l'ensemble, nous avons suggéré que la PEGylation n'a pas modifié le microenvironnement de liaison des modulateurs. Cependant, la modification des structures secondaires pour certains

bioconjugués avait eu un impact sur la liaison et la modulation du GTP ainsi que de l'ATP. Néanmoins, les changements anticipés des structures hélicoïdales ne pouvaient pas être directement corrélés à l'activité.

Tableau S2: Effet des inhibiteurs sur l'activité de la GDH.

Bioconjugué	Concentration inhibitrice médiane (CI50) (µM)				
	Hexachlorophène	Bithionol	GTP	Zinc	ATP
GDH	1.5 ± 0.3	1.9 ± 0.02	19 ± 8	49 ± 3	55 ± 19
<b>3</b>	1.7 ± 0.3	1.9 ± 0.02	17 ± 2	42 ± 13	– <sup>1</sup>
<b>4</b>	– <sup>2</sup>	1.8 ± 0.08	30 ± 12	– <sup>2</sup>	– <sup>1</sup>
<b>7</b>	2.3 ± 0.1	1.7 ± 0.6	45 ± 3 *	38 ± 0.0	– <sup>1</sup>
<b>8</b>	2.3 ± 0.1	2.0 ± 0.0	76 ± 12 *	41 ± 19	– <sup>1</sup>
<b>11</b>	1.6 ± 0.06	1.7 ± 0.6	41 ± 6 *	34 ± 0.2	– <sup>1</sup>
<b>12</b>	2.9 ± 0.5 *	– <sup>1</sup>	– <sup>1</sup>	– <sup>1</sup>	– <sup>1</sup>
<b>13</b>	1.4 ± 0.1	1.8 ± 0.0	15 ± 7	41 ± 0.6	– <sup>1</sup>

\*: différence statistiquement significative par rapport à la GDH native (Tukey, p = 0,05).

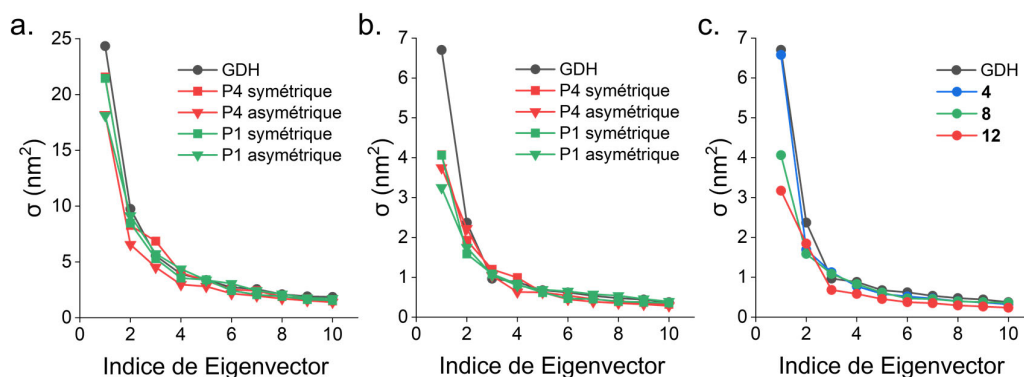
<sup>1</sup>: CI50 supérieure à 1 mM

<sup>2</sup>: pas de courbe sigmoïde

Le dernier mécanisme de désactivation étudié fut celui de l'effet de la PEGylation sur les mouvements dynamiques de la GDH, un mécanisme très peu reporté dans la littérature. Tout comme plusieurs autres enzymes, l'activité catalytique de la GDH dépend fortement des changements conformationnels ainsi que des mouvements moléculaires rotationnels et translationnels <sup>56-58</sup>. Dans ce contexte, considérant le grand nombre de mPEG attachés à la GDH, extraire expérimentalement des informations sur la dynamique globale, fut extrêmement difficile. Par conséquent, des simulations ont été entretenues (Figure S5). Quatre paramètres ont été étudiés: (1) la configuration du mPEG (« P1 » dans laquelle le mPEG adhère partiellement à la surface protéique ou « P4 » où les chaînes du polymère ne collaient pas à la surface de la GDH); (2) la distribution du mPEG (« symétrique » ou « asymétrique »); (3) la proportion de la GDH considérée (soit le squelette de la protéine uniquement ou la totalité de l'enzyme (squelette et chaînes latérales)), et finalement (4) l'effet du PM du mPEG. Nos résultats ont montré que la réduction de la dynamique de la GDH était plus prononcée pour la configuration « P1 » que « P4 » et pour la distribution « asymétrique » que « symétrique » (Figure S5 a et b). Les effets observés avec la configuration « P1 » pourraient être attribués aux propriétés du mPEG. En effet, il a été reporté, qu'étant donné que les parties hydrophiles

du mPEG interagissaient hautement avec les molécules d'eau, une déshydratation partielle de la surface de la protéine ait lieu, ce qui révélait une structure protéique plus compacte et plus rigide<sup>59</sup>. Une structure qui aurait potentiellement des permutations conformationnelles réduites<sup>39,59,60</sup>. Par ailleurs, considérant que l'activité catalytique de la GDH requiert le déplacement coopératif des six sous-unités, la présence concentrée du mPEG d'un côté de l'enzyme et pas de l'autre (distribution asymétrique) avait éventuellement altéré cette coopération. Ceci est en accord avec une étude rapportant que l'inhibition d'une seule sous-unité produisait une réduction considérable de l'activité associée à la perte de coopération entre les six monomères de la GDH<sup>49</sup>.

En outre, nos données ont démontré que la PEGylation affectait plutôt la dynamique du squelette de la GDH et cela étant d'une manière dépendante du PM du mPEG (Figure S5 c). En effet, la présence de 25 chaînes de mPEG a considérablement atténué la dynamique de la GDH notamment pour le 5 kDa mPEG. Cependant, les changements conformationnels de la GDH portant 25 x 0.5 kDa mPEG n'étaient pas affectés. Dans l'ensemble, nos données théoriques corrélées parfaitement avec les résultats correspondants aux mesures des activités catalytiques des bioconjugués. Ceci suggérait que, pour les bioconjugués 12 (~25 x 5 kDa) et 8 (~25 x 2 kDa), la désactivation de la GDH pouvait être associée à la réduction de sa dynamique structurale.



FigureS5: (a) Simulations relatives à la structure protéique entière. (b) Simulations avec le squelette protéique uniquement. (c) Effet du PM du mPEG sur la dynamique de la GDH.

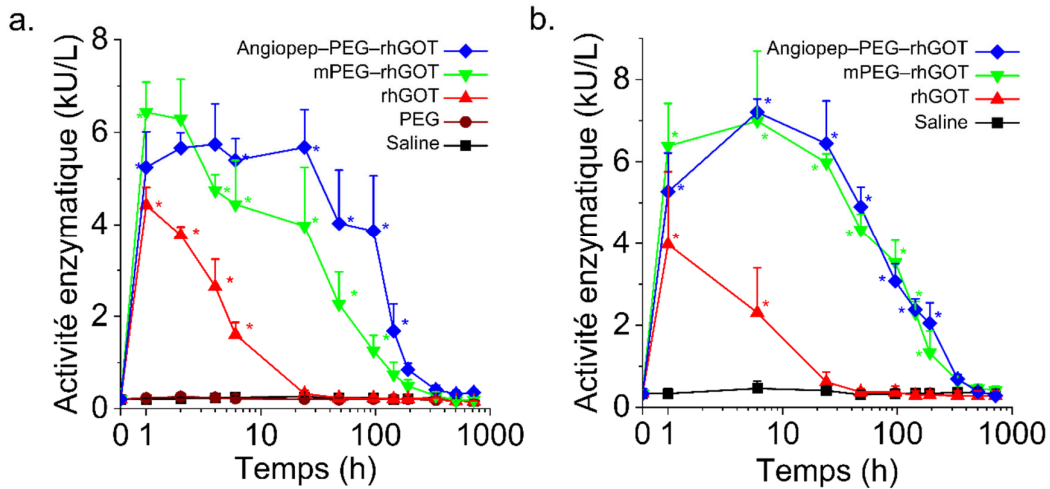
Une fois les causes de la perte d'activité de la GDH définies, nous avons décidé d'étudier l'efficacité thérapeutique de certains bioconjugués *in vivo*. En se basant sur les résultats obtenus, nous avons choisi de tester les bioconjugués 4 (25 x 0,5 kDa), 7 (10 x 2 kDa) et 13 (3 x 20 kDa). Pour le bioconjugué 4 et 7, aucune réduction significative de l'activité n'a été observée. De surcroît, les propriétés structurales et dynamiques de la GDH ont été maintenues, malgré des degrés élevés de PEGylation. En outre, bien que l'activité du

bioconjugué 13 ait diminué à la suite de la PEGylation, nos expériences ont suggéré que les aspects structuraux et micro-environnementaux à la surface de la GDH étaient préservés. Donc, considérant que, dans certains cas, une réduction de l'activité biologique pourrait être compensée par une augmentation de la demi-vie, il semblait raisonnable de tester ce bioconjugué.

Dans ce cadre, nous avons commencé par l'évaluation de l'effet du « piégeage » du glutamate de la GDH native (non-PEGylée). Contre toute attente, à la suite de l'injection intraveineuse de la GDH, nous n'avons pas observé une réduction des concentrations du glutamate ni au niveau du sang ni dans le liquide céphalorachidien (LCR). Nous avons donc supposé que soit la dose de la GDH n'était pas adéquate ou que la GDH n'était pas efficace en tant que « piègeur » du glutamate. Rétrospectivement, sur la base de nos prochains résultats (voir ci-dessous) et d'après une étude récemment publiée <sup>61</sup>, les effets thérapeutiques des « piègeurs » ne pouvaient pas être déterminés uniquement en mesurant les niveaux du glutamate dans le sang et le LCR. Par conséquent, une étude plus avancée devrait permettre de mieux discerner les doses thérapeutiques et les effets potentiels de la GDH. Dans le cadre de cette thèse, la rhGOT a été choisie comme alternative pour ses effets de « piégeage » relativement connus.

Dans le projet suivant, nous avons étudié l'efficacité thérapeutique de la rhGOT multi-PEGylée chez des rats Sprague-Dawley soumis à un protocole d'ischémie-reperfusion qui consiste à occlure transitoirement (75 minutes) l'artère cérébrale moyenne (MCAo). Deux constructions de bioconjugués ont été produites à savoir le mPEG-rhGOT et l'Angiopep-PEG-rhGOT. Dans les deux cas, les deux bioconjugués portaient ~22 chaînes de PEG et possédaient 80-90% de l'activité de la rhGOT native. Pour examiner l'effet de la PEGylation sur la biodisponibilité de l'enzyme, la rhGOT, le mPEG-rhGOT ou l'Angiopep-PEG-rhGOT ont été injectés par voie intraveineuse à des rats sains et ischémiques. Le sang a ensuite été prélevé sur une période de 30 jours pour analyser les paramètres pharmacocinétiques et pharmacodynamiques. Comme l'illustre la Figure S6, les profils de l'activité enzymatique observés chez les rats sains étaient très similaires à ceux observés pour les rats ischémiques. Aucune différence n'a été observée entre le groupe ayant reçu la solution saline et celui recevant uniquement le mPEG, ce qui indique que le mPEG en-soi n'a aucun effet sur l'activité enzymatique endogène de la GOT. En outre, la rhGOT native a été rapidement éliminée de la circulation sanguine, avec une disparition complète de l'activité en moins de 6 heures. En revanche, l'administration du mPEG-rhGOT et de l'Angiopep-PEG-rhGOT a permis de maintenir des niveaux élevés d'activité enzymatique sanguine pour une période d'environ 6 jours. Cela suggère que la PEGylation avait bloqué ou retardé l'internalisation cellulaire (notamment par les cellules du système réticulo-endothélial) et la métabolisation de la rhGOT

<sup>18-20</sup>. De plus, éventuellement la présence du polymère avait réduit l'immunogénicité de cette enzyme ainsi que sa dégradation protéolytique. Néanmoins, cet effet serait moins important que celui relatif à l'absorption tissulaire.



FigureS6: (a) Activité enzymatique *in vivo* chez les rats sains. (b) Activité enzymatique *in vivo* chez les rats ischémiques. (\*) Indique des différences statistiquement significatives par rapport au temps 0 (Tukey,  $p = 0,05$ ). Les résultats sont exprimés en moyennes + SD,  $n=3-5$ .

Afin de vérifier si l'augmentation de la biodisponibilité de la rhGOT avait eu des effets neuroprotecteurs chez les rats ischémiques, le volume cérébral infarcté a été mesuré par résonance magnétique nucléaire (RMN). L'analyse de la taille de l'infarctus 1, 7, 14, 21, et 30 jours après le MCAo est présentée à la Figure S7. Avant l'administration des traitements et pour tous les groupes, les volumes initiaux de l'infarctus étaient d'environ 35–45% du volume de l'hémisphère ipsilatéral. Pour la dose de rhGOT choisie, aucune différence significative n'a été observée entre le groupe traité par la rhGOT native et celui ayant reçu la solution saline. À l'opposé, le traitement avec le mPEG-rhGOT ainsi que l'Angiopep-PEG-rhGOT a entraîné une réduction significative du volume de l'infarctus par rapport au groupe traité avec la solution saline. Ce résultat suggérait que l'activité sanguine soutenue de la rhGOT procurait une neuroprotection considérable. Remarquablement, les bioconjugués ont réduit de 70% le volume cérébral infarcté (par rapport à sa valeur au jour 0), ce qui suggère que cette stratégie est prometteuse. En effet, une réduction des dommages ischémiques d'au moins 50% a été définie comme seuil pour considérer et soumettre le traitement à des essais cliniques <sup>62</sup>.

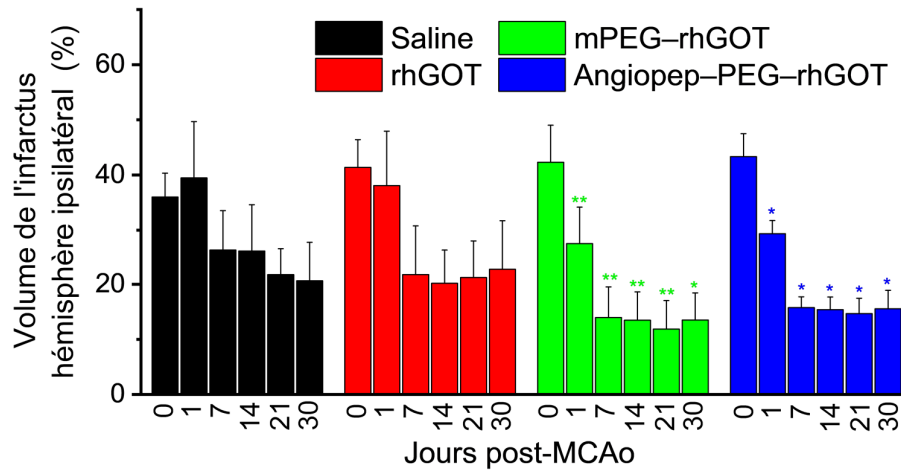


Figure S7: Volume cérébral infarci. (\*) Indique des différences statistiquement significatives par rapport au groupe salin (ANOVA, Bonferroni,  $p = 0,05$ ). Les résultats sont exprimés en moyennes + SD,  $n=5$ .

Pour encore confirmer les propriétés neuroprotectrices des bioconjugués, les fonctions motrices des rats ischémiques ont été évaluées par le test du Rotarod et le test du cylindre (Figure S8). Collectivement, nous avons démontré que les rats ischémiques qui ont été traités avec les bioconjugués ont présenté une meilleure récupération des fonctions motrices que ceux qui ont été traités avec la rhGOT native ou la solution saline.

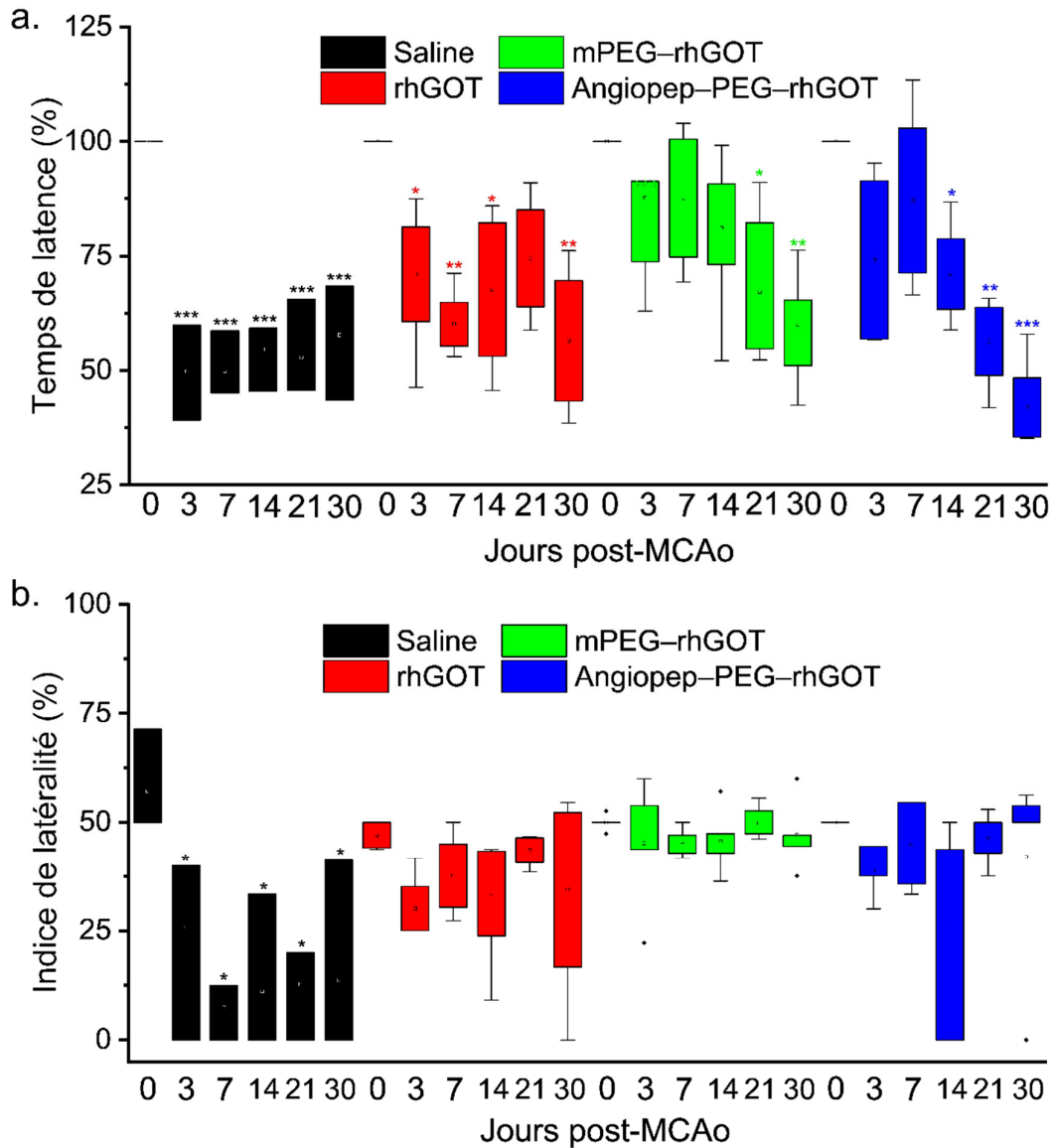


Figure S8: (a) Déficit moteur évalué par le test du Rotarod. (b) Fonctions motrices évaluées par le test du cylindre. (\*) Indique des différences statistiquement significatives par rapport au jour 0 (avant ischémie) (ANOVA, Bonferroni,  $p = 0,05$ ). Les résultats sont exprimés en moyennes + SD,  $n=5$ .

Étonnamment, les bioconjugués ciblés avaient présenté des effets thérapeutiques similaires à ceux des bioconjugués non ciblés (Figure S6, S7 et S8). Cela suggérait que l'accumulation cérébrale ne représentait qu'une très faible fraction de la dose totale administrée et ne contribuait pas aux améliorations thérapeutiques. Par ailleurs, cela pourrait également suggérer que l'efficacité du ciblage et l'interaction de l'Angiopep-2 avec le LRP1 étaient soit affectées par les chaînes du PEG, soit potentiellement altérées par la densité élevée du ligand. En effet, des études antérieures avaient démontré que, même si la présence d'une densité

élevée augmenterait l'avidité et la sélectivité pour les cellules cibles <sup>63</sup>, l'élévation du nombre de ligands de ciblage pourrait également entraîner une diminution de la transcytose et une réduction de l'accumulation dans le parenchyme cérébral <sup>64</sup>. Par conséquent, l'évaluation des profils de liaison de nos bioconjugués serait importante pour pouvoir tirer des conclusions par rapport aux données observées.

Finalement, contrairement à ce qui a été rapporté par certaines études <sup>65</sup>, les concentrations plasmatiques du glutamate n'ont pas été affectées après administration des traitements (Figure S9). En effet, aucune corrélation entre l'activité enzymatique et les niveaux du glutamate dans le sang n'a pu être identifiée. Néanmoins, nos données étaient cohérentes avec les études suggérant la rapidité de la mise en place des mécanismes périphériques impliqués dans l'homéostasie du glutamate <sup>66,67</sup>. En fait, il a été démontré que la radioactivité associée au glutamate et à ses métabolites (aspartate) diminuait précipitamment (demi-vie de ~3 minutes) après une injection intraveineuse. Ceci a été associé à la présence ubiquitaire des transporteurs au niveau des organes périphériques (notamment le foie et les muscles) qui assurent la capture rapide de ceux-ci <sup>68</sup>.

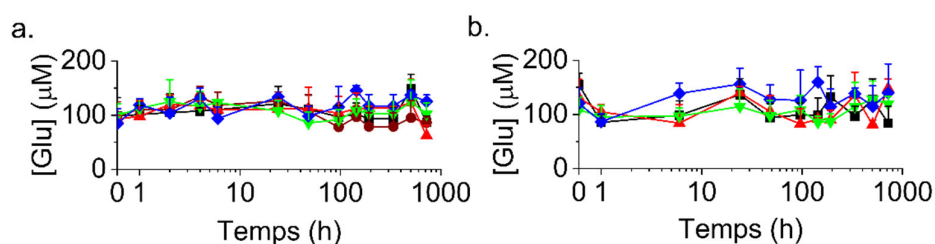


Figure S9: (a) Concentrations sériques du glutamate chez les rats sains. (b) Concentrations sériques du glutamate chez les rats ischémiques. Les résultats exprimés en moyennes + SD, n=3-5.

Dans ce cadre, et afin de déterminer si un effet plus localisé pourrait être observé, les niveaux du glutamate ont été mesurés dans le LCR de rats sains recevant soit la rhGOT ou le mPEG-rhGOT (Figure S10). Tout comme les observations faites dans le sang, aucun effet sur les concentrations du glutamate dans le LCR n'a été observé. Ces résultats étaient en accord avec une étude récemment publiée montrant que l'administration successive de la GOT (toutes les 12 heures pendant 4 jours) a significativement amélioré la plasticité synaptique *via* la diminution des concentrations du glutamate dans le liquide interstitiel, mais pas dans le LCR <sup>61</sup>. Dans l'ensemble, nous avons suggéré que la non-variation des niveaux du glutamate pourrait être associée à l'installation rapide des mécanismes de l'homéostasie.

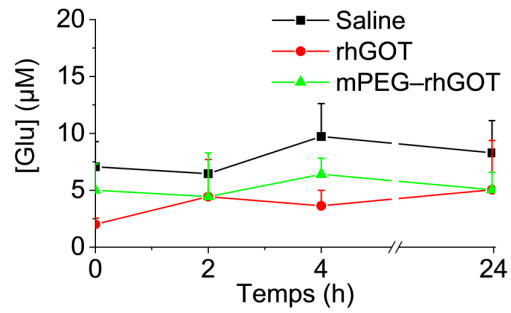


Figure S10: (a) Concentrations du glutamate dans le LCR. Les résultats exprimés en moyennes + SD, n=3-5.

#### 4. Conclusion

Dans le cadre de thèse, nous avons démontré que le maintien d'une activité enzymatique sanguine prolongée de la rhGOT avait un effet bénéfique significatif sur le volume de l'infarctus ainsi que sur les fonctions sensorimotrices. De plus, sur la base des nouvelles connaissances acquises dans le cadre de cette thèse, les effets neuroprotecteurs de la GDH pourraient être étudiés, d'une manière plus approfondie. Finalement, l'efficacité de cette stratégie offre un grand potentiel en tant que thérapie pour l'ischémie cérébrale, ainsi que pour d'autres pathologies associées à l'excitotoxicité telles que les maladies neurodégénératives.

## **CHAPTER 1: Ischemia, Glutamate Excitotoxicity, and Enzymatic Glutamate Degradation Approaches**

Sections 1.2. and 2.1.1. of this chapter are published as part of a manuscript titled “Treating Brain Diseases using Systemic Parenterally-administered Protein Therapeutics: Dysfunction of the Brain Barriers and Potential Strategies” accepted for publication in Biomaterials and formatted to enhance the flow of this Chapter.

## **Part 1: Literature Review**

### **1. Physiology of the central nervous system**

#### **1.1. Arterial vascularisation**

Although the brain represents only 2% of the body's total mass, approximately 25% of the glucose and 20% of the oxygen consumed by the human body are devoted to neuronal functions<sup>69</sup>. Due to this constant high energy requirement, the brain needs a significant blood supply and consumes about 15% of total cardiac output<sup>70</sup>.

The cerebral circulation is formed by a network of arteries providing metabolites and oxygenated blood to the brain. Generally, the brain receives blood from two sources: the vertebral arteries (20% of the total blood supply to the brain) and the internal carotid arteries (80% of the total blood supply to the brain)<sup>71</sup>. The vertebral arteries arise from the subclavian artery and transmit blood into the posterior circulation including the basilar artery that supplies the brainstem, cerebellar, and posterior cerebral arteries. The internal carotid arteries are branches of the common carotid arteries and carry blood into the anterior cerebral circulation, including the middle and the anterior cerebral arteries (MCA and ACA). These latter arteries represent the terminal branches of the internal carotid arteries and supply a wide territory of the lateral aspects of the cerebral hemispheres<sup>71</sup>. The two ACA (left and right) connect *via* the anterior communicating artery, which stabilizes blood flow. The anterior and posterior circulations communicate through the circle of Willis *via* anterior and posterior communicating arteries<sup>72</sup>. Presumably, this circle allows the cerebral perfusion to endure *via* collaterals if one of the major arteries becomes occluded by an event or disease, such as ischemia.

In rats, the cerebral arterial vascularization is relatively similar to that of humans: the anatomic distributions of the posterior cerebral artery, ACA, and MCA are identical. Nevertheless, the anterior communicating artery is absent in rats and the posterior cerebral artery and intracranial portion of the internal carotid artery are directly connected (Figure 1)<sup>73</sup>. The high anatomical and physiological resemblance between rat and human brains makes the rat the most common animal model used in stroke studies.

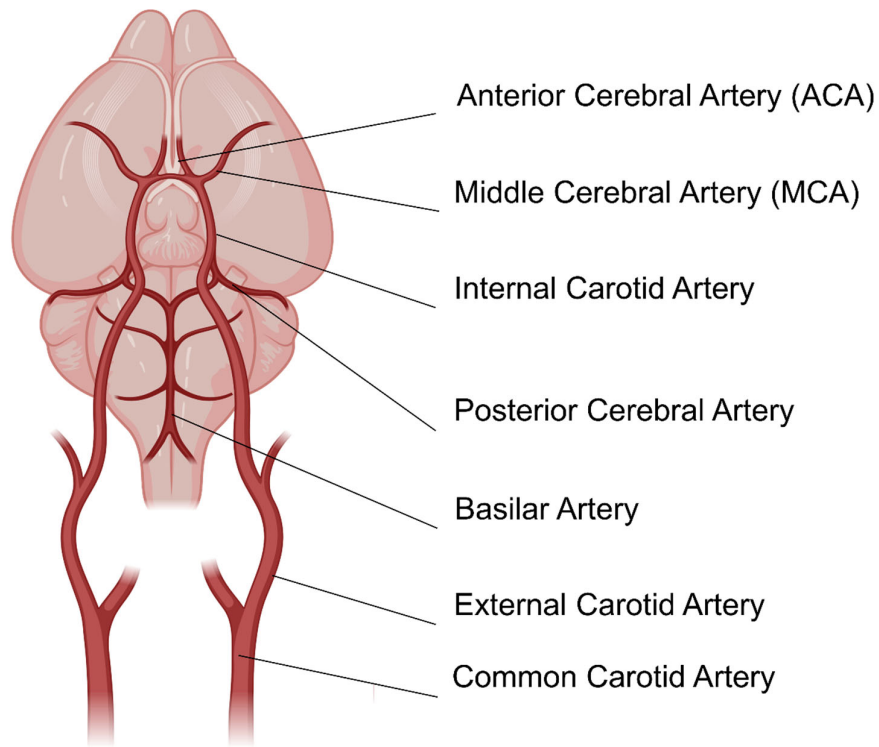


Figure 1: Illustration of cerebrovascular anatomy in rats.

## 1.2. Physical barriers of the central nervous system

The blood vessels that vascularize the brain possess unique properties. Termed the blood-brain interfaces, these vessels tightly regulate the movement of diverse molecules between the blood and the brain. The concept of a barrier between the blood and the nervous system was established by Paul Ehrlich, following the demonstration that a systemically administered dye could stain most organs, but not the brain or spinal cord <sup>74</sup>. From these early observations, much knowledge was gained on how these barriers participate in brain–periphery crosstalk, protect the brain, and maintain cerebral homeostasis. There are three main interfaces: the blood-brain barrier (BBB), the blood-cerebrospinal fluid barrier (BCSFB), and the arachnoid barrier. Jointly, these barriers are termed ‘blood–brain interfaces.’ Similar interfaces can be found in multiple locations in the body, including the blood–retinal barrier and the blood–spinal cord barrier (Figure 2) <sup>75,76</sup>.

The BBB and the BCSFB differ on a cellular level, reflecting the difference in their principal functions. For instance, the BBB is a discriminatory barrier that protects the brain from molecules in the blood than can interfere with neurotransmission, and dampens the effect of physiological fluctuations of solutes within the plasma. Moreover, it provides routes for the

exchange of nutrients, signaling molecules, ions, and metabolic waste products between the interstitial fluid of the brain and the blood. In contrast, the BCSFB secretes cerebrospinal fluid (CSF) and plays a role in the exchange of various solutes and molecules between the blood and the CSF <sup>77</sup>.

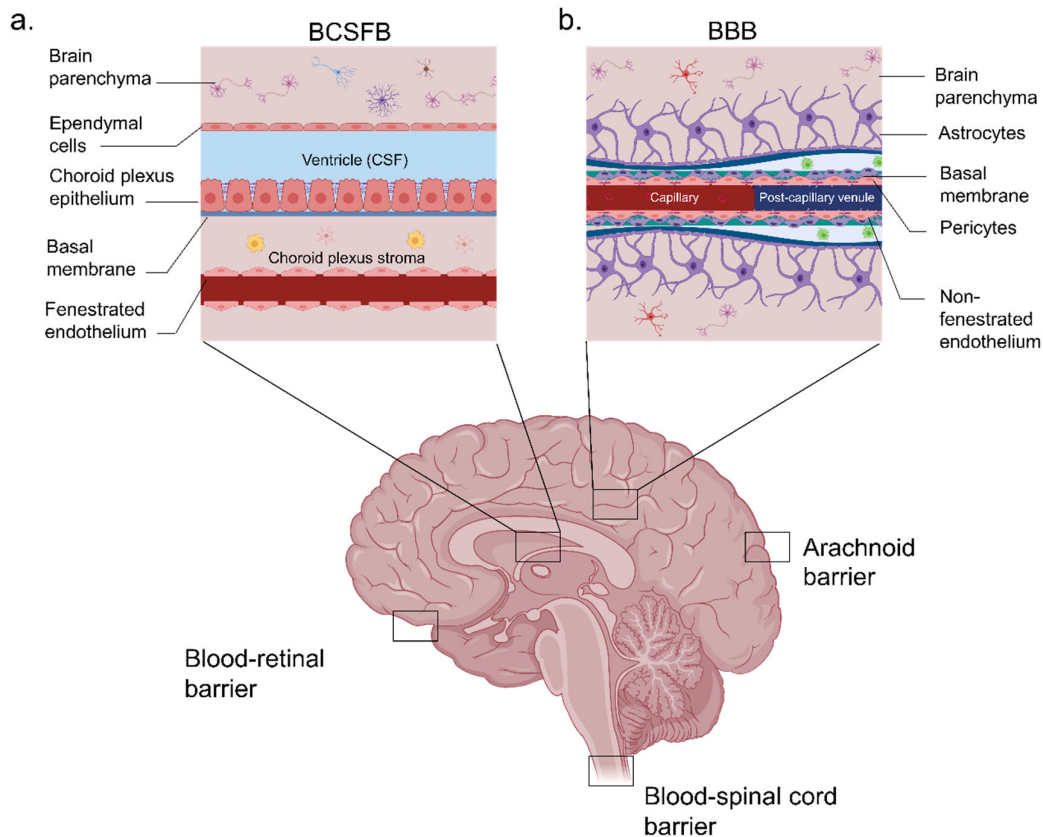


Figure 2: Location of the barriers of the nervous system and structure of the BBB and BCSFB. The five barriers are represented in a longitudinal brain section. (a) Schematic representation of the BCSFB: the capillaries in the choroid plexus permit the facile diffusion of molecules *via* intracellular fenestrations. Epithelial cells are joined by adherens and tight junctions. The presence of microvilli increases the surface area of the CSF-facing side of the epithelial cells. (b) Schematic representation of the BBB: the BBB is composed of endothelial cells that are surrounded by a basal membrane in close association with astrocyte end feet and pericytes. Neurons and microglia are also important mediators of BBB integrity. Cerebral endothelial cells are sealed together by tight junctions.

The formation and function of the BBB depend on close cell-to-cell connections at the neurovascular unit. The neurovascular unit is composed of specialized microvascular endothelial cells with their basal lamina covered with pericytes, smooth muscular cells, astrocyte end feet, neurons, and an extracellular matrix <sup>78</sup>. The restrictive characteristics of this barrier come from the complex structures expressed by the brain capillaries. Indeed, brain

endothelial cells express many active efflux transport proteins. Furthermore, the tight junctions between cells are among the most restrictive sealing elements in the body. They comprise three integral membrane proteins (claudin, occludin, and junction adhesion molecules) and multiple accessory proteins including zona occludens, cingulin, and others <sup>79,80</sup>. The spatial positioning of these junctional scaffolding proteins affects the anchoring to the cytoskeleton of the cells as well as downstream signaling events that regulate junctional dynamics. The BBB also has additional enzymatic components that can degrade compounds, which can either prevent their accumulation in the brain or accelerate their elimination. Molecules crossing the cerebral endothelial cells are thus exposed to various ecto- and endo-enzymes present within endothelial cells. In addition, brain endothelial cells display low pinocytotic activity and the endothelium is separated by non-neuronal cells on the brain side (e.g., pericytes), which places additional restrictions on permeability <sup>77</sup>.

The selectivity and permeability properties of the choroid plexus membrane are strongly associated with the BCSFB. The choroid plexus is a vascular tissue localized in cerebral ventricles. The functional unit of the choroid plexus tissue at the blood side is composed of somewhat leaky fenestrated and highly permeable capillaries <sup>81</sup>. This capillary wall is bordered by a monolayer of epithelial cells linked together by tight junctions and facing the CSF. Therefore, all molecules traversing the endothelium must pass through the epithelium in order to reach the CSF. The choroid plexus is roughly one hundred-fold leakier than the BBB, based on their respective electrical resistance and on lanthanum ion transport experiments <sup>82</sup>. Therefore, alongside other roles of the choroidal plexus (such as active production and secretion of CSF, drug metabolism, and antioxidant capacities), this tissue has a substantial surface area for exchange.

### **1.2.1. Transport across the blood–brain interfaces**

Depending on their physiochemical properties, the penetration of molecules into the brain may occur by the following routes: (1) paracellular transport (small hydrophilic molecules); (2) transcellular passive diffusion (lipophilic and nonpolar solutes such as carbon dioxide and oxygen); (3) carrier-mediated transport by diverse transporters; (4) adsorptive-mediated transcytosis (internalization of molecules following a nonspecific interaction), and (5) receptor-mediated transcytosis (RMT) ([Figure 3.a](#)). In the following sections, transporter-mediated passage, adsorptive endocytosis, and especially RMT-mediated transport mechanisms will be discussed.

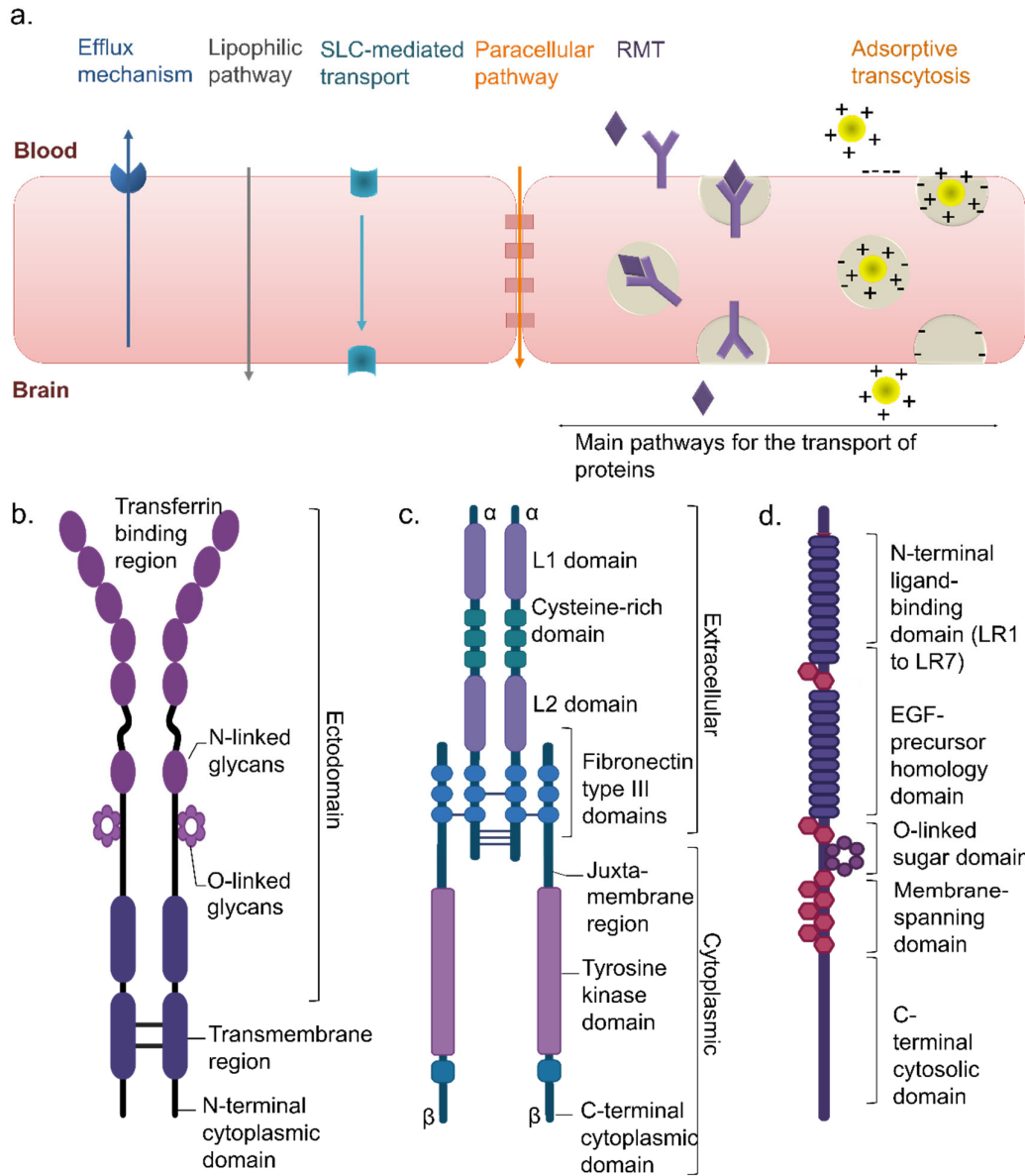


Figure 3: Transport mechanisms across brain barriers (a) and the general structure of the transferrin receptor (TfR) (b), insulin receptor (c), and low-density lipoprotein receptor (LDLR) (d). These receptors have been largely explored as brain targeting entities for proteins *via* a RMT.

### a. Carrier-mediated transport

The exchange of low molecular weight (MW) organic molecules between the brain and the blood is regulated by specific plasma membrane transporters located on the wall of the endothelial/choroidal epithelial cells forming the BBB/BCSFB. The direction of transport is dictated by the subcellular localization of the transporter (luminal or basolateral side), as well

as by the transport mechanism (energy-dependent or energy-independent). Nutrients are provided to the brain by blood-to-brain influx transporters, whereas efflux transporters remove potentially deleterious metabolites and neurotoxins from the brain parenchyma. Moreover, drug efflux pumps expressed on the luminal side actively transport a huge variety of drugs out of the BBB/BCSFB and back into the blood, thereby restricting their distribution to the brain. The transporters mostly belong to two super-families: the adenosine triphosphate (ATP) binding cassette (ABC) transporters and the solute carrier transporters. The superfamily of ABC transporters directly couple ATP hydrolysis to the active efflux of molecules against unfavourable concentration gradients and across the cell membrane <sup>83</sup>. The ABC active transporters are primarily found at the blood-facing membranes of brain microvasculature cells <sup>84</sup>. They involve ~48 distinct transporters categorized into seven families (ABC A through G) <sup>85</sup>. Relevant ABC transporters include multidrug-resistance proteins (MDR), multidrug resistance-related proteins (MRP), and breast cancer-resistance proteins (BCRP) <sup>85</sup>. These multi-specific efflux transporters are distributed between the BBB and the BCSFB and prevent the brain accumulation of a vast array of lipophilic and amphipathic molecules *via* an energy-dependent and outwardly directed (unidirectional) transport mechanism. The first and most investigated MDR protein is the P-glycoprotein (also referred to as MDR1 or ABCB1), a 170 kDa phosphorylated glycoprotein that is greatly expressed on the endothelial cells of capillaries, and poorly expressed on epithelial cells of the choroid plexus <sup>86,87</sup>. Recently, it has been further detected on the abluminal surface of the BBB, although little is known about its function at this location <sup>88</sup>. Its localization and substrate promiscuity make it an effective defense mechanism against a wide spectrum of endogenous ligands, therapeutic drugs, and xenobiotics <sup>89</sup>. The second superfamily (solute carrier transporters) includes facilitated transporters, ion-coupled transporters, and exchangers that are ATP-independent <sup>90</sup>. Some of these SLC are bidirectional and others are unidirectional. These transporters are mainly responsible for the transport of molecules that are unable to diffuse across the blood-brain interfaces due to their hydrophilicity, such as amino acids <sup>91</sup>.

#### **b. Adsorptive endocytosis**

The discovery of adsorptive endocytosis within the BBB came from the observation that polycationic molecules can bind to the vascular endothelium and penetrate the BBB <sup>92,93</sup>. Furthermore, the cationization of proteins (e.g., albumin) or their mixing with cationic molecules (e.g., protamine (small, arginine-rich, nuclear protein) or poly-L-lysine) greatly increases their permeability across the BBB <sup>94,95</sup>. In adsorptive endocytosis, the interaction between a ligand and cell surface is required, such as when a positively-charged molecule interacts with the negatively-charged cell membrane <sup>96</sup>. Following endocytosis, the intracellular transport of molecules occurs by the vesicular system, with the formation of clathrin-coated,

caveolae-coated, or macropinocytotic vesicles<sup>97</sup>. While caveolae-dependent endocytosis appears to be the most common mode for adsorptive endocytosis, the vesicle carrier has remained unidentified in many papers<sup>23,94</sup>. Once the vesicle is internalized, it progresses into an early endosome. Thereafter, the content of the vesicles can either be delivered directly to the cytoplasm, degraded in lysosomes, or released into the extracellular space by exocytosis<sup>98,99</sup>. The exocytosis of compounds from these vesicles occurs by fusion of its membrane with the plasma membrane and is believed to be regulated by protein dephosphorylation<sup>100,101</sup>. Contrary to endothelial cells, cells of the choroidal epithelium are strongly endocytic, which might be associated with the active metabolism of the choroid plexus, as well as its synthetic functions. Though, exploiting this particularity for the efficient transport of therapeutic proteins and macromolecules across the BCSFB remains elusive<sup>78,102</sup>.

### **c. Receptor-mediated transcytosis**

Specific receptors, highly expressed by endothelial/epithelial cells forming the BBB and BCSFB, are responsible for the transport of proteins required for the normal functioning of the brain. These include, for example, the insulin receptor, transferrin receptor (TfR), and low-density lipoprotein receptor (LDLR). These RMT mechanisms are currently used as delivery strategies for drugs to the brain. Of course, many receptors responsible for RMT in the brain and choroid epithelium are also ubiquitously expressed, which limits the potential for selective brain targeting.

- **Transferrin Receptor**

The delivery of iron to the brain occurs by the trafficking of iron-loaded transferrin (holo-transferrin)<sup>103</sup>. The iron–transferrin complex binds to TfR on the exterior of microvascular endothelial cells and is transported across the brain-blood interface into the brain parenchyma, ensuring the maintenance of iron homeostasis, which is important for metabolism, neuronal transmission, and appropriate brain function<sup>103</sup>. As such, iron deficiency and excess are both linked to neuronal dysfunction<sup>103</sup>.

The best-characterized receptor of transferrin is the promiscuous and widely expressed TfR1 (CD71)<sup>104</sup>. TfR1, or more simply TfR, is a ~180 kDa homodimeric type II transmembrane protein. This receptor possesses a short N-terminal cytoplasmic domain, one hydrophobic transmembrane region, and a complex extracellular C-terminal domain ([Figure 3.b](#)). Structural analysis revealed that for the butterfly-shaped dimeric TfR ectodomain, each monomer is subdivided into a protease-like domain that has contact with the cell membrane, a helical domain where the monomers contact each other, and a membrane-distal apical domain<sup>105</sup>. TfR is expressed by brain microvessels as well as the cells of the choroid epithelium<sup>106,107</sup>.

Owing to the elevated presence of TfR in cerebral endothelial cells, this receptor has been explored to deliver drugs to the brain, using transferrin as a targeting ligand. However, since high blood levels of endogenous transferrin compete with drugs for TfR, alternative methods have been explored, including anti-TfR monoclonal antibodies (TfRMAb) <sup>108</sup>. TfRMAb have been shown to bind to TfR and internalize into the endothelial cells of the brain without interfering with the uptake of iron-bound transferrin. Other approaches for exploring TfR-based delivery involve the use of small peptide binders <sup>109,110</sup>. Such peptides hold the advantage of circumventing the side effects that could be generated by the Fc effector domain of the anti-TfR antibody <sup>111</sup>. Moreover, owing to their small size, they might be easier to use, conjugate, manufacture, or store. Nevertheless, they are usually not stable in circulation and have low binding affinity.

- **Insulin Receptor**

Insulin is a ~5 kDa protein that is secreted by the pancreas and plays a vital role in the regulation of carbohydrate metabolism <sup>112,113</sup>. The transport of insulin is guaranteed by insulin receptors that are widely distributed throughout the body. In the endothelial cells of the brain, binding to its receptor not only allows insulin transport across the BBB *via* the receptor itself, but further activates signaling pathways through for example, the insulin-like growth factor 1 (IGF-1) receptor <sup>114,115</sup>.

The insulin receptor is a cylindrical homodimeric glycoprotein (MW ~300 kDa) that consists of two  $\alpha$ -subunits and two  $\beta$ -subunits <sup>116</sup>. The extracellular  $\alpha$ -subunit contains an insulin-binding site and the cytoplasmic portion of the transmembrane  $\beta$ -subunit possesses tyrosine kinase activity. The ectodomain comprises seven extracellular domains. Starting from the N-terminus, these domains are: the first leucine-rich repeat domain (L1), the cysteine-rich domain, the second leucine-rich repeat domain (L2), and the three fibronectin type III domains (FnIII-1, FnIII-2, and FnIII-3), with the seventh domain (a relatively disordered insert domain) lying within FnIII-2 and containing the  $\alpha\beta$  proteolytic processing site ([Figure 3.c](#)) <sup>117</sup>.

Insulin receptor-mediated transport has been explored to deliver various molecules across the BBB/BCSFB. The use of insulin as a scaffold for drug delivery is difficult because of its short serum half-life (~10 minutes) and rapid degradation in the bloodstream. Moreover, interfering with the normal serum insulin equilibrium could generate hypoglycaemia <sup>23</sup>. As such, the general strategy for exploiting the TfR has also been adopted for the insulin receptor, namely the development of antibodies targeting the insulin receptor <sup>118</sup>. Initially, a mouse monoclonal antibody targeting the human insulin receptor (83-14) was tested <sup>118</sup>. However, as 83-14 is a mouse antibody, it triggers an immunogenic reaction in humans <sup>119</sup>. Therefore, engineered forms of 83-14 have been developed. First, a chimeric antibody was produced by adding

mouse variable binding regions onto a human antibody scaffold <sup>120,121</sup>. Then, more recently, a fully humanized version was produced by grafting the complementary determining regions onto human immunoglobulins (Ig) <sup>122</sup>. The reactivity of these constructions towards the human insulin receptor demonstrated that in comparison to 83-14, the chimeric antibody had similar affinity <sup>120,121</sup>, whereas the fully humanized antibody had 27% lower affinity <sup>122</sup>. Despite this reduction of affinity, intravenous injection of a radiolabeled (<sup>125</sup>Iodine) humanized antibody to adult Rhesus monkeys showed rapid uptake by the gray and white matter (2 hours post-administration) <sup>122</sup>.

- **Low-density lipoprotein Receptors**

The LDLR, a large glycoprotein (MW ~160 kDa) <sup>123</sup>, was first recognized as a cell surface endocytic receptor responsible for the intracellular uptake of LDL particles. The LDLR has five functionally distinct regions: an N-terminal ligand-binding domain, an epidermal growth factor (EGF)-precursor homology domain, a region containing O-linked sugars at the cell surface, a membrane-spanning domain, and a C-terminal cytosolic domain. The ligand-binding domain possesses seven cysteine rich repeats (R1–R7), each of which are ~40 residues in length (known as the LDL-A repeats) <sup>124</sup>. The second region consists of three EGF-like repeats (A, B and C) <sup>125</sup>. The third region of the ectodomain is the site at which carbohydrate moieties attach to the receptor and possesses many serine and threonine residues that undergo O-glycosylation <sup>126,127</sup>. This domain is followed by a hydrophobic domain that anchors the LDLR to the lipid bilayer. The last domain is the cytoplasmic tail containing ~50 residues that includes an NPXY targeting sequence (asparagine, proline, unspecific amino acid, tyrosine), which regulates and assures the endocytosis and the intracellular transport of the receptor ([Figure 3.d](#)) <sup>128-130</sup>.

Nowadays, LDLR is included in a large family that includes many other relatives with RMT activity and roles in cell signaling processes <sup>131</sup>. Family members share a modular domain structure as well as one or multiple copies of a conserved cysteine-rich domain. The LDLR family can be subdivided into at least four groups <sup>132</sup>. The LDLR itself, the very-low density lipoprotein receptor (VLDLR) and the apolipoprotein E receptor 2 (ApoER2), belong to the first group. The well-investigated low-density lipoprotein receptor-related protein 1 (LRP1 or CD91 or  $\alpha$ 2-macroglobulin receptor), LRPB1B, and LRP2 are members of the second group. The third group includes LRP5 and LRP6. Finally, the fourth group comprise more distantly related members such as SorLA-1 (also called LR11), ST7, LRP4, and LRP3 <sup>132</sup>.

The mechanism of endocytosis and trafficking of LDLR family ligands to the lysosomal compartment has been widely described, particularly in peripheral cells where the cargo taken in clathrin-coated pits is released in the late endosomes and then degraded in lysosomes <sup>133</sup>.

The receptor recycles back to the cell surface after ligand dissociation in the early endosomes<sup>133,134</sup>. Although much is known about LDL uptake and trafficking in peripheral tissues, less is known for the brain and this is currently the subject of extensive investigations. At the BBB, the different members of the LDLR not only assure the use and clearance of LDL<sup>135</sup>, but also mediate the transcytosis of their cargo<sup>136-138</sup>. The non-degradation of the cargo after internalization indicates that the route of transcytosis in endothelial cells differs from the classical LDLR pathway of endocytosis<sup>138</sup>. This receptor-mediated process, which bypasses lysosomes, seems to be a specific feature of brain endothelial cells that are equipped with a RMT implicating specialized endocytic vesicles<sup>139,140</sup>.

The presence of multiple variants of the LDLR in apical membranes of the endothelial cells of the brain as well as their role in RMT raise interest for their use for the transendothelial transfer of therapeutics. As for the TfR, natural apolipoprotein (Apo) ligands as well as peptides consisting of minimal sequences of the binding domains of the latter have been investigated, despite the fact that the mechanism by which such vectors transport across the BBB remains to be clarified. To the best of our knowledge, antibodies have not been developed to target the LDLR system.

Several endogenous ligands of the LDLR family have been investigated for brain delivery of therapeutics and have shown successful transfer across the blood-brain interfaces. These include Apo ligands (such as Apo B and E) that showed an efficient delivery of therapeutically relevant agents across the BBB. The use of peptides derived from the binding domains of endogenous full-sized ligands has also been explored. This approach allowed for the reduction in size of the delivery system and competition with endogenous serum ligands. For instance, targeting members of the LRP1, such as Angiopep-2 peptide, have been investigated. Angiopep peptides were designed through the alignment of LRP1 binding proteins harboring a Kunitz-type domain and were proposed as a potential peptide-based vector to deliver drugs to the central nervous system<sup>141</sup>. These peptides, and particularly Angiopep-2, displayed higher transcytosis capacity and parenchymal accumulation (Figure 4). Indeed, the distribution of Angiopep-2 in the brain was 2.5 and 5 times higher than that of transferrin and aprotinin, respectively<sup>141</sup>.

a.

Aprotinin	G L C Q T F V Y G G C R A K R N N F K S A E D C M R T C G G A
Bikunin	M A C E T F Q Y G G C M G N G N N F V T E K E C L Q T C R T V
$\beta$ -amyloid precursor protein	G K C A P F F Y G G C G G N R N N F D T E E Y C M A V C G S A
kunitz-inhibitor precursor	Q I C K S F V Y G G C L G N K N N Y L R E E E C I L A C R G V



Peptides	Amino-acid sequence
Angiopep-2	TFFYGGSRGKRNNFKTEEY
Angiopep-5	TFFYGGs*RGKRNNFR*TEEY
Angiopep-7	TFFYGGs*RGR*RNNFR*TEEY

b.

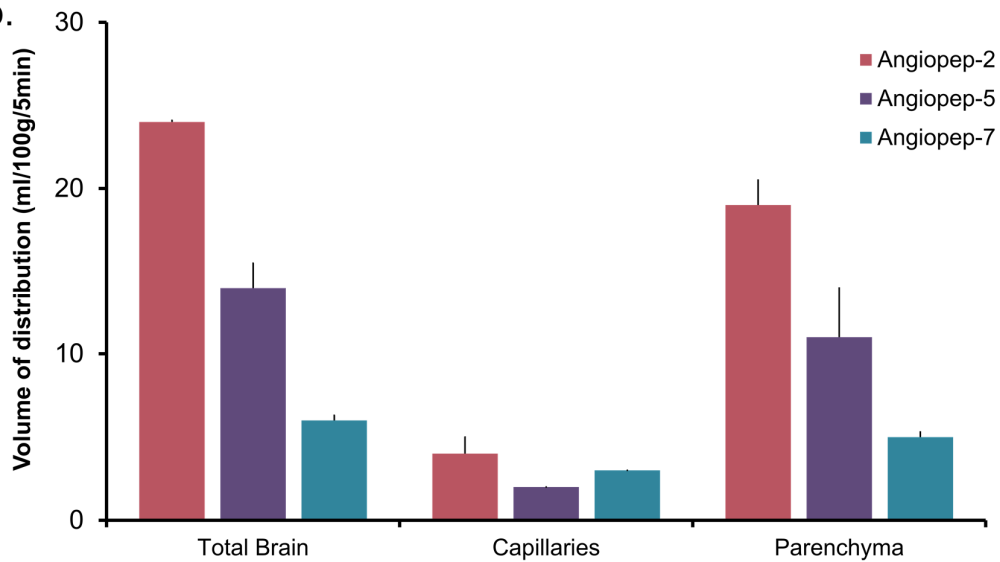


Figure 4: Angiopep peptides designs as targeting members of LRP1. (a) The amino acid sequences of tested Angiopep peptides are presented. Changes in the amino acid sequence (when compared to Angiopep-2) are indicated with an asterisk. (b) Volumes of distribution of Angiopep peptides in the brain parenchyma measured by *in situ* brain perfusion. Reprinted with permission from reference <sup>141</sup>.

Overall, the BBB and BCSFB are more than simple anatomical obstacles. They are also active tissues that express a diverse range of transporters, receptors, and enzymes. They can recognize therapeutic brain agents, such as proteins, and lower their brain bioavailability. However, under different pathological conditions such as stroke, these barriers may experience damage.

## **2. Ischemic stroke: Generalities and prevalence**

Stroke is a cerebrovascular disease, an alteration of normal cerebral blood flow, which results in neurological deficits. The World Health Organization (WHO) defines stroke as “rapidly developing clinical signs of focal (or global) disturbance of cerebral function, with symptoms lasting 24 hours or longer, or leading to death, with no apparent cause other than of vascular origin”<sup>142</sup>. Worldwide, stroke is the second leading cause of death, dementia, and depression, as well as the third leading cause of disability<sup>143</sup>. In Canada, stroke is the third leading cause of death and the largest contributor to adult disability with over 400,000 people living with the sequela of stroke<sup>1</sup>. By 2038, the number of Canadians living with the effects of stroke is expected to increase (with the changing demographics of an aging population) to between 654,000 and 726,000 people<sup>1</sup>.

At the most basic level, there are two main types of stroke: hemorrhagic and ischemic. Hemorrhagic stroke, found in about 20% of cases, occurs when an artery ruptures (usually due to an aneurysm) and blood is no longer delivered to the brain. Ischemic stroke, the focus of this thesis, is far more common and accounts for approximately 80% of strokes. Ischemic stroke results from a transient or permanent reduced or interrupted cerebral blood flow that is restricted to the corresponding irrigated brain area. The alteration of flow is typically caused by the occlusion of a cerebral artery either by an embolus or by a thrombus. Depending on the size and the affected area, ischemic stroke can be divided into focal brain ischemia (occlusion of specific arteries of the brain) or global brain ischemia (systemic and complete cessation of blood flow in the whole parenchyma of the brain). The duration of the ischemic insult determines whether the ischemia is classified as transitory or permanent. Transitory ischemia occurs if the artery occlusion is followed by reperfusion. In permanent ischemia, blood flow is not restored. The origin of ischemic stroke could be cardiogenic, atherosclerotic, lacunar, hemodynamic or cryptogenic. In the case of cardiogenic embolic stroke, for example, cardiac abnormalities can cause the formation of a thrombus in the heart that can travel *via* the bloodstream to the internal carotid artery or its branches, most commonly the MCA<sup>144</sup>. In over half of all ischemic strokes, occlusion of the territory served by the MCA was reported<sup>145</sup>. In this work, we will focus on the focal cerebral ischemic model, which normally results in an ischemia in the cortex and striatum from occlusion of the MCA.

### **2.1. Pathophysiology of ischemic stroke**

During ischemic injury, the arterial occlusion and the lack of cerebral blood supply results in oxygen and glucose deprivation in the brain. This initiates a series of detrimental processes that compromise tissue viability and ultimately lead to cell death and brain damage (Figure 5).

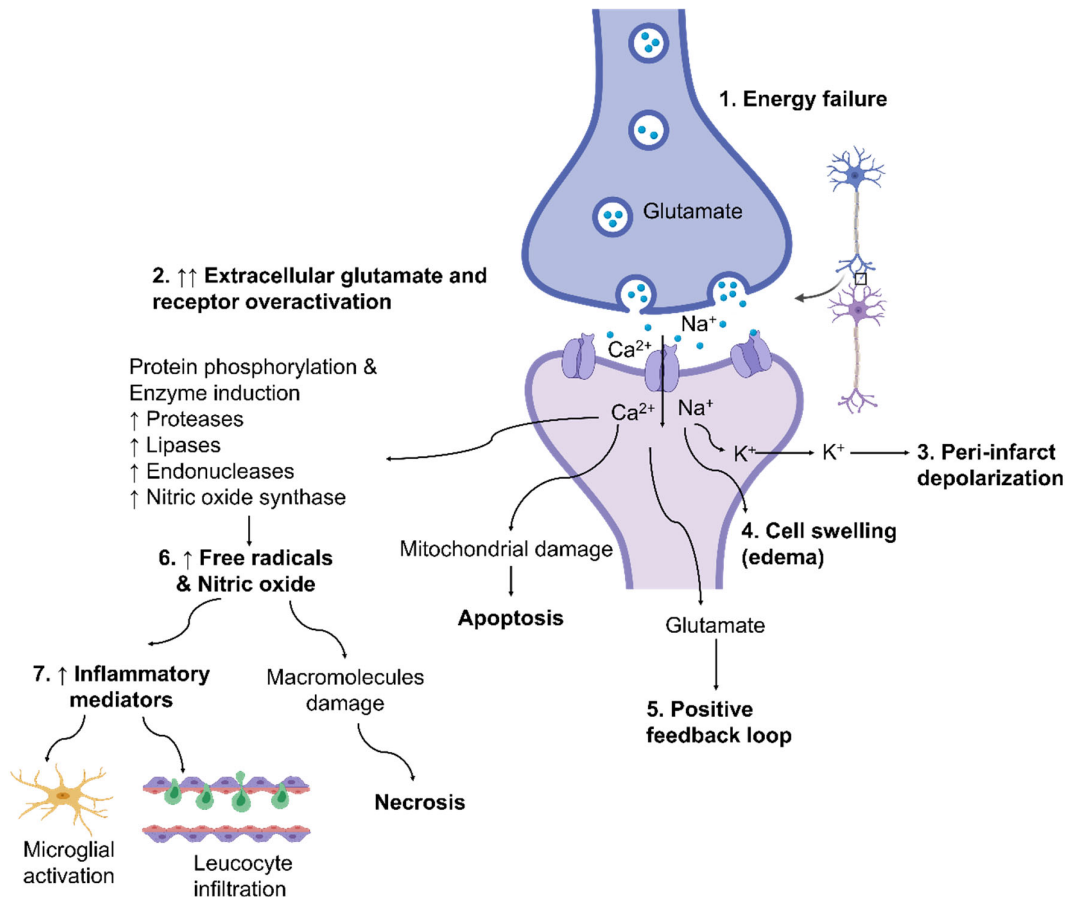


Figure 5: Simplified overview of the pathophysiological mechanisms of ischemic stroke. Energy failure leads to depolarization of neurons, excessive release of glutamate, and failure of ionic pumps. These events lead to an over-activation of specific glutamate receptors, an intracellular accumulation of Na<sup>+</sup> and Ca<sup>2+</sup>, an efflux of potassium, a spreading wave of depolarization, and cell swelling. Increased calcium concentrations cause numerous damages (oxidative stress, inflammation, cell death).

Within the affected ischemic region, two distinct zones can be distinguished: the “core” and the “penumbra”. The core, defined as the portion of the tissue where the blood flow is strictly reduced leading to an irreversible injury essentially by necrosis <sup>146</sup>. This zone is characterized by a depletion of cellular ATP stores, altered distribution of ions, intracellular acidification, high concentrations of glutamate, and generation of reactive oxygen species <sup>147,148</sup>. The area surrounding the necrotic core is severely hypoperfused and represents potentially salvageable brain tissue, in which neuronal activity is suppressed but the cells remain metabolically active (i.e., lowered levels of ATP and maintenance of ionic balance) <sup>149</sup>. This zone, termed “penumbra” or “peri-infarct zone”, is at risk of tissue death as damage spreads from the core, but is transiently maintained by collateral blood supply. Within this zone, apoptotic processes are progressively established during the subacute phase, and thus neurons are potentially

recoverable for some time (several hours or days) after the onset of stroke <sup>146,150</sup>.

The mechanisms mediating ischemic stroke damage likely involve multiple factors. In the following sections, the alterations of the blood–brain interfaces and the mechanisms related to the excitotoxicity will be discussed.

### **2.1.1. Dysfunction of the blood–brain interfaces**

The disruption of the blood–brain interfaces is common in ischemic stroke. The extent of damage is associated with the type, severity, and duration of ischemic insults. Because of the damage to the BBB, ischemic stroke results in the leakage of blood-borne cells, chemicals, and fluid into the parenchyma of the brain. This deterioration is caused by, but not limited to, endothelial cell degeneration and to increased paracellular and transcellular permeability <sup>151,152</sup>. Indeed, soon after ischemia and before BBB impairment, the dysfunction of endothelial cells and the successive increase in the activity of ion transporters (such as Na<sup>+</sup>/H<sup>+</sup> exchangers or Na<sup>+</sup>/K<sup>+</sup>/Cl<sup>-</sup> co-transporters) enhance the transport of Na<sup>+</sup>/Cl<sup>-</sup> from the blood into the brain by a transcellular pathway, causing an ionic imbalance that may play a major role in ischemia-induced edema formation and BBB breakdown <sup>153-159</sup>.

In preclinical models of ischemic stroke, the “opening” of the BBB was found to occur in two phases, even when normal blood flow was restored to neuronal tissue <sup>160,161</sup>. The first phase is controlled by endothelial cytoskeleton modifications after ischemia/reperfusion injury, and consists of recruitment and infiltration of immune cells as well as enzymatic cleavage of tight junctions. This phase is accompanied by a second phase implicating a cascade of cellular and vascular damage. For example, in a transient MCA occlusion (MCAo) rat model, a biphasic course of BBB opening (at 4 hours and 48 hours) was demonstrated by Pillai et al., with a significant reduction in BBB permeability at 24 hours <sup>162</sup>. Changes in transcriptional and translational regulation as well as the reorganisation of brain endothelial tight junction proteins have been demonstrated following ischemic insults. The active remodelling of tight junction complexes in the endothelial cells of the brain is responsible for both phases of BBB breakdown <sup>163,164</sup>. RMT, which is an energy-dependent vesicular transport process, is likewise affected during ischemia/reperfusion. In the permanent MCAo model and in the initial phase of ischemic stroke (6 hours post-ischemia), LDLR and scavenger receptor class B member 1 were significantly upregulated in endothelial cells, whereas expression of LDLR significantly decreased from 3 days after MCAo <sup>165</sup>. Furthermore, it has been reported that LRP1 is upregulated in both brain endothelial cells and neurons in the ischemic cortex within 6 hours of transient MCAo in mice <sup>166,167</sup>.

Compared to the BBB, the impact of cerebral ischemia on the BCSFB has received less attention. Disintegration of the choroidal epithelium has been reported. Indeed, BCSFB

leakiness was revealed by the 3-fold increase in  $^3\text{H}$ -inulin permeability at 6 hours post-occlusion, and had a major effect on tissues near the ventricular system <sup>168</sup>. Stroke-induced BCSFB disruption was associated with the free diffusion of proteins, cytokines, and potentially toxic plasma molecules into the ventricles, and subsequently to the closest brain structures <sup>169</sup>. The injury to the choroidal epithelium recovered within 18 hours, and was assisted by hormones and growth factors secreted by the choroid plexus <sup>168,170-172</sup>.

Typically, the "permeabilization" of the blood–brain interfaces has a deleterious effect on brain tissue and is associated with poor outcome.

## **2.1.2. Glutamate excitotoxicity**

### **a. Glutamate homeostasis**

Glutamate is the principal excitatory neurotransmitter of the central nervous system. Indeed, ~60–70% of all synapses are glutamatergic <sup>173</sup>. The concentration of glutamate varies dramatically depending upon the biological compartment. In the brain, the levels are in a dynamic equilibrium that is highly sensitive to changes in the energy supply. In fact, glutamate levels are maintained at approximately 0.5–5  $\mu\text{M}$  and 3–10  $\mu\text{M}$  in the brain interstitial fluid and the CSF, respectively <sup>174-177</sup>. These levels are much higher inside the cytosol of brain cells (~10 mM) and in the synaptosomal vesicle (~100 mM). <sup>178</sup> The tight control of glutamate levels is achieved through the presence various uptake and sequestration systems (i.e., plasma membrane glutamate transporters and vesicular glutamate transporters), as well as the strict control of glutamate catabolism and synthesis enzymes (glutaminase, glutamate decarboxylase, ...) in distinct cellular and subcellular compartments. The maintenance of low extracellular glutamate is essential because its concentration must be kept below 2–5  $\mu\text{M}$  in order to ensure normal synaptic transmission and prevent excitotoxicity <sup>179-181</sup>

### **b. Glutamate receptors**

Glutamate neurotransmission is mediated through and regulated by various categories of receptors and transporters. Stimulation of glutamatergic synapses and extracellular release of glutamate from presynaptic terminals is typically followed by the activation of highly complex membrane receptors. These receptors belong to two main classes, ionotropic (fast-acting receptors) and metabotropic (slower-acting receptors) (Figure 6) <sup>182</sup>. Each class is further divided into three main categories, depending on structural and pharmacological properties (e.g., binding specificity, ion permeability, conductance properties, ...). Glutamate receptors are widely distributed in the central nervous system, where they can be localized at synaptic and extra synaptic levels in neurons, glia, microvascular endothelial cells, pericytes, and choroidal ependymal cells <sup>183-186</sup>.

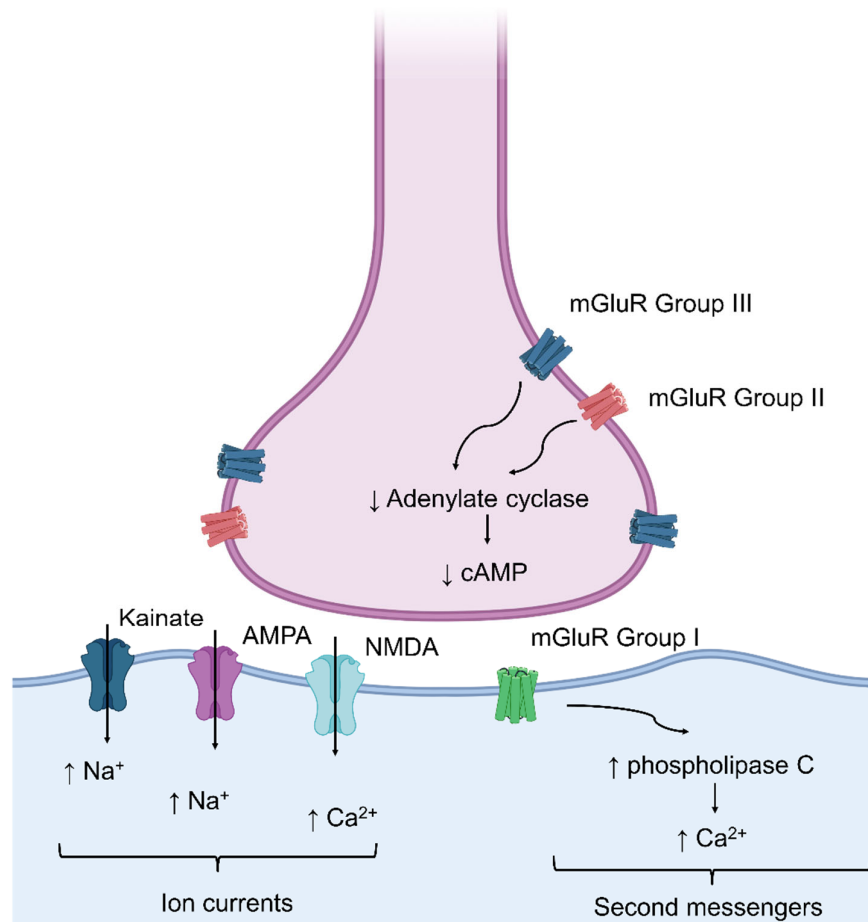


Figure 6: Illustration of a hypothetical synapse showing glutamatergic receptors.

Metabotropic glutamate receptors are G-protein-coupled receptors that produce their effects through intracellular signaling mechanisms and *via* gene expression and protein synthesis. So far, a total of eight metabotropic glutamate receptor subtypes have been identified and classified into three groups according to their structural homology, pharmacological profile, and signal transduction properties. The amino-acid sequence identity of metabotropic receptors belonging to the same group is ~70% and between groups is ~45%<sup>187</sup>. Group I receptors are formed from mGluR1 or mGluR5 subunits and typically associated with activation of phospholipase C and production of second messengers such as inositol triphosphate. Once formed, this messenger diffuses in the cytoplasm and binds to its receptor, localized primarily in the endoplasmic reticulum, resulting in calcium release into the lumen of the cell<sup>188</sup>. Group II receptors are composed of mGluR2 and mGluR3 subunits. Group III is comprised of mGluR4, mGluR6, mGluR7, and mGluR8 subunits. Both Group II and Group III generally suppress adenylate cyclase activity, thus inhibiting the production of cyclic adenosine

monophosphate (cAMP) from ATP<sup>189,190</sup>. Their primary function is to reduce glutamate release in the synaptic cleft, inhibiting excitatory transmission<sup>187</sup>. It is becoming gradually recognized that these receptors also couple to further signaling pathways, providing additional complexity to the mechanisms by which they regulate glutamate neurotransmission<sup>191</sup>. Activation of the above-mentioned signaling pathways upon glutamate binding is important for regulating glutamate release and uptake, modulating neuronal excitability, and contributing to synaptic plasticity<sup>192</sup>. For example, evidence has revealed that the internalization of the ionic glutamate receptor  $\alpha$ -amino-3-hydroxy-5-methyl-4-isoazolepropionic acid (AMPA) can be regulated by Group I receptors (mGluR1/5)<sup>193,194</sup>. Similarly, Group II upregulates glutamate transporters (i.e., excitatory amino acid transporter 1: EAAT1)<sup>195</sup>. Therefore, as the activity of metabotropic receptors is greatly affected during ischemic stroke (for instance, decreased ATP levels affect the production of cAMP and interrupts the intracellular signaling processes), their regulation of the glutamate uptake/release functions might be greatly compromised.

Ionotropic receptors are divided into three classes which are named after the agonists that were originally identified to selectively activate them: N-methyl-D-aspartate (NMDA), AMPA, and 2-carboxy-3-carboxymethyl-4-isopropenylpyrrolidine (kainate) receptors. Classically, all these receptors are tetrameric, and each receptor subtype is assembled from a different set of subunit proteins<sup>196</sup>. Therefore, there is a substantial diversity in the assemblage of the subunits and an extraordinary functional variety in the ionotropic receptors.

After glutamate binding, ionotropic receptors undergo conformational changes to allow an immediate influx of extracellular ions ( $\text{Na}^+$  and/or of  $\text{Ca}^{2+}$ ) along with an efflux of  $\text{K}^+$  ions. Unlike NMDA receptors, AMPA and kainate receptors are responsible for an immediate and rapid response, permitting post-synaptic membrane depolarization and signal transmission<sup>174,197</sup>. NMDA receptors display a high permeability towards calcium and are important for the regulation of neuronal plasticity by activating specific calcium-dependent signaling cascades<sup>197</sup>. In normal conditions, when the energy supply is sufficient, the ATP-driven ion pumps restore the equilibrium of ions in the cells<sup>198</sup>. However, under ischemic conditions, the activity of these pumps is reduced, leading to a significant reduction of active calcium efflux and producing a massive increase in intracellular calcium. This calcium overload is particularly neurotoxic, leading to the activation of enzymes that degrade proteins, membranes and nucleic acids<sup>199-201</sup>.

### **c. Glutamate transporters**

#### **- Excitatory amino acid transporters (EAATs)**

To regulate the extracellular concentration of glutamate, set the stage for the next transmission, and prevent glutamate excitotoxicity, EAATs capture synaptic glutamate. In the

brain, five EAATs, previously known as Na<sup>+</sup>-dependent high-affinity glutamate transporters, have been identified: EAAT1–5. In rodents, the EAAT1 analogue is referred to as GLAST, EAAT2 as GLT-1, and EAAT3 as EAAC1<sup>199</sup>. EAAT family members share ~50–55% amino acid sequence homology<sup>202</sup>. These transporters are homotrimeric complexes and their expression pattern greatly differs in between brain regions, cells and subcellular compartments<sup>203</sup>. EAAT4 is highly expressed in Purkinje cells of the cerebellum<sup>204,205</sup>, while EAAT5 dominates in bipolar cells and retinal photoreceptors<sup>206</sup>. Both EAAT1 and EAAT2 predominately display a glial distribution, whereas EAAT3 is enriched in the soma and dendrites of neurons<sup>207</sup>, though less so in the synaptic terminals of axons<sup>208-210</sup>.

Glial cells, most often astrocytes but also microglia and oligodendrocytes, perform a critical role in the spatial buffering of extracellular glutamate levels in brain. The major transporter is EAAT2, expressed predominantly in astrocytes and responsible for more than 90% of total glutamate uptake<sup>211</sup>. Along with glial cells, microvascular endothelial cells significantly adjust the extracellular concentration of glutamate. At least three EAAT members were detected in the abluminal membrane of the BBB (EAAT1–3)<sup>212</sup>. These transporters promote the accumulation of glutamate into the endothelial cells<sup>213</sup>. Then, when the intracellular levels of glutamate becomes higher than the blood glutamate concentration, glutamate is moved *via* facilitated diffusion through the luminal side of the BBB into the blood stream<sup>214</sup>. Moreover, neurons exclusively express EAAT3 and EAAT5 and contribute to the modulation of glutamate levels<sup>206,215</sup>. In addition to these EAATs regulating glutamate levels in the brain's interstitial fluid, further EAATs (i.e., EAAT1 and EAAT3) were detected in the apical membrane of the choroidal ependymal cells, where they participate in glutamate removal from the CSF<sup>216</sup>. Undeniably, the presence of transporters on various cell types suggests that a high level of cooperation is necessary to avoid any glutamate toxicity.

The uptake of glutamate by EAATs is thought to occur *via* an “alternating access” model<sup>217-219</sup>. According to this model, the EAATs undergo structural transitions that alternately expose their ligand binding site to the inside and the outside of the membrane (outward-open and inward-open conformations). Indeed, the binding of the ligand to the extracellular domain of the transporter triggers a series of conformational transitions allowing exposure of the binding site to the intracellular side, followed by the subsequent release of the cargo inside the cells. Thereafter, additional conformational changes occur to re-orientate the transporter and to complete the cycle. Hence, the transport performance of each EAAT will greatly depend on various parameters such as the affinity and the synaptic density of the EAAT, the initial binding rates, and the EAAT turnover rates. For instance, it was demonstrated that the EAAT4 turnover rate was significantly slower than those of EAATs 1–3. However, its affinity for glutamate was 10-fold higher than that of EAATs 1–3<sup>220</sup>.

Generally, the EAAT is activated by the sequential binding of Na<sup>+</sup> and glutamate. Glutamate uptake is driven by the co-transport of three Na<sup>+</sup> ions and one H<sup>+</sup>, into the cell, followed by the counter-transport of K<sup>+</sup> <sup>220-223</sup>. This process provides a net positive charge to glutamate transport that is compensated by an uncoupled flux of Cl<sup>-</sup> through the transporter <sup>204,224</sup>. The dependence of glutamate uptake on ions makes this mechanism highly vulnerable to any alteration of the ionic gradients. It has been estimated that more than 80% of the brain's total glucose oxidation is used to maintain the electrochemical gradients and the processes of glutamate uptake/cycling <sup>225,226</sup>. At this time, the data relative to the EAAT expression/activity following ischemic stroke are inconsistent with both downregulation and upregulation reported during an ischemic insult <sup>227-230</sup>.

- *Vesicular glutamate transporters (VGLUTs)*

Three types of VGLUTs (1, 2 and 3) assure the packaging of recycled glutamate into the synaptic vesicles at presynaptic nerve terminals. These transporters share a high degree of structural homology (~76% amino acid sequence identity) and are functionally similar <sup>231</sup>. Nonetheless, their expression varies across different regions of the brain <sup>231</sup>. The glutamate uptake by VGLUTs is an active process relying on the membrane potential established by vacuolar H<sup>+</sup>-ATPase (V-ATPase) across the vesicular membrane <sup>232,233</sup>. Therefore, similar to the rest of the glutamate receptors and transporters, disturbance of the energy metabolism is detrimental to their activity.

**d. Glutamate metabolism, catabolism and cycling**

In addition to its role as a neurotransmitter, glutamate plays important roles in intermediary metabolism – connecting carbohydrate and amino acid metabolism *via* the Krebs cycle. In the brain, glutamate metabolism is extremely complex <sup>234</sup>. Here, only the main metabolic pathways will be presented (Figure 7).

Under physiological conditions, glutamate is mainly derived by synthesis from glutamine or from citric acid cycle intermediates within the brain <sup>235</sup>. Production of glutamate from glutamine is catalyzed by phosphate-activated glutaminase, present in neurons and astrocytes <sup>236</sup>. The production of glutamate from plasma-derived glucose takes place primarily in astrocytes and begins with the entry of glucose into cells *via* glucose transporters (GLUT) <sup>237</sup>. Once inside the cytoplasm, glucose is converted *via* glycolysis to pyruvate, which can be reduced to lactate (in the cytoplasm) or enter the Krebs cycle as acetyl coenzyme (Acetyl-CoA) to provide  $\alpha$ -ketoglutarate as a carbon backbone for glutamate (in the mitochondria). The subsequent conversion of  $\alpha$ -ketoglutarate to glutamate is catalyzed by numerous enzymes, such as glutamate oxaloacetate transaminase (GOT), glutamate pyruvate transaminase (GPT), and



Taken together, astrocytes produce glutamate, reduce pyruvate to lactate (that is released to the extracellular space and taken up by neurons), or transform glutamate to glutamine (which is transferred to the extracellular fluid by electroneutral transporters and then taken up by electrogenic transporters into neurons) <sup>243-245</sup>. Neurons, on the other hand, use glucose, lactate, or glutamine as precursors to synthesize glutamate. The resulting glutamate is loaded inside vesicles *via* the VGLUTs and released in the synaptic cleft by a calcium- and energy-dependent exocytotic process during synaptic transmission <sup>246</sup>.

The metabolism of glutamate in microvascular endothelial cells has not been thoroughly identified and the exact clearance pathways of glutamate from the brain to the blood *via* the BBB remain to be characterized. It was reported that the uptake and accumulation of extracellular glutamate into these cells is an imperative step for glutamate metabolism <sup>247</sup>. Accordingly, accumulated glutamate can be directly transported to the blood compartment or metabolized with subsequent transport of the resulting metabolites (e.g., lactate) <sup>248,249</sup>. Indeed, endothelial cells express branched chain aminotransferases <sup>250</sup>, which may catalyze the conversion of glutamate to  $\alpha$ -ketoglutarate.  $\alpha$ -ketoglutarate enters the citric acid cycle and ultimately produces lactate that can be transported across the BBB through MCT1 <sup>251</sup>. Moreover, glutamine (originally produced and released by astrocytes) can also be pumped from the brain interstitial fluid into the endothelial cells by a  $\text{Na}^+$ -dependent transporter. Thereafter, within the cytoplasm, glutaminase converts glutamine back to glutamate <sup>252</sup>. The transport of intact glutamate from the cytoplasm of the microvascular endothelial cells to the blood was supported by *in vivo* studies demonstrating the presence of a facilitative glutamate transporter at the luminal membrane, termed  $x_{\text{G}^-}$ . This transporter has low affinity for glutamate and thus depends on high intracellular concentrations to enable the transport <sup>248,253</sup>.

Overall, tight regulation of glutamate metabolism, catabolism and cycling in the brain is important for the preservation of cellular and mitochondrial integrity and function. Aberrations in glutamate metabolism are tightly linked to ischemia <sup>254</sup>.

### **2.1.3. Mechanism of glutamate excitotoxicity**

Ischemic conditions deprive neurons of oxygen and glucose. Oxygen deficiency disrupts mitochondrial oxidative phosphorylation, and glucose insufficiency causes ATP loss. The depletion of ATP hampers the activity of ATP-driven ion pumps and, as the electrochemical gradients collapse, it results in cell membrane depolarization <sup>2,3</sup>. This depolarization leads to a large and sustained release of glutamate, activating numerous glutamate receptors such as the NMDA, and overwhelming the regulating mechanisms leading to a build-up of the neurotransmitter in the extracellular milieu <sup>4-6</sup>. Subsequently, a positive feedback loop is initiated as the released glutamate stimulates additional glutamate release <sup>255</sup>. This cascade

of events represents a major gateway for a myriad of downstream effects and culminates in a pathological increase in intracellular calcium that overexcites neurons <sup>256</sup>. The processes underlying glutamate-triggered, calcium-mediated excitotoxicity principally involve activation of calcium-dependent degradative enzymes. Activation of such enzymes and generation of feedback loops rapidly accelerates a downward spiral toward neuronal death (*via* overproduction of reactive oxygen species and mitochondrial damage, for example) <sup>7-10</sup>. Given the ubiquitous presence of glutamate receptors/transporters in different cellular components, as well as the widespread involvement of glutamate in various energy metabolism processes, excitotoxic cascades do not only involve neurons, but also compromise all cell types, such as astrocytes, oligodendrocytes, and microvascular endothelial cells (Figure 8) <sup>257,258</sup>.

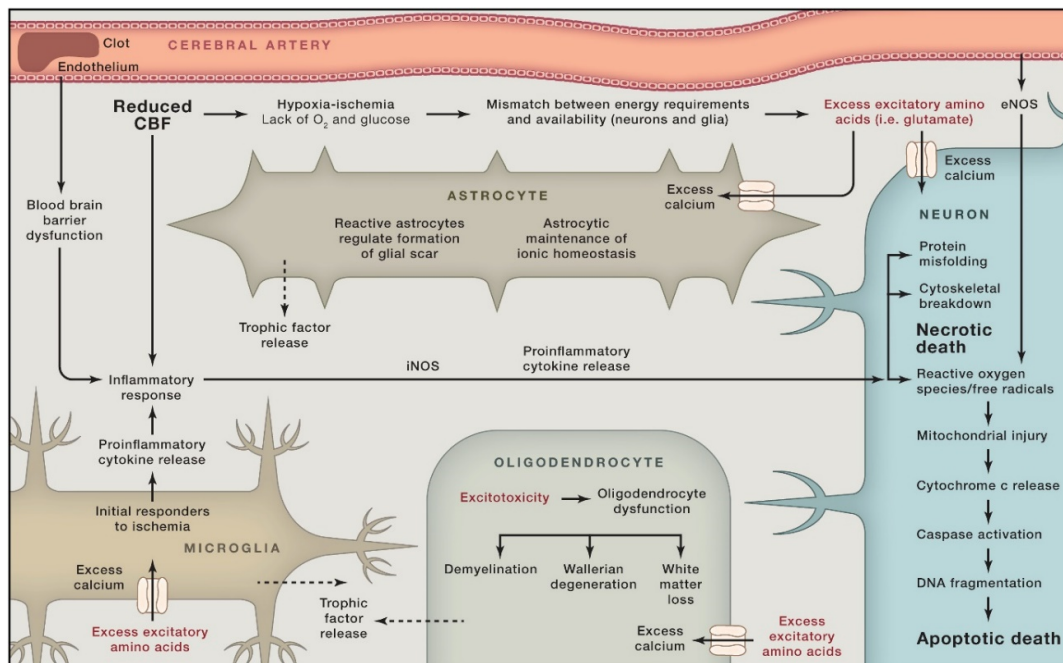


Figure 8: Implication of astrocytes, microglia, and oligodendrocytes in excitotoxicity. Reprinted with permission from reference <sup>259</sup>.

Overall, several data clearly demonstrate the contribution of glutamate homeostasis alteration to the development and progression of ischemic insult. Therefore, acting on steps of the process of glutamate excitotoxicity could confer neuroprotection by stopping numerous downstream death-signaling cascades at their converging upstream start process.

Initially, the major focus of research centred on glutamate receptor antagonism and numerous classes of NMDA antagonists were developed. While showing therapeutic efficacy, they have limited usefulness because of their difficulty in passing through the BBB. As such, they have

low cerebral bioavailability despite administration of large doses. Additional problems arise due to a lack of discrimination between the diverse actions of the receptor, as they interfere with both the negative and positive aspects of its signaling <sup>15</sup>. For instance, it was shown that inhibition of NMDA receptors lead to cognitive impairments, hallucinations, and even coma <sup>14</sup>. In addition to these drugs, Ca<sup>2+</sup> and Na<sup>+</sup> channel blockers were developed and used in clinical trials <sup>11</sup>. However, no feasible treatment candidates have passed the clinical testing required for broad clinical use. Indeed, many of these compounds lack sufficient brain penetration and exhibit significant dose-limiting toxicities. In Phase II stroke trials, Na<sup>+</sup> channel blocker “Sipatrigine”, for example, caused several side effects (nausea and vomiting, irritation at the injection site, reduced consciousness, agitation, confusion, and hallucination) and failed to improve outcome compared to placebo <sup>12,13</sup>. Thus, its further clinical investigation was interrupted <sup>12,13</sup>.

In opposition to the extensive investigation of antagonists as neuroprotectants, there have been relatively few studies exploring strategies aiming to directly reduce synaptic glutamate levels. One of these approaches relies on enzymatic glutamate degradation. The rationale of such a strategy is based on the kinetics of synaptic glutamate removal, which is normally and primarily mediated by EAATs <sup>260</sup>. Three enzymes with the capacity to degrade glutamate (GS, GDH, and GPT) have been suggested as possible neuroprotectants in *in vitro* models of glutamate excitotoxicity, but these findings were not followed by *in vivo* studies <sup>261-263</sup>. One of the main reasons could be the expected inability of such macromolecules to pass through blood–brain interfaces. Indeed, it has been reported that close to 100% of large pharmaceutical molecules (including proteins) are unable to enter the central nervous system, in the absence of specific transporters <sup>264</sup>.

Lately, alternative strategies comprising the investigation of allosteric activation of GDH activity in the brain and the exploration of GOT as a blood-resident enzyme were proposed in order to preserve mitochondrial activity and concurrently rescue neurons from glutamate excitotoxicity.

### 3. Enzymatic glutamate degradation approaches

#### 3.1. Glutamate dehydrogenase (GDH)

##### 3.1.1. Structure

Mammalian GDH is a hexameric protein composed of six identical monomers, each with a MW of around 56 kDa <sup>265,266</sup>. Its structure has been described as a 'dimer of trimers.' While GDH in mammals has long been thought to be encoded by a single gene, studies have revealed the presence of two GDH isozymes with distinct regulation and tissue expression patterns: GDH1 and GDH2 <sup>267</sup>. In the brain, GDH1 is mainly expressed in glial cells (astrocytes and oligodendrocytes) but not in neurons. GDH2 is found in both glial and neuronal cells <sup>267</sup>.

Each monomer contains three main domains: (1) a catalytic (substrate binding) cleft, (2) a coenzyme (nicotinamide adenine dinucleotide (NAD<sup>+</sup>) or nicotinamide adenine dinucleotide phosphate (NADP<sup>+</sup>)) binding domain, and (3) a regulatory 'antenna' domain extending from the coenzyme binding domain <sup>268</sup>. The latter domain is only present in mammalian GDH and consists of an ascending  $\alpha$ -helix, a random coil and a short C-terminal  $\alpha$ -helix <sup>56,269</sup>. It exhibits a remarkable conformational change on opening and closure of the active site, and plays an important role in allosteric regulation <sup>56,266</sup>.

##### 3.1.2. Dynamics

During each catalytic cycle, a large conformational change occurs throughout the hexamer (Figure 9). During this process, the coenzyme binds to its binding site in the catalytic cleft of GDH and is followed by glutamate binding to its own site (located between the coenzyme binding domain and the lower domain). A rotation of 18–20° of the coenzyme binding domain wedges the substrate and the coenzyme together, leading to the closure of the catalytic cleft. As the catalytic cleft closes, the bases of the long ascending helices in the antenna rotate out and compress the whole hexamer by pushing against the pivot helix of the adjacent subunit. As the 'mouth' closes, the short helix in the descending loops of the antenna becomes distorted and shorter. Through these movements, the pivot helix, located on the top of the hexamer, rotates in a counter-clockwise manner along the helical axes, and around the 3-fold symmetry axis of the trimer. The dimer of trimers stacked on top of each other move as rigid units towards each other, squeezing the core of the hexamer <sup>56,268,270</sup>. Once the product is formed, GDH reverses these motions to release the substrates and prepare the enzyme for another cycle <sup>271</sup>.



and the respective concentrations of substrates <sup>179</sup>. In brain tissues, for example, the physiological existence of high glutamate concentrations along with low ammonia levels are assumed to favor glutamate catabolism (oxidative deamination direction) rather than glutamate synthesis <sup>274,275 273,276</sup>.

#### **3.1.4. Homotropic and heterotropic regulation**

Mammalian GDH exhibits several unusual kinetic properties and complex homotropic and heterotropic modulation. Work to determine the role of such an allosteric network has been frustrated by its sheer complexity. A complex pattern of kinetics was observed and deviations from Michaelis-Menten behaviour were noticed with increasing concentrations of coenzyme or substrate <sup>277</sup>. In the oxidative deamination reaction, GDH shows substrate inhibition at high glutamate concentrations <sup>278</sup>. This inhibition was explained by the fact that glutamate replaces  $\alpha$ -ketoglutarate before the reduced coenzyme is released, forming an abortive or dead-end complex (GDH·NADH·Glutamate). These complexes saturate GDH, which is then slowly recycled for the next round of catalysis <sup>268,278-280</sup>.

In the steady-state, a distinct negative cooperativity was reported when coenzyme concentration was varied <sup>278</sup>. Subsequent studies demonstrated that the two sets of trimers in GDH are functionally different, and it was proposed that they either have distinct intrinsic affinity for the coenzyme or have negative interactions between their respective subunits. In the latter case, the binding of the coenzyme to the initial trimer presumably induces a conformational change that weakens the affinity to the remaining, 'free' trimer <sup>281,282</sup>. This was further confirmed by a follow-up study showing that one set of trimer covers about 82% of the total GDH activity and that the remaining set accounts for the remaining 18% <sup>283</sup>. More importantly, it was shown that these negative interactions operate not only between, but also within, the trimers. Indeed, the first subunit of the enzyme that takes part in catalysis makes the largest contribution to the overall catalysis, while the last subunit makes the smallest contribution. Therefore, inhibition of 1, 2, or 3 catalytic sites of GDH leads to the progressive loss of 54%, 20%, and 10% of activity <sup>49</sup>. The purpose of these homotropic regulation processes is difficult to ascertain. Probably, such mechanisms permit the maintenance of a certain catalytic rate and responsiveness as substrate/coenzyme levels vary.

In order to provide the versatility required for dynamic adaptation to any changes in the cellular environment, the control of GDH activity is further accomplished by an extremely sophisticated and multifactorial heterotropic regulation. Indeed, mammalian GDH is allosterically regulated by a wide range of ligands acting on its motions during the catalysis. Guanosine triphosphate (GTP) acts as a potent allosteric inhibitor and binds, mainly *via* interactions with its triphosphate moiety, to the base of the antenna (near the hinge region between the pivot helix and the

coenzyme binding domain)<sup>56,284</sup>. As its binding site becomes available when the catalytic cleft is closed, GTP can only bind to the closed conformation of the enzyme<sup>53</sup>. With this binding, GTP inhibits the reaction by stabilizing the abortive complexes, slowing down the product release, and preventing the movement of the coenzyme-domain associated with the opening of the catalytic cleft and enzymatic turnover<sup>53,285</sup>. In addition to GTP, other endogenous inhibitors, namely ATP and zinc, were shown to bind to the same GTP binding site<sup>52,286</sup>. Thus, after catalytic cleft closure, the allosteric binding site becomes accessible and binding of these molecules inhibits catalytic activity similarly to GTP. In fact, compared to GTP, ATP has a lesser binding affinity (~100-fold lower)<sup>287</sup>. Furthermore, although the major binding site for zinc is located within the GTP binding site, it can also bind to a dynamic region between the two trimers of subunits and disrupt subunit interactions required for catalytic competence<sup>288</sup>. A variety of chemically diverse compounds were also shown to influence the GDH's velocity and to interact at particular flex points on the enzyme<sup>280</sup>. For instance, hexachlorophene and bithionol, two aromatic agents, inhibit GDH by restricting the compression/expansion motions of the core of the hexamer during catalytic cleft closure/opening<sup>271,289</sup>. More specifically, hexachlorophene diffuses into the cavity in the core of the protein, where it blocks expansion by forming a ring-like structure that links the two fold-related subunits together<sup>270,285</sup>. Likewise, bithionol binds to each monomer in a binding pocket located halfway between the core and the exterior of the hexamer<sup>270</sup>. By binding, bithionol decreases the rate of the catalytic turnover by preventing the free movement of the stacked trimers<sup>271</sup>.

Conversely, GDH can be activated by a variety of allosteric activators, namely adenosine diphosphate (ADP) and leucine. ADP binds behind the coenzyme-binding domain, immediately under the pivot helix<sup>266</sup>. Upon binding, ADP activates GDH by facilitating the rotation of the NAD-binding domain and product release<sup>266</sup>. Furthermore, it was reported that by decreasing the affinity of the enzyme for coenzyme at the active site, ADP abrogates the abortive complexes<sup>279</sup>. The mechanism of activation of GDH by leucine is similar to that of ADP, but it acts at a site distinct from ADP<sup>290</sup>.

The allosteric regulation of GDH1 and GDH2 works differently: although ADP and leucine effectively activate GDH2, it has little effect on GDH1<sup>291</sup>. In contrast, GTP induces a greater inhibition of GDH1 than GDH2<sup>292</sup>. At physiological levels, such observations explain the fact that while these two isozymes diverge markedly in their regulation, they display comparable catalytic properties<sup>267</sup>. *In vivo*, these metabolic intermediates (GTP, ATP, ADP) act as energy sensors. When the cells are at a high energy state (sufficient supply of glucose, low ADP levels and high GTP/ATP levels), GDH is inhibited. However, in conditions of low energy state, GDH is activated and metabolizes glutamate to  $\alpha$ -ketoglutarate, which fuels the Krebs cycle to produce energy.

### 3.1.5. Exploitation of GDH for treating ischemia

The regulation of glutamate metabolism *via* the modulation (activation) of GDH activity was proposed as a therapeutic approach to treat ischemic stroke. Indeed, it was shown that, in an MCAo model, mice over-expressing GDH exhibited smaller ischemic lesions and reduced edema volume compared to mice with normal GDH expression <sup>293</sup>. Moreover, in an *in vitro* oxygen/glucose depletion cellular model, GDH activators (an analog of leucine, 2-aminobicyclo-(2,2,1)-heptane-2-carboxylic acid (BCH) and  $\beta$ -lapachone) increased the intracellular levels of  $\alpha$ -ketoglutarate and the subsequent ATP production in both neurons and astrocytes. In addition, GDH activation concomitantly decreased the levels of extracellular glutamate. The ensemble of these effects resulted in neuronal survival <sup>28</sup>. Consequently, administration of these GDH activators to an MCAo mouse model improved the intracellular energy state, diminished the total infarction volume, and decreased animal mortality 24 hours post-ischemia (by increasing the GDH-mediated glutamate catabolism) <sup>28</sup>.

Although the exploitation of GDH has been clearly established, this approach has limitations. In fact, the use of BCH and  $\beta$ -lapachone, even at high intravenous doses results in low cerebral bioavailability because of the inability of these activators to cross the BBB. Indeed, more than 98% of small-molecule drugs are unable to reach the brain <sup>264</sup>. Importantly, previous studies showed that these molecules are pharmacologically active and presented cytotoxic effects.  $\beta$ -lapachone was associated with poor solubility, necroptosis, and systemic toxicity <sup>294-297</sup>. Likewise, BCH caused cell cycle arrest and apoptosis <sup>298-301</sup>. Therefore, although the allosteric modulation of GDH is an appealing concept, inducing GDH activation *via* different modulators or increasing its activity by direct parenteral administration may be more appropriate.

## 3.2. Glutamate oxaloacetate transaminase (GOT)

### 3.2.1. Structure

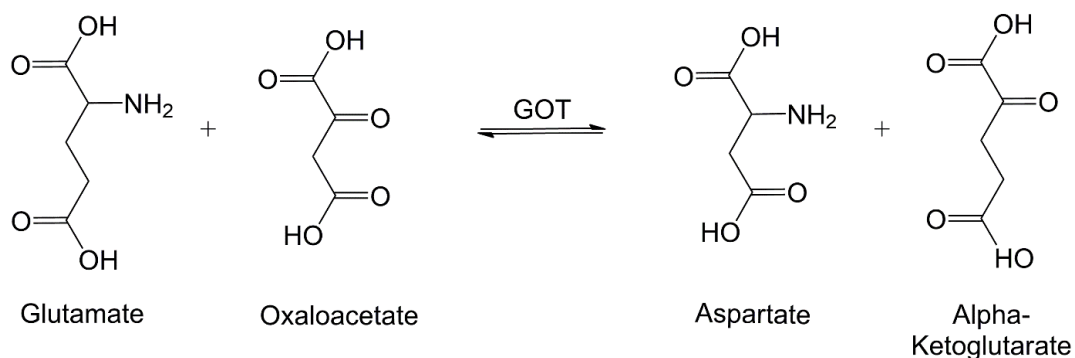
GOT, also known as aspartate aminotransferase, is a homodimeric enzyme with a MW of around 90 kDa <sup>302</sup>. GOT exists as two isoenzymes (genetically and immunologically independent): cytoplasmic (GOT1) and mitochondrial (GOT2) <sup>303</sup>.

Structurally, each monomer of human GOT1 is formed by two domains: a large and a small domain <sup>304</sup>. The large domain (core) includes seven  $\beta$ -sheets and several short  $\alpha$  helices. The small domain consists of four  $\alpha$ -helices, three  $\beta$ -strands, and the N- and C- termini <sup>304</sup>. The two active sites are formed at the interface of the large domains of each monomer <sup>305</sup>. The coenzyme resides at the bottom of the active site pocket and is stabilized by the surrounding residues (e.g., the D223 residue forms a hydrogen bond with the positively charged nitrogen in the pyridine of pyridoxal 5'-phosphate) <sup>304</sup>. At the entrance to the binding site, the two primary

substrate-binding arginine residues are localized<sup>304</sup>. The carboxylate group of the dicarboxylic substrates binds to R386 located at the small domain and to R292 located at the large domain<sup>305</sup>.

### 3.2.2. Activity

GOT catalyzes the reversible transfer of the amino group from glutamate to oxaloacetate while replacing the amino group of glutamate with a carbonyl group (Reaction 2).



Reaction 2: Reversible reaction catalyzed by GOT.

The reaction is catalyzed in the presence of pyridoxal 5'-phosphate as a cofactor and is accomplished *via* two half-reactions in a ping-pong mechanism: (1) the pyridoxal 5'-phosphate enzyme reacts with glutamate to generate the pyridoxamine 5'-phosphate enzyme and  $\alpha$ -ketoglutarate, then (2) the oxaloacetate regenerates the pyridoxal 5'-phosphate enzyme and releases aspartate<sup>306</sup>. *In vivo*, as the  $\Delta G^{\circ}$  of the reaction is  $\sim 0$  kJ/mol, the direction of this catalysis is strictly dependent on current biochemical conditions<sup>307,308</sup>. During ischemic stroke, for example, as the levels of glutamate increase, the reaction equilibrium would be shifted toward glutamate catabolism<sup>309,310</sup>.

### 3.2.3. Exploitation of GOT for treating ischemia

Similarly to GDH, overexpression of GOT in the brain of ischemic mice reduced the infarct volume, attenuated neurodegeneration, and improved post-stroke sensorimotor function<sup>310</sup>. GOT was proposed as a treatment to decrease glutamate concentrations in the brain's interstitial fluid. In this treatment, GOT is systemically administrated and acts in the periphery

(blood), affecting the central nervous system through a mechanism called the “scavenging effect” (Figure 10).

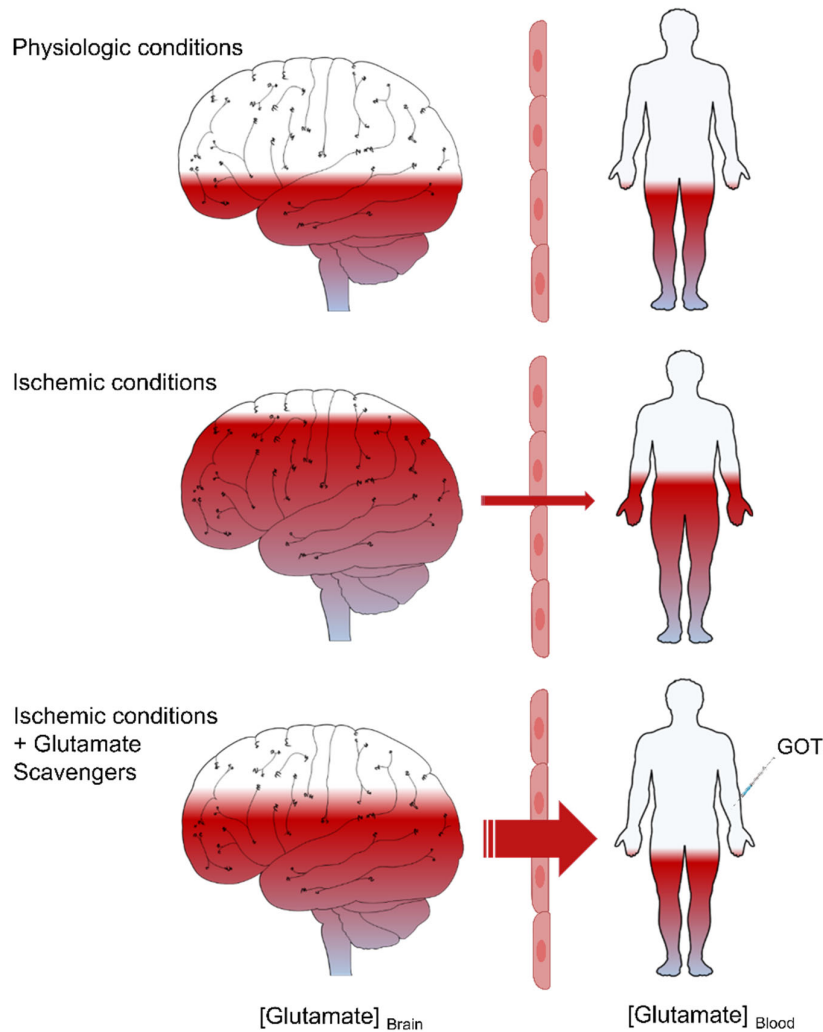


Figure 10: Mechanism of the scavenging effect. Under physiological conditions, the efflux of glutamate is practically absent. During ischemia, as the concentration of glutamate in the brain increases, the efflux of glutamate into the blood is enhanced. In the presence of a glutamate scavenger (such as GOT), the efflux is much more pronounced.

This mechanism relies on the natural diffusion of glutamate from the brain to the blood through the blood–brain interfaces. Indeed, it has been shown that a reduction in blood glutamate concentration could induce a shift in the concentration gradient of glutamate across the BBB, followed by the efflux of glutamate from the brain to the periphery. Therefore the excess glutamate in the brain extracellular fluid that occurred during an ischemic insult might be safely transported towards the blood *via* the cerebral endothelial transporter systems (as seen in the

previous sections) <sup>311-313</sup>. Subsequently, it was shown that the intravenous injections of GOT alone or alongside its co-substrate (oxaloacetate) reduced blood glutamate concentration in rats <sup>314-316</sup>. When administered after MCAo in rats, the peripheral injection of human GOT not only reduced blood and cerebral glutamate levels, but also reduced the infarct size compared to controls. Interestingly, lowering glutamate levels by means of GOT treatment had protective effects even when the treatment was delayed 1-hour after reperfusion <sup>317</sup>.

The described therapeutic strategy greatly differs from other drug treatments targeting the BBB and represents a promising paradigm for treating excitotoxicity-brain diseases. Indeed, to exert its therapeutic effect, GOT does not need to cross the BBB. Furthermore, it was hypothesized that the advantage of using such approaches is that the removal of glutamate occurs only from areas in which glutamate is pathologically elevated <sup>16</sup>. Additionally, scavenging may be a safer treatment, as it is a self-limiting process that slows down and eventually stops as the concentration of brain glutamate decreases <sup>17</sup>.

The main limitation of the glutamate blood scavenging approach is that the effect of GOT administration is short-lived, mostly because of its rapid uptake and degradation in the body <sup>18-20</sup>. Indeed, intravenous administration of <sup>125</sup>I-labeled GOT revealed that this enzyme can be taken up and metabolized by many different tissues, such as the liver, spleen, kidney, and intestines. The radioactivity associated with liver and spleen reached its maximum 2 hours post-injection and the time course coincided with that for the plasma clearance in the fast phase <sup>18</sup>. The subsequent decrease in the radioactivity of these tissues was accompanied by an increase in urinary radioactivity <sup>18</sup>. Therefore, the liver was the major structure involved in plasma clearance of GOT and the results indicated that this enzyme was exclusively taken up by sinusoidal liver cells (Kupffer cells and endothelial cells) *via* a typical endocytic pathway (i.e., initial binding, internalization, and subsequent degradation in the lysosomes) <sup>18,19</sup>. In this context, repeated administration or continuous infusion of GOT could extend the therapeutic dose of the treatment, though the use of high amounts of such enzyme is not always desirable because of the risk of secondary effects and the development of an adverse immune response. In order to achieve an effective and sustained activity in the body, several strategies can be used <sup>21-23</sup>, including PEGylation.

## Part 2: Contextualization

From this literature review, important points can be made:

- The tight control of glutamate levels, achieved through various processes, is necessary to ensure normal synaptic transmission and prevent excitotoxicity.
- Excitotoxicity, triggered by high levels of glutamate in the brain interstitial fluid, is well recognized as a central trigger and source of tissue injury during ischemic stroke.
- Reducing excitotoxicity has been a prime goal for stroke therapy and different therapeutic approaches were tested in order to alleviate the deleterious effects of glutamate.
- The established approaches failed or displayed severe adverse effects when tested in clinical trials, and the primary source of such failure has been and remains the inability of drugs to pass through blood–brain interfaces.
- Exploiting drugs that act on the blood and reduce toxic levels of glutamate in the brain raised the hope for development of clinically relevant therapeutics that circumvent the brain physiological barriers.
- Intravenously injected glutamate-degrading enzyme GOT has been investigated as a neuroprotectant, presumably without the need to reach the brain.
- Evidently, other enzymes such as GDH might also provide neuroprotection, although its effect as a blood scavenging therapeutic has not yet been tested.
- The therapeutic performance of such enzymes are highly reduced by their unfavorable pharmacokinetic properties (e.g., rapid serum degradation and/or clearance).
- To improve the stability and increase the *in vivo* half-life of enzymes, several strategies might be explored, and one of best-known approaches is PEGylation.

## CHAPTER 2: PEGylation

## Part 1: Literature Review

### 1. Overview

Polyethylene glycol (PEG),  $\text{HO}-(\text{CH}_2\text{CH}_2\text{O})_n-\text{H}$ , is a flexible, hydrophilic, biocompatible, and FDA-approved polymer <sup>318,319</sup>. Bioconjugation with PEG, also known as PEGylation, is the process by which PEG chains are covalently attached to drugs (i.e., producing bioconjugates). Initially pioneered by Davis and co-workers, the PEGylation of proteins has enabled the reduction of their immunogenicity <sup>320</sup>. Importantly and unexpectedly, grafting of methoxy-PEG (mPEG) on the surface of proteins further improved their pharmacokinetic and pharmacodynamic properties <sup>321-323</sup>. Since then, PEGylation has expanded and advanced tremendously, gaining importance in the generation of new bioconjugates from existing therapeutics. As of 2020, several PEGylated proteins have been approved for therapeutic use in humans (Table 1) and many more are in the development pipeline <sup>324,325</sup>. Many of these bioconjugates are considered blockbuster drugs (generating annual sales of at least \$1 billion for the company selling it) <sup>325-327</sup>.

Many potential mPEG derivatives are now available, providing options to modulate pharmacological output for different therapeutics. Indeed, mPEG can be produced in different MW (from 200 to tens of thousands), configurations (e.g., linear, branched, and multi-arm structures), and chemistries (e.g., protein-reactive functional groups: succinimidyl carbonate, aldehyde, and maleimide). By varying these parameters, the characteristics of the corresponding bioconjugate changes, allowing its pharmacokinetic parameters to be tuned <sup>328,329</sup>. The choice of functional end-group is directed by the functional moieties available on the polypeptide surface (e.g., amine, carboxyl, or sulfhydryl groups) (Figure 11) <sup>330,331</sup>.

Table 1: Approved PEGylated protein therapeutics.

<b>Trade name</b>	<b>Conjugate</b>	<b>Disease</b>	<b>Approval date</b>	<b>References</b>
<b>Adagen®</b>	mPEG–adenosine Deaminase	Severe combined immunodeficiency disease	1990	332
<b>Oncaspar®</b>	mPEG–asparaginase	Leukaemia	1994	333
<b>PegIntron®</b>	mPEG–interferon- $\alpha$ 2b	Hepatitis C	2000	334
<b>Pegasys®</b>	mPEG–interferon- $\alpha$ 2a	Hepatitis C	2002	335
<b>Somavert®</b>	mPEG-human growth hormone mutein antagonist	Acromegaly	2002	336
<b>Neulasta®</b>	mPEG–granulocyte colony stimulating factor	Neutropenia	2002	337
<b>Mircera®</b>	mPEG–erythropoietin	Anaemia associated with chronic kidney disease	2007	338
<b>Cimzia®</b>	mPEG–anti-tumor necrosis factor Fab'	Rheumatoid arthritis and Crohn's disease	2008	339
<b>Krystexxa®</b>	mPEG–uricase	Chronic gout	2010	340
<b>Sylatron®</b>	mPEG–interferon- $\alpha$ 2b	Melanoma	2011	327,341
<b>Plegridy®</b>	mPEG–interferon- $\beta$ 1a	Multiple sclerosis	2014	327,342
<b>Adynovate®</b>	mPEG–antihemophilic factor	Hemophilia A	2015	327,343
<b>Palynziq®</b>	mPEG–phenylalanine ammonia lyase	Phenylketonuria	2018	344,345
<b>Bayer®</b>	mPEG–factor VIII	Hemophilia A	2018	345,346

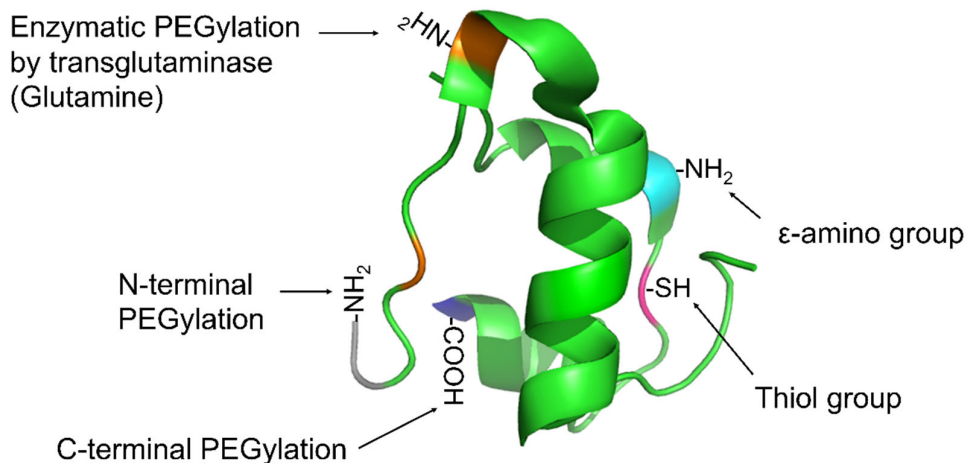
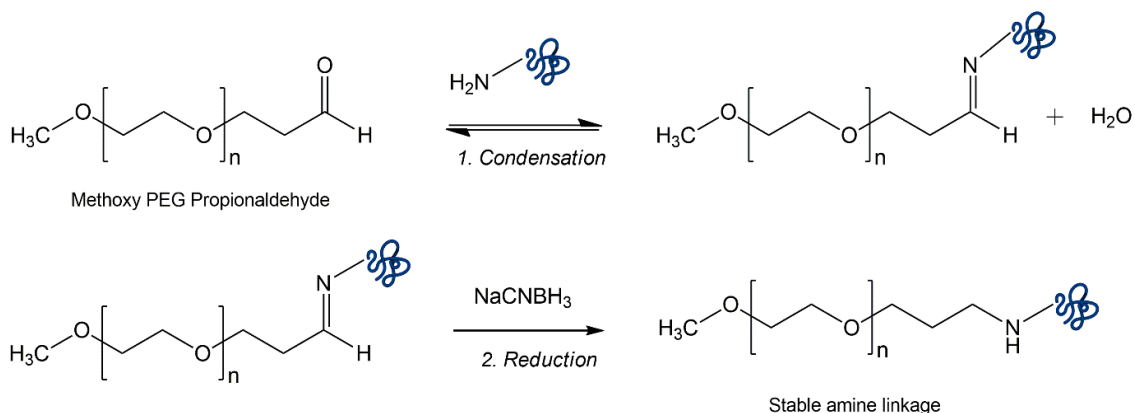


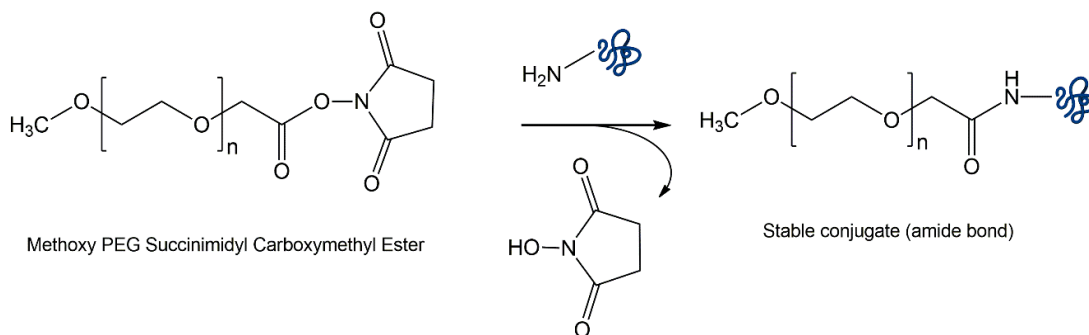
Figure 11: Most common potential sites of PEGylation in proteins.

Most mPEG derivatives target the amino groups of proteins, most frequently the  $\epsilon$ -amino groups of lysine residues. Lysines are relatively abundant amino acid residues (10% of the total amino acids on a typical protein) and are generally exposed to the solvent, which make them available for chemical reactions with mPEG reagents<sup>330</sup>. Random PEGylation is the most frequently used approach targeting these groups. While this method is convenient for creating PEGylated proteins, it often generates a heterogeneous mixture of bioconjugates with different numbers and attachment sites of mPEG chains (i.e., mono-, di-, tri-, and highly-PEGylated forms). In this context, numerous conjugation approaches exist, such as reductive alkylation (Reaction 3), which maintains the positive charge of the starting amino group, or acylation (Reaction 4), which is accompanied by loss of charge (producing a neutral amide)<sup>26,325</sup>.

Changing the bioconjugation chemistry generally alters the functional properties of proteins. For instance, PEGylation of granulocyte colony-stimulating factor through acylation with an active ester decreased the stability of the protein in comparison to PEGylation through alkylation with mPEG–aldehyde<sup>347</sup>. Extensive literature on the chemistry of mPEG, as well as on the benefits and potential drawbacks of PEGylation, is available<sup>26,319,324-326,331,348</sup>.



Reaction 3: Reductive alkylation of proteins (in blue). This reaction is advantageous due to the formation of a hydrolytically stable bond as well as preservation of the protonatable character of the lysine residue.



Reaction 4: Acylation of proteins (in blue). This reaction is advantageous due to the formation of a hydrolytically stable bond.

## 2. Benefits of PEGylation

PEGylation of biologically active macromolecules generally offers significant and distinct benefits over unmodified forms. PEGylation may: (1) enhance the physical and thermal stabilities as well as the solubility of proteins (e.g., by altering their physicochemical properties), and (2) increase the hydrodynamic size of parent proteins, preventing their tissue-organ uptake, reducing their glomerular filtration, decreasing their immunogenicity, antigenicity, enzymatic degradation (proteolysis), and prolonging their blood circulation time<sup>349-353</sup>. The extension of the circulation half-life of therapeutics allows a reduction of the frequency of dosing while maintaining the pharmaceutical effects.

## 2.1. Influence of PEGylation on protein stability

During manufacturing, storage or handling of therapeutic proteins, several physical and chemical degradation processes might be encountered. Numerous factors, such as pH, temperature, agitation, or freezing procedures have been shown to affect protein thermal and physical stability. Studies have demonstrated that PEGylation increases stability and decreases aggregation in proteins. For example, PEGylated ribonuclease, catalase, asparaginase, and trypsin were more stable over a wide range of pH and temperature changes compared with their unPEGylated forms<sup>354</sup>. Similarly, PEGylated granulocyte colony stimulating factor and monoclonal antibody antigen-binding fragments exhibited enhanced thermal and mechanical stability and reduced aggregation<sup>355-357</sup>. Likewise, mPEG attachment significantly enhanced insulin's resistance to aggregation<sup>358</sup>, and increased the transition midpoint temperatures of several PEGylated proteins when compared to their unmodified counterparts<sup>40,359,360</sup>. Increased solubility and stability upon mPEG modification were attributed to the increased water solubility of the polar mPEG groups and to the steric shielding of hydrophobic patches that stabilize against intermolecular interactions<sup>356,357</sup>. Interestingly, the removal of water molecules from the protein's surface and the subsequent reduction of the protein structural dynamics was further associated with the thermodynamic stability of PEGylated proteins<sup>359,361</sup>. Indeed, by measuring hydrogen/deuterium exchange for different bioconjugates (with varying degrees of PEGylation: 1 to 9 mPEG chains per  $\alpha$ -chymotrypsin), it was demonstrated that the stabilization of protein correlated with an altered rate of exchange and a more rigid protein core. However, the effect plateaued at four chains of conjugated mPEG<sup>361</sup>. Such an effect was further established by molecular dynamics simulations of mono-PEGylated insulin and staphylokinase: the enhanced stability of PEGylated proteins was related to the dual role played by the mPEG molecule wrapped around the protein's surface (i.e., while the ethylene moieties interact with the hydrophobic clusters, the oxygen atoms interact with hydrophilic side chains)<sup>362,363</sup>.

## 2.2. Influence of PEGylation on the kidney clearance of proteins

PEGylation has the potential to alter the biodistribution of conjugated proteins, an effect derived from its role in modifying the properties of parent therapeutics. Small proteins (ca. <60 kDa) are typically cleared through glomerular filtration (renal cut-off size for globular proteins is approximately 50–60 kDa)<sup>364</sup>. Conjugation of polymers, such as mPEG, increases the MW and hydrodynamic volume of the parent proteins, consequently resulting in decreased glomerular excretion. PEGylated proteins occupy a considerably greater volume than would be predicted based on the combined MW of the protein and mPEG alone. Indeed, owing to the strong coordination of water molecules (~3–7 per ethylene oxide unit), the hydrodynamic

volume of mPEG is higher than that of a globular protein of the same MW<sup>319,365</sup>. Furthermore, this effect becomes more magnified as the MW of the mPEG molecule increases (e.g. 10 and 40 kDa mPEG have hydrodynamic volumes corresponding to that of proteins of 65 and 670 kDa, respectively)<sup>366</sup>.

Interferon- $\alpha$  (IFN- $\alpha$ ) is a cytokine largely exploited for its antiviral effects in the context of the treatment of chronic hepatitis C infections<sup>367</sup>. Unfortunately, native IFN- $\alpha$  (MW ~19 kDa) has poor *in vivo* efficacy, mainly because of its rapid renal clearance (half-life ~5 hours)<sup>368</sup>. In order to overcome this issue, two IFN- $\alpha$  bioconjugates were developed: mPEG-IFN- $\alpha$ 2a (Pegasys®) and mPEG-IFN- $\alpha$ 2b (PegIntron®) consisting of 40 kDa branched mPEG and 12 kDa linear mPEG polymers grafted to IFN- $\alpha$ , respectively. Both bioconjugates showed significant improvement in clinical performance over the native protein<sup>369</sup>. For instance, mPEG-IFN- $\alpha$ 2a displayed an 100-fold reduction in its clearance rate<sup>368,370</sup>, an effect that manifested through sustained blood levels of IFN- $\alpha$ 2a<sup>368,370</sup>. This allowed once-weekly injections instead of three times a week as for conventional native protein<sup>371</sup>. Similarly, long-acting growth hormones, with improved clearance properties, have also been produced through conjugation with mPEG<sup>372</sup>.

### **2.3. Influence of PEGylation on immunogenicity and antigenicity of proteins**

Recognition and uptake of molecules by the immune system plays a crucial role in their pharmacokinetics and pharmacodynamics, especially for therapeutic proteins of non-human origin. As such, reducing immunogenicity has traditionally been one of the major driving forces behind research in the field of PEGylation<sup>364</sup>. When compared to their non-PEGylated counterparts, an alteration in the immunogenicity and antigenicity patterns of PEGylated proteins was noticed. Indeed, mPEG chains form a protective and highly hydrated shell that sterically shields antigenic epitopes and hinders binding of neutralizing antibodies as well as recognition by immune cells. In their pioneering studies, Abuchowski et al. demonstrated that PEGylation suppressed the immunogenicity and antigenicity of bovine liver catalase when injected into rabbits. They also reported a correlation with the degree of PEGylation: the more mPEG chains attached to the protein surface, the lower its asserted immunogenicity<sup>373</sup>. Since then, the beneficial effect of PEGylation on reducing immunogenicity has been established by several studies carried out with diverse recombinant and non-recombinant proteins<sup>358,374-377</sup>. For instance, the immunogenicity of mono-PEGylated recombinant human insulin with distinct sites of substitution (N-terminus of A-chain, N-terminus of B-chain, C-terminus of B-chain) and varying mPEG MW (0.6, 0.75, or 2kDa) was studied in mice. All bioconjugates, irrespective of MW or site of conjugation, reduced the levels of circulating insulin-specific IgG by 10 to 1000 times<sup>358</sup>.

## 2.4. Influence of PEGylation on proteolytic degradation of proteins

Proteolysis of therapeutics greatly limits their systemic application. Therefore, huge efforts are typically devoted to stabilizing proteins towards enzymatic degradation. PEGylation is thought to protect therapeutic proteins from proteolytic degradation by much the same mechanism as it diminishes immunogenicity: by sterically shielding the protein domains susceptible to proteolytic attack and reducing protease access. In this sense, grafting of five mPEG chains (5 kDa each) to the surface of human growth hormone increased its serum half-life from ~30 minutes to ~10 hours<sup>372</sup>. Considering that the contribution of the kidney to the clearance of growth hormone has been estimated to be 67% in rats<sup>378</sup>, the authors proposed that prolongation of the blood residence time did not rely solely on the hindrance of the renal filtration, but also on other mechanisms, such as reduction of the proteolysis rate<sup>372</sup>.

## 3. Potential drawbacks of PEGylation

Notwithstanding the numerous advantages conferred by PEGylation, there are still some disadvantages which, if addressed, might further increase the benefits of PEGylation. Issues related to excretion from the body as well as to the potential hypersensitivity and immune reactions of particular bioconjugates were reported<sup>24-26</sup>. More importantly, since one or multiple mPEG chains are usually linked to random residues on the protein surface, the biological activity of a protein can be reduced upon PEGylation. However, in many cases, this is compensated in biological systems by an increased half-life. For instance, attaching branched 20 kDa mPEG chains to recombinant human interleukin 11 reduced its *in vitro* biological activity by ~86%, but increased its mean residence time 50- to 60-times in comparison to the native protein<sup>379</sup>. Another example is the bioconjugate mPEG-IFN- $\alpha$ 2a, that retained only ~7% of the original antiviral activity, but, as a result of the improved pharmacokinetics, displayed an enhanced *in vivo* performance in comparison to the unPEGylated protein<sup>380</sup>. Similar observations were made for PEGylated IFN- $\beta$ 1a<sup>381</sup>. Consequently, it is difficult to extrapolate the *in vivo* performance of bioconjugates from *in vitro* data. Nonetheless, identifying key factors leading to the reduction of activity might allow them to be circumvented, which could improve the performance of protein therapeutics without sacrificing their activity.

The loss of protein activity could result from a combination of one or more of the following mechanisms: (1) direct PEGylation of bioactive sites, (2) steric effects from mPEG causing restricted diffusion near the protein's surface, (3) a conformational change of the protein, (4) a micro-environmental effect in the immediate vicinity of the protein, or (5) restricted protein movements or dynamics<sup>382</sup>. Consequently, for each new bioconjugate, it is necessary to refine the parameters (e.g., degree of grafting, MW of mPEG, chemistry of PEGylation) in order to

maximize both the biological activity and the bioavailability.

Recombinant IFN- $\beta$ 1b, clinically used for the treatment of multiple sclerosis, contains 11 lysine residues, in addition to the N-terminal amine. Over 50% of lysine residues are located within the  $\alpha$ -helical regions that are involved in receptor binding<sup>383,384</sup>. Random modification of IFN- $\beta$ 1b with two amine-reactive 40 kDa branched mPEG or three amine-reactive 12 kDa linear mPEG diminished antiviral activities by ~100%. This deactivation was attributed to direct modification of the active site of the protein<sup>40</sup>. Indeed, such a loss was circumvented by selective modification of the N-terminal amino acid of IFN- $\beta$ 1b with a branched 40 kDa mPEG<sup>40</sup>. Therewith, several papers related the decreased activity of mono-PEGylated proteins to the presence of mPEG chains that sterically hinder substrate/ligand accessibility to the active/binding site and changes the local environment necessary for the interaction<sup>363,385-387</sup>. Of these, activity reduction of phosphoglycerate kinase modified with 5–20 kDa mPEG was attributed to local crowding effects created by the polymer that delayed the diffusion time of a ligand to its binding site<sup>385</sup>. Similarly, grafting of 5 or 10 kDa mPEG chains to lysozyme produced mono-PEGylated bioconjugates having residual activities of 70% and 10% compared to the native protein, respectively. This decrease was attributed to the reduced accessibility to the active site, and was dependant on the MW of mPEG<sup>388</sup>. Moreover, conjugation of 5 kDa mPEG chain at valine-1 ( $\alpha$ ) of the human adult hemoglobin significantly destabilized the tetramer stability and altered the quaternary structure of the protein<sup>389</sup>.

While many works, both experimental and computational, have investigated the mechanism of activity loss for mono-PEGylated proteins, much less data exists regarding the mechanisms of activity loss for multi-PEGylated proteins. Furthermore, only a few studies have highlighted the effect of mPEG bioconjugation on the dynamics of the protein. This is unfortunate because multi-PEGylated proteins represent an important subset of clinically-approved PEGylated proteins.

## **Part 2: Research proposal, hypothesis and objectives**

Based on the evidence provided above, we hypothesized that extending the circulation half-life of GDH and GOT by grafting mPEG chains to their surface may lead to better health outcomes in the context of ischemic stroke (i.e., reducing excitotoxicity, along with any pathophysiological consequences).

Moreover, while peripheral depletion of glutamate appears to be well tolerated, accumulation of either enzymes at the blood side of the BBB (and potentially crossing to the brain parenchyma) would offer better neuroprotection by promoting a more significant glutamate efflux. Therefore, we further hypothesize that modification of GDH and GOT with multiple chains of mPEG bearing at their extremity a targeting ligand for the BBB (Angiopep-2) would confer both a long circulation lifetime and an accumulation near the ischemic region. Using this approach, the bioconjugates would not actually have to cross the BBB to produce a neuroprotective effect. Crossing the BBB, which is substantially more challenging, would represent a bonus of selectively depleting glutamate in the brain.

Therefore, our initial objectives were the following:

(1) Assess the scavenging effects of native (unPEGylated) GDH and evaluate the therapeutic effectiveness of multi-PEGylated GDH in a model of ischemic stroke.

- Synthesize, purify, and characterize GDH bioconjugates.
- Study the pharmacokinetics and pharmacodynamics of unPEGylated GDH in healthy rats.
- Study the pharmacokinetics and pharmacodynamics of GDH bioconjugates and study their protective effects in MCAo rats.

(2) Assess the therapeutic efficacy of multi-PEGylated human recombinant (hrGOT) in a model of ischemic stroke.

- Synthesize, purify, and characterize hrGOT bioconjugates (non-targeted mPEG–hrGOT and targeted Angiopep–PEG–hrGOT).
- Study their pharmacokinetics and pharmacodynamics in healthy rats.
- Validate their pharmacokinetics and study their protective effects in MCAo rats: Determination of the infarct size and assessment of the functional deficit.

## CHAPTER 3: Article 1

### Mechanisms of activity loss for a multi-PEGylated protein by experiment and simulation

Ahlem Zaghmi, Eduardo Mendez-Villuendas, Andrea A Greschner, Jun Yang Liu, Hendrick  
W de Haan, and Marc A Gauthier

A version of this chapter has been published in  
Materials Today Chemistry, Volume 12, June 2019, Pages 121-131  
Reprint permission is not required.

The formatting of this article conforms to the specifications of the scientific journal.

## 1. Preface

As mentioned in the previous section, our first objective was to synthesize, purify, and characterize GDH bioconjugates. However, upon PEGylation of GDH using 5 kDa mPEG, a significant decrease of catalytic activity was observed for the forms bearing high number of polymer chains per enzyme (Figure 12). Unfortunately, mechanisms related to the loss of activity of such multi-PEGylated protein are rarely investigated, possibly due to the added difficulty of characterizing these systems and singling-out individual effects. Therefore, we hypothesized that several mechanisms could be involved in the reduction of activity of multi-PEGylated GDH.

Consequently, the following objectives were set:

- Design and characterize a library of bioconjugates (with different grafting density and distinct MW of mPEG).
- Through a combination of experimental design and simulation, study the effect of multi-PEGylation on the (a) enzyme's active site, (b) GDH's secondary and tertiary structure, (c) local microenvironment of the binding partners (e.g., allosteric inhibitors), and (d) GDH's dynamic motions.

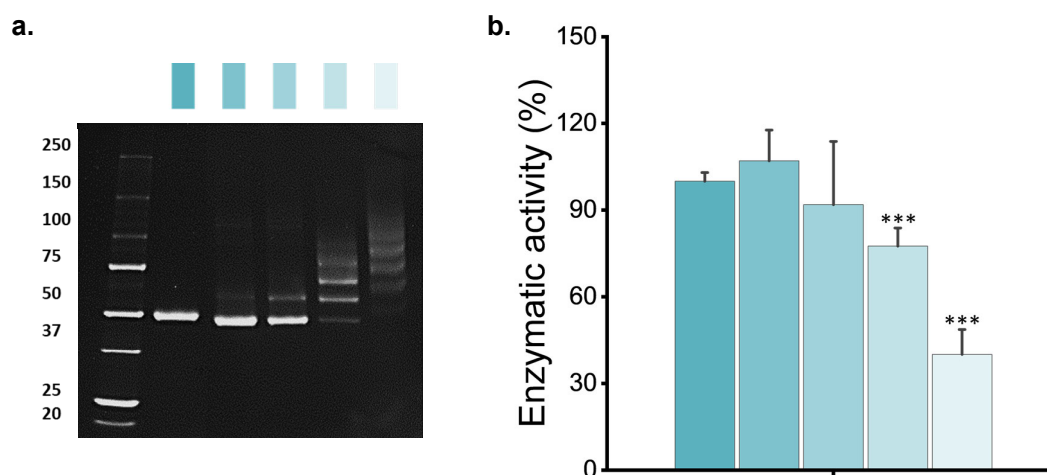


Figure 12: (a) Visualization of GDH bioconjugates. (b) *In vitro* enzymatic activity of the bioconjugates. Asterisk denote statistical differences with respect to native enzyme (0 mPEG) (ANOVA, Tukey,  $p < 0.05$ ). Data presented as Mean + SD,  $n = 3$ .

# Mechanisms of activity loss for a multi-PEGylated protein by experiment and simulation

Ahlem Zaghmi<sup>1</sup>, Eduardo Mendez-Villuendas<sup>2</sup>, Andrea A Greschner<sup>1</sup>, Jun Yang Liu<sup>1</sup>,  
Hendrick W de Haan<sup>2,\*</sup>, and Marc A Gauthier<sup>1,\*</sup>

<sup>1</sup> Institut National de la Recherche Scientifique (INRS), EMT Research Center, Varennes, Qc, J3X 1S2, Canada

<sup>2</sup> University of Ontario Institute of Technology, Faculty of Science, Oshawa, Ontario, L1H 7K4, Canada

Corresponding authors:

Marc A. Gauthier

Institut National de la Recherche Scientifique (INRS), EMT Research Center, 1650 boul. Lionel-Boulet, Varennes, J3X 1S2, Canada

E-mail: gauthier@emt.inrs.ca

Telephone: +1 514 228 69 32

Fax: +1 450 929 81 02

Hendrick de Haan

University of Ontario Institute of Technology, Faculty of Science, Oshawa, Ontario, L1H 7K4, Canada

E-mail: Hendrick.deHaan@uoit.ca

Telephone: +1 905 721 86 68 ext: 6237

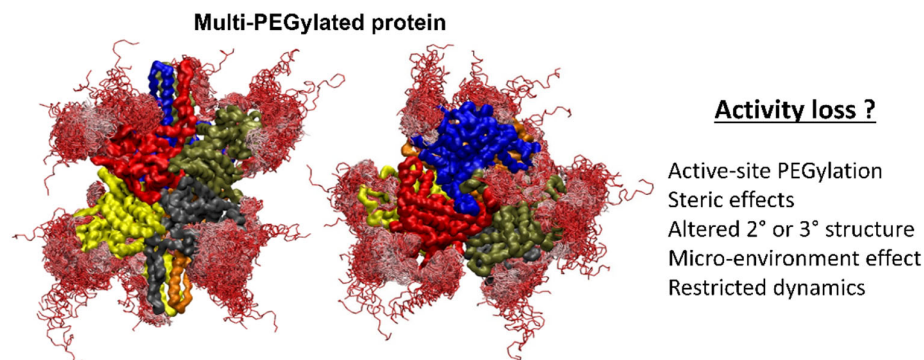
Fax: +1 905 721 33 04

Conflict of interest: None to declare

## Abstract

Over the past five decades, one of the most investigated strategies to increase the circulatory half-life and to reduce the immunogenicity of non-human therapeutic proteins has been to cover their surface with multiple copies of methoxy poly(ethylene glycol) (mPEG). This multi-‘PEGylation’ strategy, however, is often associated with loss of protein activity, which is most often rationalized as direct modification of the protein’s active site or to steric hindrance near its surface. While these mechanisms are generally accepted and likely valid, very few studies investigate other possible mechanisms of activity loss. To answer this question, this study investigates the mechanisms of activity loss for glutamate dehydrogenase (GDH) bearing up to 25 chains of mPEG per protein. Through a combination of experimental design and simulation, the most common proposed causes of protein inactivation (i.e., active-site PEGylation and steric hindrance near the surface of the protein) are circumvented to shed light on less characterized mechanisms such as: altered protein structure, altered microenvironment at the surface of the protein, and altered protein dynamics. Experiments suggest that the secondary and tertiary structure of GDH was (sometimes significantly) affected by PEGylation, though these changes do not necessarily result in a loss of activity. Structure–activity correlations could not reconcile all trends within the library of bioconjugates tested. Moreover, by measuring catalytic activity in the presence of five different allosteric modulators, loss of activity could not be ascribed to an altered local microenvironment at the protein’s surface. As such, coarse-grained simulations were exploited to reveal the effect of PEGylation on protein dynamics, which are long-ranged, cooperative, and essential for GDH catalytic activity. Normal mode analysis of native bovine GDH (i.e., not PEGylated) revealed that the lowest ranking mode displayed several features that bore similarity to movements known for the native protein. These included rotation/distortion of the ‘antenna’ regions, closure of the ‘catalytic cleft’, and constriction of the internal cavity. A reduced magnitude of this mode was observed as a function of degree of PEGylation and mPEG molecular weight, and correlated well with trends observed for the library of bioconjugates tested experimentally. Overall, this study provides new insight into fundamental considerations associated with loss of activity, which will contribute to the design of future bioconjugates by providing a better understanding of possible mechanisms of loss of activity.

## Graphical abstract (5 × 13 cm)



**Keywords** (6): PEGylation, Enzyme, Bioconjugate, Dynamics, Coarse-grained simulation, MARTINI

### 1. Introduction

Global trends in the pharmaceutical sector suggest that therapeutic proteins (i.e., in the family of ‘Biologics’) will be among the drugs of the future<sup>390</sup>. This is in part because proteins possess complex chemical structures that allow them to e.g., catalyze specific reactions (enzymes), bind specifically to target molecules (monoclonal antibodies), modulate protein–protein interactions (several classes of proteins), and edit genes (enzymes + nucleic acids)<sup>391,392</sup>. These mechanisms of action are not typically available to small-molecule drugs, which provides interesting opportunities for treating ‘undruggable’ diseases. However, proteins suffer from inherent shortcomings that can limit their efficiency as therapeutics. More specifically, proteins can fold into compact structures that are rapidly eliminated from the body by the kidneys, and non-human proteins can be recognized as ‘foreign agents’ by the immune system<sup>393</sup>. Moreover, proteins can unfold or be degraded by several mechanisms. Over the past five decades, one of the most investigated strategies to address these challenges has been to covalently modify proteins with methoxy poly(ethylene glycol) (mPEG), a process referred to as ‘PEGylation’<sup>325</sup>. Over twelve PEGylated proteins are currently approved by the US Food and Drug Administration and many others are in clinical trials<sup>394,395</sup>. PEGylation strategies fall into two main categories, which offer complementary solutions to different sets of protein-specific challenges<sup>395</sup>. The first strategy involves ‘randomly’ modifying a therapeutic protein with several copies of mPEG, and is most often employed to mask the multiple epitopes on an immunogenic protein’s surface (as well as to increase its circulatory half-life). Examples

include PEGylated adenosine deaminase (Adagen®) used for adenosine deaminase deficiency and PEGylated L-asparaginase (Oncaspar®) used in the frontline treatment of acute lymphoblastic leukemia<sup>396-398</sup>. The second strategy involves site-specifically modifying a therapeutic protein with a single mPEG chain, and is most often employed to increase the circulatory half-life of non-immunogenic proteins in a manner that does not interfere with e.g., protein–protein interactions required for activity. For example, N-terminally PEGylated human recombinant granulocyte colony-stimulating factor (Neulasta®) is used to fight infections in patients undergoing chemotherapy<sup>396,399</sup>. One general observation from the literature is that, irrespective of the strategy used, PEGylation often leads to a loss of the protein bioactivity. Even site-specifically modified proteins may lose activity, especially for small proteins or peptides<sup>400,401</sup>. This not only drives up the cost of manufacturing but can also increase the risk of side-reactions as more bioconjugate must be administered compared to the native protein to achieve an equivalent effect. As such, in parallel to the exploration of innovative bioconjugation or polymer chemistry concepts to minimize loss of activity<sup>402-404</sup>, substantial efforts are also underway to better understand the mechanisms causing loss of protein activity by polymers.

To the extent of current knowledge, loss of protein activity results from a combination of one or more of the following possible mechanisms: i) direct PEGylation of bioactive site (i.e., binding, catalytic, etc.)<sup>41</sup>; ii) steric effects from mPEG that cause restricted diffusion near the protein's surface (binding partners, enzymatic substrates, etc.)<sup>405</sup>; iii) a conformational change of the protein<sup>406</sup>; iv) restricted protein movements or dynamics; or v) a micro-environmental effect in the immediate vicinity of the protein (e.g., influences enzymatic substrate accumulation, binding constants, etc.)<sup>407,408</sup>. At present, experimental and computational studies regarding the structure of PEGylated proteins almost exclusively involve site-specifically mono- or di-PEGylated proteins, and often study structural changes and steric hindrance of the protein<sup>409-412</sup>. However, these studies rarely correlate findings to activity. Of these, activity reduction of phosphoglycerate kinase modified with 5–20 kDa mPEG was associated to local steric effects created by the polymer that increased/delayed the diffusion time of a ligand to its binding site<sup>385</sup>. Similarly, grafting of 5 or 10 kDa mPEG chains to lysozyme produced mono-PEGylated bioconjugates having residual activities of 70% and 10% compared to the native protein, respectively. This decrease was attributed to the reduced accessibility to the active site, and was mPEG molecular-weight dependant<sup>388</sup>. The activity of di-PEGylated hemoglobin was maintained upon modification with 10 kDa mPEG. Above this length, lower *in vivo* efficiency of the bioconjugates was observed, which the authors hypothesize as resulting from a change of conformation of mPEG and its wrapping around the protein<sup>413</sup>. In contrast, much less data exists regarding the mechanisms of loss of activity of

multi-PEGylated proteins, possibly due to the added difficulty of characterizing these systems and singling-out individual effects. This is unfortunate because such bioconjugates represent an important subset of clinically-approved PEGylated proteins<sup>414</sup>. Most studies attribute loss of activity to a combination of active-site PEGylation and steric hindrance<sup>415,416</sup>.

Through a combination of experimental design and simulation, this study circumvents the most common proposed causes of protein inactivation (i.e., active-site PEGylation and steric hindrance near the surface of the protein) in order to shed light on less characterized mechanisms such as: altered protein structure, altered protein dynamics, and altered microenvironment at the surface of the protein. To accomplish this, glutamate dehydrogenase (GDH) was selected as model protein. GDH is a highly dynamic enzyme that reversibly catalyzes the conversion of glutamate to  $\alpha$ -ketoglutarate and ammonia while reducing NAD(P)<sup>+</sup> to NAD(P)H. It participates in catabolic and anabolic reactions and plays an important role in energy production<sup>417</sup>. Owing to its primordial functions in the body, its activity is tightly regulated not only by its own substrate and coenzyme but also by many other allosteric modulators, which provides opportunities for experimentally-probing different binding sites on the protein, and selectively influencing different protein movements<sup>58</sup>. Moreover, because of the lack of high-resolution tools to directly correlate protein dynamics to bioactivity, this study will be complemented by coarse-grained simulations of the bioconjugates, to provide insight into the effect of PEGylation on protein dynamics, which are very well characterized for GDH and essential for its activity.

## 2. Material and Methods

**2.1 Materials.** Adenosine 5'-triphosphate disodium salt hydrate (ATP), ammonium formate, amicon ultra centrifugal filter units (molecular weight cut-off (MWCO) 50 kDa and 100 kDa), bithionol, bromophenol blue, deuterium oxide, dimethyl sulfoxide (DMSO), ethylenediaminetetraacetic acid (EDTA), guanosine 5'-triphosphate sodium salt hydrate (GTP), glycerol, glycine, L-glutamic dehydrogenase from bovine liver (GDH), hexachlorophene, monosodium glutamate, sodium bicarbonate, sodium dodecyl sulphate (SDS), sodium phosphate monobasic, sodium phosphate dibasic, tris(hydroxymethyl)aminomethane hydrochloride (TRIS-buffer), 2,4,6-trinitrobenzenesulfonic acid solution (TNBS), deuterium oxide (D<sub>2</sub>O), and zinc acetate were purchased from Sigma Aldrich (Oakville, Canada). Sodium cyanoborohydride (NaCNBH<sub>3</sub>) and nicotinamide adenine dinucleotide (NAD<sup>+</sup>) were purchased from Santa Cruz Biotechnology (Dallas, USA). Methoxypoly(ethylene glycol) (mPEG) propionaldehyde (5 kDa and 20 kDa) was purchased from JenKem Technology (Plano, USA). mPEG aldehyde (0.5 kDa and 2 kDa) was purchased from Creative PEGWorks (Durham, USA). Vivapure® Q mini H ion exchange (IEX) spin

columns were purchased from Sartorius Corporation (New York, USA). Mini-PROTEIN TGX Stain-Free Precast Gels (4–15% acrylamide) and Bio-Rad precision plus protein unstained standards were purchased from Bio-Rad (Saint-Laurent, Canada). All buffers were prepared using MilliQ water (mean resistivity 18.2 M $\Omega$ -cm). All chemicals were purchased at the highest grade possible, and used as received.

**2.2 Equipment.**  $^1\text{H}$  NMR spectra were recorded using a Bruker Av300 spectrometer operating at 300 MHz for protons. UV-Vis absorption spectra were recorded with either a NanoDrop 2000c absorbance spectrometer (Thermo Fisher Scientific) or a Cary 60 UV-Vis spectrophotometer (Agilent Technologies, Mississauga, Canada). Fluorescence spectra were recorded with a Cytation 5 microplate reader (Biotek Instrument, Vermont, USA). CD spectra were recorded by a Chirascan<sup>™</sup> Circular Dichroism spectrometer. Size-exclusion chromatography (SEC) was performed using an AKTA Start fast protein liquid chromatographer (FPLC) equipped with a HiPrep 16/60 Sephacryl<sup>™</sup> S200 HR column and an Agilent Technologies 1260 HPLC equipped with two Agilent Bio-SEC5 columns mounted in series (5  $\mu\text{m}$ , 7.8  $\times$  300 mm), with 1000 and 2000  $\text{\AA}$  nominal pore sizes, a 1200 Infinity photodiode array detector VL, and a 1290 Infinity II evaporative light scattering detector (ELSD).

**2.3 Determination of exposed amino groups.** Considering that GDH is a homo-hexameric protein, several of its constituent amino groups (e.g., lysine residues or N-termini) may be hidden within the structure of the protein. Therefore, to estimate the number of solvent-accessible amino groups on the surface of GDH, a TNBS assay was used. TNBS reacts with amino groups to form a chromophore with a strong absorbance at 335 nm. Briefly, GDH was dissolved in 0.5 mL of 0.1 M sodium bicarbonate, pH 8.5 at a concentration of 0.25 mg $\cdot$ mL $^{-1}$  and mixed with 0.25 mL 0.01% TNBSA solution. The reaction was allowed to proceed at 37  $^{\circ}\text{C}$  for 2 h in a sealed tube. The reaction was stopped by addition of 0.25 mL of 10% SDS and 0.125 mL of 1 N HCl, and the absorbance was measured at 335 nm. Results were compared to a calibration curve prepared with glycine.

**2.4 Preparation of mPEG–GDH bioconjugates.** To prepare the mPEG–GDH bioconjugates, a solution of GDH (1 mg $\cdot$ mL $^{-1}$ ) was prepared in 5 mL sodium phosphate buffer (100 mM, pH 6) containing 20 mM NaCNBH<sub>3</sub>. To this solution was added the different solid protein-reactive mPEGs (0.5–20 kDa) at several molar equivalents relative to GDH (1:5, 1:30, 1:300, 1:1500) to achieve different degrees of PEGylation. The reaction was allowed to proceed for 24 h at 4  $^{\circ}\text{C}$  in a sealed tube. After this period, the bioconjugates prepared with 0.5–5 kDa mPEG were purified by centrifugal dialysis (MWCO 50 kDa and 100 kDa), while the bioconjugates prepared with 20 kDa were purified by anion-exchange spin column according to the manufacturer's

instructions and by SEC. For SEC purification, filtered sodium phosphate buffer (100 mM, pH 6) was used to elute samples through a HiPrep 16/60 Sephacryl™ S200 HR column at a flow rate of 0.8 mL·min<sup>-1</sup>. The column was allowed to equilibrate for 0.2 column volumes (CV) before sample injection. Elution occurred over 120 mL (1 CV), while continuously collecting 4 mL fractions.

**2.5 Characterization of mPEG–GDH bioconjugates.** Because of the difficulty in analyzing the protein–polymer bioconjugates, the degree of PEGylation was determined by three complementary techniques: <sup>1</sup>H NMR spectroscopy, SEC, and sodium dodecyl sulfate polyacrylamide gel electrophoresis (SDS–PAGE) (**Table S1**). <sup>1</sup>H NMR spectroscopy: A solution of mPEG–GDH in D<sub>2</sub>O was prepared and the concentration of the protein component determined by its absorbance at 280 nm ( $\epsilon = 48,820 \text{ cm}^{-1}\cdot\text{M}^{-1}$ ). Then, a known amount (ca. 10  $\mu\text{L}$ ) of a reference compound (DMSO) was spiked into the solution. <sup>1</sup>H NMR spectroscopy of this solution permitted the integration of the ethylene glycol backbone peak of mPEG as well as the methyl groups of DMSO. The comparison of these two peaks yielded the concentration of the mPEG component in the solution. Knowing the concentration of both protein and mPEG, the degree of PEGylation could be calculated. SEC: The molecular weight of mPEG–GDH was analyzed by aqueous SEC using both UV and ELSD detectors. 100  $\mu\text{L}$  of 0.5 mg·mL<sup>-1</sup> sample solution prepared in ammonium formate buffer (100 mM, pH 3.5) were injected and eluted with ammonium formate buffer (100 mM, pH 3.5) at 1 mL·min<sup>-1</sup> at 25 °C. Retention times were compared to those of Agilent EasiVial PEG/PEO calibration standards (640–1327 kDa). Once the apparent number-average molecular weight ( $M_n$ ) was established, the degree of PEGylation was calculated. SDS–PAGE: GDH (5  $\mu\text{g}$  in 3  $\mu\text{L}$  water) and PEGylated GDH (5  $\mu\text{g}$  protein in 3  $\mu\text{L}$  water) were mixed with 5  $\mu\text{L}$  of loading buffer (65 mM Tris-HCl, pH 6.8, 2% SDS, 10% glycerol, and 0.1% bromophenol blue). Gels were run in Tris/glycine/SDS (3.0/14.4/1.0 g·L<sup>-1</sup>) buffer (pH 8.3), under constant voltage (100 V) for ~90 min. The gels were imaged using an UVP Biodoc-it imaging system running UVP VisionWorksLS™ software. Analysis of the resulting gels using ImageJ software enabled an assessment of the distribution of PEGylated species within a given sample, from which a weighted-average was calculated.

**2.6 Catalytic activity in the absence and presence of allosteric modulators.** The catalytic activity of GDH was evaluated in the absence of allosteric modulators using a modified protocol from Li et al <sup>418</sup>. Briefly, a GDH solution (~1 mg·mL<sup>-1</sup>) was prepared using 100 mM sodium phosphate buffer (pH 7.5), containing 1 mM EDTA and then dialyzed against the same buffer without EDTA. Enzyme activity was assayed in freshly prepared 0.1 ionic strength sodium phosphate buffer (16.7 mM, pH 7.5) containing either varied glutamate concentration (0.12, 0.2, 1, 2, 4, 8, 16, 32, 64, 128, or 256 mM) and fixed NAD<sup>+</sup> concentration (0.2 mM) or varied

NAD<sup>+</sup> concentrations (0.066, 0.02, 0.025, 0.033, 0.05, 0.1, 0.2, 0.4, or 1 mM) and fixed glutamate concentration (50 mM). The reaction was initiated by adding GDH from the stock solution above (final concentration 100 nM) and the production of NADH was monitored for 3–5 min at 340 nm using a Cary 60 UV-Vis spectrophotometer. The resulting velocity vs. [glutamate] or [NAD<sup>+</sup>] plots were created using the linear region from the reaction plot, and used to determine the kinetic parameters of the enzyme.

The velocity of the catalytic reaction was also measured in the presence of allosteric modulators (hexachlorophene, bithionol, GTP, and ATP) at increasing concentrations between 0.1–1000  $\mu$ M, as appropriate for each compound. At varied NAD<sup>+</sup> concentrations, kinetic parameters were extracted by linear regression from Lineweaver–Burk plots (**Fig. S1**). At varied glutamate concentrations, kinetic parameters (Michaelis constant ( $K_m$ ) and maximal velocity ( $V_{max}$ )) were extracted by non-linear regression analysis using the SubstrateInhib equation in Microcal Origin<sup>®</sup> (**Table S2**).

The catalytic activity of mPEG–GDH bioconjugates was assayed in 1 mL cuvettes in 0.1 ionic strength sodium phosphate buffer (16.7 mM, pH 7.5) containing 50 mM glutamate and 0.2 mM NAD<sup>+</sup>. Dose–activity curves for the effect of the different allosteric modulators were established (**Figs. S2–S6**) and analyzed by non-linear regression using the Sigmoidal function supplied with Microcal Origin<sup>®</sup>. Reported IC<sub>50</sub> values correspond to concentrations of modulators yielding 50% of the activity difference between the initial and final plateaus.

**2.7 Circular dichroism spectroscopy.** Circular dichroism (CD) spectra were recorded for native GDH and for selected mPEG–GDH bioconjugates. Protein concentration was 0.1 mg·mL<sup>-1</sup> in a total volume of 150  $\mu$ L of 16.7 mM sodium phosphate buffer, pH 7.5. Measurements were performed on a Chirascan CD spectrometer in 0.5 mm quartz cuvettes at 25 °C. The spectra were recorded from 260–183 nm at 1 nm step intervals and at 0.5 s time intervals. CD signals are presented in terms of ellipticity in millidegrees and are represented as an average of the three spectra obtained for each sample. Blank spectra were subtracted from the CD spectra. The CD spectra were deconvoluted using the CDNN (Circular Dichroism analysis using Neural Networks) software.

**2.8 Tryptophan fluorescence spectroscopy.** Fluorescence analyses were performed for native and selected mPEG–GDH bioconjugates. Spectra were recorded using a Cytation 5 microplate reader with  $\lambda_{ex}$  = 280 nm and  $\lambda_{em}$  = 300–450 nm, using a 9 nm bandwidth and excitation/emission slits at 4.5 nm. The concentration of GDH was adjusted to 0.25 mg·mL<sup>-1</sup> in 16.7 mM sodium phosphate buffer, pH 7.5. Spectra are presented as an average of the three spectra for each sample.

**2.9 Simulation Setup.** Molecular dynamics (MD) were conducted to explore the effect of PEGylation on the dynamics of GDH. All atom MD simulations were conducted in GROMACS<sup>419,420</sup> using the PDB structure 3etd for GDH. While these simulations contain a great degree of detail, the number of atoms required (including explicit water molecules) makes exploring large-scale dynamics prohibitively expensive. The atomistic simulations were therefore used to construct a MARTINI coarse-grained (CG) model of the protein. In brief, the MARTINI force-field combines 4 heavy atoms into a single bead (see details in the Supporting Information). The water was also modeled in a CG manner to greatly reduce the number of particles in the simulations, thus enabling simulations of protein dynamics over greater time and length scales.

Known force fields were employed for both the protein<sup>421</sup> and the mPEG chains<sup>422</sup>. The latter was slightly modified to prevent artefacts arising from a size mismatch between the polymer and solvent beads. The polymer beads were set to be of the 'polar' type, denoted as 'P' in the MARTINI framework. The mPEG chains are polar and known to be soluble in water. However, there are non-polar regions along the chain and thus the bead parameters were set such that the well-depth of the attractive part of the potential was deeper for water–water interactions than for water–polymer interactions. Hence, while still polar, this subcategory (denoted as 'P1') contains a small amount of hydrophobicity. To test the effects of using the P1 beads for mPEG, simulations in which mPEG was constructed out of 'P4' beads were also performed. P4 is the bead type used for the solvent, and thus the PEG–water interactions are the same as water–water interactions, yielding a fully hydrophilic model.

A total of 25 mPEG chains were attached to the protein hexamer in two different manners. In the first, sites were chosen at random from among the solvent-accessible lysine residues, ensuring that the distribution of polymers among the subunits is relatively equal (**Tables S3 and S4**). This is referred to as the 'symmetric' case. In the second manner, all subunits are still modified with mPEG, but the distribution is such that one or two particular subunits have many more than the other subunits ('asymmetric' case). While the CGMD approach is more efficient than the all-atom models, the simulations are still quite costly in terms of the time required to obtain the results. A length of 2 kDa for mPEG was used for most simulations as this is the shortest (and thus easiest to simulate) length for which significant loss of activity was measured experimentally. The effect of mPEG length was also explored (0.5 and 5 kDa) using the P1 bead type.

Normal mode analysis was employed to quantify the effect of PEGylation on protein dynamics. In this approach, the normal modes of the protein were calculated and ordered as a function of amplitude of motion. Low rank normal modes thus correspond to large-scale motions that generally involve the concerted motion of many parts of the protein. In the present case of

GDH, the lowest mode corresponded to motions involving the cooperative movement of all monomers within the hexameric protein, and showed similarity to the movements expected for the catalytic activity of GDH (see Section 3.4). Higher ranking modes typically had low movement amplitudes that eventually become indistinguishable from noise.

### 3. Results

#### 3.1 Design of bioconjugates to avoid the active-site PEGylation and mPEG steric effects

Bovine GDH is a hexameric protein composed of 6 identical monomers, each with a molecular weight of around 56 kDa<sup>265,266</sup>. As seen in **Fig. 1**, it is organized as a 'dimer of trimers' and each monomer contains three main domains: (1) a catalytic (substrate binding) cleft, (2) a coenzyme (NAD<sup>+</sup>) binding domain, and (3) a regulatory 'antenna' domain extending from the coenzyme binding domain<sup>58</sup>. The latter domain is only present in mammalian GDH and plays an important role in allosteric regulation<sup>56,266</sup>. The enzymology of GDH reveals some particularities that make it an interesting choice for avoiding deactivation due to active-site PEGylation. Firstly, GDH possesses six identical catalytic sites that are unlikely to be simultaneously PEGylated, due to the low degrees of PEGylation targeted (*vide infra*) and the lower solvent-accessibility of the lysine residues in these regions based on its crystal structure (**Table S3**)<sup>43</sup>. Further, and more importantly, previous studies have shown that the relative contribution of each monomeric unit to the overall catalytic process is not equivalent. Binding of the coenzyme NAD<sup>+</sup> to a given monomeric unit weakens the affinity of substrate towards the catalytic clefts on the remaining five monomeric units. Thus, binding of coenzyme and substrate to one of the monomers activates large scale movements of the protein responsible for catalysis, while simultaneously decreasing the affinity for the remaining monomers<sup>44-46</sup>. This mechanism can be observed on Lineweaver-Burk plots by a marked break from linearity (**Fig. S1**). More importantly, because of this mechanism, prior studies have shown that inhibition of 1, 2, or 3 catalytic sites of GDH lead to the progressive loss of 54%, 20%, and 10% of activity<sup>49</sup>. This suggests that bioconjugates with residual activity >46% vs. the native protein intrinsically possess all six free catalytic sites (i.e., not PEGylated).

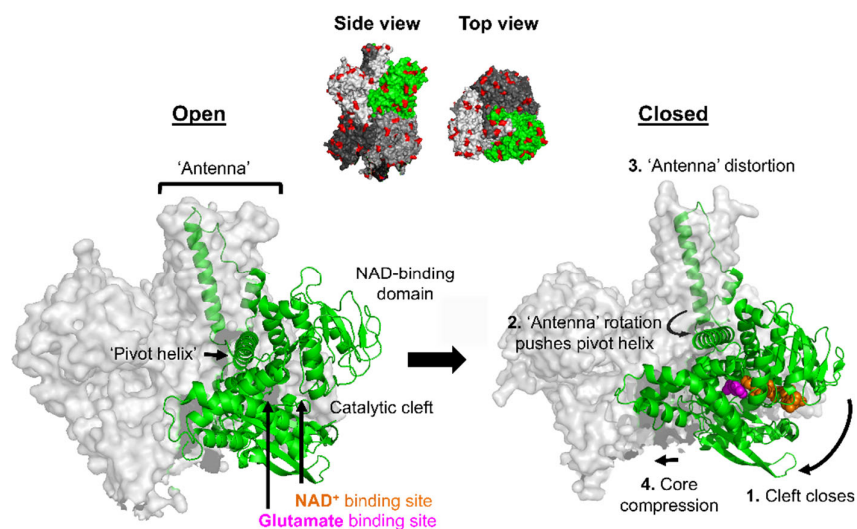


Figure 1| **Structure of bovine GDH and major movements associated with catalysis.** Inset shows hexameric structure of GDH, with lysine residues colored in red. GDH coordinates were taken from PDB entries 1nr7 (open conformation) and 6DHQ (closed conformation). The main movements associated with catalysis are: NAD<sup>+</sup> and glutamate bind to their sites, the NAD-binding domain closes the catalytic cleft (1), the bases of 'antenna' push against the 'pivot helix' (2), the 'antenna' becomes distorted (3), and the core of the hexamer compresses (4). The reverse process frees the product and consumed coenzyme.

As seen in **Fig. 1 (inset)**, the lysine residues of GDH are homogeneously distributed on the surface of the protein and were selected as targets for random (i.e., statistical) modification with mPEG. Hexameric GDH possesses 204 pendant amino groups (i.e., 198 lysine residues and 6 N-termini), though only  $160 \pm 9$  are accessible using a TNBS assay, which is comparable to the 123 residues predicted to be solvent-accessible from the protein's crystal structure. In order to circumvent loss of activity arising from mPEG steric effects and active-site PEGylation, a library of bioconjugates was prepared to identify minimal degrees of PEGylation leading to partial inactivation of GDH for mPEG molecular weights ranging from 0.5 to 20 kDa. As presented in **Fig. 2**, thirteen different bioconjugates were produced by reductive alkylation of GDH with mPEG aldehydes, the majority of which possessed monomodal size distribution profiles with dispersities in the range of 1.02–1.13 (Table S1). Minor shoulders were sometimes observed for bioconjugates with very low degrees of PEGylation (e.g., **9–10**) representing individual PEGylated species within the distribution, and tailing was sometimes observed for bioconjugates prepared with the shortest mPEG, due to enthalpic interaction with the column. Degrees of PEGylation were determined by three complementary methods (SEC, SDS-PAGE, and <sup>1</sup>H NMR spectroscopy) that were in reasonably good agreement with one another (**Table S1, and Figs. S7 and S8**).

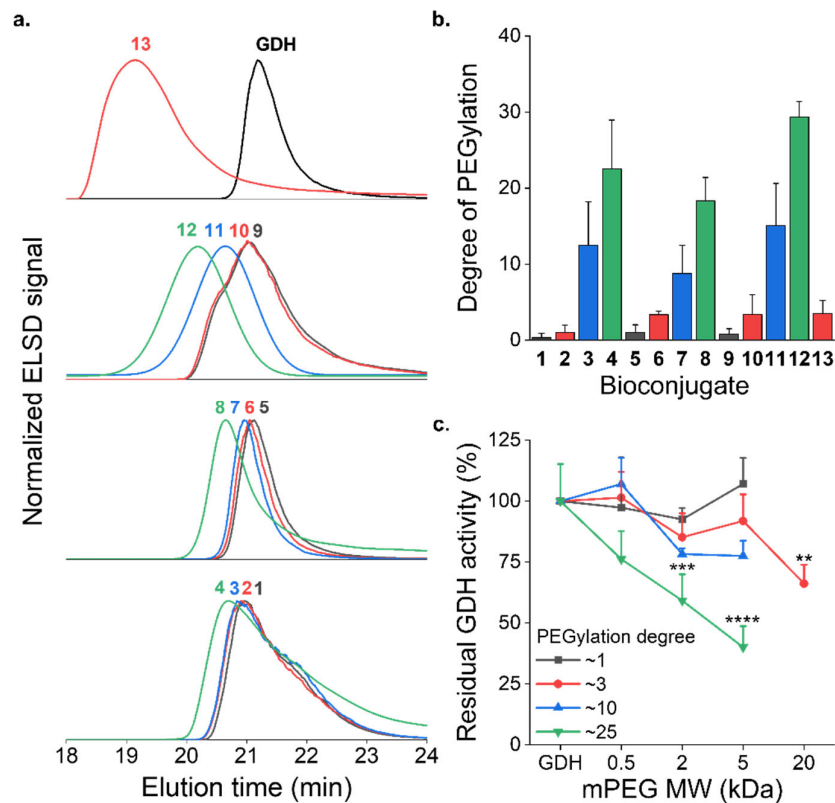


Figure 2| **Characteristics of mPEG–GDH bioconjugates.** (a) Size-exclusion chromatograms of the bioconjugates. (b) Degree of PEGylation determined by SEC, SDS-PAGE, and  $^1\text{H}$  NMR spectroscopy. (c) Enzymatic activity of GDH and mPEG–GDH bioconjugates. (\*) Denotes statistically significant differences with respect to native GDH (Tukey,  $p = 0.05$ ). Data presented as Mean  $\pm$  SD,  $n = 3$ .

Because GDH does not possess classic Michaelis-Menten behavior due to its ‘substrate inhibition’ mechanism, a variety of conditions for measuring catalytic activity were first screened, in terms of glutamate and  $\text{NAD}^+$  concentrations, to establish conditions to best study the bioconjugates <sup>423</sup>. Indeed, due to the complexity of these kinetics, a full analysis of variable glutamate and  $\text{NAD}^+$  conditions were explored for GDH, in the absence and presence of allosteric modulators, so that the bioconjugates could be analyzed under a more restricted number of conditions (**Fig. S1**). These conditions were selected to be 50 mM glutamate and 0.2 mM  $\text{NAD}^+$ , which enable analysis of enzyme kinetics in a reasonable time and avoided substrate inhibition that occurs at higher glutamate concentration. Considering the low degrees of PEGylation explored within the library, as well as the relatively low molecular weight of some of the mPEG explored, many of the bioconjugates displayed 100% of activity of the native protein (**Fig. 2c**). Exceptions included bioconjugates with very low degrees of PEGylation bearing long mPEG chains (i.e., **13** bearing  $3 \times 20$  kDa mPEG), as well as bioconjugates with

higher degrees of PEGylation and shorter mPEG chains (i.e., **8/12** bearing  $\sim 25 \times 2/5$  kDa mPEG, respectively). Interestingly, the activity of bioconjugate **4**, which bears  $\sim 25 \times 0.5$  kDa mPEG was not statistically different from that of the native protein. In light of the discussion above, this suggests that none of the bioconjugates within the library are PEGylated at any of their six active sites.

To support the argument that the surface of GDH remains highly exposed and accessible to the substrate, coenzyme, and allosteric modulators simulations were performed. For this purpose, 25 chains of mPEG were randomly distributed on the solvent-accessible lysine residues predicted by the crystal structure of GDH. An mPEG molecular weight of 2 kDa was selected for the simulation, which is mid-way between the shortest and longest values investigated at this degree of PEGylation. As can be seen on the bundle representation of the bioconjugate in **Fig. 3**, most of the protein's surface remains highly solvent-accessible. In fact, this illustration is a worst-case scenario in the sense that the regions that are occluded by the polymers are shown as a superposition of multiple frames over a 100 ns period, and thus at any one point in time the polymer chains would block much less of the protein's surface. Thus, analyzing the mechanisms of partial deactivation for selected bioconjugates within the library (namely, **3**, **4**, **7**, **8**, **11**, **12**, and **13**) provides new perspectives on deactivation that are not distinguishable for multi-PEGylated proteins with higher degrees of PEGylation or longer mPEG chains, where direct modification of the catalytic site or steric hindrance are likely to become important.

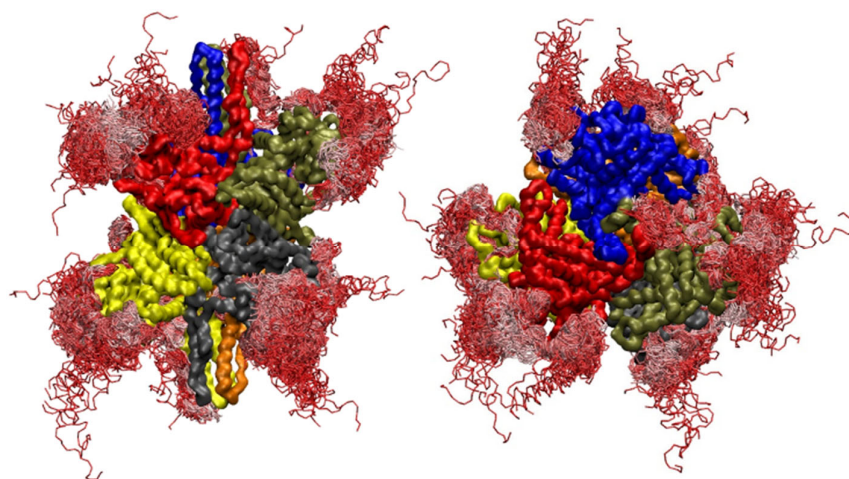


Figure 3| **Simulated structure of a representative mPEG–GDH bioconjugate.** Bundle representation of an mPEG–GDH bioconjugate bearing  $25 \times 2$  kDa mPEG, with overlapped polymer frames in a 100 ns trajectory (2 frames per nanosecond). A single hexamer frame is shown. Details of the simulation are provided in supporting information. (Left) Side view and (Right) Top view.

### 3.2 Change of protein structure

Conformational changes to GDH due to PEGylation were investigated by CD spectroscopy as well as tryptophan fluorescence (**Fig. 4**). According to the literature, GDH is predominantly  $\alpha$ -helical<sup>50</sup>, and this was confirmed by a strong positive peak at 193 nm and a double minimum at 222 and 210–208 nm for the native protein. Deconvolution revealed that ~45% of its structure was  $\alpha$ -helical, and the second most dominant feature were random coils (~30%). Analysis of the library of bioconjugates globally revealed that PEGylation caused a loss of  $\alpha$ -helical character that was dependant both on degree of PEGylation and on mPEG molecular weight (**Table S5**). This was accompanied by a proportionate increase in random coil content. Changes to  $\beta$ -sheet content were quite small, even for bioconjugate **12** that displayed the greatest changes to secondary structure, and might reflect the fact that these structures are less solvent-accessible in GDH. At low degrees of PEGylation (i.e., ~10 chains of mPEG per protein) loss of  $\alpha$ -helical character was small (ca. ~4–8%). Considering that the activity of these bioconjugates was indistinguishable from that of the native protein, this result suggests that conformational changes of this extent are not functionally relevant, at least for mPEG < 5 kDa. Indeed, while bioconjugates **7** and **13** displayed similar ellipticity profiles, the partial loss of activity observed for **13** (3 × 20 kDa) provides an indication that a mechanism beyond altered structure might be responsible for loss of activity (e.g., dynamics or micro-environment; *vide infra*). Increasing the degree of PEGylation to ~25 resulted in a more pronounced loss of ellipticity as well as a more pronounced effect of mPEG molecular weight. For these bioconjugates, the loss of  $\alpha$ -helical character might be a contributing factor to loss of activity. However, remarkably, bioconjugate **4** (~25 × 0.5 kDa mPEG) maintained the full activity of the native protein despite a ~14% loss of its helical character. To complement these experiments and to gauge the effect of PEGylation on the tertiary structure of GDH, tryptophan fluorescence spectroscopy was performed (**Fig. 4b**). The maximal tryptophan fluorescence emission wavelength ( $\lambda_{\text{max}}$ ) of native GDH was 320 nm, suggesting that tryptophan residues are buried and not solvent-accessible<sup>424</sup>. In contrast to CD spectroscopy, the loss of tryptophan fluorescence observed for the bioconjugates appeared to be more sensitive to changes of mPEG molecular weight at low degrees of PEGylation, and insensitive to this variable at higher degrees of PEGylation. The bioconjugate whose tertiary structure was most affected by PEGylation was **12** (~25 × 5 kDa), which exhibited a ~60% loss of fluorescence intensity and a 10-nm red-shift of fluorescence, suggesting greater exposure of the tryptophan to the solvent. Finally, fluorescence spectra of bioconjugate **13** (~3 × 20 kDa) and **7** (~10 × 2 kDa) overlapped, demonstrating a similar effect on GDH tertiary structure.

Globally, the results above suggest that GDH, possibly because of its highly dynamic nature, can for certain PEGylation parameters accommodate relatively significant changes to its

secondary and tertiary structure with minimal impact on its catalytic activity. This result may reflect the great conformational flexibility of GDH, which is indispensable for exerting its vital metabolic role in cellular homeostasis<sup>425</sup>. Moreover, it is noteworthy that bioconjugates **3+13** as well as **4+12** possess very similar CD/fluorescence spectra (reflecting similar steady-state conformations), respectively, but different catalytic activity. Thus, loss of activity for some bioconjugates such as **8**, **12**, and **13** may result from other phenomena, such as an altered micro-environment or molecular dynamics, which will be discussed below.

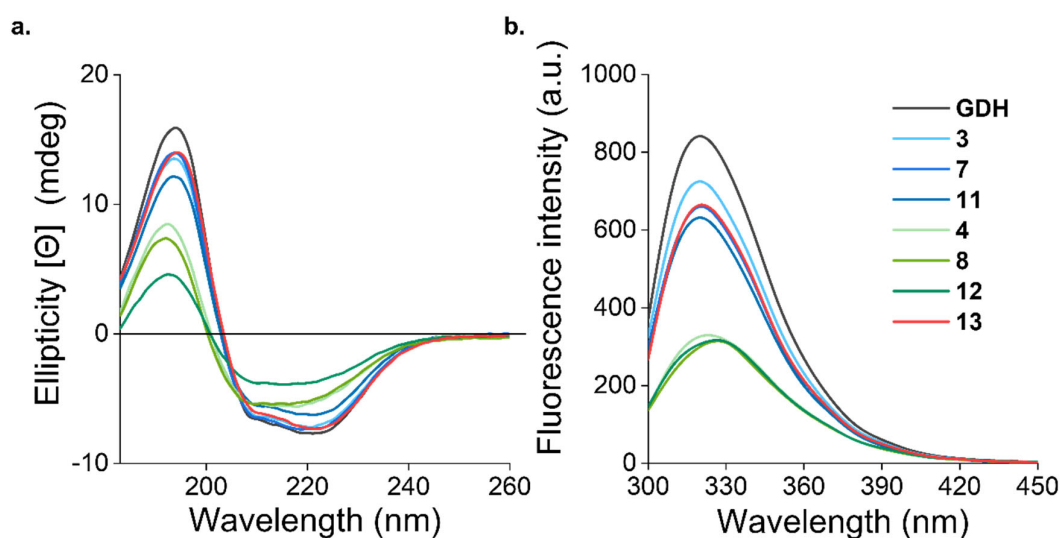


Figure 4| **Effect of the PEGylation on the secondary and tertiary structure of GDH.** (a) Far-UV Circular Dichroism spectra and (b) tryptophan fluorescence spectra of GDH and mPEG–GDH bioconjugates. Altered protein structure was found to depend on degree of PEGylation and mPEG molecular weight.

### 3.3 Change of local microenvironment caused by polymer

To shed more light on conformation as well as micro-environmental effects, the binding affinity of two series of allosteric modulators towards their respective binding sites on GDH was characterized. The catalytic activity of the bioconjugates was measured and dose-activity curves were established for each modulator. These small molecule modulators bind to different locations on GDH and inhibit its activity by restricting different protein movements. The first series of allosteric modulators includes hexachlorophene and bithionol, which prevent or restrict the compression/expansion motions of the core of the hexamer during catalytic cleft closure/opening<sup>53,418</sup>. More specifically, hexachlorophene diffuses into the cavity in the core of the protein, where it blocks expansion by forming a ring-like structure that links all the six

subunits together<sup>57</sup>. Similarly, bithionol binds to each monomer in a binding pocket located halfway between the core and the exterior of the hexamer<sup>57</sup>. By binding, bithionol decreases the rate of the catalytic turnover by preventing the free movement of the stacked dimers and by interfering with the compression/expansion motions of the hexamer<sup>53</sup>. As can be seen in **Table 1 and Figs. S2,3**, very little or no change in IC<sub>50</sub> or magnitude of the inhibitory effect of hexachlorophene or bithionol was observed within the library of bioconjugates. This result confirms arguments above and indicates that the buried binding sites for these modulators were also unaffected by steric or micro-environmental effects resulting from PEGylation (might alter modulator partition coefficients or binding constants). Only two exceptions were observed, bioconjugates **4** and **12** (~25 × 0.5/5 kDa, respectively), for which a marked loss of effect of both modulators was observed alongside non-sigmoidal dose-activity curves (**Figs. S2,3**). This observation suggests that the short mPEG used to prepare this bioconjugate may to a certain extent be modifying lysine residues that are deeper in the protein's structure and partially block the buried binding sites for these modulators, located in these regions, though this was not further explored.

The second series of allosteric modulators included GTP, ATP, and Zn<sup>2+</sup>, which all bind near the hinge region between the NAD-binding domain and the pivot helix<sup>52-54</sup>. After glutamate and NAD<sup>+</sup> binding and catalytic cleft closure, this allosteric site becomes accessible and binding of these molecules inhibits catalytic activity by slowing down product release (i.e., by stabilizing the abortive complexes and by decreasing the catalytic competence)<sup>54,426</sup>. In **Table 1**, an increase of IC<sub>50</sub> for GTP was generally observed as a function of both degree of PEGylation and mPEG molecular weight, and trends were consistent with those observed from CD or tryptophan spectroscopy. This result suggests that changes of protein structure observed in the previous section may at least partially be affecting the structure of the 'antenna' region of GDH, resulting in the loss of affinity of these modulators. These observations are consistent with previous studies demonstrating that the 'antenna' is necessary for GTP allostery and that mutations in this area resulted in loss of this mechanism of regulation<sup>427,428</sup>. In fact, while ATP shares the same binding site as GTP, its lesser affinity compared to the latter resulted in its complete loss of inhibitory effect. Nevertheless, the effect of PEGylation on IC<sub>50</sub> values obtained with GTP are relatively small compared to the native protein. The major binding site for the last modulator, Zn<sup>2+</sup>, is located within the GTP binding site, though it can also bind to a dynamic region between the two trimers of subunits and suppress movement required for catalytic competence<sup>55</sup>. As for hexachlorophene and bithionol, no effect of PEGylation on the IC<sub>50</sub> value measured for Zn<sup>2+</sup> was observed, except possibly for **12**. Overall, while it is tempting to attribute loss of catalytic activity to a modified structure in the 'antenna' region, this conclusion does not reconcile comparisons between bioconjugates such as **3** and

**13**, or **11** and **12**, which show similar structural perturbation by CD/fluorescence spectroscopy, yet different activity. Thus, the results appear to reflect that PEGylation (under in the range of parameters investigated) does not alter microenvironment, though is responsible for an altered structure of GDH near its 'antenna' region, which impacts GTP and ATP allosteric modulation. However, this altered structure cannot be directly correlated to activity. In a broader context, this result suggests that PEGylation may be altering the activity of other therapeutic proteins, by influencing allosteric regulation *via* mechanisms either known or unknown.

**Table 1:** Effect of allosteric modulators on the activity of GDH and mPEG–GDH bioconjugates. Data presented as Mean  $\pm$  SD, n = 3.

Bioconjugate	IC <sub>50</sub> ( $\mu$ M)				
	Hexachlorophene	Bithionol	GTP	Zinc	ATP
GDH	1.5 $\pm$ 0.3	1.9 $\pm$ 0.02	19 $\pm$ 8	49 $\pm$ 3	55 $\pm$ 19
<b>3</b>	1.7 $\pm$ 0.3	1.9 $\pm$ 0.02	17 $\pm$ 2	42 $\pm$ 13	– <sup>1</sup>
<b>4</b>	– <sup>2</sup>	1.8 $\pm$ 0.08	30 $\pm$ 12	– <sup>2</sup>	– <sup>1</sup>
<b>7</b>	2.3 $\pm$ 0.1	1.7 $\pm$ 0.6	45 $\pm$ 3 *	38 $\pm$ 0.0	– <sup>1</sup>
<b>8</b>	2.3 $\pm$ 0.1	2.0 $\pm$ 0.0	76 $\pm$ 12 *	41 $\pm$ 19	– <sup>1</sup>
<b>11</b>	1.6 $\pm$ 0.06	1.7 $\pm$ 0.6	41 $\pm$ 6 *	34 $\pm$ 0.2	– <sup>1</sup>
<b>12</b>	2.9 $\pm$ 0.5 *	– <sup>1</sup>	– <sup>1</sup>	– <sup>1</sup>	– <sup>1</sup>
<b>13</b>	1.4 $\pm$ 0.1	1.8 $\pm$ 0.0	15 $\pm$ 7	41 $\pm$ 0.6	– <sup>1</sup>

\*: denotes statistically significant difference with respect to the native GDH (Tukey, p = 0.05).

<sup>1</sup>: IC<sub>50</sub> above 1 mM

<sup>2</sup>: non-sigmoidal dose-activity curve

### 3.4 Effect of PEGylation on protein dynamics

During each catalytic cycle, a large conformational change occurs throughout the hexamer. Indeed, in the course of this process, NAD<sup>+</sup> binds to its binding site in the catalytic cleft, and is

followed by glutamate binding to its site. A rotation of 18–20° of the coenzyme binding domain reinforces and wedges the substrate and the coenzyme together, leading to the closure of the catalytic cleft. Through these movements, the pivot helix, located on the top of the hexamer, rotates in a counter clockwise manner along the helical axes, and around the 3-fold symmetry axis of the trimer. Once the catalytic cleft is closed, the bases of the ‘antenna’ helices rotate out and compress the whole hexamer, which further squeezes the core of the enzyme<sup>56-58</sup>. Once the product is formed, GDH reverses these movements to release the substrates and to prepare the enzyme for substrate uptake<sup>53</sup>. As the catalytic mouth opens and closes, the core of GDH expands and contracts. It is therefore an interesting model system for studying the effect of PEGylation on protein dynamics. Normal mode analysis of native bovine GDH (i.e., not PEGylated) revealed that the lowest ranking mode displayed several features that bore similarity to movements associated with catalytic activity above. As shown in the **Movies 1 and 2**, rotation/distortion of the ‘antenna’ regions and closure of the ‘catalytic cleft’ are seen in the simulations. The central cavity in the hexameric protein also constricts during the motion (see **Fig. S9**). This suggests that, at minimum, analyzing the effect of PEGylation on this mode may provide some insight into the effect of PEGylation on catalytic activity.

Movie 1| **Lowest normal mode motion for a GDH monomer projected onto the atomistic (3etd coordinates) structure.** Shown in a cartoon representation. Prepared with PYMOL<sup>429</sup>. Modes are projected with online server tools<sup>430</sup> where the amplitude of the movement is emphasized to aid visualization. Link: <https://ars.els-cdn.com/content/image/1-s2.0-S2468519418302647-mmc3.mp4>

Movie 2| **Animation of the lowest normal mode (full hexamer)** for the native protein, the P1 bead PEGylated protein, and the P4 bead PEGylated protein. Projections were made with eigenvectors from the CG simulations showing displacement amplitudes of the first eigenvalue. GDH monomers are represented by different colors. Movies prepared with VMD<sup>431</sup>. Link: <https://ars.els-cdn.com/content/image/1-s2.0-S2468519418302647-mmc3.mp4>

To model the bioconjugates, CGMD simulations were performed using the ‘P1’ (small amount of hydrophobicity) and ‘P4’ (water–water like interactions) type beads for GDH modified with 25 × 2 kDa mPEG (**Fig. 5**). For ‘P1’, the polymers partially adhere to the surface of GDH but also extend somewhat into the fluid. Conversely, for ‘P4’ type beads, mPEG did not adhere at all to the protein and rather extended into the solvent with a distinct helical conformation. Examples of simulations from the literature generated for different mPEG lengths and proteins have reported mPEG as either attaching to proteins<sup>39,432</sup> or extending out into the solvent, or both, depending on the shape and composition of the proteins<sup>433</sup>. The CGMD results

presented herein indicate that both situations can be produced as a result of subtle free energy differences in mPEG–protein–water interactions. Similarly, the observation that mPEG forms helices has already been observed in simulations and experimentally<sup>409</sup>, but not in all studies<sup>434,435</sup>. Exploring these results in more detail is the subject of ongoing work, and is not essential for this study. Indeed, because resolving the structure of PEGylated proteins computationally is not the objective of this work, the influence of both ‘P1’ and ‘P4’ type mPEG on molecular dynamics was assessed, to provide insight into the effects of these two extreme situations, under the expectation that the real situation lies somewhere in between.

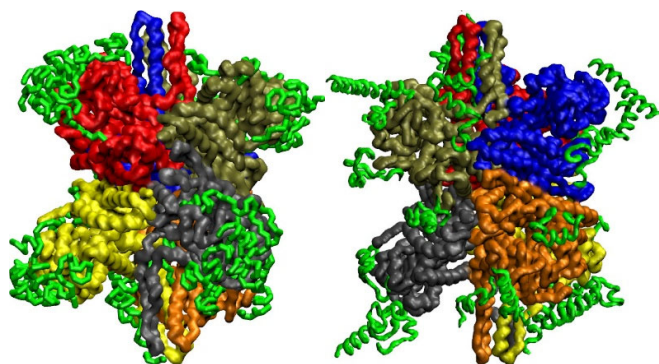


Figure 5| **Structure of a mPEG–GDH bioconjugate** bearing  $25 \times 2$  kDa mPEG chains, simulated using either ‘P1’ (small amount of hydrophobicity; left) or ‘P4’ (water–water-like interactions; right) type mPEG chains.

The normal mode analysis for native GDH as well as bioconjugates simulated with ‘P1’ or ‘P4’ mPEG chains is shown in (**Fig. 6**). Normal mode analysis was performed either for the entire protein (i.e., polyamide backbone + amino acids side-chains; **Fig. 6a**) or for the backbone alone (**Fig. 6b**). A cursory inspection of both plots shows that PEGylation affects protein dynamics in terms of reduced magnitude of the lowest modes. This observation is evident for both ‘P1’ and ‘P4’-type mPEG, and is more pronounced for the backbone than for the side-chains. Two trends emerge: ‘P1’ mPEG (partially hydrophobic) has a greater impact than ‘P4’ mPEG on protein dynamics, and the asymmetric distribution of mPEG has a greater impact than the symmetric attachments. Considering that ‘P1’ mPEG partially adheres to the surface of the protein, this result is not surprising as the adhered portions of the polymer are expected to more strongly dampen motions of the protein. The observation that ‘P4’ mPEG also significantly impacts protein dynamics suggests that polymers that simply extend out into the solution can similarly reduce large-scale motions. The effect of the polymers is thus not necessarily through direct interference of the internal degrees of freedom of the protein, but could arise from the extra drag and concomitant extra fluctuations of the polymers that extend

into solution (that is, they can act as so-called “noisy anchors”). Indeed, this could be the nanoscale manifestation of the ‘parachute effect’ observed by Gokarn et al. for PEGylated proteins analyzed by analytical ultracentrifugation <sup>411</sup>.

Considering that GDH catalysis requires that all six monomers move in a cooperative manner, the effect of how mPEG is distributed on the surface of the protein was investigated. Compared to the situation in which mPEG is distributed evenly amongst the six monomers (‘symmetric’), skewing this distribution to favor the PEGylation of one of the monomers (‘asymmetric’, see details in Supporting Information) leads to a more pronounced loss of motion. This situation, which is difficult to replicate experimentally, corroborates observations from others that the inhibition of a single catalytic site of GDH using a small molecule inhibitor results in an important, 54% loss of catalytic activity <sup>49</sup>. This disproportional high loss of activity has been interpreted as a loss of cooperativity between monomers. An asymmetric distribution of mPEG on GDH, could therefore more significantly affect the dynamics of the more PEGylated monomer, which has repercussions on the rest of the protein. Finally, given that mPEG molecular weight was shown to influence the loss of activity of the bioconjugates, the effect of this parameter was evaluated by simulation. As illustrated in **Fig. 6c**, the shortest mPEG (25 × 0.5 kDa) had little effect on the lowest normal mode, which is consistent with the native-like activity observed for this bioconjugate (**Fig. 2c**). Although simulations were only performed for ‘P1’ type mPEG, this result fits with either ‘P1’ or ‘P4’ model. Indeed, the length of mPEG adhered to GDH is unlikely to be long enough to couple two monomers or disparate parts of the same monomer. For ‘P4’ mPEG, the polymers are small and thus their effect as ‘noisy anchors’ would be proportionately small. That being said, an effect on the 2<sup>nd</sup> lowest normal mode was observed. While interpreting this result would be interesting, direct comparison between normal modes is difficult as there are many parts in motion, and a more involved analysis beyond the qualitative aspect sought after herein would be required to fully contextualize this observation. The higher molecular weight mPEG significantly dampen the 1<sup>st</sup> and 2<sup>nd</sup> lowest modes in a molecular weight dependent manner, qualitatively analogous to the loss of activity observed for conjugates **8** and **12** in **Fig. 2c**. No effect is observed for the higher order modes.

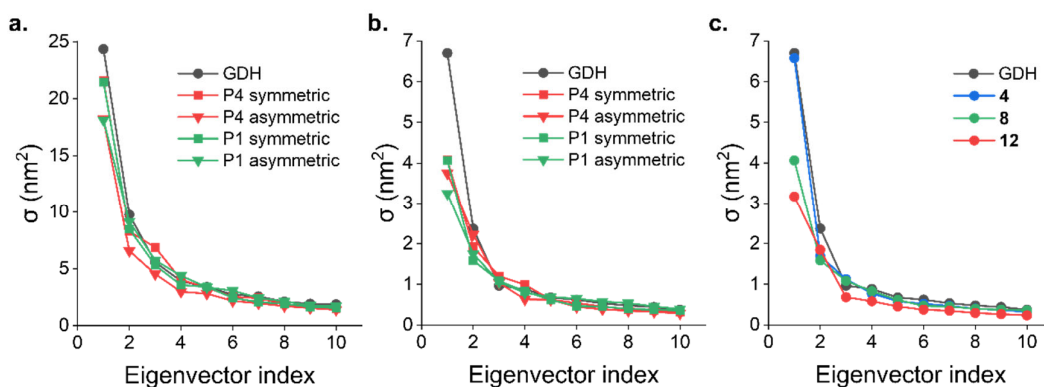


Figure 6| **Effect of PEGylation on the normal modes of GDH.** Simulations for (a) the entire protein structure (polyamide backbone + amino acid side-chains) or for (b) protein backbone alone (25 × 2 kDa mPEG). (c) Effect of mPEG molecular weight on the normal modes of GDH (symmetric distribution of mPEG). PEGylation decreases the magnitude of the lowest modes, and is more pronounced when mPEG interacts with the protein ('P1' type mPEG) and when mPEG is asymmetrically distributed on the surface of the protein.

#### 4. Conclusions

This study revealed that the secondary and tertiary structure of GDH was (sometimes significantly) affected by PEGylation, though these changes do not necessarily result in a loss of activity. Indeed, structure–activity correlations could not reconcile all trends within the library of bioconjugates tested, suggesting that other mechanisms of activity loss were at play, and that changes of structure are dynamic rather than permanent. By measuring catalytic activity in the presence of five different allosteric modulators, loss of activity could not be ascribed to an altered local microenvironment at the protein's surface. In a broader perspective, this suggests that PEGylation may be influencing the activity of therapeutic proteins *in vivo*, by altering the accessibility or structure of binding sites for allosteric modulators, both known or unknown. Coarse-grained simulations showed that PEGylation reduced the magnitude of the lowest normal mode of GDH, in a manner that depended on degree of PEGylation and mPEG molecular weight. The simulations correlated well with trends in catalytic activity observed for the library of bioconjugates tested experimentally, and suggested that loss of activity was mainly caused by restricted protein dynamics. Of course, while GDH is a prototypical example of a highly dynamic protein whose catalytic activity relies on concerted long-range movements involving the entire protein, similar phenomena may exist for other proteins at smaller or more local scales. For example, the therapeutic enzyme L-asparaginase is thought to lose activity as a result of antibodies binding to a 'flexible loop' near the enzyme's catalytic site<sup>436</sup>. Thus, modified dynamics of this loop potentially caused by PEGylation may result in loss of activity or substrate specificity, as already demonstrated by point mutations in this area<sup>437</sup>. As such,

this study provides new insight into fundamental considerations associated with loss of activity of multi-PEGylated proteins, which will contribute to the design of future bioconjugates by providing a better understanding of possible mechanisms of loss of activity.

### **Acknowledgements**

This work was supported by the Natural Science and Engineering Council of Canada (RGPIN-2015-04254 and RGPIN-2014-06091). AZ acknowledges a doctoral scholarship from the Tunisian Ministry of Education. AAG acknowledges postdoctoral scholarships from the Fonds de Recherche du Québec Nature et Technologies (FRQNT) and the Canadian Institutes for Health Research (CIHR). Further, she acknowledges the Chu Family Scholarship for a career award.

### **Supporting Information**

Supporting movies showing the simulated movement of GDH and mPEG–GDH bioconjugates, additional details on CGMS, and supporting results for mPEG–GDH bioconjugates (molecular characteristics, enzymatic properties in the absence and presence of allosteric modulators, calculated solvent-accessibility of lysine residues for GDH, unedited images of SDS-PAGE gels, secondary structure estimation).

### **Data availability**

The raw/processed data required to reproduce these findings cannot be shared at this time due to technical or time limitations. Readers are encouraged to contact the corresponding authors for access to this information.

## 2. Follow-up

Following this fundamental study, we moved to our next objective related to the assessment of the scavenging effects of intravenously injected native GDH. This was a pilot assay to establish basic dose-response relationships, in order to plan the corresponding pharmacokinetics, pharmacodynamics, and neuroprotection experiments. Indeed, even though some *in vivo* studies showed that MCAo mice over-expressing GDH exhibited smaller ischemic lesions compared to mice with normal GDH expression<sup>27</sup>, the capacity of GDH to reduce glutamate and CSF levels has not been yet demonstrated. Therefore, a necessary step would be to confirm such an outcome. To accomplish this, groups of three healthy rats were administered 1 mL of sterile saline (0.9% of NaCl) and 12.88  $\mu\text{g}/100\text{g}$  of GDH in 1 mL saline by intravenous injection. Thereafter, blood was sampled from the tail vein and CSF was sampled from the cisterna magna repeatedly over a period of 14 days (0, 2, and 6 hours, 1, 4, 7, and 14 days) and catalytic activity as well as glutamate levels were measured. As seen in Figure 13, unfortunately, no obvious reduction of the glutamate concentrations was noticed for the GDH-treated group.

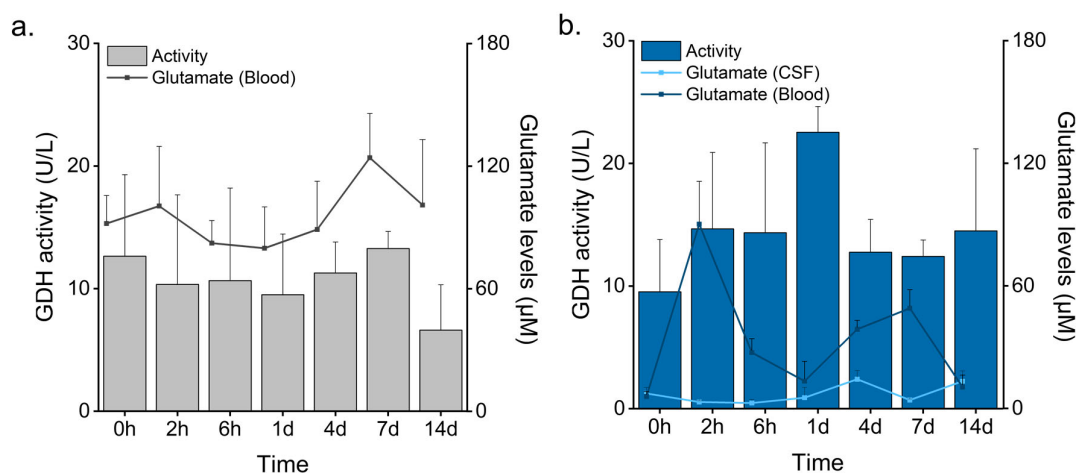


Figure 13: GDH activity and glutamate levels in the blood. Saline (a) and unPEGylated GDH (b) were administered to healthy rats. Data presented as Mean + SD, n = 3. Note: No statistical tests are shown here for simplification.

Considering these preliminary results, as well as the fact that GDH is known to promote both directions of the catalytic reaction, it was feared that this stage GDH would not reduce the concentration of glutamate *in vivo* without the co-administration of cofactors. In light of these results, as well as the suspected reason for lack of activity *in vivo* (at least under these conditions), it was not considered reasonable to plan/pursue more extensive *in vivo*

experiments with GDH or GDH bioconjugates. As such, our research was directed towards bioconjugates of hrGOT, for which more extensive precedence of exogenous administration exists in the literature.

## CHAPTER 4: Article 2

### Sustained blood glutamate scavenging enhances protection in ischemic stroke

Ahlem Zaghmi, Antonio Dopico-López, María Pérez-Mato, Ramón Iglesias-Rey, Pablo Hervella, Andrea A Greschner, Ana Bugallo-Casal, Andrés da Silva, María Gutiérrez-Fernández, José Castillo, Francisco Campos Pérez, and Marc A. Gauthier

A version of this chapter has been accepted for publication in  
Communications Biology.

The formatting of this article conforms to the specifications of the scientific journal.

# **Sustained blood glutamate scavenging enhances protection in ischemic stroke**

Ahlem Zaghmi,<sup>1</sup> Antonio Dopico-López,<sup>2</sup> María Pérez-Mato,<sup>2,3</sup> Ramón Iglesias-Rey,<sup>2</sup> Pablo Hervella,<sup>2</sup> Andrea A Greschner,<sup>1</sup> Ana Bugallo-Casal,<sup>2</sup> Andrés da Silva,<sup>2</sup> María Gutiérrez-Fernández,<sup>3</sup> José Castillo,<sup>2</sup> Francisco Campos Pérez,<sup>2,\*</sup> and Marc A. Gauthier<sup>1,\*</sup>

<sup>1</sup> Institut National de la Recherche Scientifique (INRS), EMT Research Center, Varennes, Qc, J3X 1S2, Canada

<sup>2</sup> Clinical Neuroscience Research Laboratory, Health Research Institute of Santiago de Compostela (IDIS), Santiago de Compostela, Spain.

<sup>3</sup> Neuroscience and Cerebrovascular Research Laboratory, Department of Neurology and Stroke Center, La Paz University Hospital, Neuroscience Area of IdiPAZ Health Research Institute, Universidad Autónoma de Madrid, Madrid, Spain.

Corresponding authors:

Marc A. Gauthier

Institut National de la Recherche Scientifique (INRS), EMT Research Center, 1650 boul. Lionel-Boulet, Varennes, J3X 1S2, Canada

E-mail: gauthier@emt.inrs.ca

Telephone: +1 514 228 69 32

Francisco Campos Pérez

Clinical Neuroscience Research Laboratory, Hospital Clínico Universitario, Travesa da Choupana s/n, 15706 Santiago de Compostela, Spain

Email: francisco.campos.perez@sergas.es

Phone: +34 981951097

Fax: +34 981951086

Conflict of interest: None to declare

## **Abstract**

Stroke is a major cause of morbidity, mortality, and disability. During ischemic stroke, a marked and prolonged rise of glutamate concentration in the brain causes neuronal cell death. This study explores the protective effect of a bioconjugate form of glutamate oxaloacetate transaminase (hrGOT), which catalyzes the depletion of blood glutamate in the bloodstream for ~6 days following a single administration. When treated with this bioconjugate, a significant reduction of the infarct volume and a better retention of sensorimotor function was observed for ischemic rats compared to those treated with saline. Moreover, the equivalent dose of native hrGOT yielded similar results to the saline treated group for some tests. Targeting the bioconjugate to the blood-brain-barrier did not improve its performance. The data suggest that the bioconjugates draw glutamate out of the brain by displacing homeostasis between the different glutamate pools of the body.

**Keywords:** Angiopep-2, Aspartate aminotransferase; Brain targeting; Efflux; Excitotoxicity; Glutamate oxaloacetate transaminase; PEGylation; Stroke.

## 1. Introduction

Stroke is the second leading cause of death and the third leading cause of disability in the world.<sup>143</sup> According to the World Health Organization, ~5.7 M deaths and 16 M first-ever strokes occurred in 2005 and these numbers may reach 7.8 M and 23 M by 2030, respectively.<sup>438</sup> Current therapeutic approaches for this disease are limited to pharmacological or mechanical recanalization treatments (<15-20% of patients) and unfortunately, even in the best of cases, 80% of stroke patients receive no treatment whatsoever. As a result, less than 40% of stroke patients have good clinical outcomes. After ischemic stroke, a rapid increase of extracellular glutamate levels results in a permanent influx of calcium and sodium, an overdepolarization of the postsynaptic neuron, and ultimately neuronal death through excitotoxicity.<sup>439,440</sup> Glutamate, the major excitatory neurotransmitter in the brain, is functionally involved in almost all activities of the nervous system but is especially important for learning, memory, and behavior. Unlike other neurotransmitters, the regulation of extracellular glutamate is unique in that there are no extra-synaptic enzymes for its degradation.<sup>441</sup> Instead, homeostasis of the extracellular glutamate concentration is maintained through cellular fast uptake by transporters. Consequently, substantial effort has been devoted to develop protective drugs that either inhibit glutamate receptors (e.g., N-methyl-D-aspartate receptor [NMDA] receptor antagonists) or to reduce the increase of calcium ions within neurons (e.g., blockers of voltage sensitive calcium channels). Unfortunately, the administration of such molecules leads to serious clinical side effects. For example, in the case of NMDA receptor antagonists, the lack of discrimination between the diverse actions of the receptor interferes with both the negative and positive aspects of its signalling.<sup>440,442</sup> Furthermore, NMDA antagonists affect glutamate transporters that reside in many extra-cerebral peripheral tissues and play an important role in the metabolic regulation of glutamate.<sup>443-445</sup>

In light of the shortcomings of the current therapeutic approaches and the central role of glutamate in the ischemic cascade, an alternative therapeutic strategy is necessary to address glutamate excitotoxicity. One such approach relies on exploiting the natural diffusion of cerebral glutamate across the BBB for therapeutic purposes. This is an emerging, conceptually novel protective strategy to reduce the excitotoxic effect of excess extracellular glutamate that accumulates in the brain after ischemic damage. The blood/brain glutamate scavenging mechanism is based on depleting blood glutamate to increase the natural glutamate concentration gradient between the brain and the blood, thereby promoting the efflux of extracellular brain glutamate towards the blood. The main advantage of this strategy is that it involves manipulation of blood chemistry (outside the brain), and therefore does not affect normal brain neurophysiology as happened with drugs antagonists against glutamate receptors. This differs significantly from other drug treatments used to address glutamate

excitotoxicity. One of the most efficient pharmacological strategies developed to scavenge blood glutamate consists on the exogenous administration of the blood-resident enzyme, glutamate oxaloacetate transaminase 1 (GOT1, clinically known as well as aspartate aminotransferase [AST]). GOT1 has a critical role in the regulation of glutamate levels in blood by catalyzing the reversible transformation of oxaloacetate and glutamate to aspartate and  $\alpha$ -ketoglutarate. Thus, the administration of the purified recombinant form of human GOT1 (hrGOT) in ischemic animal models leads to metabolization and reduction of glutamate in the blood and consequently also in the cerebral parenchyma, which is associated with a reduction of the ischemic lesion and better sensorimotor recovery.<sup>65,441,446</sup> However, one major shortcoming of this approach is that the effect of hrGOT administration is short-lived (~3 hours), compared with the therapeutic time window required to attenuate glutamate toxicity in brain (~6–9 hours after stroke), mainly because of its rapid degradation in the body.<sup>316</sup> In this context, repeated administration or continuous infusion of hrGOT could extend the therapeutic dose of the treatment, though the use of high amounts of a recombinant protein such as hrGOT is not always desirable because of the risk of an immune response. Moreover, although attempts to reduce glutamate levels in the blood are of great importance, the proposed mechanism of protection – glutamate efflux – has not been completely elucidated. Indeed, while it has been shown that high blood GOT levels yield better neurological outcomes, the overexpression of GOT in the brain of ischemic mice has also been shown to reduce the volume of the ischemic stroke lesion, attenuate neurodegeneration, and improve post-stroke sensorimotor function.<sup>310</sup> As such, targeting hrGOT to the brain may have a greater localized effect on the brain glutamate pool, leading to better protection.

This study is the first to evaluate protection of the brain after ischemic stroke using protein bioconjugates with sustained activity in the bloodstream following a single administration. As the transport across the BBB of various drugs or carriers remains a great challenge, the described therapeutic strategy represents a promising paradigm for treating glutamate-brain diseases. Substantially greater protection was achieved using the hrGOT bioconjugates compared to the native hrGOT, in terms of infarct size and retention of motor functions using sensorimotor tests, which are important clinical outputs. Moreover, insight into the mechanism of protection (glutamate efflux) as well as factors for improving the therapy are assessed by examining glutamate levels in the blood and CSF, as well as by targeting the hrGOT bioconjugates to the BBB in order to explore a possible localized effect on the brain.

## 2. Material and methods

### 2.1 Reagents.

Amicon ultra centrifugal filter units (molecular weight cut-off [MWCO] 30 kDa), dimethyl sulfoxide (DMSO), potassium phosphate monobasic, potassium phosphate dibasic, sodium tetraborate decahydrate, sodium acetate, o-phathaldialdehyde, 2-mercaptoethanol, and deuterium oxide (D<sub>2</sub>O) were purchased from Sigma Aldrich (Oakville, Canada).  $\alpha$ -Methoxy,  $\omega$ -succinimidyl carboxymethyl ester PEG (mPEG-NHS; 5 kDa) and  $\alpha$ -maleimide,  $\omega$ -succinimidyl carboxymethyl ester PEG (Mal-PEG-NHS; 5 kDa) were purchased from JenKem Technology (Plano, USA). Aspartate Aminotransferase Activity Assay Kits were purchased from Abcam (Cambridge, UK). Angiopep (TFFYGGSRGKRNNFKTEEYC; 2.4 kDa) was purchased from Zhejiang Ontores Biotechnologies (China). Mini-PROTEIN TGX Stain-Free Precast Gels (4–15% acrylamide) and Bio-Rad precision plus protein unstained standards were purchased from Bio-Rad (Saint-Laurent, Canada). BD Microtainer<sup>®</sup> blood collection SST tubes and BD IV catheter Insyte 24GA × 0.75" YLW BX/50 were purchased from Becton Dickinson (New Jersey, USA). All buffers were prepared using MilliQ water (mean resistivity 18.2 M $\Omega$ ·cm). All chemicals were purchased at the highest grade possible and used as received. hrGOT (~1kU/mg) was used.

### 2.2 Synthesis of mPEG–hrGOT and Angiopep–PEG–hrGOT.

To prepare mPEG–hrGOT, a 3-mL solution of hrGOT (7 mg·mL<sup>-1</sup>) was prepared in potassium phosphate buffer (100 mM, pH 7.2). To this solution was added mPEG–NHS (50 eq.) and the reaction mixture was mildly stirred for 30 min at room temperature in a sealed glass vial. After this period, mPEG–hrGOT was purified by size-exclusion chromatography (SEC) using an ÄKTA Start fast protein liquid chromatographer (FPLC) equipped with a HiPrep 16/60 Sephacryl<sup>™</sup> S200 HR column (**Figure S1a**). Filtered (0.2  $\mu$ m) potassium phosphate buffer (100 mM, pH 7.2) was used to elute samples at a flow rate of 0.8 mL·min<sup>-1</sup>. The column was equilibrated for 0.2 column volumes (CV) before sample injection and elution occurred over 120 mL (1 CV) while continuously collecting 4 mL fractions. To prepare Angiopep–PEG–hrGOT, hrGOT was modified with Mal–PEG–NHS and purified according to the procedure above. Following purification by SEC, the collected fractions containing Mal–PEG–hrGOT (**Figure S1b**) were concentrated by centrifugal dialysis (MWCO 30 kDa) and added directly to a vial containing Angiopep (2 eq. relative to the expected amount of Mal on the conjugate). The solution was left for 30 min at room temperature, then incubated for 24 hours at 4 °C in the dark. Angiopep–PEG–hrGOT was isolated from residual Angiopep by centrifugal dialysis (MWCO 30 kDa) at 5000 *g* for 60 min at 4 °C. The conjugates were stored frozen at –20 °C until used.

To determine the degree of PEGylation of the bioconjugates, SDS–PAGE was performed. hrGOT (5 µg in 3 µL water) and hrGOT bioconjugates (5 µg protein in 3 µL water) were mixed with 5 µL of loading buffer (65 mM Tris-HCl, pH 6.8, 2% SDS, 10% glycerol, and 0.1% bromophenol blue). Gels were run in Tris/glycine/SDS (3.0/14.4/1.0 g·L<sup>-1</sup>) buffer pH 8.3, under constant voltage (100 V) for ~90 min. The gels were imaged using an UVP Biodoc-it imaging system running UVP VisionWorksLS™ software.

The degree of PEGylation was determined by <sup>1</sup>H NMR spectroscopy using a Bruker Av300 spectrometer operating at 300 MHz for protons, as described elsewhere.<sup>447</sup> This parameter was also determined by UV-Vis spectroscopy. For this, a known mass of bioconjugate was dissolved in a known volume of distilled water. The number of moles of the hrGOT component of the bioconjugate in the solution was determined *via* the absorbance at 280 nm and the extinction coefficient of hrGOT (140,000 M<sup>-1</sup> cm<sup>-1</sup>). Dividing the mass of the bioconjugate by the number of moles of the hrGOT component yields the molecular weight of the bioconjugate, from which can be determined the degree of PEGylation ( $[MW_{\text{Bioconjugate}} \text{ (kDa)} - MW_{\text{hrGOT}} \text{ (kDa)}] \div MW_{\text{PEG}} \text{ (5 kDa)}$ ). mPEG does not absorb significantly at this wavelength and thus does not interfere with quantification of molecular weight in this manner.

The molecular weight distribution of the bioconjugates was analyzed by aqueous SEC using an Agilent Technologies 1260 HPLC equipped with two Agilent Bio-SEC5 columns mounted in series (5 µm, 7.8 × 300 mm), with 1000 Å and 2000 Å nominal pore sizes, a 1200 Infinity photodiode array detector VL, and a 1290 Infinity II evaporative light scattering detector (ELSD). One hundred-µL of a 0.5 mg·mL<sup>-1</sup> sample solution prepared in ammonium formate buffer (100 mM, pH 3.5) was injected and eluted with ammonium formate buffer (100 mM, pH 3.5) at 1 mL·min<sup>-1</sup> at 25 °C.

### **2.3 Animals, surgical procedures, and inclusion criteria.**

Experimental protocols were approved by the local Animal Care Committee according to the requirements of the European Union (86/609/CEE, 2003/65/CE and 2010/63/EU). Male Sprague–Dawley rats (Harlan Laboratories, Barcelona, Spain) weighing 250–300 g (8–10 weeks old) were housed individually at an environmental temperature of 23 °C with 40% relative humidity and had a 12 hours light–dark cycle. They were watered and fed *ad libitum*. All surgical procedures were performed under sevoflurane anesthesia (6% induction and 4% maintenance in a mixture of 70% NO<sub>2</sub> and 30% O<sub>2</sub>). Rectal temperature was maintained at 37 ± 0.5 °C during surgery using a thermostat-controlled electric pad (Neos Biotec, Pamplona, Spain).

Transient focal ischemia was induced in rats by transient middle cerebral artery occlusion (MCAo) following surgical procedures previously described.<sup>65,448</sup> Briefly, under an operating

microscope, following a midline neck incision, the left common, the external, and the internal carotid arteries were separated from the connective tissues. Using a 5–0 silk sutures, the left external carotid artery as well as the pterygopalatine artery of the internal carotid were ligated. A silicon rubber-coated size 4–0 monofilament (diameter 0.19 mm, length 23 mm; diameter with coating  $0.37 \pm 0.02$  mm; coating length 3–4 mm) (Docol Corporation, Sharon, MA) was inserted into the stump of the left common carotid artery and advanced into the internal carotid artery to 20 mm from the bifurcation to occlude the origin of the MCA. The suture was removed after 75 min of occlusion. A laser Doppler flow probe (tip diameter 1 mm) attached to a PeriFlux 5000 Laser Doppler Flowmeter (Perimed AB, Stockholm, Sweden) was placed over the thinned skull in the MCA territory (4 mm lateral to bregma) to obtain a continuous measure of relative cerebral flow during the experiment. Occlusion and reperfusion were monitored by laser doppler monitoring and by diffusion weighed imaging (DWI) by MRI. In combination with DWI, magnetic resonance angiography (MRA) was performed to ensure that the artery remained occluded throughout the procedure and to confirm the exclusive occlusion of the MCA. Ischemic lesions were determined from  $T_2$  maps, according with the MCAo model described in our previous study.<sup>449</sup>

Experimental procedures were performed following five criteria derived from the Stroke Therapy Academic Industry Roundtable (STAIR)<sup>450</sup> group guidelines for pre-clinical evaluation of stroke therapeutics: (1) cerebral serum flow was monitored to confirm the vascular occlusion as an index of the reliability of the ischemic model; (2) animals were randomly assigned to treatment groups of the study; (3) researchers were blinded to treatment administration; (4) researchers were blinded to treatments during result assessment; and (5) temperature was controlled during the ischemic period. The only animals included in this study had: (1) cerebral serum flow reduction of  $>70\%$  by laser Doppler monitoring; (2) DWI hemispheric infarct volume between 30% and 45% (indicated as the percentage of ischemic damage with respect to the ipsilateral hemisphere volume); (3) MRA of the MCAo; and (4) complete reperfusion ( $>60\%$ ) after MCAo.

In this study, a total of 46 animals were included. Four animals were excluded because of bleeding and spontaneous death during surgery. Based on doppler monitoring, the remaining animals ( $n = 42$ ) had successful MCAo ( $>70\%$  with respect to the basal level). However, when these animals were analyzed by MRA during arterial occlusion, 13 were excluded because both the MCA and the anterior cerebral artery had been occluded. Moreover, when DWI was performed on the remaining 29 animals, 9 of them were excluded because the infarcted regions were out of the established range (35–45%). The DWI volume of 20 rats that were ultimately included in the study was  $41.3 \pm 5.4\%$ .

### **3.4 Pharmacokinetics and pharmacodynamics in healthy rats.**

Groups of three healthy rats were administered 1 mg·kg<sup>-1</sup> (protein equivalent) of hrGOT, mPEG–hrGOT, or Angiopep–PEG–hrGOT in 1 mL sterile saline by intravenous injection *via* the tail vein. Control groups (n = 3 each) received either 1 mL of saline (0.9% of NaCl) or 1.3 mg·kg<sup>-1</sup> mPEG (equivalent to the amount administered for the bioconjugates, *vide infra*). Approximately 300 µL of blood was sampled from the tail vein repeatedly over a period of one month (1, 2, 4 and 6 hours, 1, 2, 4, 6, 8, 14, 21, and 30 days). To investigate the efflux hypothesis, CSF was collected from rats treated with 1 mg·kg<sup>-1</sup> (protein equivalent) hrGOT, mPEG–hrGOT, or sterile saline (control). The CSF was obtained from the cistern magna and was carried out using the protocol described by Pegg et al.<sup>451</sup> Briefly, using the occipital crest as a reference point, a midline incision was made beginning between the ears and ending approximately 2 cm caudally. The fascia was retracted, and muscles were dissected until the cistern magna was exposed, which appeared as a tiny inverted triangle, outlined by the cerebellum above and the medulla below, behind the translucent dural membrane. Once the cistern magna was identified, a glass capillary was inserted and a volume of 3–5 µL of CSF was collected at every puncture. CSF was collected at different time points, transferred to a tube, and kept frozen at –80 °C until used.

### **3.5 Pharmacokinetics in ischemic rats and protective study.**

Rats were randomly attributed to one of four experimental groups (n = 5 each): Saline, hrGOT (1 mg·kg<sup>-1</sup> protein), mPEG–hrGOT (1 mg·kg<sup>-1</sup> protein), or Angiopep–PEG–hrGOT (1 mg·kg<sup>-1</sup> protein). Treatments were administered *via* tail vein injection immediately after reperfusion. The serum GOT activity was determined under basal conditions (before surgery) and at different times after reperfusion (1 and 6 hours, 1, 2, 3, 4, 6, 8, 14, 21, and 30 days). T<sub>2</sub>-weighted (T<sub>2</sub>W) images were acquired at different time points (1, 3, 7, 14, 21, and 30 days) after the onset of ischemia. Recovery of functionality was studied by means of the cylinder and accelerated rotarod tests, which were carried out under basal conditions (before surgery) and 3, 7, 14, 21, and 30 days after ischemia.

### **3.6 Analysis of GOT activity in serum and CSF.**

Blood samples were collected in test tubes and immediately centrifuged at 3,000 rpm for 7 min for collection of serum that was stored frozen (–80 °C) until analyzed. GOT activity, in serum and CSF, was determined by means of an Aspartate Aminotransferase activity assay kit (Abcam, Cambridge, UK) following the manufacturer's recommended protocol.

### 3.7 Monitoring of glutamate concentration in serum and CSF by HPLC.

The concentration of glutamate was determined using a pre-column derivatization high performance liquid chromatography (HPLC) method. For serum, samples (7.5  $\mu\text{L}$ ) were deproteinized with 30  $\mu\text{L}$  ice-cold methanol. The solution was vortexed and then centrifuged at 20,000  $g$  for 5 min at 4  $^{\circ}\text{C}$ . The pellet was discarded and 25  $\mu\text{L}$  of the supernatant was collected and mixed with 5  $\mu\text{L}$  20% SDS in water and 25  $\mu\text{L}$  0.1 M sodium tetraborate (pH 9.5). Thereafter, 50  $\mu\text{L}$  o-phathaldialdehyde/2-mercaptoethanol derivatization solution (freshly prepared by dissolving 50 mg of o-phathaldialdehyde in 1.25 mL of absolute methanol, followed by the addition of 50  $\mu\text{L}$  of 2-mercaptoethanol and 11.2 mL of 0.1 M sodium tetraborate, pH 9.5) was added and mixed thoroughly. Subsequently, 50  $\mu\text{L}$  of 1 M sodium acetate (pH 7.2) was added and the mixture was injected onto the equilibrated HPLC column. For the CSF, the same volume ratios were followed using a sample volume of 3.5  $\mu\text{L}$ . A gradient elution of 40 mM  $\text{NaH}_2\text{PO}_4$  (pH 7.8) and acetonitrile: methanol: water (45:45:10, v/v/v) with a flow rate of 2  $\text{mL}\cdot\text{min}^{-1}$  was employed. The gradient was (% 40 mM  $\text{NaH}_2\text{PO}_4$ ) (% acetonitrile: methanol: water): 0 min (100), 1.9 min (100), 18.1 min (43), 18.6 min (0), 22.3 min (0), 23.2 min (100), and 26 min (100). Analytes were separated at  $30 \pm 2$   $^{\circ}\text{C}$  on a ZORBAX Eclipse AAA  $\text{C}_{18}$  reverse-phase column (4.6  $\times$  150 mm, 3.5  $\mu\text{m}$ ) and detected by fluorescence ( $\lambda_{\text{ex}} = 340$  nm and  $\lambda_{\text{em}} = 450$  nm). A glutamate standard curve was established with concentrations ranging between 0 and 400  $\mu\text{M}$  (**Figure S2**). All determinations were performed at least in duplicate. A typical HPLC chromatogram is shown in **Figure S3**. Note: minimal loss of glutamate was observed during protein precipitation by comparing precipitation using different organic solvents and acids as well as ultrafiltration (instead of protein precipitation); and bioconjugates were also removed during this step, owing to their absence in the chromatograms used for glutamate quantification.

### 3.8 Magnetic resonance imaging and image analysis.

MRI studies were conducted on a 9.4 T horizontal bore magnet (Bruker BioSpin, Ettlingen, Germany) with 12-cm wide actively shielded gradient coils (440  $\text{mT}\cdot\text{m}^{-1}$ ). Radiofrequency (RF) transmission was achieved with a birdcage volume resonator and signal was detected using a four-element arrayed surface coil positioned over the head of the animal. The latter was fixed with a teeth bar, earplugs, and adhesive tape. Transmission and reception coils were actively decoupled from each other. Gradient-echo pilot scans were performed at the beginning of each imaging session for accurate positioning of the animal inside the magnet bore. Apparent diffusion coefficient (ADC) maps were acquired during MCAo (75 min after the onset of ischemia) from diffusion-weighted images (DWI) using a spin echo echo-planar imaging sequence (DTI-EPI) with the following acquisition parameters: echo time (ET) = 24.89 ms,

repetition time (RT) = 4.5 s, spectral bandwidth (SW) = 200 kHz, 7 b-values of 0, 300, 600, 900, 1200, 1600, and 2000 s·mm<sup>-2</sup>, flip angle (FA) = 90°, number of averages (NA) = 3, 14 consecutive slices of 1 mm, 24 × 16 mm<sup>2</sup> FOV (with saturation bands to suppress signal outside this FOV), a matrix size of 96 × 64 (isotropic in-plane resolution of 250 μm·pixel<sup>-1</sup> × 250 μm·pixel<sup>-1</sup>) and implemented with fat suppression option. MCAo status was evaluated in a non-invasive manner with the time-of-flight MRA (TOF-MRA). The TOF-MRA scan was performed with a 3D-Flash sequence with an ET = 2.8 ms, RT = 15 ms, FA = 30°, NA = 2, SW = 98 kHz, 1 slice of 14 mm, 30.72 × 30.72 × 14 mm<sup>3</sup> FOV (with saturation bands to suppress signal outside this FOV), a matrix size of 256 × 256 × 58 (resolution of 120 μm·pixel<sup>-1</sup> × 120 μm·pixel<sup>-1</sup> × 241 μm·pixel<sup>-1</sup>) and implemented without fat suppression option. The progression of ischemic lesions and infarct volumes were determined from T<sub>2</sub>-maps calculated from T<sub>2</sub>W images acquired 1, 7, 14, 21, and 30 days after the onset of ischemia using a MSME sequence with an ET = 9 ms, RT = 3 s, 16 echoes with 9 ms echo spacing, FA = 180°, NA = 2, SW = 75 kHz, 14 slices of 1 mm, 19.2 × 19.2 mm<sup>2</sup> FOV (with saturation bands to suppress signal outside this FOV), a matrix size of 192 × 192 (isotropic in-plane resolution of 100 μm·pixel<sup>-1</sup> × 100 μm·pixel<sup>-1</sup>) and implemented without fat suppression option. All images were processed, and maps were constructed with ImageJ (<https://imagej.nih.gov/ij/>). Infarct volumes were determined from ADC maps and T<sub>2</sub> relaxation maps by manually selecting areas of reduced ADC values or hyperintense T<sub>2</sub> signal by a researcher blinded to the animal protocols.<sup>449</sup> Infarct size was indicated as the percentage of ischemic damage with respect to the ipsilateral hemispheric volume, corrected for brain edema. For each brain slice, the total areas of both hemispheres and the areas of infarction were calculated. An edema index was measured by quantifying the midline deviation (MD) calculated as the ratio between the volume of the ipsilateral hemisphere and the volume of the contralateral hemisphere. The actual infarct size was adjusted for edema by dividing the area of infarction by the edema index [mm<sup>3</sup>/MD]. Thereafter, the presented infarct volume was calculated as following: (infarct volume [mm<sup>3</sup>/MD]/ipsilateral hemispheric area [mm<sup>3</sup>]) × 100. These procedures have been used repeatedly in the literature to measure and evaluate stroke outcome in experimental models.

### **3.9 Motor and somatosensory tests.**

To examine the effect of hrGOT, mPEG–hrGOT, and Angiopep–PEG–hrGOT on functional outcomes of ischemic rats, a battery of behavioral tests was performed pre-MCAo and at 3, 7, 14, 21, and 30 days post-MCAO by an independent investigator blinded to the experimental groups. All tests were performed during the darkness cycle of animal housing.<sup>452,453</sup>

For the cylinder test, somatosensory deficits were evaluated by examination of the asymmetry of limbs during exploratory activity. For this test, rats were introduced in a Plexiglas cylinder

(diameter 20 cm; height 40 cm) and a video camera located under this transparent cylinder was used to record the vertical exploratory movement of the rats during 5 min. For the analysis, the VirtualDub software was used and, during slow-motion video playback, instances of the sole use of the ipsilateral or contralateral forelimb or the simultaneous bilateral use of both forelimbs for upright support were recorded. Following each forelimb placement, the subsequent movements (such as lateral exploration) were not scored until the rat returned to the ground, the next placement was then scored. Forelimb contacts while rearing up were scored with a total of 10 contacts recorded for each animal. Laterality index was calculated as following: (number of times that the animal touches the cylinder with the impaired forelimb during the ascendant movement divided the number of total forelimb contacts) ×100. This index is close to 50% for healthy animals and tends to be 0 or 100% for animals that have a preferential use of the left or the right paw, respectively.

The accelerating rotarod test was performed using rotarod apparatus (47650, Ugo Basile, Comerio, Italy) to evaluate motor balance and coordination impairment. Before surgery, the animals were pre-trained for 7 consecutive days (each animal received three training sessions per day). Rats were placed on the rotarod and the speed of the spindle was slowly increased from 5 to 40 rpm over a period of 5 min. All animals were required to stay on the accelerating rotarod for a minimum of 180 seconds. If they were unable to reach this criterion, the trial was repeated for a maximum of 5 times instead of 3 times. Animals achieving the baseline criteria were included from the subsequent study. After surgery, the time that an animal was able to hold itself on the spindle was recorded as the latency to fall. The average of the three fall latency values was used for analysis and the motor test data were presented as percentage of mean latency compared with the internal baseline (prior to surgery, considered as 100%).

**3.10. Statistics.** Results from pharmacokinetic data were compared by one-way ANOVA followed by a Tukey post-hoc test. Infarct volume and motor tests data were compared by repeated measures ANOVA followed by a Bonferroni post-hoc test was used. p values considered for statistically significance are identified in relevant figure legends.

## **4. Results**

### **4.1 Bioconjugate design for sustained blood activity and BBB-targeting**

HrGOT is a dimeric protein composed of two identical monomers, each with a molecular weight of ~46 kDa.<sup>454</sup> As seen in **Figure 1a**, the lysine residues of hrGOT (green) are homogeneously distributed on the surface of the protein and were selected as targets for random modification with methoxy poly(ethylene glycol) (mPEG). Dimeric hrGOT possesses 46 pendant amino groups (i.e., 44 lysine residues and 2 N-termini), though only 22 are predicted to be solvent-accessible from the protein's crystal structure (**Table S1**). These were quantitatively modified

with either amino-reactive mPEG (5 kDa) or  $\alpha$ -maleimide,  $\omega$ -succinimidyl carboxymethyl ester PEG (Mal-PEG-NHS; 5 kDa) as determined by two complementary methods that were in good agreement with one another (**Figure 1a**). Thus, the bioconjugates bore ~22 polymer chains and possessed monomodal size-distribution profiles with dispersities ( $\mathcal{D}$ ) in the range of 1.4–1.9 (**Figure 1b**). To target hrGOT to the BBB and potentially promote transport into the brain, the terminal maleimide groups on Mal-PEG-hrGOT were modified with a brain-targeting peptide Angiopep-2, which possesses a single thiol group. Angiopep-2 is a 19-amino acid peptide derived from the common sequence of the low-density lipoprotein receptor-related protein-1 (LRP1) ligands. It is used to target a wide variety of nanocarriers, proteins, or genetic material to the central nervous system.<sup>455</sup> LRP1 is highly-expressed on the luminal side of the BBB and exhibits higher transcytosis efficacy and parenchymal accumulation than other receptors, including those for transferrin, lactoferrin, and avidin.<sup>456</sup> Grafting of Angiopep-2 to the protein bioconjugate was quantitative by <sup>1</sup>H NMR spectroscopy (*via* the disappearance of the peak at 6.86 ppm; **Figure 1d**) and resulted in an increase in hydrodynamic size as observed by size-exclusion chromatography (**Figure 1b**). SDS-PAGE analysis of hrGOT bioconjugates under denaturing conditions is shown in **Figure 1c**. Two populations of bands were observed for the bioconjugates, representing both the monomeric or dimeric protein (due to incomplete denaturation) modified with polymer chains. No residual unmodified protein was observed, and the size of both bioconjugate populations increased slightly upon modification with Angiopep-2.

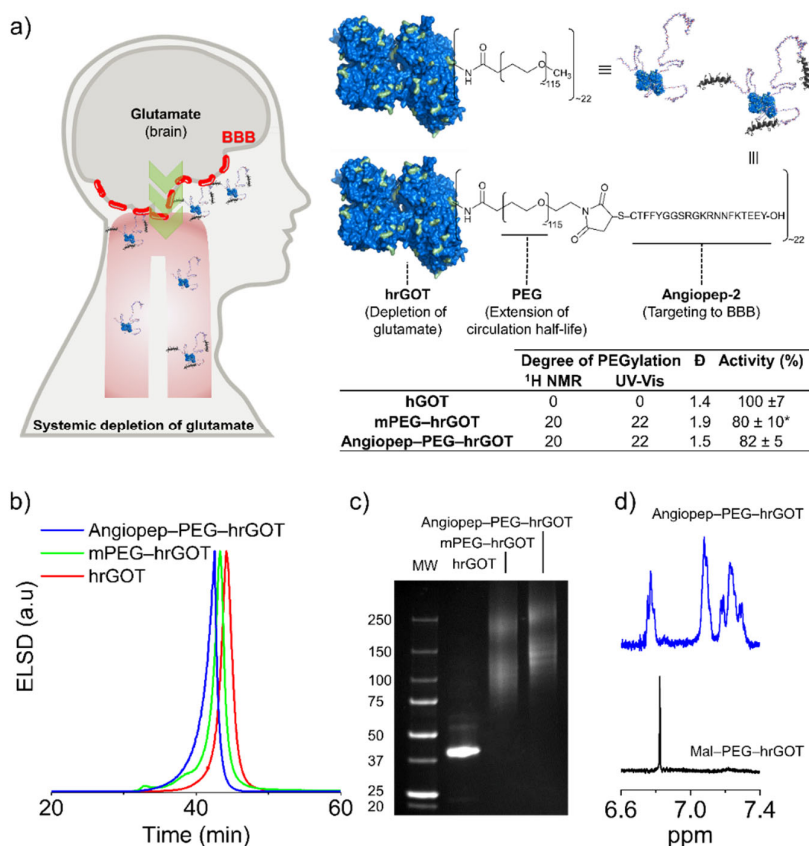


Figure 1| **Design and characterization of protective bioconjugates.** (a) hrGOT was modified with mPEG or PEG bearing terminal Angiopep-2 ligands, with low loss of catalytic activity. The bioconjugates were designed for extended blood circulation and for BBB accumulation (*via* Angiopep-2). The degree of PEGylation was determined by UV-Vis and <sup>1</sup>H NMR spectroscopy. Dispersity was determined by size-exclusion chromatography. Representative (b) size-exclusion chromatograms and (c) SDS-PAGE of the bioconjugates. (d) <sup>1</sup>H NMR spectra demonstrating quantitative modification of maleimide groups with Angiopep-2. ELSD: evaporative light scattering detector. In pane (a), the star denotes a statistically significant difference with respect to native hrGOT (ANOVA, Tukey,  $p < 0.05$ ). Data presented as Mean ± SD,  $n = 3$ .

GOT catalyzes the reversible reaction of L-aspartate and  $\alpha$ -ketoglutarate into oxaloacetate and L-glutamate *via* a ping-pong mechanism, with pyridoxal 5-phosphate as an essential cofactor.<sup>306</sup> Considering that PEGylation is often associated with loss of catalytic activity,<sup>382</sup> the activity of mPEG-hrGOT and Angiopep-PEG-hrGOT was analyzed by an aspartate aminotransferase assay. Both bioconjugates possessed ~80% of the activity of the native protein (**Figure 1a**). To examine the effect of polymer conjugation on blood exposure, equivalent amounts of native hrGOT, mPEG-hrGOT, or Angiopep-PEG-hrGOT (protein basis, similar activity) were intravenously injected into healthy and ischemic rats. Blood was then withdrawn over a period of 30 days to analyze pharmacokinetics and pharmacodynamics.

Note that prior to inducing the ischemic lesion by MCAo, there were no significant differences in endogenous GOT activity between the different treatment groups. As illustrated in **Figure 2a**, the initial activity (<1 h) for the hrGOT and bioconjugates groups were similar, in line with the similar enzymatic activity of hrGOT bioconjugates and native hrGOT, as discussed above. Native hrGOT was rapidly cleared from the body of both healthy and MCAo rats, with complete loss of activity in under 6 hours. Moreover, no difference was observed between the saline group and the free mPEG group, indicating that mPEG itself has no effect on the enzymatic activity of endogenous GOT. In contrast, the administration of mPEG–hrGOT and Angiopep–PEG–hrGOT maintained high levels of GOT activity between 3–6 kU·L<sup>-1</sup> over a period of ~6 days. This suggests a tentative protection of hrGOT from degradation (by serum proteases), as has been shown for other PEGylated proteins.<sup>457,458</sup> Very little difference, if any, was observed between the mPEG–hrGOT and Angiopep–PEG–hrGOT groups. The pharmacokinetic profiles observed in healthy rats were also very similar to those observed for ischemic rats (**Figure 2b**), with negligible differences in half-lives of circulation/elimination or in area under the curves (AUCs) (**Table S2**). This suggests that routes of distribution and elimination of the bioconjugates were not affected by MCAo and that the extended blood residence time correlated with a delayed elimination half-life.

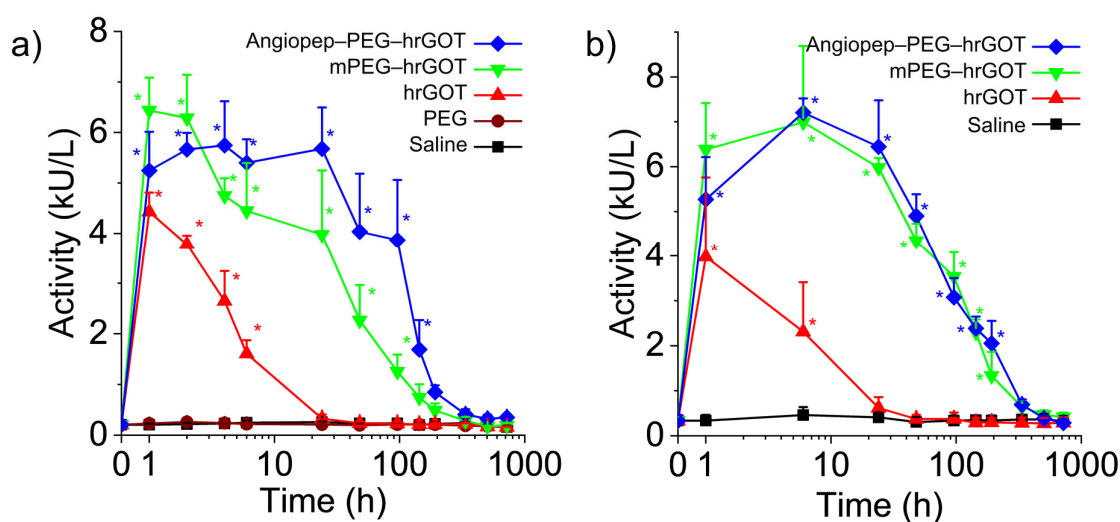


Figure 2| **Blood pharmacokinetics in (a) healthy and (b) MCAo rats.** Stars denote statistically significant differences (ANOVA, Tukey,  $p < 0.05$ ) with respect to the basal GOT activity. Data presented as Mean + SD,  $n = 3-5$ .

## 4.2 Protection

To evaluate the effect of enhanced hrGOT blood exposure imparted by PEGylation, infarct volume was measured by MRI at different times after MCAo. Representative segmented images from a central brain slices for each group are shown in **Figure 3a** to illustrate the evolution of infarct area with time. These slices show the occluded territory of the MCA, which is where the main ischemic region is located. The corresponding full stacks of these images are available in **Table S3** of the Supporting Information. MRI-based infarct size analysis from the full stacks of images was performed at Day 1 and at Days 7, 14, 21, and 30 after ischemic inductions and presented in **Figure 3b**. MRI data determined using ADC maps confirmed similar baseline lesion volumes between 35% and 45% of the ipsilateral hemisphere in all included animals before treatment administration. T<sub>2</sub>W images were used to measure infarct volume (**Figure 3a**). At the dose of hrGOT chosen for these experiments, no statistically significant difference was observed between the hrGOT and saline treated groups, one day after MCAo, in terms of infarct volume. In contrast, treatment with either bioconjugate resulted in a significant ~40% reduction in infarct volume in comparison to saline group ( $p \leq 0.01$ ). From Day 7 onwards, the reduction of the infarct volume remained significant (when compared to saline) and evolved to a lesser extent (for all the groups). When looking closely at the pharmacokinetic curves, one can notice that the enzymatic activity is substantially higher for the bioconjugates than for hrGOT within the first 24 hours after ischemia. Knowing that excitotoxicity is a process that starts within the first few minutes/hours after ischemia, the initial 24 hours are critical for an effective reduction of the cell death. Therefore, maintaining high and sustained enzymatic activity during the initial 24 hours is most likely the explanation for the significant impact of the bioconjugates on the size of the infarct at Day 1. Obviously, this does not exclude the fact that maintenance of such activity during the next few days following ischemia continues to provide neuroprotection, and may also contribute to healing processes yet to be identified. Indeed, at Day 30, the infarct volume for the bioconjugate groups was ~30% of its Day 0 value, compared to ~60% for the saline and hrGOT groups, which is comparable to that obtained with hrGOT elsewhere (combined or not with oxaloacetate).<sup>65</sup> This result thus suggests that sustained GOT activity in the blood, achieved with the bioconjugates, is beneficial for recovery post-MCAo.

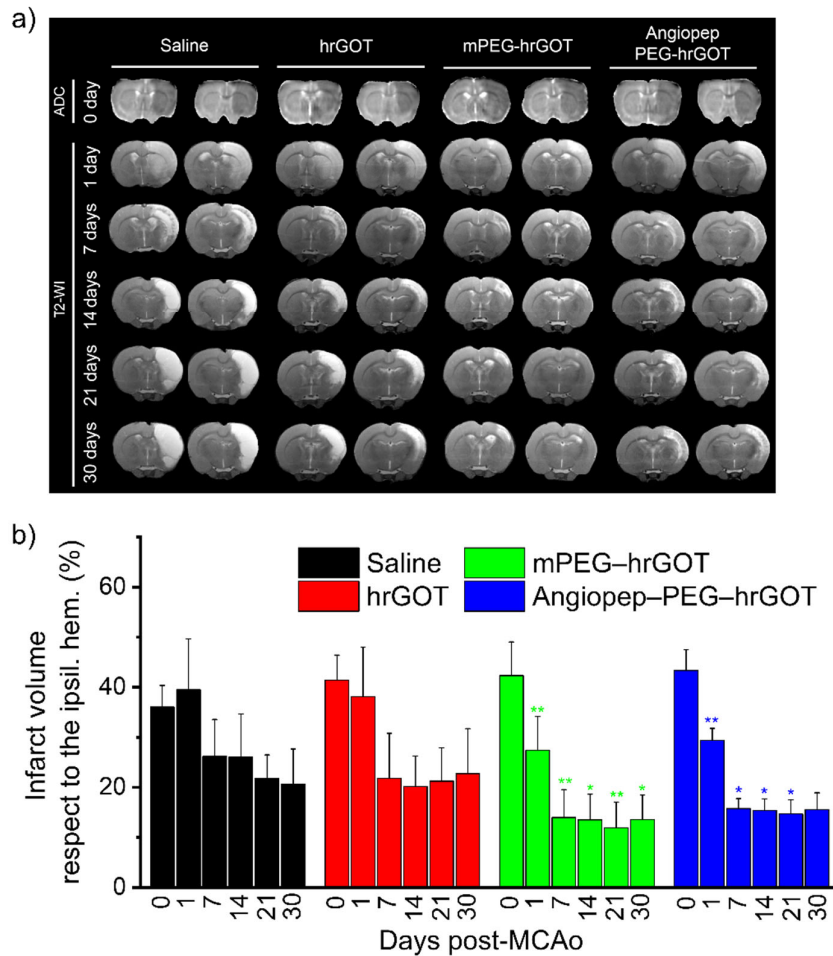


Figure 3| **Protective effects assessed by MRI.** (a) Representative T<sub>2</sub>W images (slices 7-8 at each per time point) for rats post-MCAo (all other slices are in **Table S3**). (b) Infarct expressed as percent infarct of total ipsilateral cortex. Stars denote statistically significant differences with respect to the saline group (Repeated measures ANOVA, Bonferroni, \*:  $p \leq 0.05$ , \*\*:  $p \leq 0.01$ ). Data presented as Mean + SD,  $n = 5$ .

To confirm the protective properties of the bioconjugates, the motor functions of ischemic rats were assessed using the accelerated rotarod and cylinder tests. The sensitivity of the accelerated rotarod test to detect motor impairments in ischemic models has been well established.<sup>452,453</sup> Prior to surgery, all groups spent the same time on the accelerating rotarod and thus the time spent on the apparatus for the different test groups was expressed as a percentage of pre-surgery values (**Figure 4a**). At Day 3, MCAo caused impairment in rotarod performance for the saline and hrGOT treated groups, though not for the bioconjugate groups. Retention time remained relatively stable for all groups until day 21 or 30, after which it decreased for all groups because the rats likely lost their motivation to perform the physical exercise required to remain on the cylinder (lost their fear of falling), which is one of the main limitations of this test. Intriguingly, performance appeared to degrade to a greater extent for

the bioconjugate treated groups compared to the other groups at these late time points. This decline in performance is believed to result from the caveat above rather than from real functional impairment, as it is not seen in the other functional test. Nevertheless, while the data available does not hint towards long term side-effects caused by the sustained depletion of blood glutamate, such a phenomenon cannot be excluded at this stage and should be considered in the context of future toxicological tests. In comparison to the saline group, animals treated with hrGOT bioconjugates displayed a significant increase in the use of contralateral (left) paw ( $p \leq 0.001$ ). Interestingly, rats having received the bioconjugates also showed improved exploratory activity from Day 3 onwards, as evidenced by an increased amount of rearing. Moreover, there was an increase in left forelimb usage for hrGOT-treated rats compared to control animals at Day 7, 14, and 21 (**Figure 4b**). To the best of our knowledge, there is no clear association between functional recovery and the reduction of the lesion size in the literature for the MCAo model employed in this work. For example, several studies have demonstrated that stem cell therapies improve functional outcome without reducing the infarct volume.<sup>459-462</sup> Thus, while the motor tests in the present study mostly reflect the reduction in the volume of the infarct, the possible lack of correlation between these parameters does exist in the literature for this model. Overall, rats that underwent MCAo and were treated with hrGOT bioconjugates had a better recovery than those treated with native hrGOT, which in turn had better recovery than those receiving saline. These combined results confirm that maintaining sustained GOT activity in the blood is an important factor contributing to protection following MCAo.

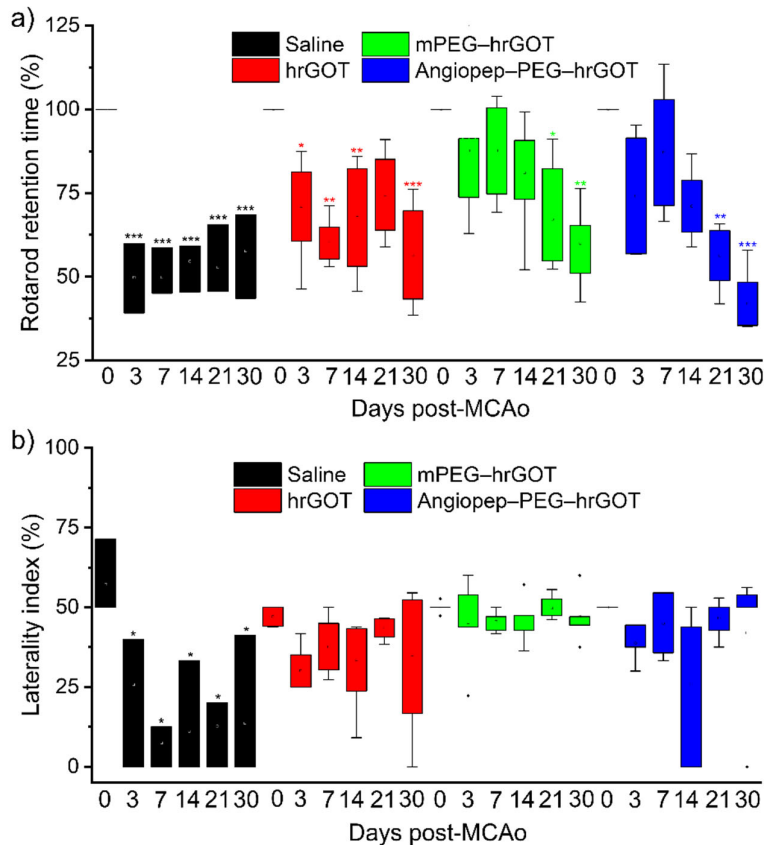


Figure 4| **Protective effects assessed by sensorimotor tests.** (a) Motor deficits evaluated by the accelerating rotarod test and expressed as the percentage of time that rats remained on the rotarod after ischemia compared to pre-ischemia testing. (b) Sensorimotor deficits assessed using the cylinder test and quantified by laterality index as a function of time after MCAo. Stars denote statistically significant differences with respect to pre-ischemia (Repeated measures ANOVA, Bonferroni, \*:  $p \leq 0.05$ , \*\*:  $p \leq 0.01$ , \*\*\*:  $p \leq 0.001$ ). Data presented as Mean + SD,  $n = 5$ .

### 4.3 Glutamate homeostasis

At the administered dose of hrGOT, the steady-state concentration of blood glutamate was not significantly affected by any of the treatments, and thus no correlation between enzymatic activity and blood glutamate levels could be identified (**Figure 2a,b and S4a,b**). This result might suggest a rapid homeostasis between blood and peripheral tissue. Moreover, similar to the observations in blood, no effect on CSF glutamate concentration was observed (**Figure S5**), suggesting once again rapid glutamate homeostasis in the brain. Nevertheless, GOT activity increased very slightly at 2 hours in the CSF after administration of the native protein, possibly indicating that a very small portion of the dose is reaching the CSF (**Figure 5**). It should be noted, however, that the  $\sim 25 \text{ U}\cdot\text{L}^{-1}$  increase observed in the CSF is very small

compared to the 3000–6000 U·L<sup>-1</sup> activity observed in the blood. mPEG–hrGOT, in contrast, did not alter GOT activity in the CSF (not statistically significant) suggesting that the presence of the polymer corona prevented passage through the brain or the blood–cerebrospinal fluid barrier. The non-variation of glutamate CSF levels following administration of either hrGOT or mPEG–hrGOT can be rationalized by the glutamate homeostasis system existing in the different parts of the central nervous system including the BBB, the circumventricular organs, and the choroid plexus.<sup>463</sup> Indeed, the BBB as well as the brain–CSF barrier work in concert to maintain and restore the homeostatic balance of neurotransmitters such as glutamate.<sup>464</sup> The pharmacokinetics/pharmacodynamics observed for the targeted (Angiopep–PEG–hrGOT bearing ~22 copies of Angiopep-2) and non-targeted bioconjugates (mPEG–hrGOT) (**Figure 2a,b and S4a,b**) were not statistically different from one another, suggesting that brain or near-brain accumulation of the targeted bioconjugate represents only a very minor fraction of the total administered dose and does not contribute significantly to the results.

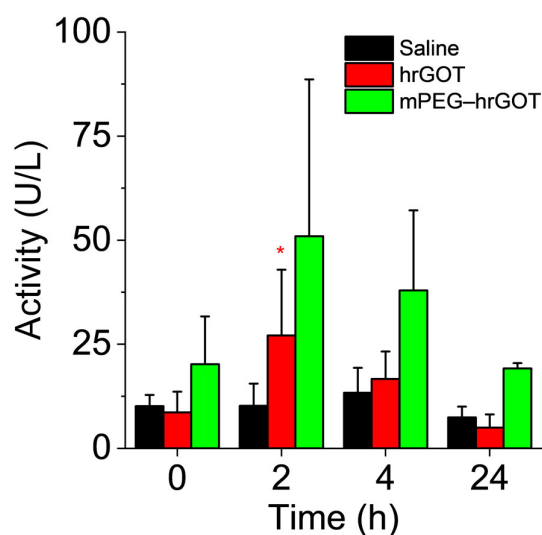


Figure 5| **Pharmacokinetics in CSF.** Saline, hrGOT, and mPEG–hrGOT were administered to healthy rats. The catalytic activity was monitored in CSF samples taken at specific time points. Stars denote statistically significant differences with respect to basal GOT activity of the CSF. (ANOVA, Tukey, \*:  $p < 0.05$ ). Data presented as Mean + SD,  $n = 3–5$ .

## 5. Discussion

Preclinical testing criteria for protective agents define a reduction of the ischemic damage by at least 50%, or even better to 80% before it can be considered for clinical trials.<sup>62</sup> In light of the fact that the hrGOT bioconjugates reduced the infarct size by ~70% relative to its Day 0 value, this protective strategy appears very promising. The increase in circulation half-life from hours to days achieved by modifying hrGOT with polymers promoted blood exposure and increased the therapeutic effect. The rapid clearance of hrGOT might be related to its peripheral uptake. Indeed, previous studies have shown that intravenously administrated <sup>125</sup>I-labeled GOT can be taken up and metabolized by different tissues (liver, spleen, kidney, and intestines). Interestingly, the radioactivity associated with liver and spleen reached its maximum 2 hours post-injection and the time course coincided with that for the plasma clearance in the fast phase.<sup>18</sup> The subsequent decrease in radioactivity of these tissues was accompanied by an increase in urinary radioactivity.<sup>18</sup> Therefore, the prolonged blood residence time of the bioconjugates was likely due to the hindrance of hrGOT uptake by peripheral organs. Moreover, conceivably, the presence of PEG chains around the enzyme surface reduced the immunogenicity of hrGOT (if existent) as well as its rate of proteolytic degradation. Nevertheless, such effects are less prominent than those implicating the liver, spleen, and kidney.

While measuring lesion size provides some evidence of protection, this parameter differs substantially from functional impairment, which is the most important parameter for patients. MCAo results in a marked deficit in neurological function and motor performance, with animals generally demonstrating weakened limbs. Based on numerous rodent studies reporting that lesion size does not necessarily correlate with functional deficits, lesion size alone is insufficient to characterize the protective character of the hrGOT preparations.<sup>453,465-467</sup> The improvement of the motor functions recorded by the accelerated rotarod test following treatment with the bioconjugates was pronounced compared to other groups, and correlated with those obtained by the cylinder test, though a slight difference in the outcomes of the two sensorimotor tests was noticed. Targeting the hrGOT bioconjugates to the BBB, via the appended Angiopep-2 ligands did not have additional therapeutic value compared to stabilizing and increasing the circulation lifetime of hrGOT using mPEG. This result suggests that glutamate transport across the BBB is not the rate-limiting step to protection. Nevertheless, future studies may investigate strategies to achieve brain accumulation, which is very challenging indeed, or explore methods to over-express endogenous GOT directly in the brain so as to investigate whether localized GOT treatment offers enhanced protection by outcompeting glutamate homeostasis with peripheral tissue.

Contrary to what has been reported in some studies,<sup>65</sup> a clear effect of hrGOT or hrGOT

bioconjugates on serum glutamate levels was not observed. It should be noted that many published works do not mention the specific activity of their rhGOT protein, which makes it impossible to compare doses between studies. Future dose escalation studies with the bioconjugates will resolve whether dose is indeed responsible for this discrepancy. Nevertheless, the present results are consistent with the observations from others of a clockwise hysteresis on the pharmacokinetics/pharmacodynamics curves, suggesting that it takes a certain time to deplete peripheral glutamate sufficiently for there to be a noticeable difference in the blood.<sup>468</sup> In general, the homeostasis of glutamate is rapid and maintained through a variety of peripheral transporters and receptors,<sup>67,469</sup> yielding rapid efflux of glutamate towards the blood from organs (e.g., brain) and peripheral tissues. In fact, prior work has shown that the radioactivity of intravenously injected (radioactive) glutamate decayed with a half-life of ~3 min, owing to metabolic reactions occurring in the liver or in the plasma, which provides some insight into the timescale of glutamate homeostasis.<sup>470</sup> This is the most probable explanation for the lack of observable depletion of glutamate in the blood concurrent with neuroprotection in the brain. To investigate whether a more localized effect may be observed, GOT activity and glutamate levels were measured in the CSF of healthy rats receiving either native hrGOT or mPEG–hrGOT. Very little or no effect on the CSF glutamate concentrations was also observed. These results are in accordance with a recently published study showing that the daily administration of recombinant GOT (each 12 hours on days 1–4) reversed the disruption of synaptic plasticity in a rat model of traumatic brain injury by decreasing the glutamate level in hippocampus interstitial fluid, but not ventricular CSF.<sup>61</sup> Overall, these observations provide strong support for the effect of sustained blood glutamate depletion by the bioconjugates on ischemic damage, which merits further investigation. Indeed, these findings raise new questions related to the safety and tolerability of such treatments. Indeed, new protection or healing mechanisms (yet to be identified) may be involved in addition to those expected for hrGOT.

## **6. Conclusions**

Glutamate scavenging strategies are highly suited to overcome many of the drawbacks of the receptor-based therapies (e.g., cognitive impairments, hallucinations and even coma)<sup>471</sup> and this concept is an attractive protective strategy to remove excess glutamate in the brain interstitium. The most significant observation of this study is that maintaining high and relatively stable hrGOT blood activity over a period of several days had a very beneficial effect on infarct volume as well as sensorimotor function.<sup>65,472-474</sup> This was achieved with a single administration of hrGOT bioconjugate. Remarkably, equivalent doses of native hrGOT alone yielded results equivalent to saline controls for certain tests, and did not alter blood or CSF glutamate levels. Overall, the efficacy of this strategy holds great potential as a therapy for stroke,<sup>475</sup> as well as

other pathologies associated with acute excitotoxicity such as spinal cord injury<sup>476</sup> or traumatic brain injury.<sup>61</sup>

## **7. Acknowledgements**

This study was supported by the Natural Science Engineering Council of Canada (NSERC; RGPIN-2015- 76104254), the MITACS Globalink Research Award Program, Bourses d'excellence pour étudiants étrangers (MEES-INRS), Ministère de l'Éducation et de l'Enseignement supérieur of Quebec, and Instituto de Salud Carlos III PI17/01103, ICI19/00032, the Miguel Servet program (CPII19/00020), and the European Union program FEDER and the European Regional Development Fund – ERDF. AZ acknowledges a doctoral scholarship from the INRS/Tunisian Ministry of Education. MAG is a Research Scholar of the Fonds de Recherche du Québec Santé (FRQS, Canada). MP is a Sara Borrell Researcher (CD19/00033). AAG acknowledges postdoctoral scholarships from the Fonds de Recherche du Québec Nature et Technologies (FRQNT) and the Canadian Institutes for Health Research (CIHR). Further, she acknowledges the Chu Family Scholarship for a career award. This study was partially supported by the Spanish Ministry of Economy and Competitiveness (SAF2014-56336-R; SAF2017-84267-R), Xunta de Galicia (GRC2014/027, IN607A2018/3). This project was supported by the FRQS, Instituto de Salud Carlos III (AC19/00066), the Scientific and Technological Research Council of Turkey (TUBITAK), and the Research Council of Norway (RCN), under the frame of EuroNanoMed III.

## **8. Author contributions**

AZ, FC, and MAG designed and conceived the study.

AZ, MP-M, and AD-L performed all experiments, with the help and advice of RI, PH.

AZ, MP-M, FC, and MAG wrote the manuscript.

AZ, MP-M, FC, and MAG discussed the results and their implications and commented on the manuscript at all stages.

All authors have given approval to the final version of the manuscript.

## **9. Supporting Information**

FPLC chromatograms for the purification of the bioconjugates, Glutamate concentration in serum and CSF, Solvent accessibility of lysine residues of hrGOT, Pharmacokinetic profiles, Representative ADC maps and T<sub>2</sub>W images of the 14 consecutive coronal rat brain slices, and Multiple pairwise means comparison tables for Figures 2–5, and S4–5.

## **CHAPTER 5: General Discussion, Conclusion, and Perspectives**

## 1. General discussion

Ischemic stroke is characterized by a multitude of complex processes, of which massive glutamate release plays a key role. Blocking glutamate receptors, a common therapeutic approach, dramatically failed to demonstrate efficacy in clinical trials<sup>477,478</sup>. This has led to a growing interest in developing blood glutamate scavengers. These scavengers stimulate the brain-to-blood glutamate efflux mechanism by reducing the blood glutamate levels and increasing the rate at which excess glutamate is cleared. In this context, investigation of the enzymatic degradation of glutamate (by means of exogenous injection of GOT) has been an emerging approach aiming to reduce the pathological effects of excitotoxicity. Originally, the hypothesis that GOT may exert a neuroprotective role comes from clinical studies demonstrating an association between high blood GOT levels and good outcome in ischemic stroke patients<sup>479,480</sup>. Interestingly, the efficacy of intravenously administered GOT has been demonstrated in different diseases implicating excitotoxicity mechanisms (i.e., ischemia, traumatic brain injury, and glioma)<sup>61,312,481</sup>.

On the other hand, even though GOT has been the sole enzyme used so far to explore its glutamate scavenging properties, other enzymes are able to metabolize glutamate and could potentially represent interesting therapeutics (e.g., GPT, GDH, and glutamate decarboxylase). One particular challenge is that many of these enzymes require co-substrates or cofactors in addition to glutamate<sup>482-485</sup>, and the only enzyme requiring glutamate as its unique substrate is glutamate decarboxylase. However, active mammalian glutamate decarboxylase is not easily available. This, and its relatively low specific activity for glutamate degradation compared with the other enzymes (1–2 U/mg *versus* 50–100 U/mg for GDH and GPT) make its therapeutic use unrealistic<sup>486</sup>. Currently, the major limitation to using glutamate-degrading enzymes as neuroprotectants is their unfavorable pharmacokinetic properties (e.g., rapid serum degradation and/or clearance, cellular uptake followed by proteolytic degradation, etc.)<sup>487</sup>. Conjugation of polymers (such as mPEG) has been investigated as a means to improve the pharmacokinetic and pharmacodynamic profiles of proteins, with studies demonstrating that the *in vivo* half-lives of proteins bearing multiple mPEG chains can be extended from hours to days<sup>488,489</sup>. The purpose of this thesis was to develop multi-PEGylated enzymes (bioconjugates) to treat ischemic stroke. In addition to GOT, we selected GDH as a potential therapeutic enzyme. Our choice was based on *in vivo* studies showing that MCAo mice over-expressing GDH exhibited smaller ischemic lesions and reduced edema volume compared to mice with normal GDH expression<sup>27</sup>. Additionally, allosteric activation of GDH improved the intracellular energy state, diminished the total infarction volume, and decreased animal mortality 24 hours post-ischemia in MCAo mice<sup>28</sup>.

With this in mind, we proceeded to PEGylate these enzymes using 5 kDa mPEG, and observed a substantial decrease of GDH activity in comparison to hrGOT. Concurrently we noticed that despite the large number of multi-PEGylated proteins, the very little research has explored how PEG chains and proteins interact, and how those interactions could affect activity. Therefore, in the first chapter of this thesis, we focused on the rational design and development of a model PEGylated enzyme (multi-PEGylated GDH) to investigate the possible mechanisms of activity loss.

Overall, thirteen different bioconjugates were prepared by randomly targeting the amino groups of GDH. Characterization confirmed the production of a library of bioconjugates possessing about 1, 3, 10, and 25 chains of 0.5 kDa, 2 kDa, and 5 kDa mPEG. PEGylation with 20 kDa mPEG was also attempted, but the maximum degree of PEGylation was 3 polymers per enzyme. This was in accordance with the majority of papers reporting that PEGylation of proteins with high MW mPEG results in a lower degree of PEGylation, usually attributed to steric hindrance<sup>37,38</sup>. Indeed, it was proposed that when the size of mPEG increases, it excludes water from the surface of proteins<sup>39</sup>, and may impede accessibility of the remaining reactive-groups of the protein. From a therapeutic point of view, there is little interest in PEGylating proteins with several molecules of 20 kDa mPEG, as no further improvements of the pharmacokinetic parameters of PEGylated proteins was observed with mPEG MW higher than 20 kDa<sup>490</sup>. Additionally, it was reported that such high MW mPEG is cleared more slowly in the body<sup>330,491</sup>. Thus, taken together, our designed library accurately represents most of the sets of multi-PEGylated proteins.

Bioconjugates with very low degrees of PEGylation and long mPEG chains ( $\sim 3 \times 20$  kDa mPEG) as well as bioconjugates with higher degrees of PEGylation and shorter mPEG chains ( $\sim 25 \times 2$  or 5 kDa mPEG, respectively) both demonstrated a significant decrease in catalytic activity. Interestingly, activity of the bioconjugates bearing up to  $25 \times 0.5$  kDa mPEG was not statistically different from that of the native protein. Based on these observations, we explored each potential cause of enzyme deactivation. Evidently, as our ultimate objective would be to use these bioconjugates for therapeutic applications, we expected that the bioconjugates bearing 1 and 3 chains of 0.5–5 kDa mPEG might be less relevant than those having more than 10 mPEG molecules per GDH. Therefore, in what followed, we have been focusing on bioconjugates that could theoretically be more interesting for *in vivo* experiments.

First, we assessed if activity loss was due to the direct modification of the active site of GDH, a common hypothesis in the literature. Considering the residual activity of the bioconjugates as well as some particularities of the enzymology of GDH (e.g., inhibition of just one catalytic

site of GDH lead to a loss of activity of 54%)<sup>44-49</sup>, we suggested that none of the bioconjugates within the library are PEGylated at any of its six active sites, and the loss of activity cannot be attributed to the modification of the active site. Evidently, this does not exclude this possibility for other enzymes, where evidence of active site deactivation due to polymers conjugation has been largely reported in the literature<sup>40-42</sup>. For instance, deactivation of uricase was attributed to the direct modification of its catalytic site through conjugation to either mPEG or poly(N-acryloylmorpholine)<sup>41</sup>. Such a loss can be avoided by, for example, protecting the active site during conjugation or by scanning through the many possible conjugation sites<sup>40,41</sup>.

Our second theory of deactivation was the alteration of the secondary or tertiary structures of GDH. Modifications of the structure of proteins are dependent on many factors such as the properties of the proteins and the grafting density of mPEG. Indeed, while, unfolding and loss of secondary structures was reported for some proteins (i.e.,  $\beta$ -lactoglobulin grafted with two and three 20 kDa chains)<sup>492</sup>, this was not the case for many others (e.g., mono-PEGylated bovine serum albumin (using 5–60 kDa mPEG))<sup>59,385,411,493,494</sup>. Importantly, most studies exploring the structural modification of proteins upon PEGylation did not necessarily correlate changes to the biological activity. In this context, examination of the secondary structures of GDH bioconjugates revealed that PEGylation caused a minimal loss of  $\alpha$ -helical character that was dependant both on the degree of PEGylation and on the MW of mPEG. Moreover, the tertiary structure appeared to be more sensitive to the mPEG MW at low degrees of PEGylation and insensitive at higher degrees of PEGylation, suggesting that above a certain threshold, the changes to tertiary structure of GDH plateaued. Remarkably, while changes of secondary/tertiary structures might be a contributing factor to loss of activity, bioconjugates bearing ~25 chains of 0.5 kDa mPEG maintained the full catalytic activity despite the apparent alteration of their structures. Furthermore, although GDH bearing ~3 chains of 20 kDa mPEG and ~10 molecules of 2–5 kDa mPEG had distinct activities, similar effects on their tertiary structures were observed. Therefore, possibly because of its highly dynamic properties, GDH can accommodate relatively significant alterations to its structures with minimal impact on its catalytic activity. Hence, alternate mechanisms are likely responsible for the activity loss of these bioconjugates.

The most popular mechanistic explanation for the loss in activity is that mPEG hinders access to the active site due to crowding effects or alteration of the binding environment. This is applicable, not only for PEGylated proteins, but for proteins modified by different polymers<sup>495-497</sup>. The longer the polymer chain is, the lower the activity is expected as steric hindrance increases. Likewise, higher grafting density is also expected to decrease activity, as a larger area of the protein surface will be shielded. For instance, a successive reduction of the activity

of mono-PEGylated phosphoglycerate kinase was observed with 5 kDa, 10 kDa, and 20 kDa mPEG. The authors surmised that the presence of mPEG chains might increase the time the ligands need to diffuse to the binding site even without directly blocking the binding site <sup>385</sup>. Moreover, a decrease to 10% and 1% of the activity of lysozyme grafted with one and two 10 kDa mPEG molecules was reported and attributed to a reduction of the accessibility to the active site <sup>388</sup>. In contrast to these findings, trypsin decorated with 4–5 iterations of 2 kDa, 5 kDa, and 10 kDa mPEG chains displayed an increased activity over the native enzyme, demonstrating that the presence of the polymer did not sterically interfere with the substrate <sup>494</sup>. Interestingly, the authors reported a decrease in activity when trypsin was conjugated to 20 kDa mPEG and supposed that, at a certain length, the polymer might interfere with the substrate's access to the active site <sup>494</sup>. Whilst the crowding effects suggested by these papers are entirely plausible, the loss of activity could also be associated with other mechanisms that have not necessarily been explored by these studies.

The first step in addressing the effects of crowding is to investigate the potential distribution of mPEG around the surface of the protein. Two prevailing models were used to designate mPEG conformations: the dumbbell model, where the polymer molecules dangle away from the protein, or; the shroud model, where polymers wrap around the protein <sup>498,499</sup>. The first configuration has no contact with the protein surface and the second arrangement may generate a shielding effect as it partially or totally covers the surface of the protein <sup>495,498,499</sup>. While transition from the dumbbell to the shroud model was reported with increasing mPEG size, conflicting studies have observed both conformations at high MW mPEG (20 kDa) <sup>366,498,499</sup>. To support the argument that the surface of GDH remained highly exposed and accessible to its binding partners, the distribution of mPEG at the highest degree of PEGylation and in both conformations was computationally investigated. For this purpose, 25 chains of 2 kDa mPEG were randomly distributed on the solvent-accessible lysine residues, and analysis clearly showed that most of the GDH's surface remained highly solvent-accessible.

In order to further investigate the effect of PEGylation on the micro-environmental effects, the binding of two series of allosteric modulators (inhibitors) towards their respective binding sites on GDH was characterized. The binding site of the first series of modulators is located inside the core (hexachlorophene) and in the binding pocket situated halfway between the core and the exterior of the hexamer (bithionol) <sup>51</sup>. In contrast, the main binding location of the second series of modulators (GTP, ATP, and zinc) is positioned on the surface of GDH at the base of the 'antenna' region <sup>52-54</sup>. We first demonstrated that the buried binding sites of the first series of inhibitors were mostly unaffected by the steric and micro-environmental effects resulting

from PEGylation. On the other hand, the binding of the second series of modulators (particularly GTP) correlated with the trends related to changes in the secondary/tertiary structures of GDH. Therefore, changes of GDH structure might affected the 'antenna' region, resulting in the loss of binding of these modulators. This was further confirmed with the last modulator (zinc) whose binding patterns were not affected. Unlike the other modulators of the second series, which can only bind at the base of the 'antenna', zinc can also bind to a region between the two trimers of subunits (a region that was potentially unaltered by PEGylation)<sup>55</sup>. Taken together, we suggested that PEGylation did not alter the microenvironment, though it was responsible for an altered structure of GDH near its 'antenna' region, which impacted GTP and ATP allosteric modulation. Nevertheless, the anticipated changes of the 'antenna' structure cannot be directly correlated to activity.

We therefore investigated the effect of PEGylation on the dynamics of GDH. Indeed, enzymes usually display dynamical dependency, and their activity is widely considered as being correlated to a wide range of movements from rapid local motions of individual groups to slow movements of large regions<sup>500,501</sup>. The influence of both configurations of mPEG (dumbbell and shroud) on the molecular dynamics of GDH was assessed, to provide insight into the effects of these two situations, under the expectation that reality lies somewhere in between. Computational data clearly demonstrated that PEGylation affected the GDH dynamics for both configurations (with the shroud configuration having the greatest impact) and was more pronounced for the backbone than for the side-chains. The decrease observed with the dumbbell configuration might be related to extra drag and concomitant extra fluctuations of polymers that extend into solution. In contrast, considering that in the shroud configuration, the mPEG chains wrap around the GDH surface, adhered portions are expected to more strongly dampen the motions of GDH. This has been reported by some studies relating the reduction of protein dynamics to the amphiphilic nature of mPEG<sup>39,59,60</sup>. Indeed, as the hydrophobic parts of mPEG interact with the hydrophobic clusters on the protein surface and the hydrophilic regions interact with water molecules, the removal of water molecules from the surface of the protein could generate a more rigid structure (displaying reduced protein dynamics).

In addition to the mPEG configuration, the effect of its distribution on the GDH surface (symmetric or asymmetric) was investigated. Indeed, considering that GDH catalysis requires that all six subunits move in a cooperative manner, the pattern of mPEG distribution might influence GDH dynamics. As expected, the asymmetric distribution of mPEG had a greater impact than the symmetric distribution. This observation correlated with a study proposing that the disproportionately high loss of activity occurring with the inhibition of a single catalytic site might be associated to the loss of cooperativity between the six monomers of GDH<sup>49</sup>.

Therefore, the asymmetric distribution of mPEG could more significantly affect the dynamic of the most PEGylated monomer, which had repercussions on the rest of the protein. Moreover, given that the MW of mPEG was associated with the loss of activity, the effect of this parameter was evaluated by simulation of the bioconjugates bearing 25 chains per GDH. As suspected, mPEG significantly dampened the dynamics of GDH in a MW dependent manner, and the trends correlated with the effects on the catalytic activity. To the best of our knowledge, this was the first study computationally investigating the correlation between the catalytic activity and the protein dynamics at high degrees of PEGylation. Our observations did not necessarily concur with an experimental study demonstrating that the structural dynamics of  $\alpha$ -chymotrypsin bioconjugates was independent of the MW of mPEG (assessed by the measurement of the kinetics of hydrogen/deuterium (H/D) exchange)<sup>59</sup>. Even though the bioconjugates differed between the studies (e.g., dissimilar protein and different degrees of PEGylation), this might indicate that, while there might be some general trends observed upon PEGylation, the exact outcome cannot be accurately predicted.

In summary, in this study, we showed that structure–activity correlations could not reconcile all trends within the library of bioconjugates tested, signifying that other mechanisms of activity loss were at play. The simulations suggested that loss of activity was mainly caused by restricted protein dynamics (at least for the highly PEGylated forms). Hence for dynamic proteins, such mechanism of deactivation should be always considered.

Finally, as the causes of activity loss of GDH were defined, we aimed to test the therapeutic efficacy of some of our GDH bioconjugates *in vivo*. According to the above presented findings, we decided to test the therapeutic effects of bioconjugates with 25 x 0.5 kDa mPEG, 10 x 2 kDa mPEG, and 3 x 20 kDa mPEG. The first two bioconjugates were included because our data had shown no significant reduction of activity as well as a preservation of the structural and dynamic properties of GDH, despite high degrees of PEGylation. Furthermore, although the activity of GDH carrying 3 x 20 kDa mPEG decreased significantly, our experiments suggested that the structure and the microenvironment on the surface of the GDH were preserved. Considering that, in some cases, a reduction in biological activity is compensated by an increase in circulating half-life, it was reasonable to expect that these bioconjugates could provide an enhanced *in vivo* performance in comparison to the unPEGylated GDH.

Thus, as an initial step, we proceeded to assess the glutamate scavenging effect of intravenously injected native GDH<sup>317</sup>. Unexpectedly, we didn't observe an effect on the concentrations of glutamate neither in the blood nor in the CSF. We therefore surmised that either the chosen dose was therapeutically irrelevant or that the GDH was not efficient as a

scavenging enzyme for unknown reasons. Retrospectively, based on the results obtained with hrGOT in Chapter 4, as well as a recently published study <sup>61</sup>, the therapeutic effects of glutamate-degrading enzymes cannot be determined only by measuring the blood/CSF glutamate levels. Therefore, a more advanced study should provide a better discernment of the therapeutic doses and the potential effects of GDH. As this could not be foreseen at the conclusion of Chapter 3, hrGOT was chosen as a replacement enzyme for its relatively better-known glutamate scavenging effects upon exogenous administration.

In Chapter 4 we explored the therapeutic efficiency of multi-PEGylated hrGOT in healthy and ischemic rats. Two different designs were produced (mPEG–hrGOT and Angiopep–PEG–hrGOT targeted to the BBB), and both bioconjugates bore ~22 polymer chains and possessed 80–90% of the activity of the native hrGOT. This minimal reduction in hrGOT activity following PEGylation reflects the less dynamic nature of this enzyme in comparison to the GDH.

Intravenous administration of the treatments demonstrated an increase in circulation time from less than 6 hours for native hrGOT to ~6 days for the PEGylated forms. The rapid elimination of hrGOT from the blood compartment was in accordance with the literature, which reported a fast uptake of this enzyme by the peripheral organs (with a maximal uptake by the liver 2 hours post-injection) <sup>18,19</sup>. Therefore, the prolonged blood residence time of the bioconjugates was likely due to the hindrance of hrGOT uptake by peripheral organs. Moreover, the presence of mPEG chains around the enzyme surface likely reduced the immunogenicity of hrGOT (if existent), as well as its rate of proteolytic degradation. Nevertheless, such effects are less prominent than those implicating the uptake by peripheral organs. Additionally, the pharmacokinetic profiles observed in healthy rats were also very similar to those observed for ischemic rats, suggesting that the routes of distribution and elimination of the bioconjugates were not affected by the MCAo.

Contrary to what has been reported in some studies <sup>65</sup>, a clear effect of native hrGOT or hrGOT bioconjugates on serum glutamate levels was not detected. Indeed, at the administered dose, the steady-state concentration of blood glutamate was not significantly affected by any of the treatments, and thus no correlation between enzymatic activity and blood glutamate levels could be identified. It should be noted that the published works do not mention the specific activity of their hrGOT, making a comparison of the doses impossible. Nevertheless, our data were consistent with the studies proposing that the homeostasis of glutamate is rapid and maintained through a variety of peripheral transporters and receptors <sup>66,67</sup>. In fact, prior work has shown that the radioactivity of intravenously injected (radioactive) glutamate and its metabolites (e.g., aspartate) decayed with a half-life of ~3 min, owing to metabolic reactions

occurring in the liver or in the plasma, which provides some insight into the timescale of glutamate homeostasis. This study further demonstrated that the major sequestering organs, serving as depots for the eliminated glutamate and/or its metabolites were skeletal muscle, liver and gut<sup>68</sup>. Thus, we proposed that the existence of a rapid homeostasis of glutamate between blood and peripheral tissue (e.g., muscles, liver) maintained steady glutamate levels (Figure 14).

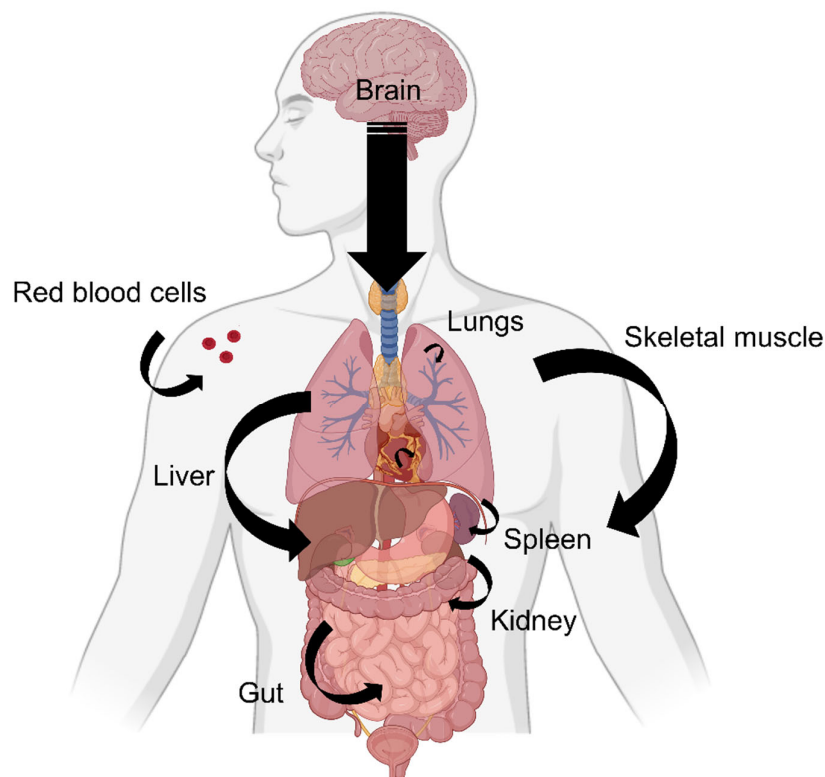


Figure 14: Overview of the homeostasis of glutamate and/or its metabolites between the different parts of the body following administration of GDH bioconjugates. The size of the arrows indicates the expected respective contribution of each compartment.

In order to investigate whether a more localized effect may be observed, glutamate levels were measured in the CSF of healthy rats receiving either native hrGOT or mPEG-hrGOT. No effect on the CSF glutamate concentrations was detected. These data were in accordance with a recently published study showing that the daily administration of recombinant GOT (each 12 hours on days 1–4) reversed the disruption of synaptic plasticity in a rat model of traumatic brain injury by decreasing the glutamate level in hippocampus interstitial fluid, but not

ventricular CSF <sup>61</sup>. Taken together, the non-variation of glutamate levels can be rationalized by the glutamate homeostasis systems that work to maintain the homeostatic balance of glutamate. Probably, these fast-paced homeostasis mechanisms have not allowed the quantification of the levels of degraded glutamate.

On the other hand, we observed an increase in enzyme activity in the CSF at 2 hours post-administration of the native hrGOT, possibly indicating that a very small portion of the dose reached the CSF. mPEG–hrGOT bioconjugates, in contrast, did not alter hrGOT activity in the CSF suggesting that the presence of the polymer corona prevented passage through the brain barriers. These data were measured in healthy rats, and potentially would have changed in ischemic animals, though this was not further explored. Indeed, promotion of passage of PEGylated proteins across the brain barriers would not be expected, unless the barriers were compromised. Studies exploring the crossing of PEGylated proteins across damaged brain barriers are inconsistent in the literature, with some research showing they were impeded <sup>502,503</sup>, and one study showing their passage (dependent on the “opening” phases of the barriers) <sup>504</sup>. Evidently, these data were not demonstrated in ischemic models and could be specific to certain types of brain injury as well as to the investigated bioconjugate. Moreover, extrapolation to the case of human ischemia would be difficult. Nevertheless, in all cases, the scavenging effects would be the primary mechanism of hrGOT neuroprotection, with passage across the brain barriers potentially providing an additional advantage (i.e., ensure the delivery of proteins only in the damaged areas of the brain).

Following analysis of pharmacokinetic/pharmacodynamic, we demonstrated that sustained hrGOT activity in the blood, achieved with the bioconjugates, provided neuroprotection and significantly reduced the infarct volume when compared to saline and hrGOT groups. Remarkably, the bioconjugates reduced the infarct size by ~70% relative to its Day 0 value, suggesting that this protective strategy might be present a promising treatment. Indeed, preclinical testing criteria for neuroprotective agents defined a reduction of the ischemic damage of at least 50%, or even better by 80%, for consideration for clinical trials <sup>62</sup>. It should be noted that the achievement of a relatively similar reduction in the infarct size has also been reported elsewhere <sup>505,506</sup>. Nevertheless, the passage of these suggested neuroprotective molecules through the BBB represents a necessary and essential step to obtain the desired therapeutic effect. Therefore, as for many drugs targeting the brain, these molecules could possibly be ineffective during clinical trials. Indeed, although evidence from preclinical studies has been exciting and many neuroprotective molecules have progressed to clinical trials, none of these agents has been proven to be clinically beneficial <sup>507</sup>. One of the main reasons is the difference in the composition and the anatomy of brain between rodents (small lissencephalic

brain) and primates (large gyrencephalic brain)<sup>508</sup>. In fact, predicting the brain penetration of these drugs from rodents to humans represents a critical translational step that hindered the translation of preclinical success into clinical practice. Consequently, considering that the passage of our bioconjugates through the BBB is not required, we anticipate that the effectiveness of the treatment would not be potentially compromised.

To further confirm the neuroprotective properties of the bioconjugates, the motor functions of ischemic rats were assessed. Our results globally showed that rats that underwent MCAo and were treated with hrGOT bioconjugates had a better recovery than those treated with saline or native hrGOT. This finding was very important, because even though measuring lesion size might provide some evidence of protection, this parameter differs substantially from functional impairment, which is the most important parameter for patients.

Interestingly, our findings regarding the effects of targeted bioconjugates were rather unexpected. Indeed, targeting the hrGOT bioconjugates to the BBB, *via* appended Angiopep-2 ligands, did not have an additional therapeutic value compared to stabilizing and increasing the circulation lifetime of hrGOT using mPEG. This suggested that brain or near-brain accumulation of the Angiopep-PEG-hrGOT represented only a very minor fraction of the total administered dose and did not contribute significantly to the outcomes. Alternatively, it might suggest that the targeting efficiency of the bioconjugates was either somehow affected by the mPEG chains or potentially altered by the high density of the ligand (Angiopep-2). Indeed, while some studies have shown that mPEG molecules could improve the elasticity of the ligand (and presumably the interaction between the ligand and its receptor)<sup>509-511</sup>, it is also possible that this flexibility hindered such interactions. Additionally, it was shown that a certain density of ligand is usually required for an efficient brain targeting delivery. Even though the higher ligand density showed higher avidity and selectivity with target cells<sup>63</sup>, increasing the density could also inhibit the disassociation from cells, resulting in decreased transcytosis and reduced accumulation in brain parenchyma<sup>64</sup>. Therefore, assessing the binding patterns of our bioconjugates will be important in future work before pursuing new hypotheses using brain-targeted bioconjugates.

In summary, this study demonstrated that hrGOT bioconjugates induced a significant reduction of the infarct volume, and an increased retention of sensorimotor function for ischemic rats compared to those treated with native hrGOT or saline. Moreover, our data suggested that the bioconjugates drew glutamate out of the brain by displacing homeostasis between the different glutamate pools in the body.

## 2. Conclusion and perspectives

In the context of this thesis, we have:

(1) Provided an outline of the complexity of factors causing inactivation of multi-PEGylated proteins. Indeed, while GDH is a prototypical example of a highly dynamic enzyme whose catalytic activity relies on concerted long-range motions, similar phenomena might exist for other proteins. We also highlighted the necessity for more comprehensive investigations that will allow for more accurate prediction of the mechanism of activity loss, potentially by comparing sets of structurally related protein entities. Overall, the new insight into these fundamental considerations could contribute to the design of future bioconjugates.

(2) Developed a neuroprotective therapy for ischemic stroke, with potential applicability in other diseases. This was the first study to evaluate the sustained therapeutic effect in the brain, *via* bioconjugates that remain in the blood stream. As the transport across the BBB of various drugs remains a great challenge, the described therapeutic strategy represented a promising paradigm as it does not necessarily require BBB transport. Importantly, our work provided a completely new perspective on the treatment of excitotoxicity. While the specific benefits for ischemic stroke were assessed herein, the concept is equally applicable for many other diseases implicating excitotoxicity mechanisms (traumatic brain injury, Parkinson's disease, Alzheimer's disease, etc.). Therefore, this therapeutic approach will benefit a large proportion of the population in addition to reducing a huge socio-economic burden.

Future experimental and computational studies on the effect of PEGylation of dissimilar proteins can be investigated in order to identify some trends related to the effects of polymer chains on particular structural or dynamical properties.

Concerning the therapeutic effects of the hrGOT bioconjugates, we are interested in exploring and understanding the neuroprotective mechanisms. For this purpose, we are planning to study the biodistribution of native hrGOT and hrGOT bioconjugates by radiolabeling. This will provide us with an insight into the location and the differential accumulation of our targeted and non-targeted bioconjugates.

Furthermore, considering that excitotoxicity induces cell death and various physiopathological mechanisms (e.g., oxidative stress, inflammation), we are planning to perform biochemical and histological analyses of the brains (e.g., detect and quantify the necrotic and apoptotic cells, the markers of the glial activation (e.g., cytokines specific to anti and pro-inflammatory microglial cells), and the levels of oxidized macromolecules).

Recently, as many studies highlighted the prevalence of neutralizing anti-mPEG antibodies in the general human population, it is becoming relevant to assess the presence of anti-mPEG

antibodies following treatment. Of note, assessing the levels of Ig will be undoubtedly very important especially if we plan to use our bioconjugates for the treatment of neuronal diseases displaying a chronic excitotoxicity. Evidently, we can also investigate the conjugation of dissimilar polymers to hrGOT (polymer chains with comb architectures) and assess their therapeutic effectiveness.

Finally, looking at the unsuccessful *in vivo* results of the native GDH in decreasing the glutamate levels, and considering our results with hrGOT, we are now interested in investigating the effect of GDH. As such, we will need to adjust the doses and test the effects on ischemic animals.

## APPENDIX PAGES

## **APPENDIX A: Supplementary Information of Paper 1**

### **Mechanisms of activity loss for a multi-PEGylated protein by experiment and simulation**

Ahlem Zaghmi, Eduardo Mendez-Villuendas, Andrea A Greschner, Jun Yang Liu, Hendrick  
W de Haan, and Marc A Gauthier

A version of this chapter has been published in

Materials Today Chemistry, Volume 12, June 2019, Pages 121-131

Reprint permission is not required.

The formatting of this article conforms to the specifications of the scientific journal.

Electronic Supporting Information

for

**Mechanisms of activity loss for a multi-PEGylated protein by  
experiment and simulation**

Ahlem Zaghmi<sup>1</sup>, Eduardo Mendez-Villuendas<sup>2</sup>, Andrea A Greschner<sup>1</sup>, Jun Yang Liu<sup>1</sup>,  
Hendrick W de Haan<sup>2,\*</sup>, and Marc A Gauthier<sup>1,\*</sup>

<sup>1</sup> Institut National de la Recherche Scientifique (INRS), EMT Research Center, Varennes, Qc,  
J3X 1S2, Canada

<sup>2</sup> University of Ontario Institute of Technology, Faculty of Science, Oshawa, Ontario, L1H 7K4,  
Canada

Corresponding authors:

Marc A. Gauthier

Institut National de la Recherche Scientifique (INRS), EMT Research Center, 1650 boul.  
Lionel-Boulet, Varennes, J3X 1S2, Canada

E-mail: gauthier@emt.inrs.ca

Telephone: +1 514 228 69 32

Fax: +1 450 929 81 02

Hendrick de Haan

University of Ontario Institute of Technology, Faculty of Science, Oshawa, Ontario, L1H 7K4,  
Canada

E-mail: Hendrick.deHaan@uoit.ca

Telephone: +1 905 721 86 68 ext: 6237

Fax: +1 905 721 33 04

Conflict of interest: None to declare

## 1. Supporting methods

**2.1 Coarse grained (CG) simulations.** For large structures, atomistic simulations are insufficient to prove large scale motions within a reasonable computational expense, and hence, molecular simplifications to the atomistic representations are in order. The atomistic model was translated into a CG representation with four heavy atoms to one bead, described by the MARTINI force field. Solvent is represented explicitly, with four TIP3P molecules now represented by a single martini bead. This CG representation is at the limit where chemical specificity is maintained. In the MARTINI force field<sup>512,513</sup>, mapping takes a group of four heavy atoms and replaces them with beads modeled *via* van der Waals interactions characterized by a discrete set of ten well-depth levels from “super-repulsive”  $2.0 \text{ kJ} \cdot \text{mol}^{-1}$ , to “supra-attractive”  $5.6 \text{ kJ} \cdot \text{mol}^{-1}$ , and beads that may take various diameters ( $\sigma = 0.47$  for normal beads, and  $\sigma = 0.43$  for small beads, typically representing parts of rings). Interaction between bead types should be chosen according to combination rules, hence a matrix of interactions results in a huge set of possibilities. To help define chemical specificity, beads are divided into four main categories (P, polar; N, intermediate; C, apolar; Q, charged) with a number of sub-levels. It is possible in principle to introduce additional bead types according to the need in particular, while trying to maintain chemical specificity.

**CG model of GDH.** In the MARTINI force field, an elastic network needs to be adjusted to reproduce the secondary structure of the reference atomistic simulation’s trajectory<sup>514</sup>. This fit is enforced *via* an Elastic Network model, and described *via* harmonic restraint functions, given by  $K_b(r - r_0)^2$ , applied in between backbone amino acid bead pairs. For the tunable parameters, equilibrium distances  $r_0$  are found within a small and a large cut-off radii  $r_{\text{small}} \leq r_0 < r_{\text{large}}$ , and the force constant  $K_b$  can be adjusted among all pairs. We employed a cut-off between 0.9 and 1.2 nm to define the elastic network, with a harmonic force constant of  $500 \text{ kJ} \cdot \text{nm}^{-2}$ , which has been found to produce the correct dynamics for a great variety of systems as an appropriate approximation. Although it is possible to tune the force constant for every pair of backbone beads of the system, the aim of this study was to produce a general picture with which the mechanism and dynamics of the enzyme could be tested. A picture with the elastic network is shown in **Fig. S10**. The elastic network of the force field for the protein alone is validated *via* comparison to the normal modes of atomistic representations and comparison to molecular dynamic (MD) trajectories at the atomistic level. The MARTINIZE python script was used to translate atomistic groups of atoms into beads (<https://github.com/cgmartini/martinize.py>) using the crystallographic coordinates derived from the pdb structure 3etd with cofactors removed. The final model consisted of six units with the same representative topology. The MARTINI model has 1,103 beads per unit compared to

4,561 atom particles in the atomistic model counterpart (CHARMM36 force field).

**Atomistic Simulation Details.** For the atomistic simulations, the system was solvated with 75,473 water molecules and sufficient ions to neutralize and to obtain a zero-total charge. Positional restraints on the backbone atoms were applied with a force constant of 5,000 kJ·mol<sup>-1</sup>. A 2 fs integration time step was used. The charmm36 force field was employed to model the interactions. The Coulomb and rVdW cut-offs were set to 1.2 nm and a modified rvdw-switch was applied at 1.0 nm. Simulations were carried out in the NPT ensemble (constant number of particles, Pressure = 1 bar, T = 300 K). Pressure was held maintained *via* a Berendsen isotropic thermostat with a 3.0 ps time constant, a compressibility of  $4.5 \times 10^{-5}$ , and semi-isotropic pressure conditions. Temperature was maintained by a Nose-Hoover thermostat with a 0.5 ps time constant. Simulations were carried out for 0.5 ns, and then the positional restrains on the backbone were removed. The system was still restrained to fix its central position and to avoid rotations around the main axis, as the system box was not cubic but had equilibrated dimensions of about 11 × 11 × 17 nm per side. An initial equilibration stage was carried out for 2 ns of simulations. A production run consisted of 2 ns simulation where pressure, box size, and rms displacements with respect to the structure after 2 ns simulation were set approximately constant. A total of five hundred frames per nanosecond, saving all coordinates including solvent, were output during these simulations. A second trajectory was saved containing only the coordinates for the protein. Normal mode analysis was later performed using the protein trajectory by carrying out calculations with the covar utility in GROMACS. The backbone atoms are used as a reference to remove displacements.

**Preliminary CG simulations of GDH.** The resulting hexamer was held *via* positional restraints (harmonic force constant of 2,500 kJ · mol<sup>-1</sup>). Of particular note is the preservation of the water structure inside the hexamer and thus the cavity was filled by a triple row of solvent beads (type P4). In the crystallographic structure, one may find conserved waters inside the transversal channel that runs from the center of the top trimer to the bottom trimer. Since the protein is held *via* positional restraints, extra solvent beads will eventually equilibrate with the protein and the surrounding environment. Equilibrium simulations were performed in the NPT ensemble (fixed number of particles, constant pressure, constant temperature). In the CG MD simulations, a time step of 10 fs was used, with a Berendsen thermostat was applied every 0.5 ns. The barostat was coupled *via* a 2 ns restitution constant using the Parrinello-Rahman scheme. A single cut-off of 1.4 was used for van der Waals interactions. Pressure coupling was done with the Berendsen algorithm<sup>515</sup> at semi-isotropic conditions with 1 bar reference pressures and a pressure relaxation time  $\tau_p = 2.5$  ps. Temperature coupling was fixed *via* the V-rescale<sup>516</sup> temperature algorithm using a relaxation time of  $\tau_T = 0.5$  ps. The endpoint of

these simulations is used as the GDH model for the native and PEGylated proteins studied below.

**PEG model.** It is possible to adjust new bead types to better fit the predictions from atomistic-reference calculations. In an earlier study<sup>422</sup>, PEG monomers were represented by parameters optimized *via* atomistic molecular simulations to reproduce various measures such as radius of gyration and diffusion constant. These parameters, however, were merely used as a device to introduce a new interaction potential to be used by the GROMACS MD software, and the test incorporated interactions in solvent with other polymer species but not for polymer–protein interactions. In our simulations the bond, angle, and dihedral interaction potentials of this model were used. However, when using small beads with  $\epsilon$  values close to those used in [7], large discrepancies were found with the expected behavior. Using small beads resulted in the model polymer strongly adhering to the protein for a system with  $25 \times 2$  kDa PEG (46 PEG monomers per polymer). The mismatch between the polymer bead and solvent bead sizes yielded artefacts in which the small polymer was forced into small crevices on the surface of the protein to enhance the volume available for the solvent bead. To alleviate this, the polymer beads were changed from SP1 to P1 beads, which are the same diameter as the P4 solvent beads. Note that only the bead size is changed and not the well depths of the interactions. Polymers were constructed *via* the bonded interactions described in ref.<sup>422</sup>. Simulations were also performed using the P4 beads for the polymer. This results in a fully hydrophilic polymer without the partial hydrophobic character of the P1 beads.

**PEGylated proteins.** A python script was produced to select a set of lysine sites within a list of solvent-accessible residues available for PEGylation (**Table S3**). The entire list was cast into an absolute list from 1 to N, with N the number of possible PEGylation sites in the hexamer. Next, the target number of polymers to be added  $N_{\text{poly}}$  were chosen within the N set at random. It is obvious that the realization of these random selections would lead to selections where the polymers were evenly distributed on all six monomers (symmetric case) or unevenly distributed (asymmetric case), with most of the residues selected in only one of the monomers. The goal was to obtain one symmetric and one asymmetric realization for various sizes and coverages, as an initial exploration of the role played by PEGylation. **Table S4** lists all relevant PEGylated hexamer simulations carried out at the MARTINI CG level. The nature of the random selection led to some of the polymers being attached in points that could be important for the lowest normal mode dynamics. These include, near the antennae of the upper and lower trimers, sites near the large clefts on each of the hexamers, and near the large clefts of individual monomers.

**Simulations of the bioconjugates.** Once the polymers were attached to the protein, the

systems required an initial process of energy minimization. First, the thermodynamic integration scheme was used as a device to zero the electrostatic and van der Waals interactions between solvent and the protein–polymer(s) system. The protein hexamer is clamped *via* positional restraints and only polymers and solvent are allowed to move. Solvent interactions are slowly turned on from zero to one (full hydration). Next, equilibrium MD simulations in the NPT ensemble were carried out for 50 ns, with positional restraints on the protein backbone still activated, with a force constant of  $1,000 \text{ kJ} \cdot \text{nm}^{-2}$ . This was followed by a stage of equilibration for 100 ns where positional restraints are removed. Finally, production runs were performed where solvent-free trajectories are saved every 0.25 ns. Equilibration of the total system was measured *via* rmsd and total energy values. Post-equilibration data was used for the normal mode analysis.

**Normal mode calculations.** In standard normal mode calculations, one defines interacting beads that are linked by harmonic bonds. These are used to build interaction matrices that can be symmetrized to obtain eigenvalues and eigenvectors. The set of all the eigenvectors defines a translational space, and the magnitude given by the eigenvectors denotes the intensity of the motion along a particular direction. It becomes convenient to arrange the modes by intensity resulting in a monotonically decreasing sequence. The normal modes with higher index are very small and can be associated to noise. Thus, only the first ten or so non-trivial modes are analyzed. The net effect of these modes constitutes between 70 and 80% of the total movement of the network representing the protein. Note that the first six modes are discarded as these correspond to rigid body rotation (3) and rigid body rotations (3). If the first normal mode has a high eigenvalue compared to the second, then much of the total motion can be attributed to this mode. Conversely, when the first mode is reduced such that it is comparable to the second (and often higher) modes, then the motion is spread among many modes. Normal modes were calculated *via* a single frame perturbation, given by the Anisotropic Network Mode server <sup>517</sup> (<http://anm.csb.pitt.edu/>) with a network defined by cut-off interactions between  $C_{\alpha}$  atoms.

**Central Water Cavity.** **Fig. S9** displays cross-sections of the protein such that the interior water pockets can be seen. The sample representations have been cut as a section along the main axis and colored according to radial distance from the center of the protein and thus indicate depth. The dark regions correspond to the plane that crosses through the hexamer. Since each trimer has three-fold symmetry within the hexamer, the figures are not exactly symmetric. The images were rendered using VMD <sup>431</sup>. The top panel corresponds to the native protein and the bottom to P1 bead  $25 \times 2$  kDa PEG symmetric case.

## 2. Supporting Results

**Table S1.** Characteristics of the mPEG–GDH bioconjugates investigated in this study.

Bioconjugate	mPEG MW (kDa)	GDH: mPEG ratio <sup>1</sup>	Degree of PEGylation <sup>2</sup>			M <sub>n</sub> , SEC (Da)	Đ <sup>3</sup>
			SDS PAGE	<sup>1</sup> H NMR	SEC		
1	0.5	1:5	0 – 1	0	0	116,400	1.07
2		1:30	0 – 1	2	0	120,600	1.07
3		1:300	9 – 15	7	18	121,800	1.07
4		1:1500	18 – 24	17	30	128,400	1.14
5	2	1:5	0 – 1	2	1	120,000	1.04
6		1:30	0 – 2	3	4	125,400	1.03
7		1:300	10 – 16	7	6	129,600	1.02
8		1:1500	19 – 23	15	19	148,800	1.12
9	5	1:5	0 – 1	1	1	126,600	1.1
10		1:30	1 – 2	3	6	139,800	1.1
11		1:300	18 – 24	10	14	184,800	1.09
12		1:1500	27 – 35	30	27	245,400	1.07
13	20	1:30	2 – 3	3	6	279,000	1.13

<sup>1</sup>: Feed molar ratio of mPEG to GDH used to prepare the bioconjugate

<sup>2</sup>: Number of mPEG chains per protein hexamer

<sup>3</sup>: Dispersity of the bioconjugate determined by size-exclusion chromatography (SEC)

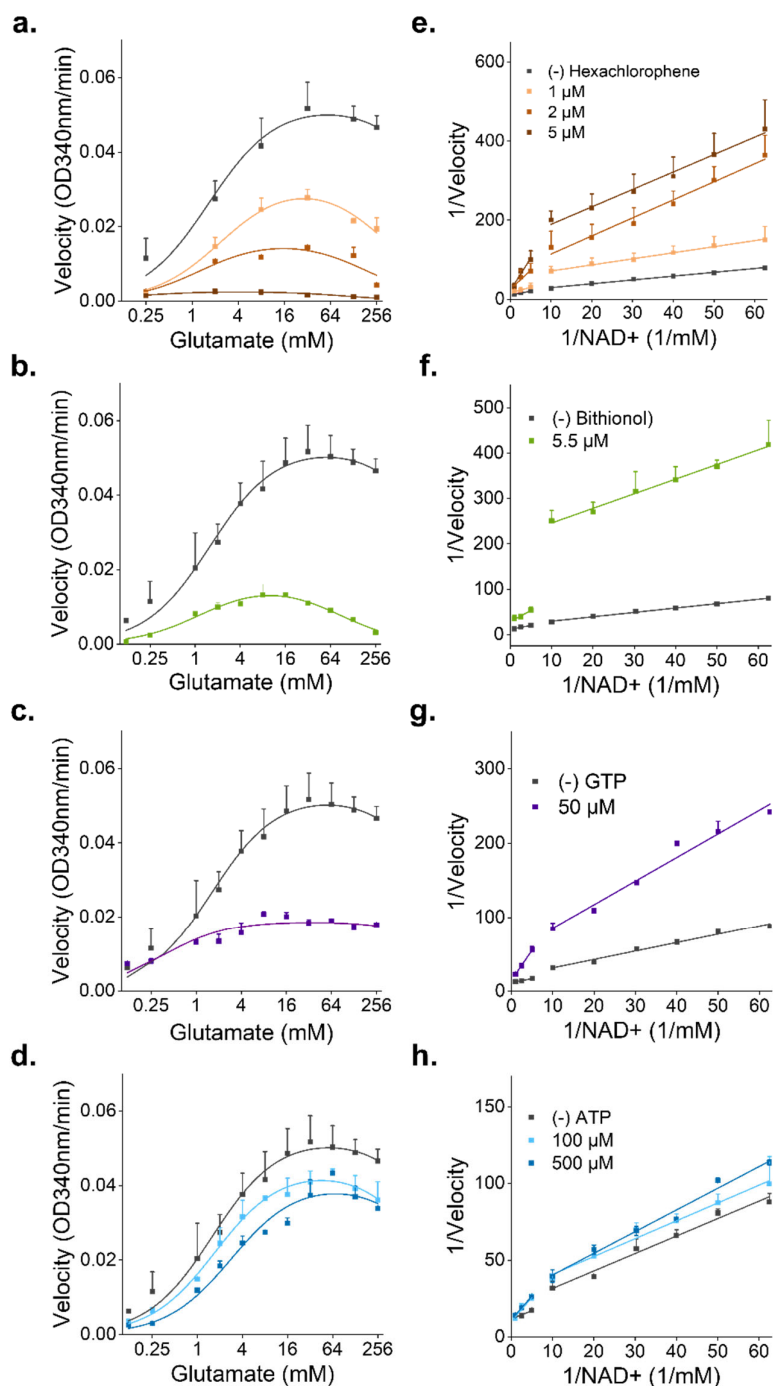


Figure S1| **Kinetic analysis of GDH activity.** Michaelis-Menten plots with glutamate as varied substrate in the absence/presence of (a) Hexachlorophene, (b) Bithionol, (c) GTP, and (d) ATP. The marked downward trend in the curve at 64 mM of glutamate is due to substrate inhibition. The  $V_{\max}$  and  $K_m$  values obtained by curve fitting are summarized in Table S2. Lineweaver-Burk plots with NAD<sup>+</sup> as varied coenzyme in the absence/presence of (e) Hexachlorophene, (f) Bithionol, (g) GTP, and (h) ATP. The marked break from the expected linearity at 0.1–0.2 mM NAD<sup>+</sup> is due to negative cooperativity. Mean + SD,  $n = 3$ .

**Table S2.** Curve fitting parameters obtained from plots in **Figure S1**.

	Concentration ( $\mu\text{M}$ )	$V_{\text{max}}$	$K_m$ (mM)	$R^2$
(-) Inhibitor	0	$0.050 \pm 0.008$	$1.6 \pm 0.2$	0.98
Hexachlorophene	1	$0.030 \pm 0.001$	$2.4 \pm 0.4$	0.98
	2	$0.020 \pm 0.002$	$1.5 \pm 0.6$	0.84
	5	$0 \pm 3$	$0.16 \pm 0.09$	0.86
Bithionol	5.5	$0.02 \pm 0.01$	$1.2 \pm 0.2$	0.97
GTP	50	$0.020 \pm 0.001$	$0.3 \pm 0.1$	0.86
ATP	100	$0.040 \pm 0.001$	$1.7 \pm 0.2$	0.99
	500	$0.040 \pm 0.002$	$2.9 \pm 0.7$	0.96

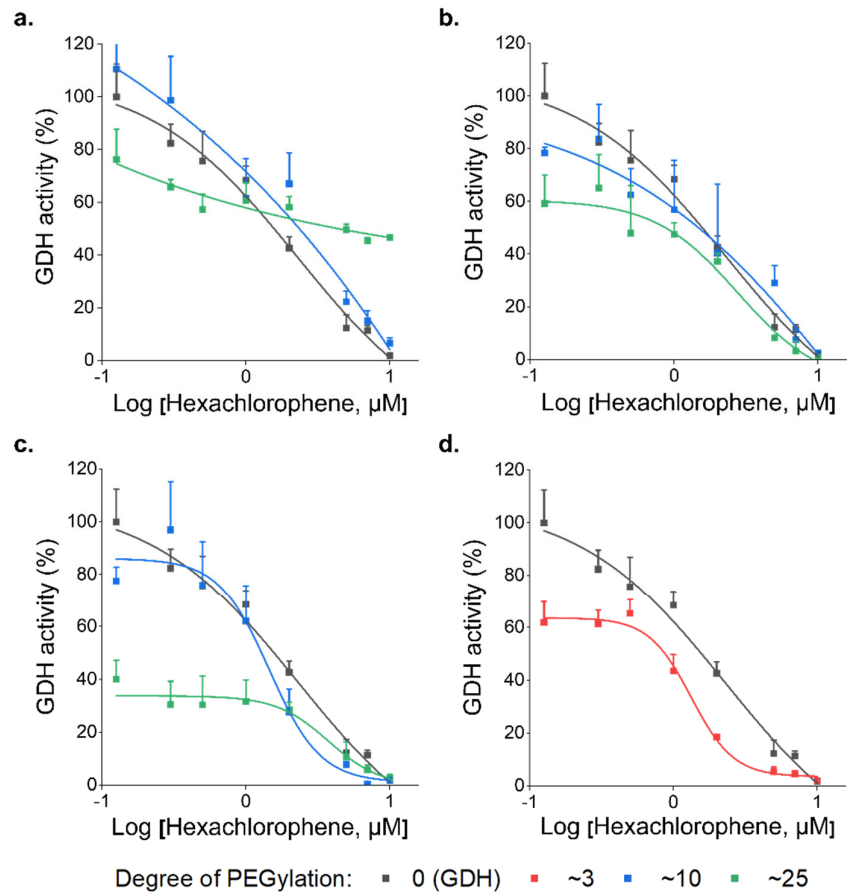


Figure S2| **Dose-activity curves of GDH and mPEG–GDH bioconjugates in the presence of hexachlorophene.** Panel (a) 0.5 kDa, (b) 2 kDa, (c) 5 kDa, and (d) 20 kDa mPEG. Mean + SD, n = 3.

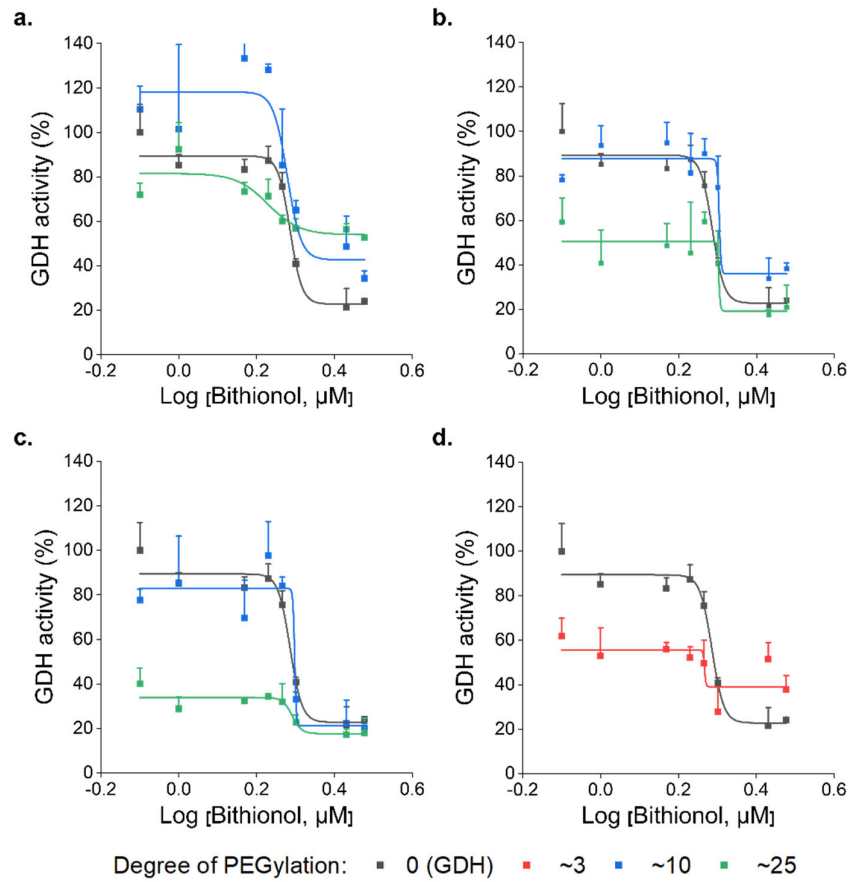


Figure S3| **Dose-activity curves of GDH and mPEG–GDH bioconjugates in the presence of bithionol.** Panel (a) 0.5 kDa, (b) 2 kDa, (c) 5 kDa, and (d) 20 kDa mPEG. Mean + SD, n = 3.

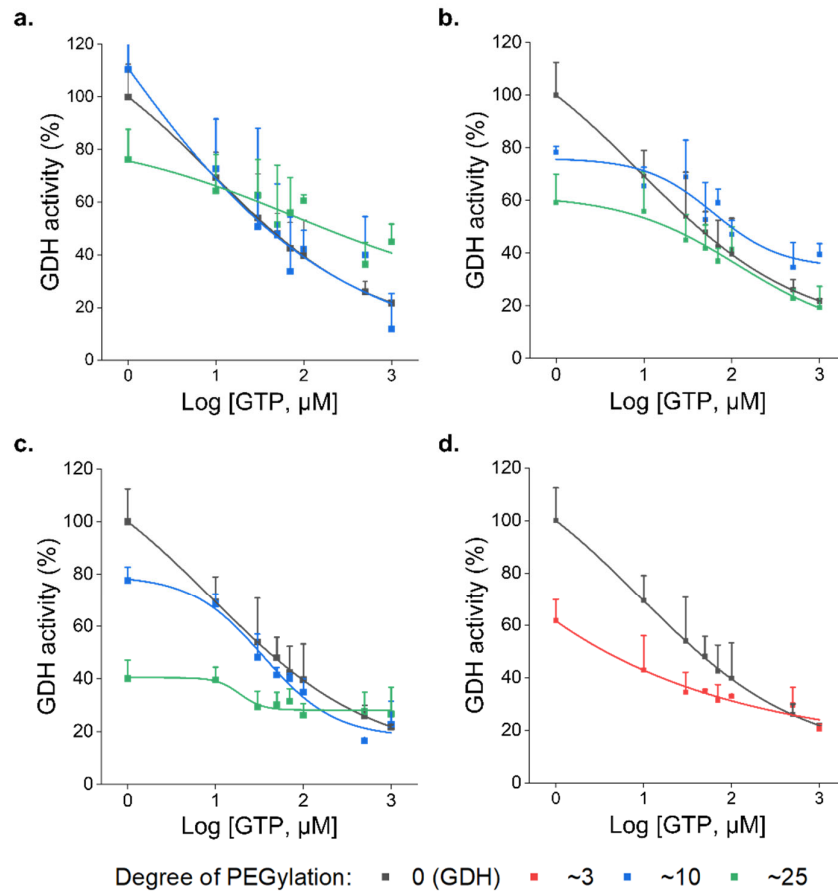


Figure S4| **Dose-activity curves of GDH and mPEG–GDH bioconjugates in the presence of GTP.** Panel (a) 0.5 kDa, (b) 2 kDa, (c) 5 kDa, and (d) 20 kDa mPEG. Mean + SD, n = 3.

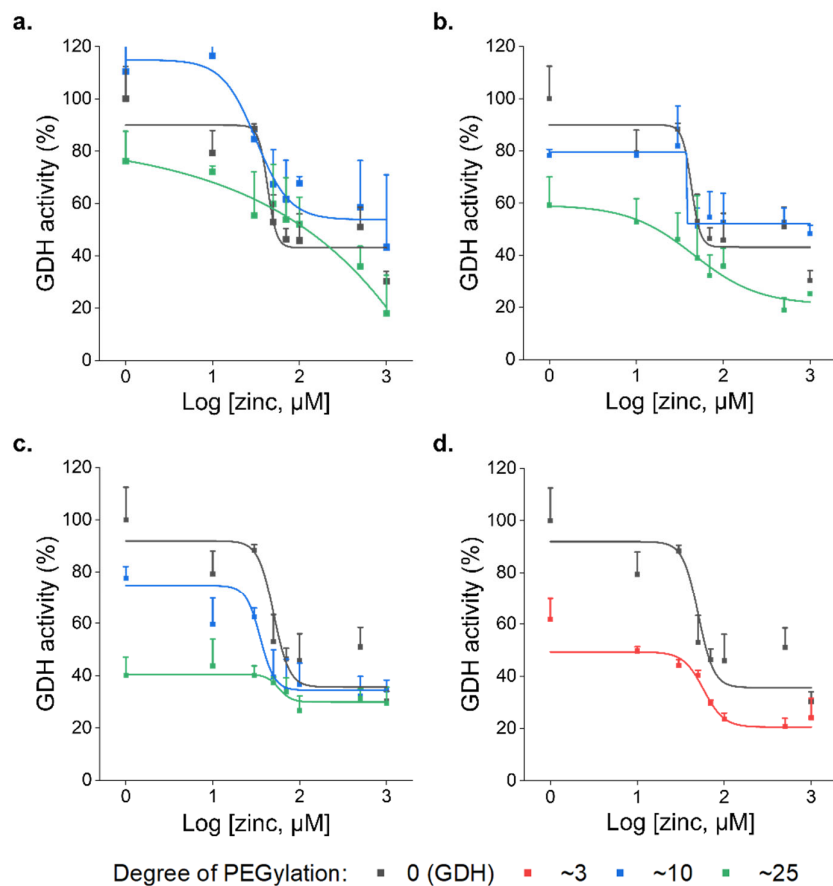


Figure S5| **Dose-activity curves of GDH and mPEG-GDH bioconjugates in the presence of Zn<sup>2+</sup>.** Panel (a) 0.5 kDa, (b) 2 kDa, (c) 5 kDa, and (d) 20 kDa mPEG. Mean + SD, n = 3.

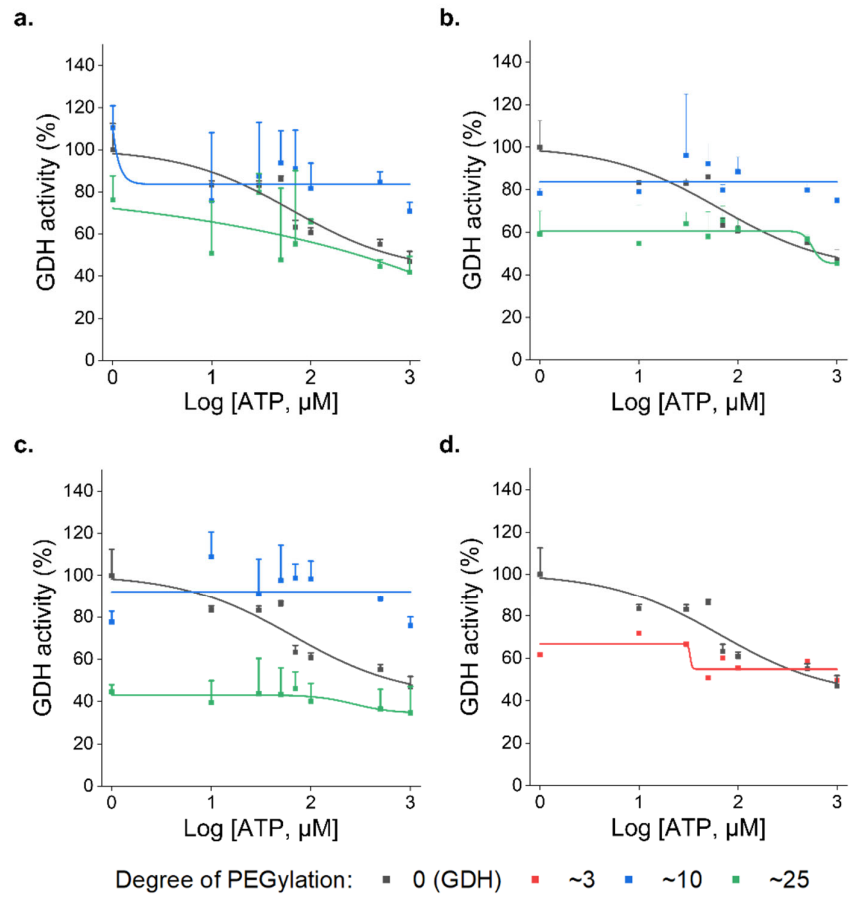


Figure S6| **Dose-activity curves of GDH and mPEG–GDH bioconjugates in the presence of ATP.** Panel (a) 0.5 kDa, (b) 2 kDa, (c) 5 kDa, and (d) 20 kDa mPEG. Mean + SD, n = 3.

**Table S3.** Solvent-accessibility of the lysine residues in the glutamate binding site, NAD-binding domain, antenna, and other regions. Calculated using the PDBePISA (Proteins, Interfaces, Structures and Assemblies) tool on [http://www.ebi.ac.uk/msd-srv/prot\\_int](http://www.ebi.ac.uk/msd-srv/prot_int), using PDB 3etg.

Region	Lysine residue	Degree of accessibility of residue on monomers 1–6 (Å <sup>2</sup> )					
		1	2	3	4	5	6
Glutamate binding domain	11	127.78	130.01	121.09	129.12	124.63	127.26
	27	77.12	76.94	74.51	75.89	75.99	76.49
	33	110.60	85.98	92.32	136.70	111.27	92.57
	41	18.41	18.53	18.86	17.93	18.80	19.51
	53	44.84	44.66	45.21	44.87	45.02	46.31
	90	0.00	0.00	0.00	0.00	0.00	0.00
	105	37.51	37.34	37.47	37.56	37.95	37.39
	114	0.32	0.34	0.17	0.50	0.16	0.17
	126	0.34	70.23	0.34	70.10	0.33	0.67
	130	70.47	3.44	69.21	3.81	70.84	69.72
	134	0.00	0.00	0.00	0.00	0.00	0.00
	143	0.00	0.00	0.00	0.00	0.00	0.00
	154	0.00	0.00	0.00	0.00	0.00	0.00
155	0.00	0.00	0.00	0.00	0.00	0.00	
201	4.17	0.00	3.55	0.00	3.80	4.17	
NAD	245	7.64	7.16	7.63	7.71	7.52	7.84

binding domain	269	0.00	80.76	80.32	80.01	79.66	79.29
	289	0.00	0.00	0.00	0.00	0.00	0.00
	295	0.00	0.00	0.00	0.00	0.00	0.00
	306	124.37	123.41	124.98	124.74	124.82	0.00
	308	0.00	0.00	0.00	120.63	0.00	121.34
	306	0.00	0.00	0.00	0.00	0.00	0.00
	329	32.04	42.28	35.09	26.62	30.70	33.66
	333	112.33	93.01	111.05	108.07	94.82	111.06
	340	0.00	0.00	0.00	103.60	103.26	102.80
	342	50.48	52.03	51.40	50.77	50.90	50.89
	358	103.19	103.32	100.78	102.43	104.38	103.76
	387	44.85	44.82	44.04	46.63	43.58	44.99
	Antenna, and other	423	200.65	0.00	0.00	0.00	199.77
470		138.63	137.70	139.48	139.65	137.07	139.45
488		32.13	39.93	44.74	39.98	38.66	41.22

**Table S4.** Details of the different PEGylated CG hexamer systems that were simulated.

PEG MW (kDa)	N <sub>bead/poly</sub>	N <sub>poly</sub>	PEG Distribution		
			Sim. N°	(Unit A/B/C/D/E/F)	PEG bead
0.5	12	25	1	5/3/4/6/4/3 (symmetric)	P1
			2	5/1/3/1/5/10 (asymmetric)	P1
2	46	25	3	3/4/4/4/5/5 (symmetric)	P1
			4	3/8/6/3/3/2 (asymmetric)	P1
			5	3/4/4/4/5/5 (symmetric)	P4
			6	3/8/6/3/3/2 (asymmetric)	P4
5	114	25	9	4/5/5/3/3/5 (symmetric)	P1
			10	7/6/3/3/3/3 (asymmetric)	P1

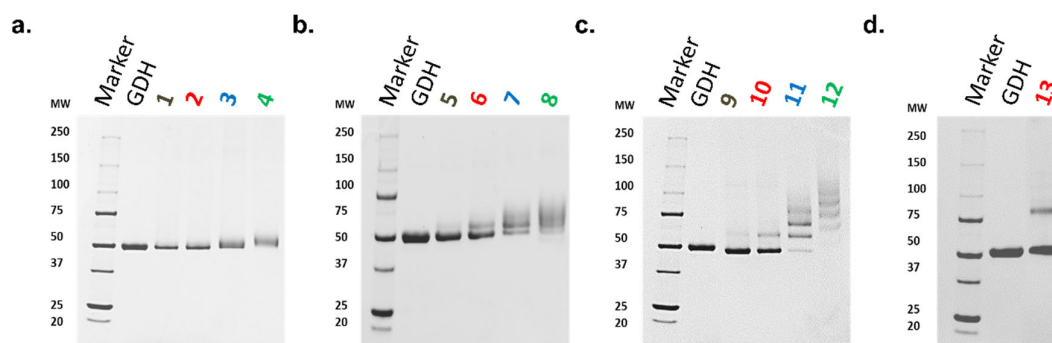


Figure S7| **Visualization of bioconjugates by SDS-PAGE.** Native GDH (lane 2) and mPEG–GDH bioconjugates (lane 3, 4, 5 and 6) were loaded into 4–15% polyacrylamide gels and compared to the molecular weight marker (lane 1). Bioconjugates prepared with varying mPEG lengths: (a) 0.5, (b) 2, (c) 5, and (d) 20 kDa.

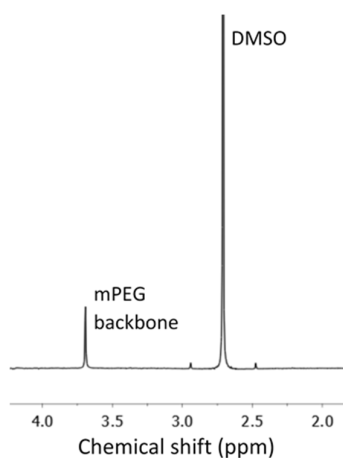


Figure S8| **Representative  $^1\text{H}$  NMR spectrum of mPEG–GDH bioconjugates in  $\text{D}_2\text{O}$** , with peaks corresponding to the backbone of mPEG and DMSO (internal concentration standard) identified. A known mass of mPEG–GDH bioconjugates was dissolved in 500  $\mu\text{L}$  of  $\text{D}_2\text{O}$  containing 10 $\mu\text{L}$  DMSO. By comparing the integral of the mPEG to that of DMSO, the number of moles of mPEG can be determined. This in turn can be used to ultimately determine the number of mPEG chains grafted on the GDH.

**Table S5.** Estimation of secondary structure of GDH and mPEG–GDH bioconjugates from CD spectra presented in **Fig. 4** (main article) calculated using CDNN (Circular Dichroism analysis using Neural Networks).

Bioconjugate	Helix (%)	$\beta$ -sheet (%)	Turn (%)	Random Coil (%)
GDH	45.5	9.3	14.3	30.1
<b>3</b>	41.2	11.1	15.1	31.1
<b>7</b>	42.3	10.5	14.9	30.6
<b>11</b>	37.2	13.2	15.8	33.5
<b>4</b>	31.5	14.3	17.4	35
<b>8</b>	30.3	11.4	17.8	41.5
<b>12</b>	24.9	13.9	18.7	43.5
<b>13</b>	41.5	10.9	14.8	33

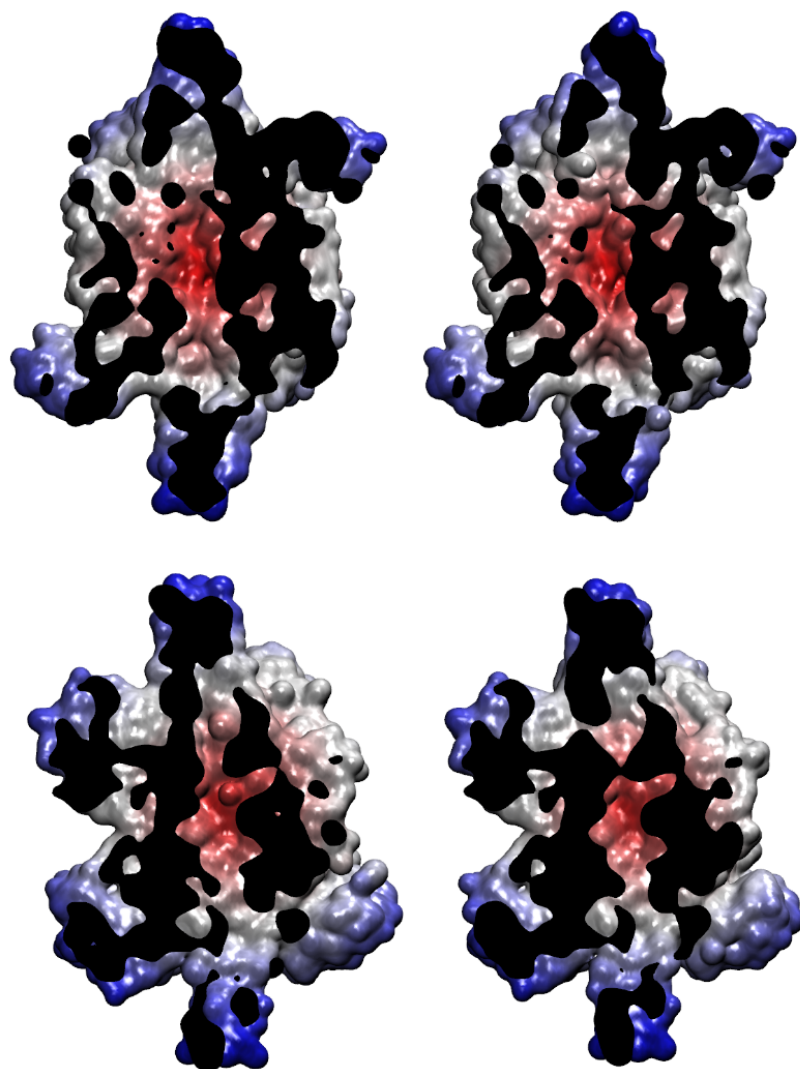


Figure S9| **Water cavity comparison.** Cross-section of the hexamer showing changes in the cavity in the lowest (left) and highest amplitudes (right) of movement for the first normal mode. The figure shows a coordinated movement of water molecules along the main axis. For the native protein (top frames), we are able to see three connected cavities: one for the top trimer, one for the bottom trimer, and one central cavity in the hexamer. The water cavities and constriction thereof during normal mode motion are significantly less pronounced in the P1 bead PEGylated protein (bottom frames).

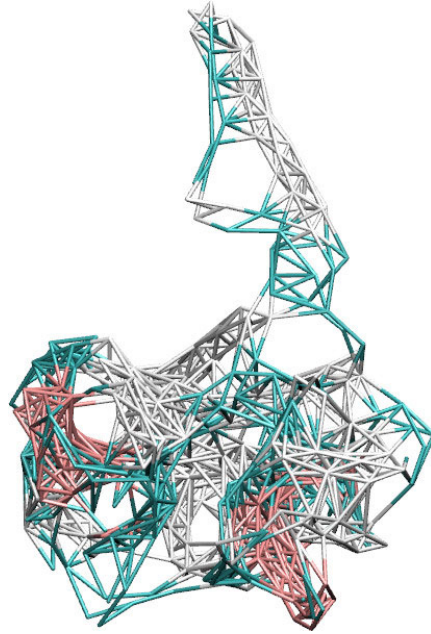


Figure S10| **Elastic network model associated to the protein units and linking backbone beads within the cut-off radii.** One of the six subunits is displayed. Pink lines denote links between  $\beta$  strand –  $\beta$  strand backbone beads, white lines denote  $\alpha$  helix –  $\alpha$  helix backbone bead links, and white links everything else, including coil–coil,  $\beta$  strand – coil and  $\alpha$  helix – coil backbone contacts.

## **APPENDIX B: Supplementary Information of Paper 2**

### **Sustained blood glutamate scavenging enhances protection in ischemic stroke**

Ahlem Zaghmi, Antonio Dopico-López, María Pérez-Mato, Ramón Iglesias-Rey, Pablo Hervella, Andrea A Greschner, Ana Bugallo-Casal, Andrés da Silva, María Gutiérrez-Fernández, José Castillo, Francisco Campos Pérez, and Marc A. Gauthier

A version of this chapter has been accepted for publication in  
Communications Biology.

The formatting of this article conforms to the specifications of the scientific journal.

Electronic Supporting Information

for

## **Sustained blood glutamate scavenging enhances protection in ischemic stroke**

Ahlem Zaghmi,<sup>1</sup> Antonio Dopico-López,<sup>2</sup> María Pérez-Mato,<sup>2,3</sup> Ramón Iglesias-Rey,<sup>2</sup> Pablo Hervella,<sup>2</sup> Andrea A Greschner,<sup>1</sup> Ana Bugallo-Casal,<sup>2</sup> Andrés da Silva,<sup>2</sup> María Gutiérrez-Fernández<sup>3</sup>, José Castillo,<sup>2</sup> Francisco Campos Pérez,<sup>2,\*</sup> and Marc A. Gauthier<sup>1,\*</sup>

<sup>1</sup> Institut National de la Recherche Scientifique (INRS), EMT Research Center, Varennes, Qc, J3X 1S2, Canada

<sup>2</sup> Clinical Neuroscience Research Laboratory, Health Research Institute of Santiago de Compostela (IDIS), Santiago de Compostela, Spain.

<sup>3</sup> Neuroscience and Cerebrovascular Research Laboratory, Department of Neurology and Stroke Center, La Paz University Hospital, Neuroscience Area of IdiPAZ Health Research Institute, Universidad Autónoma de Madrid, Madrid, Spain.

Corresponding authors:

Marc A. Gauthier

Institut National de la Recherche Scientifique (INRS), EMT Research Center, 1650 boul. Lionel-Boulet, Varennes, J3X 1S2, Canada

E-mail: gauthier@emt.inrs.ca

Telephone: +1 514 228 69 32

Francisco Campos Pérez

Clinical Neuroscience Research Laboratory, Hospital Clínico Universitario, Travesía da Choupana s/n, 15706 Santiago de Compostela, Spain

Email: francisco.campos.perez@sergas.es

Phone: +34 981951097

Fax: +34 981951086

Conflict of interest: None to declare

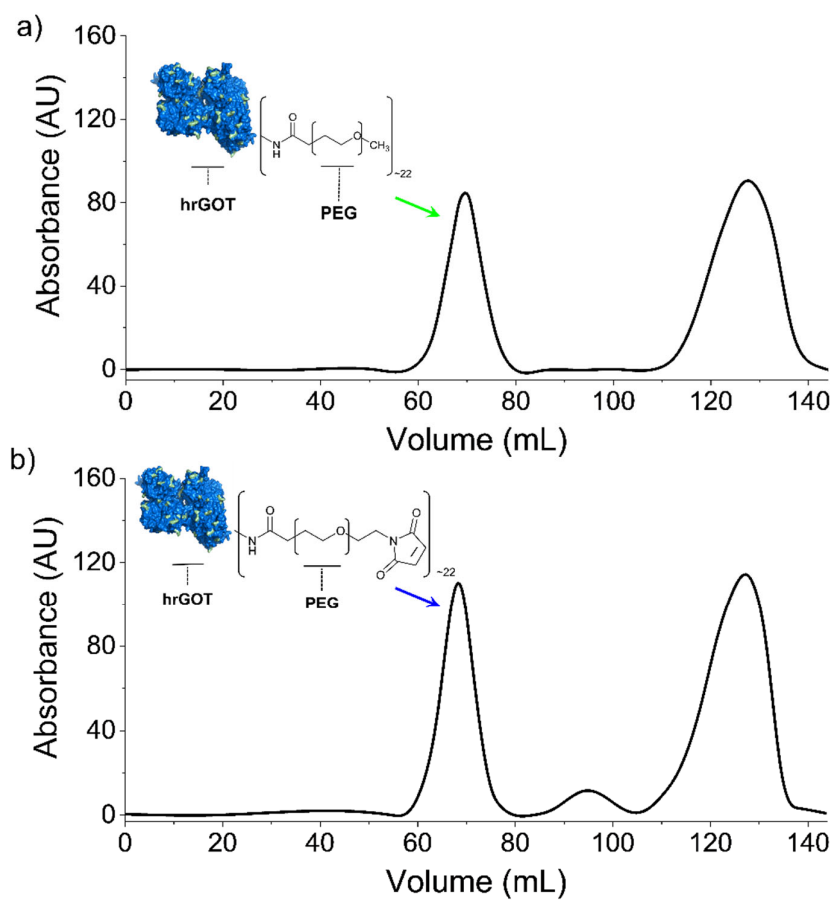


Figure S1| **FPLC chromatograms for the purification of (a) mPEG-hrGOT and (b) Mal-PEG-hrGOT.** Size exclusion chromatography was used to purify the bioconjugates after each reaction (peaks corresponding to mPEG-hrGOT and Mal-PEG-hrGOT are identified).

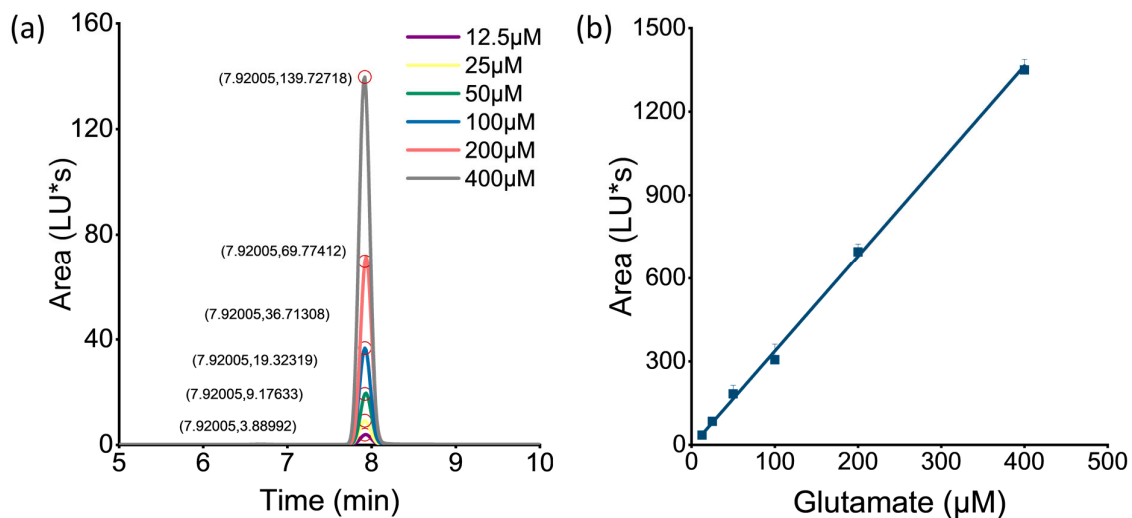


Figure S2| Quantification of Glutamate in serum by HPLC. (a) Representative chromatograms of glutamate (pre-column derivatized with o-pathaldialdehyde/2-mercaptoethanol) at different concentrations. (b) Calibration curves for glutamate.

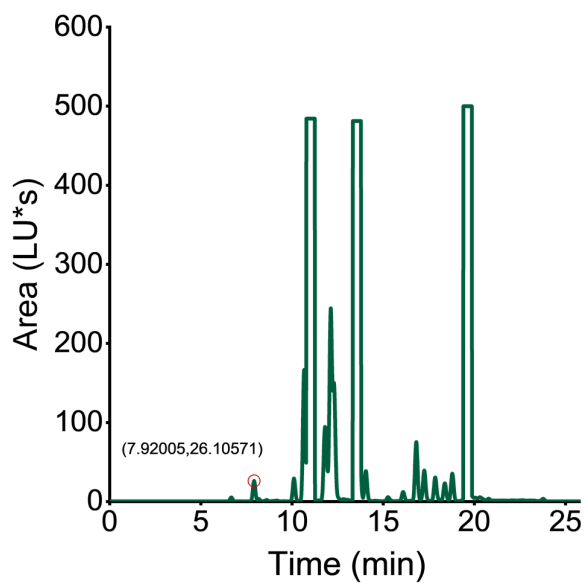


Figure S3| Representative chromatogram of serum (pre-column derivatized with o-pathaldialdehyde/2-mercaptoethanol). Fluorescence detection ( $\lambda_{ex} = 340 \text{ nm}$  ;  $\lambda_{em} = 450 \text{ nm}$ ). Peak of glutamate identified.

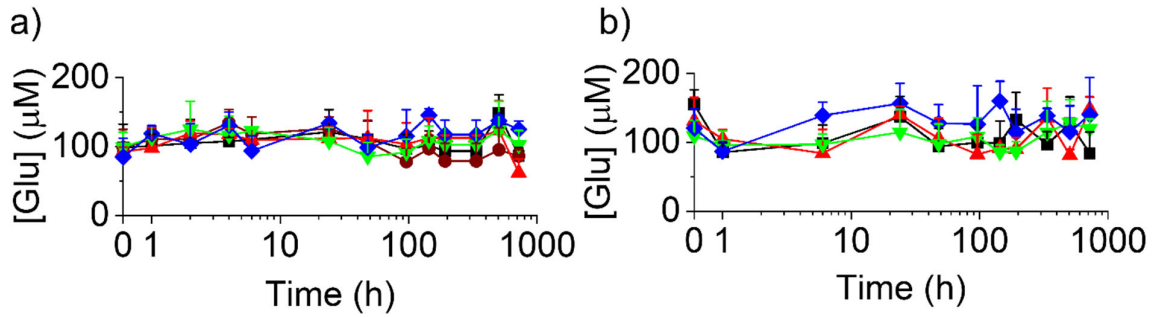


Figure S4| Effects of native hrGOT, mPEG-hrGOT, and Angiopep-PEG-hrGOT on serum glutamate levels in (a) healthy and (b) MCAo rats. No change in steady-state blood glutamate concentrations was observed following intravenous administration in rats. Data presented as Mean + SD, n = 3–5.

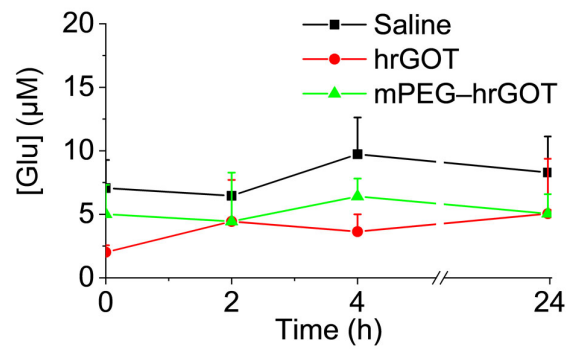


Figure S5| Effects of native hrGOT, mPEG-hrGOT, and Angiopep-PEG-hrGOT on CSF glutamate levels in healthy rats. The glutamate levels were monitored in CSF samples taken at specific time points. Data presented as Mean + SD, n = 3–5.

**Table S1.** Solvent-accessibility of the lysine residues in hrGOT. Calculated using the PDBePISA (Proteins, Interfaces, Structures and Assemblies) tool on [http://www.ebi.ac.uk/msd-srv/prot\\_int](http://www.ebi.ac.uk/msd-srv/prot_int), using PDB 3ii0.

Lysine residue	Degree of accessibility of residue on monomers 1–2 (Å <sup>2</sup> )	
	1	2
6	114.19	114.31
19	57.83	57.42
41	119.16	116.69
42	93.84	94.65
46	115.58	112.54
83	144.05	143.32
85	85.31	152.84
116	60.19	62.76
140	155.38	153.29
152	104.20	79.79
193	76.49	98.74
200	64.43	76.20
245	31.24	29.45
262	124.65	126.17
276	81.82	79.99
311	90.74	89.94
332	164.97	164.25
355	46.27	69.25
364	28.43	27.38
382	126.24	127.80
397	142.26	141.95
405	126.84	123.39

**Table S2.** Pharmacokinetic parameters (half-life ( $t_{1/2}$ ) and Area under the curve (AUC)) of native hrGOT, mPEG–hrGOT, and Angiopep–PEG–hrGOT following intravenous administration in rats (data extracted from Figure 2).

	Circulation $t_{1/2}$ (h)	Elimination $t_{1/2}$ (h)	AUC ((U/L) × h)
hrGOT	2	6	52542
mPEG–hrGOT	92	192	843805
Angiopep–PEG–hrGOT	92	192	866182

**Table S3.** Representative ADC maps (Day 0) and T2-weighted images (Day 1 –30) of the 14 consecutive coronal rat brain slices (hind brain to fore brain) from each group at each time point investigated. Regions of interest including the motor cortex (M1/M2), the primary sensory cortex (S1), and the secondary sensory cortex (S2) are identified on one image for illustrative purposes. Note the background was subtracted from Slices 7 and 8 for use as display items in Figure 3 of the Main article.

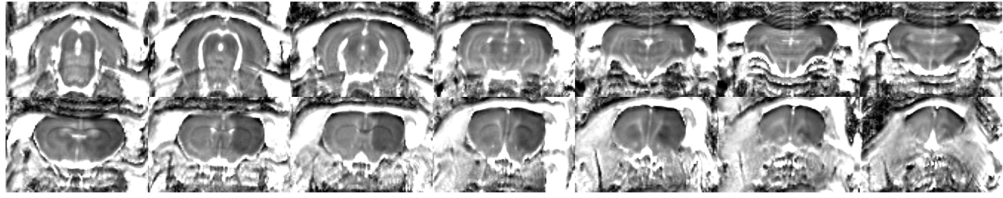
Slice 1	Slice 2	Slice 3	Slice 4	Slice 5	Slice 6	Slice 7
Slice 8	Slice 9	Slice 10	Slice 11	Slice 12	Slice 13	Slice 14

---

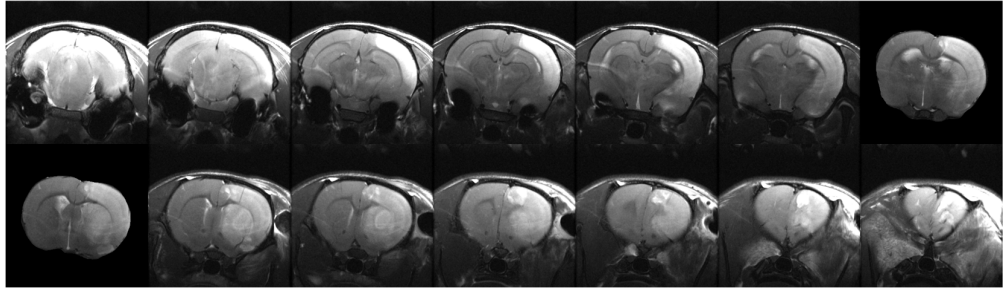
**Saline**

---

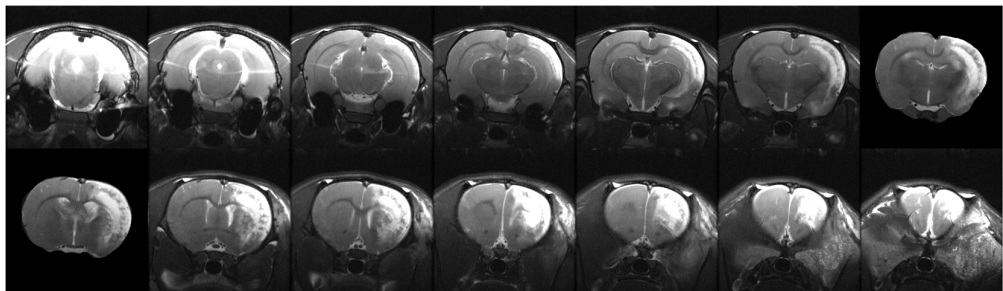
**Day 0**



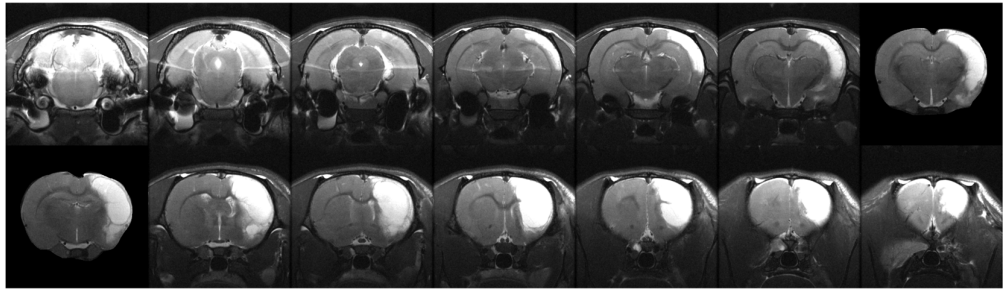
**Day 1**



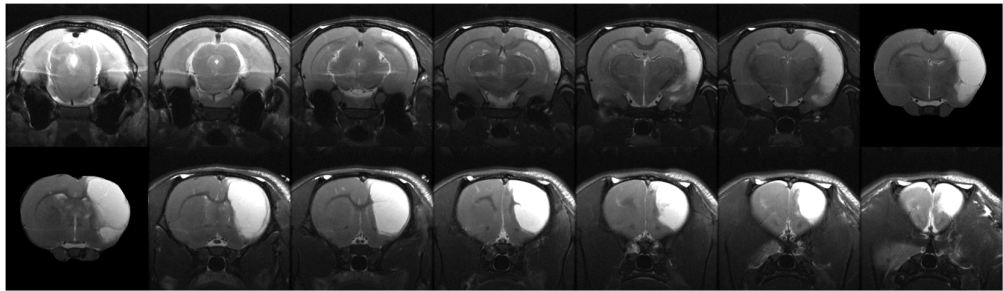
**Day 7**



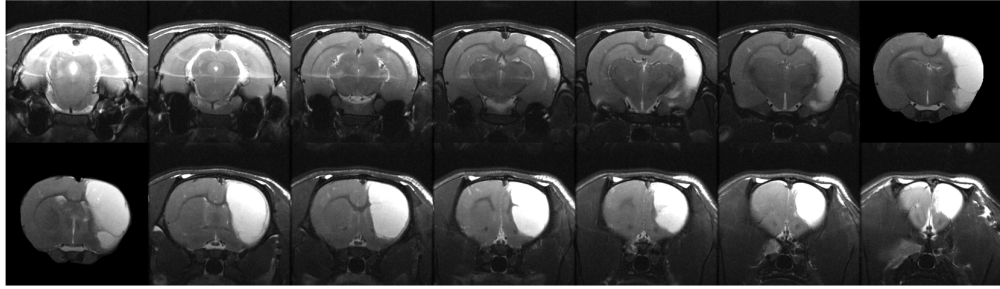
**Day  
14**



**Day  
21**

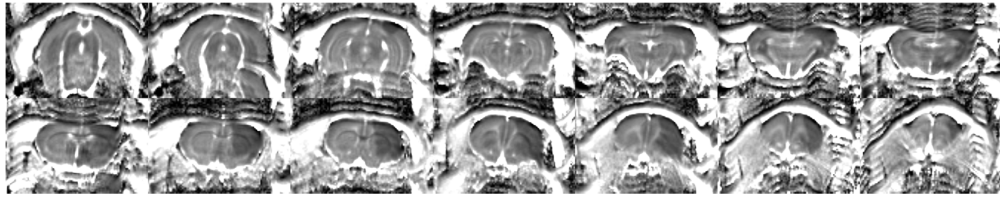


Day  
30

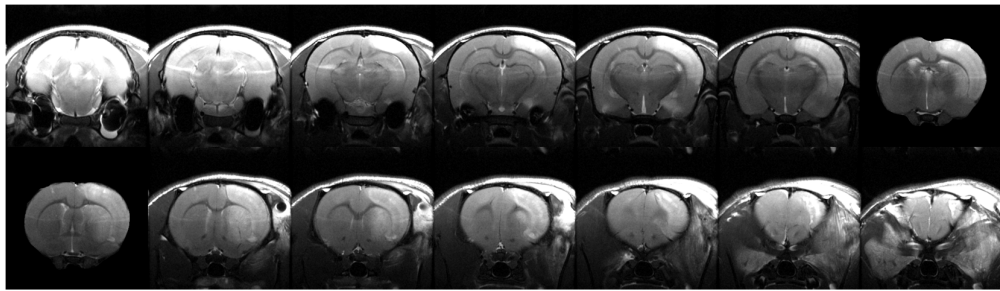


hrGOT

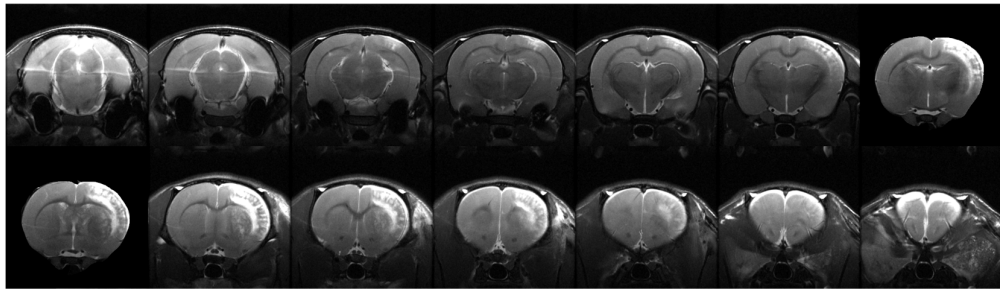
Day 0



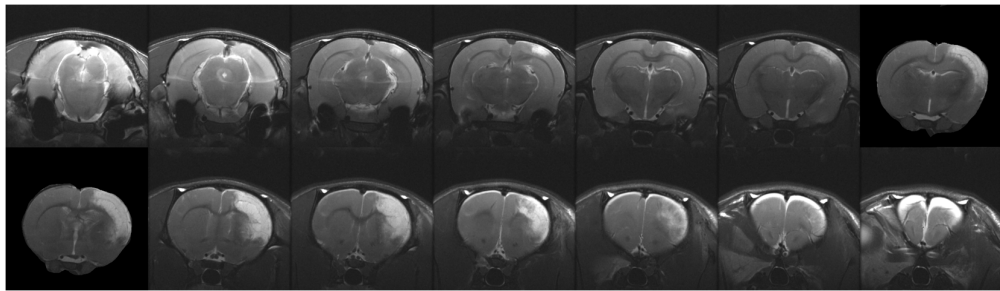
Day 1



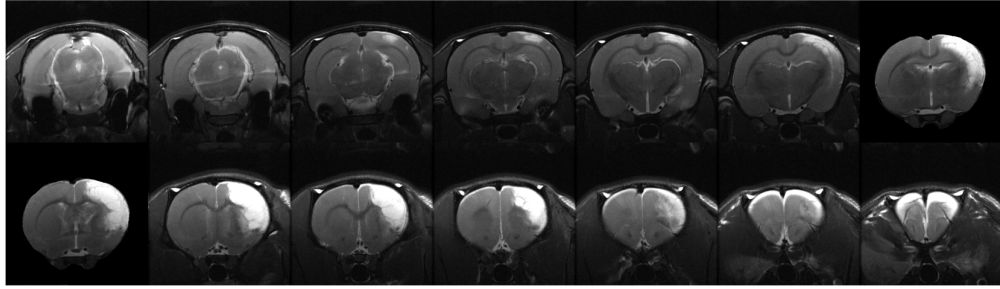
Day 7



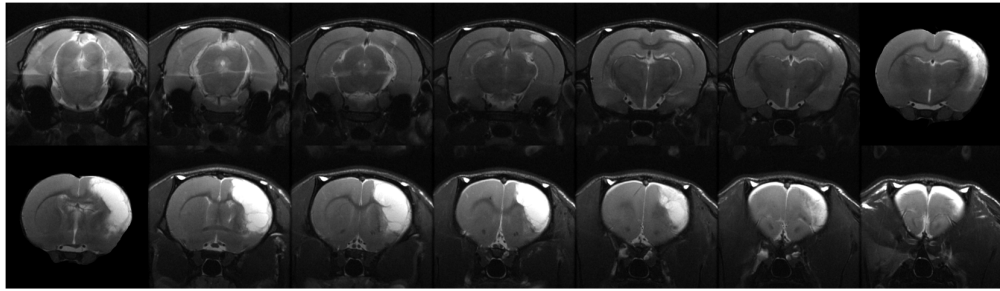
Day  
14



Day  
21

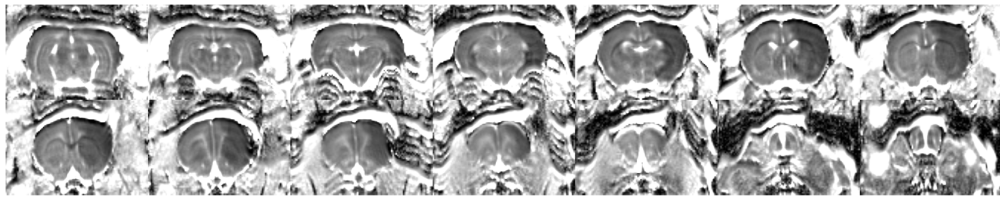


Day  
30

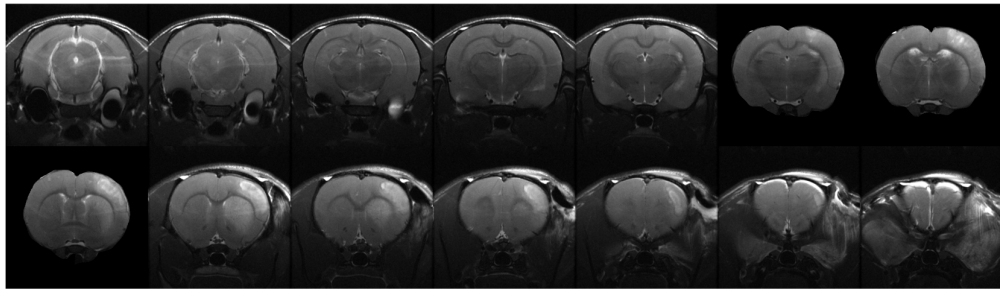


mPEG-hrGOT

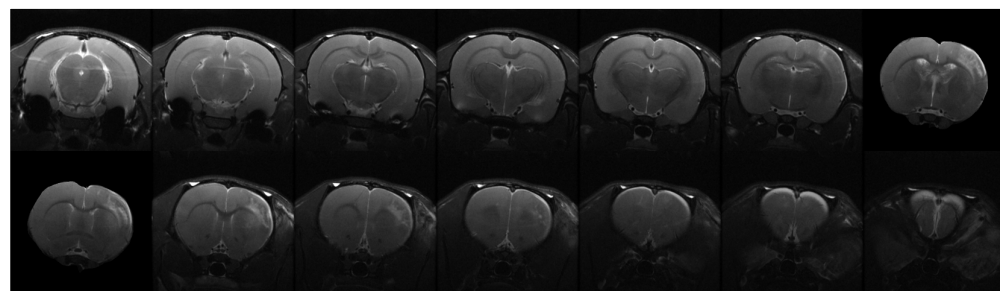
Day 0



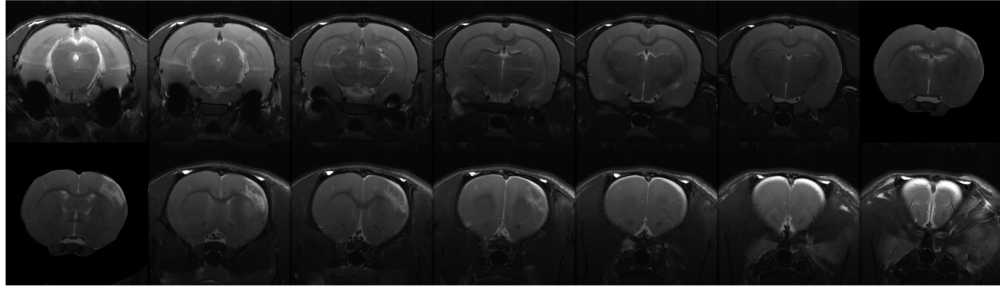
Day 1



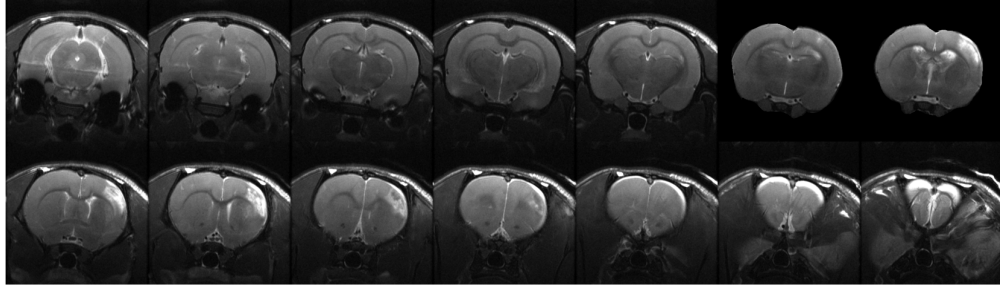
Day 7



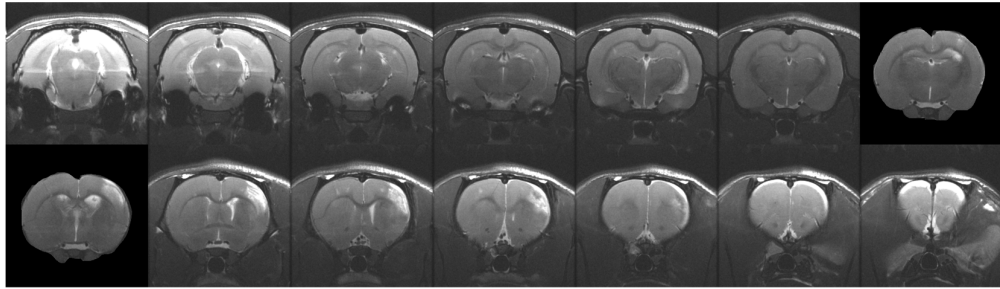
Day  
14



Day  
21

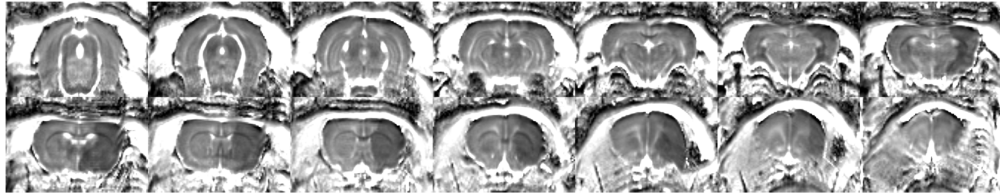


Day  
30

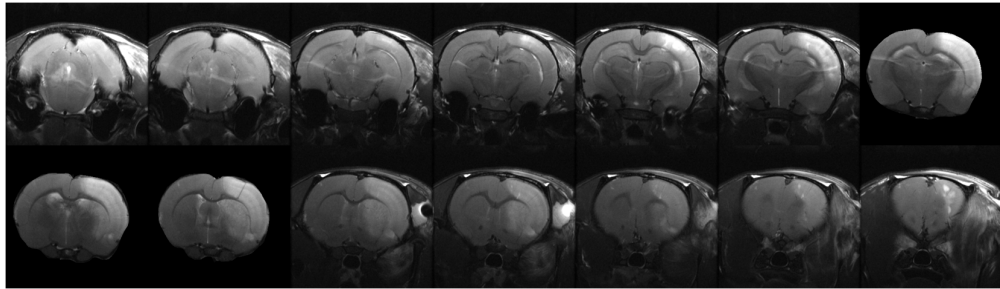


mPEG-hrGOT

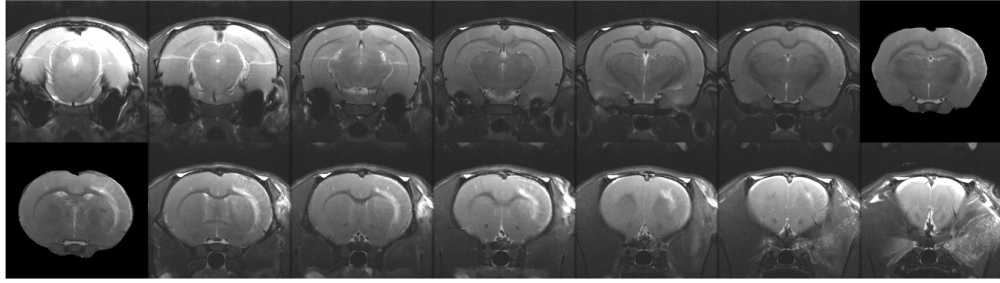
Day 0



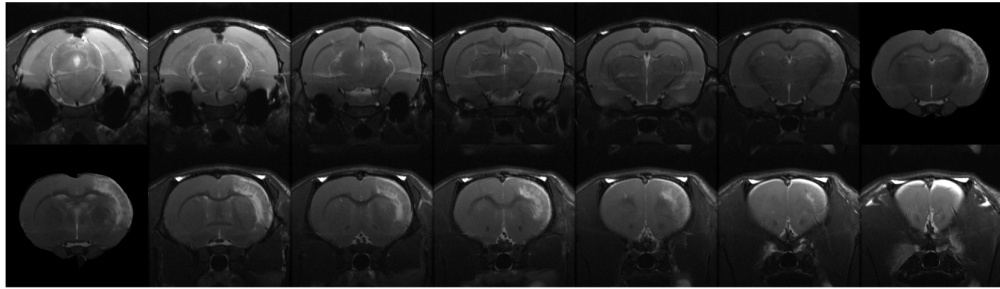
Day 1



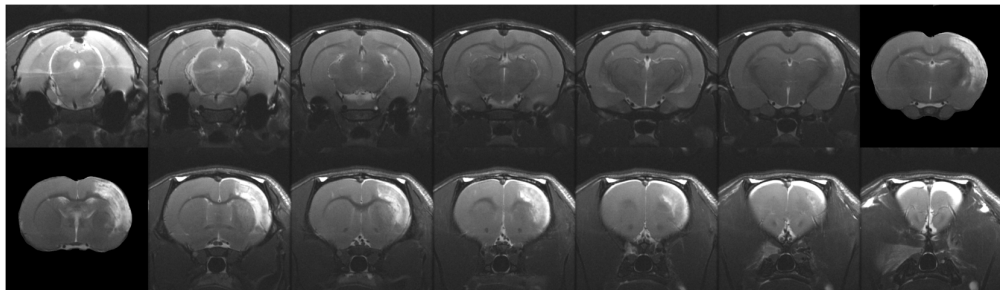
**Day 7**



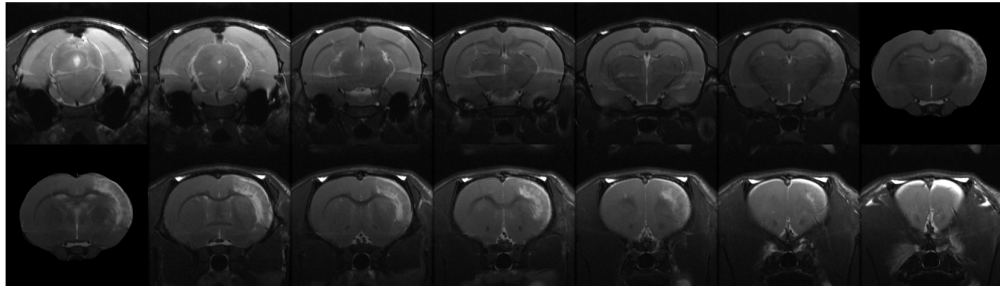
**Day  
14**



**Day  
21**



**Day  
30**



## **APPENDIX C: Review Paper**

### **Treating Brain Diseases using Systemic Parenterally-administered Protein Therapeutics: Dysfunction of the Brain Barriers and Potential Strategies**

A Zaghmi, J Drouin-Ouellet, D Brambilla, and MA Gauthier

A version of this chapter has been accepted for publication in  
Biomaterials.

The formatting of this article conforms to the specifications of the scientific journal.

# Treating Brain Diseases using Systemic Parenterally-administered Protein Therapeutics: Dysfunction of the Brain Barriers and Potential Strategies

A Zaghmi<sup>1</sup>, J Drouin-Ouellet<sup>2</sup>, D Brambilla<sup>2</sup>, and MA Gauthier<sup>1,\*</sup>

<sup>1</sup> Institut National de la Recherche Scientifique (INRS), EMT Research Center, Varennes, Qc, J3X 1S2, Canada

<sup>2</sup> Faculty of Pharmacy, Université de Montréal, CP 6128, succ. Centre-ville, Montréal, QC H3C 3J7, Canada

## Abstract

The parenteral administration of protein therapeutics is increasingly gaining importance for the treatment of human diseases. However, the presence of practically impermeable blood–brain barriers greatly restricts access of such pharmaceuticals to the brain. Treating brain disorders with proteins thus remains a great challenge, and the slow clinical translation of these therapeutics may be largely ascribed to the lack of appropriate brain delivery system. Exploring new approaches to deliver proteins to the brain by circumventing physiological barriers is thus of great interest. Moreover, parallel advances in the molecular neurosciences are important for better characterizing blood–brain interfaces, particularly under different pathological conditions (e.g., stroke, multiple sclerosis, Parkinson's disease, and Alzheimer's disease). This review presents the current state of knowledge of the structure and the function of the main physiological barriers of the brain, the mechanisms of transport across these interfaces, as well as alterations to these concomitant with brain disorders. Further, the different strategies to promote protein delivery into the brain are presented, including the use of molecular Trojan horses, the formulation of nanosystems conjugated/loaded with proteins, protein-engineering technologies, the conjugation of proteins to polymers, and the modulation of intercellular junctions. Additionally, therapeutic approaches for brain diseases that do not involve targeting to the brain are presented (i.e., sink and scavenging mechanisms).

## Introduction

Over the last three decades, considerable advances have been made in unravelling the very specific and complex role proteins play as key molecules in the regulation of most cellular and molecular physiological processes. As a result of this progress, proteins have been proposed

as potential therapeutic molecules for treating many disorders of the central nervous system (CNS) such as neurovascular, neuroinflammatory, and neurodegenerative diseases. Nevertheless, proteins face several challenges that can render them ineffective as therapeutic agents for brain diseases, especially when delivered *via* the systemic route. Indeed, while systemic parenteral delivery is not the most efficient route for achieving high protein concentrations in the CNS, it is clinically the most convenient and widely used one. Obstacles to targeting proteins to the brain include the unfavorable pharmacokinetic properties of exogenous proteins (e.g., rapid serum degradation and/or clearance). Indeed, proteins are generally charged, large, hydrophilic, and have a high potential for forming hydrogen bonds<sup>518</sup>, which according to Lipinski's "Rule of 5" usually correlate to poor membrane absorption and permeation (i.e., not conducive for passive diffusion *via* transcellular and paracellular pathways)<sup>519</sup>. Furthermore, the presence of various physiological blood–brain interfaces such as the blood-brain barrier (BBB) prevent unwanted molecules from penetrating the brain. For instance, it has been reported that molecules with hydrodynamic diameters larger than 11 Å or molecular weight of 500 Da are too large to pass through this barrier<sup>520,521</sup>. Accordingly, in order to address and to overcome these issues, many strategies have been evaluated to achieve effective and sustained delivery of proteins to the diseased area of the brain, in a non-invasive manner. In addition to this, much effort has been devoted to understand the pathological processes accompanying neurological disorders (mainly those related to the alteration of the blood-brain interfaces), which might offer some opportunities (or reveal new challenges) for promoting brain delivery.

This review covers strategies explored thus far to deliver therapeutic proteins to the brain using systemic parenteral administration. Herein, parenteral administration refers to all the parenteral routes with the exception of those that physically bypass the blood-brain physiological interfaces (i.e., direct CNS administration). The efficacy of various approaches used to deliver proteins to the brain will be discussed, and the advantages and disadvantages of each strategy will be exposed. In addition, the *in vivo* therapeutic effectiveness of proteins delivered to treat neurological disorders will be presented. The administration of peptides and proteins *via* intranasal or direct CNS administration/injection as well as strategies using gene or cell approaches for CNS delivery of peptides and proteins will not be covered and are reviewed elsewhere<sup>21-23,522-524</sup>.

## **1. The Blood-Brain Barrier and the Blood-Cerebrospinal Fluid Barrier**

The concept of a barrier between the blood and the CNS was established by Paul Ehrlich, following the demonstration that a systemically administered dye could stain most organs, but

not the brain or spinal cord<sup>74</sup>. From these early observations, much knowledge was gained on how these barriers participate in brain-periphery crosstalk, protecting the brain, and maintaining cerebral homeostasis. There are three main interfaces: the blood-brain barrier (BBB), the blood-cerebrospinal fluid barrier (BCSFB), and the arachnoid barrier. These barriers are communally named blood-brain interfaces and can be found in multiple locations in the body. Additional interfaces include the blood-retinal barrier and the blood-spinal cord barrier (Figure 1)<sup>75,76</sup>.

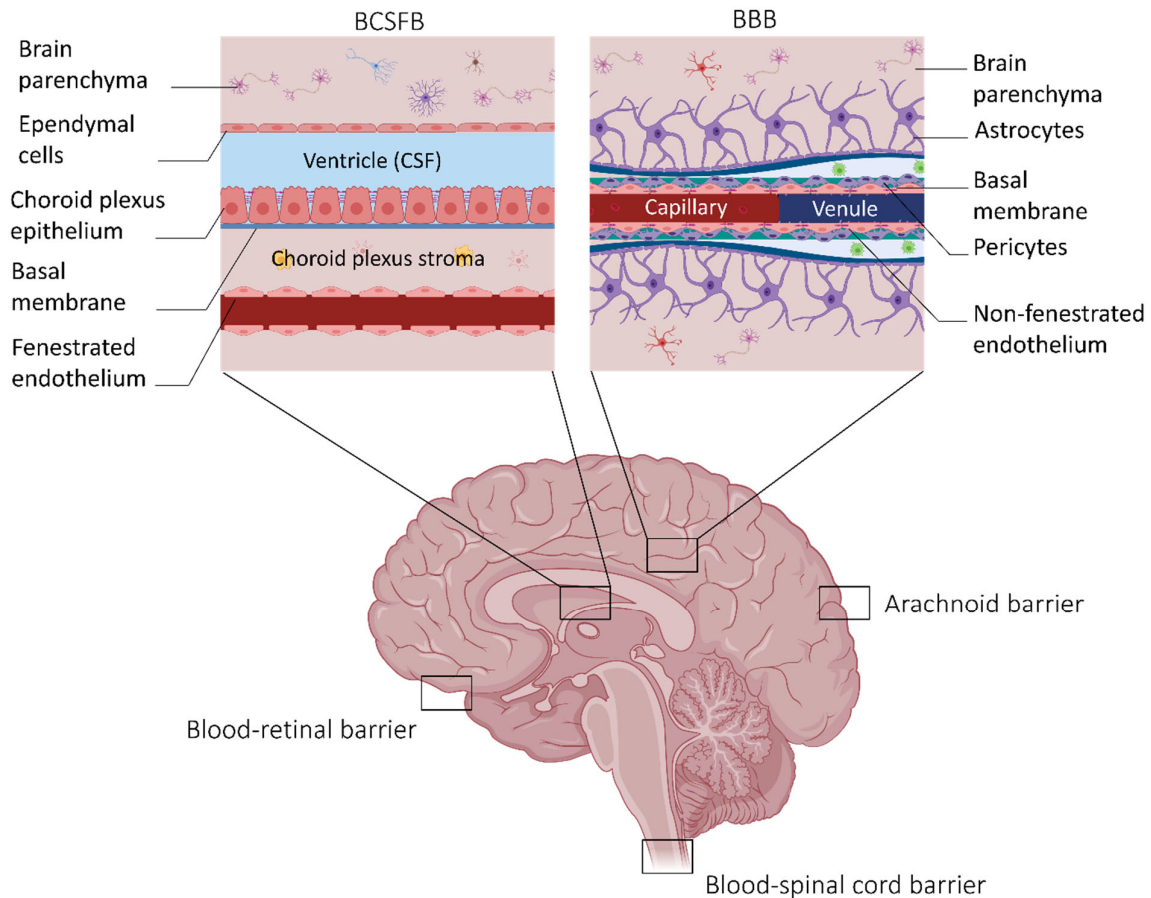


**Figure 1: Location of the barriers of the nervous system and structure of the BBB and BCSFB.** The five barriers include the BBB, the BCSFB, the arachnoid barrier, the brain-retinal barrier, and the blood-spinal cord barrier. All of these are represented in a longitudinal brain section. **(a)** Schematic representation of the BCSFB: the capillaries in the choroid plexus permit the facile diffusion of molecules *via* intracellular fenestrations. Epithelial cells are joined by adherens and tight junctions. The presence of microvilli increases the surface area of the CSF-facing side of the epithelial cells, secrete CSF into the ventricles. **(b)** Schematic representation of the BBB: the BBB is composed of a high density of cells that restrict the passage of substances to the brain parenchymal tissues and protect neurons from systemically circulating toxins. The BBB is composed of endothelial cells that are surrounded by a basal membrane in close association with astrocyte end feet and pericytes. Neurons and microglia

are also important mediators of BBB integrity. Cerebral endothelial cells are sealed together by tight junctions. These proteins are anchored to endothelial cells by protein complexes comprising zona occludens (ZO-1, -2, and -3).

The difference regarding the cellular basis of the structures of the BBB and the BCSFB reflects the dissimilarity in their principal functions. For instance, the BBB is a discriminatory barrier that protects the brain from molecules in the blood that can interfere with neurotransmission, in addition to dampening the effect of physiological fluctuations in plasma levels of other solutes. Moreover, it provides routes for the exchange of nutrients, signaling molecules, ions, and metabolic waste products between the interstitial fluid in the brain and the blood. In contrast, the BCSFB secretes CSF (a process that could be considered as the main function of this epithelium) and plays a role in the exchange of various solutes and molecules between the blood and the CSF <sup>77</sup>.

The formation and function of the BBB depend on close cell-to-cell connections at the neurovascular unit. The neurovascular unit is composed of specialized microvascular endothelial cells with their basal lamina covered with pericytes, smooth muscular cells, astrocyte end feet, neurons, and an extracellular matrix <sup>78</sup>. The restrictive characteristics of this barrier come from the complex structures expressed by the brain capillaries. Indeed, brain endothelial cells possess many active efflux transport proteins (see section 1.1). Furthermore, the tight junctions (TJs) between cells are among the most restrictive sealing elements in the body. They comprise three integral membrane proteins (claudin, occludin, and junction adhesion molecules (JAM)) and multiple accessory proteins such as zona occludens (ZO), cingulin, and others <sup>79,80</sup>. The spatial positioning of these junctional scaffolding proteins affects anchoring to the cytoskeleton as well as the downstream signaling events regulating junctional dynamics. The BBB also has additional enzymatic components that can degrade compounds, which can prevent their accumulation in the brain or accelerate their elimination. Molecules crossing the cerebral endothelial cells are thus exposed to ecto- and endo-enzymes present within endothelial cells containing a high density of metabolically active organelles (such as mitochondria). In addition, brain endothelial cells display low pinocytotic activity and the endothelium is separated by non-neuronal cells on the brain side (e.g., pericytes), which places additional restrictions on permeability <sup>77</sup>.

The selectivity and permeability properties of the choroid plexus membrane are strongly associated with the BCSFB. The choroid plexus is a vascular tissue localized in cerebral ventricles. The functional unit of the choroid plexus tissue at the blood side is composed of somewhat leaky fenestrated and highly permeable capillaries <sup>81</sup>. This capillary wall is bordered by a monolayer of epithelial cells linked together by TJs and facing the CSF. Therefore, all

molecules traversing the endothelium should pass by the epithelium in order to reach the CSF. The choroid plexus is roughly one hundred-fold leakier than the BBB, based on their respective electrical resistance and on lanthanum ion transport experiments<sup>82</sup>. Therefore, alongside other roles of the choroidal plexus (such as active production and secretion of CSF, drug metabolism, and antioxidant capacities), this tissue develops a substantial surface area of exchange.

Overall, these barriers are more than simple anatomical obstacles. They are also active tissues that express a diverse range of transporters, receptors, and enzymes. They can recognize therapeutic CNS agents, such as proteins, which in turn can reduce their efficacy due to lower brain bioavailability. Furthermore, considering the general physicochemical properties of proteins (e.g., charged, large, hydrophilic) that further hinder their ability to cross physiological barriers, the delivery of these pharmacologically active macromolecules is highly challenging.

### **1.1. Transport Across the BBB and the BCSFB**

Depending on their physicochemical properties, the penetration of molecules into the brain may occur by the following routes: (1) paracellular transport (small hydrophilic molecules); (2) transcellular passive diffusion (lipophilic and nonpolar solutes such as carbon dioxide and oxygen); (3) carrier-mediated transport by the diverse members of the solute carrier (SLC) family of transporters; (4) adsorptive-mediated transcytosis (internalization of molecules following a nonspecific interaction); and (5) receptor-mediated transcytosis (RMT) ([Figure 2.a](#)). In the following sections, transporter-mediated passage, adsorptive endocytosis, and especially RMT-mediated transport mechanisms will be discussed.

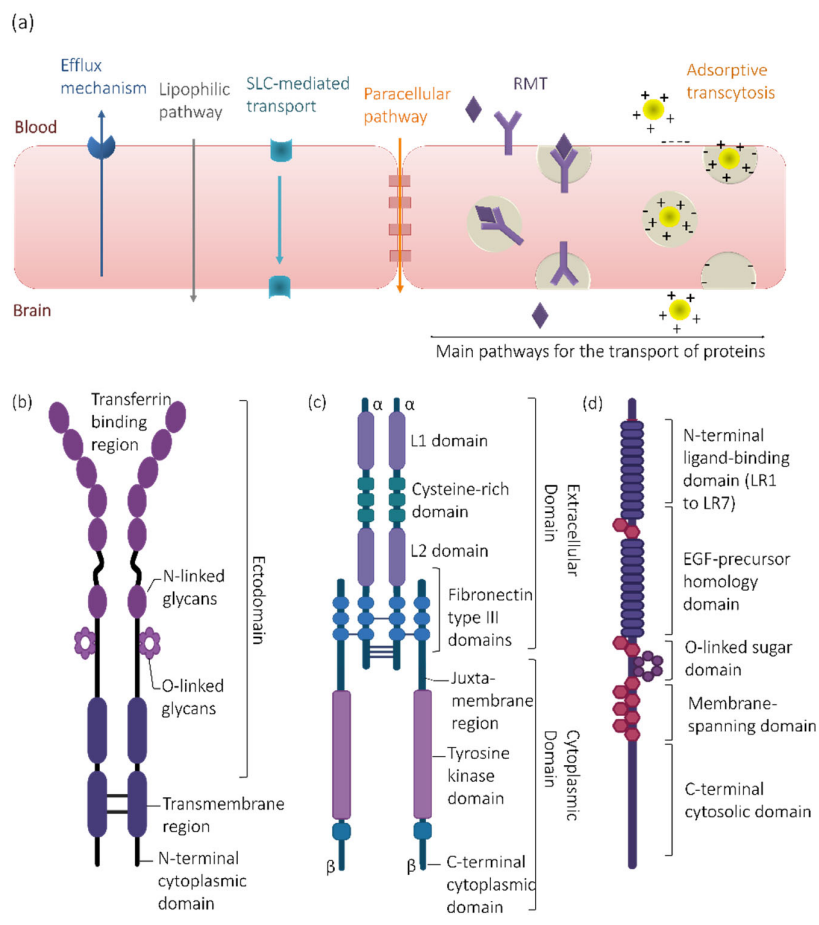


**Figure 2: Transport mechanisms across brain barriers (a) and the general structure of the transferrin receptor (TfR) (b), Insulin receptor (c), and Low-density lipoprotein receptor (LDLR) (d).** Scheme of the possible mechanisms for drug transport across brain interfaces. Efflux transporters are located on the luminal side of the cellular barriers and restrict brain uptake of therapeutics. Small and lipid-soluble molecules passively diffuse across the cell membrane. Small compounds such as amino acids, nucleosides, and glucose are transported by solute carrier (SLC) transporters. Paracellular transport of small hydrophobic molecules is essentially negligible in healthy barriers. Endogenous plasma proteins cross the cells by adsorptive-mediated endocytosis. Endogenous large molecules (such as proteins) can bind to receptors on the luminal side, be endocytosed, transported across the cell, and ultimately released at the abluminal side. The structure of the most characterized and investigated receptors present within the physiological interfaces is presented (see main text for more details). These receptors have been largely explored as brain targeting entities for proteins *via* a receptor-mediated transcytosis mechanism (RMT).

### 1.1.1. Carrier-mediated transport

The exchange of low molecular weight (MW) organic molecules between the brain and the blood is regulated by specific plasma membrane transporters located on the wall of the endothelial/choroidal epithelial cells forming the BBB/BCSFB. The direction of transport is

dictated by the subcellular localization of the transporter (luminal or basolateral side), as well as by the transport mechanism (energy-dependent or energy-independent). Nutrients are provided to the brain by blood-to-brain influx transporters, whereas efflux transporters remove potentially deleterious metabolites and neurotoxins from the brain parenchyma. Moreover, drug efflux pumps expressed on the luminal side actively transport a huge variety of drugs out of the BBB/BCSFB and back into blood, thereby restricting their distribution to the brain. The transporters mostly belong to two super-families: the adenosine triphosphate binding cassette (ABC) transporters and the SLC transporters. The superfamily of ABC transporters directly couple ATP hydrolysis to the active efflux of molecules against unfavourable concentration gradients and across the cell membrane<sup>83</sup>. The ABC active transporters are primarily found at the blood-facing membranes of brain microvasculature cells<sup>84</sup>. They involve ~48 distinct transporters categorized into seven families (ABC A through G)<sup>85</sup>. Relevant ABC transporters include multidrug-resistance proteins (MDRs or ABCB111), multidrug resistance-related proteins MRPs (ABCC15), and breast cancer-resistance proteins (BCRP or ABCG18)<sup>85</sup>. These multi-specific efflux transporters are differently distributed between the BBB and the BCSFB and prevent the brain accumulation of a vast array of lipophilic and amphipathic molecules *via* an energy-dependent and outwardly directed (unidirectional) transport mechanism. ABCB1 and ABCG2 are highly expressed at the BBB, while ABCC1 is enriched at the BCSFB<sup>87,525</sup>. The first and most investigated MDR protein is the P-glycoprotein (also referred to as MDR1 or ABCB1), a 170 kDa phosphorylated glycoprotein<sup>86</sup> that is greatly expressed on the endothelial cells of capillaries, and poorly expressed on epithelial cells of the choroid plexus<sup>87</sup>. Recently, it has been further detected on the abluminal surface of the BBB, although little is known about its function at this location<sup>88</sup>. Its localization and substrate promiscuity make it an effective defense mechanism against a wide spectrum of endogenous ligands, therapeutic drugs, and xenobiotics<sup>89</sup>. The second superfamily named SLC includes facilitated transporters, ion-coupled transporters, and exchangers that are ATP-independent<sup>90</sup>. Some of these SLC are bidirectional and others are unidirectional. These transporters are mainly responsible for the transport of molecules that are unable to diffuse across the blood-brain interfaces due to their hydrophilicity, such as amino acids<sup>91</sup>.

### **1.1.2. Adsorptive endocytosis**

Endocytosis can be described as the invagination of the cell membrane that leads to the creation and trafficking of intracellular vesicles ultimately leading to the cytoplasm. Endocytosis can be divided into fluid-phase endocytosis, adsorptive endocytosis, and RMT. For the two first modes, uptake does not require mediation by membrane receptors, while the third mode requires induction by the binding of specific ligands to their respective membrane receptors

<sup>526</sup>. Both adsorptive endocytosis and RMT are saturable transport processes, with adsorptive endocytosis being saturated at much higher concentration (i.e., maximum binding capacities for adsorptive endocytosis and RMT range from nanomoles to < 1 picomoles per milligram of membrane protein, respectively) <sup>23,527</sup>. However, by adjusting these values by their affinity constants, the affinity–capacity product for adsorptive endocytosis is somewhat similar to that for RMT <sup>527</sup>. While the uptake mechanism of molecules does not always require energy, transcytosis is an energy-requiring process (either for transport across the cell or for exocytosis at the basolateral side of the up-taken molecules). Energy-dependent transcapillary vesicular transport correlates to enhanced cerebral capillary activity, as established by a greater density of mitochondria present in cerebral endothelial cells (i.e., roughly five times greater than in peripheral endothelium) <sup>528</sup>. Unlike small or lipophilic molecules, macromolecule transport appears to proceed exclusively *via* the vesicular system. Over six distinct categories of endocytic vesicles exist, and major specific types have been identified for macromolecules at the blood-brain interfaces: clathrin-coated pits responsible for the majority of RMT; caveolae vesicles that facilitate nonselective adsorptive-mediated endocytosis of extracellular proteins as well as the trafficking of some membrane receptors; clathrin/caveolin-independent endocytosis; and macropinocytotic vesicles mediating the uptake of various extracellular components <sup>529</sup>.

The discovery of adsorptive endocytosis within the BBB came from the observation that polycationic molecules can bind to the vascular endothelium and penetrate the BBB <sup>92,93</sup>. Furthermore, the cationization of proteins (e.g., albumin) or their mixing with cationic molecules (e.g., protamine (small, arginine-rich, nuclear protein) or poly-L-lysine) greatly increases their permeability across the BBB <sup>94,95</sup>. In adsorptive endocytosis, the interaction between a ligand and cell surface is required, such as when a positively-charged molecule interacts with the negatively-charged cell membrane <sup>96</sup>. Following endocytosis, the intracellular transport of molecules occurs by the vesicular system, with the formation of clathrin-coated, *caveolae*-coated, or *macropinocytotic vesicles* <sup>97</sup>. While *caveolae*-dependent endocytosis appears to be the most common mode for adsorptive endocytosis, the vesicle carrier remained unidentified in many papers <sup>23,94</sup>. Once the vesicle is internalized, it progresses into an early endosome. Thereafter, the contents of the vesicles can either be delivered directly to the cytoplasm, degraded in lysosomes, or released into the extracellular space by exocytosis <sup>98,99</sup>. The exocytosis of compounds from these vesicles occurs by fusion of its membrane with the plasma membrane and is believed to be regulated by protein (de)phosphorylation <sup>100,101</sup>. Contrary to endothelial cells, cells of the choroidal epithelium are strongly endocytic, which might be associated with the active metabolism of the choroid plexus, as well as its synthetic functions. However, exploiting this particularity for the efficient transport of therapeutic proteins

and macromolecules across the BCSFB remains elusive <sup>78,102</sup>.

### 1.1.3. Receptor-mediated transcytosis

Specific receptors, highly expressed by endothelial/epithelial cells forming the BBB and BCSFB, are responsible for the transport of proteins required for the normal functioning of the brain (Table 1). These include, for example, the insulin receptor, transferrin receptor, low-density lipoprotein (LDL) receptor, and its related protein. These RMT mechanisms are currently used as delivery strategies for macromolecules to the brain. Compared to the BBB, protein transfer mechanisms occurring at the BCSFB are much less explored. Therefore, research on these pathways could result in new delivery strategies. Of course, many receptors responsible for RMT in the brain and choroid epithelium are also ubiquitously expressed, which limits the potential for selective brain targeting. Another important aspect that is usually neglected in drug delivery studies is that, apart from the binding to the target receptor, the designed targeting agent (e.g., ligand) needs to activate an endocytosis process to be used as a transporter.

**Table 1:** Main receptors involved in receptor-mediated transcytosis for brain delivery.

Receptor	Features	Main ligands	References
<b>Transferrin receptor (TfR)</b>	Glycoprotein consisting of two ~90 kDa subunits joined by intermolecular disulfide bonds	Transferrin 8D3 OX26	108,530
<b>Insulin receptor</b>	~300 kDa glycoprotein formed by two $\alpha$ -subunits and two $\beta$ -subunits	Insulin HIRMAb	531,532
<b>Low Density Lipoprotein Receptor (LDLR)</b>	~160 kDa glycoprotein formed by a single subunit with five distinct regions	Apolipoprotein B Apolipoprotein E Melanotransferrin Angiopep-2	123,533,534
<b>Leptin Receptor (LepR)</b>	Glycoprotein consisting of a single membrane-spanning receptor with four distinct domains  Two splice variants: (1) an isoform with a long cytoplasmic domain and	Leptin Leptin-derived peptides	535-538

	signal transduction ability, (2) an isoform with a short cytoplasmic domain, presumably with no signal transduction function		
<b>Nicotinic Acetylcholine Receptor (nAChR)</b>	~290 kDa glycoprotein formed by five subunits arranged around a water-filled pore  All subunits are organized as following: a conserved long extracellular N-terminal domain, followed by three hydrophobic transmembrane regions (M1–M3), a large cytoplasmic loop, a fourth transmembrane region (M4), and ultimately a variable short extracellular C-terminus	Acetylcholine  Rabies virus glycoprotein-derived peptides : RDP and RVG-29	539-542
<b>Diphtheria toxin receptor (DtR) or Membrane-bound precursor of heparin-binding epidermal growth factor (HB-EGF)</b>	~22 kDa glycoprotein	Diphtheria toxin  CRM197	543-545
<b>Neonatal Fc receptor (FcRn)</b>	Glycoprotein consisting of a type I transmembrane heavy chain non-covalently associated with the soluble light chain, $\beta$ 2-microglobulin.	Anti-FcRn  monoclonal antibodies or  antigen-binding fragments	546,547

#### - **Transferrin Receptor**

The delivery of iron to the brain occurs by the trafficking of iron-loaded transferrin (holo-transferrin) <sup>103</sup>. The iron–transferrin complex binds to transferrin receptors (TfR) on the exterior of microvascular endothelial cells and transport across the brain-blood interface into the brain parenchyma to ensure the maintenance of iron homeostasis, which is important for metabolism, neuronal transmission, and appropriate brain function <sup>103</sup>. As such, iron deficiency and excess are both linked to neuronal dysfunction <sup>103</sup>.

Transferrin is a bilobed glycoprotein (MW ~80 kDa) that belongs to a family of proteins containing a preserved amino acid motif, a three-dimensional structure, and a putative function (i.e., transport of iron from plasma to cells, regulation of iron levels) <sup>548</sup>. Most of the protein members contain two lobes termed N- and C-domain (of ~340 amino acids and 40% sequence identity) connected by a flexible hinge <sup>548</sup>. Transferrin is a very abundant plasma protein (25–50 μM) <sup>549</sup>.

The best-characterized receptor of transferrin is the promiscuous and widely expressed TfR1 (CD71) <sup>104</sup>. TfR1, or more simply TfR, is a ~180 kDa homodimeric type II transmembrane protein. This receptor possesses a short N-terminal cytoplasmic domain, one hydrophobic transmembrane region, and a complex extracellular C-terminal domain ([Figure 2.b](#)). Structural analysis revealed that for the butterfly-shaped dimeric TfR ectodomain, each monomer is subdivided into a protease-like domain that contacts the cell membrane, a helical domain where the monomers contact each other, and a membrane-distal apical domain <sup>105</sup>. TfR is expressed by brain microvessels as well as the cells of the choroid epithelium <sup>106,107</sup>.

Recent evidence shows that iron transport through the BBB does not involve full transport of the TfR to the abluminal side. Rather, TfR is internalized and then either transported back to the luminal membrane or sorted to the cytoplasm <sup>550</sup>. This process has been well described and reviewed elsewhere. <sup>551</sup> The delivery process starts with iron uptake through binding and internalization of the transferrin-diferric iron complex by TfR-mediated endocytosis *via* a clathrin-dependent pathway. Then, iron dissociates from transferrin upon acidification of the endosome, while the apo-transferrin remains tightly bound to TfR. Thereafter, reduction to ferrous iron by ferrireductases is followed by translocation by the divalent metal transporter (DMT1) to the cytoplasm. Subsequently, apo-transferrin together with the TfR are either recycled to the apical membrane or become stored inside the endothelial cells of the brain. At extracellular pH, apo-transferrin dissociates from TfR and is replaced by diferric transferrin. Cytoplasmic iron can be used by the endothelial cells of the brain, stored as ferritin, or exported by ferroportin at the basolateral membrane (alongside oxidation to its ferric state by ferroxidases). Similarly to the BBB, TfR mediates iron transport across the BCSFB. Importantly, the BCSFB not only buffers the CSF against fluctuating iron plasma levels, but also responds to higher brain requirements for iron, in the eventuality that the BBB has an insufficient transport capacity <sup>81,552,553</sup>.

Owing to the high presence of TfR in cerebral endothelial cells, this receptor has been explored to deliver drugs to the brain, using transferrin as a targeting ligand. However, since high blood levels of endogenous transferrin compete with drugs for TfR, alternative methods have been

explored, including anti-TfR monoclonal antibodies (TfRMAb) <sup>108</sup>. TfRMAb have been shown to bind to TfR and internalize into the endothelial cells of the brain without interfering with the uptake of iron-bound transferrin. Protein engineering has been used to alter affinity, avidity, and pH-sensitivity of the binding interaction, which has led to improved TfRMAb transport<sup>554-556</sup>. For example, reducing the binding affinity to TfR has been studied for TfRMAb (OX26) <sup>556</sup>, though it should be noted that this approach remains controversial <sup>557</sup>, and that some studies suggest that the affinity needs to be adjusted for optimal endothelial cell uptake and transcytosis across the BBB without TfR degradation <sup>558</sup>. Indeed, several lines of evidence suggest that high-affinity TfR antibodies do not reach the brain and remain trapped within the brain vasculature [82-84]. In contrast, TfR antibodies with lower affinity have been reported to better enhance brain uptake because they can more readily dissociate from TfR <sup>57</sup>. For instance, *in vitro* live imaging and colocalization experiments showed that high-affinity anti-TfR promoted trafficking of TfR to lysosomes and its consequent degradation. This observation was further confirmed *in vivo* <sup>559</sup>. Other approaches for exploring TfR-based delivery involve the use of small peptides binders <sup>109,110</sup>. Such peptides hold the advantage of circumventing the side effects that could be generated by the Fc effector domain of the anti-TfR antibody <sup>111</sup>. Moreover, owing to their small size, they might be easier to use, conjugate, manufacture, or store. Nevertheless, they are usually not stable in circulation and have low binding affinity.

#### - **Insulin Receptor**

Insulin is a ~5 kDa protein that is secreted by the pancreas and plays a vital role in the regulation of the carbohydrate metabolism <sup>112,113</sup>. The transport of insulin is guaranteed by insulin receptors that are widely distributed throughout the body. In the endothelial cells of the brain, binding to its receptor not only allows insulin transport across the BBB *via* the receptor itself, but further activates signalling pathways through e.g., the insulin-like growth factor 1 (IGF-1) receptor <sup>114,115</sup>.

The insulin receptor is a cylindrical homodimeric glycoprotein (MW ~300 kDa) that consists of two  $\alpha$ -subunits and two  $\beta$ -subunits <sup>116</sup>. The extracellular  $\alpha$ -subunit contains an insulin-binding site and the cytoplasmic portion of the transmembrane  $\beta$ -subunit possesses tyrosine kinase activity. The ectodomain comprises seven extracellular domains. Starting from the N-terminus, these domains are: the first leucine-rich repeat domain (L1), the cysteine-rich domain, the second leucine-rich repeat domain (L2), and the three fibronectin type III domains (FnIII-1, FnIII-2, and FnIII-3), with the seventh domain (a relatively disordered insert domain) lying within FnIII-2 and containing the  $\alpha\beta$  proteolytic processing site ([Figure 2.c](#)) <sup>117</sup>.

Insulin transport at the BBB is a dynamic process regulated by the current physiological state of the body <sup>560</sup>. Insulin binding causes conformational changes to the receptor. The quaternary structure of the  $\beta$ -subunit changes to allow the autophosphorylation of its tyrosine residues, the subsequent endocytosis of the insulin-receptor complex, and the downstream stimulation of signaling pathways <sup>116,532,561</sup>. Although it is now confirmed that brain insulin transport requires a vesicular endocytotic process <sup>562</sup>, very little data regarding insulin uptake and trafficking are available, especially in brain endothelial cells. Indeed, the exact uptake process as well as the regulation of intracellular vesicle trafficking and exocytosis remain poorly understood, and therefore the mechanisms involved require further study.

Insulin receptor-mediated transport has been explored to deliver various molecules across the BBB/BCSFB. The use of insulin as a scaffold for drug delivery is difficult because of its short serum half-life (~10 min) and rapid degradation in the bloodstream. Moreover, interfering with the normal serum insulin equilibrium could generate hypoglycaemia <sup>23</sup>. Henceforward, the general strategy for exploiting the transferrin receptor has also been adopted for the insulin receptor, namely the development of antibodies targeting the insulin receptor <sup>118</sup>. Initially, a mouse monoclonal antibody targeting the human insulin receptor (83-14) was tested <sup>118</sup>. However, as 83-14 is a mouse antibody, it triggers an immunogenic reaction in humans <sup>119</sup>. Therefore, engineered forms of 83-14 have been developed. First, a chimeric antibody was produced by adding mouse variable binding regions onto a human antibody scaffold <sup>120,121</sup>. Then, more recently, a fully humanized version was produced by grafting the complimentary determining regions onto human immunoglobulins (Igs) <sup>122</sup>. The reactivity of these constructions towards the human insulin receptor demonstrated that in comparison to the 83-14, the chimeric antibody had comparable affinity <sup>120,121</sup>, whereas the fully humanized antibody had 27% lower affinity <sup>122</sup>. Intravenous injection of a radiolabeled (<sup>125</sup>Iodine) humanized antibody to adult Rhesus monkey showed rapid uptake by the gray and white matter (2 hours post-administration), and that ~1% of the injected dose was retained by the brain (that weighs ~100 g) <sup>122</sup>. Additionally, considering the relative affinities of these antibodies, the uptake of the humanized antibody by the Rhesus monkey brain was about ~50% of that of the chimeric antibody <sup>120,122</sup>.

#### - **Low-density lipoprotein Receptors**

The LDL receptor (LDLR), a large glycoprotein (MW ~160 kDa) <sup>123</sup>, was first recognized as a cell surface endocytic receptor responsible for the intracellular uptake of LDL particles. The LDLR has five functionally distinct regions: an N-terminal ligand-binding domain, an epidermal growth factor (EGF)-precursor homology domain, a region containing O-linked sugars at the cell surface, a membrane-spanning domain, and a C-terminal cytosolic domain. The ligand-

binding domain possesses seven cysteine rich repeats (R1–R7), each of which are ~40 residues in length (known as the LDL-A repeats) <sup>124</sup>. The second region consists of three EGF-like repeats (A, B, and C) <sup>125</sup>. The third region of the ectodomain is the site at which carbohydrate moieties attach to the receptor and possesses many serine and threonine residues that undergo O-glycosylation <sup>126,127</sup>. This domain is followed by a hydrophobic domain that anchors the LDLR to the lipid bilayer. The last domain is the cytoplasmic tail containing ~50 residues that includes an NPXY targeting sequence (asparagine, proline, unspecific amino acid, tyrosine), which regulates and assures the endocytosis and the intracellular transport of the receptor (Figure 2.d) <sup>128-130</sup>.

Nowadays, LDLR is included in a large family that counts many other relatives with RMT activity and playing roles in cell signalling processes <sup>131</sup>. Family members share a modular domain structure as well as one or multiple copies of a conserved cysteine-rich domain (LDLR class A (LDL-A) repeats). The LDLR family can be subdivided into at least four groups <sup>132</sup>. The LDLR itself, the very-low density lipoprotein receptor (VLDLR), and the apolipoprotein E receptor 2, also called LDLR-related protein 8 (ApoER2 or LRP8), belong to the first group. The well investigated receptor LRP1 (CD91 or  $\alpha$ 2-macroglobulin receptor), LRPB1B, LRP2 (Megalin also known as gp330) are members of the second group. The third group include LRP5 and LRP6. Finally, the fourth group comprise more distantly related members such as SorLA-1 (also called LR11), ST7, LRP4, and LRP3 <sup>132</sup>.

The mechanism of endocytosis and trafficking of LDLR family ligands to the lysosomal compartment has been widely described, particularly in peripheral cells where the cargo taken in clathrin-coated pits is released in the late endosomes and then degraded in lysosomes <sup>133</sup>. The receptor recycles back to the cell surface after ligand dissociation in the early endosomes <sup>133,134</sup>. Although much is known about LDL uptake and trafficking in peripheral tissues, less is known for the brain and this is currently the object of extensive investigations. At the BBB, the different members of the LDLR not only assure the use and clearance of LDL <sup>135</sup>, but also mediate the transcytosis of their cargo <sup>136-138</sup>. The non-degradation of the cargo after internalization indicates that the route of transcytosis in endothelial cells differs from the classical LDLR pathway of endocytosis <sup>138</sup>. This receptor-mediated process, which bypasses lysosomes, seems to be a specific feature of brain endothelial cells that are equipped with a RMT implicating specialized endocytic vesicles <sup>139,140</sup>.

The presence of multiple variants of the LDLR in apical membranes of the endothelial cells of the brain as well as their role in RMT raise interest for their use for the transendothelial transfer of therapeutic proteins. As for the TfR, natural apolipoprotein (Apo) ligands as well as peptides

consisting of minimal sequences of the binding domains (BDs) of the latter have been investigated, despite the fact that the mechanism by which such vectors transport across the BBB remains to be clarified. To the best of our knowledge, antibodies have not been developed to target the LDLR system. Several endogenous ligands of the LDLR family have been investigated for brain delivery of therapeutics and have shown successful transfer across the blood-brain interfaces. These include Apo ligands (such as Apo B and E) that showed an efficient delivery of therapeutically relevant agent across the BBB (see section 2.1.3). Similar observations have been reported for melanotransferrin (MW ~80 kDa) (so-called p97 protein) binding to the LRP subfamily (see section 2.1.3). The use of peptides derived from the binding domains of endogenous full-sized ligands has also been explored. This approach allowed for the reduction of the size of the delivery system and competition with endogenous serum ligands. For instance, Apo B-BD, Apo E-BD peptides, and other targeting members of the LRP1 (such as Angiopep-2 (19 residues)) have been investigated. It should be mentioned here that, for instance, targeting the LRP1 by Angiopep-2, sometimes leads to divergent results. Indeed, it was reported that the transport peptide Angiopep-2 could engage in different endocytosis mechanisms (unrelated to the LRP1 pathway) depending on the moiety to which it is conjugated <sup>563</sup>. For example, *in vitro* uptake efficiency and kinetics of Angiopep-2 as well as Angiopep-2 conjugated to  $\beta$ -secretase inhibitor was not altered when downregulating the expression of LRP1. Interestingly, pharmacological inhibition of different endocytosis pathways demonstrated that unconjugated Angiopep-2 was internalized by a combination of endocytic pathways that differ from those used by the conjugate <sup>563</sup>.

## 1.2. Dysfunction of the barriers in brain diseases

In a variety of neurological diseases (neuroinflammatory, neurovascular, neoplastic, or neurodegenerative), the disruption of blood-brain interfaces has been described as a part of the pathophysiological process (not only as an early event, but also in late stages of disease) <sup>564-566</sup>. For many of these pathologies, whether barrier dysfunctions are a cause or a consequence is still unclear. These alterations may affect ion balance, disrupt transport systems, alter the enzymatic barrier, and lead to the homing of immune blood cells to the brain. Furthermore, the inflammation that is associated with the progression of several CNS disorders promotes an aberrant neuro-vascular remodelling, likely contributing to neuronal dysfunction and degeneration (Figure 3). Thus, unravelling of the molecular mechanisms associated with brain endothelium/ choroidal epithelium alteration are important for finding a potential common factor that would enable the design of more general therapeutic approaches, applicable to multiple disease states.

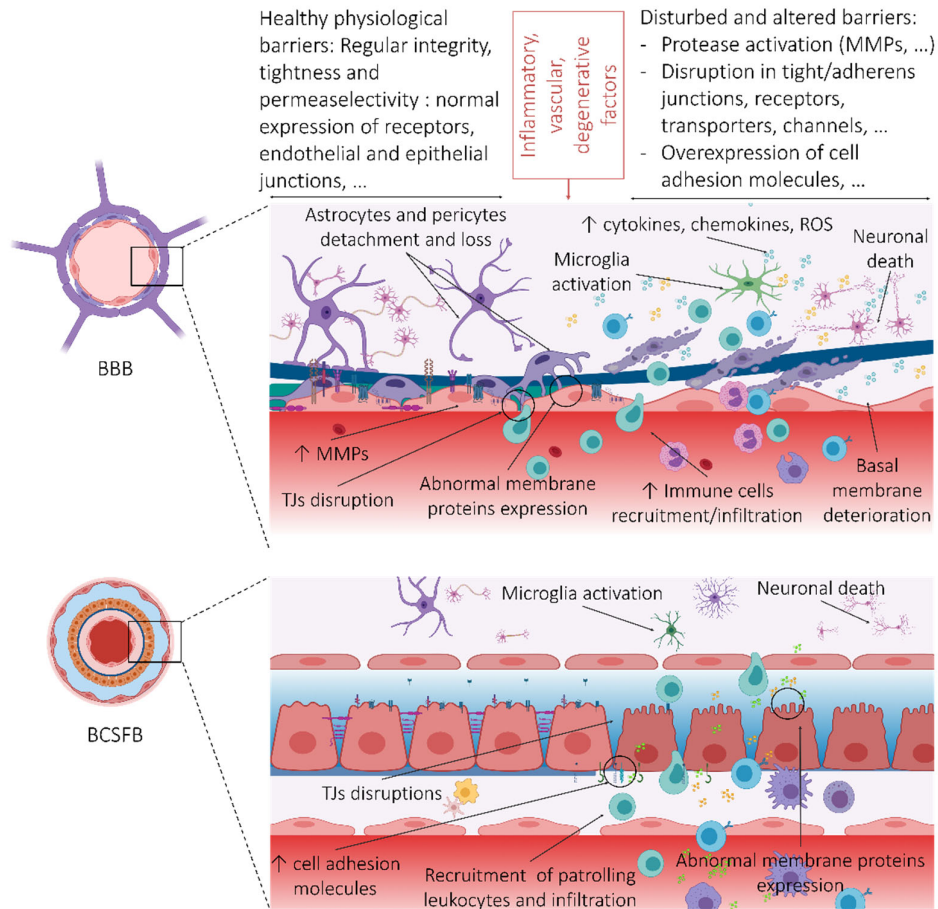


**Figure 3: General overview of the main alterations to the BBB and BCSFB under pathological conditions.** Under normal physiological conditions, the physical and functional properties of the barriers are maintained. Under pathological conditions that can occur following a combination of various disease-specific triggers, several alterations happen: dysregulation of the cells of the neurovascular unit (e.g., detachment and loss of astrocytes), alteration of the expression of transmembrane proteins (e.g., tight junctions (TJs), receptors), increased activity of the matrix metalloproteinases (e.g., MMP-9), activation of immune cells, release of cytokines and chemokines, overproduction of reactive oxygen species (ROS), upregulation of cell adhesion molecules), recruitment and brain parenchyma invasion of circulating leukocytes. All these events ultimately lead to neuronal injury and neurodegeneration.

Alterations to the barrier may also affect the diffusion of therapeutics from the capillary to the brain parenchyma, as a result of structural changes and associated changes to equilibrium dynamics.<sup>567</sup> Therefore, the impact of disorder-related barrier disruptions on drug delivery systems must be considered, especially when designing active-targeting systems (where accumulation in the brain irrespective of a targeting molecule should be evaluated). Moreover, as some of the alterations are specific to a given pathology, the development of therapeutics is more challenging. Additionally, disease progression and disruption of the BBB/BCSFB could

yield different performance for a drug delivery system. In the following sections, an overview of prominent brain diseases will be presented with focus on associated modifications occurring within the BBB/BCSFB.

### **1.2.1. Multiple sclerosis**

The disruption and loss of proper function of neuroprotective barriers are critical events in numerous neurological disorders including multiple sclerosis (MS), a chronic neuroimmune disease characterized by the infiltration of auto-reactive T-lymphocytes and monocytes in the CNS, which in turn locally attack the myelin sheath<sup>568</sup>. The invasion of immune cells involves numerous steps, each involving a variety of BBB receptors and transporters, and thus provides multiple targets that could be used to prevent immune cell trafficking into the CNS.

The progressive loss of BBB integrity, as indicated by a persistent vascular leakage and an alteration of the integrity of TJs, has been largely reported in MS patients and the consequent increase in BBB permeability at the active MS lesion can be imaged by magnetic resonance imaging (MRI), *via* the extravasation of a contrast agent (e.g., gadolinium-DTPA (diethylenetriamine penta-acetic acid); MW ~545 Da) to the brain parenchyma<sup>569,570</sup>. Various degrees of alteration (from mild to severe) can be observed, from minimal and delayed to massive and early gadolinium enhancement<sup>569-574</sup>. This “loosening” of the BBB has been correlated to augmented levels of matrix metalloproteinases (MMPs). MMPs are versatile endopeptidases critical for neuronal network remodelling, degradation of TJ proteins, and BBB integrity/permeability, whose roles in the pathophysiology of MS were clearly highlighted in various animal and clinical studies<sup>575,576</sup>.

The increase in the levels of MMPs in MS has been associated to an increase in transmigration of circulating leukocytes into the CNS<sup>577</sup>, which occurs when endothelial barrier function is compromised. Indeed, the expression level, the distribution, and the post-translational modifications of many TJ proteins in patients and in animal models have been reported<sup>578,579</sup>. For example, the migration of leukocytes can reorganize the actin cytoskeleton and lead to a loss or redistribution of TJs such as claudin-5, claudin-3, and occludin, alongside disruption of both the BBB and BCSFB<sup>580-583</sup>. Moreover, in a common mouse model of MS, experimental autoimmune encephalomyelitis (EAE), occludin dephosphorylation coincided with the onset of inflammation and slightly preceded visible impairments<sup>581</sup>. This suggests an association between the apparent TJs alteration with changes in BBB permeability and MS-related symptoms<sup>581,584</sup>. Alteration in the TJ proteins occludin, VE-cadherin, and ZO-1 was also observed in the brain tissue from MS patients. This also suggests a loss of BBB integrity in this disease<sup>584,585</sup>. While the obliteration of the TJs was largely reported, additional investigations

are needed to determine the expression pattern of the transporters and receptors on the barrier's interfaces in MS. Considering the pathological mechanisms of MS, current therapies aim to target the blood-brain interfaces by reducing leakage as well as limit the local inflammation and the infiltration of CNS-specific leukocytes<sup>586,587</sup>.

### **1.2.2. Lysosomal storage diseases**

Lysosomal storage diseases (LSDs) are caused by the mutation of proteins that are critical for lysosomal function, and are rare inherited metabolic disorders. The proteins affected can include integral lysosomal membrane proteins, enzymes, as well as proteins that regulate the post-translational modification and the trafficking of lysosomal proteins<sup>588</sup>. Mutations can produce an accumulation of specific “undigested” products that lead to progressive cellular and organ dysfunction. Most LSDs involve accumulation of substrate molecules in brain tissue, which can lead to neuropathy and cell death in the CNS<sup>588</sup>. Multiple types of LSDs are recognized, such as the mucopolysaccharidoses (MPS). MPS result from a deficiency in lysosomal hydrolases needed for the catabolism of complex carbohydrates (glycosaminoglycans)<sup>589,590</sup>. Each specific deficiency defines what substrate(s) will accumulate, the tissues affected, as well as symptom severity. There are seven distinct types of MPS (I, II, III, IV, VI, VII, and IX), which are further divided into subtypes<sup>591</sup>. For example, in MPS type IIIA (MPS IIIA), the deficiency in sulfamidase results in lysosomal accumulation of heparan sulfate, causing severe and progressive CNS dysfunction.

The potential contribution of BBB dysfunction to the neuropathology of LSDs has been investigated. To date, there have been few studies about the molecular changes of the BBB in LSDs. Most studies have used animal models with genetic mutations presenting a relatively well-defined pathology to either study BBB integrity *via* the passive extravasation of solutes, or to examine markers of neuroinflammation. Extravasation of fluorescent dextran (3 kDa, 40 kDa, or 500 kDa) after intravenous administration has been observed in a mouse model of juvenile Batten disease (neuronal ceroid-lipofuscinosis-3 knockout mouse (Cln3<sup>-/-</sup>))<sup>592</sup>. Additional studies have demonstrated the BBB alteration in Sandhoff disease ( $\beta$ -hexosaminidase B <sup>-/-</sup>) and Gangliosidosis-1 ( $\beta$ -galactosidase ( $\beta$ -GAL) <sup>-/-</sup>) mouse models, where the extravasation of Evans blue albumin (~67 kDa) and endogenous IgG (~150 kDa) was associated to CNS inflammatory processes observed in the model<sup>593</sup>. However, such studies are further complicated considering that BBB dysfunctions are different as function of MPS type. For example, in a mouse model of MPS IIIB, BBB structural and functional impairments (e.g., ultrastructural abnormalities, presence of large cytoplasmic vacuoles in endothelial and perivascular cells, and vascular leakage) were clearly detected.

This was suggested to be attributed to an accumulation of the storage product (GM3 ganglioside) in the cells themselves or to a secondary event following microglial activation and inflammatory cascade <sup>594-596</sup>. In contrast, the BBB remained intact in a mouse model of late onset MPS IIIA, even at late stages of the disease <sup>597,598</sup>. Therefore, clearly, the fact that the barrier appears to be damaged in only some models of neuronopathic LSDs requires further investigation. Nevertheless, a common feature in animal models is neuroinflammation <sup>599,600</sup>, suspected to be one of the major causes of BBB dysfunction.

Overall, besides neuropathology resulting in the accumulation of storage products, BBB damage and extensive neuroinflammation can further contribute to CNS dysfunction, and the correlation between these processes needs to be further clarified. In addition, it should be noted that while data on the molecular deterioration of the BBB in LSDs are scarce, data on BCSFB dysfunction are currently lacking. In conclusion, BBB/BCSFB breakdown concurrent with LSDs as well its underlying cellular and molecular changes need to be further understood before new treatments can be proposed. Nonetheless, so far, various strategies have been considered for the treatment of LSDs, for instance stem cell transplantation, enzyme/gene replacement therapy, substrate elimination, or anti-inflammatory therapy.

### **1.2.3. Ischemic stroke**

Blood–brain interface dysfunction is a common pathological aspect of ischemic stroke and is associated with poor outcome. Ischemic stroke (85% of all stroke cases) exhibits extravasation of blood solutes into the parenchyma of the brain across a defective BBB. This deterioration is caused by, but not limited to, endothelial cell degeneration and to increased paracellular and transcellular permeability <sup>151,152</sup>. Indeed, early after ischemia and before BBB impairment, the dysfunction of endothelial cells and the successive increase in the activity of ion transporters (such as Na<sup>+</sup>/H<sup>+</sup> exchangers, Na<sup>+</sup>-K<sup>+</sup>-Cl<sup>-</sup> co-transporters, or the calcium-activated potassium channel KCa3.1) enhance the transport of Na<sup>+</sup>/Cl<sup>-</sup> from blood into the brain by a transcellular pathway and cause an ionic imbalance that may play a major role on ischemia-induced edema formation and BBB breakdown <sup>153-159</sup>.

In preclinical models of ischemic stroke, the “opening” of the BBB was biphasic despite adequate reperfusion aimed to support the affected neuronal tissue and to restore normal blood flow <sup>160,161</sup>. The first phase is controlled by endothelial cytoskeleton modifications after ischemia/reperfusion injury, and is later accompanied by a cascade of cellular and vascular damage after enzymatic cleavage of TJs by recruitment and massive infiltration of immune cells. For example, in a transient Middle Cerebral Artery Occlusion (MCAo) rat model, a biphasic course of BBB opening (at 4 hours and 48 hours) was demonstrated by Pillai et al.,

with a significant reduction in BBB permeability at 24 hours<sup>162</sup>. These time-courses related to the opening of the BBB and did not completely correlate with other studies<sup>162,601-605</sup>, possibly due to the use of different stroke models. Nevertheless, these observations reveal the diversity of the pathological mechanisms in stroke and suggest the need to clarify the time-course for BBB opening.

RMT, which is an energy-dependent vesicular transport process, is likewise affected during ischemia/reperfusion. For example, TfR is sensitive to the reduction of blood supply but remains partially functional for several hours post-ischemia. Indeed, at early time points after onset of permanent MCAo, TfR-mediated brain binding/uptake is reduced. Then, at late time points (24 hours), this process is virtually abolished. However, reperfusion after occlusion (in transient MCAo model) re-establishes energy supply and leads to immediate recovery of binding/uptake processes<sup>606</sup>. Moreover, in the permanent MCAo model and in the initial phase of ischemic stroke (6 hours post-ischemia), LDLR and scavenger receptor class B member 1 (SRB1) were significantly upregulated in endothelial cells, whereas expression of LDLR significantly decreased from 3 days after MCAo<sup>165</sup>. Furthermore, it has been reported that LRP1 is upregulated in both brain endothelial cells and neurons in the ischemic cortex within 6 hours of transient MCAo in mice<sup>166,167</sup>. Furthermore, changes in transcriptional and translational regulation as well as the reorganisation of brain endothelial TJ proteins have been largely demonstrated following ischemic insults. Though defective TJ morphology was noticed 3 hours post-ischemia in rodents, ultrastructural analysis of TJ proteins during the progression of the disease did enable the authors to conclude that their disturbance is responsible for early BBB breakdown<sup>163,164</sup>. This suggests that the active remodelling of TJ complexes in the endothelial cells of the brain is responsible for both phases of BBB breakdown<sup>163,164</sup>.

Compared to the BBB, the impact of cerebral ischemia on the BCSFB has received less attention. Disintegration of the choroidal epithelium has been reported. Indeed, BCSFB leakiness was revealed by the 3-fold increase in <sup>3</sup>H-inulin permeability at 6 hours post-occlusion, and had a major effect on tissues near the ventricular system<sup>168</sup>. Stroke-induced BCSFB disruption was associated to the free diffusion of proteins, cytokines, and potentially toxic plasma molecules into the ventricles, and subsequently to the closest brain structures<sup>169</sup>. The injury to the choroidal epithelium recovered within 18 hours, and was assisted by hormones and growth factors secreted by the choroid plexus<sup>168,170-172</sup>. In terms of drug delivery, ischemia-induced BCSFB disruption might be interesting for some drugs acting during the “early” phase of the barrier breakdown, considering that it occurs earlier than for the BBB

<sup>168</sup>.

Taken together, the properties of blood-brain interfaces following stroke should be taken into consideration when designing a drug delivery system. For example, erythropoietin (EPO) and fibroblast growth factor-2 (FGF-2), two neuroprotective polypeptides that do not easily enter the brain, were able to pass the breached BBB/BCSFB after intravenous administration following stroke <sup>607</sup>. This shows that the barriers' dynamics after injury might be a potential factor permitting the delivery of some high-MW therapeutics to the brain.

#### **1.2.4. Traumatic brain injury**

Traumatic brain injury (TBI) is a severe neurological disorder commonly caused by e.g., car accidents, sporting activities, or violence, and is an important risk factor for neurodegenerative disorders. Primary brain injury initiates a secondary process that spreads by various molecular mechanisms. According to the insult, TBI can be divided as: closed head, penetrating, and explosive blast TBI <sup>608</sup>. Following TBI, a series of events occur: (1) primary injury disrupting brain tissues, (2) secondary injury causing pathophysiology in the brain, (3) inflammatory response exasperating the neurodegeneration, and (4) a repair–regeneration phase contributing to neuronal repair (to some extent).

Similar to stroke, BBB alteration and increase of permeability after TBI occur in two phases (primary damage and secondary damage), also known as immediate and delayed dysfunction. In animal models of TBI, the severity and degree of breakdown is directly associated to the method by which the insult is delivered to the head. Globally, in experimental models, the first stage is rapid with BBB permeability typically occurring at 4–6 hours and subsequently declines, and the second is delayed, starting 3 days following injury <sup>609</sup>. Early opening of the BBB is caused by contusions and shear forces on the brain resulting in mechanical deformation of the BBB neurovascular unit, followed by vascular and parenchymal dysfunctions (i.e., disorganization of TJ proteins, energy failure and cell death, edema formation, and neuroinflammation) <sup>609</sup>. Although the actual processes involved leading to secondary BBB breakdown remain controversial for TBI (owing to scattered methodology) <sup>610,611</sup>, it is still considered a potentially treatable stage <sup>612</sup>.

In contrast to the extensive literature on the modification of protein expression/organization in ischemia, the available data for TBI is rather limited. In a rat model of TBI, the expression of claudin-5, occludin, and ZO-1 proteins was significantly lower (3 to 72 hours) than for controls and returned to the levels of the control group within 168 hours <sup>613</sup>. Similarly, the levels of mRNA transcription and protein expression of these proteins were significantly reduced 72 hours post-TBI, changes that were consistent with the BBB permeability <sup>614</sup>.

A variety of pharmacological therapeutics have been tested for TBI. Most of these aim to stabilize the injury and prevent secondary damage. Indeed, the progressive nature of the secondary injury provides a window of opportunity for planning an intervention to reduce the inflammatory response, excitotoxicity, oxidative stress, or apoptotic cell death<sup>615</sup>. Unfortunately, while many of the tested drugs have shown promising results in animal models, they have failed to influence outcome following TBI when translated into the clinical setting<sup>616,617</sup>. Therefore, much work has been dedicated elucidating the underlying phenomena associated with secondary brain injuries and to developing strategies that focus on the manipulation of barrier dynamics after injury.

### **1.2.5. Neurodegenerative diseases**

Neurodegenerative diseases are incurable and debilitating pathologies that result in a progressive degeneration and death of nerve cells. Examples of neurodegenerative diseases include Alzheimer's disease (AD; ~60 to 80% of dementia cases)<sup>618</sup>, Parkinson's disease (PD), and Huntington's disease (HD). Each of these diseases manifest themselves as an abnormal accumulation of proteins in the brain, concomitantly with neuronal death in specific brain regions.

BBB impairment in AD and other dementia is increasingly recognized as an early and intrinsic part of its pathophysiology<sup>619</sup>. Although not as extensively characterized, BBB permeability has also been shown in PD<sup>620,621</sup>, and HD<sup>622</sup>. Neurodegenerative diseases often display a disorganization and/or destruction of TJs as well as adherens junctions<sup>164</sup>. TJ alterations are related to a dysregulation of the phosphorylation and degradation mechanisms, an alteration of translocation processes, and a downregulation of TJ protein expression<sup>623,624</sup>. Additionally, because of cell degeneration, the loss of transporters and/or receptors at the BBB has been widely documented<sup>160,566,625-627</sup>. For example, autoradiography on post-mortem human brain specimens have shown changes in TfR expression in PD and AD<sup>628-632</sup>. Nevertheless, these changes did not often reflect the expression of TfR at the capillary level<sup>628</sup>, suggesting that TfR expression might be maintained in this compartment, as recently demonstrated<sup>633,634</sup>. Similarly, patients with AD have shown decreased activity and/or protein levels of LRP1<sup>635,636</sup>, insulin receptor<sup>637,638</sup>, and P-glycoprotein in their barrier cells<sup>639,640</sup>. Recently, the role of the BCSFB on the pathogenesis of neurodegenerative diseases has received increased attention<sup>641,642</sup>. Briefly, just as for the BBB, increased transcellular and paracellular permeability as well as BCSFB breaching have been described<sup>643,644</sup>. Of note, alterations of the blood-brain interfaces in neurodegenerative diseases are complex and have been properly addressed and reviewed elsewhere<sup>566,567</sup>.

Given the multifactorial mechanisms of neurodegenerative diseases (permanent neuroinflammation, excitotoxicity, oxidative stress, etc.), finding effective therapeutics is still a challenge. Prominently, changes in the amount and/or ratio of transporters and/or receptors would significantly affect the properties and functionalities of brain barriers, and therefore performance and fate of drug delivery systems. Furthermore, the lack of understanding of the disease mechanisms as well as the chronology of the underlying events, hinders the development of an effective treatment. Consequently, there is a need to further investigate the pathological processes related to the blood-brain interfaces and to develop new therapeutic strategies to combat these devastating diseases.

## **2. Strategies for the treatment of brain diseases using protein therapeutics**

Due to existence of blood–brain interfaces, the delivery of traditional therapeutic proteins with large MW to the brain is generally not possible. Systemic parenteral administration, especially by intravenous injection is relatively safe and generally preferred to local brain administration. However, the efficiency of delivery to the brain is much lower than for local delivery due to these barriers. In contrast, delivery in the CSF through intracerebroventricular or intrathecal injections bypass the BBB to reach the brain, though these are somewhat complex, invasive, and clinically impractical especially with the need for repeated dosing. The following sections will review *in vivo* studies involving the delivery of proteins to the brain following systemic parenteral administration, mainly by the intravenous route ([Figure 4](#)). All of these strategies carry their own advantages and disadvantages (Table 2).

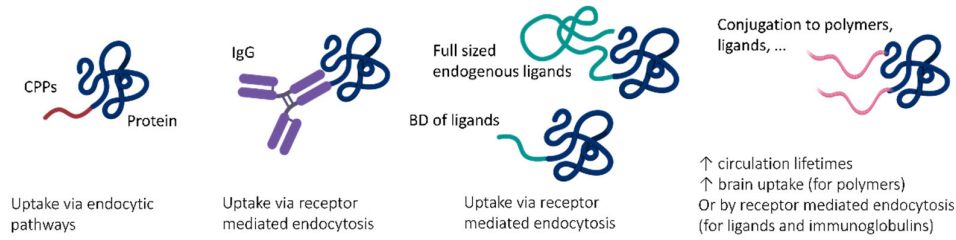
**Table 2:** Advantages and disadvantages of the main strategies proposed for delivery of proteins to the brain

Strategies		Advantages	Disadvantages
<b>Fusion proteins</b>	Cell penetrating peptides (CCPs)	<ul style="list-style-type: none"> <li>- Improved blood–brain interfaces permeability</li> <li>- Fusion to proteins with minimum risks of jeopardizing their therapeutic functions</li> </ul>	<ul style="list-style-type: none"> <li>- Neurotoxicity, inflammation, and immunogenicity (cationic nature of the CCPs)</li> <li>- Off-target effects (penetration into various cell types)</li> </ul>
	Immunoglobulins	<ul style="list-style-type: none"> <li>- Improved blood–brain interfaces transcytosis</li> <li>- Exploration of the physiological presence of receptors on the brain</li> <li>- Avoid competition with endogenous ligands</li> <li>- Tuning of the binding mode in terms of affinity, avidity, or pH-sensitivity</li> </ul>	<ul style="list-style-type: none"> <li>- Toxicity (particularly at high doses)</li> <li>- Immunogenicity and hypersensitivity reactions (especially for long-term treatment)</li> <li>- Affinity/activity loss</li> <li>- Off-target effects (extended distribution of the receptor-targeted therapeutics)</li> </ul>
	Endogenous ligands	<ul style="list-style-type: none"> <li>- Improved blood–brain interfaces transcytosis</li> <li>- Exploration of the receptor-mediated transcytosis mechanism</li> </ul>	<ul style="list-style-type: none"> <li>- Competition with/mimicking of endogenous ligands</li> <li>- Affinity/activity loss</li> <li>- Off-target effects</li> </ul>
	Binding domain of endogenous ligands (short homing peptides)	<ul style="list-style-type: none"> <li>- Improved blood–brain interfaces transcytosis</li> <li>- Fusion to proteins with minimum risks of</li> </ul>	<ul style="list-style-type: none"> <li>- Low binding affinity in comparison to full-length ligands</li> <li>- Instability in physiological environment</li> </ul>

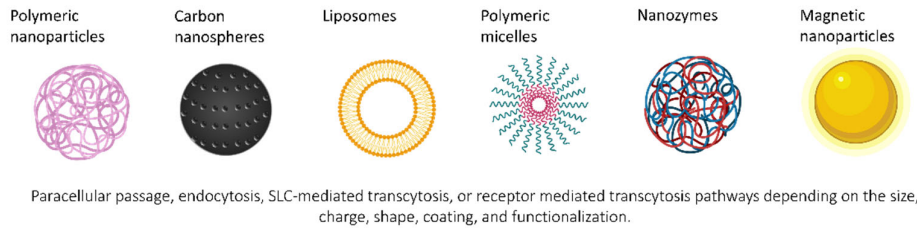
		jeopardizing their therapeutic function	- Off-target effects
		- Reduction of the size of the delivery system	
<b>Bioconjugates</b>	Endogenous ligands	- Exploration of a physiological mechanism (receptor-mediated transcytosis)	- Loss of affinity/activity during conjugation - Off-target effects
	Polymers	- Improved pharmacokinetic properties - Tuning of the grafting density/targeted functional groups/shape of conjugated polymers	- Toxicity and immunogenicity (of some polymers) - Loss of activity during conjugation - Off-target effects
<b>Nano-formulations</b>	Polymeric nanoparticles	- Protection of the protein's structure	- Low protein loading efficiency
	Carbon nanospheres	- Avoid some limitations related to the direct injection of native proteins in the blood (immunologic reactions, denaturation, and degradation)	- Inactivation of proteins during encapsulation processes
	Liposomes		- Toxicity and immunogenicity (magnetic nanocarriers)
	Polymeric micelles		- Poor stability (liposomes)
	Nanozymes		- Initial "burst" release and irreversible adsorption of proteins to the polymer matrix (PLGA)
			- Instability issues and formation of aggregates (pluronic micelles)
			- Off-target effects
<b>Modifications of</b>	Glycation/glycosylation	- Potentially safe (glycol-groups and oligosaccharides are ubiquitously expressed)	- Loss of affinity/activity

<b>proteins</b>		throughout the body and are easily broken down)	- Immunogenicity and proteolytic degradation of proteins - Off-target effects
		- Improved solubility and stability	
	Acylation	- Improved blood–brain interfaces permeability	- Immunogenicity and proteolytic degradation of proteins - Off-target effects and intracellular sequestration of acylated proteins
	Cationization	- Improved blood–brain interfaces permeability	- Clearance and toxicity of cationized proteins (interaction with other proteins and cell membranes (negatively charged))
<b>Sink or scavenging mechanisms</b>	Antibodies	- The mechanism is a self-limiting process and slows down and eventually stops as the concentration of the toxic molecules in the brain decreases	- Potential immunological reactions
	Enzymes		- Potential denaturation, and degradation of proteins
<b>Modulation of the intercellular junctions</b>	Osmotic agents: hypertonic mannitol solution or cadherin peptides	- Increased permeability of blood–brain interfaces within a certain duration of time and for a certain size of proteins	- Off-target effects

### Fusion Proteins & bioconjugates



### Nanosystems (proteins loaded into or adsorbed on)



### Protein modifications

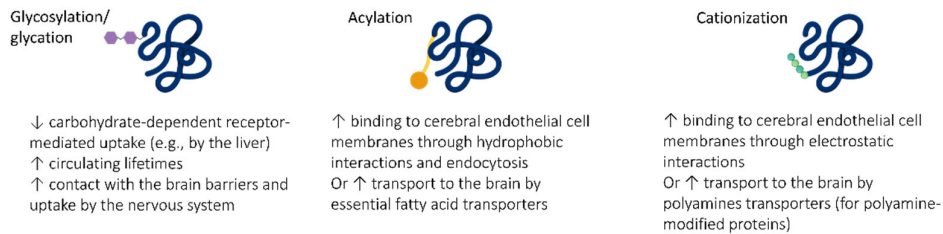


**Figure 4: Brain protein-delivery strategies exploiting endogenous pathways across the brain–blood interfaces.** RMT is the common mechanism of transport for proteins fused to or chemically linked to ligands, binding domain (BD) of ligands, or to antibodies against brain receptors. Similarly, nanoparticles (NPs) functionalized with ligands or surfactants (such as polysorbate 80 that adsorbs Apolipoproteins E) are able to bind targeted receptors on the brain, which promotes the transport of the NPs. The interaction between ligands/antibodies and their respective receptors at the luminal side triggers plasma membrane invaginations followed by vesicle formation, which facilitates the release of the proteins in the parenchymal side. Endocytosis (following electrostatic or hydrophobic interactions with the cell membranes) allows the passage of proteins coupled to cell penetrating peptides (CPPs), liposomes, charged NPs, and polymeric micelles across brain interfaces. Likewise, glycated, acylated, and cationized proteins are taken-up by the brain *via* endocytic routes. Finally, transporter-mediated delivery has been proposed as mechanism for acylated and cationized proteins, as well as for NPs functionalized with a substrate of a specific transporter. Of note, loosened tight junctions, due to pathological conditions, might override the need for a specific transport system to achieve brain accumulation.

## 2.1. Targeting: Fusion Proteins

Fusion proteins are created by joining two or more genes that originally code for separate proteins/peptides. These genetically-engineered constructs can exploit multiple physiological pathways by which macromolecules can be taken up into the brain (RMT/adsorptive endocytosis). Most of them involve generating a conjugate containing the protein of interest and a targeting entity, which might be a cell penetrating peptide, an antibody targeting an endogenous receptor, a ligand, or a mimetic peptide ligand.

### 2.1.1. Cell Penetrating Peptides

Cell penetrating peptides (CPPs) have been studied to promote brain delivery by adsorptive endocytosis. The process is based on the potential of CPPs to electrostatically interact with and bind to the lipid bilayer of cerebral endothelial cells. CPPs are heterogeneous in size (5–30 amino acid residues) and sequence, and generally possess several positive charges at physiological pH<sup>645</sup>. The importance of the basic residues on CPP translocation has been largely demonstrated<sup>646-648</sup>. Although CPPs have been used *in vivo* delivering therapeutics across the BBB, different mechanisms have been proposed including rapid direct penetration across the plasma membrane and slow endosomal uptake *via* one or several endocytic pathways<sup>649-652</sup>. These uptake mechanisms might occur simultaneously and depend on the biophysical properties of the cargo<sup>653</sup>. Many peptides with cell-penetrating properties have been reviewed in great detail<sup>527,654-657</sup>. While CPP vector-mediated strategies have shown efficacy in carrying low MW cargo into the brain<sup>658,659</sup>, evidence demonstrating their capacity to transport macromolecules, such as proteins, through the BBB/BCSFB remains limited.

The transcription activating factor-derived peptides (Tat peptides) were the first CPPs to be reported, and were derived from the human immunodeficiency virus type I (HIV-1). They demonstrated an ability to be rapidly taken up by cells and to concentrate in the nucleus<sup>660</sup>. Cell and nuclear import is associated with residues 49 to 58 of the sequence<sup>661</sup>. Many truncated Tat peptides have been shown to enter various cell types<sup>646,662</sup>. Some fragmentary (and sometimes controversial) studies have reported the ability of CPPs to reach the brain parenchyma<sup>662,663</sup>. Most studies have involved CPPs attached to cargoes and resulted in divergent outcomes given that the cargo may influence cell-penetration and BBB transport of the CCPs. Tat peptides have been conjugated to proteins to promote crossing of blood–brain interfaces. The capability of Tat to deliver proteins to the brain was investigated by Schwarze et al.<sup>664</sup>, who assessed the biodistribution of Tat-derived peptide (47–57) fused to  $\beta$ -GAL (MW ~120 kDa) in mice. Following intraperitoneal injection of the Tat- $\beta$ -GAL constructs, analysis of  $\beta$ -GAL activity demonstrated that the fusion protein had not only passed into the brain but also

reached all examined organs (liver, kidney, lung, heart muscle, and spleen). These results conflicted with earlier work in which Tat peptides (1–72 or 37–72) were chemically cross-linked to  $\beta$ -GAL and showed no penetration into the brain following intravenous injection<sup>665</sup>. This contradiction could be related to the use of different peptide sequences, although this interpretation requires further exploration to clarify this discrepancy. Following this study, the intravenous administration of recombinant glial cell line-derived neurotrophic factor (GDNF)-Tat fusion protein, significantly reduced infarct size after ischemia in mice<sup>666</sup>. In contrast, the neuroprotection of dopaminergic neurons was not achieved using Tat-GDNF in a PD mouse model, even though the fusion protein succeeded in reaching the brain (as shown by immunohistochemical staining). This effect was attributed to the probable insufficient amount of the fusion protein reaching the striatal nerve endings of surviving dopaminergic neurons<sup>667</sup>.

Using genetic engineering, heat shock protein70 (Hsp70) was linked to Tat and administered in a transient MCAo animal model at the moment of reperfusion as well as 2 weeks later. Tat-Hsp70 treated groups displayed a significant decrease of the infarct volume in comparison to non-treated groups<sup>668</sup>. Furthermore, intraperitoneal injection into a murine stroke model of Bcl-xL, a death-suppression molecule, fused to Tat resulted in transduction of protein in neurons and a decrease of infarction<sup>669</sup>. Similar results as well as improved neurological deficits were seen after intravenous injection of Tat-Bcl-xL one hour before or right after MCAo in a rat model<sup>670</sup>. Comparable conclusions have been drawn for Tat-Neuroglobin following intravenous injection in focal cerebral ischemia in mouse models (i.e., treatment two hours before MCAo reduced brain infarct volume, increased neuronal survival in the striatum, and improved neurologic outcomes compared to controls)<sup>671</sup>. Taken together, these studies clearly demonstrated that Tat-enhanced delivery of proteins through the BBB is promising. However, the BBB is compromised in these models. Therefore, while not elaborated in these studies, the enhanced passage of proteins might be related to the damaged nature of the BBB rather than the ability of Tat to promote BBB passage. In addition to Tat, other CPPs such as the Rabies virus glycoprotein derived peptide (RDP), have been used to deliver systemically-administrated proteins across BBB<sup>672,673</sup>. While the beneficial effects of fusing CPPs to proteins have been clearly demonstrated, most of the papers on BBB targeting based their results on microscopy or whole animal fluorescence images, without providing actual quantification. Therefore, this parameter needs to be further investigated and reported in order to allow a measurable appreciation of the delivered dose (% in comparison to the total dose).

Overall, while several studies have demonstrated an increased therapeutic effect of proteins fused to CPPs, the capacity of CPPs to penetrate various cell types at the same time greatly restricts their pharmaceutical application for specific brain delivery. Moreover, the use

of CPPs for brain targeting was associated with issues such as neurotoxicity, endothelial cell apoptosis, inflammation, and immunogenicity due to the cationic nature, as well as the instability of peptides in the biological environment <sup>674</sup>.

### 2.1.2. Immunoglobulins

Molecular Trojan horses (MTH) have been shown to efficiently deliver therapeutic proteins to the brain, *via* RMT <sup>675,676</sup>. The MTH method consists of an endogenous ligand or genetically-engineered monoclonal antibody against a receptor on the targeted cells that is fused to a large therapeutic protein to be delivered to the CNS <sup>675</sup>. Of the receptors expressed on brain endothelial cells, TfR and the insulin receptor have been those most commonly targeted by MTHs.

The use of monoclonal antibodies against TfR originated from the ability of this receptor to mediate the passage of transferrin through blood-brain interfaces <sup>677</sup>. These monoclonal antibodies bind to epitopes on the extracellular domain of TfR distal to the transferrin binding site, and thus do not compete with transferrin for TfR binding. Various studies using the monoclonal antibody OX26 have demonstrated that TfR can mediate the passage of TfRMAb from blood to the brain <sup>678-680</sup>. Indeed, owing to its interaction with TfR, the brain distribution of OX26 was 18-fold higher than that of a control mouse IgG2a, at 5 hours post-injection <sup>679</sup>. In addition to OX26, various TfRMAb have been developed, namely 8D3 and RI7-217 <sup>678</sup>, as well as single chain variable fragments (scFv) and chimeric TfR antibodies (cTfRMAb) that can be fused to other proteins <sup>681-683</sup>. The affinity towards TfR, brain uptake, and consequent transport across the BBB of different fusion constructs based on OX26 <sup>684-686</sup> was considerably different from those based on cTfRMAb <sup>687-693</sup> (0.12–0.15% *versus* 2.2–3.5% of the injected dose/g, respectively) <sup>678</sup>. Furthermore, the brain uptake of dissimilar cTfRMAb fusion proteins yielded different values in mice. For instance, cTfRMAb fused with therapeutic ScFv, GDNF, TNF receptor (TNFR), and EPO exhibited  $3.5 \pm 0.7$ ,  $3.1 \pm 0.2$ ,  $2.8 \pm 0.5$ ,  $2.0 \pm 0.1\%$  of the injected dose/g, respectively (brain uptake is expressed per gram of brain tissue) <sup>687,691,694,695</sup>.

Biologic TNF inhibitors, such as etanercept (a soluble form of the TNFR 2; TNFR2), that represent a potential new intravenous treatment for acute stroke <sup>696,697</sup> were not developed as pharmaceuticals because they cannot cross the BBB <sup>698</sup>. To achieve brain delivery for etanercept, an IgG fusion protein designated as cTfRMAb-TNFR was engineered by joining the extracellular domain of TNFR2 C-terminally to the heavy chain of a genetically-engineered monoclonal antibody against mouse TfR <sup>695,696</sup>. Results demonstrated that cTfRMAb-TNFR rapidly crossed the BBB in mice *via* RMT mediated by TfR <sup>695</sup>. Passage through the BBB resulted in therapeutic improvement in an experimental stroke model. Indeed, in the transient

MCAo mouse model, treatment with cTfRMAb-TNFR significantly reduced (40–50%) hemispheric, cortical, and subcortical stroke volumes as well as in the neural deficit score (24 h or 7 days post-occlusion). In contrast, free etanercept had no therapeutic effect<sup>696</sup>. Similar neuroprotective properties have been drawn from other investigations on ischemia (combined cTfRMAb-TNFR and cTfRMAb-GDNF treatment) and on AD (chronic treatment with cTfRMAb-TNFR)<sup>699,700</sup>. Likewise, GDNF was fused to cTfRMAb as it possesses neuroprotective and restorative properties in animal models of PD<sup>701,702</sup>. The fusion protein cTfRMAb-GDNF indeed possessed neuroprotective properties in an experimental mouse model of PD generated by intra-striatal injection of 6-hydroxydopamine. Indeed, after daily administration of the fusion protein for 3 weeks, the treated group had increased dopaminergic activity as well as marked improvements in motor functions<sup>703</sup>. Another fusion protein composed of iduronate 2-sulfatase (IDS) linked N-terminally to the Fc domain of a humanized anti-human TfR antibody has shown a high brain distribution in mice and monkeys, and a reduction of the glycosaminoglycans levels in the brain of a mouse model of MPS II<sup>704</sup>. Similar results were obtained in MPS I mice with cTfRMAb-iduronidase (IDUA), where increased enzyme activity levels in the brain and decreased vacuolation/ glycosaminoglycans storage were reported<sup>705</sup>. There is a significant body of literature demonstrating the efficacy of genetically engineered cTfRMAb for brain delivery of a broad range of proteins, such as TNFR,<sup>690,699,706-708</sup> GDNF<sup>691,699,709,710</sup>, EPO<sup>711</sup>, N-sulfoglucosamine sulfohydrolase (SGSH)<sup>712</sup>, iduronate-2-sulfatase (IDS)<sup>688</sup>, interleukin-1 receptor antagonist (IL-1RA)<sup>713</sup>, and anti- $\beta$ -amyloid scFv therapeutic antibody<sup>687,689</sup>. Clinical trials for some of these constructs were recently launched. Phase 1/2 clinical trials show that high affinity binding of anti-TfR antibodies fused to IDS reduce the concentration of heparan sulfate in the CSF of patients suffering from MPSII<sup>714</sup>. It should be mentioned however that the number of participants in this study was extremely low, leading to an inevitable lack of statistical power. Consequently, further clinical studies are needed to confirm (or not) these data.

Considering that 83-14 undergoes transcytosis in rhesus monkeys, anti-insulin receptor monoclonal antibodies (IRMAb) have been studied to deliver proteins to the brain. A single intravenous injection resulted in 3.8% of dosed 83-14 being delivered to the brain, while no brain uptake was observed for a control antibody<sup>118</sup>. Likewise, chimeric and fully humanized forms of IRMAb (both referred to as HIRMAb) internalized and crossed blood–brain interfaces<sup>120,122,715</sup>. Subsequently, fusion proteins based on HIRMAb molecules were developed to deliver relevant therapeutic proteins to the brain, with examples including lysosomal enzymes (arylsulfatase A (ASA), GUSB, IDS, IDUA), TNFR, EPO, GDNF, and murine anti-A $\beta$  ScFv<sup>691,698,716-723</sup>.

The use of HIRMAb-fusion proteins as enzyme replacement therapies for MPS diseases in non-human primate models has generated stunning results <sup>716,724-726</sup>, allowing it to move to clinical studies. One example is the HIRMAb-IDUA (also designated AGT-181) <sup>727</sup>. Recombinant IDUA or HIRMAb-IDUA were iodinated with <sup>125</sup>I and (separately) intravenously administered to Rhesus monkeys <sup>728</sup>. At 2 hours post-injection, brain scans showed no measurable brain uptake of IDUA and a significant brain uptake of HIRMAb-IDUA (~1% of injected dose/brain tissue). From these results, the authors suggested that an infused dose of ~1 mg/kg of the fusion protein was expected to restore IDUA activity in the brain <sup>716</sup>. Recent clinical reports with HIRMAb-IDUA are of great interest. HIRMAb-IDUA represents the first clinical example of the exploitation of RMT to deliver a drug to the brain in pediatric and adult patients with MPSI <sup>729-731</sup>. So far, positive neurocognitive and somatic effects were observed (e.g., stabilization of the severe mental retardation from a further decline), albeit adverse events were also reported (e.g., reaction at infusion site, transient hypoglycaemia) <sup>731</sup>. The success of these trials will surely provide the basis for the future design of IgG fusion proteins for various brain diseases.

While the MTH strategy allows efficient brain delivery of relevant therapeutic proteins that are originally not able to cross blood-brain interfaces, it still suffers from downsides <sup>607</sup>. Firstly, antibodies targeted to specific receptors might, in some cases, mimic or antagonize endogenous ligands and can exhibit toxicity, especially at high doses. For example, chronic administration of HIRMAb-IDUA caused hypoglycemia at doses of 30 mg/kg in pre-clinical models <sup>724</sup>, but not at doses of 3–10 mg/kg <sup>732</sup>. The second important aspect to consider for the MTH strategy is related to receptor expression. For example, while the targeted receptors are enriched at blood-brain interfaces, they are also expressed in other tissues leading to unwanted, extended distribution of receptor-targeted therapeutics <sup>733</sup>. Thirdly, an immune response and hypersensitivity reaction could be generated, especially for long-term treatment. So far, increased plasmatic levels of anti-HIRMAb-IDUA antibodies and the development of hypersensitivity reactions have been reported in monkeys over the course of six months of treatment. While this immune response did not alter pharmacokinetic parameters of the fusion protein (e.g., plasma bioavailability), similar considerations should be underlined for each specific fusion protein <sup>732</sup>. Furthermore, when engineering the MTH, functionality of each fusion partner should be maintained (i.e., high antibody affinity towards the targeted receptor and retained therapeutic activity of therapeutic protein). For instance, human  $\beta$ -glucuronidase (GUSB) was fused to the heavy chain of the chimeric HIRMAb. Two different fusion proteins were generated: HIRMAb-GUSB (fusion to the C-terminus of HIRMAb heavy chain) and GUSB-HIRMAb (fusion to the N-terminus of the heavy chain of the HIRMAb). The first construct retained high affinity towards the insulin receptor but lost >95% enzymatic activity.

In contrast, the second fusion protein displayed a high enzymatic activity but lost 95% binding affinity towards the insulin receptor <sup>720</sup>. Therefore, the design of fusion proteins is critical and should take into account the activity of both fused proteins. Furthermore, in the case where the therapeutic protein is also an antibody, the binding properties of the fusion protein acting as a bi-specific molecule might be compromised. In this context, the monovalent binding of scFv targeting TfR has been found to be more advantageous than the bivalent binding of the whole TfRMAb <sup>554</sup>. Thus far, a bispecific fusion protein based on two scFv of TfRMAb (8D3) attached C-terminally to the light chains of mAb158 (binds to A $\beta$  protofibrils associated with the pathophysiology of AD) greatly improved the brain uptake of the fusion protein. Indeed, three days post-injection, the concentration of fusion protein in transgenic AD mouse brains was 9-fold higher than in wild-type mice <sup>734</sup>. Higher or equal brain uptake was achieved compared to previously reported BBB shuttles, and with a less pronounced decline in uptake at therapeutic doses <sup>57,554,735,736</sup>. Additionally, as the TfR and insulin receptor-mediated endocytosis are generally species specific, the selection of the right antibodies for the MTH based brain delivery should be considered <sup>737</sup>. Finally, for cerebral diseases the chronology of the alteration of blood-brain interfaces as well as the consecutive alteration of certain receptors should be taken into consideration when designing the Ig entities (e.g., affinity, structure) as well as the fusion proteins (e.g., dose and timing of injection). In addition, the full transcytosis of the fusion protein to the brain might be limited <sup>733</sup>.

### **2.1.3. Endogenous ligands**

Natural physiological transport mechanisms have been exploited to achieve brain delivery, by using endogenous ligands as promoters of RMT. Although full-length ligands have been used to transport low MW molecules and nanosystems <sup>738,739</sup>, the peptides derived from these entities have been applied to high MW molecules. Compared with the entire ligand molecules or anti-receptor antibodies, such short homing peptides can be readily fused to proteins with minimum risks of jeopardizing their therapeutic function. Moreover, only using the segment associated with transport reduces the risk of altering the homeostasis of the ligand, of disrupting its important physiological function(s), or stimulating an immune response against the fusion protein. Nevertheless, further evaluation is needed to demonstrate this and to evaluate the affinity of such homing peptides in comparison to full-length ligands.

The number of studies using fusion proteins based on ligands or peptides targeting receptors on the BBB/BCSFB are limited. The majority of studies have used lentivirus vector systems to deliver fusion protein genes to the liver or spleen, which transforms their cells into sites of expression and secretion of the targeted therapeutic proteins. One example, Apo B-BD fusion promotes the brain delivery glucocerebrosidase, green fluorescent protein, and the

metalloprotease neprilysin<sup>740,741</sup>.

Melanotransferrin belongs to the transferrin family and has been investigated as carrier for the transport of drugs across blood–brain interfaces<sup>548</sup>. Despite its homology with transferrin, LRP1 (and not TfR) was suggested to be involved in its transcytosis across the BBB<sup>742</sup>. Recent *in vivo* studies have demonstrated effective brain delivery of a fusion protein composed of a control antibody (NIP228) and either full-length melanotransferrin or a twelve amino acid peptide (460–471) derived from melanotransferrin (melanotransferrin peptide). In this study, melanotransferrin and melanotransferrin peptide were genetically fused to the C-terminus and to the N-terminus of the antibody's heavy chain (NIP228), respectively. Following intravenous administration to mice, both fusion proteins distributed to a greater extent to the brain compared to the free antibody (95% of fluorescence in the brain parenchyma vs. capillary blood vessels). Interestingly, a NIP228-melanotransferrin peptide fusion protein had a significantly extended brain exposure when compared to NIP228-full-length melanotransferrin and NIP228 alone, with a peak exposure of ~4% of the injected dose/g 24 hours post-injection (in comparison, the brain uptake of NIP228- melanotransferrin and free NIP228 was ~2% and <1%, respectively). To further validate the apparent ability of these molecules to deliver proteins to the CNS, fusion of an analgesic compound IL-1RA was conducted and pharmacodynamic studies were performed in a mouse model of neuropathic pain. Brain exposure of both fusion proteins was very similar with a maximum exposure of 2.2% of injected dose/g at 2 hours post-administration. The resulting brain delivery of IL-1RA enabled the measurement of analgesia through a reduction in mechanical hypersensitivity following partial sciatic nerve ligation. The magnitude of the response was very similar for both fusion proteins tested<sup>743</sup>. Moreover, the potential brain delivery of different fusion proteins formed by arylsulfatase A (ASA) linked to five presumed brain uptake enhancer peptides (Tat, Angiopep-2, Apo B-BD, and Apo E-BD (two versions Apo E-BD-I (148–170) and Apo E-BD-II (159–167))) were evaluated. All fusion proteins maintained their enzymatic activity and were able to target the lysosomes of cultured cells. In contrast to free ASA, which is taken up by mannose-6-phosphate receptors, mannose-6-phosphate-independent routes were also observed for all fusion proteins. For instance, for ASA-Angiopep-2 and ASA fused with the two versions of Apo E-BD, the uptake was partially due to LRP1. Although Apo E-BD-II did not show the best *in vitro* endocytosis performance, it was the only shuttle to increase the brain delivery of ASA compared to Angiopep-2, Apo B-BD, and Apo E-BD-I fused ASA. Apo E-BD-II fused with ASA also performed better than the native protein in the CNS of ASA-knock-out mice. Interestingly, this shuttle did not compete with the endogenous protein in ApoE-knock out mice because transport efficiency did not increase<sup>744</sup>. This study reflects the lack of correlation between the mechanisms of endocytosis and transcytosis encountered in most studies. Indeed,

endocytosis of molecules does not necessarily reflect their transcellular passage, and this aspect should be considered in the development of brain delivery systems.

Although the diversity of peptides that promote cellular uptake has dramatically increased, very few have led to efficient brain delivery of protein therapeutics over the last two decades. As mentioned above, the use of ligands/peptides fused to therapeutic proteins to target the brain remains very restricted and has its own drawbacks. Furthermore, comparative and quantitative data on their performance are currently lacking.

## 2.2. Bioconjugates

Covalently linking a brain-impermeable therapeutic protein to a brain targeting molecule (IgG, endogenous ligands, ...) or a polymer (polyethylene glycol (PEG), pluronics, ...) has been widely investigated. Depending on the conjugated molecule, the resulting bioconjugates can either target proteins to the brain interfaces (and therefore increase their brain uptake) or possess a longer blood residence time, which consequently increases the contact time and potentially the passage through the blood-brain interfaces.

A series of studies have been published by Pardridge and colleagues in which they investigated the methods of conjugation of TfRMAb (predominantly OX26) to different proteins (e.g., brain-derived neurotrophic factor (BDNF), EGF, and FGF)<sup>685,745-748</sup>, the pharmacokinetic profiles of various bioconjugates after systemic delivery<sup>749,750</sup>, along with the possibility of using TfRMAb for the transport of proteins across the BBB<sup>678,745,746,749,751-753</sup>. For example, 60 min after intravenous bolus injection to rats, radiolabeled bFGF was avidly taken up by peripheral organs and displayed a low brain uptake. However, the administration of a radiolabeled FGF–OX26 bioconjugate exhibited a decrease in the peripheral uptake along with a 5-fold increase in brain uptake ( $0.050 \pm 0.011\%$  of injected dose/g)<sup>749</sup>. Most prominently, these TfRMAb-based bioconjugates demonstrated efficient transport into the brain and provided obvious therapeutic effects. For instance, BDNF linked to the OX26 *via* an avidin-biotin coupling strategy and further conjugated to 2 kDa PEG (at carboxyl residues of BDNF) was intravenously injected to permanent MCAo rats, and resulted in a dose-dependent decrease of infarct volume. Importantly, significant reduction in stroke volume was still observed with the delayed administration (1–2 hours after MCAo) of the bioconjugate, although the pharmacological effects were reduced. With the same doses, unconjugated BDNF and unconjugated OX26 were ineffective<sup>754</sup>. Comparable improvements using the BDNF–OX26 bioconjugate (produced by the same or different chemistry) were reported for cerebral ischemia and stroke models as well as for dissimilar brain diseases (e.g., neurodegenerative diseases of the spinal cord or midbrain dopaminergic neurons)<sup>755-757</sup>. Other neurotrophic factors were

conjugated to OX26, including nerve growth factor (NGF). Indeed, the efficient brain delivery of the NGF–OX26 biconjugate was demonstrated<sup>758</sup>. This effective transport across the BBB resulted in increased survival for both cholinergic and non-cholinergic neurons, which is of importance for the treatment for various neuronal diseases<sup>758-763</sup>.

In addition to OX26, other TfRMAb were successfully conjugated to proteins. Bacterial  $\beta$ -GAL was conjugated to rat 8D3 by streptavidin–biotin chemistry. Native  $\beta$ -GAL or the  $\beta$ -GAL–8D3 bioconjugate were injected systemically to mice, and activity measured in the brain and peripheral organs. Unconjugated  $\beta$ -GAL rapidly accumulated in the liver and spleen, with minimal brain uptake. In contrast,  $\beta$ -GAL–8D3 had ten times greater brain uptake (evaluated by enzyme activity measurement) and intra-endothelial localization in the brain compartment by histochemical analysis<sup>764</sup>.

The conjugation of horseradish peroxidase (HRP), which by itself does not cross the BBB, to transferrin (diferric form), OX26 (MW ~150 kDa), and the Fab fragment of OX26 (MW ~50 kDa) has also been performed. OX26, OX26(Fab)–HRP, and transferrin were coupled to HRP in a stoichiometric ratio. OX26–HRP and transferrin–HRP underwent transcytosis through the BBB, while OX26(Fab)–HRP did not. Interestingly, clear differences in the intra/extracellular distributions were observed for OX26–HRP and transferrin–HRP, which suggests that the RMT of transferrin–HRP was more efficient than for OX26–HRP. The non-transcytosis of OX26(Fab)–HRP might be because the monovalent form of IgG was not able to crosslink TfRs and thus circumvented the implication of the Golgi complex and subsequent transcytosis<sup>765</sup>.

As mentioned in previous sections, the use of peptides derived from endogenous ligands (instead of the full-length ligand molecules) has yielded some success. These targeting peptides could likewise be conjugated directly to therapeutic proteins of interest. Melanotransferrin peptide (460–471) was attached to the NIP288 antibody *via* a cysteine residue engineered on the Fc domain of NIP288. This study demonstrated that, following intravenous administration, NIP288–melanotransferrin peptide induced sufficient transport through the brain capillary endothelium to achieve sufficient levels in the brain parenchyma. Importantly, when injected to a mouse model of neuropathic pain, melanotransferrin peptide conjugated to NIP288–IL-1RA resulted of mechanical hyperalgesia at four days post dose<sup>743</sup>. Furthermore, conjugation of angiopep-2 to anti-HER2 as well as anti-EGFR antibody was undertaken. In both cases, an increase in the transport rate of the antibody across a mouse BBB was observed by *in situ* brain perfusion and fluorescence imaging<sup>766,767</sup>.

The modification of proteins with hydrophilic (e.g., PEG) or amphiphilic block copolymers (e.g. pluronics or poly(2-oxazoline)s (POx)) was used as a strategy to improve protein brain delivery. PEGylation (attachment of PEG to molecules) has been used to increase the stability, improve

serum bioavailability, limit the passage of small drugs through the BBB, eliminate rapid clearance and potential side effects (e.g., clinically approved Naloxegol) <sup>768</sup>. Thus, although PEGylation can alter pharmacokinetic properties, promotion of passage across the BBB/BCSFB would not be expected, unless the barriers are compromised. Nevertheless, increasing the circulation time (and therefore increasing the exposure of proteins to the brain capillaries) might indirectly promote passage to the brain. So far, PEGylated hemoglobin was tested in an animal model of stroke <sup>769</sup>. PEG–haemoglobin (SB1; total MW ~104 kDa with a size of 30–50 nm), was infused after transient MCAo through the femoral artery. Compared to an MCAo control (displaying a corrected infarct volume of  $145.1 \pm 9.2 \text{ mm}^3$ ), SB1 reduced the infarct size by a dose-dependent manner (decrease to  $19.9 \pm 4.6$  and  $1.9 \pm 0.5 \text{ mm}^3$  for an SB1 dose of 240 and 480 mg/kg, respectively) and prevented the accompanying behavioural deficits. The observed neuroprotective effect was related to either the passage of SB1 through the openings between cerebral blood vessels and thrombus (hence providing oxygen to hypoxic cells), or to the supply of oxygen *via* collateral blood vessels and thus preventing hypoxic brain injury in the affected areas <sup>769</sup>. Of note, while SB1 was effective at preventing neural injury caused by MCAo, comparison to free hemoglobin was not made. Such comparison is important because it would determine whether the recorded improvements were due to the PEGylation of this protein. Apart from this study, PEGylation was not successful in transporting other proteins across the brain barriers. Possible explanations include increase of hydrophilicity and hydrodynamic radius concurrent with PEGylation, which might offset their permeability across the blood-brain interfaces <sup>770</sup>. PEGylation of leptin (a treatment for obesity that failed due in part to unfavourable transport across the pathological BBB), for example, increased its blood circulation half-life but not brain uptake <sup>771-773</sup>. Additionally, PEGylated superoxide dismutase (SOD) was injected in piglets in the absence and presence of global cerebral ischemia and reperfusion <sup>502</sup>. In this experiment, PEG–SOD administration increased serum SOD activity without increasing the brain activity. It was concluded that the bioconjugate did not reach the brain despite expected disruptions to the BBB <sup>774</sup>. Nonetheless, while the non-passage of PEGylated SOD across blood-brain interfaces was clearly demonstrated, the lower limit of sensitivity for the SOD assay may have prevented the detection of a very small increase in activity. Therefore, a study of the brain distribution of PEG–SOD was undertaken to investigate whether distribution of radiolabelled PEG–SOD (<sup>125</sup>I-PEG–SOD) injected intravenously was altered by acute norepinephrine induced hypertension <sup>504</sup>. This study included: (1) control group : healthy animals receiving PEG–SOD, (2) pre-injury group: animals receiving PEG–SOD 30 min before norepinephrine induced hypertensive injury, and (3) post-injury group: animals injected with PEG–SOD 30 min after norepinephrine-induced hypertensive injury. Ninety minutes post-injection, CSF samples were collected by cisternal puncture, the brains as well as various organs were removed, and <sup>125</sup>I was counted by

scintillation. The data showed that in the control group (intact blood-brain interfaces) and in the post-treated group, no major uptake of PEG–SOD into the brain or CSF was noticed. In contrast, a ~2.5-fold increase in brain PEG–SOD concentration was recorded in the pre-treated group. The difference between pre- and post-treated groups was explained by the transient increase in the permeability of blood-brain interfaces only during the hypertensive phase. Moreover, CSF analysis provided different results. A significant increase in the levels of PEGylated SOD was observed irrespective of whether the injection was given before or after the hypertensive injury, implying a longer-lasting disruption of the BCSFB by the acute hypertension<sup>504</sup>. Taken together, this study showed that when the integrity of various barriers is breached, an increased brain distribution of PEG–SOD might be observed. Of course, these results could be specific to this case rather than apply to more dramatic types of brain injury or for dissimilar PEGylated enzymes. Overall, PEG–protein bioconjugates generally have extended circulation time and greater serum stability in comparison to their native forms. However, PEGylation appears to significantly hinder their ability to cross intact blood-brain interfaces. From a clinical perspective, the fact that they do not pass intact physiological barriers could be advantageous for the treatment of neuronal diseases (i.e., ensure the delivery of proteins only in the damaged areas of the brain).

The conjugation of amphiphilic block copolymers to proteins rather than hydrophilic polymers efficiently promoted delivery across the blood-brain interfaces. More specifically, the ability of pluronics to interact with hydrophobic surfaces such as cell membranes has been explored to promote crossing<sup>775</sup>. Interestingly, pluronics can inhibit drug efflux transporters (notably the P-glycoprotein)<sup>776-778</sup>.

Pluronics have been conjugated to several proteins, including HRP<sup>779</sup>, leptin<sup>780,781</sup>, and SOD<sup>782</sup>. More specifically, Pluronic L81, P85, L121, and P123 have been conjugated to HRP *via* either a biodegradable disulfide linker, or a permanent linker. The bioconjugates bore ~1–2 pluronic chains per HRP and generally retained less than 70% of the activity of the native enzyme<sup>783</sup>. *In vitro* uptake by primary bovine brain microvessel endothelial cells (BBMEC) and Mardin-Derby canine kidney (MDCK) cells showed that bioconjugates with shorter PPO chains (L81 and P85) exhibited the highest cellular uptake<sup>783</sup>. Despite these results, conjugation of P85 *via* a degradable SS bond to HRP and the subsequent intravenous administration did not show a considerable difference in comparison to unconjugated HRP<sup>779</sup>. In contrast, protein modification with pluronics has shown to be a promising strategy for the development of an anti-obesity bioconjugate<sup>780,781,784</sup>. Indeed, to overcome peripheral leptin resistance and to promote penetration of leptin to the brain independently of its transporter, the latter was conjugated to pluronic P85. Pharmacokinetic data demonstrated that intravenously injected

bioconjugate containing a disulfide bond (leptin(ss)–P85) was transported across the BBB *via* a non-saturable mechanism independent of the leptin transporter <sup>780</sup>. Consequently, two different leptin(ss)–P85 bioconjugates were generated. Lep(ss)–P85(H) contains several P85 chains, while Lep(ss)–P85(L) only contains a single P85 chain. Lep(ss)–P85(H) and Lep(ss)–P85(L) were intravenously administered to *ob/ob* mice, a leptin-sensitive model of obesity, as well as in a diet-induced model of obesity demonstrating both central and peripheral resistance to leptin. In *ob/ob* mice, Lep(ss)–P85(L) crossed the BBB *via* the leptin transporter and exhibited enhanced peripheral pharmacokinetics along with increased brain accumulation relative to native leptin. In contrast, insufficient transport to the brain was most likely responsible for the lack of response to Lep(ss)–P85(L) and native leptin. In contrast, Lep(ss)–P85(H) penetrated the BBB independently of the leptin transporter *via* a non-saturable mechanism and led to reduced food intake in the diet-induced obese mice ([Figure 5](#)). Based on these data, the authors suggested that Lep(ss)–P85(H) might be a promising anti-obesity bioconjugate due to its improved peripheral bioavailability and greater brain uptake achieved independently of the leptin transporter <sup>781</sup>.

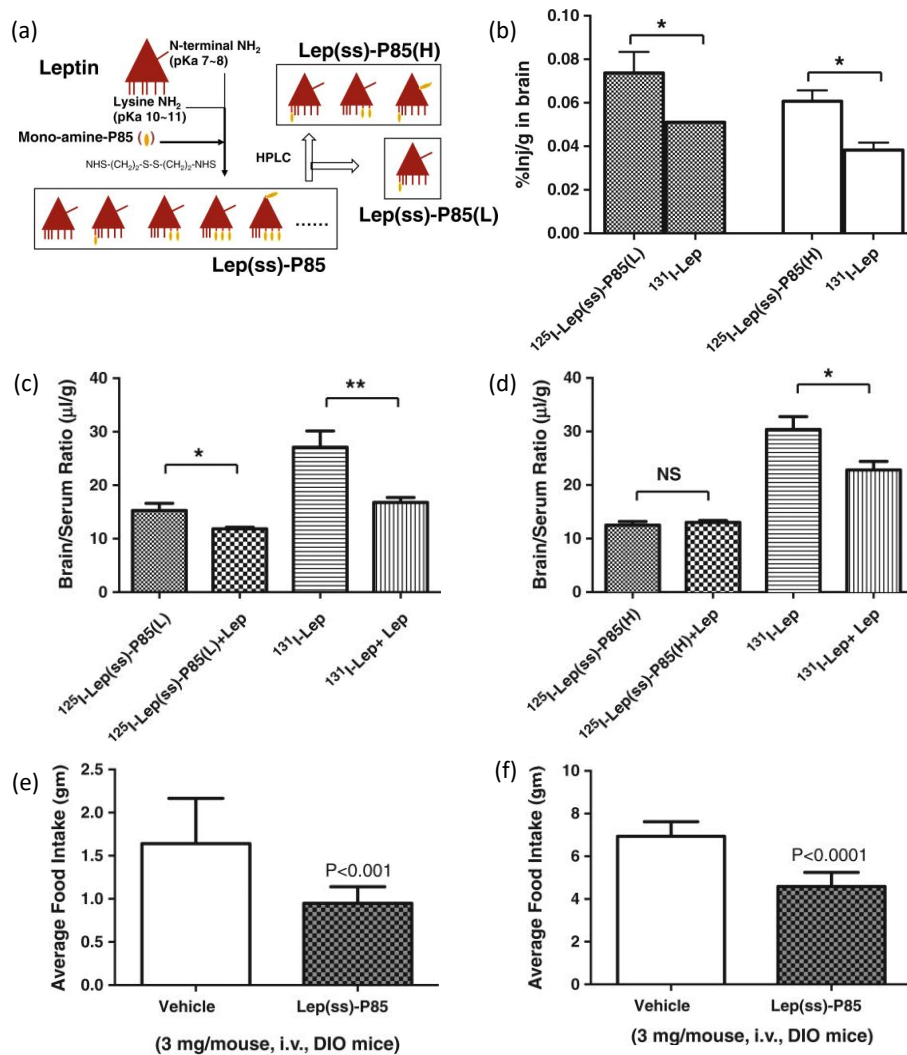


**Figure 5: Leptin modified with pluronic possesses increased systemic circulation, brain uptake, and efficacy for treatment of obesity relative to native leptin. (a)** Preparation and purification of Lep(ss)-P85(H) and Lep(ss)-P85(L), which contains high and low numbers of P85 per leptin molecule, respectively. **(b)** Brain exposure of <sup>125</sup>I-Lep(ss)-P85(L) or <sup>125</sup>I-Lep(ss)-P85(H) was significantly higher than that of radiolabeled leptin (<sup>131</sup>I-Lep) four hours after intravenous administration. **(c, d)** Co-injection of non-radioactive leptin decreased the brain/serum ratio of both <sup>125</sup>I-Lep(ss)-P85(L) and <sup>131</sup>I-Lep 30 min after injection. The brain/serum ratio of <sup>125</sup>I-Lep(ss)-P85(H) when co-injected with leptin. **(e, f)** Intravenous injection of Lep(ss)-P85 significantly reduced food intake of DIO mice (at 2 and 24 hours after food induction). Adapted with permission from <sup>781</sup>.

Protein modification with amphiphilic POx block copolymers has also been explored to promote brain accumulation <sup>785-787</sup>. SOD1 was modified with POx, P(MeOx-b-BuOx) or P(EtOx-b-BuOx), which are composed of hydrophilic 2-methyl-2-oxazoline (MeOx) and hydrophobic 2-butyl-2-oxazoline (BuOx) or hydrophilic 2-ethyl-2-oxazoline (EtOx) and BuOx repeating units <sup>788</sup>. The conjugates bore ~2–3 POx chains per SOD1 linked *via* reducible disulfide bond (SS) or a non-reducible (cc) linker at the BuOx block terminus. After intravenous administration to mice, SOD1–P(EtOx-b-BuOx) possessed ~1.75 times longer circulation half-life compared to native SOD1, crossed the BBB by non-saturable mechanism (*via* caveolae-mediated and/or clathrin and caveolae-independent endocytosis), and reached brain parenchyma (0.08% of injected dose/g at 4 hours post-injection) <sup>788</sup>. It was reported that, in comparison to PEG and pluronics, POx copolymers have a great versatility because of the ability of introducing various functional side-chain groups <sup>21</sup>. Future research with POx might explore how this versatility could be exploited for the brain delivery of proteins.

Recent studies have started to explore other polymers. For example, polymer chemistry and immunotherapy were combined to systemically deliver a nanoscale immunoconjugate (NIC) IgG across the BBB and activate a local anti-glioblastoma immune response. In this study, humanized monoclonal antibodies against T-lymphocyte-associated antigen 4 (CTLA-4 IgG2b) or programmed cell death-1 (PD-1 IgG) were covalently conjugated to poly( $\beta$ -L-malic acid) (PMLA) to promote stability during blood circulation. Furthermore, additional molecules were attached to these conjugates, including (1) brain targeting molecules (TfRMAb or Angiopep-2) to enable the passage across the BBB, (2) 5 kDa mPEG for solubility and stability, and (3) trileucine peptide to stabilize PMLA against hydrolysis. Administration of the bioconjugates to mice bearing intracranial GL261 glioblastoma stimulated the brain resident immune system and with an increase of CD8<sup>+</sup> T-cells, naturel killer cells, and macrophages and a decrease of regulatory T-cells in the tumor. Interestingly, survival of glioblastoma-bearing mice treated with a combination of both NIC was longer compared to animals treated with single nanoscale immunoconjugates treatment or only free CTLA-4 IgG2b or PD-1 IgG. Overall, these nanoscale immunoconjugates were able to deliver immunotherapy and other therapeutics to brain tumors ([Figure 6](#)) <sup>789</sup>.

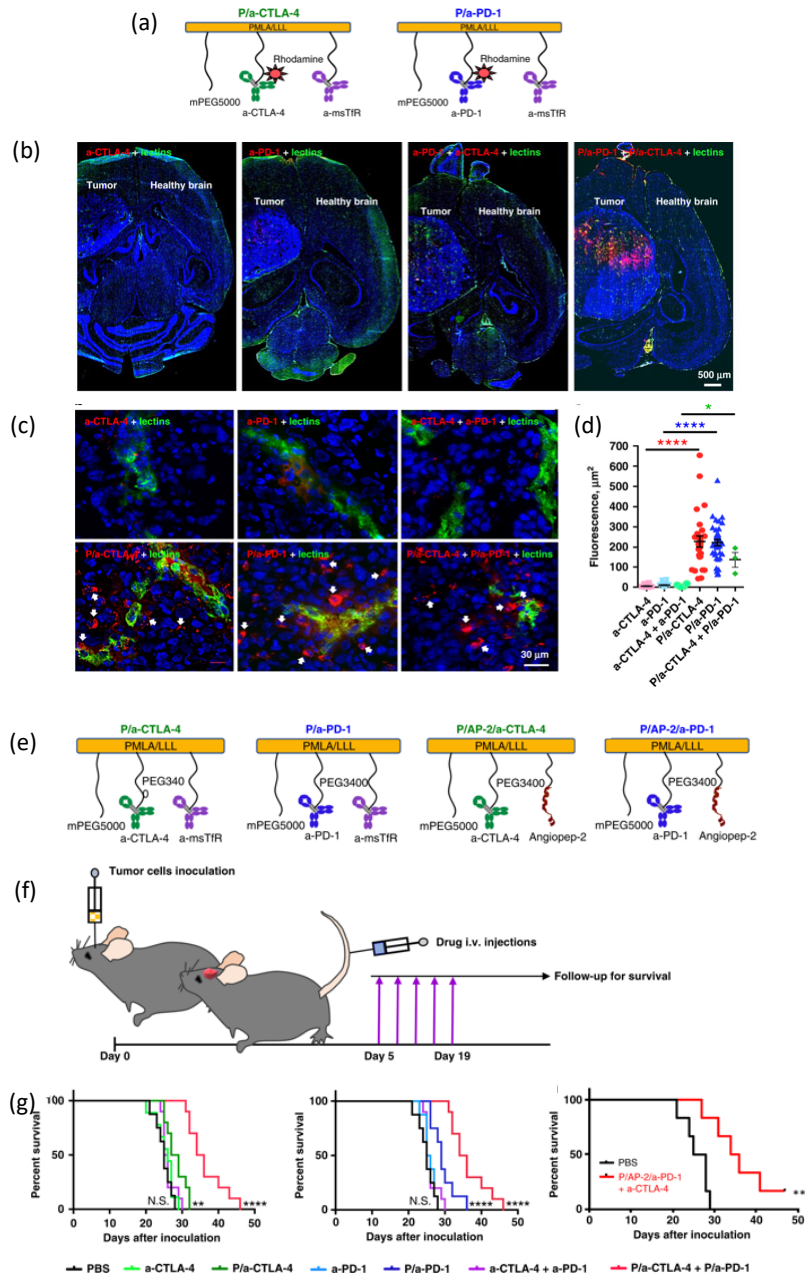


**Figure 6: Blood–brain barrier permeable NICs improved the survival of animals bearing intracranial GL261 glioblastoma. (a)** Structures of treatment NIC. **(b, c, d)** Fluorescently labelled NIC cross the BBB and accumulate in the glioma. **(b)** Combined rhodamine-labelled NIC (a-CTLA-4+a-PD-1) displayed significant BBB crossing and tumor accumulation (right panel, red). Rhodamine-labelled IgG (a-CTLA-4 or a-PD-1 or their combination) presented low tumor accumulation, mostly inside the stained blood vessels (left and middle, green). No accumulation was recorded in healthy brain. **(c)** Distribution in brain tumor sections. Rhodamine-labelled IgG (a-CTLA-4 or a-PD-1 or their combination) are absent out of the blood vessels (top row, green). NIC (red, arrows) are mostly distributed out of blood vessels and in the tumor parenchyma (bottom row). **(d)** NIC treatments produced

higher doses in the tumor parenchyma than treatments with only IgG. **(e, f, g)** Increased survival of animals bearing intracranial GL261 after treatment with NIC. **(e)** Structures of treatment NIC. **(f)** Schematic depiction of the experimental setup: tumor cells were inoculated intracranially and five intravenous treatments were given at 5 days post-inoculation. **(g)** Kaplan–Meier plot of animal survival after treatment. Treatment with P/a-CTLA-4, P/a-PD-1 and P/a-CTLA-4+P/a-PD-1 significantly increased survival compared with IgG and PBS. Combined treatment of NIC containing tumor vasculature targeting Angiopep-2 (AP-2) as an alternative to TfRMAb (a-TfR antibody) significantly improved animal survival (similar to TfRMAb-mediated BBB delivery) (right graph). Adapted with permission from <sup>789</sup>.

### 2.3. Nano-formulations

Nanoscale particles ranging from 1–100 nm are an attractive option for brain drug delivery owing to their ability to pass through the BBB/BCSFB or to damage the BBB vasculature in a manner that would temporarily facilitate drug permeation <sup>790-792</sup>. Various nanoparticles (NPs) have been considered for brain drug delivery, including polymeric NPs, liposomes, micelles, dendrimers, as well as a variety of inorganic nanomaterials <sup>793</sup>. Following intravenous administration, these NPs might potentially reach the brain by two main routes: unspecific cerebral uptake and adsorptive endocytosis (for untargeted NPs such as liposomal formulations), or RMT (NPs decorated with a brain-targeting ligand) <sup>794-796</sup>.

In comparison to small molecule drugs, proteins generally possess complex three-dimensional structures than can be damaged during formulation, leading to inactivation. For instance, as proteins are generally amphipathic, emulsion methods usually promote their unfolding. Hence, distinct loading procedures are generally required for proteins, such as the addition of additional proteins (e.g., albumin) to minimize the fraction of the protein at the interface and to stabilize it during emulsification <sup>797</sup>. Despite the additional complexities associated with encapsulation procedures and achieving a high loading capacity, much interest has arisen for the development of protein-loaded NPs. The encapsulation of proteins within NPs could provide protection of structure/function/activity, which thereby removes some of the limitations related to the direct injection of native proteins in the blood (immunologic reactions, denaturation, and degradation), and thus improving their pharmacokinetic and pharmacodynamic properties. Many studies have produced protein-loaded NPs and tested their stability, cellular uptake, and function. However, few of these studies have specifically investigated brain delivery <sup>798,799</sup>. Moreover, the hazardous effects that these nanocarriers could have on the brain should be taken into consideration. Indeed, some NPs might induce neuroinflammation, neurotoxicity, and cause damage to the cognitive process <sup>800-802</sup>.

### 2.3.1. Polymeric nanoparticles

NPs prepared with poly(d,l-lactide-co-glycolide) (PLGA) have been studied for sustained and targeted delivery of various drugs <sup>803</sup>, owing to their biocompatibility and GRAS status characteristics <sup>804</sup>. Although it has been shown to be possible to encapsulate small molecules <sup>803</sup>, effective encapsulation of proteins within PLGA NPs remains an active area of research. Additionally, even though PLGA NPs loaded with proteins has garnered attention, to the extent of our knowledge no studies have yet reported their intravenous administration for brain delivery. Indeed, most reports involve the administration of these nanosystems by other, potentially more effective, routes. For example, a fifteen-fold greater brain uptake was observed by intracarotid administration of SOD-loaded PLGA NPs compared to the intravenous route. Furthermore, an improved therapeutic outcome (reduction of brain infarct size and prevention of neuronal death) for these NPs was only observed for intracarotid injection and not for intrajugular or tail vein administration in a rat model of transient ischemic stroke (Figure 7) <sup>805</sup>. Similar improvements have been described by intraperitoneal administration of EPO-loaded PLGA NPs <sup>806</sup>. In all cases above, the observed neuroprotection might possibly be due to sustained protein release from the NPs, which subsequently accumulate in the brain due to ischemia associated BBB impairment.

The possibility of directing NPs to the CNS with cerebral targeting ligands has provided a promising option for intravenous administration. Indeed, several studies have shown that up to 10% of the injected dose of PLGA NPs decorated with a glycopeptide (g7) cross the BBB <sup>803,807-810</sup>. This encouraged the use of g7-NPs for brain delivery of intravenously injected albumin-loaded g7-NPs, as evaluated in two murine models for MPS I and MPS II. In this study, the capacity of g7-NPs to deliver fluorescein isothiocyanate (FITC)-albumin (MW ~67 kDa) was assessed. The NPs crossed the BBB and localized in brain parenchyma, which suggests that g7-NPs are useful for the delivery of macromolecules to the brain <sup>811</sup>. Importantly, even though the localization of g7-NPs was clearly demonstrated in this study, the detection of NPs at the cerebral parenchyma was done by measuring the fluorescence in extracted brains without perfusing the animals. Therefore, the results may not necessarily reflect the presence of NPs only at cerebral level but also within the vascular area, suggesting the necessity of further analysis. Additionally, quantification of the dose reaching the brain relative to that injected was not performed.

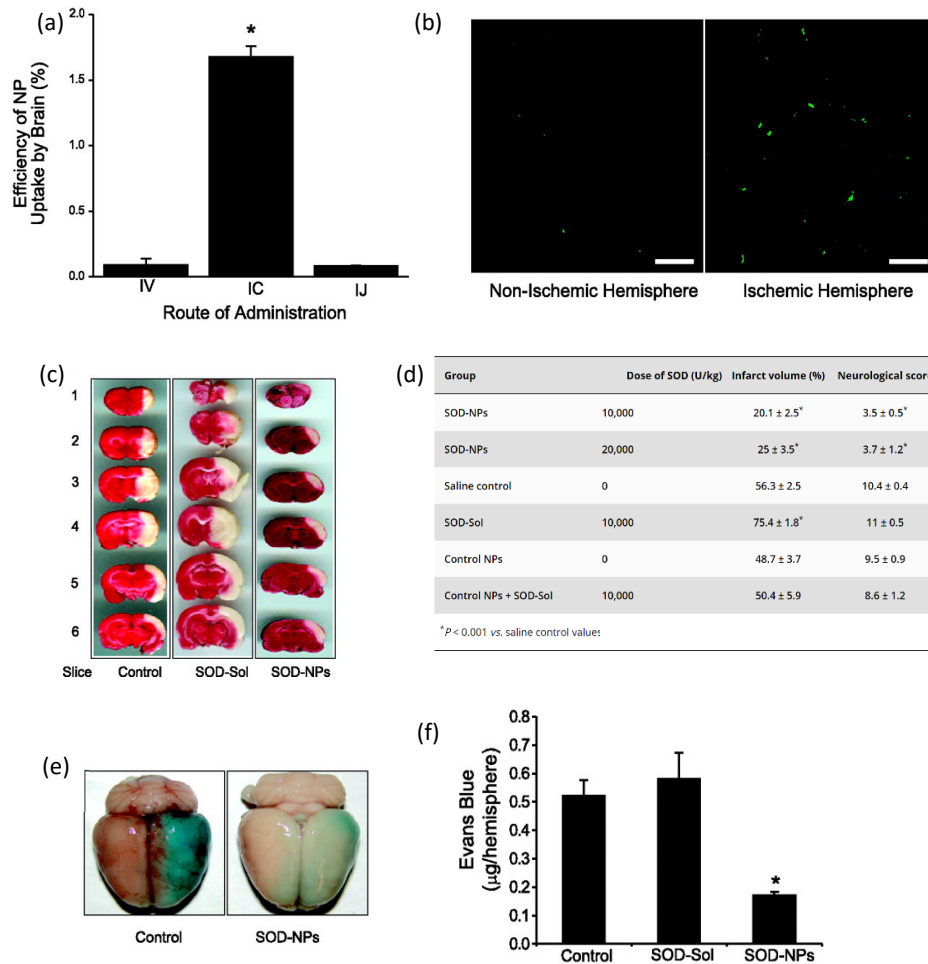


**Figure 7: PLGA NP-mediated delivery of SOD1 to the brain to reduce ischemia-reperfusion injury.** (a) Uptake of NPs by the intravenous (IV), intracarotid (IC), and intrajugular (IJ) routes. (b) Fluorescence photomicrographs of brain sections: ischemic area displayed higher fluorescence from dye-loaded NPs (green) compared to the non-ischemic side. (c, d) Therapeutic efficacy of SOD-NPs in a rat MCAo model after carotid administration: SOD-NPs significantly reduced infarct size and improved functional outcome. (c) Triphenyl tetrazolium chloride (TTC)-stained brain slices from each of the treatment groups. (d) Quantitative infarct volume analysis and neurological score. (e, f) Protection of the BBB in animals treated with SOD-NPs: extravasation of Evans blue from the ischemic hemisphere was lower in the SOD-NPs group compared to the control or native SOD (SOD-Sol) groups. (e) Brain showing Evans blue leakage for SOD-NPs and control groups 6 hours post-reperfusion. (f) Analysis of Evans blue in rats receiving saline, native SOD, or SOD-NPs. Adapted with permission from <sup>805</sup>.

Coating NPs with surfactants, such as the non-ionic surfactant polysorbate 80 (Ps80; Tween 80) can facilitate brain delivery <sup>812</sup>. Despite the potential toxicity of Ps80, PLGA NPs loaded with tissue inhibitor of matrix metalloproteinases 1 (TIMP-1) and coated with Ps80, have been tested. TIMP-1 (MW ~28 kDa), a potent inhibitor of MMPs with strong affinity for MMP-9, has therapeutic interest for the treatment of brain diseases <sup>813</sup>. Ps80-coated PLGA NPs had higher binding/penetration to endothelial cells (compared to un-coated NPs) *in vitro* as well as good biocompatibility. Intravenous injection to mice indicated that TIMP-1-loaded PLGA NPs coated with Ps80 penetrated the brain, as revealed by the His tag signal in brain sections <sup>813</sup>. Of note, the pharmacological effects of the formulation were not evaluated and the control group of uncoated PLGA NPs was lacking in this study. Rather, a comparison was made with a group of mice receiving saline solution. Nevertheless, the brain uptake of Ps80-coated NPs was demonstrated, and two main mechanisms have been hypothesized for this process. The first is the solubilisation of the endothelial cell-membrane lipids by the surfactants resulting in an increase of NP passage through the blood-brain interfaces <sup>814</sup>. Another possible mechanism is the adsorption of plasma proteins, especially Apo E and Apo B on the surface of the Ps80-coated NPs and their subsequent taken-up *via* an LRP1-mediated transcytosis mechanism <sup>815</sup>.

Overall, despite its extensive use for protein delivery, very little pharmacokinetic data is available to demonstrate that PLGA NPs can enhance the delivery of encapsulated proteins to the brain. To date, disadvantages of PLGA nanocarriers include low protein loading due to the hydrophobic matrix of the NPs, initial “burst” release, irreversible protein adsorption, as well protein inactivation during encapsulation <sup>816</sup>. These drawbacks might be attenuated by altering the composition of the polymer or excipients, modifying encapsulation steps, or adjusting the ratio of the lactic to glycolic acid and degree of polymerization <sup>816,817</sup>. For example, a new encapsulation strategy to efficiently load enzymes has recently been developed. More specifically, cross-linked enzyme aggregates were encapsulated into PLGA NPs to promote retention of enzymatic activity (~60%). This approach was validated for different therapeutically relevant enzymes (e.g., palmitoyl protein thioesterase 1 (PPT1), galactosylceramidase (GALC),  $\alpha$ -glucosidase, and  $\beta$ -glucosidase). Importantly, cross-linked enzyme aggregate NPs efficiently delivered PPT1 in cultured neuronal ceroid-lipofuscinosis type 1 primary fibroblasts, with a complete enzyme release occurring in 48 hours <sup>818</sup>. Although this study has shown positive outcomes *in vitro*, *in vivo* studies are required to confirm the ability of these nanoparticles to deliver proteins efficiently.

In 2009, Hasadsri and colleagues designed poly(butyl cyanoacrylate) (PBCA) NPs and demonstrated their ability to deliver proteins into neuronal cell lines <sup>819</sup>. Following this study, surface modification of PBCA NPs with Ps80 promoted crossing of blood-brain interfaces *in*

*vivo*. For example, it has been suggested that brain uptake of NGF adsorbed onto PBCA NPs coated with Ps80 increases upon intravenous injection relative to the native protein. The beneficial effects of this formulation were further assessed in a rat model of acute amnesia induced by scopolamine as well as in a 1-methyl-4-phenyl-1,2,3,6-tetrahydropyridine (MPTP)-induced Parkinsonian syndrome model. In this study, intravenous injection of the NGF-loaded Ps80-coated PBCA NPs successfully reduced PD symptoms in the PD model<sup>820</sup>. Similarly, Lin et al. reported that Ps80-coated PBCA NPs loaded with HRP or enhanced green fluorescent protein (EGFP) can achieve brain accumulation in a rat model of TBI<sup>821</sup>. Interestingly, histological evidence proved that 45 min post-injection, both formulations were hardly detected in the brain of normal rats, and that small amount of EGFP carried by PBCA NPs could be detected at much later timepoints (48 hours after administration). In contrast, at 4 hours post-trauma and with a short circulation time (45 min), the PBCA NPs-loaded HRP or EGFP were widely distributed near injured sites in the TBI rats, though free HRP or EGFP hardly passed through the disrupted blood-brain interfaces. The inability of the formulations to cross the intact physiological barriers of the brain (in parallel to their passage through the damaged blood-brain interfaces) is certainly interesting from a therapeutic point of view as it would prevent the encapsulated proteins from reaching and accumulating in healthy tissues. This would therefore reduce possible undesirable side effects in healthy tissues.

Similarly to the Ps80-coated PLGA NPs, the brain entry mechanism of Ps80-coated PBCA NPs through the blood-brain interfaces after intravenous administration remains unclear and might be related to different phenomena. Firstly, probable damage to blood vessels (occurring in various brain disorders, including TBI) may allow the PBCA NPs to bind to vasculature and transport the associated proteins into the brain<sup>821</sup>. Secondly, the toxic effect on the BBB of the surfactant coated PBCA NPs and the resulting opening of TJs<sup>822</sup>. Thirdly, once in the blood, the surface of the Ps80-coated PBCA NPs becomes further coated with Apo E or Apo B and then taken up through the BBB *via* a RMT<sup>823</sup>. Although no study has yet provided direct proof that Apo E/B are responsible for brain uptake of Ps80-coated PBCA NPs, the pre-coating of these NPs with Apo B or Apo E has generated the best therapeutic effect of the loaded drug. This effect was attenuated in Apo E-deficient mice<sup>823</sup>. Though the adsorption of Apo E on the surface of the NPs appears to increase delivery to the brain, it might further severely affect the targeting yields and direct unfavorable biodistribution (i.e., to the liver for example). For instance, the recently approved ONPATTRO™ made of lipid NPs has been shown to interact with ApoE in the blood and deliver its cargo to hepatocytes<sup>824,825</sup>. Though these studies appear encouraging, quantitative assessment of the amount of NPs present in the brain in terms of the total injected dose is missing. Furthermore, numerous questions regarding the brain transport mechanisms of PBCA NPs, brain delivery and release of proteins, as well as the

toxicity associated with PBCA NPs would need to be thoroughly investigated<sup>826</sup>. In addition to this, cyanoacrylate polymers have yet to be FDA-approved and parenterally administered to humans<sup>21</sup>. Moreover, in addition to these nanocarriers, other types of materials have been used to encapsulate proteins. For instance, pH-sensitive poly(oligo(ethylene glycol) methyl methacrylate)-co-poly(2-(diisopropylamino)ethyl methacrylate) (POEGMA-PDPA) polymersomes modified with Angiopep-2 have been tested as vehicle for the transport of a model protein (IgG). Intravenous injection into mice of Angiopep-2 targeted POEGMA-PDPA loaded-IgG lead to an increased brain accumulation of polymersomes compared to IgG. Interestingly, the antibody was detected inside glia and neurons in the midbrain and hippocampus, suggesting good penetration in brain parenchyma<sup>827</sup>. In another study, a fibrin-targeted NP delivery system was developed for recombinant tissue plasminogen activator (rtPA; the most known treatment for embolic or thrombotic stroke)<sup>828</sup>. rtPA was conjugated to poly(ethylene glycol)-poly( $\epsilon$ -caprolactone) (PEG-PCL) NPs. Subsequent to the development of rtPA-PEG-PCL NPs and their *in vitro* characterization, the pharmacokinetics and pharmacodynamics were evaluated in healthy and MCAo rats. The results showed that the pharmacokinetics of rtPA conjugated to PEG-PCL NPs (having a diameter of ~129 nm) was significantly improved in comparison to free rtPA. For instance, after intravenous injection of rtPA-NPs, the nanocarriers exhibited a half-life 18 times longer than that of free rtPA (~5 min). Interestingly, the initial distribution phase,  $t_{1/2\alpha}$ , was ~3 min, indicating rtPA-NPs were rapidly distributed to blood circulation after administration. Importantly, injection of free rtPA (1 mg/kg) at 2 hours post-MCAo did not significantly reduce infarct size compared to controls. However, rtPA-NPs treatment (20 mg/kg equivalent to 1mg/kg conjugated rtPA) reduced infarct size to one third of the controls. Better functional outcomes were thus observed in the rtPA-NPs group. Overall, as mentioned for the PLGA and PBCA NPs, quantification of the brain uptake (in terms of % of injected dose/g) is not available in the above-cited studies, making the comparison of the performance of each type of polymeric NPs difficult.

### **2.3.2. Carbon nanospheres**

Carbon nanospheres are emerging carbon-rich nanoparticles (size range between 50 nm and 1  $\mu$ m) that are generally produced by the decomposition of precursor molecules by hydrothermal synthesis<sup>829</sup>. Depending on the precursors chosen, carbon nanospheres are generally colloidally stable in water and exhibit fluorescence properties. SMAR1 (Scaffold/Matrix Attachment region 1) is a 60 kDa protein reported to be a transcriptional regulator<sup>830,831</sup>. The C-terminal 350–548 amino acid region is characterized as a DNA binding domain (DBD)<sup>832</sup>, and displays an anti-inflammatory function<sup>830</sup>. SMAR1 DBD was conjugated with hydrothermally synthesized carbon nanospheres (spherical forms and exposing carboxylic acid and hydroxyl groups on their surface), and intravenously injected to EAE

induced conditional SMAR1<sup>-/-</sup> mice. Conjugation of SMAR1 to carbon nanospheres significantly decreased the production of IL-17 and demyelination reduction. They thus contributed a significant biological effect in combating the Th17 mediated EAE disease progression<sup>830</sup>. Although the carbon nanospheres were not targeted to the brain and instead delivered SMAR1 DBD inside the T-cells, their effects on reversing the progression of MS-like manifestations in mice were clearly demonstrated in this study. To our knowledge, no other study has used these nanospheres to treat neuronal diseases.

### 2.3.3. Liposomes

Liposomes are small spherical vesicles that are formed by an aqueous core encapsulated by one or multiple concentric lipid bilayers. They are sometimes made with cholesterol or combinations of different natural or synthetic lipids<sup>833-835</sup>. While the investigation of liposomes as drug carriers has attracted substantial attention<sup>836</sup>, their use as brain delivery systems for proteins remains limited. The first *in vivo* experiments showing that liposomes can promote accumulation of proteins in the brain after intravenous administration probably date back to 1980, with the encapsulation of thyrotropin releasing hormone (TRH) in neutral (phosphatidylcholine, cholesterol), cationic (phosphatidylcholine, cholesterol, and stearylamine), or anionic (phosphatidylcholine, cholesterol, phosphatidylserine) liposomes<sup>837</sup>. TRH loaded into cationic and neutral liposomes had greater brain uptake (i.e., the brain uptake of liposome-transported TRH was 0.27% (cationic) and 0.32% (neutral) of the dose injected at 3 hours post-injection) and physiological effect (increase in body temperature) than TRH in anionic liposomes. However, epileptic seizures and cerebral tissue necrosis were observed due to stearylamine<sup>837</sup>. Three years later, the encapsulation of a model protein,  $\beta$ -GAL, in anionic liposomes was carried-out. This study demonstrated that after injection into the tail vein of rats, liposomes containing  $\beta$ -GAL were predominantly taken up by the liver, spleen, and lungs but could also cross the BBB more effectively than the free enzyme<sup>838</sup>. The cationic liposomes were also used to deliver an antioxidant enzyme, SOD1, to the brain. Globally, the results showed a reduced cerebral infarct volume size in ischemic stroke and TBI animal models upon intravenous injection of liposomes entrapped SOD1<sup>839,840</sup>. In a different study, the passive tumor targeting property of PEGylated liposomes loaded with two anti-cancer drugs (tumor necrosis factor-related apoptosis-inducing ligand (TRAIL) (MW ~32 kDa) and doxorubicin) were exploited. While previous reports indicated that the enhanced permeability and retention (EPR) effect of brain tumors is weak compared with peripheral tumors,<sup>841</sup> the synchronous systemic administration of these latter liposomes caused a significant suppression of tumor growth of human U87MG xenografts and a prolonged median survival time of brain tumor-bearing mice from 32 to 48 days<sup>842</sup>. To increase accumulation in the brain,

liposomes bearing targeting ligands toward the transporters/receptors expressed on the BBB/BCSFB were used and resulted in higher transcytosis across these blood-brain interfaces. Intravenously administered PEGylated liposomes functionalized with RMP-7, a ligand to the B2 receptor on brain endothelial cells, efficiently carried NGF to the brain (i.e., the average concentration in the brain was ~10 times more than that of free NGF)<sup>843</sup>. Moreover, glutathione (a tripeptide actively transported across the BBB)-targeted PEGylated liposomes delivered  $\beta$ -amyloid targeting antibody fragments to the brain of AD mice<sup>844</sup>. In this study, two different formulations of liposomes based on 1,2-dimyristoyl-sn-glycero-3-phosphocholine (DMPC) and egg-yolk phosphatidylcholine (EYPC) were tested. Both formulations encapsulated  $\beta$ -amyloid binding llama single domain antibody fragments (VHH-pa2H). Radiolabelled liposomes were administered intravenously to APP<sup>swe</sup>/PS1dE9 double transgenic mice, a mouse model of AD, as well as wild-type control mice. In comparison to free VHH-pa2H, both DMPC and EYPC loaded-liposomes significantly increased the uptake of VHH-pa2H, with the EYPC loaded-liposomes yielding the highest brain exposure in transgenic animals (i.e., 24 hours after injection, the brain uptake of VHH-pa2H, DMPC, and EYPC loaded-liposomes was ~0.001%, ~0.008%, and ~0.165% of the injected dose/g, respectively). Importantly, the brain distribution in transgenic mice was 2-fold higher than that in the brain of wild-type mice (~0.026% *versus* ~0.165% of the injected dose/g for EYPC loaded-liposomes at 24 hours post-administration), demonstrating that the system could deliver single domain antibody fragments to brains with AD-like pathology<sup>844</sup>.

Liposomes might represent biodegradable/biocompatible NPs that offer brain delivery and protection of encapsulated proteins. Nevertheless, their practical use has been hindered by toxicity issues and many questions regarding their properties need to be addressed. First, such as for many nanoparticulate systems, the mechanism behind the improved brain delivery of protein-loaded liposomes remains unclear. It was suggested that liposomes could interact with the membranes of brain endothelial cells<sup>837</sup>, and that adsorptive-mediated endocytosis could be promoted by electrostatic interactions<sup>845</sup>. Second, poor stability and the potential *in vivo* toxicity limit their systemic applicability to some extent, especially for cationic liposomes<sup>846,847</sup>.

Although PEGylation reduces the immunogenicity of liposomes, this approach also reduces interactions between the liposomes and the brain endothelium, which could hinder delivery to the brain<sup>21</sup>. To improve this, further modification with brain-specific targeting ligands has been tried. While, surface-functionalization approaches improved, at least in part, the distribution of protein-loaded liposomes into the brain, the majority, if not all, of the animal studies have not reported or measured a beneficial effect. Additionally, aside from the therapeutic effect, quantification of liposomes that across the blood-brain interfaces is sometimes lacking.

Moreover, the comparison of different types of nanosystems has not yet been a subject of study and therefore investigations need to be performed. For instance, the efficiency of PLGA, PBCA, or liposomes loaded with SOD and targeted with anti-NMDA (N-methyl-D-aspartate) receptor 1 antibody was assessed in a mouse model of ischemia and reperfusion injury<sup>848</sup>. The intracarotid administration of nanocarriers at 25 U of SOD activity per injection, showed a 50% to 60% reduction in infarct size, a reduction in inflammatory markers, and improved behaviors with no difference between the diverse formulations. In addition, as expected, these ameliorations were superior to those related to untargeted nanocarriers and nanocarriers conjugated to a nonspecific IgG. Although no difference in the biological effects was reported for the nanosystems tested, the SOD loading of the PLGA NPs was significantly higher than that of liposomes and PBCA NPs (SOD activity of >4,000 U/mL *versus* <2000 U/mL). However, while the loading yield of the PLGA NPs was higher, its 'current' activity was much lower (~150 to 200 U/mL), as only a small fraction of SOD was available on the surface of PLGA NPs.

#### **2.3.4. Polymeric micelles**

Polymeric micelles are self-assembled colloids of amphiphilic copolymers in an aqueous solvent, that have a hydrophobic core and a hydrophilic corona structure. Few studies have explored protein delivery to the brain using such micelles. Poloxamers are poly(ethylene oxide)-poly(propylene oxide) (PEO-PPO) block copolymers, characterized by an amphiphilicity and self-assembly properties in aqueous solution. The most investigated poloxamers for brain delivery are pluronics, which have a triblock PEO-PPO-PEO structure. Pluronic molecules self-associate in aqueous solution above a given temperature and concentration to form spherical micelles with PPO cores and PEO coronas<sup>777,849</sup>. Mixed micelles composed of pluronic F127 and D- $\alpha$ -tocopheryl PEG succinate (TPGS) were shown to improve the delivery of  $\beta$ -GAL to the brain. In contrast, intravenous administration of free  $\beta$ -GAL did not show any detectable enzymatic activity in the brain<sup>850</sup>. However, no quantification data regarding the % of the brain uptake was provided in this study. Moreover, chitosan-conjugated pluronic F127-based nanocarriers decorated with a brain targeting peptide (rabies virus glycoprotein (RVG29)) were produced. *In vivo* brain accumulation of these nanocarriers following intravenous injection to mice was monitored optically. Results showed that F127-based nanocarriers conjugated to both chitosan and RVG29 accumulated in brain tissue and were significantly better (~3 times greater) than F127 nanocarriers only conjugated to RVG29.  $\beta$ -GAL, spontaneously loaded inside these nanocarriers, maintained its bioactivity, and displayed a high and prolonged brain enzyme activity with RVG29-chitosan-functionalized F127-based nanocarriers (~25% of injection dose/g after 48 hours post-injection)<sup>851</sup>. Although reports demonstrating that mixed micelles/pluronic-based nanocarriers show promise for brain

targeting, these were not necessarily followed by other studies, probably because of the instability and formation of aggregates of pluronic micelles <sup>852</sup>.

### 2.3.5. “Nanozymes” and other nanocarriers

Polyion complex micelles, formed by coacervation of two hydrophilic block copolymers of opposite charge, have been investigated as a class of nanocarriers for the delivery of charged proteins <sup>853,854</sup>. Indeed, the incorporation (under physiological conditions) of positively charged (trypsin, lysozyme) or negatively charged (SOD1, catalase) proteins into a polyion complexes with anionic (PEG-poly(aspartic acid) (PEG-PAA) or cationic (PEG-polyethyleneimine (PEG-PEI) or PEG-poly(L-lysine) (PEG-PLL)) copolymers was reported <sup>853,855-857</sup>, and such complexes form a core-shell type NPs with a polyion complex core and an outer shell of PEG. Polyion complex micelles encapsulating antioxidant enzymes, SOD1 and catalase (so-called nanozymes) were developed. Catalase, incorporated in a block ionomer complex with a cationic block copolymer (PEG-PEI), generated self-assembled complexes (~60–100 nm) that retained antioxidant activity. Intravenous administration of the nanozyme to MPTP mice showed that some labelled catalase was found in the brain (~0.3% of the injected dose). The authors proposed an uptake mechanism involving circulating monocytes, which then carry the enzyme to the brain. In order to confirm this hypothesis, they showed that after injection of adoptively transferred nanozyme-loaded bone-marrow-derived macrophage, the amount found in the brain was doubled <sup>855</sup>. Although these results are interesting, it might be worth considering that uptake did not just increase in the brain but also in other tissues (liver, spleen, kidney, and lung). Furthermore, additional experiments are necessary to examine the neuroprotective effects in PD models. Cross-linked nanozymes containing SOD1 were evaluated in healthy and ischemic animals <sup>856,858</sup>. These nanocarriers were assembled by mixing cationic block copolymers and SOD1 and cross-linking to stabilize the complex. Intravenous injection to mice demonstrated that cross-linked nanozymes exhibited improved stability in both blood and brain as well as an increased brain uptake (1.7- and 10-fold increase to serum ratios in brain parenchyma and brain capillaries, respectively), as compared to native SOD1 and non-cross-linked nanozymes <sup>856</sup>. The rise in brain delivery translated into improved therapeutic efficacy in a transient MCAo rat model. A single intravenous dose of the cross-linked nanozymes resulted in a 59% reduction of the infarct volume and improved sensorimotor outcomes (significant 70% enhancement in the functional performances) compared to vehicle and native SOD1 groups (Figure 8) <sup>858</sup>. In addition to the incorporation of antioxidant enzymes, butyrylcholinesterase was packaged into cross-linked polyion complex micelles (formed by cationic PLL-graft-PEO (PLL-g-PEO)) and delivered to the brain of a butyrylcholinesterase<sup>-/-</sup> mouse model (i.e., 23 hours post-intramuscular injection, butyrylcholinesterase levels in the

brain homogenates of mice treated with the complexes were ~2.5 times higher than those of animals treated with the free enzyme). In this study, the delivery of butyrylcholinesterase appeared to be more efficient with an intramuscular injection in comparison to an intravenous one<sup>859</sup>. The authors suggested that the intramuscular administration allows the brain delivery *via* neuromuscular junctions by retrograde transport. The studies above suggest that nanozymes might be interesting nanocarriers for proteins in terms of loading efficiency and preservation of the enzyme activity.

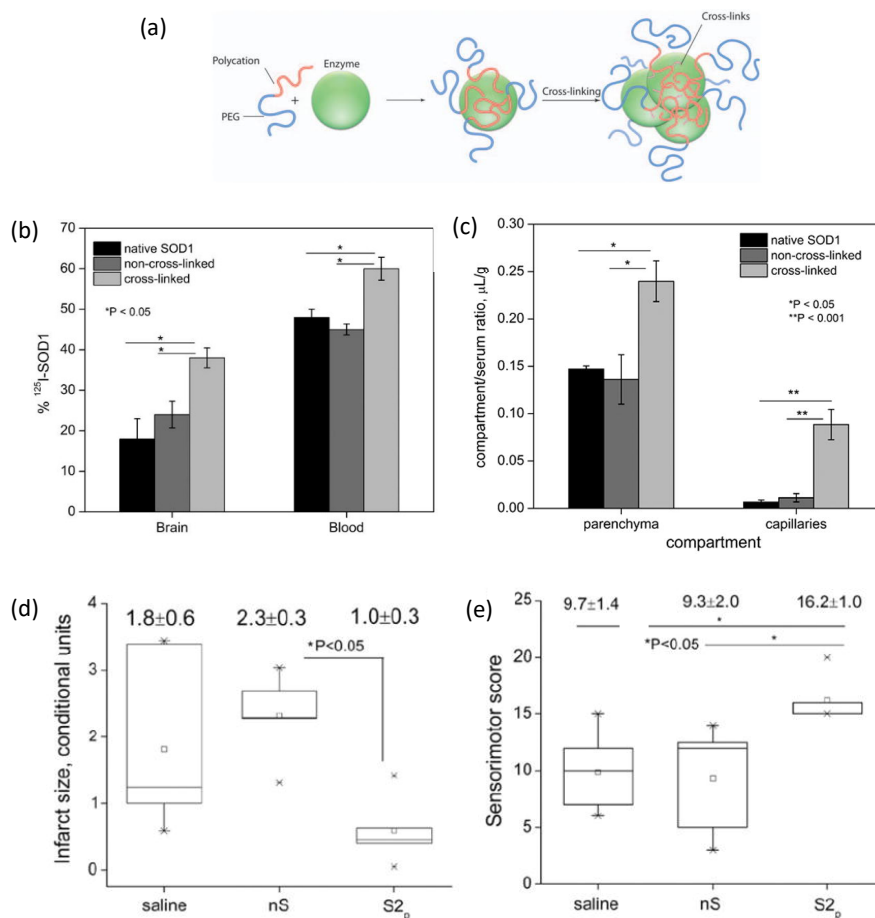


**Figure 8: Cross-linked SOD1 nanozymes with increased stability, brain uptake, and efficacy for treatment of ischemic stroke. (a)** Illustration of nanozymes, which form in aqueous solution due to electrostatic coupling of SOD1 and cationic block copolymer. Cross-linker (EDC/S-NHS) was added to pre-formed complexes to produce cross-linked nanozymes. **(b)** *In vivo* stability of native SOD1 and nanozyme formulations at 1-hour post-intravenous injection: cross-linked nanozymes displayed the highest stability in blood and brain. **(c)** Brain delivery of native SOD1 and nanozyme formulations at 1-hour post-intravenous injection: cross-linked nanozymes exhibited an increased brain uptake. **(d, e)** Therapeutic efficacy in MCAo rat model at 22 hours after reperfusion: native SOD1 (nS) and cross-linked nanozymes (S2<sub>p</sub>) were intravenously administered at the onset of reperfusion

(2 hours post-occlusion): S2p generated a significant reduction of the infarct volume **(d)** and an improvement of the functional outcomes **(e)**. Adapted with permission from <sup>858</sup>.

Recently, functionalized layered double hydroxide NPs were used to deliver bovine serum albumin (BSA) to the brain <sup>860</sup>. Layered double hydroxides possess a structure based on brucite-like layers and their interlayer spaces are electrostatically filled and form a lamellar structure <sup>861</sup>. Thus, layered double hydroxide NPs provide high chemical versatility, anionic exchange properties, and the ability to intercalate a large amount of charged biological molecules. In this study, coating of BSA and cross-linking with glutaraldehyde was used to achieve colloidal stability and to avoid aggregation in serum or blood. Moreover, subsequent ligand functionalization with Angiopep-2 and RVG29 was explored to increase the brain delivery. After intravenous administration, BSA-loaded NPs accumulated in the brain of mice. Indeed, 2 and 48 hours post injection, Angiopep-2 functionalized NPs displayed a significantly higher brain accumulation than un-functionalized NPs and NPs decorated with RVG29 (e.g., at 2 hours after injection, the fluorescence signal in the brain for BSA-NPs-Angiopep-2 was ~75% higher than BSA-NPs and BSA-NPs-RVG29). Interestingly, the efficient brain targeting of Angiopep-2 decorated NPs (in comparison to RVG29) was in good agreement with *in vivo* confocal neuroimaging observation where BSA-NPs-Angiopep-2 was retained much longer in the blood-retina barrier area compared to BSA-NPs-RVG29 and to control BSA-NPs <sup>860</sup>. The authors suggest that the increase in retention time assessed in the blood-retina barrier (virtually identical to the BBB) reflects indirectly the accumulation to the BBB. Indeed, the blood-retina barrier is genetically derived from the CNS and the retinal epithelial cells express Angiopep-2/RVG ligand receptors.

Magnetic nanocarriers coated with different biocompatible matrices have been also used to deliver proteins such as rtPA for the treatment of stroke <sup>862,863</sup>. However, issues with limited protein loading as well as toxicity occurring when some magnetic nanoparticles are degraded might be the reasons of their limited use <sup>864,865</sup>. The potential toxicity problems might be limited by targeting the NPs using a magnetic field, which would lead to reduced doses <sup>864</sup>. Nevertheless, additional studies are required to validate the safety of such nanocarriers.

Finally, we should mention that the “dual targeting delivery” strategy is gaining increasing importance for improving intra-brain selectivity of brain delivery nanosystems <sup>866,867</sup>. This approach, also termed “cascade targeting delivery”, was designed to allow the sequential penetration of NPs-loaded drugs through the BBB and then to the specific targeted diseased cells in the brain. However, to the best of our knowledge, this strategy has not yet been applied to NPs delivering protein therapeutics.

## 2.4. Protein modifications

As reported previously, intrinsic physicochemical (molecular instabilities) and inherently poor pharmacological properties (adverse pharmacodynamic responses and limited pharmacokinetic profiles) greatly limit the delivery of proteins to the brain *via* non-invasive routes. In order to alter these properties and consequently increase the brain accumulation of therapeutic proteins, various chemical and biochemical methods have been investigated.

### 2.4.1. Glycosylation/glycation

Glycosylation typically corresponds to the modification of proteins with carbohydrate-based molecules (glycans). The impact of glycosylation on protein pharmacokinetics can be ascribed to the discovery of the hepatic asialoglycoprotein receptor by the Ashwell group<sup>868-871</sup>. Indeed, a pronounced difference between circulatory half-life of natively glycosylated protein with sialic acid terminated glycans (~56 hours) and a partially de-glycosylated variant (galactose terminated glycans) was observed (< 30 minutes)<sup>872</sup>.

Subsequent studies extended the generality of these observations<sup>873,874</sup>, and nowadays it is well known that glycosylation improves the solubility and stability of proteins in addition to improving their *in vivo* bioavailability (by reducing immunogenicity and proteolytic degradation)<sup>875-878</sup>. For example, proteolytic stabilization of numerous therapeutically relevant glycosylated proteins has been demonstrated, with examples including human hematopoietic cytokine granulocyte colony stimulating factor (G-CSF)<sup>879,880</sup>, human protein C<sup>881</sup>, ranpirnase<sup>882</sup>, thyroid-stimulating hormone<sup>883</sup>, human IFN- $\gamma$ <sup>884</sup>, and various IgG-like antibodies<sup>885</sup>. These effects have been attributed to type, number, length, and branching of glycans bound to the protein surface as well as the charge of their terminal end glycans<sup>875,886</sup>. For example, it has been demonstrated that sialic acid increases of the circulating lifetime of proteins<sup>887</sup>. In contrast, glycosylated proteins exposing terminal galactose, mannose, N-acetyl-glucosamine, or fucose can be rapidly removed from circulation through interaction with specific receptors, and targeting to certain organs might be possible by modifying the glycosylation patterns of proteins<sup>888-891</sup>. While glycosylation appears to be an effective strategy to improve brain delivery of therapeutic peptides (i.e., mainly by increasing the circulation life-time)<sup>892,893</sup>, its use for proteins remains limited. To our knowledge, the only reports showing that glycation of proteins can increase their distribution in the CNS are those by Poduslo et al. where increased permeability across blood-brain interfaces (BBB and blood-nerve barrier) of human plasma albumin, NGF, and human IgG after glycation with D-glucose was demonstrated<sup>894,895</sup>. The permeability of these glycated proteins at blood-brain interfaces after intravenous administration was assessed by calculating the permeability coefficient multiplied by surface area. The permeability surface area-product is a reliable pharmacokinetic measure of brain

entry that measures the permeability of the blood-brain interfaces to contrast material. It is expressed in the equation:  $PS = q(T) / \int_0^T C_p dt$ , where  $T$  is the circulation time,  $q(T)$  is the extravascular  $^{125}\text{I}$  activity in endoneurium/endothelium at time  $T$ , and  $\int_0^T C_p dt$  is the plasma concentration time integral of  $^{125}\text{I}$ -labeled protein. The unit for  $PS$  is  $\text{ml}\cdot\text{g}^{-1}\cdot\text{s}^{-1}$ . For instance, the permeability coefficient–surface area of glycosylated NGF across the blood-nerve barrier significantly increased compared to native NGF, and a similar rise was described for the BBB<sup>895</sup>. The authors postulated that since glycosylation did not affect the proteins' activities, systemic administration of glycosylated proteins might be an efficient approach to deliver therapeutics into the CNS and peripheral nervous system for the treatment of a variety of neurological diseases. However, there was no follow-up for these studies.

The chemical modification of the exposed carbohydrates on a glycoprotein, human GUSB, has been explored to inactivate carbohydrate-dependent receptor-mediated uptake (by galactose receptor, mannose 6-phosphate receptor, and mannose receptor) and subsequently improve its pharmacokinetic and pharmacodynamic parameters<sup>891,896,897</sup>. In this study, the terminal sugars were chemically inactivated by treatment with sodium metaperiodate and borohydride (to prevent aggregation resulting from cross-linking). In cultured cells, chemical modification of human GUSB eliminated uptake by mannose 6-phosphate and mannose receptors. Moreover, when intravenously administered to mice, the plasma clearance of the modified enzyme dramatically slowed from a *half-life* of <10 min to ~18 hours. Interestingly, modified GUSB infused weekly for 12 weeks was more effective in clearing CNS storage than native GUSB in an MPS VII mouse model<sup>898</sup>. This effect resulted from an altered biodistribution of GUSB following its modification. Indeed, the brain exposure of modified GUSB was ~5 times higher than that of native GUSB. In contrast, modified GUSB levels were ~4-fold lower in liver and spleen, which are rich in mannose 6-phosphate (hepatocytes) and mannose receptors (Kupffer cells and macrophages). The authors proposed that the decrease in uptake by the liver and spleen displayed by modified GUSB is probably due to reduced elimination by these abundant carbohydrate receptors. Of note, in addition to increased brain uptake, modified GUSB reached other tissues (namely the heart, kidney, muscle, lung, and eye) better than native GUSB, suggesting that the uptake of modified GUSB is a non-specific process.

The relevance of this approach was further demonstrated for other enzymes<sup>899,900</sup>. All these studies provide evidence that long-circulating enzymes, modified to escape carbohydrate-mediated clearance, may present therapeutic opportunities for some brain diseases. Overall, glycosylation appears to improve the efficacy of protein therapeutics *in vivo*, and this strategy appears safe as many of the glycol-groups and oligosaccharides (such as polysialic acid) are ubiquitously expressed throughout the body and are easily broken down<sup>901,902</sup>. Nevertheless,

precautions should be taken to ensure the preservation of the biological properties of the protein and avoid potential immune reactions <sup>903</sup>. Furthermore, the off-target effects of these proteins especially when they are systematically administered should be considered.

#### 2.4.2. Acylation

Acylation corresponds to the covalent attachment of fatty acids to proteins. Acylation of proteins with fatty acids (e.g., stearate or palmitate) enhanced cellular uptake in vitro <sup>904</sup>. Hydrophobically-modified proteins can remain water-soluble, but are better able to anchor to mammalian cells *via* their lipid moieties, which can help hydrophilic molecules to enter the cell <sup>905</sup>. The first studies investigating the effects of acylation on brain accumulation concerned the modification of Fab antibody fragments against gliofibrillar acid protein (GFA) and brain-specific  $\alpha$ 2-glycoprotein ( $\alpha$ 2-GP) with stearate moieties <sup>906,907</sup>. Intracarotid injection of modified Fab fragments resulted in an increased accumulation in rat brains. Moreover, trifluoperazine (a neuroleptic drug) conjugated with stearylated Fab fragments targeting neurospecific antigens exhibited a high brain accumulation and neuroleptic activity. Interestingly, in this study, Fab of nonspecific antibodies accumulated in the liver rather than in the brain when modified with fatty acids ( $\sim$ 0.37% *versus*  $<$ 0.01% of introduced label/g at 3 hours post-injection), while stearate-modified Fab of brain-specific antibodies displayed preferential accumulation in the brain ( $\sim$ 0.45% *versus*  $\sim$ 0.07% of introduced label/g at 3 hours post-injection). The authors suggested that the accumulation of nonspecific stearylated conjugates in the liver was due to the presence of large amount of fatty acid binding proteins in this tissue. In contrast, the effective accumulation of the specific fatty acid modified conjugates in the brain could be explained by the presence of both the hydrophobic anchor and the antigen recognizing site (the brain-specific Fab fragments). Therefore, stearyl residues provided an enhancement of the conjugate binding to the cerebral endothelium, which in turn increased the apparent binding constant of the Fab fragment <sup>908</sup>. Subsequently, point modification of a BBB-impermeable protein HRP with lipophilic (stearyl) moieties slightly enhanced the transport and the accumulation in the brain (the maximum brain exposure was  $\sim$ 0.17% (at 1-hour post-injection) and  $\sim$ 0.1% (at 2 hours post-injection) of injected dose/g for of HRP and stearylated HRP, respectively) following intravenous administration. Importantly, modification of HRP significantly decreased its catalytic activity (i.e., stearylated HRP retained only 50% of the original activity), but this activity was preserved after the passage across the BBB <sup>779</sup>.

The increase in brain penetration of stearylated proteins might be explained by the enhancement of their binding to cerebral endothelial cell membranes through hydrophobic interactions <sup>909</sup>, or to transporter-mediated uptake for proteins modified with essential fatty acids. For instance, linoleic acid reaches the brain by an essential fatty acid transporter

positioned (mainly) on the abluminal membrane of microvascular endothelial cells <sup>910,911</sup>. Similar to glycosylation, the field of protein acylation has not experienced a considerable expansion, possibly because of the non-selective organ uptake and the intracellular sequestration of acylated proteins. Additionally, the intravenous injection of acylated proteins could confront them to the physiological protein degradation/elimination mechanisms (proteolysis, induction of the immune system, etc.).

### 2.4.3. Cationization

The simplest way to chemically cationize a protein is by amidation (mainly carbodiimide-mediated) of its carboxylic acid groups (glutamic and aspartic acid side chain groups and C-terminal acid) with diamines or polyamines <sup>912</sup>. These positively-charged amines might be natural (e.g., putrescine (PUT), spermidine (SPD), and spermine (SPM)) or synthetic (e.g., hexamethylenediamine (HMD)). The extent of cationization mainly depends on the protein's sequence and conformation and might be tailored as required <sup>92,912</sup>. Additionally, amidation can be limited by adjusting solution pH to control the level of protonation of the carboxyl groups <sup>913</sup>. If necessary, radiolabeled polyamines could be used to quantitatively determine the extent of cationization of the protein <sup>912,914</sup>. It has been suggested that cationization increases the brain delivery of proteins by promoting their interaction with cerebral endothelial/epithelial cells and their transcytosis across blood-brain interfaces. However, the precise mechanisms involved remain unknown as permeability did not directly correlate polyamine charge <sup>95,915</sup>. In contrast, permeability decreased with the number of positively charged amino groups on the polyamines (PUT>SPD>SPM), suggesting a probable implication of polyamine transporters for the polyamine-modified proteins <sup>95</sup>. This mechanism is also supported by the results showing that the uptake of cationized proteins in the brain was a saturable process <sup>916,917</sup>.

Various therapeutic proteins have been cationized in order to enhance the brain delivery in healthy as well as diseased animals (e.g., amyotrophic lateral sclerosis, AD, and ischemia models). Most of them showed successful brain delivery and sometimes a better therapeutic effect following intravenous administration. Among these proteins are (1) anti-*ras* oncogene <sup>92</sup>, anti-EGF receptor, and anti-tenascin-antibodies (by HMD cationization) <sup>92</sup>, (2) anti- $\beta$ -amyloid antibodies<sup>918,919</sup>, NGF <sup>920</sup>, SOD <sup>921</sup>, and catalase (by PUT cationization) <sup>922-924</sup>, (3) SOD and NGF (by SPD and SPM cationization) <sup>95</sup>. In an early study, the modification of albumin (isoelectric point of 4) with HMD was conducted. The resulting cationized albumin (isoelectric point >8) was conjugated to  $\beta$ -endorphin and injected to the rat carotid. Autoradiography data showed that  $\beta$ -endorphin-cationized albumin chimeric peptide (isoelectric point >9) successfully crossed the capillaries and distributed in the brain

parenchyma, contrarily to native  $\beta$ -endorphin that showed a negligible BBB uptake <sup>916,925</sup>. Two years later, the same team explored the possibility of enhancing IgG (isoelectric point from 5–6) delivery through the BBB by cationization with HMD. An increase in brain uptake was also observed for cationized IgG (isoelectric point 10.5) <sup>917</sup>. Subsequently, the ability to reach the nervous system of a variety of cationized proteins (albumin, SOD, insulin, IgG) intravenously injected was demonstrated <sup>95</sup>. In this study, the permeability at blood-brain interfaces of these proteins modified with PUT, SPD, and SPM was determined by calculating the permeability coefficient–surface area in rats <sup>95</sup>. Essentially, results showed that the permeability coefficient–surface area values at the BBB and at the blood-nerve barrier increased for all cationized proteins when compared to their native forms. For example, for PUT-IgG the increase ranged from ~111 to ~349-fold for nerve and different brain regions compared with native IgG. In a similar manner, when compared to native SOD, PUT-SOD showed ~21-fold increase in permeability coefficient–surface area at the blood-nerve barrier and >17.6-fold enhancement at the BBB of different brain regions <sup>95</sup>. Of note, no activity test was performed for these proteins in this report. Consequently, the relationship between the brain permeability, the enzymatic activity of cationized SOD, and the pH of the modification reaction was examined. Indeed, PUT increased the permeability of SOD 4-fold when the reaction was conducted at pH 6.7 (80% residual activity), while permeability increased 22-fold for a reaction conducted at pH 4.7 (less than 5% residual activity) <sup>915</sup>. Although these results are specific for SOD, measurement of enzymatic activity and optimization of the pH of the reaction should be considered for amidation reactions involving biologically active proteins. Some therapeutic effects of cationized SOD in a global cerebral ischemia rat model were reported. For example, intravenous administration (twice daily for 3 days) of a PUT-modified SOD, with increased BBB permeability and preserved enzymatic activity resulted in neuroprotective effects in the hippocampus. In contrast, saline and inactive PUT-modified SOD-injected animals did not show significant neuroprotective effects when compared to sham rats <sup>921</sup>.

Taken together, cationization can significantly increase the net cationic charge of proteins, allowing their promote brain delivery without having to rely on a cationic import carrier. Moreover, natural polyamines are ubiquitously present in mammalian cells, which reduces the risk of toxicity <sup>926</sup>. Some authors claim that the increased brain uptake observed for cationized proteins is not related to BBB breakdown, suggesting that their penetration into the brain should be efficient even if blood-brain interfaces are altered during neuronal diseases <sup>917</sup>. Despite these benefits, cationization has some disadvantages. Firstly, cationized proteins strongly interact with other proteins and cell membranes (negatively charged), which might induce clearance and toxicity. Indeed, cationized proteins are generally rapidly cleared from

the blood. For example, when albumin, insulin, and IgG were modified by natural polyamines their serum half-life time decreased dramatically (e.g., from  $30.2 \pm 5.8$  to  $0.9 \pm 0.1$  min for IgG and PUT-IgG)<sup>95</sup>. This decrease could counterbalance improved BBB permeability and reduce brain accumulation of cationized proteins. Moreover, concerns about the potential toxicity of cationized proteins exist. For example, while low doses of cationized IgG appeared to be safe<sup>917</sup>, considerable toxicities (immune complex formation in the choroid plexus of rats, membranous nephropathy in rabbits) were described after injecting therapeutic doses to rabbits<sup>927,928</sup>. Similarly, administration of a high dose of protamine increased cerebral and peripheral vascular alteration/penetrability<sup>929-931</sup>. Therefore, these aforementioned factors might limit the clinical development of this strategy for the brain delivery of therapeutically relevant proteins.

## **2.5. Acting on the blood: sink or scavenging mechanisms**

As seen in the previous sections, many considerations should be taken when designing a brain delivery system because of the presence of highly restrictive barriers. It has been reported that close to 100 % of large pharmaceutical molecules (including proteins) were unable to enter the CNS<sup>264</sup>. In order to circumvent blood-brain interfaces, other strategies have been developed. These alternative treatment modalities consist in the systemic administration of proteins acting in the periphery (blood) and affecting the CNS through a mechanism called “sink or scavenging effect”. In the next section, strategies to promote the brain clearance of toxic molecules that accumulate during neuronal diseases will be described.

The pathological emblem of AD is the accumulation of A $\beta$  plaques and neurofibrillary tangles<sup>932</sup>. The neurotoxic accretion of A $\beta$  and hyperphosphorylated tau has been hypothesized to result from an alteration of the clearance mechanisms in the aged and damaged brain<sup>933,934</sup>. Apart from local cellular uptake and enzymatic degradation, soluble A $\beta$  might be removed from the brain by various mechanisms, such as transport across blood-brain interfaces (BBB and BCSFB), absorption into the blood and lymphatic systems by CSF, and interstitial fluid bulk flow (mainly in the peri-vascular space)<sup>636,933,935-937</sup>. However, the relative contribution of these systems to A $\beta$  clearance remains unknown. The rapid transport of exogenous A $\beta$  between the CNS and plasma has been clearly demonstrated<sup>636,937,938</sup>. For example, after intracerebral injection in mice, radiolabeled A $\beta_{1-40}$  was rapidly removed from the brain (half-life  $\leq 25$  minutes), mainly by transport across the BBB/BCSF<sup>636,938</sup>. This A $\beta$  clearance mechanism has been explored through systemic injection of anti-A $\beta$  antibodies. These antibodies bind soluble A $\beta$  in the blood circulation and thus promote A $\beta$  efflux from the brain to the blood, a so-called “peripheral sink” effect. For example, systemic injection of the middle portion of anti-A $\beta$

monoclonal antibody (whose epitope lies in A $\beta$ <sub>13-28</sub> (so called m266)) resulted in a rapid 1000-fold increase in plasma A $\beta$ . Moreover, the peripheral administration of m266 to transgenic mice overexpressing mutant human amyloid precursor protein V717F (PDAPP) markedly decreased brain levels of soluble A $\beta$  and prevented plaque formation without binding to A $\beta$  deposits in the brain<sup>939</sup>. This shows that peripheral m266 altered the equilibrium of A $\beta$  between the plasma and the brain. The new equilibrium favours clearance rather of deposition within the brain. Moreover, the possibility that small amounts of monoclonal antibodies or other anti-peptide antibodies enter the brain and sequester a soluble toxic A $\beta$  species could not be excluded, as shown by other reports<sup>940-942</sup>. The clearance mechanisms of the protein tau are less well known than those of A $\beta$ <sup>933</sup>. The peripheral passive immunization with antibodies towards tau oligomer support that the latter can be eliminated from the brain by the peripheral sink mechanism<sup>943</sup>. The exploration of clearance systems has been similarly entertained for treatment of excitotoxicity generated by the presence of high concentrations of glutamate in the brain<sup>944</sup>. It has been shown that the reduction in blood glutamate concentration could induce a shift in the concentration gradient of glutamate across the BBB, followed by efflux of glutamate from the brain to the periphery (neuroprotection by blood glutamate scavenging). Indeed, Teichberg *et al.* postulated that excess of glutamate in the brain extracellular fluid might be safely transported towards the blood *via* the cerebral endothelial transporter systems<sup>311-313</sup>. Subsequently, Gottlieb *et al.* demonstrated that the peripheral use of glutamate-specific enzymes such as glutamate oxaloacetate transaminase (GOT) and glutamate pyruvate transaminase (GPT) can decrease glutamate levels in both the blood and, as a result of efflux, the CSF<sup>945</sup>. Likewise, intravenous injections of GOT and GPT in rats alone or alongside its co-substrates (oxaloacetate and pyruvate, respectively) reduced blood glutamate concentration<sup>314-316</sup>. After MCAo in rats, it was demonstrated that peripheral injection of human GOT1 reduced blood and cerebral glutamate levels, alongside reduction in infarct size and smaller sensorimotor deficits compared to controls. Interestingly, lowering glutamate by means of GOT1 treatment had protective effects even when the treatment was delayed 1-hour after reperfusion (Figure 9)<sup>317</sup>. Similarly, peripheral infusion of GPT 1 hour after MCAo reduced blood glutamate concentration, decrease infarct size, reduced brain edema, improved neurological outcome, and reduced mortality rate compared to controls<sup>946</sup>. Moreover, repeated dosing of recombinant GOT1 with oxaloacetate significantly reversed the disruption of synaptic plasticity 4 days post-TBI<sup>947</sup>. Interestingly, the authors demonstrated that the systemic injection of recombinant GOT1 reversed the inhibition of long-term potentiation by decreasing glutamate levels in hippocampus interstitial fluid (without affecting expression of major glutamate transporters, EAAT1 and EAAT2), but not ventricular CSF<sup>947</sup>. Similar improvements were reported in a rat model of amyotrophic lateral sclerosis<sup>948</sup>. The advantage of using such approaches is that the removal of glutamate occurs only from areas in which

glutamate is pathologically elevated<sup>16</sup>. Furthermore, it was reported that scavenging is a self-limiting process that slows down and eventually stops as the concentration of brain glutamate decreases<sup>17</sup>.

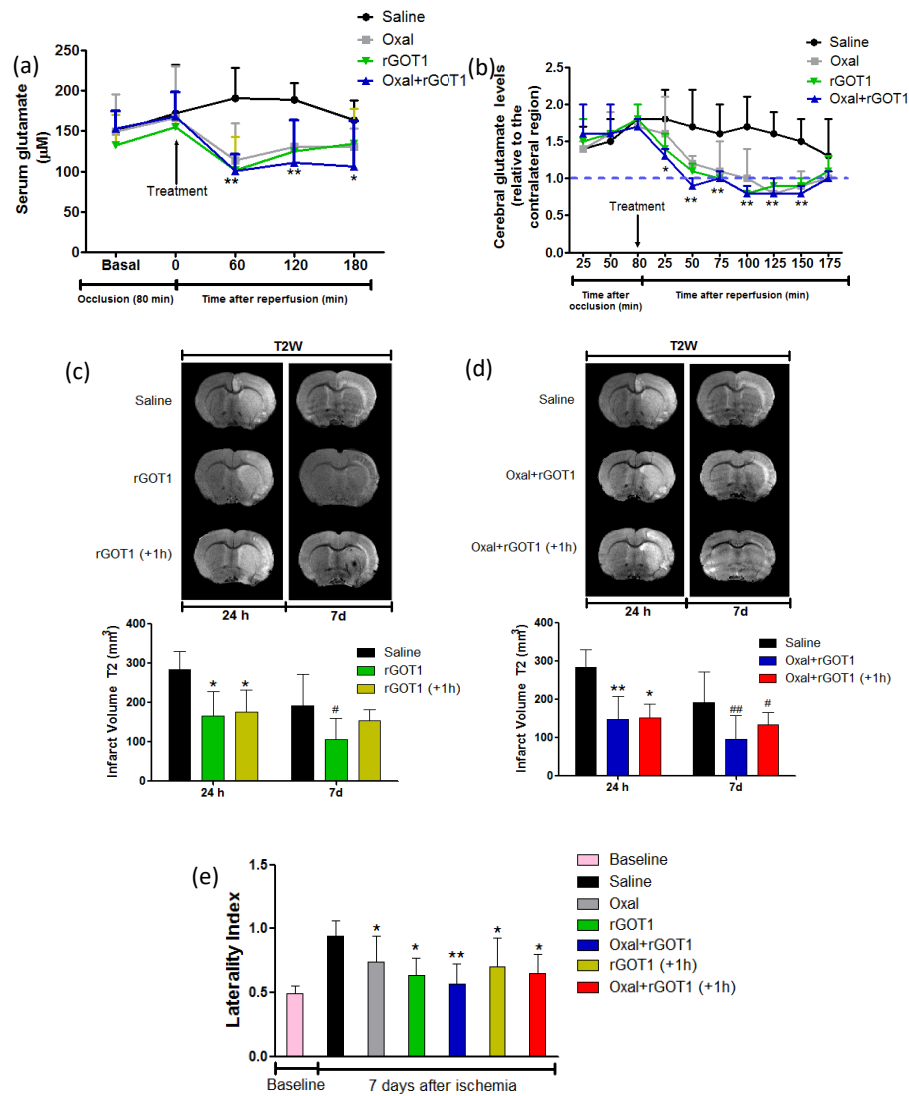


**Figure 9: Protective effects of intravenously injected GOT1 via glutamate scavenging mechanism.** (a, b) Time course of serum and brain glutamate levels in MCAo rats: intravenous administration of oxaloacetate (Oxal), rGOT1, or rGOT1 plus oxaloacetate induced a significant decrease in serum and brain glutamate concentrations (in comparison to saline group). (c, d) Infarct size assessed by means of MRI: administration of rGOT1 or rGOT1 plus oxaloacetate at the moment of reperfusion (c) or 1-hour after reperfusion generated a reduction in the infarct volume (d). (e) Sensorimotor deficits assessed using cylinder test: a significant improvement of the motor functions was measured for rGOT1 and rGOT1 plus oxaloacetate. Adapted with permission from<sup>317</sup>.

## 2.6. Delivery of proteins *via* the paracellular pathway: modulation of intercellular junctions

One alternative strategy to deliver proteins into the brain is *via* the paracellular pathway (i.e., through the intercellular junctions of the BBB). Indeed, it was demonstrated that the administration of osmotic agents (such as a hypertonic mannitol solution) induced a shrinking of the vascular endothelial cells, thereby increased the porosity of the paracellular space and enhancing the passage of various therapeutics to the brain<sup>949-953</sup>. Such an approach, termed “osmotic BBB delivery”, has been explored in order to deliver antitumor drugs to patients with brain tumors<sup>949,950</sup>.

In the same context, there have been recent developments of using cadherin peptides (e.g., ADTC5, HAV6, and cHAVc3) to improve brain delivery of proteins in healthy and animal models of brain diseases<sup>954-956</sup>. These peptides were designed to inhibit cadherin–cadherin interactions and to reversibly increase paracellular permeability<sup>957-959</sup>. For instance, in healthy Balb/c mice, cadherin peptides (10  $\mu\text{mol/kg}$ ) significantly enhanced the delivery of galbumin (MW  $\sim 65$  kDa) when administered at a high dose (600 nmol/kg). Indeed, following intravenous injection, galbumin was detected in the posterior, midbrain, and anterior regions of the brain. Interestingly, the time window of the BBB opening achieved with these peptides was different: less than 10 minutes for HAV6, and between 10–40 minutes for ADTC5<sup>960</sup>. In another report, ADTC5 was intravenously co-administrated with BDNF to healthy and EAE mice. When compared to BDNF alone, the group ADTC5 + BDNF displayed a (1) significant improvement in the delivery of BDNF to the brain, (2) neuroregeneration (e.g., activation of oligodendrocytes, remyelination), (3) suppression of the EAE relapse, and (4) lower clinical body scores<sup>955</sup>. Therefore, overall, this study demonstrated that ADTC5 modulated the BBB and allowed the noninvasive delivery of BDNF to the brain of EAE mice where it exerted its therapeutic activity. Recently, the effectiveness of HAV6 and ADTC5 for delivering intravenously injected proteins of different sizes was assessed in healthy C57BL/6 mice. The tested proteins were lysozyme, albumin, IgG, and fibronectin (with MW of  $\sim 15$  kDa,  $\sim 65$  kDa,  $\sim 150$  kDa, and  $\sim 220$  kDa, respectively)<sup>956</sup>. Mostly, the results showed that while HAV6 only enhanced the brain delivery of lysozyme (when compared to the control receiving only the protein), ADTC5 allowed the passage of lysozyme, albumin, and IgG but not fibronectin. Moreover, the passage of lysozyme through the BBB for ADTC5 group was significantly higher than that for HAV6 group (i.e., when injecting 54 nmol/kg of lysozyme with 13  $\mu\text{mol/kg}$  of either peptides, the amount of lysozyme in the brain was  $37.8 \pm 7.1$  and  $8.3 \pm 2.5$  pmol/g for the ADTC5 and HAV6 group, respectively)<sup>956</sup>.

The ensemble of the data relative to the cadherin peptides suggests that depending on the peptide employed, variable ranges of pore sizes (small, medium, and large) can be generated before they collapse in a time-dependent manner. Thus, depending on the size of the formed pores, each peptide has a particular cut-off size for molecules that can be transported across the BBB<sup>955,960</sup>. In contrast, one major and potential disadvantage of such strategy is the non-specificity of action of these peptides, as they can also increase the depositions of the delivered therapeutics in other organs (liver, kidney, spleen, lung, and heart)<sup>955,956</sup>.

## **Conclusion**

The delivery of proteins to the CNS has been a challenging area of research for several decades. Achieving optimized *in vivo* brain delivery profiles for a given protein therapeutic will involve aspects of stability, pharmacokinetics, and specific targeting strategies. Chemical or biological conjugation of proteins to brain-targeting moieties (immunoglobulins, ligands, or peptides) was largely explored in the context of parenteral administration. Nevertheless, the endocytosis of proteins coupled to such targeting molecules does not necessarily reflect their transcellular passage, and this aspect should be carefully considered in the development of these brain delivery systems. Modification of the sequence of proteins in order to alter their intrinsic properties (by glycosylation, acylation, cationization) effectively improved their pharmacokinetic profiles and increased their membrane permeabilities. However, the potential loss of protein activity, the exact mechanism of transport through cell membranes, and some toxicological issues have hindered the clinical development of many of these approaches. While, the delivery of proteins using functionalized nanosystems was effective in some cases, several technical, toxicological, and immunological aspects should be considered and exploring new nanosystems would represent a future direction for an efficient delivery of proteins to the brain. Grafting polymers to proteins certainly improves their pharmacokinetic properties, but the available results are still inconsistent and exploring different types of polymers is needed for targeting proteins to the brain. Definitely, the off-target effects observed for all the above-mentioned strategies have greatly delayed their clinical development. On the other hand, exploration of some natural physiological mechanisms such as the glutamate scavenging mechanisms has shown considerable potential, but this approach remains limited to certain specific therapeutic proteins. Additionally, the delivery of proteins by altering the paracellular pathway might be promising, but precautions should be taken as undesired large molecules (e.g., toxins) may also pass to reach the brain. Probably, the identification of paracellular permeability modulators that are more specific to the brain and that allow the opening of paracellular spaces for shorter and well-determined duration, would be of great importance.

Overall, the investigation of a variety of strategies reflects the inherent difficulty in transporting proteins across blood–brain interfaces. Substantial progress will be achieved with continued research efforts to develop safe and more specific brain delivery systems to the damaged area in the brain. Importantly, more quantitative analysis on blood–brain interface transport and brain uptake might be necessary to better identify and select the best performing strategies. Finally, more studies that take into account alterations of the BBB and the BCSFB due to brain diseases as well as the properties of the protein delivery system and the optimal timing of administration are required before taking full advantage of these strategies.

### **Declaration of Competing Interest**

The authors declare that they have no conflict of interest related to this work.

### **Acknowledgements**

MAG is a Research Scholar of the Fonds de Recherche du Québec Santé (FRQS, Canada). The preparation of this manuscript was supported by the Natural Science Engineering Council of Canada (NSERC; RGPIN-2015– 76104254) as well as by the FRQS, Instituto de Salud Carlos III (AC19/00066), the Scientific and Technological Research Council of Turkey (TUBITAK), and the Research Council of Norway (RCN), under the frame of EuroNanoMed III. AZ acknowledges a doctoral scholarship from the INRS/ Tunisian Ministry of Education. DB is a Research Scholar of the FRQS, and gratefully acknowledges financial support from the NSERC (RGPIN-2018-05076) and the Canadian Generic Pharmaceutical Association and Biosimilars Canada (Biotherapy Chair). JDO is a Research Scholar of the FRQS in collaboration with Parkinson Quebec (268980), providing salary support and operating funds, and by the Young Investigator Award from Parkinson Canada (No. 2018-00236). Figures were made with BioRender.

## APPENDIX D: Data in Brief Paper

### Determination of the degree of PEGylation of protein bioconjugates using data from proton nuclear magnetic resonance spectroscopy

Ahlem Zaghmi, Andrea A Greschner, Eduardo Mendez-Villuendas, Jun Yang Liu, Hendrick W de Haan, and Marc A Gauthier

A version of this chapter has been published in  
Materials Today Chemistry, Volume 12, June 2019, Pages 121-131

Reprint permission is not required.

The formatting of this article conforms to the specifications of the scientific journal.



ELSEVIER

Contents lists available at ScienceDirect

## Data in brief

journal homepage: [www.elsevier.com/locate/dib](http://www.elsevier.com/locate/dib)

## Data Article

# Determination of the degree of PEGylation of protein bioconjugates using data from proton nuclear magnetic resonance spectroscopy



Ahlem Zaghmi<sup>a</sup>, Andrea A. Greschner<sup>a</sup>,  
Eduardo Mendez-Villuendas<sup>b</sup>, Jun Yang Liu<sup>a</sup>,  
Hendrick W. de Haan<sup>b</sup>, Marc A. Gauthier<sup>a,\*</sup>

<sup>a</sup> Institut National de la Recherche Scientifique (INRS), EMT Research Center, Varennes, QC, J3X 1S2, Canada

<sup>b</sup> University of Ontario Institute of Technology, Faculty of Science, Oshawa, Ontario, L1H 7K4, Canada

## ARTICLE INFO

*Article history:*

Received 27 January 2019

Received in revised form 25 April 2019

Accepted 15 May 2019

Available online 23 May 2019

## ABSTRACT

The average number of methoxy poly(ethylene glycol) (mPEG) chains grafted to a protein – also known as the degree of PEGylation – is a fundamental parameter for characterizing a bioconjugate. The degree of PEGylation is typically determined by chromatographic or electrophoretic methods, which are subject to certain biases. This contribution describes an analytical approach alongside technical precautions for quantitatively determining the degree of PEGylation of protein bioconjugates by <sup>1</sup>H NMR spectroscopy. An accompanying dataset, corresponding to the raw <sup>1</sup>H NMR spectra of thirteen bioconjugates with different degrees of PEGylation and different mPEG molecular weights, is provided for the reader to become familiar with the analysis. The exemplary bioconjugate system used in this Data article is the enzyme glutamate dehydrogenase (GDH) modified with multiple copies of mPEG (0.5–20 kDa). These bioconjugates correspond to those discussed in-depth in the article “Mechanisms of activity loss for a multi-PEGylated protein by experiment and simulation” by Zaghmi et al., 2019. The described approach to calculate degree of PEGylation is quantitative, applicable to other proteins, and can be adapted to other types of polymers.

© 2019 The Authors. Published by Elsevier Inc. This is an open access article under the CC BY license (<http://creativecommons.org/licenses/by/4.0/>).

DOI of original article: <https://doi.org/10.1016/j.mtchem.2018.12.007>.

\* Corresponding author.

E-mail address: [gauthier@emt.inrs.ca](mailto:gauthier@emt.inrs.ca) (M.A. Gauthier).

<https://doi.org/10.1016/j.dib.2019.104037>

2352-3409/© 2019 The Authors. Published by Elsevier Inc. This is an open access article under the CC BY license (<http://creativecommons.org/licenses/by/4.0/>).

## Specifications table

Subject area	Biochemistry
More specific subject area	PEGylation, Bioconjugate chemistry, Biologics, Pharmaceutical chemistry
Type of data	Spectra, chromatogram, tables
How data was acquired	<sup>1</sup> H NMR spectra were recorded using a Bruker Av300 spectrometer operating at 300 MHz for protons. UV–Vis absorption spectra were recorded with either a NanoDrop 2000c absorbance spectrophotometer or a Cary 60 UV–Vis spectrophotometer. Size-exclusion chromatography was performed using an AKTA Start fast protein liquid chromatographer equipped with a HiPrep 16/60 Sephacryl™ S200 HR column.
Data format	Raw and processed data
Experimental factors	Starting compounds were either purchased or synthesized using published procedures [1]
Experimental features	Bioconjugates were purified and the average degree of PEGylation was determined by <sup>1</sup> H NMR spectroscopy
Data source location	INRS, Quebec, Canada
Data accessibility	Data available within accompanying Supplementary Material
Related research article	A. Zaghmi, E. Mendez-Villuendas, A.A. Greschner, J.Y. Liu, H.W. de Haan, M.A. Gauthier, Mechanisms of activity loss for a multi-PEGylated protein by experiment and simulation, Mater Today Chem. 12 (2019) 121–131, <a href="https://doi.org/10.1016/j.mtchem.2018.12.007">https://doi.org/10.1016/j.mtchem.2018.12.007</a> [1].

**Value of the data**

- The provided dataset is useful to familiarize oneself with the methodology for determining the average degree of PEGylation of protein bioconjugates by <sup>1</sup>H NMR spectroscopy.
- The Data is most useful to scientists not yet familiar with the analysis of PEGylated proteins.
- Precautions are provided regarding sample preparation, to acquire reliable Data for analysis.
- The provided dataset and accompanying analysis can be adapted to analyze bioconjugates prepared with polymers other than mPEG.
- The values obtained from the accompanying dataset highly complement those obtained by other techniques (e.g., chromatographic, electrophoretic, etc.).

**1. Data**

This article provides experimental protocols and technical precautions for obtaining reliable data, suitable for determining the average degree of PEGylation of protein bioconjugates by <sup>1</sup>H NMR spectroscopy. Precautions to be considered when purifying samples by centrifugal dialysis and size-exclusion chromatography yielded Figs. 1 and 2. Analysis of thirteen exemplary bioconjugates by <sup>1</sup>H NMR spectroscopy yielded the spectra plotted in Fig. 3. Integration of these spectra and analysis of these values yielded their average degree of PEGylation (Table 1). This article includes an accompanying dataset corresponding to the <sup>1</sup>H NMR spectra of the thirteen PEGylated proteins, which can be used to become familiar with the analysis of a variety of bioconjugates with different degrees of PEGylation and different mPEG molecular weights.

**2. Experimental design, materials and methods**

All chemicals were obtained from Sigma Aldrich (Oakville, Canada) at the highest purity available, unless otherwise specified. PEGylation of GDH using protein-reactive mPEG can be achieved by several different bioconjugate strategies [2]. For this Data article, PEGylation was achieved by reductive alkylation of bovine GDH using mPEG-propionaldehyde/mPEG-aldehyde (0.5–20 kDa; JenKem Technology (Plano, USA) and Creative PEGWorks (Durham, USA)) in the presence of sodium cyanoborohydride, as described by Zaghmi et al. [1] Other methods to prepare the PEGylated proteins could in principle be employed, as the method of protein PEGylation is not a factor that influences the calculated degree of PEGylation. Feed reaction conditions used to prepare the thirteen bioconjugates can be found in Table 1.

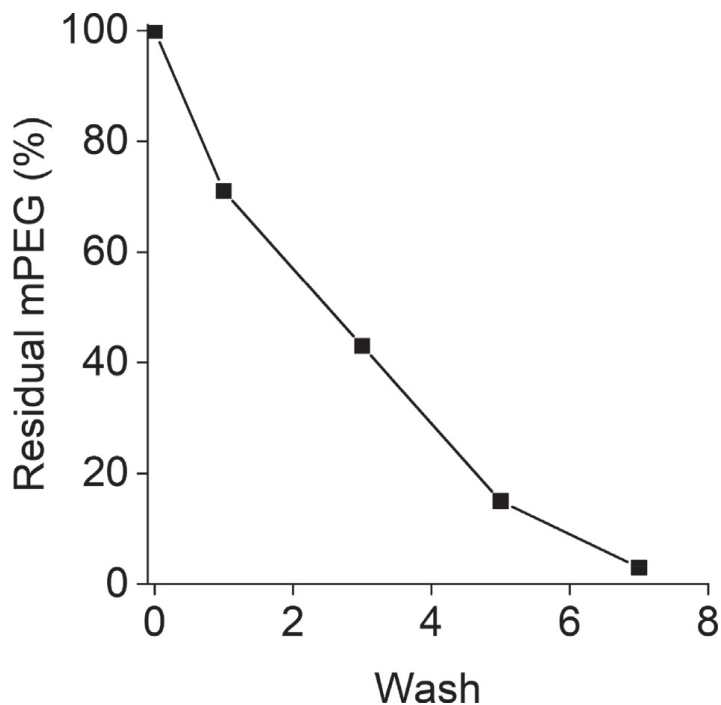


**Fig. 1. Removal of mPEG from the crude reaction mixture of exemplary bioconjugate 12 requires multiple washes.** The integrated peak area for the main-chain methylene groups of mPEG (3.69 ppm) normalized to the intensity of the first wash. Data presented as  $n = 1$ .

### 2.1. Purification of the bioconjugates

Because the described analytical method does not intrinsically involve separation of bioconjugate from starting materials (as opposed to chromatographic and electrophoretic methods), purification from residual mPEG (i.e., non-protein conjugated) is essential. Removal of non-PEGylated protein (should any remain after the reaction), may be desirable for the foreseen application of the bioconjugate. The presence or absence of residual protein will affect the degree of PEGylation measured by this method.

#### 2.1.1. Centrifugal ultrafiltration ( $m\text{PEG} \leq 5 \text{ kDa}$ )

Centrifugal ultrafiltration is the most appropriate method to eliminate residual mPEG of molecular weight below 5 kDa. However, care should be taken in the selection of the filter's Molecular Weight Cut-Off (MWCO). Most MWCOs are given in reference to globular proteins, whereas the 'random coil' character of mPEG results in a hydrodynamic radius substantially larger than a protein of similar molecular weight. If the MWCO is too small, little or no mPEG will pass through the filter. If the MWCO is too large, the bioconjugate itself will also pass through the filter. For 5 kDa mPEG, 15 mL Amicon ultra centrifugal filter units (or equivalent) with 100 kDa MWCO were found to give the best results. To ensure complete removal of mPEG, multiple washes should be used, and the filtrate of each wash should be analyzed for the presence of mPEG by (e.g.,  $^1\text{H}$  NMR spectroscopy). Following the PEGylation reaction, 1 mL of the crude reaction mixture containing bioconjugate ( $1 \text{ mg} \cdot \text{mL}^{-1}$ ) was transferred to the top compartment of the ultrafiltration unit. Seven consecutive 15-mL washes with 100 mM sodium phosphate buffer (pH 6; total volume 105 mL) were required to remove all residual mPEG (Fig. 1). The resultant solution was lyophilized to dryness to isolate the bioconjugate. It is important to note that depending upon the feed ratio of mPEG to protein, the molecular weight of mPEG, the supplier from which the filters were purchased as well as different filters from the same supplier, these results can

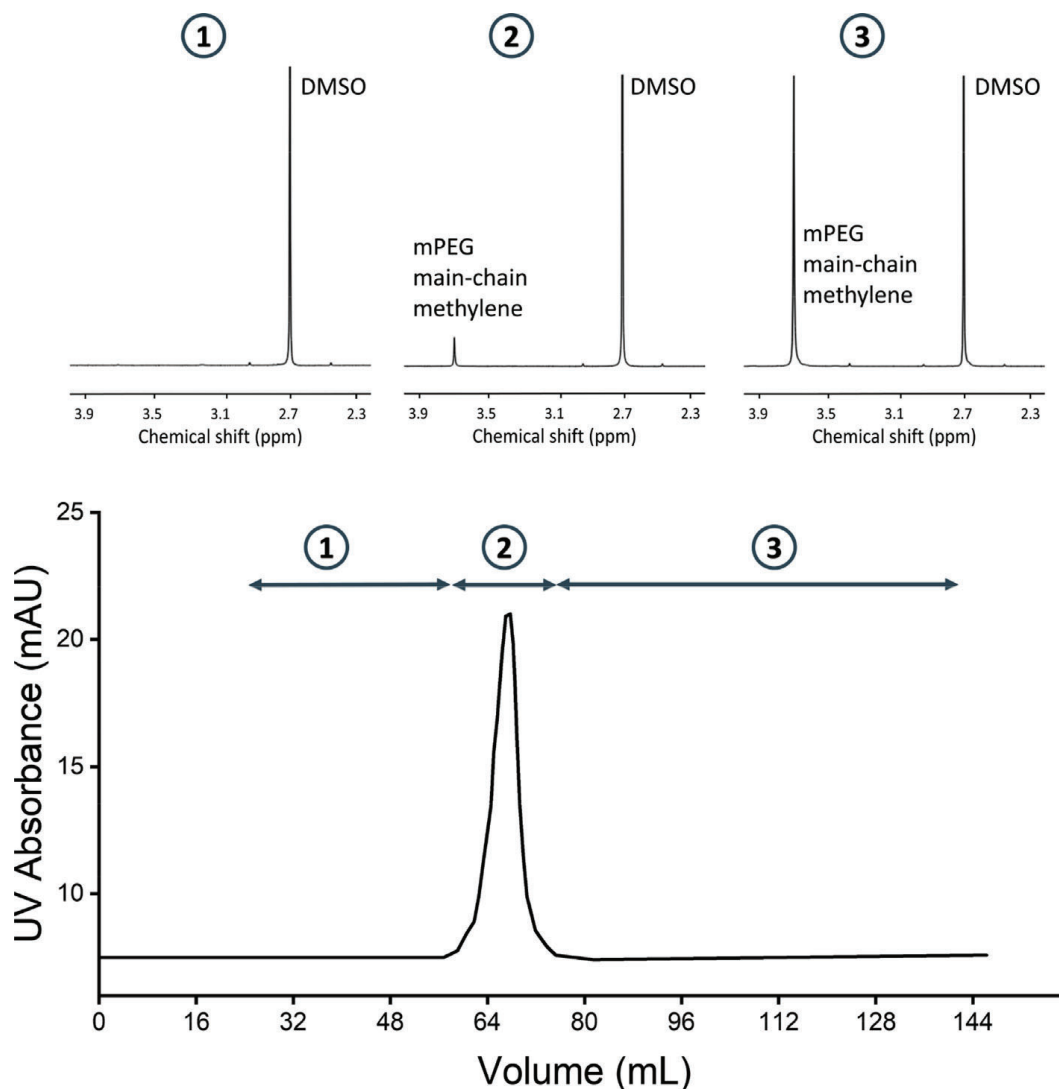


**Fig. 2. Purification of bioconjugates by size-exclusion chromatography.** Example of a size-exclusion chromatogram of the crude bioconjugation reaction mixture of bioconjugate **12**. Analysis of pooled fractions 1, 2, and 3, corresponding to 24–56 mL (buffer), 57–76 mL (bioconjugates), and 77–144 mL (residual mPEG), respectively by  $^1\text{H}$  NMR spectroscopy. Note: These spectra contain peaks of DMSO (internal integration standard, *vide infra*).

vary considerably. Therefore, optimization of this purification procedure is necessary for each new set of reaction/purification conditions.

### 2.1.2. Size-exclusion chromatography ( $m\text{PEG} \geq 5 \text{ kDa}$ )

Bioconjugates prepared with higher molecular weight mPEG (e.g.,  $\geq 5 \text{ kDa}$ ) are most easily isolated from residual mPEG by size-exclusion chromatography (SEC). SEC is more appropriate for larger mPEG because its hydrodynamic radius is too large for most ultrafiltration units. Following the PEGylation reaction, the crude reaction mixture containing bioconjugate ( $1 \text{ mg} \cdot \text{mL}^{-1}$ ) was submitted to size-exclusion chromatography. Prior to sample injection, the HiPrep 16/60 Sephacryl™ S200 HR column was equilibrated with 0.2 column volumes of filtered and degassed sodium phosphate buffer (100 mM, pH 6) at a flow rate of  $0.8 \text{ mL} \cdot \text{min}^{-1}$ . Then, the sample (1 mL) was injected and eluted over 120 mL (1 column volume) using the same eluent and flow rate, while continuously recording absorbance at 280 nm and continuously collecting 4 mL fractions (Fig. 2). Note that mPEG propionaldehyde does not absorb at 280 nm and thus the chromatogram in Fig. 2 only shows protein-containing peaks. This is not

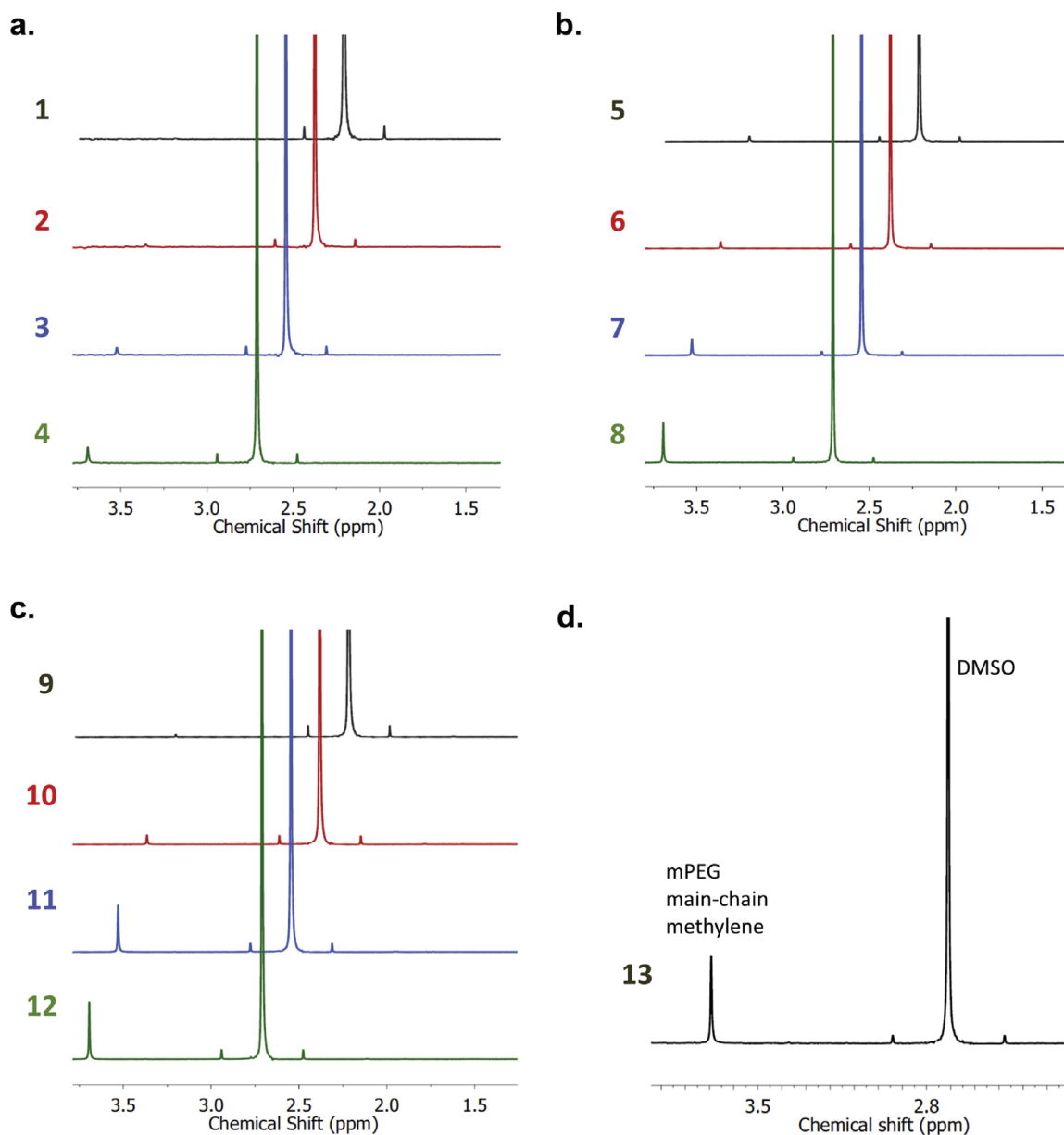


**Fig. 3.**  $^1\text{H}$  NMR spectra of bioconjugates 1–13 in  $\text{D}_2\text{O}$ . Peaks corresponding to the main-chain methylene groups of mPEG and methyl groups of DMSO are identified. Bioconjugates prepared with varying mPEG molecular weights: (a) 0.5, (b) 2, (c) 5, and (d) 20 kDa. Spectra are offset in the X-axis to improve clarity.

necessarily the case for all protein-reactive mPEGs (e.g., mPEG-orthopyridyl disulfide, used to PEGylate protein thiols *via* disulfide bond formation, absorbs at 280 nm) [3]. Upon lyophilization of the fractions, white powder was evident in some tubes: those associated with the bioconjugate peak (i.e., concurrent absorbance at 280 nm) and those associated with residual mPEG (no absorbance at 280 nm).  $^1\text{H}$  NMR spectroscopy confirms the identity of the species present in these fractions (Fig. 2). The bioconjugate peak should be resolved from the fractions containing residual mPEG to guarantee the latter is completely removed. A second round of chromatography may be necessary if a large excess of mPEG relative to protein is used during the bioconjugation reaction. The fractions associated with the bioconjugate (57–76 mL in Fig. 2) were pooled for subsequent analysis.

**Table 1**

Data used to determine the degree of PEGylation. 'Mn' is the number-averaged molecular weight, 'C' is concentration, and 'I' is the integrated peak area from <sup>1</sup>H NMR spectra.

Bioconjugate	M <sub>n</sub> of mPEG (kDa)	mPEG: GDH ratio <sup>a</sup>	A <sub>280</sub>	C <sub>Bioconjugate</sub> (μM)	I <sub>mPEG</sub> (a.u.)	I <sub>DMSO</sub> (a.u.)	C <sub>mPEG</sub> a(μM)	Degree of PEGylation
1	0.5	1:5	1.1	3.85	0	6	0	0
2		1:30	1.0	3.25	0.01	6	6.16	2
3		1:300	1.1	3.70	0.04	6	24.6	7
4		1:1500	1.2	4.00	0.11	6	67.8	17
5	2	1:5	1.3	4.50	0.05	6	7.70	2
6		1:30	0.8	2.77	0.05	6	7.70	3
7		1:300	1.0	3.40	0.15	6	23.1	7
8		1:1500	0.9	3.23	0.31	6	47.7	15
9	5	1:5	1.0	3.37	0.058	6	3.57	1
10		1:30	0.5	1.72	0.085	6	5.24	3
11		1:300	0.5	1.67	0.275	6	16.9	10
12		1:1500	0.2	0.63	0.311	6	19.2	30
13	20	1:30	0.7	2.28	0.454	6	6.99	3

<sup>a</sup> Feed molar ratio of mPEG to GDH used to prepare the bioconjugate.

## 2.2. Acquisition of data to determine the degree of PEGylation

Step 1 – Approximately ~0.2–1 mg of the purified and lyophilized bioconjugate from either Section 1.1 or 1.2 was weighed in a 1 mL Eppendorf tube.

Step 2 – Exactly 500 μL of D<sub>2</sub>O was added to the Eppendorf and quantitatively transferred to a UV-transparent cuvette. Absorbance at 280 nm was recorded using a standard UV–Vis spectrophotometer. Alternatively, a small volume (ca. 2 μL) of the bioconjugate solution was analyzed in the Nanodrop spectrometer.

Step 3 – The concentration of bioconjugate in solution was calculated using the extinction coefficient of the protein (292,920 cm<sup>-1</sup>·M<sup>-1</sup> for hexameric GDH). The concentration of protein was considered equivalent to the concentration of bioconjugate (C<sub>Protein</sub> = C<sub>Bioconjugate</sub>).

Step 4 – The bioconjugate solution was transferred quantitatively into an NMR tube and precisely 1–5 μL of dimethyl sulfoxide (DMSO) was added quantitatively, to be used as an internal integration standard. Note that DMSO is a convenient internal standard because it can be removed alongside water by lyophilization, for sample recovery.

Step 5 – A standard <sup>1</sup>H NMR spectrum was recorded of this solution. The <sup>1</sup>H NMR spectra of bioconjugates **1–13** are presented in Fig. 3, and show two major peaks of interest: a singlet at 3.69 ppm for the main-chain ethylene groups of mPEG, and a singlet at 2.71 ppm for the methyl groups of DMSO. Peaks characteristic of the protein component of the bioconjugate are not generally observed.

Step 6 – The concentration of mPEG in solution (C<sub>mPEG</sub>) is determined by integration of the peak of mPEG (I<sub>mPEG</sub>; main-chain ethylene group at 3.69 ppm) relative to the integration standard DMSO (I<sub>DMSO</sub>; methyl group at 2.71 ppm) via:

$$C_{mPEG} = \frac{6}{I_{DMSO}} \times \frac{I_{DMSO}}{4 \times DP_{mPEG}} \times C_{DMSO} \quad (1)$$

where DP<sub>mPEG</sub> is the degree of polymerization of the mPEG (113 in the case of 5 kDa mPEG), '6' is the number of protons on a molecule of DMSO, '4' is the number of protons per repeat unit in mPEG, and C<sub>DMSO</sub> is 0.084–0.28 M based the sample preparation conditions described above.

Step 7 – The average degree of PEGylation is given by:

$$\text{Degree of PEGylation} = \frac{C_{mPEG}}{C_{Bioconjugate}} \quad (2)$$

Values obtained from the spectra in Fig. 3 for bioconjugates **1–13** are found in Table 1. The accompanying dataset contains the raw data for the <sup>1</sup>H NMR spectra of the thirteen PEGylated proteins,

which can be used to become familiar with the analysis of a variety of bioconjugates with different degrees of PEGylation and different mPEG molecular weights.

### Acknowledgements

This work was supported by the Natural Science and Engineering Council of Canada (RGPIN-2015-04254 and RGPIN-2014-06091). AZ acknowledges a doctoral scholarship from the Tunisian Ministry of Education. AAG acknowledges postdoctoral scholarships from the Fonds de Recherche du Québec Nature et Technologies (FRQNT) and the Canadian Institutes for Health Research (CIHR). Further, she acknowledges the Chu Family Scholarship for a career award.

### Transparency document

Transparency document associated with this article can be found in the online version at <https://doi.org/10.1016/j.dib.2019.104037>.

### Appendix A. Supplementary data

Supplementary data to this article can be found online at <https://doi.org/10.1016/j.dib.2019.104037>.

### References

- [1] A. Zaghmi, E. Mendez-Villuendas, A.A. Greschner, J.Y. Liu, H.W. de Haan, M.A. Gauthier, Mechanisms of activity loss for a multi-PEGylated protein by experiment and simulation, *Mater. Today Chem.* 12 (2019) 121–131. <https://doi.org/10.1016/j.mtchem.2018.12.007>.
- [2] M.A. Gauthier, H.A. Klok, Peptide/protein-polymer conjugates: synthetic strategies and design concepts, *Chem. Commun.* 23 (2008) 2591–2611. <https://doi.org/10.1039/b719689j>.
- [3] Y.J. Zhao, Y.Q. Zhai, Z.G. Su, G.H. Ma, Methoxy poly (ethylene glycol) thiosulfonate: new activated polymer derivatives for thiol-specific modification, *Polym. Adv. Technol.* 21 (12) (2010) 867–873. <https://doi.org/10.1002/pat.1512>.

## **APPENDIX E: Book Chapter**

### **In vivo properties of therapeutic bioconjugates composed of proteins and architecturally/functionally complex polymers**

Ahlem Zaghmi<sup>1</sup>, Andrea A Greschner<sup>1</sup>, and Marc A Gauthier

A version of this chapter has been published in

Book: Polymer-Protein Conjugates, From PEGylation and Beyond

2020, Pages 389-406

Reprinted with permission.

The formatting of this chapter conforms to the specifications of the scientific journal.

# In vivo properties of therapeutic bioconjugates composed of proteins and architecturally/functionally complex polymers

Ahlem Zaghmi, Andrea A. Greschner, Marc A. Gauthier

*INSTITUT NATIONAL DE LA RECHERCHE SCIENTIFIQUE (INRS), EMT RESEARCH CENTER,  
VARENNES, QC, CANADA*

## 1. Introduction

Polyethylene glycol monomethyl ether (mPEG) is historically one of the first polymers ever grafted to therapeutic proteins with the goal of altering their drug-like characteristics. Arguably, this polymer was most likely selected at the time because of its hydrophilicity and unfavorable interaction with proteins, combined with the fact that it was one of the very few well-defined semitelechelic polymers available. Over its ca. 5 decade history, the “PEGylation” of proteins has received considerable attention and several PEGylated proteins are now used clinically [1,2]. As such, an abundance of data and literature is available on the effect of administration route, absorption from site of administration, distribution, immunogenicity, metabolism, and elimination of PEGylated proteins, and these subjects have been thoroughly reviewed elsewhere [3]. Indeed, the opportunities offered by mPEG, as well as limitations or challenges associated specifically with this polymer, are well-known. For instance, it is recognized that PEGylation typically confers extended blood circulation time to proteins and reduced antigenicity. However, sometimes these benefits come at the cost of reduced intrinsic activity of the protein (especially for randomly PEGylated proteins bearing high numbers of mPEG chains) and the potential of developing an immune response to mPEG [4,5].

While polymers with narrow molecular weight distributions have traditionally been prepared via fractionation techniques, advances in living radical polymerization reactions and click chemistries have greatly increased access to well-defined, protein-reactive polymers [6]. As such, it is not surprising that the field has explored new polymers as either direct replacements for mPEG or as alternatives that offer new

opportunities. Indeed, while the structure of mPEG is quite simple, many new polymers in the literature possess modular structures and pendant functional groups. These design parameters can be exploited to balance their advantages/limitations relative to mPEG or to explore new concepts such as administration via new routes, achieving stability in new environments, modifying biodistribution, etc. This chapter presents an overview of currently available data regarding the route of administration, absorption, distribution, immunology, metabolism, and elimination of therapeutic protein bioconjugates prepared with polymers other than linear mPEG (Fig. 17.1). For more detailed information on the synthesis, functionalization, and conjugation of polymers in Fig. 17.1, the reader is referred to recent literature on the topic [7–10].

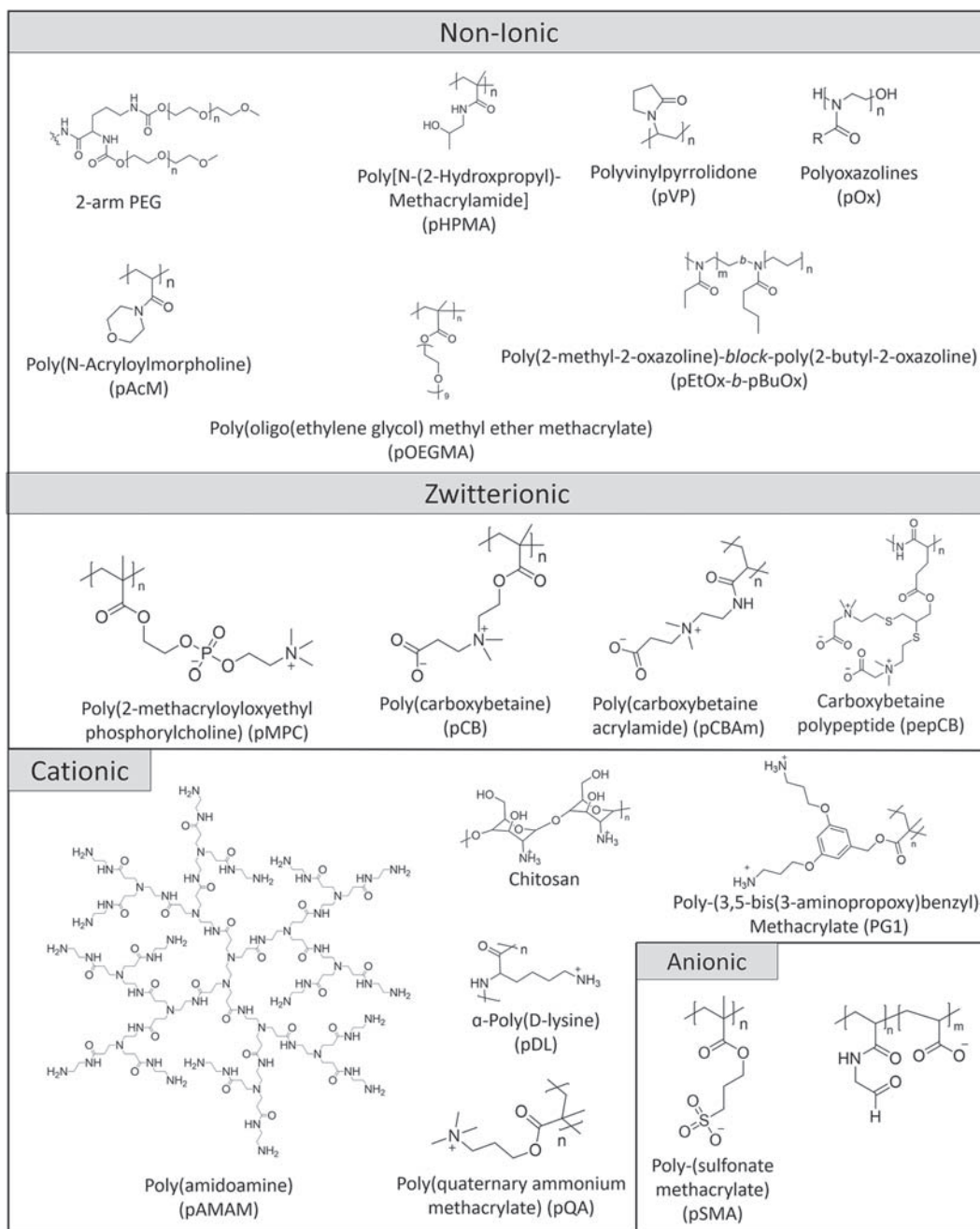
## 2. Routes of administration and absorption

At present, protein therapeutics are most often administered parenterally via the intravenous, subcutaneous, or intramuscular routes, and the same holds true for therapeutic bioconjugates. Among these routes, intravenous administration has the fewest barriers, as issues of absorption and local metabolism at the site of injection are circumvented, and the full dose is immediately available in the bloodstream. As such, polymers are not typically used with the intent to modify the absorption of the conjugate. In contrast, most other routes of administration involve a process of absorption, and the appended polymer may have a dramatic effect on diffusion, local metabolism, and transport through biological barriers.

### 2.1 Subcutaneous, intramuscular, and intraperitoneal injection

Administration via the subcutaneous and intramuscular routes typically leads to a longer duration of action than for the intravenous route, as the bioconjugate must diffuse to the bloodstream. To achieve this, it must first cross several barriers to reach either the blood capillaries or the lymphatic system. Most bioconjugates designed for nonintravenous parenteral administration (e.g., subcutaneous, intramuscular, etc.) are prepared with polymers that do not favorably interact with other biomolecules. These polymers shield the conjugated protein from attractive interactions with indigenous proteins (such as by hydrophobic interactions, van der Waals forces, and hydrogen bonding). As a result, the process of absorption is mainly affected by the hydrodynamic size of the bioconjugate. The increase of size imparted by the polymer is, for a given molecular weight, affected by architecture (i.e., branching) and conformation.

In the late 90s, efforts were undertaken to enhance the efficacy of interferon- $\alpha$ 2 by modifying it with a two-arm branched mPEG ( $2 \times 20$  kDa). While the native protein reached a maximum serum concentration ( $t_{\max}$ ) in <1 h after subcutaneous injection, the conjugate (PEGASYS) displayed a  $t_{\max}$  of 24 h, reflecting restricted diffusion because of the presence of the polymer component [11]. In a more recent study, the effect of increasing the degree of branching was explored. Compared to PEGASYS, using a



\* PAA employed in the referenced study was copolymerized with a second monomer bearing an aldehyde group, used for grafting to a protein.

FIGURE 17.1 Structures and acronyms for architecturally and functionally complex polymers that have been grafted to therapeutic proteins and discussed in this chapter.

four-armed mPEG ( $4 \times 12$  kDa) resulted in a 35% increase in  $t_{\max}$  and prolonged elimination from the body ( $\sim 2$  times smaller elimination constant) [12]. In a more systematic investigation of the effect of branched mPEG on  $t_{\max}$ , Qi et al. modified exendin-4, a GLP-1 receptor agonist that promotes insulin secretion, with pOEGMA, a comb-shaped analogue of mPEG bearing a high density of short mPEG chains connected to a poly(methacrylate) backbone. The authors examined the onset, magnitude, and duration of the effects for bioconjugates prepared with pOEGMA (one chain between  $\sim 25$  and 155 kDa; Fig. 17.2) [13]. Compared to the native exendin-4, which was only able to lower blood glucose levels for 6 h, the bioconjugates had significantly extended effects. The onset, magnitude, and duration depended on molecular weight (Fig. 17.2). Delayed onset but prolonged duration was observed for the smaller molecular weight bioconjugates. A prolonged effect (i.e., flat and steady glucose profiles) was observed with an increase of molecular weight, although with a smaller magnitude of glucose reduction. This presumably reflects hindered diffusion from the subcutaneous space. The profiles

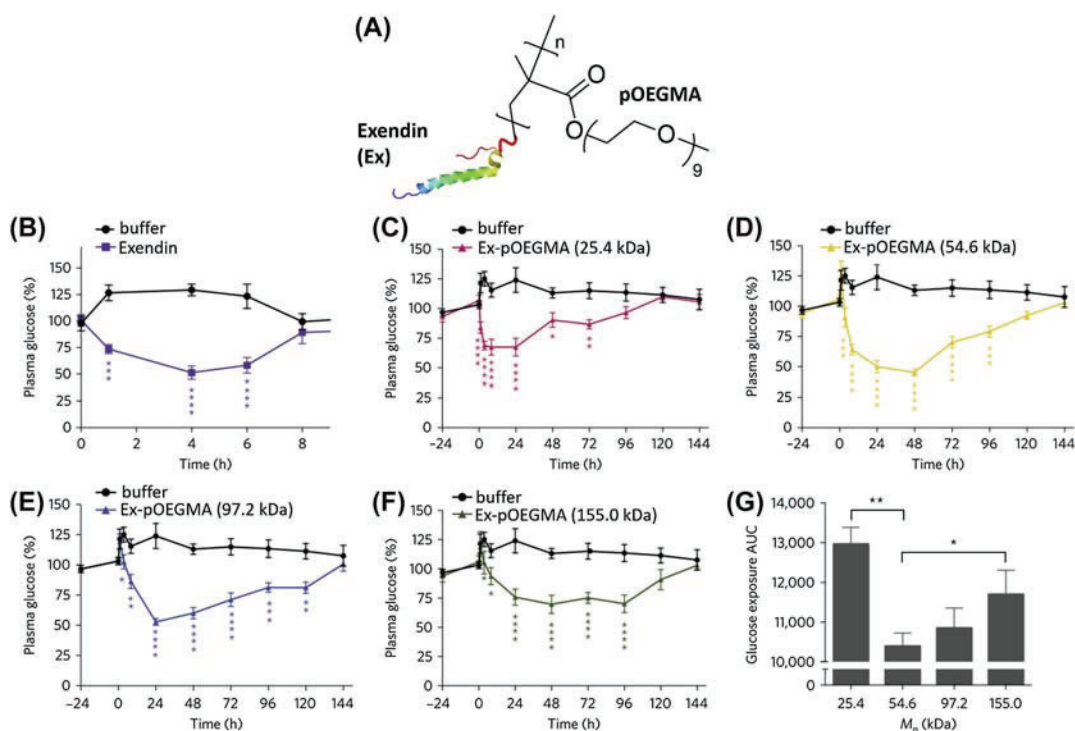


**FIGURE 17.2** (A) Structure of exendin-4-pOEGMA bioconjugate. Blood glucose lowering effect of exendin-4-pOEGMA bioconjugates in fed mice as a function of pOEGMA molecular weight; (B) unmodified exendin-4; (C) pOEGMA = 25.4 kDa; (D) pOEGMA = 54.6 kDa; (E) pOEGMA = 97.2 kDa; (F) pOEGMA = 155.0 kDa. (G) Area under the curves (AUC) of (B–F). Adapted with permission from Qi Y, Simakova A, Ganson N, Li X, Luginbuhl K, Ozer I, et al. A brush-polymer/exendin-4 conjugate reduces blood glucose levels for up to five days and eliminates poly(ethylene glycol) antigenicity. *Nat Biomed Eng.* 2017;1(1):0002.

obtained with the highest molecular weight pOEGMA resembled those of a sustained-release depot, with no peak-to-valley effect that can cause undesirable side effects.

In addition to architecture, polymer conformation can influence its “compactness,” which in turn has implications on the hydrodynamic size of bioconjugates. pMPC is an excellent example of a compact polymer. Compared to mPEG (Fig. 17.1), each repeating unit of pMPC has a pendant group with a molecular mass about 7.4 times as large as a single unit of mPEG, meaning the polymer chain can be 7.4 times shorter and still have equivalent mass. In addition, pMPC is a zwitterionic polymer that is globally neutral, despite possessing both positive and negative charges on each monomeric unit, making it superhydrophilic. These features produce different absorption effects for pMPC bioconjugates: the subcutaneous absorption of IFN- $\alpha$ 2 conjugated to a single chain of pMPC (~58 kDa; equivalent hydrodynamic radius to mPEG 20 kDa) showed a comparable absorption half-life ( $t_{1/2}$ ) to PEGASYS (~7.3 h;  $2 \times 20$  kDa mPEG chains). The absorption  $t_{1/2}$  correlated with a prolonged circulation  $t_{1/2}$ , a delayed elimination  $t_{1/2}$ , and an improved therapeutic effects (i.e., antiviral and antiproliferative activities) in comparison to native IFN- $\alpha$ 2 and to mPEG–IFN- $\alpha$ 2 (20 kDa mPEG) [14]. These observations suggest that the pMPC–IFN- $\alpha$ 2a have more difficulty diffusing in tissues and show a greater depot effect, which could explain their longer pharmacokinetic/pharmacodynamic parameters.

Globally, considering the relatively short absorption times above (on the order of 1–2 days), studies have not scrutinized local metabolism of the protein moiety of bioconjugates at the site of injection. Incidentally, polymer architecture and conformation may also play a role in more efficiently repelling enzymes and components of the immune system, as is known from in vivo work [15]. As such, the observed effects of polymer conjugation tend to reflect trends already established for mPEG and seem mostly based on restricted diffusion caused by the hydrodynamic radius of the polymer. Nevertheless, future studies involving polymers with pendant functional groups designed for interaction with the biological matrix at the site of injection may yield divergent trends and may provide new opportunities for achieving sustained release of bioconjugates (analogous to depots).

## 2.2 Oral administration

Because of the ease of oral administration, this route is generally considered to be the most convenient for the patient, especially when repetitive or chronic dosing is required. However, to reach systemic circulation, orally administered therapeutics must overcome several challenges associated with digestion (acidity, abrupt changes of pH, proteolytic enzymes, surfactants, etc.), intestinal absorption, and liver metabolism (i.e., the so-called first-pass effect). While the influence of polymer properties on the stability of bioconjugates is discussed in Section 5, polymer design also has the potential to influence absorption by slowing transit through the gastrointestinal (GI) tract. In fact, in contrast to systemic circulation, the transit time of bioconjugates through the GI tract is expected

to be mainly dictated by motility of digestive fluids, rather than the hydrodynamic radius of the bioconjugate. Therefore, altering pharmacokinetics requires the use of polymers with pendant functional groups susceptible to interact with the lining of the GI tract. Generally, it is reasoned that promoting and prolonging interaction with the intestinal epithelium favors absorption. To this end, Lee et al. [16] have conjugated low molecular weight chitosan (3–13 kDa) to insulin and have evaluated retention time in the GI tract and potential paracellular transport from the intestine to the bloodstream. For this bioconjugate, insulin (at lysine B29) was linked to the amino groups of chitosan via a short linker containing a disulfide bridge. A molecular weight dependence was observed on the blood glucose lowering effect, with larger polymers providing a greater effect. However, considering the complexity of the environment and the process of absorption, the underlying mechanism remains unexplored. Indeed, it is unknown whether absorption is occurring for the intact bioconjugate or for insulin alone and when/where insulin is released from the polymer.

Considering that absorption through the intestinal epithelium is expected to be hindered by the polymer component due to restricted diffusion, some therapeutic bioconjugates have been designed to exert their activity directly in the GI tract, where issues of absorption do not exist. Leroux and co-workers have investigated bioconjugate approaches for the oral delivery of prolyl endopeptidases, for adjuvant therapy of Celiac disease, an inflammatory disease of the small intestine triggered by gluten [17]. Modification of the enzymes with a variety of polymers, including dendritic polycations (PG1 and generation 3 pAMAM), pAA, and mPEG [18,19], yielded bioconjugates with the ability to degrade the immunogenic peptides of wheat gluten. Considering that some of the polymers used possessed multiple potential functional groups for conjugation, reaction stoichiometry was optimized to reduce the potential for cross-linking. In contrast to traditional oral delivery where the drug is intended to reach systemic circulation, the concept of the authors was to exploit the polymer to retain and stabilize the enzymes in the stomach (i.e., exert therapeutic activity in this location), where they can degrade the immunogenic peptides of gluten before they can transit to the small intestine and exert their deleterious effects. The authors observed that polycations promoted retention and full protection of the bioconjugates in the stomach for a period of ca. 3 h because of ionic interaction between positive charges on the polymers and the negatively charged sialic acid found in mucin. After 3 h, the progressive loss of activity was interpreted as being associated with the renewal of the mucus layer of the stomach (renewal time in rats is 4–6 h) [20]. In comparison to the polycations, the bioconjugates prepared with mPEG and pAA did not display activity in the stomach, likely due to the acidity of this environment (the enzyme is most active at pH ~7) [21] (Fig. 17.3). Upon reaching the small intestine, full (mPEG) or partial (pAA) recovery of activity was observed because of the increase of pH at this location. Cummings et al. have explored a similar concept by designing bioconjugates of chymotrypsin for the treatment of exocrine pancreatic insufficiency. As above, the oral administration of exogenous chymotrypsin is challenging because of its degradation in the stomach (proteases and

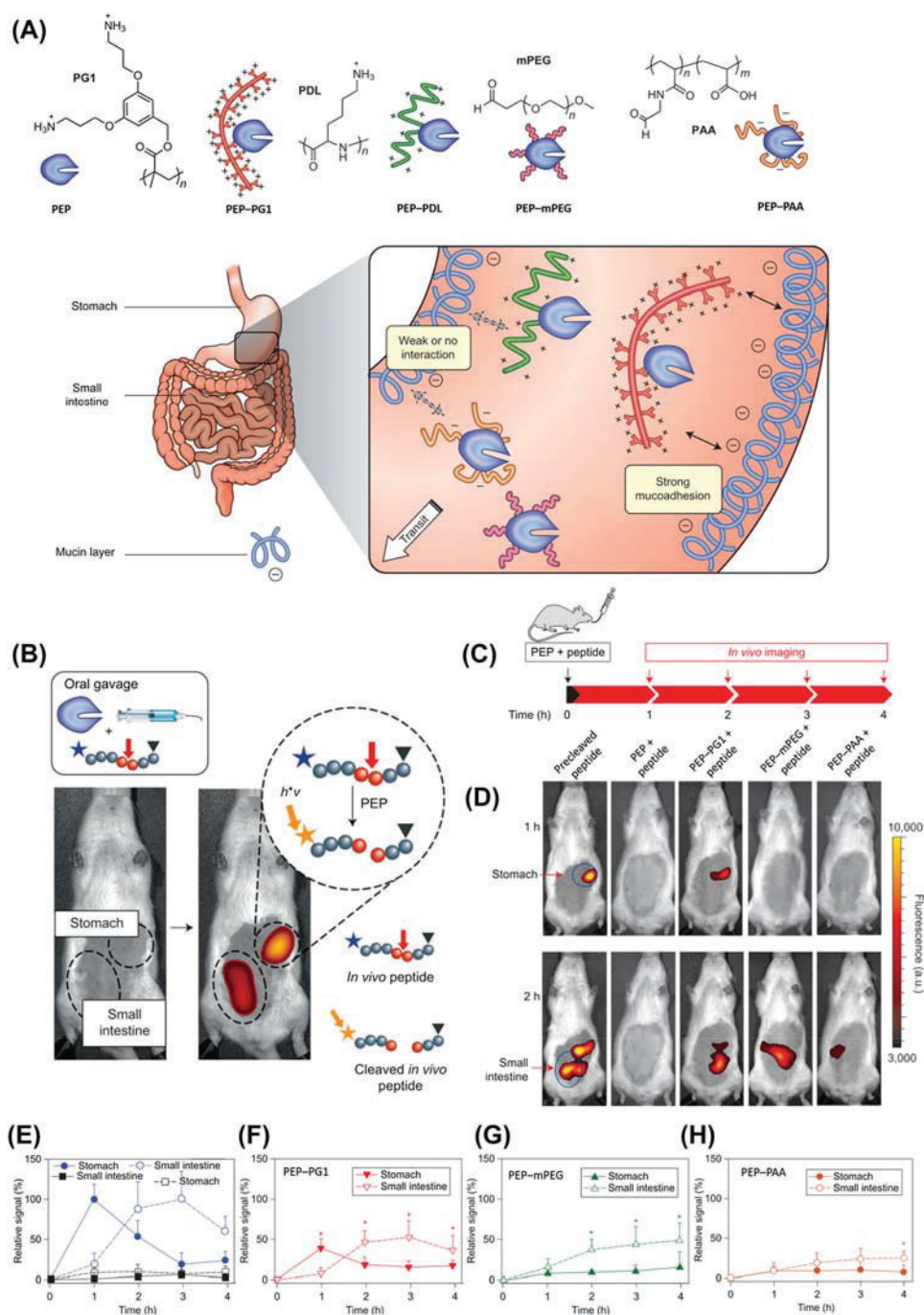


**FIGURE 17.3** The functionality of polymers grafted to prolyl endopeptidases (PEP) has a significant effect on their residence time and stability of bioconjugates in the gastrointestinal (GI) tract. (A) Schematic of the interaction between different bioconjugates and the mucin lining of the stomach. (B) Approach used to monitor the activity of bioconjugates of PEP by in vivo imaging. A peptide bearing both a fluorophore and quencher was administered to rats. Proteolysis of this peptide by the PEP or bioconjugates leads to recovery of fluorescence. (C) Experimental timeline for administration of bioconjugates and in vivo imaging. (D) Recovery of fluorescence is observed at different locations in the GI tract, due to the activity of PEP or the bioconjugates. (E–H) Quantitative analysis of data from (D) (Panel "E" represents controls for pre-cleaved peptide (blue [black in print version]) and native PEP (black)). Adapted with permission from Fuhrmann G, Grotzky A, Lukić R, Matoori S, Luciani P, Yu H, et al. Sustained gastrointestinal activity of dendronized polymer–enzyme conjugates. *Nat Chem.* 2013;5:582.

low pH) [22]. To improve on this, four different polymers with distinct physicochemical properties were tested: pOEGMA, pSMA (anionic), pQA (cationic), and pCBAm (zwitterionic) were grown from protein macroinitiators using atom-transfer radical polymerization. At extremely low pH [1–4], cationic pQA and zwitterionic pCBAm stabilized chymotrypsin while the bioconjugates prepared with pOEGMA and pSMA lost activity because of protein unfolding. Furthermore, the authors found that cationic pQA showed high mucoadhesive properties, while for zwitterionic pCBAm, mucin binding was pH-dependant (pOEGMA and pSMA did not display mucoadhesive properties). For the zwitterionic polymer, the authors rationalized the pH dependency as resulting from protonation of the polymer at low pH, yielding a net positive rather than a neutral charge.

Overall, the data suggest that, analogous to mPEG, many polymers can protect proteins from digestion in the GI tract. However, the functional groups on the polymer have a determinant role in altering GI transit time and possibly attenuating the effect of pH on the intrinsic activity of the protein. Indeed, while experimental proof *in vivo* remains to be established, polymers with protonable side chains may buffer the local pH environment as observed *in vitro* [23], which would reduce the effect of pH changes observed in the GI tract.

### 3. Circulation and distribution

The modification of proteins with polymers, such as mPEG, is known to have an important effect on their pharmacokinetics, such as by prolonging their blood residence time. This is achieved by protecting the protein from degradation, shielding it from clearing receptors and the immune system (Section 4), and preventing/slowing renal elimination. After systemic administration, bioconjugates typically display a bicompartmental pharmacokinetic pattern. Passage from the blood to the peripheral compartment is dictated by both the characteristics of biological barriers that are crossed and the characteristics of the bioconjugate itself [24]. Indeed, while the shape of a bioconjugate, its size, and flexibility have the potential to influence its *in vivo* behavior [1], the interactions between the functional groups on the polymer and blood components or tissue yield the most pronounced differences in comparison to PEGylated proteins.

Polymers known to have no interactions with proteins, like mPEG, have been shown to impart half-life extension similar to PEGylation. For instance, the comb-shaped analogue of mPEG, pOEGMA, has been reported to extend the blood circulation lifetime of several peptides and small proteins that are below the cutoff for glomerular filtration, including exendin-4, recombinant human growth hormone, salmon calcitonin, myoglobin, and green fluorescent protein [13,25–28]. In addition, Kamada et al. have modified tumor necrosis factor- $\alpha$  with either pVP (6 kDa) or mPEG (5 kDa) and, upon intravenous injection, both polymers increased the plasma  $t_{1/2}$  of the therapeutic protein to a similar extent [29]. In contrast, divergent properties can be observed as a result of interactions with biomolecules. For example, Caliceti et al. have compared the pharmacokinetics and biodistribution of bioconjugates of uricase prepared with mPEG (5 kDa), two-arm mPEG ( $2 \times 5$  kDa), pVP (6 kDa), or pAcM (6 kDa) [30]. The bioconjugates possessed similar

degrees of polymer grafting and molecular weight and showed prolonged presence in the blood following intravenous administration to mice. Interestingly, different clearance from circulation and organ distribution behaviors were observed. The bioconjugate prepared with pVP had the longest blood circulation time, reflecting low levels of tissue distribution. This bioconjugate ultimately displayed accumulation in the liver and low uptake indexes in other organs, in agreement with reports indicating the hepatic uptake by endocytosis of pVP as its main route of elimination [31]. Intriguingly, while the bioconjugate prepared with mPEG promoted the lowest distribution levels in all organs examined, the one prepared with two-arm mPEG ( $2 \times 5$  kDa) accumulated significantly in both the liver and the spleen. The authors suggest that this branched polymer could affect cell–bioconjugate interactions and, possibly because of the higher molecular volume of the latter, more efficiently stimulate phagocytosis. The bioconjugate prepared with pAcM showed practically instantaneous deposition in the liver and considerable accumulation in other organs. Nevertheless, the bioconjugate had a higher persistence in blood ( $\beta$  phase) compared to the native enzyme, probably because of a reduced degradation and a slow release from tissues. Polymer functionality can also be exploited to target specific regions in the body, such as the brain. Tong et al. have grafted polyoxazoline block copolymers to superoxide dismutase and have exploited copolymer composition to adjust the hydrophobicity/hydrophilicity balance of bioconjugates [32]. The authors conjugated p(EtOx-b-BuOx) ( $\sim 8$ – $10$  kDa) to the protein and observed a slight increase of blood residence time compared to the native form upon intravenous injection (ca. 28 vs. 16 min, respectively). While the bioconjugate prepared with mPEG circulated for a substantially longer period of time (ca. 24 h), there was an accumulation of the polyoxazoline bioconjugates in the brain and other peripheral organs, removing them from circulation. Indeed, the bioconjugate was able to cross the blood–brain barrier faster than albumin and accumulate in the parenchyma and brain capillaries. Interestingly, although the exact uptake mechanism was not identified, the authors suggested that the transport into the brain might be mediated by nonspecific transcytosis. Nevertheless, it is important to note that the uptake of the enzyme modified by polyoxazoline was very similar to that of the native enzyme; therefore, further studies should be carried out to clarify this reported trend.

Overall, beyond polymer molecular weight, which in general leads to greater blood circulation lifetimes, the functional groups of polymers can sometimes affect tissue distribution. This could be an interesting avenue to explore for more selective accumulation of bioconjugates in a given organ, although considering the general paucity of data available in the literature, a more systematic analysis of this phenomenon is warranted.

## 4. Immunology

Recognition and uptake by the immune system plays a crucial role in the biodistribution, pharmacokinetics, and pharmacodynamics of molecules, especially for therapeutic

proteins of nonhuman origin. As such, reducing immunogenicity has traditionally been one of the major driving forces behind research in the bioconjugate field, and multiple mPEG-related parameters have already been evaluated. Current research directions in this regard are divided into three major areas: achieving better shielding of epitopes, reducing loss of activity associated with polymer conjugation, and reducing polymer-related immunogenicity.

#### 4.1 Better shielding of epitopes

The typical strategy for hindering interactions between therapeutic proteins and components of the immune system is to use polymers as steric barriers. As such, one might expect polymers to exert different effects, based on their grafting density, molecular weight, and structure. For instance, Viegas et al. have evaluated the immunogenicity of bioconjugates of bovine serum albumin (BSA) prepared with pEtOx or mPEG (5 and 10 kDa) in rabbits [33]. The 10 kDa bioconjugates developed fewer anti-BSA antibodies compared to the 5 kDa bioconjugates, which was attributed to a combination of larger hydrodynamic radius and grafting density, and the bioconjugates prepared with pEtOx were less immunogenic than mPEG at each molecular weight tested. One way of increasing the density of polymer near to the conjugation site on the protein is to employ branched structures. Veronese, Caliceti, and their co-workers have demonstrated that the immunogenicity and antigenicity of uricase was reduced to a greater extent by grafting of two-arm mPEG ( $2 \times 5$  kDa) to the protein than by linear mPEG (5 kDa) [34,35]. While this effect could be related to the higher molecular weight of the two-armed versus linear mPEG, two-arm mPEG ( $2 \times 2$  kDa) was also found to reduce the antigenicity of L-asparaginase more efficiently than linear mPEG of comparable molecular weight (10 kDa) [36]. This result may arise from a better shielding of epitopes near the site of conjugation on the protein, due to the greater density of polymers at this location with the branched structures. Indeed, compared to L-asparaginase grafted with 42 mPEG (5 kDa) chains, L-asparaginase grafted with 32 pOEGMA ( $\sim 8$  kDa; a comb-shaped analogue of mPEG with a branching point at each monomer repeat unit) chains showed a substantially reduced antigenicity and immunogenicity, which supports this claim [15].

In addition to branching, another means of increasing the density of polymer at the surface of a protein is to exploit polymer conformation (i.e., expanded vs. collapsed structures). Some zwitterionic polymers, such as pMPC, adopt a more compact conformation in solution compared to mPEG, which should lead to greater polymer density at the immediate surface of the protein. As shown by Lewis et al., bioconjugates of IFN- $\alpha$ 2a prepared with pMPC were less antigenic than mPEG bioconjugates of comparable molecular weight [14]. Similarly, Liu et al. have observed a greater reduction of immunogenicity toward uricase modified with zwitterionic pCB versus mPEG, despite their similar molecular weight and conjugation chemistry [37].

Polymer functionality can mediate interactions with other biomolecules, including those of the immune system. While many polymers are chosen for their minimal

interaction with these biomolecules, this does not always end up being the case. For instance, the relative immunogenicity of bioconjugates of uricase prepared with pVP (5 kDa), pAcM (5 kDa), linear mPEG (5 kDa), and two-arm mPEG ( $2 \times 5$  kDa) was tested in Balb/c mice [35]. While all the bioconjugates (carrying  $\sim 43$  polymer chains per protein) were found to stimulate a lower antiuricase immune response compared to the native protein, differences between the polymers were observed. Indeed, pVP was the least effective in reducing protein immunogenicity, followed by pAcM, linear mPEG, and two-arm mPEG. Another interesting observation was the twofold higher *in vitro* antigenicity for pVP–uricase versus the native protein using serum from uricase-sensitized mice. The authors postulate that the antigenicity is not only related to the arrangement of the polymers around the protein but also to the protein's characteristics. Indeed, dissimilar epitopes on the protein surface could be exposed and/or masked, based on how the polymers are arranged on the surface of the protein. An interesting alternative hypothesis suggested by the authors lies in the relative stabilizing character of the polymer on the protein. Indeed, uricase is a multimeric protein, which might dissociate to produce highly immunogenic subunits during *in vitro* or *in vivo* testing.

Overall, it appears that exploiting strategies that increase the density of polymer near the surface of the protein are most efficient in reducing immunogenicity, although they may also contribute to loss of activity. As such, polymer architecture and functionality may play a large role in outperforming linear mPEG as a modifier to reduce immunogenicity.

## 4.2 Combating loss of activity

An important facet to the development of immune responses is that they are determined by the amount of protein (and thus bioconjugate) administered. As bioconjugates circulate, they are taken up by the reticuloendothelial system, which promotes accumulation in the liver and the spleen, and to a lesser extent the kidney, lung, and lymph nodes, where they are metabolized and/or eliminated according to their polymer chemical structure, size, charge, architecture, flexibility (extended or coiled conformation), and biodegradability [38]. During this process, protein epitopes initially hidden by the polymer become exposed, which can lead to an immune response. Indeed, the loss of activity of a therapeutic protein that typically occurs on polymer grafting implies that lesser-active bioconjugates must be administered at higher dose compared to bioconjugates with higher activity to achieve the same dose (i.e., activity or response).

To minimize loss of activity caused by polymer grafting, Gauthier and co-workers have investigated the dimension of polymer structure. The authors have evaluated the effect of pOEGMA grafting density and molecular weight characteristics on the activity and immunogenicity of L-asparaginase [15]. By exploring an expansive number of bioconjugates, the authors demonstrated that a large decrease of antigenicity/immunogenicity can be achieved by controlling the size and aspect ratio of the polymer on the protein. Simultaneously, they observed a substantially lower loss of therapeutic activity.

The most desirable characteristics were observed when the molecular attributes of pOEGMA were adjusted so that the polymer remained in a compact ellipsoidal conformation on the surface of the protein.

### 4.3 Combating polymer-related immunogenicity

Despite the inherently low immunogenicity of polymers used for therapeutic bioconjugate applications, this parameter can significantly increase by linkage to proteins. In this regard, a number of studies have emerged regarding the development of anti-mPEG antibodies for clinically used PEGylated proteins. PEG is omnipresent in many products used in daily life such as cosmetics, pharmaceuticals, agrochemicals, household chemicals, etc. [39]. An early study conducted in 1984 reported the preexistence of IgM anti-PEG antibodies in 0.2% of healthy blood donors [40]. A markedly higher percentage was reported in a more recent study (i.e., >25%) [41], possibly related to the growing exposure of the population to PEG.

Several studies have shown that, in comparison to mPEG, bioconjugates prepared with its comb-shaped analogue pOEGMA do not display polymer-related immunogenicity. Qi et al. have modified exendin-4 with this polymer and showed that the bioconjugate displayed lower reactivity toward patients' plasma-derived anti-PEG antibodies than two PEGylated controls (Krystexxa and Adagen) [13]. Compatible results were obtained by Liu et al., who did not observe the development of anti-pOEGMA-L-asparaginase IgG in a mouse model of L-asparaginase sensitization [15]. These results may provide some insight into what part of mPEG is recognized by antibodies (i.e., chain end, main-chain, interfacial region near protein), although more detailed studies are necessary.

## 5. Metabolism and elimination

### 5.1 Bioconjugate metabolism

The route of elimination of bioconjugates is usually related to their hydrodynamic volume, which is dictated by polymer molecular weight, the number of grafted polymer chains, and their flexibility and deformability [42]. Smaller proteins (ca. <50 kDa) are typically cleared through glomerular filtration (renal cutoff size for globular proteins is approximately 50–60 kDa). Glomerular filtration depends on the interplay of different factors, including the intrinsic permselectivity of the glomerular capillary wall that controls molecular ultrafiltration and reabsorption at the level of the proximal tubule. Both ultrafiltration and reabsorption depend not only on size and charge but also molecular deformability of the circulating molecules [43,44]. Thus, despite the fact that bioconjugates typically have a hydrodynamic radius that is larger than the pore size of the glomerular capillary, the high flexibility and deformability of the polymer nevertheless enables their filtration, albeit at low rate [43,45].

When glomerular filtration is too slow to be relevant, accumulation and metabolism (leading to elimination) become important factors to consider. Several mechanisms can be involved, including liver uptake (and subsequently hepatic metabolism), proteolytic digestion (e.g., by proteases of the blood or the interstitial fluid), endocytosis by endothelial cells, or elimination via the immune system (Section 4) [30,46]. Typically, polymer conjugation confers proteolytic stability to their protein component by sterically hindering the approach of proteases, similar to the reduction of antigenicity/immunogenicity discussed in the previous section [47]. As such, most studies observe some stabilization toward enzymatic degradation, irrespective of the nature of the polymer. Ryan et al. have conjugated pOEGMA to the N-terminal cysteine-1 of salmon calcitonin and have reported an improvement in pharmacokinetic parameters, which was correlated to the ex vivo resistance of the bioconjugate to serum, liver homogenates, and selected intestinal enzyme hydrolysis (i.e., trypsin, chymotrypsin, elastase) [48] (Fig. 17.4). Compared to linear mPEG (5 kDa), pOEGMA (6.5 kDa) provided 2.5-fold

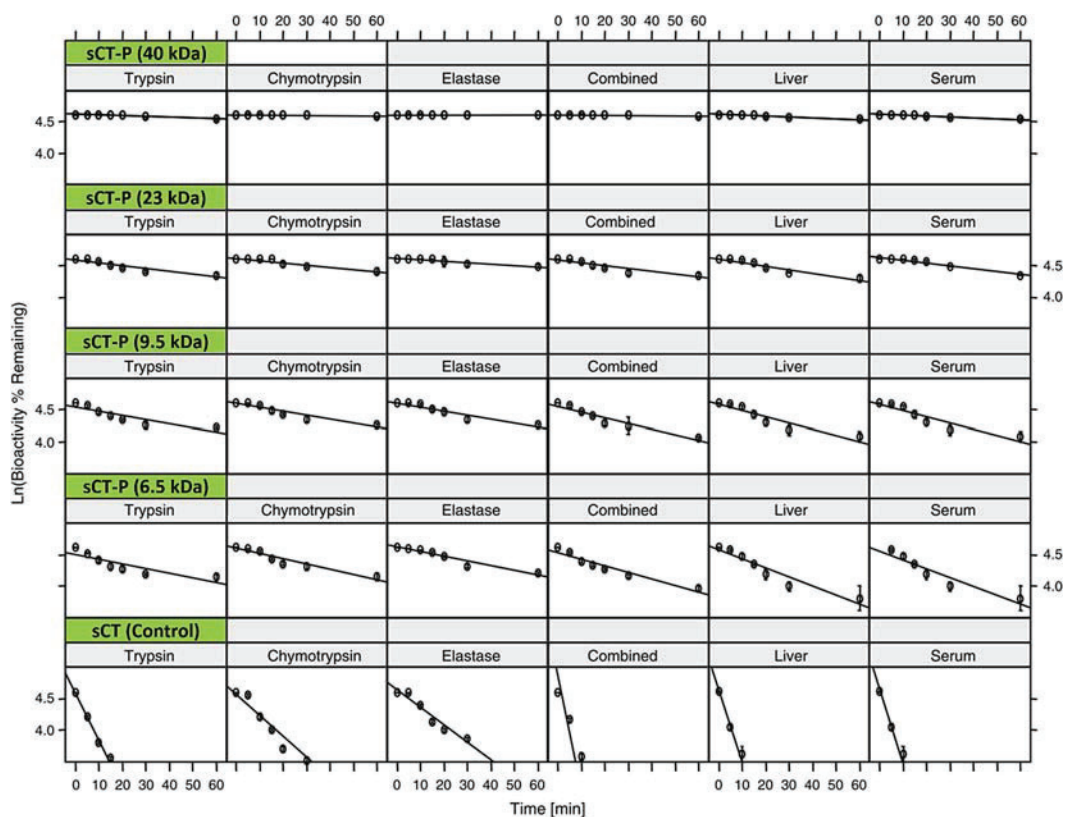


**FIGURE 17.4** Degradation profiles of salmon calcitonin–pOEGMA bioconjugates (sCT-P) incubated with enzymes, liver homogenates, or serum. Reproduced from Ryan S, Frías J, Wang X, Sayers C, Haddleton D, Brayden D. PK/IPD modelling of comb-shaped PEGylated salmon calcitonin conjugates of differing molecular weights. *J Control Release* 2011;149(2):126–32.

increase in resistance toward intestinal enzymes, as well as during incubation in excised rat intestinal sacs [25]. This polymer also offered superior protection in rat liver homogenates and serum, although linear mPEG provided little evidence of protection in liver homogenates compared to the native protein. It should be noted, however, that because the grafting method/sites were identical for both polymers, the small difference in molecular weight ( $\sim 1.5$  kDa) might possibly contribute to the observed effect. That being said, improved stability in serum and in the liver should increase the amount of bioconjugate in systemic circulation following intravenous injection, compared to mPEG. Unfortunately, beyond proteolytic degradation, very little data are available in the literature regarding the action of other types of enzymatic or nonenzymatic metabolism (i.e., oxidation, reduction, etc.).

## 5.2 Polymer elimination

The elimination of mPEG is known to depend on its molecular weight. Studies report that the main route of elimination of mPEG up to  $\sim 6$  kDa is by renal filtration, with a short circulatory  $t_{1/2}$  of about 18 min [49,50]. With increasing molecular weight, the  $t_{1/2}$  increases, with increased phagocytosis and accumulation in the Kupffer cells above ca. 50 kDa [50]. Slow clearance of large molecular weight mPEG raises concerns about potential adverse effects resulting from accumulation in tissues [3,51]. As such, alternatives to mPEG that share its nonbiodegradability also have the potential to accumulate in the body. An interesting option is to incorporate mechanisms of biodegradation that favor eventual elimination. For example, pOEGMA consists of a number of short mPEG chains grafted to the main chain via an ester bond. While these ester bonds are expected to be very stable, they potentially provide a route for biodegradation that releases oligomeric mPEG chains that are small enough for renal elimination and, upon complete hydrolysis, produces a poly(methacrylic acid), which if of proper size can be also eliminated by the kidneys. However, the kinetics of this process is not currently known and the toxicity of oligomeric mPEG remains a concern [52].

The molecular weight cutoffs for elimination of different polymers depend on their conformation in solution, which depends on their functionality. For instance, the elimination of 40 kDa mPEG was compared to that of 80 kDa zwitterionic PepCB, which is of similar hydrodynamic radius to the mPEG. Three months after intravenous injection of polymers to animals, their livers, kidneys, and spleens were examined. Vacuolation and histologic changes were clearly detected in the kidney and spleen tissues for the mPEG group. On the other hand, no histologic modifications in the PepCB group were observed [53]. Gaertner et al. studied the biodistribution and excretion of radiolabeled pMeOx and pEtOx (5 kDa) and have demonstrated rapid blood clearance (mostly after the first renal passage) and remarkably low uptake by organs of the reticuloendothelial system [54]. Regarding pVP, it has been reported that high molecular weight chains ( $>30$  kDa) may accumulate inside cells and induce a "pVP storage disease," especially if administered chronically or at high doses. The deposit of nonbiodegradable pVP might

cause bone destruction, skin lesions, and arthritis as well as liver lysosomal vacuolation [55,56]. Similarly, pHPMA is generally not biodegradable along the main chain, although it has been reported that, following intravenous injection, pHPMA with a molecular weight smaller than 40 kDa is mostly cleared from the body by renal clearance (i.e., detection of 60% of the injected dose in the urine 24 h postadministration) [57].

## 6. Conclusion

This chapter has provided an overview of the state of knowledge regarding the use of polymers other than linear mPEG for the development of therapeutic bioconjugates. While many of the trends observed with these polymers mimic those of mPEG, others do not. In general, properties associated with the “steric” nature underlying the effect of polymer conjugation, which are influenced by grafting density and molecular weight, tend to be similar to mPEG. In contrast, new properties and effects are observed when one goes to more architecturally complex polymers or polymers with pendant functional groups (e.g., charged, hydrogen bond donors, etc.), as these can influence polymer density at the surface of the protein and mediate interactions with other biomolecules. It is therefore interesting to realize that alternatives to mPEG do exist that possess similar (or greater) advantages and lesser (or different) shortcomings. Moreover, it is important to note that new polymers are emerging that offer fresh opportunities, such as the possibility of modulating interactions with biomolecules, which paves the way for the use of therapeutic bioconjugates in new applications. Overall, despite the fact that the examples discussed herein cover a long time span (ca. four decades), it is important to notice that the actual number of relevant studies in the literature is not overly abundant. It is therefore timely and important to explore replacements for mPEG to be incorporated in future generations of therapeutic bioconjugates.

## Acknowledgments

This work was supported by the Natural Science and Engineering Council of Canada (RGPIN-2015-04254). AZ acknowledges a doctoral scholarship from the Tunisian Ministry of Education. AAG acknowledges postdoctoral scholarships from the Fonds de Recherche du Québec Nature et Technologies (FRQNT) and the Canadian Institutes for Health Research (CIHR). Furthermore, she acknowledges the Chu Family Scholarship for a career award.

## References

- [1] Jevsevar S, Kunstelj M, Porekar V. PEGylation of therapeutic proteins. *Biotechnol J* 2010;5(1): 113–28.
- [2] Grigoletto A, Maso K, Mero A, Rosato A, Schiavon O, Pasut G. Drug and protein delivery by polymer conjugation. *J Drug Deliv Sci Technol* 2016;32:132–41.

- [3] Baumann A, Tuerck D, Prabhu S, Dickmann L, Sims J. Pharmacokinetics, metabolism and distribution of PEGs and PEGylated proteins: quo vadis? *Drug Discov Today* 2014;19(10):1623–31.
- [4] Zhang F, Liu M, Wan H. Discussion about several potential drawbacks of PEGylated therapeutic proteins. *Biol Pharm Bull* 2014;37(3):335–9.
- [5] Ivens I, Achanzar W, Baumann A, Brändli-Baiocco A, Cavagnaro J, Dempster M, et al. PEGylated biopharmaceuticals: current experience and considerations for nonclinical development. *Toxicol Pathol* 2015;43(7):959–83.
- [6] Zhang Q, Li M, Zhu C, Nurumbetov G, Li Z, Wilson P, et al. Well-defined protein/peptide-polymer conjugates by aqueous Cu-LRP: synthesis and controlled self-assembly. *J Am Chem Soc* 2015; 137(29):9344–53.
- [7] Grover G, Maynard H. Protein-polymer conjugates: synthetic approaches by controlled radical polymerizations and interesting applications. *Curr Opin Chem Biol* 2010;14(6):818–27.
- [8] Paeth M, Stapleton J, Dougherty M, Fischesser H, Shepherd J, McCauley M, et al. Approaches for conjugating tailor-made polymers to proteins. *Methods Enzymol* 2017;590:193–224.
- [9] Laschewsky A. Structures and synthesis of zwitterionic polymers. *Polymers* 2014;6(5):1544–601.
- [10] Pelegri-O'Day E, Lin E, Maynard H. Therapeutic protein-polymer conjugates: advancing beyond PEGylation. *J Am Chem Soc* 2014;136(41):14323–32.
- [11] Bailon P, Palleroni A, Schaffer C, Spence C, Fung W, Porter J, et al. Rational design of a potent, long-lasting form of interferon: a 40 kDa branched polyethylene glycol-conjugated interferon  $\alpha$ -2a for the treatment of hepatitis C. *Bioconjug Chem* 2001;12(2):195–202.
- [12] Costa M, Picon P, Sander G, Cuni H, Silva C, Meireles R, et al. Pharmacokinetics comparison of two pegylated interferon alfa formulations in healthy volunteers. *BMC Pharmacol Toxicol* 2018;19(1):1.
- [13] Qi Y, Simakova A, Ganson N, Li X, Luginbuhl K, Ozer I, et al. A brush-polymer/exendin-4 conjugate reduces blood glucose levels for up to five days and eliminates poly (ethylene glycol) antigenicity. *Nat Biomed Eng* 2017;1(1):0002.
- [14] Lewis A, Tang Y, Brocchini S, Choi J, Godwin A. Poly(2-methacryloyloxyethyl phosphorylcholine) for protein conjugation. *Bioconjug Chem* 2008;19(11):2144–55.
- [15] Liu M, Johansen P, Zabel F, Leroux J, Gauthier M. Semi-permeable coatings fabricated from comb-polymers efficiently protect proteins in vivo. *Nat Commun* 2014;5:5526.
- [16] Lee E, Lee J, Jon S. A novel approach to oral delivery of insulin by conjugating with low molecular weight chitosan. *Bioconjug Chem* 2010;21(10):1720–3.
- [17] Gass J, Khosla C. Prolyl endopeptidases. *Cell Mol Life Sci* 2007;64(3):345–55.
- [18] Schulz J, Patt M, Basler S, Kries H, Hilvert D, Gauthier M, et al. Site-specific polymer conjugation stabilizes therapeutic enzymes in the gastrointestinal tract. *Adv Mater* 2016;28(7):1455–60.
- [19] Fuhrmann G, Grotzky A, Lukić R, Matoori S, Luciani P, Yu H, et al. Sustained gastrointestinal activity of dendronized polymer–enzyme conjugates. *Nat Chem* 2013;5:582.
- [20] Lai S, Wang Y, Hanes J. Mucus-penetrating nanoparticles for drug and gene delivery to mucosal tissues. *Adv Drug Deliv Rev* 2009;61(2):158–71.
- [21] Brzozowski B, Lewandowska M. Prolyl endopeptidase – optimization of medium and culture conditions for enhanced production by *Lactobacillus acidophilus*. *Electron J Biotechnol* 2014;17(5): 204–10.
- [22] Cummings C, Campbell A, Baker S, Carmali S, Murata H, Russell A. Design of stomach acid-stable and mucin-binding enzyme polymer conjugates. *Biomacromolecules* 2017;18(2):576–86.
- [23] Zhang Y, Wang Q, Hess H. Increasing enzyme cascade throughput by pH-engineering the micro-environment of individual enzymes. *ACS Catal* 2017;7(3):2047–51.

- [24] Takakura Y, Fujita T, Hashida M, Sezaki H. Disposition characteristics of macromolecules in tumor-bearing mice. *Pharm Res* 1990;7(4):339–46.
- [25] Ryan S, Wang X, Mantovani G, Sayers C, Haddleton D, Brayden D. Conjugation of salmon calcitonin to a combed-shaped end functionalized poly(poly(ethylene glycol) methyl ether methacrylate) yields a bioactive stable conjugate. *J Control Release* 2009;135(1):51–9.
- [26] Magnusson J, Bersani S, Salmaso S, Alexander C, Caliceti P. In situ growth of side-chain PEG polymers from functionalized human growth hormone—a new technique for preparation of enhanced protein-polymer conjugates. *Bioconjug Chem* 2010;21(4):671–8.
- [27] Gao W, Liu W, Mackay J, Zalutsky M, Toone E, Chilkoti A. In situ growth of a stoichiometric PEG-like conjugate at a protein's N-terminus with significantly improved pharmacokinetics. *Proc Natl Acad Sci USA* 2009;106(36):15231–6.
- [28] Gao W, Liu W, Christensen T, Zalutsky M, Chilkoti A. In situ growth of a PEG-like polymer from the C terminus of an intein fusion protein improves pharmacokinetics and tumor accumulation. *Proc Natl Acad Sci USA* 2010;107(38):16432–7.
- [29] Kaneda Y, Tsutsumi Y, Yoshioka Y, Kamada H, Yamamoto Y, Kodaira H, et al. The use of PVP as a polymeric carrier to improve the plasma half-life of drugs. *Biomaterials* 2004;25(16):3259–66.
- [30] Caliceti P, Schiavon O, Veronese F. Biopharmaceutical properties of uricase conjugated to neutral and amphiphilic polymers. *Bioconjug Chem* 1999;10(4):638–46.
- [31] Seale L, Love W, Amos N, Williams B, Kellaway I. Accumulation of polyvinylpyrrolidone within the inflamed paws of adjuvant induced arthritic rats. *J Pharm Pharmacol* 1992;44(1):10–4.
- [32] Tong J, Yi X, Luxenhofer R, Banks W, Jordan R, Zimmerman M, et al. Conjugates of superoxide dismutase 1 with amphiphilic poly(2-oxazoline) block copolymers for enhanced brain delivery: synthesis, characterization and evaluation in vitro and in vivo. *Mol Pharm* 2013;10(1):360–77.
- [33] Viegas T, Bentley M, Harris J, Fang Z, Yoon K, Dizman B, et al. Polyoxazoline: chemistry, properties, and applications in drug delivery. *Bioconjug Chem* 2011;22(5):976–86.
- [34] Veronese F, Caliceti P, Schiavon O. Branched and linear poly (ethylene glycol): influence of the polymer structure on enzymological, pharmacokinetic, and immunological properties of protein conjugates. *J Bioact Compat Polym* 1997;12(3):196–207.
- [35] Caliceti P, Schiavon O, Veronese F. Immunological properties of uricase conjugated to neutral soluble polymers. *Bioconjug Chem* 2001;12(4):515–22.
- [36] Veronese F, Monfardini C, Caliceti P, Schiavon O, Scrawen M, Beer D. Improvement of pharmacokinetic, immunological and stability properties of asparaginase by conjugation to linear and branched monomethoxy poly (ethylene glycol). *J Control Release* 1996;40(3):199–209.
- [37] Liu S, Jiang S. Zwitterionic polymer-protein conjugates reduce polymer-specific antibody response. *Nano Today* 2016;11(3):285–91.
- [38] Markovsky E, Baabur-Cohen H, Eldar-Boock A, Omer L, Tiram G, Ferber S, et al. Administration, distribution, metabolism and elimination of polymer therapeutics. *J Control Release* 2012;161(2):446–60.
- [39] Fruijtier-Pöllöth C. Safety assessment on polyethylene glycols (PEGs) and their derivatives as used in cosmetic products. *Toxicology* 2005;214(1–2):1–38.
- [40] Richter A, Akerblom E. Polyethylene glycol reactive antibodies in man: titer distribution in allergic patients treated with monomethoxy polyethylene glycol modified allergens or placebo, and in healthy blood donors. *Int Arch Allergy Appl Immunol* 1984;74(1):36–9.
- [41] Armstrong J, Hempel G, Koling S, Chan L, Fisher T, Meiselman H, et al. Antibody against poly(ethylene glycol) adversely affects PEG-asparaginase therapy in acute lymphoblastic leukemia patients. *Cancer* 2007;110(1):103–11.

- [42] Hamidi M, Azadi A, Rafiei P. Pharmacokinetic consequences of pegylation. *Drug Deliv* 2006;13(6):399–409.
- [43] Arendshorst W. Renal circulation and glomerular hemodynamics. *Am J Kidney Dis* 1993;1:65–117.
- [44] Jarad G, Miner J. Update on the glomerular filtration barrier. *Curr Opin Nephrol Hypertens* 2009;18(3):226.
- [45] Duncan R. Polymer conjugates as anticancer nanomedicines. *Nat Rev Cancer* 2006;6(9):688–701.
- [46] Shi S. Biologics: an update and challenge of their pharmacokinetics. *Curr Drug Metab* 2014;15(3):271–90.
- [47] Depp V, Alikhani A, Grammer V, Lele B. Native protein-initiated ATRP: a viable and potentially superior alternative to PEGylation for stabilizing biologics. *Acta Biomater* 2009;5(2):560–9.
- [48] Ryan S, Frías J, Wang X, Sayers C, Haddleton D, Brayden D. PK/PD modelling of comb-shaped PEGylated salmon calcitonin conjugates of differing molecular weights. *J Control Release* 2011;149(2):126–32.
- [49] Shaffer C, Critchfield F, Carpenter C. Renal excretion and volume distribution of some polyethylene glycols in the dog. *Am J Physiol* 1947;152(1):93–9.
- [50] Yamaoka T, Tabata Y, Ikada Y. Distribution and tissue uptake of poly(ethylene glycol) with different molecular weights after intravenous administration to mice. *J Pharm Sci* 1994;83(4):601–6.
- [51] Rudmann D, Alston J, Hanson J, Heidel S. High molecular weight polyethylene glycol cellular distribution and PEG-associated cytoplasmic vacuolation is molecular weight dependent and does not require conjugation to proteins. *Toxicol Pathol* 2013;41(7):970–83.
- [52] Liu G, Li Y, Yang L, Wei Y, Wang X, Wang Z, et al. Cytotoxicity study of polyethylene glycol derivatives. *RSC Adv* 2017;7(30):18252–9.
- [53] Zhang P, Jain P, Tsao C, Yuan Z, Li W, Li B, et al. Polypeptides with high zwitterion density for safe and effective therapeutics. *Angew Chem Int Ed Engl* 2018;57(26):7743–7.
- [54] Gaertner F, Luxenhofer R, Blechert B, Jordan R, Essler M. Synthesis, biodistribution and excretion of radiolabeled poly(2-alkyl-2-oxazoline)s. *J Control Release* 2007;119(3):291–300.
- [55] Dunn P, Kuo T, Shih L, Wang P, Sun C, Chang M. Bone marrow failure and myelofibrosis in a case of PVP storage disease. *Am J Hematol* 1998;57(1):68–71.
- [56] Christensen M, Johansen P, Hau C. Storage of polyvinylpyrrolidone (Pvp) in tissues following long-term treatment with a Pvp-containing vasopressin preparation. *Acta Med Scand* 1978;204(4):295–8.
- [57] Seymour L, Miyamoto Y, Maeda H, Brereton M, Strohalm J, Ulbrich K, et al. Influence of molecular weight on passive tumour accumulation of a soluble macromolecular drug carrier. *Eur J Cancer* 1995;31A(5):766–70.

## BIBLIOGRAPHY

- 1 Krueger, H. *et al.* Prevalence of Individuals Experiencing the Effects of Stroke in Canada Trends and Projections. *Stroke* **46**, 2226-2231, doi:<https://doi.org/10.1161/Strokeaha.115.009616> (2015).
- 2 Silver, I. A., Deas, J. & Erecinska, M. Ion homeostasis in brain cells: Differences in intracellular ion responses to energy limitation between cultured neurons and glial cells. *Neuroscience* **78**, 589-601, doi:[https://doi.org/10.1016/S0306-4522\(96\)00600-8](https://doi.org/10.1016/S0306-4522(96)00600-8) (1997).
- 3 Hansen, A. J. & Nedergaard, M. Brain Ion Homeostasis in Cerebral-Ischemia. *Neurochem Pathol* **9**, 195-209 (1988).
- 4 Dawson, L. A., Djali, S., Gonzales, C., Vinegra, M. A. & Zaleska, M. M. Characterization of transient focal ischemia-induced increases in extracellular glutamate and aspartate in spontaneously hypertensive rats. *Brain Res Bull* **53**, 767-776, doi:[https://doi.org/10.1016/s0361-9230\(00\)00363-4](https://doi.org/10.1016/s0361-9230(00)00363-4) (2000).
- 5 Domercq, M. & Matute, C. Excitotoxicity therapy for stroke patients still alive. *Ebiomedicine* **39**, 3-4, doi:<https://doi.org/10.1016/j.ebiom.2018.12.027> (2019).
- 6 Wu, Q. J. & Tymianski, M. Targeting NMDA receptors in stroke: new hope in neuroprotection. *Mol Brain* **11**, doi:<https://doi.org/10.1186/s13041-018-0357-8> (2018).
- 7 Curcio, M., Salazar, I. L., Mele, M., Canzoniero, L. M. T. & Duarte, C. B. Calpains and neuronal damage in the ischemic brain: The swiss knife in synaptic injury. *Prog Neurobiol* **143**, 1-35, doi:<https://doi.org/10.1016/j.pneurobio.2016.06.001> (2016).
- 8 Xu, J. *et al.* Extrasynaptic NMDA Receptors Couple Preferentially to Excitotoxicity via Calpain-Mediated Cleavage of STEP. *J Neurosci* **29**, 9330-9343, doi:<https://doi.org/10.1523/Jneurosci.2212-09.2009> (2009).
- 9 Kristian, T. & Siesjo, B. K. Calcium in ischemic cell death. *Stroke* **29**, 705-718, doi:<https://doi.org/10.1161/01.Str.29.3.705> (1998).
- 10 Andreyev, A., Tamrakar, P., Rosenthal, R. E. & Fiskum, G. Calcium uptake and cytochrome c release from normal and ischemic brain mitochondria. *Neurochem Int* **117**, 15-22, doi:<https://doi.org/10.1016/j.neuint.2017.10.003> (2018).
- 11 Lai, T. W., Zhang, S. & Wang, Y. T. Excitotoxicity and stroke: identifying novel targets for neuroprotection. *Prog Neurobiol* **115**, 157-188, doi:<https://doi.org/10.1016/j.pneurobio.2013.11.006> (2014).
- 12 Muir, K. W. *et al.* A randomized, double-blind, placebo-controlled ascending dose tolerance study of 619C89 in acute stroke. *Ann N Y Acad Sci* **765**, 328-329, doi:<https://doi.org/10.1111/j.1749-6632.1995.tb16605.x> (1995).
- 13 Muir, K. W., Holzappel, L. & Lees, K. R. Phase II clinical trial of sipatrigine (619C89) by continuous infusion in acute stroke. *Cerebrovasc Dis* **10**, 431-436, doi:<https://doi.org/10.1159/000016103> (2000).
- 14 Lipton, S. A. Pathologically activated therapeutics for neuroprotection. *Nat Rev Neurosci* **8**, 803-808, doi:<https://doi.org/10.1038/nrn2229> (2007).
- 15 Lipton, S. A. Failures and successes of NMDA receptor antagonists: molecular basis for the use of open-channel blockers like memantine in the treatment of acute and chronic neurologic insults. *NeuroRx* **1**, 101-110, doi:<https://doi.org/10.1602/neurorx.1.1.101> (2004).

- 16 Gottlieb, M., Wang, Y. & Teichberg, V. I. Blood-mediated scavenging of cerebrospinal fluid glutamate. *J Neurosci* **87**, 119-126, doi:<https://doi.org/10.1046/j.1471-4159.2003.01972.x> (2003).
- 17 Leibowitz, A., Boyko, M., Shapira, Y. & Zlotnik, A. Blood Glutamate Scavenging: Insight into Neuroprotection. *Int J Mol Sci* **13**, 10041-10066, doi:<https://doi.org/10.3390/ijms130810041> (2012).
- 18 Kamimoto, Y., Horiuchi, S., Tanase, S. & Morino, Y. Plasma clearance of intravenously injected aspartate aminotransferase isozymes: evidence for preferential uptake by sinusoidal liver cells. *Hepatology* **5**, 367-375, doi:<https://doi.org/10.1002/hep.1840050305> (1985).
- 19 Horiuchi, S., Kamimoto, Y. & Morino, Y. Hepatic-Clearance of Rat-Liver Aspartate-Aminotransferase Isozymes - Evidence for Endocytotic Uptake Via Different Binding-Sites on Sinusoidal Liver-Cells. *Hepatology* **5**, 376-382, doi:<https://doi.org/10.1002/hep.1840050306> (1985).
- 20 Fleisher, G. A. & Wakim, K. G. Fate of Enzymes in Body Fluids - an Experimental Study .1. Disappearance Rates of Glutamic-Pyruvic Transaminase under Various Conditions. *J Lab Clin Med* **61**, 76-& (1963).
- 21 Yi, X., Manickam, D. S., Brynskikh, A. & Kabanov, A. V. Agile delivery of protein therapeutics to CNS. *J Control Release* **190**, 637-663, doi:<https://doi.org/10.1016/j.jconrel.2014.06.017> (2014).
- 22 Salameh, T. S. & Banks, W. A. Delivery of therapeutic peptides and proteins to the CNS. *Adv Pharmacol* **71**, 277-299, doi:<https://doi.org/10.1016/bs.apha.2014.06.004> (2014).
- 23 Bickel, U., Yoshikawa, T. & Pardridge, W. M. Delivery of Peptides and Proteins through the Blood-Brain-Barrier. *Adv Drug Deliv Rev* **10**, 205-245, doi:[https://doi.org/10.1016/s0169-409x\(00\)00139-3](https://doi.org/10.1016/s0169-409x(00)00139-3) (1993).
- 24 Yang, Q. & Lai, S. K. Anti-PEG immunity: emergence, characteristics, and unaddressed questions. *Wiley Interdiscip Rev Nanomed Nanobiotechnol* **7**, 655-677, doi:<https://doi.org/10.1002/wnan.1339> (2015).
- 25 Zhang, F., Liu, M. R. & Wan, H. T. Discussion about Several Potential Drawbacks of PEGylated Therapeutic Proteins. *Biol Pharm Bull* **37**, 335-339, doi:<https://doi.org/10.1248/bpb.b13-00661> (2014).
- 26 Veronese, F. M. & Pasut, G. PEGylation, successful approach to drug delivery. *Drug Discov Today* **10**, 1451-1458, doi:[https://doi.org/10.1016/S1359-6446\(05\)03575-0](https://doi.org/10.1016/S1359-6446(05)03575-0) (2005).
- 27 Badawi, Y., Pal, R., Hui, D. W., Michaelis, E. K. & Shi, H. L. Ischemic Tolerance in an In Vivo Model of Glutamate Preconditioning. *J Neurosci Res* **93**, 623-632, doi:<https://doi.org/10.1002/jnr.23517> (2015).
- 28 Kim, A. Y. *et al.* Glutamate Dehydrogenase as a Neuroprotective Target against Brain Ischemia and Reperfusion. *Neuroscience* **340**, 487-500, doi:<https://doi.org/10.1016/j.neuroscience.2016.11.007> (2017).
- 29 Gabathuler, R. Approaches to transport therapeutic drugs across the blood-brain barrier to treat brain diseases. *Neurobiol Dis* **37**, 48-57, doi:<https://doi.org/10.1016/j.nbd.2009.07.028> (2010).
- 30 Li, Y., Zheng, X. M., Gong, M. & Zhang, J. N. Delivery of a peptide-drug conjugate targeting the blood brain barrier improved the efficacy of paclitaxel against glioma. *Oncotarget* **7**, 79387-79393, doi:<https://doi.org/10.18632/oncotarget.12708> (2016).
- 31 Endo-Takahashi, Y. *et al.* Preparation of Angiopep-2 Peptide-Modified Bubble

- Liposomes for Delivery to the Brain. *Biol Pharm Bull* **39**, 977-983, doi:<https://doi.org/10.1248/bpb.b15-00994> (2016).
- 32 Shi, X. X. *et al.* Angiopep-2 conjugated nanoparticles loaded with doxorubicin for the treatment of primary central nervous system lymphoma. *Biomater Sci-Uk* **8**, 1290-1297, doi:<https://doi.org/10.1039/c9bm01750j> (2020).
- 33 Demeule, M. *et al.* Involvement of the low-density lipoprotein receptor-related protein in the transcytosis of the brain delivery vector Angiopep-2. *J Neurochem* **106**, 1534-1544, doi:<https://doi.org/10.1111/j.1471-4159.2008.05492.x> (2008).
- 34 Tian, X. H. *et al.* LRP-1-mediated intracellular antibody delivery to the Central Nervous System. *Sci Rep-Uk* **5**, doi:<https://doi.org/10.1038/srep11990> (2015).
- 35 Kristensen, M. & Brodin, B. Routes for Drug Translocation Across the Blood-Brain Barrier: Exploiting Peptides as Delivery Vectors. *J Pharm Sci* **106**, 2326-2334, doi:<https://doi.org/10.1016/j.xphs.2017.04.080> (2017).
- 36 Zhang, W. *et al.* Differential expression of receptors mediating receptor-mediated transcytosis (RMT) in brain microvessels, brain parenchyma and peripheral tissues of the mouse and the human. *Fluids Barriers CNS* **17**, 47, doi:<https://doi.org/10.1186/s12987-020-00209-0> (2020).
- 37 Piedmonte, D. M. & Treuheit, M. J. Formulation of Neulasta (R) (pegfilgrastim). *Adv Drug Deliv Rev* **60**, 50-58, doi:<https://doi.org/10.1016/j.addr.2007.04.017> (2008).
- 38 Alconcel, S. N. S., Baas, A. S. & Maynard, H. D. FDA-approved poly(ethylene glycol)-protein conjugate drugs. *Polym Chem* **2**, 1442-1448, doi:<https://doi.org/10.1039/c1py00034a> (2011).
- 39 Yang, C., Lu, D. & Liu, Z. How PEGylation Enhances the Stability and Potency of Insulin: A Molecular Dynamics Simulation. *Biochemistry* **50**, 2585-2593, doi:<https://doi.org/10.1021/bi101926u> (2011).
- 40 Basu, A. *et al.* Structure-function engineering of interferon-beta-1b for improving stability, solubility, potency, immunogenicity, and pharmacokinetic properties by site-selective mono-PEGylation. *Bioconjug Chem* **17**, 618-630, doi:<https://doi.org/10.1021/bc050322y> (2006).
- 41 Schiavon, O., Caliceti, P., Ferruti, P. & Veronese, F. M. Therapeutic proteins: a comparison of chemical and biological properties of uricase conjugated to linear or branched poly(ethylene glycol) and poly(N-acryloylmorpholine). *Farmaco* **55**, 264-269, doi:[https://doi.org/10.1016/S0014-827X\(00\)00031-8](https://doi.org/10.1016/S0014-827X(00)00031-8) (2000).
- 42 Gauthier, M. A. & Klok, H. A. Polymer-protein conjugates: an enzymatic activity perspective. *Polym Chem* **1**, 1352-1373, doi:<https://doi.org/10.1039/c0py90001j> (2010).
- 43 Thevenot, D. R., Godinot, C., Gautheron, D. C., Branlant, G. & Biellmann, J. F. Binding of L-glutamate to glutamate dehydrogenase in the presence of 1, 4, 5, 6-tetrahydronicotinamide adenine dinucleotide. *FEBS Lett* **54**, 206-211, doi:[https://doi.org/10.1016/0014-5793\(75\)80075-5](https://doi.org/10.1016/0014-5793(75)80075-5) (1975).
- 44 Syed, S. E. & Engel, P. C. Ox liver glutamate dehydrogenase. The use of chemical modification to study the relationship between catalytic sites for different amino acid substrates and the question of kinetic non-equivalence of the subunits. *Biochem J* **222**, 621-626, doi:<https://doi.org/10.1042/bj2220621> (1984).
- 45 Engel, P. & Dalziel, K. Kinetic studies of glutamate dehydrogenase with glutamate and norvaline as substrates. Coenzyme activation and negative homotropic interactions in allosteric enzymes. *Biochem J* **115**, 621-631, doi:<https://doi.org/10.1042/bj1150621> (1969).

- 46 Bell, J. E. & Dalziel, K. A conformational transition of the oligomer of glutamate dehydrogenase induced by half-saturation with NAD<sup>+</sup> or NADP<sup>+</sup>. *Biochim Biophys Acta* **309**, 237-242, doi:[https://doi.org/10.1016/0005-2744\(73\)90336-7](https://doi.org/10.1016/0005-2744(73)90336-7) (1973).
- 47 Koshland, D. E., Jr., Nemethy, G. & Filmer, D. Comparison of experimental binding data and theoretical models in proteins containing subunits. *Biochemistry* **5**, 365-385, doi:<https://doi.org/10.1021/bi00865a047> (1966).
- 48 Koshland, D. E., Jr. The structural basis of negative cooperativity: receptors and enzymes. *Curr Opin Struct Biol* **6**, 757-761, doi:[https://doi.org/10.1016/s0959-440x\(96\)80004-2](https://doi.org/10.1016/s0959-440x(96)80004-2) (1996).
- 49 Rasool, C. G., Nicolaidis, S. & Akhtar, M. The asymmetric distribution of enzymic activity between the six subunits of bovine liver glutamate dehydrogenase. Use of d- and l-glutamyl  $\alpha$ -chloromethyl ketones (4-amino-6-chloro-5-oxohexanoic acid). *Biochem J* **157**, 675-686, doi:<https://doi.org/10.1042/bj1570675> (1976).
- 50 Wells, B. D. Circular dichroism estimate of secondary structure of glutamate dehydrogenase. *J Mol Biol* **97**, 391-394, doi:[https://doi.org/10.1016/s0022-2836\(75\)80047-7](https://doi.org/10.1016/s0022-2836(75)80047-7) (1975).
- 51 Li, M., Li, C., Allen, A., Stanley, C. A. & Smith, T. J. The structure and allosteric regulation of glutamate dehydrogenase. *Neurochem Int* **59**, 445-455, doi:<https://doi.org/10.1016/j.neuint.2010.10.017> (2011).
- 52 Smith, T. J., Peterson, P. E., Schmidt, T., Fang, J. & Stanley, C. A. Structures of bovine glutamate dehydrogenase complexes elucidate the mechanism of purine regulation. *J Mol Biol* **307**, 707-720, doi:<https://doi.org/10.1006/jmbi.2001.4499> (2001).
- 53 Li, M., Li, C., Allen, A., Stanley, C. A. & Smith, T. J. The structure and allosteric regulation of mammalian glutamate dehydrogenase. *Arch Biochem Biophys* **519**, 69-80, doi:<https://doi.org/10.1016/j.abb.2011.10.015> (2012).
- 54 Koberstein, R. & Sund, H. Studies of glutamate dehydrogenase. The influence of ADP, GTP, and L-glutamate on the binding of the reduced coenzyme to beef-liver glutamate dehydrogenase. *Eur J Biochem* **36**, 545-552, doi:<https://doi.org/10.1111/j.1432-1033.1973.tb02942.x> (1973).
- 55 Bailey, J. *et al.* A novel mechanism of V-type zinc inhibition of glutamate dehydrogenase results from disruption of subunit interactions necessary for efficient catalysis. *FEBS J* **278**, 3140-3151, doi:<https://doi.org/10.1111/j.1742-4658.2011.08240.x> (2011).
- 56 Peterson, P. E. & Smith, T. J. The structure of bovine glutamate dehydrogenase provides insights into the mechanism of allostery. *Structure* **7**, 769-782, doi:Doi 10.1016/S0969-2126(99)80101-4 (1999).
- 57 Yu, Y. J. *et al.* Boosting brain uptake of a therapeutic antibody by reducing its affinity for a transcytosis target. *Sci Transl Med* **3**, 84ra44, doi:<https://doi.org/10.1126/scitranslmed.3002230> (2011).
- 58 Smith, T. J. & Stanley, C. A. Untangling the glutamate dehydrogenase allosteric nightmare. *Trends Biochem Sci* **33**, 557-564, doi:<https://doi.org/10.1016/j.tibs.2008.07.007> (2008).
- 59 Rodriguez-Martinez, J. A. *et al.* Stabilization of alpha-Chymotrypsin Upon PEGylation Correlates With Reduced Structural Dynamics. *Biotechnol Bioeng* **101**, 1142-1149, doi:<https://doi.org/10.1002/bit.22014> (2008).
- 60 Rodriguez-Martinez, J. A., Rivera-Rivera, I., Sola, R. J. & Griebenow, K. Enzymatic activity and thermal stability of PEG-alpha-chymotrypsin conjugates. *Biotechnol Lett* **31**, 883-887, doi:<https://doi.org/10.1007/s10529-009-9947-y> (2009).

- 61 Zhang, D., Xiao, M., Wang, L. & Jia, W. Blood-Based Glutamate Scavengers Reverse Traumatic Brain Injury-Induced Synaptic Plasticity Disruption by Decreasing Glutamate Level in Hippocampus Interstitial Fluid, but Not Cerebral Spinal Fluid, In Vivo. *Neurotox Res* **35**, 360-372, doi:<https://doi.org/10.1007/s12640-018-9961-8> (2019).
- 62 Rother, J. Neuroprotection does not work! *Stroke* **39**, 523-524, doi:<https://doi.org/10.1161/STROKEAHA.107.494799> (2008).
- 63 Choi, C. H. J., Alabi, C. A., Webster, P. & Davis, M. E. Mechanism of active targeting in solid tumors with transferrin-containing gold nanoparticles. *P Natl Acad Sci USA* **107**, 1235-1240, doi:<https://doi.org/10.1073/pnas.0914140107> (2010).
- 64 Wiley, D. T., Webster, P., Gale, A. & Davis, M. E. Transcytosis and brain uptake of transferrin-containing nanoparticles by tuning avidity to transferrin receptor. *P Natl Acad Sci USA* **110**, 8662-8667, doi:<https://doi.org/10.1073/pnas.1307152110> (2013).
- 65 Perez-Mato, M. *et al.* Human recombinant glutamate oxaloacetate transaminase 1 (GOT1) supplemented with oxaloacetate induces a protective effect after cerebral ischemia. *Cell Death Dis* **5**, e992, doi:<https://doi.org/10.1038/cddis.2013.507> (2014).
- 66 Hinoi, E., Takarada, T., Ueshima, T., Tsuchihashi, Y. & Yoneda, Y. Glutamate signaling in peripheral tissues. *Eur J Biochem* **271**, 1-13, doi:<https://doi.org/10.1046/j.1432-1033.2003.03907.x> (2004).
- 67 Nemkov, T. *et al.* Metabolism of Citrate and Other Carboxylic Acids in Erythrocytes As a Function of Oxygen Saturation and Refrigerated Storage. *Front Med (Lausanne)* **4**, 175, doi:<https://doi.org/10.3389/fmed.2017.00175> (2017).
- 68 Klin, Y. *et al.* Distribution of radiolabeled L-glutamate and D-aspartate from blood into peripheral tissues in naive rats: Significance for brain neuroprotection. *Biochem Bioph Res Co* **399**, 694-698, doi:<https://doi.org/10.1016/j.bbrc.2010.07.144> (2010).
- 69 Belanger, M., Allaman, I. & Magistretti, P. J. Brain energy metabolism: focus on astrocyte-neuron metabolic cooperation. *Cell Metab* **14**, 724-738, doi:<https://doi.org/10.1016/j.cmet.2011.08.016> (2011).
- 70 Xing, C. Y. *et al.* Distribution of cardiac output to the brain across the adult lifespan. *J Cereb Blood Flow Metab* **37**, 2848-2856, doi:<https://doi.org/10.1177/0271678X16676826> (2017).
- 71 Yu, R. & Lui, F. in *StatPearls* (2020).
- 72 Takakuwa, T., Koike, T., Muranaka, T., Uwabe, C. & Yamada, S. Formation of the circle of Willis during human embryonic development. *Congenit Anom (Kyoto)* **56**, 233-236, doi:<https://doi.org/10.1111/cga.12165> (2016).
- 73 Lee, R. M. Morphology of cerebral arteries. *Pharmacol Ther* **66**, 149-173, doi:[https://doi.org/10.1016/0163-7258\(94\)00071-a](https://doi.org/10.1016/0163-7258(94)00071-a) (1995).
- 74 Ehrlich, P. in *Eine farbenanalytische studie* (1885).
- 75 De Bock, M. *et al.* A new angle on blood-CNS interfaces: a role for connexins? *FEBS Lett* **588**, 1259-1270, doi:<https://doi.org/10.1016/j.febslet.2014.02.060> (2014).
- 76 Neuwelt, E. A. *et al.* Engaging neuroscience to advance translational research in brain barrier biology. *Nat Rev Neurosci* **12**, 169-182, doi:<https://doi.org/10.1038/nrn2995> (2011).
- 77 Redzic, Z. Molecular biology of the blood-brain and the blood-cerebrospinal fluid barriers similarities and differences. *Fluids Barriers CNS*, doi:<https://doi.org/10.1186/2045-8118-8-3> (2011).
- 78 Strazielle, N. & Ghersi-Egea, J. F. Physiology of blood-brain interfaces in relation to brain disposition of small compounds and macromolecules. *Mol Pharm* **10**, 1473-1491,

- doi:<https://doi.org/10.1021/mp300518e> (2013).
- 79 Kniesel, U. & Wolburg, H. Tight junctions of the blood-brain barrier. *Cell Mol Neurobiol* **20**, 57-76, doi:<https://doi.org/10.1023/a:1006995910836> (2000).
- 80 Bauer, H. & Traweger, A. Tight Junctions of the Blood-Brain Barrier - A Molecular Gatekeeper. *CNS Neurol Disord Drug Targets* **15**, 1016-1029, doi:<https://doi.org/10.2174/1871527315666160915142244> (2016).
- 81 Redzic, Z. B. & Segal, M. B. The structure of the choroid plexus and the physiology of the choroid plexus epithelium. *Adv Drug Deliv Rev* **56**, 1695-1716, doi:<https://doi.org/10.1016/j.addr.2004.07.005> (2004).
- 82 Pardridge, W. M. CSF, blood-brain barrier, and brain drug delivery. *Expert Opin Drug Deliv* **13**, 963-975, doi:<https://doi.org/10.1517/17425247.2016.1171315> (2016).
- 83 Dean, M., Hamon, Y. & Chimini, G. The human ATP-binding cassette (ABC) transporter superfamily. *Genome Res* **42**, 1007-1017, doi:<https://doi.org/10.1101/gr.184901> (2001).
- 84 Morris, M. E., Rodriguez-Cruz, V. & Felmler, M. A. SLC and ABC Transporters: Expression, Localization, and Species Differences at the Blood-Brain and the Blood-Cerebrospinal Fluid Barriers. *Aaps J* **19**, 1317-1331, doi:<https://doi.org/10.1208/s12248-017-0110-8> (2017).
- 85 Schinkel, A. H. & Jonker, J. W. Mammalian drug efflux transporters of the ATP binding cassette (ABC) family: an overview. *Adv Drug Deliv Rev* **55**, 3-29, doi:[https://doi.org/10.1016/s0169-409x\(02\)00169-2](https://doi.org/10.1016/s0169-409x(02)00169-2) (2003).
- 86 Juliano, R. L. & Ling, V. A surface glycoprotein modulating drug permeability in Chinese hamster ovary cell mutants. *Biochim Biophys Acta* **455**, 152-162, doi:[https://doi.org/10.1016/0005-2736\(76\)90160-7](https://doi.org/10.1016/0005-2736(76)90160-7) (1976).
- 87 Gazzin, S. *et al.* Differential expression of the multidrug resistance-related proteins ABCb1 and ABCc1 between blood-brain interfaces. *J Comp Neurol* **510**, 497-507, doi:<https://doi.org/10.1002/cne.21808> (2008).
- 88 Bendayan, R., Ronaldson, P. T., Gingras, D. & Bendayan, M. In situ localization of P-glycoprotein (ABCB1) in human and rat brain. *J Histochem Cytochem* **54**, 1159-1167, doi:<https://doi.org/10.1369/jhc.5A6870.2006> (2006).
- 89 Miller, D. S., Bauer, B. & Hartz, A. M. S. Modulation of P-glycoprotein at the blood-brain barrier: Opportunities to improve central nervous system pharmacotherapy. *Pharmacol Rev* **60**, 196-209, doi:<https://doi.org/10.1124/pr.107.07109> (2008).
- 90 Redzic, Z. Molecular biology of the blood-brain and the blood-cerebrospinal fluid barriers: similarities and differences. *Fluids Barriers CNS* **8**, 3, doi:10.1186/2045-8118-8-3 (2011).
- 91 Hawkins, R. A., O'Kane, R. L., Simpson, I. A. & Vina, J. R. Structure of the blood-brain barrier and its role in the transport of amino acids. *J Nutr* **136**, 218s-226s, doi:<https://doi.org/10.1093/jn/136.1.218S> (2006).
- 92 Bickel, U. Antibody Delivery through the Blood-Brain-Barrier. *Adv Drug Deliv Rev* **15**, 53-72, doi:[https://doi.org/10.1016/0169-409X\(95\)00005-R](https://doi.org/10.1016/0169-409X(95)00005-R) (1995).
- 93 Kumagai, A. K., Eisenberg, J. B. & Pardridge, W. M. Absorptive-mediated endocytosis of cationized albumin and a beta-endorphin-cationized albumin chimeric peptide by isolated brain capillaries. Model system of blood-brain barrier transport. *J Biol Chem* **262**, 15214-15219, doi:PMID: 2959663 (1987).
- 94 Pardridge, W. M., Buciak, J. L., Kang, Y. S. & Boado, R. J. Protamine-Mediated Transport of Albumin into Brain and Other Organs of the Rat - Binding and Endocytosis

- of Protamine-Albumin Complex by Microvascular Endothelium. *J Clin Invest* **92**, 2224-2229, doi:<https://doi.org/10.1172/Jci116825> (1993).
- 95 Poduslo, J. F. & Curran, G. L. Polyamine modification increases the permeability of proteins at the blood-nerve and blood-brain barriers. *J Neurochem* **66**, 1599-1609, doi:<https://doi.org/10.1046/j.1471-4159.1996.66041599.x> (1996).
- 96 Lu, W. Adsorptive-mediated brain delivery systems. *Curr Pharm Biotechnol* **13**, 2340-2348, doi:<https://doi.org/10.2174/138920112803341851> (2012).
- 97 Mayor, S., Parton, R. G. & Donaldson, J. G. Clathrin-independent pathways of endocytosis. *Cold Spring Harb Perspect Biol* **6**, doi:<https://doi.org/10.1101/cshperspect.a016758> (2014).
- 98 Rodriguez-Boulan, E., Kreitzer, G. & Musch, A. Organization of vesicular trafficking in epithelia. *Nat Rev Mol Cell Biol* **6**, 233-247, doi:<https://doi.org/10.1038/nrm1593> (2005).
- 99 Brooks, D. A. The endosomal network. *Int J Clin Pharmacol Ther* **47 Suppl 1**, S9-17, doi:<https://doi.org/10.5414/cpp47009> (2009).
- 100 Almers, W. Exocytosis. *Annu Rev Physiol* **52**, 607-624, doi:<https://doi.org/10.1146/annurev.ph.52.030190.003135> (1990).
- 101 Pardridge, W. M., Yang, J. & Eisenberg, J. Blood-brain barrier protein phosphorylation and dephosphorylation. *J Neurochem* **45**, 1141-1147, doi:<https://doi.org/10.1111/j.1471-4159.1985.tb05534.x> (1985).
- 102 Peters, A., Palay, S. L. & Webster, H. d. *The fine structure of the nervous system : neurons and their supporting cells*. 3rd edn, (Oxford University Press, 1991).
- 103 Mills, E., Dong, X. P., Wang, F. & Xu, H. Mechanisms of brain iron transport: insight into neurodegeneration and CNS disorders. *Future Med Chem* **2**, 51-64, doi:<https://doi.org/10.4155/fmc.09.140> (2010).
- 104 Enns, C. A., Rutledge, E. A. & Williams, A. M. The transferrin receptor. *Biomembranes: A Multi-Volume Treatise* **4**, 255-287, doi:[https://doi.org/10.1016/S1874-5342\(96\)80012-2](https://doi.org/10.1016/S1874-5342(96)80012-2) (1996).
- 105 Lawrence, C. M. *et al.* Crystal structure of the ectodomain of human transferrin receptor. *Science* **286**, 779-782, doi:<https://doi.org/10.1126/science.286.5440.779> (1999).
- 106 Kissel, K. *et al.* Immunohistochemical localization of the murine transferrin receptor (TfR) on blood-tissue barriers using a novel anti-TfR monoclonal antibody. *Histochem Cell Biol* **110**, 63-72, doi:<https://doi.org/10.1007/s004180050266> (1998).
- 107 Connor, J. R. *et al.* Profile of altered brain iron acquisition in restless legs syndrome. *Brain* **134**, 959-968, doi:<https://doi.org/10.1093/brain/awr012> (2011).
- 108 Qian, Z. M., Li, H. Y., Sun, H. Z. & Ho, K. Targeted drug delivery via the transferrin receptor-mediated endocytosis pathway. *Pharmacol Rev* **54**, 561-587, doi:<https://doi.org/10.1124/pr.54.4.561> (2002).
- 109 Kuang, Y. Y. *et al.* Dual Functional Peptide-Driven Nanoparticles for Highly Efficient Glioma-Targeting and Drug Codelivery. *Mol Pharm* **13**, 1599-1607, doi:<https://doi.org/10.1021/acs.molpharmaceut.6b00051> (2016).
- 110 Wang, Z. *et al.* Enhanced anti-ischemic stroke of ZL006 by T7-conjugated PEGylated liposomes drug delivery system. *Sci Rep* **5**, 12651, doi:<https://doi.org/10.1038/srep12651> (2015).
- 111 Couch, J. A. *et al.* Addressing Safety Liabilities of TfR Bispecific Antibodies That Cross the Blood-Brain Barrier. *Sci Transl Med* **5**, doi:<https://doi.org/10.1126/scitranslmed.3005338> (2013).

- 112 Smith, M. W. & Gumbleton, M. Endocytosis at the blood-brain barrier: From basic understanding to drug delivery strategies. *J Drug Target* **14**, 191-214, doi:<https://doi.org/10.1080/10611860600650086> (2006).
- 113 Weiss, M., Steiner, D. F. & Philipson, L. H. in *Endotext* (eds K. R. Feingold *et al.*) (2000).
- 114 van Houten, M. & Posner, B. I. Insulin binds to brain blood vessels in vivo. *Nature* **282**, 623-625, doi:<https://doi.org/10.1038/282623a0> (1979).
- 115 Jialal, I. *et al.* Characterization of the receptors for insulin and the insulin-like growth factors on micro- and macrovascular tissues. *Endocrinology* **117**, 1222-1229, doi:<https://doi.org/10.1210/endo-117-3-1222> (1985).
- 116 Yamaguchi, Y., Flier, J. S., Benecke, H., Ransil, B. J. & Moller, D. E. Ligand-binding properties of the two isoforms of the human insulin receptor. *Endocrinology* **132**, 1132-1138, doi:<https://doi.org/10.1210/endo.132.3.8440175> (1993).
- 117 Croll, T. I. *et al.* Higher-Resolution Structure of the Human Insulin Receptor Ectodomain: Multi-Modal Inclusion of the Insert Domain. *Structure* **24**, 469-476, doi:<https://doi.org/10.1016/j.str.2015.12.014> (2016).
- 118 Pardridge, W. M., Kang, Y. S., Buciak, J. L. & Yang, J. Human Insulin-Receptor Monoclonal-Antibody Undergoes High-Affinity Binding to Human Brain Capillaries in-Vitro and Rapid Transcytosis through the Blood-Brain-Barrier in-Vivo in the Primate. *Pharm Res* **12**, 807-816, doi:<https://doi.org/10.1023/A:1016244500596> (1995).
- 119 Pardridge, W. M., Kang, Y. S., Buciak, J. L. & Yang, J. Human insulin receptor monoclonal antibody undergoes high affinity binding to human brain capillaries in vitro and rapid transcytosis through the blood-brain barrier in vivo in the primate. *Pharm Res* **12**, 807-816, doi:<https://doi.org/10.1023/a:1016244500596> (1995).
- 120 Coloma, M. J. *et al.* Transport across the primate blood-brain barrier of a genetically engineered chimeric monoclonal antibody to the human insulin receptor. *Pharm Res* **17**, 266-274, doi:<https://doi.org/10.1023/A:1007592720793> (2000).
- 121 Morrison, S. L., Johnson, M. J., Herzenberg, L. A. & Oi, V. T. Chimeric Human-Antibody Molecules - Mouse Antigen-Binding Domains with Human Constant Region Domains. *P Natl Acad Sci USA* **81**, 6851-6855, doi:<https://doi.org/10.1073/pnas.81.21.6851> (1984).
- 122 Boado, R. J., Zhang, Y. F., Zhang, Y. & Pardridge, W. M. Humanization of anti-human insulin receptor antibody for drug targeting across the human blood-brain barrier. *Biotechnol Bioeng* **96**, 381-391, doi:<https://doi.org/10.1002/bit.21120> (2007).
- 123 Melmed, S., Auchus, R. J., Goldfine, A. B., Koenig, R. J. & Rosen, C. J. *Williams textbook of endocrinology*. 14. edn, (Elsevier, Inc, 2019).
- 124 Sudhof, T. C., Goldstein, J. L., Brown, M. S. & Russell, D. W. The LDL receptor gene: a mosaic of exons shared with different proteins. *Science* **228**, 815-822, doi:<https://doi.org/10.1126/science.2988123> (1985).
- 125 Russell, D. W. *et al.* Domain map of the LDL receptor: sequence homology with the epidermal growth factor precursor. *Cell* **37**, 577-585, doi:[https://doi.org/10.1016/0092-8674\(84\)90388-x](https://doi.org/10.1016/0092-8674(84)90388-x) (1984).
- 126 Yamamoto, T. *et al.* The human LDL receptor: a cysteine-rich protein with multiple Alu sequences in its mRNA. *Cell* **39**, 27-38, doi:[https://doi.org/10.1016/0092-8674\(84\)90188-0](https://doi.org/10.1016/0092-8674(84)90188-0) (1984).
- 127 Cummings, R. D. *et al.* Biosynthesis of N- and O-linked oligosaccharides of the low density lipoprotein receptor. *J Biol Chem* **258**, 15261-15273, doi:PMID: 6317691 (1983).

- 128 Davis, C. G. *et al.* The J.D. mutation in familial hypercholesterolemia: amino acid substitution in cytoplasmic domain impedes internalization of LDL receptors. *Cell* **45**, 15-24, doi:[https://doi.org/10.1016/0092-8674\(86\)90533-7](https://doi.org/10.1016/0092-8674(86)90533-7) (1986).
- 129 Chen, W. J., Goldstein, J. L. & Brown, M. S. Npxy, a Sequence Often Found in Cytoplasmic Tails, Is Required for Coated Pit-Mediated Internalization of the Low-Density-Lipoprotein Receptor. *J Biol Chem* **265**, 3116-3123, doi:PMID: 1968060 (1990).
- 130 Yokode, M. *et al.* Cytoplasmic Sequence Required for Basolateral Targeting of Ldl Receptor in Livers of Transgenic Mice. *J Cell Biol* **117**, 39-46, doi:<https://doi.org/10.1083/jcb.117.1.39> (1992).
- 131 Herz, J. & Bock, H. H. Lipoprotein receptors in the nervous system. *Annu Rev Biochem* **71**, 405-434, doi:<https://doi.org/10.1146/annurev.biochem.71.110601.135342> (2002).
- 132 Roslan, Z., Muhamad, M., Selvaratnam, L. & Ab-Rahim, S. The Roles of Low-Density Lipoprotein Receptor-Related Proteins 5, 6, and 8 in Cancer: A Review. *J Oncol* **2019**, 4536302, doi:<https://doi.org/10.1155/2019/4536302> (2019).
- 133 Hussain, M. M., Strickland, D. K. & Bakillah, A. The mammalian low-density lipoprotein receptor family. *Annu Rev Nutr* **19**, 141-172, doi:<https://doi.org/10.1146/annurev.nutr.19.1.141> (1999).
- 134 Dunn, K. W., McGraw, T. E. & Maxfield, F. R. Iterative fractionation of recycling receptors from lysosomally destined ligands in an early sorting endosome. *J Cell Biol* **109**, 3303-3314, doi:<https://doi.org/10.1083/jcb.109.6.3303> (1989).
- 135 Goti, D. *et al.* Effects of lipoprotein lipase on uptake and transcytosis of low density lipoprotein (LDL) and LDL-associated alpha-tocopherol in a porcine in vitro blood-brain barrier model. *J Biol Chem* **277**, 28537-28544, doi:<https://doi.org/10.1074/jbc.M203989200> (2002).
- 136 Dehouck, B., Dehouck, M. P., Fruchart, J. C. & Cecchelli, R. Upregulation of the low density lipoprotein receptor at the blood-brain barrier: intercommunications between brain capillary endothelial cells and astrocytes. *J Cell Biol* **126**, 465-473, doi:<https://doi.org/10.1083/jcb.126.2.465> (1994).
- 137 Candela, P. *et al.* Physiological pathway for low-density lipoproteins across the blood-brain barrier: transcytosis through brain capillary endothelial cells in vitro. *Endothelium* **15**, 254-264, doi:<https://doi.org/10.1080/10623320802487759> (2008).
- 138 Dehouck, B. *et al.* A new function for the LDL receptor: transcytosis of LDL across the blood-brain barrier. *J Cell Biol* **138**, 877-889, doi:<https://doi.org/10.1083/jcb.138.4.877> (1997).
- 139 Candela, P. *et al.* Physiological Pathway for Low-Density Lipoproteins across the Blood-Brain Barrier: Transcytosis through Brain Capillary Endothelial Cells In Vitro. *Endothelium-J Endoth* **15**, 254-264, doi:Pii 906496590  
10.1080/10623320802487759 (2008).
- 140 Simionescu, M., Popov, D. & Sima, A. Endothelial transcytosis in health and disease. *Cell Tissue Res* **335**, 27-40, doi:<https://doi.org/10.1007/s00441-008-0688-3> (2009).
- 141 Demeule, M. *et al.* Identification and design of peptides as a new drug delivery system for the brain. *J Pharmacol Exp Ther* **324**, 1064-1072, doi:<https://doi.org/10.1124/jpet.107.131318> (2008).
- 142 Investigators, W. M. P. P. The World Health Organization MONICA Project (monitoring trends and determinants in cardiovascular disease): a major international collaboration. *J Clin Epidemiol* **41**, 105-114, doi:[https://doi.org/10.1016/0895-4356\(88\)90084-4](https://doi.org/10.1016/0895-4356(88)90084-4) (1988).

- 143 Johnson, W., Onuma, O., Owolabi, M. & Sachdev, S. Stroke: a global response is needed. *B World Health Organ* **94**, 634-634, doi:<https://doi.org/10.2471/Blt.16.181636> (2016).
- 144 Nogles, T. E. & Galuska, M. A. in *StatPearls* (2020).
- 145 Ng, Y. S., Stein, J., Ning, M. & Black-Schaffer, R. M. Comparison of clinical characteristics and functional outcomes of ischemic stroke in different vascular territories. *Stroke* **38**, 2309-2314, doi:<https://doi.org/10.1161/STROKEAHA.106.475483> (2007).
- 146 Ginsberg, M. D. The new language of cerebral ischemia. *AJNR Am J Neuroradiol* **18**, 1435-1445, doi:PMID: 9296184 (1997).
- 147 Belov Kirdajova, D., Kriska, J., Tureckova, J. & Anderova, M. Ischemia-Triggered Glutamate Excitotoxicity From the Perspective of Glial Cells. *Front Cell Neurosci* **14**, 51, doi:<https://doi.org/10.3389/fncel.2020.00051> (2020).
- 148 Rossi, D. J., Brady, J. D. & Mohr, C. Astrocyte metabolism and signaling during brain ischemia. *Nat Neurosci* **10**, 1377-1386, doi:<https://doi.org/10.1038/nn2004> (2007).
- 149 Moskowitz, M. A., Lo, E. H. & Iadecola, C. The science of stroke: mechanisms in search of treatments. *Neuron* **67**, 181-198, doi:<https://doi.org/10.1016/j.neuron.2010.07.002> (2010).
- 150 Broughton, B. R., Reutens, D. C. & Sobey, C. G. Apoptotic mechanisms after cerebral ischemia. *Stroke* **40**, e331-339, doi:<https://doi.org/10.1161/STROKEAHA.108.531632> (2009).
- 151 Tadi, P. & Lui, F. in *StatPearls* (2020).
- 152 Knowland, D. *et al.* Stepwise Recruitment of Transcellular and Paracellular Pathways Underlies Blood-Brain Barrier Breakdown in Stroke. *Neuron* **82**, 603-617, doi:<https://doi.org/10.1016/j.neuron.2014.03.003> (2014).
- 153 Chen, Y. J. *et al.* Blood-brain barrier KCa3.1 channels: evidence for a role in brain Na uptake and edema in ischemic stroke. *Stroke* **46**, 237-244, doi:<https://doi.org/10.1161/STROKEAHA.114.007445> (2015).
- 154 O'Donnell, M. E. Blood-brain barrier Na transporters in ischemic stroke. *Adv Pharmacol* **71**, 113-146, doi:<https://doi.org/10.1016/bs.apha.2014.06.011> (2014).
- 155 O'Donnell, M. E. *et al.* Intravenous HOE-642 reduces brain edema and Na uptake in the rat permanent middle cerebral artery occlusion model of stroke: evidence for participation of the blood-brain barrier Na/H exchanger. *J Cereb Blood Flow Metab* **33**, 225-234, doi:<https://doi.org/10.1038/jcbfm.2012.160> (2013).
- 156 Dharmasaroja, P. A. Fluid Intake Related to Brain Edema in Acute Middle Cerebral Artery Infarction. *Transl. Stroke Res.* **7**, 49-53, doi:<https://doi.org/10.1007/s12975-015-0439-1> (2016).
- 157 Stokum, J. A., Gerzanich, V. & Simard, J. M. Molecular pathophysiology of cerebral edema. *J Cereb Blood Flow Metab* **36**, 513-538, doi:<https://doi.org/10.1177/0271678X15617172> (2016).
- 158 Rosenberg, G. A. Ischemic brain edema. *Prog Cardiovasc Dis* **42**, 209-216, doi:[https://doi.org/10.1016/s0033-0620\(99\)70003-4](https://doi.org/10.1016/s0033-0620(99)70003-4) (1999).
- 159 Giraud, M. *et al.* Early Blood Brain Barrier Changes in Acute Ischemic Stroke: A Sequential MRI Study. *J Neuroimaging* **25**, 959-963, doi:<https://doi.org/10.1111/jon.12225> (2015).
- 160 Keaney, J. & Campbell, M. The dynamic blood-brain barrier. *FEBS J* **282**, 4067-4079, doi:<https://doi.org/10.1111/febs.13412> (2015).

- 161 Sweeney, M. D., Zhao, Z., Montagne, A., Nelson, A. R. & Zlokovic, B. V. Blood-Brain Barrier: From Physiology to Disease and Back. *Physiol Rev* **99**, 21-78, doi:<https://doi.org/10.1152/physrev.00050.2017> (2019).
- 162 Pillai, D. R. *et al.* Cerebral ischemia-reperfusion injury in rats-A 3 T MRI study on biphasic blood-brain barrier opening and the dynamics of edema formation. *J Cereb Blood Flow Metab* **29**, 1846-1855, doi:<https://doi.org/10.1038/jcbfm.2009.106> (2009).
- 163 Sandoval, K. E. & Witt, K. A. Blood-brain barrier tight junction permeability and ischemic stroke. *Neurobiol Dis* **32**, 200-219, doi:<https://doi.org/10.1016/j.nbd.2008.08.005> (2008).
- 164 Luissint, A. C., Artus, C., Glacial, F., Ganeshamoorthy, K. & Couraud, P. O. Tight junctions at the blood brain barrier: physiological architecture and disease-associated dysregulation. *Fluids Barriers CNS* **9**, 23, doi:<https://doi.org/10.1186/2045-8118-9-23> (2012).
- 165 Li, F. *et al.* Upregulation of lipoprotein receptors on brain endothelial cells and neurons in the early phase of ischemic stroke in mice. *J Med Dent Sci* **65**, 59-71, doi:<https://doi.org/10.11480/jmds.650203> (2018).
- 166 Suzuki, Y. *et al.* Tissue-type plasminogen activator (t-PA) induces stromelysin-1 (MMP-3) in endothelial cells through activation of lipoprotein receptor-related protein. *Blood* **114**, 3352-3358, doi:<https://doi.org/10.1182/blood-2009-02-203919> (2009).
- 167 Suzuki, Y. *et al.* Recombinant tissue-type plasminogen activator transiently enhances blood-brain barrier permeability during cerebral ischemia through vascular endothelial growth factor-mediated endothelial endocytosis in mice. *J Cereb Blood Flow Metab* **35**, 2021-2031, doi:<https://doi.org/10.1038/jcbfm.2015.167> (2015).
- 168 Ennis, S. R. & Keep, R. F. The effects of cerebral ischemia on the rat choroid plexus. *J Cereb Blood Flow Metab* **26**, 675-683, doi:<https://doi.org/10.1038/sj.jcbfm.9600224> (2006).
- 169 Ferrand-Drake, M. Cell death in the choroid plexus following transient forebrain global ischemia in the rat. *Microsc Res Tech* **52**, 130-136, doi:[https://doi.org/10.1002/1097-0029\(20010101\)52:1<130::AID-JEMT14>3.0.CO;2-6](https://doi.org/10.1002/1097-0029(20010101)52:1<130::AID-JEMT14>3.0.CO;2-6) (2001).
- 170 Johanson, C. E. *et al.* Choroid plexus recovery after transient forebrain ischemia: role of growth factors and other repair mechanisms. *Cell Mol Neurobiol* **20**, 197-216, doi:<https://doi.org/10.1023/a:1007097622590> (2000).
- 171 Palm, D. E., Knuckey, N. W., Primiano, M. J., Spangenberg, A. G. & Johanson, C. E. Cystatin C, a protease inhibitor, in degenerating rat hippocampal neurons following transient forebrain ischemia. *Brain Res* **691**, 1-8, doi:[https://doi.org/10.1016/0006-8993\(95\)00520-z](https://doi.org/10.1016/0006-8993(95)00520-z) (1995).
- 172 Johanson, C. *et al.* *Blood-Spinal Cord and Brain Barriers in Health and Disease*. (2003).
- 173 Nadler, J. V. Plasticity of glutamate synaptic mechanisms. *Epilepsia* **51**, 17-17, doi:<https://doi.org/10.1111/j.1528-1167.2010.02803.x> (2010).
- 174 Featherstone, D. E. & Shippy, S. A. Regulation of synaptic transmission by ambient extracellular glutamate. *Neuroscientist* **14**, 171-181, doi:<https://doi.org/10.1177/1073858407308518> (2008).
- 175 Tucci, S., Pinto, C., Goyo, J., Rada, P. & Hernandez, L. Measurement of glutamine and glutamate by capillary electrophoresis and laser induced fluorescence detection in cerebrospinal fluid of meningitis sick children. *Clin Biochem* **31**, 143-150, doi:[https://doi.org/10.1016/S0009-9120\(98\)00003-4](https://doi.org/10.1016/S0009-9120(98)00003-4) (1998).
- 176 Danbolt, N. C. Glutamate uptake. *Prog Neurobiol* **65**, 1-105,

- doi:[https://doi.org/10.1016/S0301-0082\(00\)00067-8](https://doi.org/10.1016/S0301-0082(00)00067-8) (2001).
- 177 Rainesalo, S. *et al.* Plasma and cerebrospinal fluid amino acids in epileptic patients. *Neurochem Res* **29**, 319-324, doi:<https://doi.org/10.1023/B:NERE.0000010461.34920.0c> (2004).
- 178 Castillo, J. *et al.* A novel mechanism of neuroprotection: Blood glutamate grabber. *J Cerebr Blood F Met* **36**, 292-301, doi:<https://doi.org/10.1177/0271678x15606721> (2016).
- 179 Cooper, A. J. & Jeitner, T. M. Central Role of Glutamate Metabolism in the Maintenance of Nitrogen Homeostasis in Normal and Hyperammonemic Brain. *Biomolecules* **6**, doi:<https://doi.org/10.3390/biom6020016> (2016).
- 180 Meldrum, B. & Garthwaite, J. Excitatory amino acid neurotoxicity and neurodegenerative disease. *Trends Pharmacol Sci* **11**, 379-387, doi:[https://doi.org/10.1016/0165-6147\(90\)90184-a](https://doi.org/10.1016/0165-6147(90)90184-a) (1990).
- 181 Rosenberg, P. A., Amin, S. & Leitner, M. Glutamate uptake disguises neurotoxic potency of glutamate agonists in cerebral cortex in dissociated cell culture. *J Neurosci* **12**, 56-61, doi:<https://doi.org/10.1523/JNEUROSCI.12-01-00056.1992> (1992).
- 182 Huang, H. & van den Pol, A. N. Rapid direct excitation and long-lasting enhancement of NMDA response by group I metabotropic glutamate receptor activation of hypothalamic melanin-concentrating hormone neurons. *J Neurosci* **27**, 11560-11572, doi:<https://doi.org/10.1523/JNEUROSCI.2147-07.2007> (2007).
- 183 Ribeiro, F. M., Vieira, L. B., Pires, R. G. W., Olmo, R. P. & Ferguson, S. S. G. Metabotropic glutamate receptors and neurodegenerative diseases. *Pharmacol Rev* **115**, 179-191, doi:<https://doi.org/10.1016/j.phrs.2016.11.013> (2017).
- 184 Gillard, S. E., Tzaferis, J., Tsui, H. C. T. & Kingston, A. E. Expression of metabotropic glutamate receptors in rat meningeal and brain microvasculature and choroid plexus. *J Comp Neurol* **461**, 317-332, doi:<https://doi.org/10.1002/cne.10671> (2003).
- 185 Parfenova, H., Fedinec, A. & Leffler, C. W. Ionotropic glutamate receptors in cerebral microvascular endothelium are functionally linked to heme oxygenase. *J Cerebr Blood F Met* **23**, 190-197, doi:<https://doi.org/10.1097/01.Wcb.000004823561824.C4> (2003).
- 186 Hoft, S., Griemsmann, S., Seifert, G. & Steinhauser, C. Heterogeneity in expression of functional ionotropic glutamate and GABA receptors in astrocytes across brain regions: insights from the thalamus. *Philos T R Soc B* **369**, doi:<https://doi.org/10.1098/rstb.2013.0602> (2014).
- 187 Conn, P. J. & Pin, J. P. Pharmacology and functions of metabotropic glutamate receptors. *Annu Rev Pharmacol Toxicol* **37**, 205-237, doi:<https://doi.org/10.1146/annurev.pharmtox.37.1.205> (1997).
- 188 Ribeiro, F. M., Paquet, M., Cregan, S. P. & Ferguson, S. S. Group I metabotropic glutamate receptor signalling and its implication in neurological disease. *CNS Neurol Disord Drug Targets* **9**, 574-595, doi:<https://doi.org/10.2174/187152710793361612> (2010).
- 189 Crupi, R., Impellizzeri, D. & Cuzzocrea, S. Role of Metabotropic Glutamate Receptors in Neurological Disorders. *Front Mol Neurosci* **12**, 20, doi:<https://doi.org/10.3389/fnmol.2019.00020> (2019).
- 190 Willard, S. S. & Koochekpour, S. Glutamate, Glutamate Receptors, and Downstream Signaling Pathways. *Int J Biol Sci* **9**, 948-959, doi:<https://doi.org/10.7150/ijbs.6426> (2013).
- 191 Niswender, C. M. & Conn, P. J. Metabotropic glutamate receptors: physiology, pharmacology, and disease. *Annu Rev Pharmacol Toxicol* **50**, 295-322,

- doi:<https://doi.org/10.1146/annurev.pharmtox.011008.145533> (2010).
- 192 Ferraguti, F. & Shigemoto, R. Metabotropic glutamate receptors. *Cell Tissue Res* **326**, 483-504, doi:<https://doi.org/10.1007/s00441-006-0266-5> (2006).
- 193 Snyder, E. M. *et al.* Internalization of ionotropic glutamate receptors in response to mGluR activation. *Nat Neurosci* **4**, 1079-1085, doi:<https://doi.org/10.1038/nn746> (2001).
- 194 Xiao, M. Y., Zhou, Q. & Nicoll, R. A. Metabotropic glutamate receptor activation causes a rapid redistribution of AMPA receptors. *Neuropharmacology* **41**, 664-671, doi:[https://doi.org/10.1016/s0028-3908\(01\)00134-4](https://doi.org/10.1016/s0028-3908(01)00134-4) (2001).
- 195 Gegelashvili, G., Dehnes, Y., Danbolt, N. C. & Schousboe, A. The high-affinity glutamate transporters GLT1, GLAST, and EAAT4 are regulated via different signalling mechanisms. *Neurochem Int* **37**, 163-170, doi:[https://doi.org/10.1016/s0197-0186\(00\)00019-x](https://doi.org/10.1016/s0197-0186(00)00019-x) (2000).
- 196 Rosenmund, C., Stern-Bach, Y. & Stevens, C. F. The tetrameric structure of a glutamate receptor channel. *Science* **280**, 1596-1599, doi:<https://doi.org/10.1126/science.280.5369.1596> (1998).
- 197 Blanke, M. L. & VanDongen, A. M. J. in *Biology of the NMDA Receptor* (ed Van Dongen AM) Ch. 13, (Taylor & Francis Group, LLC., 2009).
- 198 Kumagai, A. *et al.* Monitoring of glutamate-induced excitotoxicity by mitochondrial oxygen consumption. *Synapse* **73**, doi:<https://doi.org/10.1002/syn.22067> (2019).
- 199 Hazell, A. S. Excitotoxic mechanisms in stroke: An update of concepts and treatment strategies. *Neurochem Int* **50**, 941-953, doi:<https://doi.org/10.1016/j.neuint.2007.04.026> (2007).
- 200 Tymianski, M., Charlton, M. P., Carlen, P. L. & Tator, C. H. Source Specificity of Early Calcium Neurotoxicity in Cultured Embryonic Spinal Neurons. *J Neurosci* **13**, 2085-2104 (1993).
- 201 Girling, K. D. *et al.* Activation of caspase-6 and cleavage of caspase-6 substrates is an early event in NMDA receptor-mediated excitotoxicity. *J Neurosci Res* **96**, 391-406, doi:<https://doi.org/10.1002/jnr.24153> (2018).
- 202 Hu, W. H., Walters, W. M., Xia, X. M., Karmally, S. A. & Bethea, J. R. Neuronal glutamate transporter EAAT4 is expressed in astrocytes. *Glia* **44**, 13-25, doi:<https://doi.org/10.1002/glia.10268> (2003).
- 203 Gendreau, S. *et al.* A trimeric quaternary structure is conserved in bacterial and human glutamate transporters. *J Biol Chem* **279**, 39505-39512, doi:<https://doi.org/10.1074/jbc.M408038200> (2004).
- 204 Fairman, W. A., Vandenberg, R. J., Arriza, J. L., Kavanaugh, M. P. & Amara, S. G. An excitatory amino-acid transporter with properties of a ligand-gated chloride channel. *Nature* **375**, 599-603, doi:<https://doi.org/10.1038/375599a0> (1995).
- 205 Massie, A. *et al.* High-affinity Na<sup>+</sup>/K<sup>+</sup>-dependent glutamate transporter EAAT4 is expressed throughout the rat fore- and midbrain. *J Comp Neurol* **511**, 155-172, doi:<https://doi.org/10.1002/cne.21823> (2008).
- 206 Arriza, J. L., Eliasof, S., Kavanaugh, M. P. & Amara, S. G. Excitatory amino acid transporter 5, a retinal glutamate transporter coupled to a chloride conductance. *P Natl Acad Sci USA* **94**, 4155-4160, doi:<https://doi.org/10.1073/pnas.94.8.4155> (1997).
- 207 Rothstein, J. D. *et al.* Localization of neuronal and glial glutamate transporters. *Neuron* **13**, 713-725, doi:[https://doi.org/10.1016/0896-6273\(94\)90038-8](https://doi.org/10.1016/0896-6273(94)90038-8) (1994).
- 208 Coco, S. *et al.* Non-synaptic localization of the glutamate transporter EAAC1 in cultured

- hippocampal neurons. *Eur J Neurosci* **9**, 1902-1910, doi:<https://doi.org/10.1111/j.1460-9568.1997.tb00757.x> (1997).
- 209 Shashidharan, P. *et al.* Immunohistochemical localization of the neuron-specific glutamate transporter EAAC1 (EAAT3) in rat brain and spinal cord revealed by a novel monoclonal antibody. *Brain Res* **773**, 139-148, doi:[https://doi.org/10.1016/s0006-8993\(97\)00921-9](https://doi.org/10.1016/s0006-8993(97)00921-9) (1997).
- 210 Holmseth, S. *et al.* The density of EAAC1 (EAAT3) glutamate transporters expressed by neurons in the mammalian CNS. *J Neurosci* **32**, 6000-6013, doi:<https://doi.org/10.1523/JNEUROSCI.5347-11.2012> (2012).
- 211 Kim, K. *et al.* Role of Excitatory Amino Acid Transporter-2 (EAAT2) and Glutamate in Neurodegeneration: Opportunities for Developing Novel Therapeutics. *J Cell Physiol* **226**, 2484-2493, doi:<https://doi.org/10.1002/jcp.22609> (2011).
- 212 O'Kane, R. L., Martinez-Lopez, I., DeJoseph, M. R., Vina, J. R. & Hawkins, R. A. Na<sup>+</sup>-dependent glutamate transporters (EAAT1, EAAT2, and EAAT3) of the blood-brain barrier - A mechanism for glutamate removal. *J Biol Chem* **274**, 31891-31895, doi:<https://doi.org/10.1074/jbc.274.45.31891> (1999).
- 213 Leibowitz, A., Boyko, M., Shapira, Y. & Zlotnik, A. Blood Glutamate Scavenging: Insight into Neuroprotection. *Int J Mol Sci* **13**, 10041-10066, doi:10.3390/ijms130810041 (2012).
- 214 Jia, M., Njapo, S. A. N., Rastogi, V. & Hedna, V. S. Taming Glutamate Excitotoxicity: Strategic Pathway Modulation for Neuroprotection. *Cns Drugs* **29**, 153-162, doi:<https://doi.org/10.1007/s40263-015-0225-3> (2015).
- 215 Holmseth, S. *et al.* The Density of EAAC1 (EAAT3) Glutamate Transporters Expressed by Neurons in the Mammalian CNS. *J Neurosci* **32**, 6000-6013, doi:<https://doi.org/10.1523/Jneurosci.5347-11.2012> (2012).
- 216 Akanuma, S., Sakurai, T., Tachikawa, M., Kubo, Y. & Hosoya, K. Transporter-mediated L-glutamate elimination from cerebrospinal fluid: possible involvement of excitatory amino acid transporters expressed in ependymal cells and choroid plexus epithelial cells. *Fluids Barriers CNS* **12**, doi:ARTN 11  
10.1186/s12987-015-0006-x (2015).
- 217 Jardetzky, O. Simple allosteric model for membrane pumps. *Nature* **211**, 969-970, doi:<https://doi.org/10.1038/211969a0> (1966).
- 218 Reyes, N., Ginter, C. & Boudker, O. Transport mechanism of a bacterial homologue of glutamate transporters. *Nature* **462**, 880-885, doi:<https://doi.org/10.1038/nature08616> (2009).
- 219 Drew, D. & Boudker, O. Shared Molecular Mechanisms of Membrane Transporters. *Annu Rev Biochem* **85**, 543-572, doi:<https://doi.org/10.1146/annurev-biochem-060815-014520> (2016).
- 220 Mim, C., Balani, P., Rauen, T. & Grever, C. The glutamate transporter subtypes EAAT4 and EAATs 1-3 transport glutamate with dramatically different kinetics and voltage dependence but share a common uptake mechanism. *J Gen Physiol* **126**, 571-589, doi:<https://doi.org/10.1085/jgp.200509365> (2005).
- 221 Owe, S. G., Marcaggi, P. & Attwell, D. The ionic stoichiometry of the GLAST glutamate transporter in salamander retinal glia. *J Physiol-London* **577**, 591-599, doi:<https://doi.org/10.1113/jphysiol.2006.116830> (2006).
- 222 Zerangue, N. & Kavanaugh, M. P. Flux coupling in a neuronal glutamate transporter. *Nature* **383**, 634-637, doi:<https://doi.org/10.1038/383634a0> (1996).

- 223 Vandenberg, R. J. & Ryan, R. M. Mechanisms of Glutamate Transport. *Physiol Rev* **93**, 1621-1657, doi:<https://doi.org/10.1152/physrev.00007.2013> (2013).
- 224 Wadiche, J. I., Amara, S. G. & Kavanaugh, M. P. Ion fluxes associated with excitatory amino acid transport. *Neuron* **15**, 721-728, doi:[https://doi.org/10.1016/0896-6273\(95\)90159-0](https://doi.org/10.1016/0896-6273(95)90159-0) (1995).
- 225 Magistretti, P. J., Pellerin, L., Rothman, D. L. & Shulman, R. G. Neuroscience - Energy on demand. *Science* **283**, 496-497, doi:<https://doi.org/10.1126/science.283.5401.496> (1999).
- 226 Sibson, N. R. *et al.* Stoichiometric coupling of brain glucose metabolism and glutamatergic neuronal activity. *P Natl Acad Sci USA* **95**, 316-321, doi:<https://doi.org/10.1073/pnas.95.1.316> (1998).
- 227 Weller, M. L. *et al.* Selective overexpression of excitatory amino acid transporter 2 (EAAT2) in astrocytes enhances neuroprotection from moderate but not severe hypoxia-ischemia. *Neuroscience* **155**, 1204-1211, doi:<https://doi.org/10.1016/j.neuroscience.2008.05.059> (2008).
- 228 Arranz, A. M., Gottlieb, M., Perez-Cerda, F. & Matute, C. Increased expression of glutamate transporters in subcortical white matter after transient focal cerebral ischemia. *Neurobiol Dis* **37**, 156-165, doi:<https://doi.org/10.1016/j.nbd.2009.09.019> (2010).
- 229 Fukamachi, S. *et al.* Altered expressions of glutamate transporter subtypes in rat model of neonatal cerebral hypoxia-ischemia. *Brain Res Dev Brain Res* **132**, 131-139, doi:[https://doi.org/10.1016/s0165-3806\(01\)00303-0](https://doi.org/10.1016/s0165-3806(01)00303-0) (2001).
- 230 Rao, V. L., Bowen, K. K. & Dempsey, R. J. Transient focal cerebral ischemia down-regulates glutamate transporters GLT-1 and EAAC1 expression in rat brain. *Neurochem Res* **26**, 497-502, doi:<https://doi.org/10.1023/a:1010956711295> (2001).
- 231 Almqvist, J., Huang, Y., Laaksonen, A., Wang, D. N. & Hovmoller, S. Docking and homology modeling explain inhibition of the human vesicular glutamate transporters. *Protein Sci* **16**, 1819-1829, doi:<https://doi.org/10.1110/ps.072944707> (2007).
- 232 Krzyzanowska, W., Pomierny, B., Filip, M. & Pera, J. Glutamate transporters in brain ischemia: to modulate or not? *Acta Pharmacol Sin* **35**, 444-462, doi:<https://doi.org/10.1038/aps.2014.1>.
- 233 Martineau, M., Guzman, R. E., Fahlke, C. & Klingauf, J. VGLUT1 functions as a glutamate/proton exchanger with chloride channel activity in hippocampal glutamatergic synapses. *Nat Commun* **8**, doi:<https://doi.org/10.1038/s41467-017-02367-6> (2017).
- 234 Schousboe, A., Scafidi, S., Bak, L. K., Waagepetersen, H. S. & McKenna, M. C. Glutamate metabolism in the brain focusing on astrocytes. *Adv Neurobiol* **11**, 13-30, doi:[https://doi.org/10.1007/978-3-319-08894-5\\_2](https://doi.org/10.1007/978-3-319-08894-5_2) (2014).
- 235 Coulter, D. A. & Eid, T. Astrocytic regulation of glutamate homeostasis in epilepsy. *Glia* **60**, 1215-1226, doi:<https://doi.org/10.1002/glia.22341> (2012).
- 236 Mahan, V. L. Neurointegrity and neurophysiology: astrocyte, glutamate, and carbon monoxide interactions. *Med Gas Res* **9**, 24-45, doi:<https://doi.org/10.4103/2045-9912.254639> (2019).
- 237 Qutub, A. A. & Hunt, C. A. Glucose transport to the brain: a systems model. *Brain Res Brain Res Rev* **49**, 595-617, doi:<https://doi.org/10.1016/j.brainresrev.2005.03.002> (2005).
- 238 Pellerin, L. *et al.* Evidence supporting the existence of an activity-dependent astrocyte-neuron lactate shuttle. *Dev Neurosci* **20**, 291-299,

- doi:<https://doi.org/10.1159/000017324> (1998).
- 239 Stobart, J. L. & Anderson, C. M. Multifunctional role of astrocytes as gatekeepers of neuronal energy supply. *Front Cell Neurosci* **7**, doi:ARTN 38 10.3389/fncel.2013.00038 (2013).
- 240 Daikhin, Y. & Yudkoff, M. Compartmentation of brain glutamate metabolism in neurons and glia. *Journal of Nutrition* **130**, 1026s-1031s, doi:<https://doi.org/10.1093/jn/130.4.1026S> (2000).
- 241 Norenberg, M. D. & Martinez-Hernandez, A. Fine structural localization of glutamine synthetase in astrocytes of rat brain. *Brain Res* **161**, 303-310, doi:[https://doi.org/10.1016/0006-8993\(79\)90071-4](https://doi.org/10.1016/0006-8993(79)90071-4) (1979).
- 242 Hertz, L. The Glutamate-Glutamine (GABA) Cycle: Importance of Late Postnatal Development and Potential Reciprocal Interactions between Biosynthesis and Degradation. *Front Endocrinol (Lausanne)* **4**, 59, doi:<https://doi.org/10.3389/fendo.2013.00059> (2013).
- 243 Broer, S. & Brookes, N. Transfer of glutamine between astrocytes and neurons. *J Neurochem* **77**, 705-719, doi:<https://doi.org/10.1046/j.1471-4159.2001.00322.x> (2001).
- 244 Allaman, I., Belanger, M. & Magistretti, P. J. Astrocyte-neuron metabolic relationships: for better and for worse. *Trends Neurosci* **34**, 76-87, doi:<https://doi.org/10.1016/j.tins.2010.12.001> (2011).
- 245 Chaudhry, F. A. *et al.* Glutamine uptake by neurons: interaction of protons with system a transporters. *J Neurosci* **22**, 62-72, doi:<https://doi.org/10.1523/JNEUROSCI.22-01-00062.2002> (2002).
- 246 Nicholls, D. G. Release of glutamate, aspartate, and gamma-aminobutyric acid from isolated nerve terminals. *J Neurochem* **52**, 331-341, doi:<https://doi.org/10.1111/j.1471-4159.1989.tb09126.x> (1989).
- 247 O'Kane, R. L., Martinez-Lopez, I., DeJoseph, M. R., Vina, J. R. & Hawkins, R. A. Na(+)-dependent glutamate transporters (EAAT1, EAAT2, and EAAT3) of the blood-brain barrier. A mechanism for glutamate removal. *J Biol Chem* **274**, 31891-31895, doi:<https://doi.org/10.1074/jbc.274.45.31891> (1999).
- 248 Helms, H. C. *et al.* Characterization of the L-glutamate clearance pathways across the blood-brain barrier and the effect of astrocytes in an in vitro blood-brain barrier model. *J Cereb Blood Flow Metab* **37**, 3744-3758, doi:<https://doi.org/10.1177/0271678X17690760> (2017).
- 249 Cederberg, H. H., Uhd, N. C. & Brodin, B. Glutamate efflux at the blood-brain barrier: cellular mechanisms and potential clinical relevance. *Arch Med Res* **45**, 639-645, doi:<https://doi.org/10.1016/j.arcmed.2014.11.004>.
- 250 Hull, J. *et al.* Distribution of the branched chain aminotransferase proteins in the human brain and their role in glutamate regulation. *J Neurosci* **123**, 997-1009, doi:<https://doi.org/10.1111/jnc.12044> (2012).
- 251 Pierre, K. & Pellerin, L. Monocarboxylate transporters in the central nervous system: distribution, regulation and function. *J Neurosci* **94**, 1-14, doi:<https://doi.org/10.1111/j.1471-4159.2005.03168.x> (2005).
- 252 Lee, W. J., Hawkins, R. A., Vina, J. R. & Peterson, D. R. Glutamine transport by the blood-brain barrier: a possible mechanism for nitrogen removal. *Am J Physiol Cell Physiol* **274**, C1101-C1107 (1998).
- 253 Oldendorf, W. H. & Szabo, J. Amino acid assignment to one of three blood-brain barrier

- amino acid carriers. *Am J Physiol* **230**, 94-98, doi:<https://doi.org/10.1152/ajplegacy.1976.230.1.94> (1976).
- 254 Ishikawa, M. Abnormalities in glutamate metabolism and excitotoxicity in the retinal diseases. *Scientifica (Cairo)* **2013**, 528940, doi:<https://doi.org/10.1155/2013/528940> (2013).
- 255 Mark, L. P. *et al.* Pictorial review of glutamate excitotoxicity: fundamental concepts for neuroimaging. *AJNR Am J Neuroradiol* **22**, 1813-1824, doi:PMID: 11733308 (2001).
- 256 Schubert, P., Keller, F., Nakamura, Y. & Rudolphi, K. The use of ion-sensitive electrodes and fluorescence imaging in hippocampal slices for studying pathological changes of intracellular Ca<sup>2+</sup> regulation. *J Neural Transm Suppl* **44**, 73-85, doi:[https://doi.org/10.1007/978-3-7091-9350-1\\_6](https://doi.org/10.1007/978-3-7091-9350-1_6) (1994).
- 257 Terasaki, Y. *et al.* Mechanisms of Neurovascular Dysfunction in Acute Ischemic Brain. *Curr Med Chem* **21**, 2035-2042, doi:<https://doi.org/10.2174/0929867321666131228223400> (2014).
- 258 Basuroy, S., Leffler, C. W. & Parfenova, H. CORM-A1 prevents blood-brain barrier dysfunction caused by ionotropic glutamate receptor-mediated endothelial oxidative stress and apoptosis. *Am J Physiol Cell Physiol* **304**, C1105-1115, doi:<https://doi.org/10.1152/ajpcell.00023.2013> (2013).
- 259 George, P. M. & Steinberg, G. K. Novel Stroke Therapeutics: Unraveling Stroke Pathophysiology and Its Impact on Clinical Treatments. *Neuron* **87**, 297-309, doi:<https://doi.org/10.1016/j.neuron.2015.05.041> (2015).
- 260 Matthews, C. C., Zielke, H. R., Wollack, J. B. & Fishman, P. S. Enzymatic degradation protects neurons from glutamate excitotoxicity. *J Neurochem* **75**, 1045-1052, doi:<https://doi.org/10.1046/j.1471-4159.2000.0751045.x> (2000).
- 261 Gorovits, R., Avidan, N., Avisar, N., Shaked, I. & Vardimon, L. Glutamine synthetase protects against neuronal degeneration in injured retinal tissue. *P Natl Acad Sci USA* **94**, 7024-7029, doi:<https://doi.org/10.1073/pnas.94.13.7024> (1997).
- 262 Blitzblau, R., Gupta, S., Djali, S., Robinson, M. B. & Rosenberg, P. A. The glutamate transport inhibitor L-trans-pyrrolidine-2,4-dicarboxylate indirectly evokes NMDA receptor mediated neurotoxicity in rat cortical cultures. *Eur J Neurosci* **8**, 1840-1852, doi:<https://doi.org/10.1111/j.1460-9568.1996.tb01328.x> (1996).
- 263 Volterra, A. *et al.* The competitive transport inhibitor L-trans-pyrrolidine-2, 4-dicarboxylate triggers excitotoxicity in rat cortical neuron-astrocyte co-cultures via glutamate release rather than uptake inhibition. *Eur J Neurosci* **8**, 2019-2028, doi:<https://doi.org/10.1111/j.1460-9568.1996.tb01345.x> (1996).
- 264 Pardridge, W. M. Blood-brain barrier delivery. *Drug Discov Today* **12**, 54-61, doi:<https://doi.org/10.1016/j.drudis.2006.10.013> (2007).
- 265 Merk, A. *et al.* Breaking Cryo-EM Resolution Barriers to Facilitate Drug Discovery. *Cell* **165**, 1698-1707, doi:<https://doi.org/10.1016/j.cell.2016.05.040> (2016).
- 266 Banerjee, S., Schmidt, T., Fang, J., Stanley, C. A. & Smith, T. J. Structural studies on ADP activation of mammalian glutamate dehydrogenase and the evolution of regulation. *Biochem J* **42**, 3446-3456, doi:<https://doi.org/10.1021/bi0206917> (2003).
- 267 Plaitakis, A., Kalef-Ezra, E., Kotzamani, D., Zaganas, I. & Spanaki, C. The Glutamate Dehydrogenase Pathway and Its Roles in Cell and Tissue Biology in Health and Disease. *Biology-Basel* **6**, doi:<https://doi.org/10.3390/biology6010011> (2017).
- 268 Smith, T. J. & Stanley, C. A. Untangling the glutamate dehydrogenase allosteric nightmare. *Trends Biochem. Sci.* **33**, 557-564, doi:<https://doi.org/10.1016/j.tibs.2008.07.007> (2008).

- 269 Smith, T. J. *et al.* The structure of apo human glutamate dehydrogenase details subunit communication and allostery. *J Mol Biol* **318**, 765-777, doi:[https://doi.org/10.1016/S0022-2836\(02\)00161-4](https://doi.org/10.1016/S0022-2836(02)00161-4) (2002).
- 270 Li, M., Li, C., Allen, A., Stanley, C. A. & Smith, T. J. The structure and allosteric regulation of glutamate dehydrogenase. *Neurochem. Int.* **59**, 445-455, doi:<https://doi.org/10.1016/j.neuint.2010.10.017> (2011).
- 271 Li, M., Li, C., Allen, A., Stanley, C. A. & Smith, T. J. The structure and allosteric regulation of mammalian glutamate dehydrogenase. *Arch. Biochem. Biophys.* **519**, 69-80, doi:<https://doi.org/10.1016/j.abb.2011.10.015> (2012).
- 272 Arce, C., Canadas, S., Oset-Gasque, M. J., Castro, E. & Gonzalez, M. P. Glutamate dehydrogenase: some properties of the rat brain enzyme from different cellular compartments. *Comp Biochem Physiol C Comp Pharmacol Toxicol* **97**, 265-267, doi:[https://doi.org/10.1016/0742-8413\(90\)90139-z](https://doi.org/10.1016/0742-8413(90)90139-z) (1990).
- 273 Plaitakis, A., Kalef-Ezra, E., Kotzamani, D., Zaganas, I. & Spanaki, C. The Glutamate Dehydrogenase Pathway and Its Roles in Cell and Tissue Biology in Health and Disease. *Biology (Basel)* **6**, doi:10.3390/biology6010011 (2017).
- 274 Cooper, A. J. 13N as a tracer for studying glutamate metabolism. *Neurochem Int* **59**, 456-464, doi:<https://doi.org/10.1016/j.neuint.2010.11.011> (2011).
- 275 Westergaard, N., Drejer, J., Schousboe, A. & Sonnewald, U. Evaluation of the importance of transamination versus deamination in astrocytic metabolism of [U-13C]glutamate. *Glia* **17**, 160-168, doi:[https://doi.org/10.1002/\(SICI\)1098-1136\(199606\)17:2<160::AID-GLIA7>3.0.CO;2-6](https://doi.org/10.1002/(SICI)1098-1136(199606)17:2<160::AID-GLIA7>3.0.CO;2-6) (1996).
- 276 Cooper, A. J. & Jeitner, T. M. Central role of glutamate metabolism in the maintenance of nitrogen homeostasis in normal and hyperammonemic brain. *Biomolecules* **6**, 16 (2016).
- 277 Engel, P. & Dalziel, K. Kinetic studies of glutamate dehydrogenase with glutamate and norvaline as substrates. Coenzyme activation and negative homotropic interactions in allosteric enzymes. *Biochem. J.* **115**, 621-631, doi:<https://doi.org/10.1042/bj1150621> (1969).
- 278 Engel, P. & Dalziel, K. Kinetic studies of glutamate dehydrogenase with glutamate and norvaline as substrates. Coenzyme activation and negative homotropic interactions in allosteric enzymes. *Biochem J* **115**, 621-631 (1969).
- 279 Bailey, J., Bell, E. T. & Bell, J. E. Regulation of Bovine Glutamate-Dehydrogenase - the Effects of Ph and Adp. *J Biol Chem* **257**, 5579-5583 (1982).
- 280 Li, M., Allen, A. & Smith, T. J. High throughput screening reveals several new classes of glutamate dehydrogenase inhibitors. *Biochemistry* **46**, 15089-15102, doi:<https://doi.org/10.1021/bi7018783> (2007).
- 281 Bell, J. E. & Dalziel, K. A conformational transition of the oligomer of glutamate dehydrogenase induced by half-saturation with NAD<sup>+</sup> or NADP<sup>+</sup>. *Biochimica et Biophysica Acta (BBA)-Enzymology* **309**, 237-242 (1973).
- 282 Melzi d'Eril, G. & Dalziel, K. Negative co-operativity in glutamate dehydrogenase: coenzyme-binding studies. *Biochem J* **130**, 3P-3P (1972).
- 283 Rasool, C. G., Nicolaidis, S. & Akhtar, M. The asymmetric distribution of enzymic activity between the six subunits of bovine liver glutamate dehydrogenase. Use of d- and l-glutamyl  $\alpha$ -chloromethyl ketones (4-amino-6-chloro-5-oxohexanoic acid). *Biochem J* **157**, 675-686 (1976).
- 284 Smith, T. J., Peterson, P. E., Schmidt, T., Fang, J. & Stanley, C. A. Structures of bovine glutamate dehydrogenase complexes elucidate the mechanism of purine regulation.

- Journal of Molecular Biology* **307**, 707-720, doi:10.1006/jmbi.2001.4499 (2001).
- 285 Li, M., Smith, C. J., Walker, M. T. & Smith, T. J. Novel Inhibitors Complexed with Glutamate Dehydrogenase ALLOSTERIC REGULATION BY CONTROL OF PROTEIN DYNAMICS. *J Biol Chem* **284**, 22988-23000, doi:<https://doi.org/10.1074/jbc.M109.020222> (2009).
- 286 Bell, E. T., Stilwell, A. M. & Bell, J. E. Interaction of Zn<sup>2+</sup> and Eu<sup>3+</sup> with bovine liver glutamate dehydrogenase. *Biochem J* **246**, 199-203, doi:<https://doi.org/10.1042/bj2460199> (1987).
- 287 Frieden, C. Glutamate Dehydrogenase. Vi. Survey of Purine Nucleotide and Other Effects on the Enzyme from Various Sources. *J Biol Chem* **240**, 2028-2035, doi:PMID: 14299621 (1965).
- 288 Bailey, J. *et al.* A novel mechanism of V-type zinc inhibition of glutamate dehydrogenase results from disruption of subunit interactions necessary for efficient catalysis. *FEBS J.* **278**, 3140-3151, doi:<https://doi.org/10.1111/j.1742-4658.2011.08240.x> (2011).
- 289 Li, M., Smith, C. J., Walker, M. T. & Smith, T. J. Novel inhibitors complexed with glutamate dehydrogenase: allosteric regulation by control of protein dynamics. *J. Biol. Chem.* **284**, 22988-23000, doi:<https://doi.org/10.1074/jbc.m109.020222> (2009).
- 290 Prough, R. A., Culver, J. M. & Fisher, H. F. The mechanism of activation of glutamate dehydrogenase-catalyzed reactions by two different, cooperatively bound activators. *J Biol Chem* **248**, 8528-8533, doi:PMID: 4148674 (1973).
- 291 Kanavouras, K., Mastorodemos, V., Borompokas, N., Spanaki, C. & Plaitakis, A. Properties and molecular evolution of human GLUD2 (neural and testicular tissue-specific) glutamate dehydrogenase. *J Neurosci Res* **85**, 3398-3406, doi:<https://doi.org/10.1002/jnr.21576> (2007).
- 292 Plaitakis, A., Metaxari, M. & Shashidharan, P. Nerve tissue-specific (GLUD2) and housekeeping (GLUD1) human glutamate dehydrogenases are regulated by distinct allosteric mechanisms: implications for biologic function. *J Neurochem* **75**, 1862-1869, doi:<https://doi.org/10.1046/j.1471-4159.2000.0751862.x> (2000).
- 293 Badawi, Y., Pal, R., Hui, D. W., Michaelis, E. K. & Shi, H. L. Ischemic Tolerance in an In Vivo Model of Glutamate Preconditioning. *J Neurosci Res* **93**, 623-632, doi:10.1002/jnr.23517 (2015).
- 294 Jeong, S. Y. *et al.* Systemic delivery and preclinical evaluation of Au nanoparticle containing beta-lapachone for radiosensitization. *J Control Release* **139**, 239-245, doi:<https://doi.org/10.1016/j.jconrel.2009.07.007> (2009).
- 295 Pink, J. J. *et al.* NAD(P)H : quinone oxidoreductase activity is the principal determinant of beta-lapachone cytotoxicity. *J Biol Chem* **275**, 5416-5424, doi:<https://doi.org/10.1074/jbc.275.8.5416> (2000).
- 296 Dubin, M., Fernandez Villamil, S. H. & Stoppani, A. O. Cytotoxicity of beta-lapachone, an naphthoquinone with possible therapeutic use. *Medicina (B Aires)* **61**, 343-350, doi:PMID: 11474885 (2001).
- 297 Kung, H.-N., Lu, K.-S. & Chau, Y.-P. The chemotherapeutic effects of lapacho tree extract: β-lapachone. *Chemotherapy* **3**, 131-135 (2014).
- 298 Nawashiro, H. *et al.* L-type amino acid transporter 1 as a potential molecular target in human astrocytic tumors. *Int J Cancer* **119**, 484-492, doi:<https://doi.org/10.1002/ijc.21866> (2006).
- 299 Kaira, K. *et al.* Clinical significance of L-type amino acid transporter 1 expression as a prognostic marker and potential of new targeting therapy in biliary tract cancer. *BMC*

- Cancer* **13**, 482, doi:<https://doi.org/10.1186/1471-2407-13-482> (2013).
- 300 Kim, C. S. *et al.* BCH, an inhibitor of system L amino acid transporters, induces apoptosis in cancer cells. *Biol Pharm Bull* **31**, 1096-1100, doi:<https://doi.org/10.1248/bpb.31.1096> (2008).
- 301 Imai, H. *et al.* Inhibition of L-type amino acid transporter 1 has antitumor activity in non-small cell lung cancer. *Anticancer Res* **30**, 4819-4828, doi:PMID: 21187458 (2010).
- 302 Ndrepepa, G. *et al.* Aspartate aminotransferase and mortality in patients with ischemic heart disease. *Nutrition, Metabolism and Cardiovascular Diseases*, doi:<https://doi.org/10.1016/j.numecd.2020.07.033> (2020).
- 303 Kulecka, M. *et al.* A heterozygous mutation in GOT1 is associated with familial macroaspartate aminotransferase. *J Hepatol* **67**, 1026-1030, doi:<https://doi.org/10.1016/j.jhep.2017.07.003> (2017).
- 304 Lee, J., Gokey, T., Ting, D. L., He, Z. H. & Guliaev, A. B. Dimerization misalignment in human glutamate-oxaloacetate transaminase variants is the primary factor for PLP release. *Plos One* **13**, doi:<https://doi.org/10.1371/journal.pone.0203889> (2018).
- 305 Hayashi, H. *et al.* Conformational change in aspartate aminotransferase on substrate binding induces strain in the catalytic group and enhances catalysis. *J Biol Chem* **278**, 9481-9488, doi:<https://doi.org/10.1074/jbc.M209235200> (2003).
- 306 Toney, M. D. Aspartate aminotransferase: an old dog teaches new tricks. *Arch Biochem Biophys* **544**, 119-127, doi:<https://doi.org/10.1016/j.abb.2013.10.002> (2014).
- 307 Villa, R. F., Ferrari, F. & Gorini, A. Functional proteomics related to energy metabolism of synaptosomes from different neuronal systems of rat hippocampus during aging. *J Proteome Res* **12**, 5422-5435, doi:<https://doi.org/10.1021/pr400834g> (2013).
- 308 Ferrari, F., Gorini, A., Hoyer, S. & Villa, R. F. Glutamate metabolism in cerebral mitochondria after ischemia and post-ischemic recovery during aging: relationships with brain energy metabolism. *J Neurochem* **146**, 416-428, doi:<https://doi.org/10.1111/jnc.14464> (2018).
- 309 Phillis, J. W. & O'Regan, M. H. Mechanisms of glutamate and aspartate release in the ischemic rat cerebral cortex. *Brain Res* **730**, 150-164, doi:[https://doi.org/10.1016/0006-8993\(96\)00434-9](https://doi.org/10.1016/0006-8993(96)00434-9) (1996).
- 310 Rink, C. *et al.* Glutamate oxaloacetate transaminase enables anaplerotic refilling of TCA cycle intermediates in stroke-affected brain. *FASEB J* **31**, 1709-1718, doi:<https://doi.org/10.1096/fj.201601033R> (2017).
- 311 Teichberg, V. I. From the liver to the brain across the blood-brain barrier. *P Natl Acad Sci USA* **104**, 7315-7316, doi:<https://doi.org/10.1073/pnas.0702450104> (2007).
- 312 Teichberg, V. I., Cohen-Kashi-Malina, K., Cooper, I. & Zlotnik, A. Homeostasis of glutamate in brain fluids: an accelerated brain-to-blood efflux of excess glutamate is produced by blood glutamate scavenging and offers protection from neuropathologies. *Neuroscience* **158**, 301-308, doi:<https://doi.org/10.1016/j.neuroscience.2008.02.075> (2009).
- 313 Hawkins, R. A. & Vina, J. R. How Glutamate Is Managed by the Blood-Brain Barrier. *Biology (Basel)* **5**, doi:<https://doi.org/10.3390/biology5040037> (2016).
- 314 Zlotnik, A. *et al.* Brain neuroprotection by scavenging blood glutamate. *Exp Neurol* **203**, 213-220, doi:<https://doi.org/10.1016/j.expneurol.2006.08.021> (2007).
- 315 Boyko, M. *et al.* The effect of blood glutamate scavengers oxaloacetate and pyruvate on neurological outcome in a rat model of subarachnoid hemorrhage. *Neurotherapeutics* **9**, 649-657, doi:<https://doi.org/10.1007/s13311-012-0129-6> (2012).

- 316 Boyko, M. *et al.* Pharmacokinetics of glutamate-oxaloacetate transaminase and glutamate-pyruvate transaminase and their blood glutamate-lowering activity in naive rats. *Neurochem Res* **37**, 2198-2205, doi:<https://doi.org/10.1007/s11064-012-0843-9> (2012).
- 317 Perez-Mato, M. *et al.* Human recombinant glutamate oxaloacetate transaminase 1 (GOT1) supplemented with oxaloacetate induces a protective effect after cerebral ischemia. *Cell Death Dis.* **5**, e992, doi:<https://doi.org/10.1038/cddis.2013.507> (2014).
- 318 Moncalvo, F., Martinez Espinoza, M. I. & Cellesi, F. Nanosized Delivery Systems for Therapeutic Proteins: Clinically Validated Technologies and Advanced Development Strategies. *Front Bioeng Biotechnol* **8**, 89, doi:<https://doi.org/10.3389/fbioe.2020.00089> (2020).
- 319 Harris, J. M. & Chess, R. B. Effect of pegylation on pharmaceuticals. *Nat Rev Drug Discov* **2**, 214-221, doi:<https://doi.org/10.1038/nrd1033> (2003).
- 320 Abuchowski, A., van Es, T., Palczuk, N. C. & Davis, F. F. Alteration of immunological properties of bovine serum albumin by covalent attachment of polyethylene glycol. *J Biol Chem* **252**, 3578-3581 (1977).
- 321 Nucci, M. L., Shorr, R. & Abuchowski, A. The therapeutic value of poly (ethylene glycol)-modified proteins. *Adv Drug Deliv Rev* **6**, 133-151 (1991).
- 322 Lee, V. *Peptide and protein drug delivery*. Vol. 4 (Crc Press, 1990).
- 323 Davis, F. F. *et al.* in *Enzyme Engineering* 169-173 (Springer, 1978).
- 324 Banerjee, S. S., Aher, N., Patil, R. & Khandare, J. Poly(ethylene glycol)-Prodrug Conjugates: Concept, Design, and Applications. *J Drug Deliv* **2012**, 103973, doi:<https://doi.org/10.1155/2012/103973> (2012).
- 325 Veronese, F. M. & Mero, A. The impact of PEGylation on biological therapies. *Biodrugs* **22**, 315-329, doi:<https://doi.org/10.2165/00063030-200822050-00004> (2008).
- 326 Swierczewska, M., Lee, K. C. & Lee, S. What is the future of PEGylated therapies? *Expert Opin Emerg Dr* **20**, 531-536, doi:<https://doi.org/10.1517/14728214.2015.1113254> (2015).
- 327 Walsh, G. Biopharmaceutical benchmarks 2018. *Nature biotechnology* **36**, 1136-1145, doi:<https://doi.org/10.1038/nbt.4305> (2018).
- 328 Grayson, S. M. & Godbey, W. T. The role of macromolecular architecture in passively targeted polymeric carriers for drug and gene delivery. *Journal of Drug Targeting* **16**, 329-356, doi:<https://doi.org/10.1080/10611860801969616> (2008).
- 329 Luxenhofer, R., Bezen, M. & Jordan, R. Kinetic Investigations on the Polymerization of 2-Oxazolines Using Pluritriflate Initators. *Macromol Rapid Commun* **29**, 1509-1513 (2008).
- 330 Roberts, M. J., Bentley, M. D. & Harris, J. M. Chemistry for peptide and protein PEGylation. *Adv Drug Deliv Rev* **54**, 459-476, doi:Pii S0169-409x(02)00022-4  
Doi 10.1016/S0169-409x(02)00022-4 (2002).
- 331 Gupta, V. *et al.* Protein PEGylation for cancer therapy: bench to bedside. *J Cell Commun Signal* **13**, 319-330, doi:<https://doi.org/10.1007/s12079-018-0492-0> (2019).
- 332 Levy, Y. *et al.* Adenosine deaminase deficiency with late onset of recurrent infections: response to treatment with polyethylene glycol-modified adenosine deaminase. *J Pediatr* **113**, 312-317, doi:[https://doi.org/10.1016/S0022-3476\(88\)80271-3](https://doi.org/10.1016/S0022-3476(88)80271-3) (1988).
- 333 Graham, M. L. Pegaspargase: a review of clinical studies. *Adv Drug Deliv Rev* **55**, 1293-1302, doi:[https://doi.org/10.1016/S0169-409X\(03\)00110-8](https://doi.org/10.1016/S0169-409X(03)00110-8) (2003).

- 334 Wang, Y.-S. *et al.* Structural and biological characterization of pegylated recombinant interferon alpha-2b and its therapeutic implications. *Adv Drug Deliv Rev* **54**, 547-570, doi:[https://doi.org/10.1016/S0169-409X\(02\)00027-3](https://doi.org/10.1016/S0169-409X(02)00027-3) (2002).
- 335 Reddy, K. R., Modi, M. W. & Pedder, S. Use of peginterferon alfa-2a (40 KD)(Pegasys®) for the treatment of hepatitis C. *Adv Drug Deliv Rev* **54**, 571-586, doi:[https://doi.org/10.1016/s0169-409x\(02\)00028-5](https://doi.org/10.1016/s0169-409x(02)00028-5) (2002).
- 336 Trainer, P. J. *et al.* Treatment of acromegaly with the growth hormone-receptor antagonist pegvisomant. *N Engl J Med* **342**, 1171-1177, doi:<https://doi.org/10.1056/NEJM200004203421604> (2000).
- 337 Kinstler, O., Molineux, G., Treuheit, M., Ladd, D. & Gegg, C. Mono-N-terminal poly(ethylene glycol)-protein conjugates. *Adv Drug Deliv Rev* **54**, 477-485, doi:[https://doi.org/10.1016/S0169-409x\(02\)00023-6](https://doi.org/10.1016/S0169-409x(02)00023-6) (2002).
- 338 Macdougall, I. C. CERA (Continuous Erythropoietin Receptor Activator): a new erythropoiesis-stimulating agent for the treatment of anemia. *Current hematology reports* **4**, 436-440, doi:PMID: 16232379 (2005).
- 339 Wong, S. S. Reactive groups of proteins and their modifying agents. *Chemistry of protein conjugation and cross-linking*, 7-48 (1991).
- 340 Sherman, M. R., Saifer, M. G. & Perez-Ruiz, F. PEG-uricase in the management of treatment-resistant gout and hyperuricemia. *Adv Drug Deliv Rev* **60**, 59-68, doi:<https://doi.org/10.1016/j.addr.2007.06.011> (2008).
- 341 Patel, J. N. & Walko, C. M. Sylatron: a pegylated interferon for use in melanoma. *Ann Pharmacother* **46**, 830-838, doi:<https://doi.org/10.1345/aph.1Q791> (2012).
- 342 Calabresi, P. A. *et al.* Pegylated interferon beta-1a for relapsing-remitting multiple sclerosis (ADVANCE): a randomised, phase 3, double-blind study. *Lancet Neurol* **13**, 657-665, doi:[https://doi.org/10.1016/S1474-4422\(14\)70068-7](https://doi.org/10.1016/S1474-4422(14)70068-7) (2014).
- 343 Dunn, A., Ahuja, S. & Mullins, E. Real-world experience with use of Antihemophilic Factor (Recombinant), PEG ylated for prophylaxis in severe haemophilia A. *Haemophilia* **24**, e84-e92, doi:<https://doi.org/10.1111/hae.13403> (2018).
- 344 Thomas, J. *et al.* Pegvaliase for the treatment of phenylketonuria: Results of a long-term phase 3 clinical trial program (PRISM). *Mol Genet Metab* **124**, 27-38, doi:<https://doi.org/10.1016/j.ymgme.2018.03.006> (2018).
- 345 Ekladius, I., Colson, Y. L. & Grinstaff, M. W. Polymer-drug conjugate therapeutics: advances, insights and prospects. *Nat Rev Drug Discov* **18**, 273-294, doi:<https://doi.org/10.1038/s41573-018-0005-0> (2019).
- 346 Coyle, T. E. *et al.* Phase I study of BAY 94-9027, a PEGylated B-domain-deleted recombinant factor VIII with an extended half-life, in subjects with hemophilia A. *J Thromb Haemost* **12**, 488-496, doi:<https://doi.org/10.1111/jth.12506> (2014).
- 347 Kinstler, O. B. *et al.* Characterization and stability of N-terminally PEGylated rhG-CSF. *Pharmaceutical Research* **13**, 996-1002, doi:<https://doi.org/10.1023/A:1016042220817> (1996).
- 348 Hamidi, M., Azadi, A. & Rafiei, P. Pharmacokinetic consequences of pegylation. *Drug Deliv* **13**, 399-409, doi:<https://doi.org/10.1080/10717540600814402> (2006).
- 349 Walsh, S., Shah, A. & Mond, J. Improved pharmacokinetics and reduced antibody reactivity of lysostaphin conjugated to polyethylene glycol. *Antimicrob Agents Ch* **47**, 554-558, doi:<https://doi.org/10.1128/Aac.47.2.554-558.2003> (2003).
- 350 Caliceti, P. & Veronese, F. M. Pharmacokinetic and biodistribution properties of poly(ethylene glycol)-protein conjugates. *Adv Drug Deliv Rev* **55**, 1261-1277,

- doi:[https://doi.org/10.1016/S0169-409x\(03\)00108-X](https://doi.org/10.1016/S0169-409x(03)00108-X) (2003).
- 351 Baumann, A., Tuerck, D., Prabhu, S., Dickmann, L. & Sims, J. Pharmacokinetics, metabolism and distribution of PEGs and PEGylated proteins: quo vadis? *Drug Discov Today* **19**, 1623-1631, doi:<https://doi.org/10.1016/j.drudis.2014.06.002> (2014).
- 352 Veronese, F. M. Peptide and protein PEGylation: a review of problems and solutions. *Biomaterials* **22**, 405-417, doi:[https://doi.org/10.1016/S0142-9612\(00\)00193-9](https://doi.org/10.1016/S0142-9612(00)00193-9) (2001).
- 353 Fishburn, C. S. The pharmacology of PEGylation: Balancing PD with PK to generate novel therapeutics. *J Pharm Sci* **97**, 4167-4183, doi:<https://doi.org/10.1002/jps.21278> (2008).
- 354 Monfardini, C. *et al.* A Branched Monomethoxypoly(Ethylene Glycol) for Protein Modification. *Bioconjug Chem* **6**, 62-69, doi:<https://doi.org/10.1021/bc00031a006> (1995).
- 355 Rajan, R. S. *et al.* Modulation of protein aggregation by polyethylene glycol conjugation: GCSF as a case study. *Protein Sci* **15**, 1063-1075, doi:<https://doi.org/10.1110/ps.052004006> (2006).
- 356 Natalello, A. *et al.* Biophysical Characterization of Met-G-CSF: Effects of Different Site-Specific Mono-Pegylations on Protein Stability and Aggregation. *Plos One* **7**, doi:<https://doi.org/10.1371/journal.pone.0042511> (2012).
- 357 Roque, C., Sheung, A., Rahman, N. & Ausar, S. F. Effect of polyethylene glycol conjugation on conformational and colloidal stability of a monoclonal antibody antigen-binding fragment (Fab'). *Mol Pharm* **12**, 562-575, doi:<https://doi.org/10.1021/mp500658w> (2015).
- 358 Hinds, K. D. & Kim, S. W. Effects of PEG conjugation on insulin properties. *Adv Drug Deliv Rev* **54**, 505-530, doi:[Pii S0169-409x\(02\)00025-X](https://doi.org/10.1016/S0169-409x(02)00025-X)
- Doi [10.1016/S0169-409x\(02\)00025-X](https://doi.org/10.1016/S0169-409x(02)00025-X) (2002).
- 359 Lopez-Cruz, J. I., Viniegra-Gonzalez, G. & Hernandez-Arana, A. Thermostability of native and pegylated Myceliophthora thermophila laccase in aqueous and mixed solvents. *Bioconjug Chem* **17**, 1093-1098, doi:<https://doi.org/10.1021/bc0503465> (2006).
- 360 Nie, Y., Zhang, X., Wang, X. & Chen, J. Preparation and stability of N-terminal mono-PEGylated recombinant human endostatin. *Bioconjug Chem* **17**, 995-999, doi:<https://doi.org/10.1021/bc050355d> (2006).
- 361 Rodriguez-Martinez, J. A. *et al.* Stabilization of alpha-Chymotrypsin Upon PEGylation Correlates With Reduced Structural Dynamics. *Biotechnology and Bioengineering* **101**, 1142-1149, doi:[10.1002/bit.22014](https://doi.org/10.1002/bit.22014) (2008).
- 362 Yang, C., Lu, D. N. & Liu, Z. How PEGylation Enhances the Stability and Potency of Insulin: A Molecular Dynamics Simulation. *Biochemistry* **50**, 2585-2593, doi:<https://doi.org/10.1021/bi101926u> (2011).
- 363 Mu, Q. M., Hu, T. & Yu, J. K. Molecular Insight into the Steric Shielding Effect of PEG on the Conjugated Staphylokinase: Biochemical Characterization and Molecular Dynamics Simulation. *Plos One* **8**, doi:<https://doi.org/10.1371/journal.pone.0068559> (2013).
- 364 Zaghmi, A., Greschner, A. A. & Gauthier, M. A. In vivo properties of therapeutic bioconjugates composed of proteins and architecturally/functionally complex polymers. *Polymer-Protein Conjugates: From Pegylation and Beyond*, 389-406, doi:<https://doi.org/10.1016/B978-0-444-64081-9.00017-6> (2020).
- 365 Harris, M. & Poly, J. I. (Plenum Publishing Corporation, 1992).

- 366 Fee, C. J. & Van Alstine, J. M. Prediction of the viscosity radius and the size exclusion chromatography behavior of PEGylated proteins. *Bioconjug Chem* **15**, 1304-1313, doi:<https://doi.org/10.1021/bc049843w> (2004).
- 367 Gull, I., Samra, Z. Q., Aslam, M. S. & Athar, M. A. Heterologous expression, immunochemical and computational analysis of recombinant human interferon alpha 2b. *Springerplus* **2**, 264, doi:<https://doi.org/10.1186/2193-1801-2-264> (2013).
- 368 Kozlowski, A. & Harris, J. M. Improvements in protein PEGylation: pegylated interferons for treatment of hepatitis C. *J Control Release* **72**, 217-224, doi:[https://doi.org/10.1016/s0168-3659\(01\)00277-2](https://doi.org/10.1016/s0168-3659(01)00277-2) (2001).
- 369 Foster, G. R. Pegylated interferons for the treatment of chronic hepatitis C. *Drugs* **70**, 147-165, doi:<https://doi.org/10.2165/11531990-000000000-00000> (2010).
- 370 Algranati, N., Sy, S. & Modi, M. in *Hepatology*. 190A-190A (WB SAUNDERS CO INDEPENDENCE SQUARE WEST CURTIS CENTER, STE 300, PHILADELPHIA ...).
- 371 Dill, M. T. *et al.* Pegylated IFN- $\alpha$  regulates hepatic gene expression through transient Jak/STAT activation. *J Clin Invest* **124**, 1568-1581, doi:<https://doi.org/10.1172/JCI70408> (2014).
- 372 Clark, R. *et al.* Long-acting growth hormones produced by conjugation with polyethylene glycol. *J Biol Chem* **271**, 21969-21977, doi:<https://doi.org/10.1074/jbc.271.36.21969> (1996).
- 373 Abuchowski, A., Vanes, T., Palczuk, N. C. & Davis, F. F. Alteration of Immunological Properties of Bovine Serum-Albumin by Covalent Attachment of Polyethylene-Glycol. *J Biol Chem* **252**, 3578-3581 (1977).
- 374 Basu, A. *et al.* Structure-function engineering of interferon-beta-1b for improving stability, solubility, potency, immunogenicity, and pharmacokinetic properties by site-selective mono-PEGylation. *Bioconjug Chem* **17**, 618-630, doi:<https://doi.org/10.1021/bc050322y> (2006).
- 375 Bailon, P. *et al.* Rational design of a potent, long-lasting form of interferon: a 40 kDa branched polyethylene glycol-conjugated interferon  $\alpha$ -2a for the treatment of hepatitis C. *Bioconjug Chem* **12**, 195-202 (2001).
- 376 So, T. *et al.* Depression of T-cell epitope generation by stabilizing hen lysozyme. *J Biol Chem* **272**, 32136-32140, doi:<https://doi.org/10.1074/jbc.272.51.32136> (1997).
- 377 Katre, N. V. Immunogenicity of Recombinant IL-2 Modified by Covalent Attachment of Polyethylene-Glycol. *J Immunol* **144**, 209-213 (1990).
- 378 Johnson, V. & Maack, T. Renal extraction, filtration, absorption, and catabolism of growth hormone. *Am J Physiol Renal Physiol* **233**, F185-F196 (1977).
- 379 Takagi, A. *et al.* Enhanced pharmacological activity of recombinant human interleukin-11 (rhIL11) by chemical modification with polyethylene glycol. *J Control Release* **119**, 271-278, doi:<https://doi.org/10.1016/j.jconrel.2007.03.009> (2007).
- 380 Bailon, P. *et al.* Rational design of a potent, long-lasting form of interferon: a 40 kDa branched polyethylene glycol-conjugated interferon alpha-2a for the treatment of hepatitis C. *Bioconjug Chem* **12**, 195-202, doi:<https://doi.org/10.1021/bc000082g> (2001).
- 381 Baker, D. P. *et al.* N-terminally PEGylated human interferon-beta-1a with improved pharmacokinetic properties and in vivo efficacy in a melanoma angiogenesis model. *Bioconjug Chem* **17**, 179-188, doi:<https://doi.org/10.1021/bc050237q> (2006).
- 382 Zaghmi, A. *et al.* Mechanisms of activity loss for a multi-PEGylated protein by experiment and simulation. *Mater Today Chem* **12**, 121-131,

- doi:<https://doi.org/10.1016/j.mtchem.2018.12.007> (2019).
- 383 Karpusas, M. *et al.* The crystal structure of human interferon  $\beta$  at 2.2-Å resolution. *P Natl Acad Sci USA* **94**, 11813-11818, doi: <https://doi.org/10.1073/pnas.94.22.11813> (1997).
- 384 Runkel, L. *et al.* Systematic mutational mapping of sites on human interferon-beta-1a that are important for receptor binding and functional activity. *Biochemistry* **39**, 2538-2551, doi:<https://doi.org/10.1021/bi991631c> (2000).
- 385 Ciepluch, K. *et al.* Influence of PEGylation on Domain Dynamics of Phosphoglycerate Kinase: PEG Acts Like Entropic Spring for the Protein. *Bioconjug Chem* **29**, 1950-1960, doi:<https://doi.org/10.1021/acs.bioconjugchem.8b00203> (2018).
- 386 Ramberg, K. O., Antonik, P. M., Cheung, D. L. & Crowley, P. B. Measuring the Impact of PEGylation on a Protein-Polysaccharide Interaction. *Bioconjug Chem* **30**, 1162-1168, doi:<https://doi.org/10.1021/acs.bioconjugchem.9b00099> (2019).
- 387 Foser, S. *et al.* Isolation, structural characterization, and antiviral activity of positional isomers of monopegylated interferon alpha-2a (PEGASYS). *Protein Expr Purif* **30**, 78-87, doi:[https://doi.org/10.1016/s1046-5928\(03\)00055-x](https://doi.org/10.1016/s1046-5928(03)00055-x) (2003).
- 388 Morgenstern, J., Baumann, P., Brunner, C. & Hubbuch, J. Effect of PEG molecular weight and PEGylation degree on the physical stability of PEGylated lysozyme. *Int J Pharm* **519**, 408-417, doi:<https://doi.org/10.1016/j.ijpharm.2017.01.040> (2017).
- 389 Hu, T. *et al.* PEGylation of Val-1(alpha) destabilizes the tetrameric structure of hemoglobin. *Biochemistry* **48**, 608-616, doi:<https://doi.org/10.1021/bi801880y> (2009).
- 390 Ku, M. S. Recent trends in specialty pharma business model. *J Food Drug Anal* **23**, 595-608, doi:<https://doi.org/10.1016/j.jfda.2015.04.008> (2015).
- 391 Alberts, B. *et al.* *Essential cell biology*. (Garland Science, 2015).
- 392 Dimitrov, D. S. Therapeutic proteins. *Methods Mol Biol* **899**, 1-26, doi:[https://doi.org/10.1007/978-1-61779-921-1\\_1](https://doi.org/10.1007/978-1-61779-921-1_1) (2012).
- 393 Vugmeyster, Y., Xu, X., Theil, F. P., Khawli, L. A. & Leach, M. W. Pharmacokinetics and toxicology of therapeutic proteins: Advances and challenges. *World J Biol Chem* **3**, 73-92, doi:<https://doi.org/10.4331/wjbc.v3.i4.73> (2012).
- 394 Turecek, P. L., Bossard, M. J., Schoetens, F. & Ivens, I. A. PEGylation of Biopharmaceuticals: A Review of Chemistry and Nonclinical Safety Information of Approved Drugs. *J Pharm Sci* **105**, 460-475, doi:<https://doi.org/10.1016/j.xphs.2015.11.015> (2016).
- 395 Swierczewska, M., Lee, K. C. & Lee, S. What is the future of PEGylated therapies? *Expert Opin Emerg Drugs* **20**, 531-536, doi:<https://doi.org/10.1517/14728214.2015.1113254> (2015).
- 396 Magharla, D. D. & Sathyamoorthy, N. Clinical Implications of Molecular PEGylation on Therapeutic Proteins. *J Basic Clin Pharma* **8**, 87-90 (2017).
- 397 Graham, M. L. Pegaspargase: a review of clinical studies. *Adv Drug Deliv Rev* **55**, 1293-1302, doi:[https://doi.org/10.1016/S0169-409X\(03\)00110-8](https://doi.org/10.1016/S0169-409X(03)00110-8) (2003).
- 398 Levy, Y. *et al.* Adenosine-Deaminase Deficiency with Late Onset of Recurrent Infections Response to Treatment with Polyethylene-Glycol Modified Adenosine-Deaminase. *J Pediatr* **113**, 312-317, doi:[https://doi.org/10.1016/S0022-3476\(88\)80271-3](https://doi.org/10.1016/S0022-3476(88)80271-3) (1988).
- 399 Kinstler, O. B. *et al.* Characterization and stability of N-terminally PEGylated rhG-CSF. *Pharm Res* **13**, 996-1002, doi:<https://doi.org/10.1023/A:1016042220817> (1996).

- 400 Unterweger, B., Stoisser, T., Leitgeb, S., Birner-Grünberger, R. & Nidetzky, B. Engineering of *Aerococcus viridans* L-lactate oxidase for site-specific PEGylation: characterization and selective bioorthogonal modification of a S218C mutant. *Bioconjug Chem* **23**, 1406-1414, doi:<https://doi.org/10.1021/bc2006847> (2012).
- 401 Grace, M. *et al.* Structural and biologic characterization of pegylated recombinant IFN-alpha2b. *J Interferon Cytokine Res* **21**, 1103-1115, doi:<https://doi.org/10.1089/107999001317205240> (2001).
- 402 Gong, Y., Andina, D., Nahar, S., Leroux, J. C. & Gauthier, M. A. Releasable and traceless PEGylation of arginine-rich antimicrobial peptides. *Chem Sci* **8**, 4082-4086, doi:<https://doi.org/10.1039/c7sc00770a> (2017).
- 403 Schulz, J. D. *et al.* Site-Specific Polymer Conjugation Stabilizes Therapeutic Enzymes in the Gastrointestinal Tract. *Adv Mater* **28**, 1455-1460, doi:<https://doi.org/10.1002/adma.201504797> (2016).
- 404 Liu, M., Johansen, P., Zabel, F., Leroux, J. C. & Gauthier, M. A. Semi-permeable coatings fabricated from comb-polymers efficiently protect proteins in vivo. *Nat Commun* **5**, 5526, doi:<https://doi.org/10.1038/ncomms6526> (2014).
- 405 Bowen, S. *et al.* Relationship between molecular mass and duration of activity of polyethylene glycol conjugated granulocyte colony-stimulating factor mutein. *Exp Hematol* **27**, 425-432, doi:[https://doi.org/10.1016/S0301-472X\(98\)00051-4](https://doi.org/10.1016/S0301-472X(98)00051-4) (1999).
- 406 Chiu, K. *et al.* Effects of Polymer Molecular Weight on the Size, Activity, and Stability of PEG-Functionalized Trypsin. *Biomacromolecules* **11**, 3688-3692, doi:<https://doi.org/10.1021/bm1006954> (2010).
- 407 Ross, R. J. M. *et al.* Binding and functional studies with the growth hormone receptor antagonist, B2036-PEG (pegvisomant), reveal effects of pegylation and evidence that it binds to a receptor dimers. *J Clin Endocr Metab* **86**, 1716-1723, doi:<https://doi.org/10.1210/jcem.86.4.7403> (2001).
- 408 Kubetzko, S., Sarkar, C. A. & Pluckthun, A. Protein PEGylation decreases observed target association rates via a dual blocking mechanism. *Mol Pharmacol* **68**, 1439-1454, doi:<https://doi.org/10.1124/mol.105.014910> (2005).
- 409 Cattani, G., Vogeley, L. & Crowley, P. B. Structure of a PEGylated protein reveals a highly porous double-helical assembly. *Nat Chem* **7**, 823-828, doi:<https://doi.org/10.1038/nchem.2342> (2015).
- 410 DeBenedictis, E. P., Hamed, E. & Keten, S. Mechanical Reinforcement of Proteins with Polymer Conjugation. *ACS Nano* **10**, 2259-2267, doi:<https://doi.org/10.1021/acs.nano.5b06917> (2016).
- 411 Gokarn, Y. R., McLean, M. & Laue, T. M. Effect of PEGylation on protein hydrodynamics. *Mol Pharm* **9**, 762-773, doi:<https://doi.org/10.1021/mp200470c> (2012).
- 412 Xu, D. *et al.* Molecular insights into the improved clinical performance of PEGylated interferon therapeutics: a molecular dynamics perspective. *Rsc Adv* **8**, 2315-2322, doi:<https://doi.org/10.1039/c7ra12480e> (2018).
- 413 Le Cœur, C. *et al.* Conformation of the Poly (ethylene Glycol) chains in DiPEGylated hemoglobin specifically probed by SANS: correlation with PEG length and in vivo efficiency. *Langmuir* **31**, 8402-8410, doi:<https://doi.org/10.1021/acs.langmuir.5b01121> (2015).
- 414 Turecek, P. L., Bossard, M. J., Schoetens, F. & Ivens, I. A. PEGylation of biopharmaceuticals: a review of chemistry and nonclinical safety information of approved drugs. *J. Pharm. Sci.* **105**, 460-475 (2016).
- 415 Caliceti, P., Schiavon, O., Veronese, F. M. & Chaiken, I. M. Effects of

- monomethoxypoly(ethylene glycol) modification of ribonuclease on antibody recognition, substrate accessibility and conformational stability. *J Mol Recognit* **3**, 89-93, doi:<https://doi.org/10.1002/jmr.300030206> (1990).
- 416 Veronese, F., Sartore, L., Schiavon, O. & Caliceti, P. A comparative study of enzymatic, structural, and pharmacokinetic properties of superoxide dismutase isolated from two sources and modified by monomethoxypolyethylene glycol using different methods of coupling. *Ann N Y Acad Sci* **613**, 468-474, doi:<https://doi.org/10.1111/j.1749-6632.1990.tb18202.x> (1990).
- 417 Li, M., Li, C., Allen, A., Stanley, C. A. & Smith, T. J. Glutamate dehydrogenase: structure, allosteric regulation, and role in insulin homeostasis. *Neurochem Res* **39**, 433-445, doi:<https://doi.org/10.1007/s11064-013-1173-2> (2014).
- 418 Li, M., Smith, C. J., Walker, M. T. & Smith, T. J. Novel inhibitors complexed with glutamate dehydrogenase: allosteric regulation by control of protein dynamics. *J Biol Chem* **284**, 22988-23000, doi:<https://doi.org/10.1074/jbc.m109.020222> (2009).
- 419 Vandrunen, R., Vanderspoel, D. & Berendsen, H. J. C. Gromacs - a Software Package and a Parallel Computer for Molecular-Dynamics. *Abstr Pap Am Chem S* **209**, 49-Comp, doi:[https://doi.org/10.1016/0010-4655\(95\)00042-E](https://doi.org/10.1016/0010-4655(95)00042-E) (1995).
- 420 Kutzner, C. *et al.* Best bang for your buck: GPU nodes for GROMACS biomolecular simulations. *J Comput Chem* **36**, 1990-2008, doi:<https://doi.org/10.1002/jcc.24030> (2015).
- 421 Monticelli, L. *et al.* The MARTINI coarse-grained force field: Extension to proteins. *J Chem Theory Comput* **4**, 819-834, doi:<https://doi.org/10.1021/ct700324x> (2008).
- 422 Rossi, G., Fuchs, P. F. J., Barnoud, J. & Monticelli, L. A Coarse-Grained MARTINI Model of Polyethylene Glycol and of Polyoxyethylene Alkyl Ether Surfactants. *J Phys Chem B* **116**, 14353-14362, doi:<https://doi.org/10.1021/jp3095165> (2012).
- 423 Bailey, J., Bell, E. T. & Bell, J. E. Regulation of bovine glutamate dehydrogenase. The effects of pH and ADP. *J Biol Chem* **257**, 5579-5583, doi:PMID: 7068608 (1982).
- 424 Uversky, V. & Longhi, S. *Instrumental analysis of intrinsically disordered proteins: assessing structure and conformation*. Vol. 3 (John Wiley & Sons, 2011).
- 425 Wacker, S. A., Bradley, M. J., Marion, J. & Bell, E. Ligand-induced changes in the conformational stability and flexibility of glutamate dehydrogenase and their role in catalysis and regulation. *Protein Sci* **19**, 1820-1829, doi:<https://doi.org/10.1002/pro.459> (2010).
- 426 Bunik, V., Artiukhov, A., Aleshin, V. & Mkrtychyan, G. Multiple Forms of Glutamate Dehydrogenase in Animals: Structural Determinants and Physiological Implications. *Biology* **5**, doi:<https://doi.org/10.3390/biology5040053> (2016).
- 427 Allen, A., Kwagh, J., Fang, J., Stanley, C. A. & Smith, T. J. Evolution of glutamate dehydrogenase regulation of insulin homeostasis is an example of molecular exaptation. *Biochemistry* **43**, 14431-14443, doi:<https://doi.org/10.1021/bi048817i> (2004).
- 428 Stanley, C. A. *et al.* Hyperinsulinism and hyperammonemia in infants with regulatory mutations of the glutamate dehydrogenase gene. *N Engl J Med* **338**, 1352-1357, doi:<https://doi.org/10.1056/nejm199805073381904> (1998).
- 429 DeLano, W. L. PyMOL molecular viewer: Updates and refinements. *Abstracts of Papers of the ACS* **238** (2009).
- 430 Yang, L. W. *et al.* oGNM: online computation of structural dynamics using the Gaussian Network Model. *Nucleic Acids Res* **34**, W24-W31, doi:<https://doi.org/10.1093/nar/gkl084> (2006).

- 431 Liu, Y. X. *et al.* VMD as a Software for Visualization and Quantitative Analysis of Super Resolution Imaging and Single Particle Tracking. *Biophys J* **106**, 202a-202a, doi:<https://doi.org/10.1016/j.bpj.2013.11.1187> (2014).
- 432 DeBenedictis, E. P., Hamed, E. & Keten, S. Mechanical Reinforcement of Proteins with Polymer Conjugation. *Acs Nano* **10**, 2259-2267, doi:10.1021/acsnano.5b06917 (2016).
- 433 Giovanni, S., Jiajia, Z. & Friederike, S. Interactions between proteins and poly(ethylene-glycol) investigated using molecular dynamics simulations. *J Phys Conf Ser* **921**, 012002, doi:<https://doi.org/10.1088/1742-6596/921/1/012002> (2017).
- 434 Alessi, M. L., Norman, A. I., Knowlton, S. E., Ho, D. L. & Greer, S. C. Helical and Coil Conformations of Poly(ethylene glycol) in Isobutyric Acid and Water. *Macromolecules* **38**, 9333-9340, doi:<https://doi.org/10.1021/ma051339e> (2005).
- 435 O'Neill, S. C., Bhuiyan, Z. H. & Tu, R. S. Evolution of mechanics in  $\alpha$ -helical peptide conjugated linear- and star-block PEG. *Soft Matter* **13**, 7521-7528, doi:<https://doi.org/10.1039/c7sm00968b> (2017).
- 436 Werner, A., Röhm, K.-H. & Müller, H.-J. Mapping of B-cell epitopes in E. coli asparaginase II, an enzyme used in leukemia treatment. *Biol Chem* **386**, 535-540, doi:<https://doi.org/10.1515/bc.2005.063> (2005).
- 437 Aung, H.-P., Bocola, M., Schleper, S. & Röhm, K.-H. Dynamics of a mobile loop at the active site of Escherichia coli asparaginase. *Biochim Biophys Acta* **1481**, 349-359, doi:[https://doi.org/10.1016/s0167-4838\(00\)00179-5](https://doi.org/10.1016/s0167-4838(00)00179-5) (2000).
- 438 Strong, K., Mathers, C. & Bonita, R. Preventing stroke: saving lives around the world. *The Lancet Neurology* **6**, 182-187 (2007).
- 439 Lipton, P. Ischemic cell death in brain neurons. *Physiological reviews* **79**, 1431-1568 (1999).
- 440 Chamorro, Á., Dirnagl, U., Urra, X. & Planas, A. M. Neuroprotection in acute stroke: targeting excitotoxicity, oxidative and nitrosative stress, and inflammation. *The Lancet Neurology* **15**, 869-881 (2016).
- 441 Castillo, J. *et al.* A novel mechanism of neuroprotection: Blood glutamate grabber. *J Cereb Blood Flow Metab* **36**, 292-301, doi:10.1177/0271678X15606721 (2016).
- 442 Ginsberg, M. D. Neuroprotection for ischemic stroke: past, present and future. *Neuropharmacology* **55**, 363-389, doi:<https://doi.org/10.1016/j.neuropharm.2007.12.007> (2008).
- 443 Cryan, J. F. & Julio-Pieper, M. Metabotropic Glutamate Receptors in Peripheral and Non-Neural Tissues: Implications for Drug Discovery. *Curr Neuropharmacol* **9**, 12-13 (2011).
- 444 Julio-Pieper, M., Flor, P. J., Dinan, T. G. & Cryan, J. F. Exciting Times beyond the Brain: Metabotropic Glutamate Receptors in Peripheral and Non-Neural Tissues. *Pharmacol Rev* **63**, 35-58, doi:10.1124/pr.110.004036 (2011).
- 445 Gill, S. S. & Pulido, O. M. Glutamate receptors in peripheral tissues: Current knowledge, future research, and implications for toxicology. *Toxicol Pathol* **29**, 208-223, doi:10.1080/019262301317052486 (2001).
- 446 Gottlieb, M., Wang, Y. & Teichberg, V. I. Blood-mediated scavenging of cerebrospinal fluid glutamate. *J Neurochem* **87**, 119-126 (2003).
- 447 Zaghmi, A. *et al.* Determination of the degree of PEGylation of protein bioconjugates using data from proton nuclear magnetic resonance spectroscopy. *Data Brief* **25**, 104037, doi:<https://doi.org/10.1016/j.dib.2019.104037> (2019).
- 448 Campos, F. *et al.* Neuroprotection by glutamate oxaloacetate transaminase in ischemic

- stroke: an experimental study. *J Cerebr Blood F Met* **31**, 1378-1386, doi:10.1038/jcbfm.2011.3 (2011).
- 449 Fernandez-Susavila, H. *et al.* Inclusion criteria update for the rat intraluminal ischaemic model for preclinical studies. *Dis Model Mech* **10**, 1433-1438, doi:<https://doi.org/10.1242/dmm.029868> (2017).
- 450 Saver, J. L. *et al.* Stroke Therapy Academic Industry Roundtable (STAIR) recommendations for extended window acute stroke therapy trials. *Stroke* **40**, 2594-2600, doi:<https://doi.org/10.1161/STROKEAHA.109.552554> (2009).
- 451 Pegg, C. C., He, C., Stroink, A. R., Kattner, K. A. & Wang, C. X. Technique for collection of cerebrospinal fluid from the cisterna magna in rat. *J Neurosci Methods* **187**, 8-12, doi:<https://doi.org/10.1016/j.jneumeth.2009.12.002> (2010).
- 452 Schaar, K. L., Brenneman, M. M. & Savitz, S. I. Functional assessments in the rodent stroke model. *Exp Transl Stroke Med* **2**, 13, doi:<https://doi.org/10.1186/2040-7378-2-13> (2010).
- 453 Hunter, A. J. *et al.* Functional assessments in mice and rats after focal stroke. *Neuropharmacology* **39**, 806-816, doi:[https://doi.org/10.1016/S0028-3908\(99\)00262-2](https://doi.org/10.1016/S0028-3908(99)00262-2) (2000).
- 454 Rej, R. Aspartate aminotransferase activity and isoenzyme proportions in human liver tissues. *Clinical Chemistry* **24**, 1971-1979 (1978).
- 455 Oller-Salvia, B., Sanchez-Navarro, M., Giralt, E. & Teixido, M. Blood-brain barrier shuttle peptides: an emerging paradigm for brain delivery. *Chem Soc Rev* **45**, 4690-4707, doi:<https://doi.org/10.1039/c6cs00076b> (2016).
- 456 Bertrand, Y. *et al.* Transport characteristics of a novel peptide platform for CNS therapeutics. *J Cell Mol Med* **14**, 2827-2839, doi:<https://doi.org/10.1111/j.1582-4934.2009.00930.x> (2010).
- 457 Conover, C. D., Gilbert, C. W., Shum, K. L. & Shorr, R. G. L. The impact of polyethylene glycol conjugation on bovine hemoglobin's circulatory half-life and renal effects in a rabbit top-loaded transfusion model. *Artif Organs* **21**, 907-915 (1997).
- 458 Lawrence, P. B. & Price, J. L. How PEGylation influences protein conformational stability. *Curr Opin Chem Biol* **34**, 88-94, doi:10.1016/j.cbpa.2016.08.006 (2016).
- 459 Zhang, L. *et al.* Intravenous administration of human umbilical tissue-derived cells improves neurological function in aged rats after embolic stroke. *Cell Transplant* **22**, 1569-1576, doi:<https://doi.org/10.3727/096368912X658674> (2013).
- 460 Ramos-Cabrer, P., Justicia, C., Wiedermann, D. & Hoehn, M. Stem cell mediation of functional recovery after stroke in the rat. *Plos One* **5**, e12779, doi:<https://doi.org/10.1371/journal.pone.0012779> (2010).
- 461 Argibay, B. *et al.* Intraarterial route increases the risk of cerebral lesions after mesenchymal cell administration in animal model of ischemia. *Sci Rep* **7**, 40758, doi:<https://doi.org/10.1038/srep40758> (2017).
- 462 Zhang, L. *et al.* Delayed administration of human umbilical tissue-derived cells improved neurological functional recovery in a rodent model of focal ischemia. *Stroke* **42**, 1437-1444, doi:<https://doi.org/10.1161/STROKEAHA.110.593129> (2011).
- 463 Lee, A. *et al.* Localisation of novel forms of glutamate transporters and the cystine-glutamate antiporter in the choroid plexus: Implications for CSF glutamate homeostasis. *J Chem Neuroanat* **43**, 64-75, doi:10.1016/j.jchemneu.2011.09.006 (2012).
- 464 Conrad E. Johanson, N. L. J. Choroid Plexus Blood-CSF Barrier Major Player in Brain

- Disease Modeling and Neuromedicine. *J Neurol Neuromed*, 39-58, doi:<https://doi.org/10.29245/2572.942x/2018/4.1194> (2018).
- 465 Lyeth, B. G. Cognitive deficits after focal cerebral ischemia in mice - Editorial comment. *Stroke* **31**, 1944-1944 (2000).
- 466 Bouet, V. *et al.* Sensorimotor and cognitive deficits after transient middle cerebral artery occlusion in the mouse. *Exp Neurol* **203**, 555-567, doi:10.1016/j.expneurol.2006.09.006 (2007).
- 467 Zhang, L., Chen, J. L., Li, Y., Zhang, Z. G. & Chopp, M. Quantitative measurement of motor and somatosensory impairments after mild (30 min) and severe (2 h) transient middle cerebral artery occlusion in rats. *J Neurol Sci* **174**, 141-146, doi:10.1016/S0022-510x(00)00268-9 (2000).
- 468 Boyko, M. *et al.* Pharmacokinetics of Glutamate-Oxaloacetate Transaminase and Glutamate-Pyruvate Transaminase and Their Blood Glutamate-Lowering Activity in Naive Rats. *Neurochemical Research* **37**, 2198-2205, doi:10.1007/s11064-012-0843-9 (2012).
- 469 Hinoi, E., Takarada, T., Ueshima, T., Tsuchihashi, Y. & Yoneda, Y. Glutamate signaling in peripheral tissues. *Eur J Biochem* **271**, 1-13, doi:10.1046/j.1432-1033.2003.03907.x (2004).
- 470 Klin, Y. *et al.* Distribution of radiolabeled L-glutamate and D-aspartate from blood into peripheral tissues in naive rats: Significance for brain neuroprotection. *Biochem Biophys Res Commun* **399**, 694-698, doi:10.1016/j.bbrc.2010.07.144 (2010).
- 471 Lipton, S. A. Pathologically activated therapeutics for neuroprotection (Vol 8, pg 803, 2007). *Nat Rev Neurosci* **8**, doi:<https://doi.org/10.1038/nrn2229> (2007).
- 472 Nakajima, M. *et al.* Mesenchymal Stem Cells Overexpressing Interleukin-10 Promote Neuroprotection in Experimental Acute Ischemic Stroke. *Mol Ther Methods Clin Dev* **6**, 102-111, doi:<https://doi.org/10.1016/j.omtm.2017.06.005> (2017).
- 473 Milani, D. *et al.* Neuroprotective efficacy of poly-arginine R18 and NA-1 (TAT-NR2B9c) peptides following transient middle cerebral artery occlusion in the rat. *Neurosci Res* **114**, 9-15, doi:<https://doi.org/10.1016/j.neures.2016.09.002> (2017).
- 474 Milani, D., Knuckey, N. W., Anderton, R. S., Cross, J. L. & Meloni, B. P. The R18 Polyarginine Peptide Is More Effective Than the TAT-NR2B9c (NA-1) Peptide When Administered 60 Minutes after Permanent Middle Cerebral Artery Occlusion in the Rat. *Stroke Res Treat*, doi:<https://doi.org/10.1155/2016/2372710> (2016).
- 475 Perez-Mato, M. *et al.* Human recombinant glutamate oxaloacetate transaminase 1 (GOT1) supplemented with oxaloacetate induces a protective effect after cerebral ischemia. *Cell Death & Disease* **5**, doi:ARTN e992 10.1038/cddis.2013.507 (2014).
- 476 Goldshmit, Y. *et al.* Blood Glutamate Scavenger as a Novel Neuroprotective Treatment in Spinal Cord Injury. *J Neurotrauma* **35**, 2581-2590, doi:<https://doi.org/10.1089/neu.2017.5524> (2018).
- 477 Muir, K. W. Glutamate-based therapeutic approaches: clinical trials with NMDA antagonists. *Curr Opin Pharmacol* **6**, 53-60, doi:<https://doi.org/10.1016/j.coph.2005.12.002> (2006).
- 478 Ikonomidou, C. & Turski, L. Why did NMDA receptor antagonists fail clinical trials for stroke and traumatic brain injury? *Lancet Neurol* **1**, 383-386, doi:[https://doi.org/10.1016/S1474-4422\(02\)00164-3](https://doi.org/10.1016/S1474-4422(02)00164-3) (2002).
- 479 Campos, F. *et al.* Blood levels of glutamate oxaloacetate transaminase are more

- strongly associated with good outcome in acute ischaemic stroke than glutamate pyruvate transaminase levels. *Clin Sci* **121**, 11-17, doi:<https://doi.org/10.1042/CS20100427> (2011).
- 480 Campos, F. *et al.* High blood glutamate oxaloacetate transaminase levels are associated with good functional outcome in acute ischemic stroke. *J Cereb Blood Flow Metab* **31**, 1387-1393, doi:<https://doi.org/10.1038/jcbfm.2011.4> (2011).
- 481 Ruban, A., Berkutzki, T., Cooper, I., Mohar, B. & Teichberg, V. I. Blood glutamate scavengers prolong the survival of rats and mice with brain-implanted gliomas. *Invest New Drugs* **30**, 2226-2235, doi:<https://doi.org/10.1007/s10637-012-9799-5>.
- 482 Fahien, L. A. & Strmecki, M. Studies on gluconeogenic mitochondrial enzymes. II. The conversion of glutamate to alpha-ketoglutarate by bovine liver mitochondrial glutamate dehydrogenase and glutamate-oxaloacetate transaminase. *Arch Biochem Biophys* **130**, 456-467, doi:[https://doi.org/10.1016/0003-9861\(69\)90058-7](https://doi.org/10.1016/0003-9861(69)90058-7) (1969).
- 483 Wedler, F. C. & Horn, B. R. Catalytic mechanisms of glutamine synthetase enzymes. Studies with analogs of possible intermediates and transition states. *J Biol Chem* **251**, 7530-7538, doi:PMID: 12170 (1976).
- 484 Colanduoni, J., Nissan, R. & Villafranca, J. J. Studies of the mechanism of glutamine synthetase utilizing pH-dependent behavior in catalysis and binding. *J Biol Chem* **262**, 3037-3043, doi:PMID: 2880845 (1987).
- 485 Hudson, R. C. & Daniel, R. M. L-glutamate dehydrogenases: distribution, properties and mechanism. *Comp Biochem Physiol B* **106**, 767-792, doi:[https://doi.org/10.1016/0305-0491\(93\)90031-y](https://doi.org/10.1016/0305-0491(93)90031-y) (1993).
- 486 Erlander, M. G. & Tobin, A. J. The structural and functional heterogeneity of glutamic acid decarboxylase: a review. *Neurochem Res* **16**, 215-226, doi:<https://doi.org/10.1007/BF00966084> (1991).
- 487 Tibbitts, J., Canter, D., Graff, R., Smith, A. & Khawli, L. A. Key factors influencing ADME properties of therapeutic proteins: A need for ADME characterization in drug discovery and development. *MAbs* **8**, 229-245, doi:<https://doi.org/10.1080/19420862.2015.1115937> (2016).
- 488 Wright, T. A., Page, R. C. & Konkolewicz, D. Polymer conjugation of proteins as a synthetic post-translational modification to impact their stability and activity. *Polym Chem* **10**, 434-454, doi:<https://doi.org/10.1039/c8py01399c> (2019).
- 489 Gong, Y. H., Leroux, J. C. & Gauthier, M. A. Releasable Conjugation of Polymers to Proteins. *Bioconjug Chem* **26**, 1172-1181, doi:<https://doi.org/10.1021/bc500611k> (2015).
- 490 Holtsberg, F. W., Ensor, C. M., Steiner, M. R., Bomalaski, J. S. & Clark, M. A. Poly(ethylene glycol) (PEG) conjugated arginine deiminase: effects of PEG formulations on its pharmacological properties. *J Control Release* **80**, 259-271, doi:[https://doi.org/10.1016/S0168-3659\(02\)00042-1](https://doi.org/10.1016/S0168-3659(02)00042-1) (2002).
- 491 Rudmann, D. G., Alston, J. T., Hanson, J. C. & Heidel, S. High molecular weight polyethylene glycol cellular distribution and PEG-associated cytoplasmic vacuolation is molecular weight dependent and does not require conjugation to proteins. *Toxicol Pathol* **41**, 970-983, doi:<https://doi.org/10.1177/0192623312474726> (2013).
- 492 Zhong, J. Z. *et al.* Purification and conformational changes of bovine PEGylated beta-lactoglobulin related to antigenicity. *Food Chem* **199**, 387-392, doi:<https://doi.org/10.1016/j.foodchem.2015.12.047> (2016).
- 493 Svergun, D. I. *et al.* Solution structure of poly(ethylene) glycol-conjugated hemoglobin revealed by small-angle X-ray scattering: implications for a new oxygen therapeutic.

- Biophys J* **94**, 173-181, doi:<https://doi.org/10.1529/biophysj.107.114314> (2008).
- 494 Chiu, K. *et al.* Effects of polymer molecular weight on the size, activity, and stability of PEG-functionalized trypsin. *Biomacromolecules* **11**, 3688-3692, doi:<https://doi.org/10.1021/bm1006954> (2010).
- 495 So, T., Ueda, T., Abe, Y., Nakamata, T. & Imoto, T. Situation of monomethoxypolyethylene glycol covalently attached to lysozyme. *J Biochem* **119**, 1086-1093, doi:<https://doi.org/10.1093/oxfordjournals.jbchem.a021352> (1996).
- 496 Zhang, J. F., Shi, L. Y. & Wei, D. Z. Chemical modification of L-asparaginase from *Escherichia coli* with a modified polyethyleneglycol under substrate protection conditions. *Biotechnol Lett* **26**, 753-756, doi:<https://doi.org/10.1023/b:bile.0000024100.49716.3d> (2004).
- 497 Morgenstern, J. *et al.* Impact of Polymer Bioconjugation on Protein Stability and Activity Investigated with Discrete Conjugates: Alternatives to PEGylation. *Biomacromolecules* **19**, 4250-4262, doi:<https://doi.org/10.1021/acs.biomac.8b01020> (2018).
- 498 Pai, S. S. *et al.* The conformation of the poly(ethylene glycol) chain in mono-PEGylated lysozyme and mono-PEGylated human growth hormone. *Bioconjug Chem* **22**, 2317-2323, doi:<https://doi.org/10.1021/bc2003583> (2011).
- 499 Le Coeur, C. *et al.* Conformation of the Poly(ethylene Glycol) Chains in DiPEGylated Hemoglobin Specifically Probed by SANS: Correlation with PEG Length and in Vivo Efficiency. *Langmuir* **31**, 8402-8410, doi:<https://doi.org/10.1021/acs.langmuir.5b01121> (2015).
- 500 Brooks, C. L., Karplus, M. & Pettitt, B. M. *Advances in chemical physics, volume 71: Proteins: A theoretical perspective of dynamics, structure, and thermodynamics.* (Wiley-Blackwell, 2006).
- 501 McCammon, J. A. & Harvey, S. C. *Dynamics of proteins and nucleic acids.* (Cambridge University Press, 1988).
- 502 Haun, S. E., Kirsch, J. R., Helfaer, M. A., Kubos, K. L. & Traystman, R. J. Polyethylene glycol-conjugated superoxide dismutase fails to augment brain superoxide dismutase activity in piglets. *Stroke* **22**, 655-659, doi:<https://doi.org/10.1161/01.str.22.5.655> (1991).
- 503 Kuroiwa, T., Ting, P., Martinez, H. & Klatzo, I. The biphasic opening of the blood-brain barrier to proteins following temporary middle cerebral artery occlusion. *Acta Neuropathol* **68**, 122-129, doi:<https://doi.org/10.1007/bf00688633> (1985).
- 504 Yoshida, K., Burton, G. F., McKinney, J. S., Young, H. & Ellis, E. F. Brain and Tissue Distribution of Polyethylene-Glycol Conjugated Superoxide-Dismutase in Rats. *Stroke* **23**, 865-869, doi:<https://doi.org/10.1161/01.Str.23.6.865> (1992).
- 505 Ugidos, I. F. *et al.* Neuroprotective effect of 2-hydroxy arachidonic acid in a rat model of transient middle cerebral artery occlusion. *Biochim Biophys Acta Biomembr* **1859**, 1648-1656, doi:<https://doi.org/10.1016/j.bbamem.2017.03.009> (2017).
- 506 Inoue, S., Drummond, J. C., Davis, D. P., Cole, D. J. & Patel, P. M. Combination of isoflurane and caspase inhibition reduces cerebral injury in rats subjected to focal cerebral ischemia. *Anesthesiology* **101**, 75-81, doi:<https://doi.org/10.1097/00000542-200407000-00013> (2004).
- 507 Cheng, Y. D., Al-Khoury, L. & Zivin, J. A. Neuroprotection for ischemic stroke: two decades of success and failure. *NeuroRx* **1**, 36-45, doi:<https://doi.org/10.1602/neurorx.1.1.36> (2004).
- 508 Stanimirovic, D. B., Bani-Yaghoub, M., Perkins, M. & Haqqani, A. S. Blood-brain barrier models: in vitro to in vivo translation in preclinical development of CNS-targeting

- biotherapeutics. *Expert Opin Drug Discov* **10**, 141-155, doi:<https://doi.org/10.1517/17460441.2015.974545> (2015).
- 509 Kolate, A. *et al.* PEG - a versatile conjugating ligand for drugs and drug delivery systems. *J Control Release* **192**, 67-81, doi:<https://doi.org/10.1016/j.jconrel.2014.06.046> (2014).
- 510 Larson, T. A., Joshi, P. P. & Sokolov, K. Preventing protein adsorption and macrophage uptake of gold nanoparticles via a hydrophobic shield. *ACS Nano* **6**, 9182-9190, doi:<https://doi.org/10.1021/nn3035155> (2012).
- 511 Owens, D. E., 3rd & Peppas, N. A. Opsonization, biodistribution, and pharmacokinetics of polymeric nanoparticles. *Int J Pharm* **307**, 93-102, doi:<https://doi.org/10.1016/j.ijpharm.2005.10.010> (2006).
- 512 Marrink, S. J. & Tieleman, D. P. Perspective on the Martini model. *Chem Soc Rev* **42**, 6801-6822, doi:<https://doi.org/10.1039/c3cs60093a> (2013).
- 513 Marrink, S. J., Risselada, H. J., Yefimov, S., Tieleman, D. P. & de Vries, A. H. The MARTINI Force Field: Coarse Grained Model for Biomolecular Simulations. *J Phys Chem B* **111**, 7812-7824, doi:<https://doi.org/10.1021/jp071097f> (2007).
- 514 Periole, X., Cavalli, M., Marrink, S.-J. & Ceruso, M. A. Combining an Elastic Network With a Coarse-Grained Molecular Force Field: Structure, Dynamics, and Intermolecular Recognition. *J Chem Theory Comput* **5**, 2531-2543, doi:<https://doi.org/10.1021/ct9002114> (2009).
- 515 H. J. C., B., J. P. M., P., W. F., v. G., A., D. & J. R., H. Molecular dynamics with coupling to an external bath. *J Chem Phys*, 3684-3690, doi:<https://doi.org/10.1063/1.448118> (1984).
- 516 Bussi, G., Donadio, D. & Parrinello, M. Canonical sampling through velocity rescaling. *J Chem Phys* **126**, doi:<https://doi.org/10.1063/1.2408420> (2007).
- 517 Eyal, E., Lum, G. & Bahar, I. The anisotropic network model web server at 2015 (ANM 2.0). *Bioinformatics* **31**, 1487-1489, doi:<https://doi.org/10.1093/bioinformatics/btu847> (2015).
- 518 Zaghmi, A., Greschner, A. A. & Gauthier, M. A. in *Polymer-Protein Conjugates From PEGylation and Beyond* (ed Gianfranco Pasut and Samuel Zalipsky) Ch. 7, 389-406 (Elsevier, 2019).
- 519 Lipinski, C. A., Lombardo, F., Dominy, B. W. & Feeney, P. J. Experimental and computational approaches to estimate solubility and permeability in drug discovery and development settings. *Adv Drug Deliv Rev* **46**, 3-26, doi:[https://doi.org/10.1016/s0169-409x\(00\)00129-0](https://doi.org/10.1016/s0169-409x(00)00129-0) (2001).
- 520 Zheng, K., Trivedi, M. & Siahaan, T. J. Structure and function of the intercellular junctions: Barrier of paracellular drug delivery. *Curr Pharm Design* **12**, 2813-2824, doi:<https://doi.org/10.2174/138161206777947722> (2006).
- 521 Van Itallie, C. M. & Anderson, J. M. Measuring Size-Dependent Permeability of the Tight Junction Using PEG Profiling. *Claudins: Methods and Protocols* **762**, 1-11, doi:[https://doi.org/10.1007/978-1-61779-185-7\\_1](https://doi.org/10.1007/978-1-61779-185-7_1) (2011).
- 522 Meredith, M. E., Salameh, T. S. & Banks, W. A. Intranasal Delivery of Proteins and Peptides in the Treatment of Neurodegenerative Diseases. *Aaps J* **17**, 780-787, doi:<https://doi.org/10.1208/s12248-015-9719-7> (2015).
- 523 Huang, T. T., Smith, A., Chen, J. & Li, P. Y. Intranasal Delivery of Therapeutic Peptides for Treatment of Ischemic Brain Injury. *Spr Ser Transl Stroke*, 65-73, doi:[https://doi.org/10.1007/978-3-030-16715-8\\_6](https://doi.org/10.1007/978-3-030-16715-8_6) (2019).

- 524 Shevchenko, K. V., Nagaev, I. Y., Andreeva, L. A., Shevchenko, V. P. & Myasoedov, N. F. Molecular-Biological Problems of Drug Design and Mechanism of Drug Action Prospects for Intranasal Delivery of Neuropeptides to the Brain. *Pharm Chem J* **53**, 89-100, doi:<https://doi.org/10.1007/s11094-019-01960-x> (2019).
- 525 Daood, M., Tsai, C., Ahdab-Barmada, M. & Watchko, J. F. ABC transporter (P-gp/ABCB1, MRP1/ABCC1, BCRP/ABCG2) expression in the developing human CNS. *Neuropediatrics* **39**, 211-218, doi:<https://doi.org/10.1055/s-0028-1103272> (2008).
- 526 Doherty, G. J. & McMahon, H. T. Mechanisms of Endocytosis. *Annu Rev Biochem* **78**, 857-902, doi:<https://doi.org/10.1146/annurev.biochem.78.081307.110540> (2009).
- 527 Herve, F., Ghinea, N. & Scherrmann, J. M. CNS delivery via adsorptive transcytosis. *Aaps J* **10**, 455-472, doi:<https://doi.org/10.1208/s12248-008-9055-2> (2008).
- 528 Oldendorf, W. H., Cornford, M. E. & Brown, W. J. The large apparent work capability of the blood-brain barrier: a study of the mitochondrial content of capillary endothelial cells in brain and other tissues of the rat. *Ann Neurol* **1**, 409-417, doi:<https://doi.org/10.1002/ana.410010502> (1977).
- 529 Furtado, D. *et al.* Overcoming the Blood-Brain Barrier: The Role of Nanomaterials in Treating Neurological Diseases. *Adv Mater* **30**, doi:<https://doi.org/10.1002/adma.201801362> (2018).
- 530 Moos, T. & Morgan, E. H. Transferrin and transferrin receptor function in brain barrier systems. *Cell Mol Neurobiol* **20**, 77-95, doi:<https://doi.org/10.1023/A:1006948027674> (2000).
- 531 Gaillard, P. J., Visser, C. C. & de Boer, A. G. Targeted delivery across the blood-brain barrier. *Expert Opin Drug Deliv* **2**, 299-309, doi:<https://doi.org/10.1517/17425247.2.2.299> (2005).
- 532 Ullrich, A. *et al.* Human insulin receptor and its relationship to the tyrosine kinase family of oncogenes. *Nature* **313**, 756-761, doi:<https://doi.org/10.1038/313756a0> (1985).
- 533 Lajoie, J. M. & Shusta, E. V. Targeting receptor-mediated transport for delivery of biologics across the blood-brain barrier. *Annu Rev Pharmacol Toxicol* **55**, 613-631, doi:<https://doi.org/10.1146/annurev-pharmtox-010814-124852> (2015).
- 534 Demeule, M. *et al.* Involvement of the low-density lipoprotein receptor-related protein in the transcytosis of the brain delivery vector Angiopep-2. *J Neurochem* **106**, 1534-1544, doi:<https://doi.org/10.1111/j.1471-4159.2008.05492.x> (2008).
- 535 Schwartz, M. W., Seeley, R. J., Campfield, L. A., Burn, P. & Baskin, D. G. Identification of targets of leptin action in rat hypothalamus. *J Clin Invest* **98**, 1101-1106, doi:<https://doi.org/10.1172/Jci118891> (1996).
- 536 Sierra-Honigmann, M. R. *et al.* Biological action of leptin as an angiogenic factor. *Science* **281**, 1683-1686, doi:<https://doi.org/10.1126/science.281.5383.1683> (1998).
- 537 Golden, P. L., Maccagnan, T. J. & Pardridge, W. M. Human blood-brain barrier leptin receptor - Binding and endocytosis in isolated human brain microvessels. *J Clin Invest* **99**, 14-18, doi:<https://doi.org/10.1172/Jci119125> (1997).
- 538 Liu, C. *et al.* Expression and characterization of a putative high affinity human soluble leptin receptor. *Endocrinology* **138**, 3548-3554, doi:<https://doi.org/10.1210/endo.138.8.5343> (1997).
- 539 Huey, R., Hawthorne, S. & McCarron, P. The potential use of rabies virus glycoprotein-derived peptides to facilitate drug delivery into the central nervous system: a mini review. *J Drug Target* **25**, 379-385, doi:<https://doi.org/10.1080/1061186X.2016.1223676> (2017).

- 540 Dani, J. A. Neuronal Nicotinic Acetylcholine Receptor Structure and Function and Response to Nicotine. *Int Rev Neurobiol* **124**, 3-19, doi:<https://doi.org/10.1016/bs.im.2015.07.001> (2015).
- 541 Unwin, N. Refined structure of the nicotinic acetylcholine receptor at 4 angstrom resolution. *J Mol Biol* **346**, 967-989, doi:<https://doi.org/10.1016/j.jmb.2004.12.031> (2005).
- 542 Dineley, K. T., Pandya, A. A. & Yakel, J. L. Nicotinic ACh receptors as therapeutic targets in CNS disorders. *Trends Pharmacol Sci* **36**, 96-108, doi:<https://doi.org/10.1016/j.tips.2014.12.002> (2015).
- 543 Gaillard, P. J., Brink, A. & de Boer, A. G. Diphtheria toxin receptor-targeted brain drug delivery. *Int Congr Ser* **1277**, 185-198, doi:<https://doi.org/10.1016/j.ics.2005.02.022> (2005).
- 544 Collier, R. J. Understanding the mode of action of diphtheria toxin: a perspective on progress during the 20th century. *Toxicon* **39**, 1793-1803, doi:[https://doi.org/10.1016/S0041-0101\(01\)00165-9](https://doi.org/10.1016/S0041-0101(01)00165-9) (2001).
- 545 Vinante, F. & Rigo, A. Heparin-binding epidermal growth factor-like growth factor/diphtheria toxin receptor in normal and neoplastic hematopoiesis. *Toxins (Basel)* **5**, 1180-1201, doi:<https://doi.org/10.3390/toxins5061180> (2013).
- 546 Sockolosky, J. T. & Szoka, F. C. The neonatal Fc receptor, FcRn, as a target for drug delivery and therapy. *Adv Drug Deliv Rev* **91**, 109-124, doi:<https://doi.org/10.1016/j.addr.2015.02.005> (2015).
- 547 Ruano-Salguero, J. S. & Lee, K. H. Antibody transcytosis across brain endothelial-like cells occurs nonspecifically and independent of FcRn. *Sci Rep* **10**, doi:<https://doi.org/10.1038/s41598-020-60438-z> (2020).
- 548 Lambert, L. A., Perri, H. & Meehan, T. J. Evolution of duplications in the transferrin family of proteins. *Comp Biochem Physiol B Biochem Mol Biol* **140**, 11-25, doi:<https://doi.org/10.1016/j.cbpc.2004.09.012> (2005).
- 549 Anderson, G. J. & Vulpe, C. D. Mammalian iron transport. *Cell Mol Life Sci* **66**, 3241-3261, doi:<https://doi.org/10.1007/s00018-009-0051-1> (2009).
- 550 Johnsen, K. B. *et al.* Targeting transferrin receptors at the blood-brain barrier improves the uptake of immunoliposomes and subsequent cargo transport into the brain parenchyma. *Sci Rep* **7**, 10396, doi:<https://doi.org/10.1038/s41598-017-11220-1> (2017).
- 551 Johnsen, K. B., Burkhart, A., Thomsen, L. B., Andresen, T. L. & Moos, T. Targeting the transferrin receptor for brain drug delivery. *Prog Neurobiol* **181**, 101665, doi:<https://doi.org/10.1016/j.pneurobio.2019.101665> (2019).
- 552 Deane, R., Zheng, W. & Zlokovic, B. V. Brain capillary endothelium and choroid plexus epithelium regulate transport of transferrin-bound and free iron into the rat brain. *J Neurochem* **88**, 813-820, doi:<https://doi.org/10.1046/j.1471-4159.2003.02221.x> (2004).
- 553 Strazielle, N. & Ghersi-Egea, J. F. Physiology of Blood-Brain Interfaces in Relation to Brain Disposition of Small Compounds and Macromolecules. *Mol Pharmaceut* **10**, 1473-1491, doi:10.1021/mp300518e (2013).
- 554 Niewoehner, J. *et al.* Increased Brain Penetration and Potency of a Therapeutic Antibody Using a Monovalent Molecular Shuttle. *Neuron* **81**, 49-60, doi:<https://doi.org/10.1016/j.neuron.2013.10.061> (2014).
- 555 Sade, H. *et al.* A Human Blood-Brain Barrier Transcytosis Assay Reveals Antibody Transcytosis Influenced by pH-Dependent Receptor Binding. *Plos One* **9**,

- doi:<https://doi.org/10.1371/journal.pone.0096340> (2014).
- 556 Haqqani, A. S. *et al.* Intracellular sorting and transcytosis of the rat transferrin receptor antibody OX26 across the blood-brain barrier in vitro is dependent on its binding affinity. *J Neurochem* **146**, 735-752, doi:<https://doi.org/10.1111/jnc.14482> (2018).
- 557 Pardridge, W. M., Boado, R. J., Patrick, D. J., Hui, E. K. W. & Lu, J. Z. Blood-Brain Barrier Transport, Plasma Pharmacokinetics, and Neuropathology Following Chronic Treatment of the Rhesus Monkey with a Brain Penetrating Humanized Monoclonal Antibody Against the Human Transferrin Receptor. *Mol Pharm* **15**, 5207-5216, doi:<https://doi.org/10.1021/acs.molpharmaceut.8b00730> (2018).
- 558 Yu, Y. J. *et al.* Therapeutic bispecific antibodies cross the blood-brain barrier in nonhuman primates. *Sci Transl Med* **6**, doi:<https://doi.org/10.1126/scitranslmed.3009835> (2014).
- 559 Nga, B. L. *et al.* Transferrin receptor (TfR) trafficking determines brain uptake of TfR antibody affinity variants. *J Exp Med* **211**, 233-244, doi:<https://doi.org/10.1084/jem.20131660> (2014).
- 560 Rhea, E. M. & Banks, W. A. Role of the Blood-Brain Barrier in Central Nervous System Insulin Resistance. *Front. Neurosci.* **13**, 521, doi:<https://doi.org/10.3389/fnins.2019.00521> (2019).
- 561 Gaillard, P. J., Visser, C. C. & de Boer, A. G. Targeted delivery across the blood-brain barrier. *Expert Opin. Drug Deliv.* **2**, 299-309, doi:<https://doi.org/10.1517/17425247.2.2.299> (2005).
- 562 Gray, S. M., Aylor, K. W. & Barrett, E. J. Unravelling the regulation of insulin transport across the brain endothelial cell. *Diabetologia* **60**, 1512-1521, doi:<https://doi.org/10.1007/s00125-017-4285-4> (2017).
- 563 Kim, J. A., Casalini, T., Brambilla, D. & Leroux, J. C. Presumed LRP1-targeting transport peptide delivers beta-secretase inhibitor to neurons in vitro with limited efficiency. *Sci Rep* **6**, 34297, doi:<https://doi.org/10.1038/srep34297> (2016).
- 564 Montagne, A. *et al.* Blood-brain barrier breakdown in the aging human hippocampus. *Neuron* **85**, 296-302, doi:<https://doi.org/10.1016/j.neuron.2014.12.032> (2015).
- 565 Turjeman, K. *et al.* Nano-Drugs Based on Nano Sterically Stabilized Liposomes for the Treatment of Inflammatory Neurodegenerative Diseases. *Plos One* **10**, e0130442, doi:<https://doi.org/10.1371/journal.pone.0130442> (2015).
- 566 Zlokovic, B. V. The blood-brain barrier in health and chronic neurodegenerative disorders. *Neuron* **57**, 178-201, doi:<https://doi.org/10.1016/j.neuron.2008.01.003> (2008).
- 567 Sweeney, M. D., Sagare, A. P. & Zlokovic, B. V. Blood-brain barrier breakdown in Alzheimer disease and other neurodegenerative disorders. *Nat Rev Neurol* **14**, 133-150, doi:<https://doi.org/10.1038/nrneurol.2017.188> (2018).
- 568 Vos, C. M. P. *et al.* Blood-brain barrier alterations in both focal and diffuse abnormalities on postmortem MRI in multiple sclerosis. *Neurobiol Dis* **20**, 953-960, doi:<https://doi.org/10.1016/j.nbd.2005.06.012> (2005).
- 569 Waubant, E. Biomarkers indicative of blood-brain barrier disruption in multiple sclerosis. *Dis Markers* **22**, 235-244, doi:<https://doi.org/10.1155/2006/709869> (2006).
- 570 Bakshi, R., Minagar, A., Jaisani, Z. & Wolinsky, J. S. Imaging of multiple sclerosis: role in neurotherapeutics. *NeuroRx* **2**, 277-303, doi:<https://doi.org/10.1602/neurorx.2.2.277> (2005).
- 571 Kermode, A. G. *et al.* Breakdown of the Blood-Brain-Barrier Precedes Symptoms and

- Other Mri Signs of New Lesions in Multiple-Sclerosis - Pathogenetic and Clinical Implications. *Brain* **113**, 1477-1489, doi:<https://doi.org/10.1093/brain/113.5.1477> (1990).
- 572 Claudio, L., Raine, C. S. & Brosnan, C. F. Evidence of Persistent Blood-Brain-Barrier Abnormalities in Chronic-Progressive Multiple-Sclerosis. *Acta Neuropathologica* **90**, 228-238, doi:<https://doi.org/10.1007/BF00296505> (1995).
- 573 Kermode, A. G. *et al.* Heterogeneity of blood-brain barrier changes in multiple sclerosis: an MRI study with gadolinium-DTPA enhancement. *Neurology* **40**, 229-235, doi:<https://doi.org/10.1212/WNL.40.2.229> (1990).
- 574 Grossman, R. I. *et al.* Multiple sclerosis: serial study of gadolinium-enhanced MR imaging. *Radiology* **169**, 117-122, doi:<https://doi.org/10.1148/radiology.169.1.3420246> (1988).
- 575 Yong, V. W. Metalloproteinases: Mediators of pathology and regeneration in the CNS. *Nat Rev Neurosci* **6**, 931-944, doi:<https://doi.org/10.1038/nrn1807> (2005).
- 576 Opendakker, G., Nelissen, I. & Van Damme, J. Functional roles and therapeutic targeting of gelatinase B and chemokines in multiple sclerosis. *Lancet Neurol* **2**, 747-756, doi:[https://doi.org/10.1016/S1474-4422\(03\)00587-8](https://doi.org/10.1016/S1474-4422(03)00587-8) (2003).
- 577 Bar-Or, A. *et al.* Analyses of all matrix metalloproteinase members in leukocytes emphasize monocytes as major inflammatory mediators in multiple sclerosis. *Brain* **126**, 2738-2749, doi:<https://doi.org/10.1093/brain/awq285> (2003).
- 578 Goncalves, A., Ambrosio, A. F. & Fernandes, R. Regulation of claudins in blood-tissue barriers under physiological and pathological states. *Tissue Barriers* **1**, e24782, doi:<https://doi.org/10.4161/tisb.24782> (2013).
- 579 Pfeiffer, F. *et al.* Claudin-1 induced sealing of blood-brain barrier tight junctions ameliorates chronic experimental autoimmune encephalomyelitis. *Acta Neuropathol* **122**, 601-614, doi:<https://doi.org/10.1007/s00401-011-0883-2> (2011).
- 580 Wolburg, H. *et al.* Localization of claudin-3 in tight junctions of the blood-brain barrier is selectively lost during experimental autoimmune encephalomyelitis and human glioblastoma multiforme. *Acta Neuropathol* **105**, 586-592, doi:<https://doi.org/10.1007/s00401-003-0688-z> (2003).
- 581 Morgan, L. *et al.* Inflammation and dephosphorylation of the tight junction protein occludin in an experimental model of multiple sclerosis. *Neuroscience* **147**, 664-673, doi:<https://doi.org/10.1016/j.neuroscience.2007.04.051> (2007).
- 582 Wosik, K. *et al.* Angiotensin II controls occludin function and is required for blood-brain barrier maintenance: Relevance to multiple sclerosis. *J Neurosci* **27**, 9032-9042, doi:<https://doi.org/10.1523/Jneurosci.2088-07.2007> (2007).
- 583 Argaw, A. T., Gurfein, B. T., Zhang, Y., Zameer, A. & John, G. R. VEGF-mediated disruption of endothelial CLN-5 promotes blood-brain barrier breakdown. *P Natl Acad Sci USA* **106**, 1977-1982, doi:<https://doi.org/10.1073/pnas.0808698106> (2009).
- 584 Kirk, J., Plumb, J., Mirakhur, M. & McQuaid, S. Tight junctional abnormality in multiple sclerosis white matter affects all calibres of vessel and is associated with blood-brain barrier leakage and active demyelination. *J Pathol* **201**, 319-327, doi:<https://doi.org/10.1002/path.1434> (2003).
- 585 Minagar, A. *et al.* Serum from patients with multiple sclerosis downregulates occludin and VE-cadherin expression in cultured endothelial cells. *Mult Scler* **9**, 235-238, doi:<https://doi.org/10.1191/1352458503ms916oa> (2003).
- 586 Kraus, J. & Oschmann, P. The impact of interferon-beta treatment on the blood-brain barrier. *Drug Discov Today* **11**, 755-762,

- doi:<https://doi.org/10.1016/j.drudis.2006.06.008> (2006).
- 587 Finkelsztejn, A. Multiple sclerosis: overview of disease-modifying agents. *Perspect Medicin Chem* **6**, 65-72, doi:<https://doi.org/10.4137/PMC.S13213> (2014).
- 588 Schultz, M. L., Tecedor, L., Chang, M. & Davidson, B. L. Clarifying lysosomal storage diseases. *Trends Neurosci* **34**, 401-410, doi:<https://doi.org/10.1016/j.tins.2011.05.006> (2011).
- 589 Clarke, L. A. The mucopolysaccharidoses: a success of molecular medicine (vol 10, e1, 2008). *Expert Rev Mol Med* **11**, doi:<https://doi.org/10.1017/S1462399409001185> (2009).
- 590 Giugliani, R. *et al.* Mucopolysaccharidosis I, II, and VI: Brief review and guidelines for treatment. *Genet Mol Biol* **33**, 589-U520, doi:<https://doi.org/10.1590/S1415-47572010005000093> (2010).
- 591 Filocamo, M., Tomanin, R., Bertola, F. & Morrone, A. Biochemical and molecular analysis in mucopolysaccharidoses: what a paediatrician must know. *Ital J Pediatr* **44**, doi:<https://doi.org/10.1186/s13052-018-0553-2> (2018).
- 592 Lim, M. J. *et al.* IgG entry and deposition are components of the neuroimmune response in Batten disease. *Neurobiol Dis* **25**, 239-251, doi:<https://doi.org/10.1016/j.nbd.2006.09.005> (2007).
- 593 Jeyakumar, M. *et al.* Central nervous system inflammation is a hallmark of pathogenesis in mouse models of GM1 and GM2 gangliosidosis. *Brain* **126**, 974-987, doi:<https://doi.org/10.1093/brain/awg089> (2003).
- 594 Garbuzova-Davis, S. *et al.* Blood-brain barrier impairment in an animal model of MPS III B. *Plos One* **6**, e16601, doi:<https://doi.org/10.1371/journal.pone.0016601> (2011).
- 595 Garbuzova-Davis, S. *et al.* Blood-brain barrier impairment in MPS III patients. *BMC Neurol* **13**, 174, doi:<https://doi.org/10.1186/1471-2377-13-174> (2013).
- 596 Garbuzova-Davis, S. *et al.* Blood-Brain Barrier Impairment in an Animal Model of MPS III B. *Plos One* **6**, doi:ARTN e16601  
10.1371/journal.pone.0016601 (2011).
- 597 Mehta, A. B. & Winchester, B. *Lysosomal storage disorders: a practical guide*. (Wiley-Blackwell, 2012).
- 598 Scarpa, M., Bellettato, C. M., Lampe, C. & Begley, D. J. Neuronopathic lysosomal storage disorders: Approaches to treat the central nervous system. *Best Pract Res Clin Endocrinol Metab* **29**, 159-171, doi:<https://doi.org/10.1016/j.beem.2014.12.001> (2015).
- 599 Arfi, A. *et al.* Neuroinflammatory and oxidative stress phenomena in MPS IIIA mouse model: The positive effect of long-term aspirin treatment. *Mol Genet Metab* **103**, 18-25, doi:<https://doi.org/10.1016/j.ymgme.2011.01.015> (2011).
- 600 Killedar, S. *et al.* Mucopolysaccharidosis IIIB, a lysosomal storage disease, triggers a pathogenic CNS autoimmune response. *J Neuroinflammation* **7**, 39, doi:<https://doi.org/10.1186/1742-2094-7-39> (2010).
- 601 Sandoval, K. E. & Witt, K. A. Blood-brain barrier tight junction permeability and ischemic stroke. *Neurobiol Dis* **32**, 200-219, doi:<https://doi.org/10.1016/j.nbd.2008.08.005> (2008).
- 602 Kastrop, A., Engelhorn, T., Beaulieu, C., de Crespigny, A. & Moseley, M. E. Dynamics of cerebral injury, perfusion, and blood-brain barrier changes after temporary and permanent middle cerebral artery occlusion in the rat. *J Neurol Sci* **166**, 91-99, doi:[https://doi.org/10.1016/s0022-510x\(99\)00121-5](https://doi.org/10.1016/s0022-510x(99)00121-5) (1999).

- 603 Kidd, G. A., Hong, H., Majid, A., Kaufman, D. I. & Chen, A. F. Inhibition of brain GTP cyclohydrolase I and tetrahydrobiopterin attenuates cerebral infarction via reducing inducible NO synthase and peroxynitrite in ischemic stroke. *Stroke* **36**, 2705-2711, doi:<https://doi.org/10.1161/01.STR.0000190000.98707.6d> (2005).
- 604 Kuntz, M. *et al.* Stroke-induced brain parenchymal injury drives blood-brain barrier early leakage kinetics: a combined in vivo/in vitro study. *J Cereb Blood Flow Metab* **34**, 95-107, doi:<https://doi.org/10.1038/jcbfm.2013.169> (2014).
- 605 Durukan, A. *et al.* Post-ischemic blood-brain barrier leakage in rats: One-week follow-up by MRI. *Brain Res* **1280**, 158-165, doi:<https://doi.org/10.1016/j.brainres.2009.05.025> (2009).
- 606 Hao, J. & Bickel, U. Transferrin Receptor Mediated Brain Uptake During Ischemia and Reperfusion. *J Pharm Pharm Sci* **16**, 541-550, doi:<https://doi.org/10.18433/J3b303> (2013).
- 607 Pardridge, W. M. Delivery of Biologics Across the Blood-Brain Barrier with Molecular Trojan Horse Technology. *Biodrugs* **31**, 503-519, doi:<https://doi.org/10.1007/s40259-017-0248-z> (2017).
- 608 Ng, S. Y. & Lee, A. Y. W. Traumatic Brain Injuries: Pathophysiology and Potential Therapeutic Targets. *Front Cell Neurosci* **13**, 528, doi:<https://doi.org/10.3389/fncel.2019.00528> (2019).
- 609 Baskaya, M. K., Rao, A. M., Dogan, A., Donaldson, D. & Dempsey, R. J. The biphasic opening of the blood-brain barrier in the cortex and hippocampus after traumatic brain injury in rats. *Neurosci Lett* **226**, 33-36, doi:[https://doi.org/10.1016/s0304-3940\(97\)00239-5](https://doi.org/10.1016/s0304-3940(97)00239-5) (1997).
- 610 Smith, D. H. *et al.* Pre-Clinical Traumatic Brain Injury Common Data Elements: Toward a Common Language Across Laboratories. *J Neurotrauma* **32**, 1725-1735, doi:<https://doi.org/10.1089/neu.2014.3861> (2015).
- 611 McKee, A. C. & Daneshvar, D. H. The neuropathology of traumatic brain injury. *Handb Clin Neurol* **127**, 45-66, doi:<https://doi.org/10.1016/B978-0-444-52892-6.00004-0> (2015).
- 612 Shlosberg, D., Benifla, M., Kaufer, D. & Friedman, A. Blood-brain barrier breakdown as a therapeutic target in traumatic brain injury. *Nat Rev Neurol* **6**, 393-403, doi:<https://doi.org/10.1038/nrneurol.2010.74> (2010).
- 613 Qian, Z. Y., Li, Q. Y., Huang, S. M. & Ma, H. Protective effect of rhEPO on tight junctions of cerebral microvascular endothelial cells early following traumatic brain injury in rats. *Brain Injury* **30**, 462-467, doi:<https://doi.org/10.3109/02699052.2015.1080386> (2016).
- 614 Wen, J. *et al.* Overexpression of netrin-1 increases the expression of tight junction-associated proteins, claudin-5, occludin, and ZO-1, following traumatic brain injury in rats. *Exp Ther Med* **8**, 881-886, doi:<https://doi.org/10.3892/etm.2014.1818> (2014).
- 615 Ray, S. K., Dixon, C. E. & Banik, N. L. Molecular mechanisms in the pathogenesis of traumatic brain injury. *Histol Histopathol* **17**, 1137-1152, doi:<https://doi.org/10.14670/HH-17.1137> (2002).
- 616 Maas, A. I., Roozenbeek, B. & Manley, G. T. Clinical trials in traumatic brain injury: past experience and current developments. *Neurotherapeutics* **7**, 115-126, doi:<https://doi.org/10.1016/j.nurt.2009.10.022> (2010).
- 617 Narayan, R. K. *et al.* Clinical trials in head injury. *J Neurotrauma* **19**, 503-557, doi:<https://doi.org/10.1089/089771502753754037> (2002).
- 618 Gaugler, J. *et al.* 2019 Alzheimer's disease facts and figures. *Alzheimers Dement* **15**, 321-387, doi:<https://doi.org/10.1016/j.jalz.2019.01.010> (2019).

- 619 Nation, D. A. *et al.* Blood-brain barrier breakdown is an early biomarker of human cognitive dysfunction. *Nat Med* **25**, 270-276, doi:<https://doi.org/10.1038/s41591-018-0297-y> (2019).
- 620 Guan, J. *et al.* Vascular degeneration in Parkinson's disease. *Brain Pathol* **23**, 154-164, doi:<https://doi.org/10.1111/j.1750-3639.2012.00628.x> (2013).
- 621 Gray, M. T. & Woulfe, J. M. Striatal blood-brain barrier permeability in Parkinson's disease. *J Cereb Blood Flow Metab* **35**, 747-750, doi:<https://doi.org/10.1038/jcbfm.2015.32> (2015).
- 622 Drouin-Ouellet, J. *et al.* Cerebrovascular and blood-brain barrier impairments in Huntington's disease: Potential implications for its pathophysiology. *Ann Neurol* **78**, 160-177, doi:<https://doi.org/10.1002/ana.24406> (2015).
- 623 Dorfel, M. J. & Huber, O. Modulation of tight junction structure and function by kinases and phosphatases targeting occludin. *J Biomed Biotechnol* **2012**, 807356, doi:<https://doi.org/10.1155/2012/807356> (2012).
- 624 Cummins, P. M. Occludin: one protein, many forms. *Mol Cell Biol* **32**, 242-250, doi:<https://doi.org/10.1128/MCB.06029-11> (2012).
- 625 Carvey, P. M., Hendey, B. & Monahan, A. J. The blood-brain barrier in neurodegenerative disease: a rhetorical perspective. *J Neurochem* **111**, 291-314, doi:<https://doi.org/10.1111/j.1471-4159.2009.06319.x> (2009).
- 626 Maiuolo, J. *et al.* The "Frail" Brain Blood Barrier in Neurodegenerative Diseases: Role of Early Disruption of Endothelial Cell-to-Cell Connections. *Int J Mol Sci* **19**, doi:<https://doi.org/10.3390/ijms19092693> (2018).
- 627 Rhea, E. M. & Banks, W. A. Role of the Blood-Brain Barrier in Central Nervous System Insulin Resistance. *Front Neurosci-Switz* **13**, doi:ARTN 521 10.3389/fnins.2019.00521 (2019).
- 628 Kalaria, R. N., Sromek, S. M., Grahovac, I. & Harik, S. I. Transferrin Receptors of Rat and Human Brain and Cerebral Microvessels and Their Status in Alzheimers-Disease. *Brain Res* **585**, 87-93, doi:[https://doi.org/10.1016/0006-8993\(92\)91193-I](https://doi.org/10.1016/0006-8993(92)91193-I) (1992).
- 629 Morris, C. M., Candy, J. M., Kerwin, J. M. & Edwardson, J. A. Transferrin Receptors in the Normal Human Hippocampus and in Alzheimers-Disease. *Neuropath Appl Neuro* **20**, 473-477, doi:<https://doi.org/10.1111/j.1365-2990.1994.tb00998.x> (1994).
- 630 Faucheux, B. A., Hauw, J. J., Agid, Y. & Hirsch, E. C. The density of [I-125]-transferrin binding sites on perikarya of melanized neurons of the substantia nigra is decreased in Parkinson's disease. *Brain Res* **749**, 170-174, doi:[https://doi.org/10.1016/S0006-8993\(96\)01412-6](https://doi.org/10.1016/S0006-8993(96)01412-6) (1997).
- 631 Faucheux, B. A. *et al.* Distribution of I-125 Ferrotransferrin Binding-Sites in the Mesencephalon of Control Subjects and Patients with Parkinsons-Disease. *J Neurochem* **60**, 2338-2341, doi:<https://doi.org/10.1111/j.1471-4159.1993.tb03527.x> (1993).
- 632 Morris, C. M., Candy, J. M., Omar, S., Bloxham, C. A. & Edwardson, J. A. Transferrin Receptors in the Parkinsonian Midbrain. *Neuropath Appl Neuro* **20**, 468-472, doi:<https://doi.org/10.1111/j.1365-2990.1994.tb00997.x> (1994).
- 633 Bien-Ly, N. *et al.* Lack of Widespread BBB Disruption in Alzheimer's Disease Models: Focus on Therapeutic Antibodies. *Neuron* **88**, 289-297, doi:<https://doi.org/10.1016/j.neuron.2015.09.036> (2015).
- 634 Bourassa, P., Alata, W., Tremblay, C., Paris-Robidas, S. & Calon, F. Transferrin Receptor-Mediated Uptake at the Blood-Brain Barrier Is Not Impaired by Alzheimer's

- Disease Neuropathology. *Mol Pharm* **16**, 583-594, doi:<https://doi.org/10.1021/acs.molpharmaceut.8b00870> (2019).
- 635 Donahue, J. E. *et al.* RAGE, LRP-1, and amyloid-beta protein in Alzheimer's disease. *Acta Neuropathol* **112**, 405-415, doi:<https://doi.org/10.1007/s00401-006-0115-3> (2006).
- 636 Shibata, M. *et al.* Clearance of Alzheimer's amyloid-ss(1-40) peptide from brain by LDL receptor-related protein-1 at the blood-brain barrier. *J Clin Invest* **106**, 1489-1499, doi:<https://doi.org/10.1172/JCI10498> (2000).
- 637 Craft, S. *et al.* Cerebrospinal fluid and plasma insulin levels in Alzheimer's disease: relationship to severity of dementia and apolipoprotein E genotype. *Neurology* **50**, 164-168, doi:<https://doi.org/10.1212/wnl.50.1.164> (1998).
- 638 Talbot, K. *et al.* Demonstrated brain insulin resistance in Alzheimer's disease patients is associated with IGF-1 resistance, IRS-1 dysregulation, and cognitive decline. *J Clin Invest* **122**, 1316-1338, doi:<https://doi.org/10.1172/JCI59903> (2012).
- 639 Wijesuriya, H. C., Bullock, J. Y., Faull, R. L. M., Hladky, S. B. & Barrand, M. A. ABC efflux transporters in brain vasculature of Alzheimer's subjects. *Brain Res* **1358**, 228-238, doi:<https://doi.org/10.1016/j.brainres.2010.08.034> (2010).
- 640 van Assema, D. M. *et al.* Blood-brain barrier P-glycoprotein function in Alzheimer's disease. *Brain* **135**, 181-189, doi:<https://doi.org/10.1093/brain/awr298> (2012).
- 641 Serot, J. M., Bene, M. C. & Faure, G. C. Choroid plexus, ageing of the brain, and Alzheimer's disease. *Front Biosci-Landmrk* **8**, S515-S521, doi:<https://doi.org/10.2741/1085> (2003).
- 642 Serot, J. M., Zmudka, J. & Jouanny, P. A Possible Role for CSF Turnover and Choroid Plexus in the Pathogenesis of Late Onset Alzheimer's Disease. *J Alzheimers Dis* **30**, 17-26, doi:<https://doi.org/10.3233/Jad-2012-111964> (2012).
- 643 Bergen, A. A. *et al.* Gene expression and functional annotation of human choroid plexus epithelium failure in Alzheimer's disease. *BMC Genomics* **16**, doi:<https://doi.org/10.1186/s12864-015-2159-z> (2015).
- 644 Brkic, M. *et al.* Amyloid beta Oligomers Disrupt Blood-CSF Barrier Integrity by Activating Matrix Metalloproteinases. *J Neurosci* **35**, 12766-12778, doi:<https://doi.org/10.1523/Jneurosci.0006-15.2015> (2015).
- 645 Patel, S. G. *et al.* Cell-penetrating peptide sequence and modification dependent uptake and subcellular distribution of green florescent protein in different cell lines. *Sci Rep* **9**, 6298, doi:<https://doi.org/10.1038/s41598-019-42456-8> (2019).
- 646 Vives, E., Brodin, P. & Lebleu, B. A truncated HIV-1 Tat protein basic domain rapidly translocates through the plasma membrane and accumulates in the cell nucleus. *J Biol Chem* **272**, 16010-16017, doi:<https://doi.org/10.1074/jbc.272.25.16010> (1997).
- 647 Drin, G. *et al.* Physico-chemical requirements for cellular uptake of pAntp peptide. Role of lipid-binding affinity. *Eur J Biochem* **268**, 1304-1314, doi:<https://doi.org/10.1046/j.1432-1327.2001.01997.x> (2001).
- 648 Wender, P. A. *et al.* The design, synthesis, and evaluation of molecules that enable or enhance cellular uptake: peptoid molecular transporters. *P Natl Acad Sci USA* **97**, 13003-13008, doi:<https://doi.org/10.1073/pnas.97.24.13003> (2000).
- 649 Bechara, C. & Sagan, S. Cell-penetrating peptides: 20 years later, where do we stand? *FEBS Lett* **587**, 1693-1702, doi:<https://doi.org/10.1016/j.febslet.2013.04.031> (2013).
- 650 Pooga, M. *et al.* Cellular translocation of proteins by transportan. *FASEB J* **15**, 1451-1453, doi:<https://doi.org/10.1096/fj.00-0780fje> (2001).

- 651 Hallbrink, M. *et al.* Cargo delivery kinetics of cell-penetrating peptides. *Biochim Biophys Acta* **1515**, 101-109, doi:[https://doi.org/10.1016/s0005-2736\(01\)00398-4](https://doi.org/10.1016/s0005-2736(01)00398-4) (2001).
- 652 Zhu, X., Jin, K., Huang, Y. & Pang, Z. in *Brain Targeted Drug Delivery System* 159-183 (Elsevier, 2019).
- 653 Fischer, R., Waizenegger, T., Kohler, K. & Brock, R. A quantitative validation of fluorophore-labelled cell-permeable peptide conjugates: fluorophore and cargo dependence of import. *Biochim Biophys Acta* **1564**, 365-374, doi:[https://doi.org/10.1016/s0005-2736\(02\)00471-6](https://doi.org/10.1016/s0005-2736(02)00471-6) (2002).
- 654 Derakhshankhah, H. & Jafari, S. Cell penetrating peptides: A concise review with emphasis on biomedical applications. *Biomed. Pharmacother.* **108**, 1090-1096, doi:<https://doi.org/10.1016/j.biopha.2018.09.097> (2018).
- 655 Koren, E., Apte, A., Sawant, R. R., Grunwald, J. & Torchilin, V. P. Cell-penetrating TAT peptide in drug delivery systems: proteolytic stability requirements. *Drug Deliv* **18**, 377-384, doi:<https://doi.org/10.3109/10717544.2011.567310> (2011).
- 656 Drin, G., Rousselle, C., Scherrmann, J. M., Rees, A. R. & Tamsamani, J. Peptide delivery to the brain via adsorptive-mediated endocytosis: advances with SynB vectors. *AAPS PharmSci* **4**, E26, doi:<https://doi.org/10.1208/ps040426> (2002).
- 657 Trehin, R. & Merkle, H. P. Chances and pitfalls of cell penetrating peptides for cellular drug delivery. *Eur J Pharm Biopharm* **58**, 209-223, doi:<https://doi.org/10.1016/j.ejpb.2004.02.018> (2004).
- 658 Rousselle, C. *et al.* Improved brain uptake and pharmacological activity of dalargin using a peptide-vector-mediated strategy. *J Pharmacol Exp Ther* **306**, 371-376, doi:<https://doi.org/10.1124/jpet.102.048520> (2003).
- 659 Rousselle, C., Clair, P., Tamsamani, J. & Scherrmann, J. M. Improved brain delivery of benzylpenicillin with a peptide-vector-mediated strategy. *J Drug Target* **10**, 309-315, doi:<https://doi.org/10.1080/10611860290031886> (2002).
- 660 Prochiantz, A. Messenger proteins: homeoproteins, TAT and others. *Curr Opin Cell Biol* **12**, 400-406, doi:[https://doi.org/10.1016/s0955-0674\(00\)00108-3](https://doi.org/10.1016/s0955-0674(00)00108-3) (2000).
- 661 Vogel, B. E. *et al.* A novel integrin specificity exemplified by binding of the alpha v beta 5 integrin to the basic domain of the HIV Tat protein and vitronectin. *J Cell Biol* **121**, 461-468, doi:<https://doi.org/10.1083/jcb.121.2.461> (1993).
- 662 Stalmans, S. *et al.* Cell-Penetrating Peptides Selectively Cross the Blood-Brain Barrier In Vivo. *Plos One* **10**, e0139652, doi:<https://doi.org/10.1371/journal.pone.0139652> (2015).
- 663 Zou, L. L., Ma, J. L., Wang, T., Yang, T. B. & Liu, C. B. Cell-penetrating Peptide-mediated therapeutic molecule delivery into the central nervous system. *Curr Neuropharmacol* **11**, 197-208, doi:<https://doi.org/10.2174/1570159X11311020006> (2013).
- 664 Schwarze, S. R., Ho, A., Vocero-Akbani, A. & Dowdy, S. F. In vivo protein transduction: delivery of a biologically active protein into the mouse. *Science* **285**, 1569-1572, doi:<https://doi.org/10.1126/science.285.5433.1569> (1999).
- 665 Fawell, S. *et al.* Tat-mediated delivery of heterologous proteins into cells. *P Natl Acad Sci USA* **91**, 664-668, doi:<https://doi.org/10.1073/pnas.91.2.664> (1994).
- 666 Kilic, U., Kilic, E., Dietz, G. P. H. & Bahr, M. Intravenous TAT-GDNF is protective after focal cerebral ischemia in mice. *Stroke* **34**, 1304-1310, doi:<https://doi.org/10.1161/01.Str.0000066869.45310.50> (2003).
- 667 Dietz, G. P. H. *et al.* Application of a blood-brain-barrier-penetrating form of GDNF in a

- mouse model for Parkinson's disease. *Brain Res* **1082**, 61-66, doi:<https://doi.org/10.1016/j.brainres.2006.01.083> (2006).
- 668 Doepfner, T. R. *et al.* TAT-Hsp70-mediated neuroprotection and increased survival of neuronal precursor cells after focal cerebral ischemia in mice. *J Cereb Blood Flow Metab* **29**, 1187-1196, doi:<https://doi.org/10.1038/jcbfm.2009.44> (2009).
- 669 Cao, G. *et al.* In Vivo Delivery of a Bcl-xL Fusion Protein Containing the TAT Protein Transduction Domain Protects against Ischemic Brain Injury and Neuronal Apoptosis. *J Neurosci* **22**, 5423-5431, doi:<https://doi.org/20026550> (2002).
- 670 Kilic, E., Dietz, G. P., Hermann, D. M. & Bahr, M. Intravenous TAT-Bcl-XI is protective after middle cerebral artery occlusion in mice. *Ann Neurol* **52**, 617-622, doi:<https://doi.org/10.1002/ana.10356> (2002).
- 671 Cai, B. *et al.* TAT-mediated delivery of neuroglobin protects against focal cerebral ischemia in mice. *Neurosci Res* **71**, E105-E105, doi:<https://doi.org/10.1016/j.neures.2011.07.447> (2011).
- 672 Xiang, L. X. *et al.* Targeted delivery of large fusion protein into hippocampal neurons by systemic administration. *J Drug Target* **19**, 632-636, doi:<https://doi.org/10.3109/1061186x.2010.523788> (2011).
- 673 Fu, A. L., Wang, Y. L., Zhan, L. P. & Zhou, R. M. Targeted Delivery of Proteins into the Central Nervous System Mediated by Rabies Virus Glycoprotein-Derived Peptide. *Pharm Res* **29**, 1562-1569, doi:<https://doi.org/10.1007/s11095-012-0667-y> (2012).
- 674 Herve, F., Ghinea, N. & Schermmann, J. M. CNS Delivery Via Adsorptive Transcytosis. *Aaps J* **10**, 455-472, doi:10.1208/s12248-008-9055-2 (2008).
- 675 Pardridge, W. M. Re-engineering biopharmaceuticals for delivery to brain with molecular Trojan horses. *Bioconjug Chem* **19**, 1327-1338, doi:<https://doi.org/10.1021/bc800148t> (2008).
- 676 Pardridge, W. M. & Boado, R. J. in *Methods Enzymol* Vol. 503 269-292 (Elsevier, 2012).
- 677 Zhang, Y. & Pardridge, W. M. Rapid transferrin efflux from brain to blood across the blood-brain barrier. *J Neurochem* **76**, 1597-1600, doi:<https://doi.org/10.1046/j.1471-4159.2001.00222.x> (2001).
- 678 Lee, H. J., Engelhardt, B., Lesley, J., Bickel, U. & Pardridge, W. M. Targeting rat anti-mouse transferrin receptor monoclonal antibodies through blood-brain barrier in mouse. *J Pharmacol Exp Ther* **292**, 1048-1052, doi:PMID: 10688622 (2000).
- 679 Pardridge, W. M., Buciak, J. L. & Friden, P. M. Selective transport of an anti-transferrin receptor antibody through the blood-brain barrier in vivo. *J Pharmacol Exp Ther* **259**, 66-70, doi:PMID: 1920136 (1991).
- 680 Broadwell, R. D., Baker-Cairns, B. J., Friden, P. M., Oliver, C. & Villegas, J. C. Transcytosis of protein through the mammalian cerebral epithelium and endothelium. III. Receptor-mediated transcytosis through the blood-brain barrier of blood-borne transferrin and antibody against the transferrin receptor. *Exp Neurol* **142**, 47-65, doi:<https://doi.org/10.1006/exnr.1996.0178> (1996).
- 681 Boado, R. J., Zhang, Y., Wang, Y. T. & Pardridge, W. M. Engineering and Expression of a Chimeric Transferrin Receptor Monoclonal Antibody for Blood-Brain Barrier Delivery in the Mouse. *Biotechnol Bioeng* **102**, 1251-1258, doi:<https://doi.org/10.1002/bit.22135> (2009).
- 682 Boado, R. J., Ji, A. M. & Pardridge, W. M. Cloning and expression in pichia pastoris of a genetically engineered single chain antibody against the rat transferrin receptor. *J Drug Target* **8**, 403-412, doi:<https://doi.org/10.3109/10611860008997916> (2000).

- 683 Li, J. Y. *et al.* Genetically engineered brain drug delivery vectors: cloning, expression and in vivo application of an anti-transferrin receptor single chain antibody-streptavidin fusion gene and protein. *Protein Eng* **12**, 787-796, doi:<https://doi.org/10.1093/protein/12.9.787> (1999).
- 684 Kang, Y. S., Voigt, K. & Bickel, U. Stability of the disulfide bond in an avidin-biotin linked chimeric peptide during in vivo transcytosis through brain endothelial cells. *J Drug Target* **8**, 425-434, doi:<https://doi.org/10.3109/10611860008997918> (2000).
- 685 Pardridge, W. M., Wu, D. F. & Sakane, T. Combined use of carboxyl-directed protein pegylation and vector-mediated blood-brain barrier drug delivery system optimizes brain uptake of brain-derived neurotrophic factor following intravenous administration. *Pharm Res* **15**, 576-582, doi:<https://doi.org/10.1023/A:1011981927620> (1998).
- 686 Saito, Y., BUclAK, J., Yang, J. & Pardridge, W. M. Vector-mediated delivery of 125I-labeled beta-amyloid peptide A beta 1-40 through the blood-brain barrier and binding to Alzheimer disease amyloid of the A beta 1-40/vector complex. *P Natl Acad Sci USA* **92**, 10227-10231, doi:<https://doi.org/10.1073/pnas.92.22.10227> (1995).
- 687 Boado, R. J., Zhou, Q. H., Lu, J. Z., Hui, E. K. & Pardridge, W. M. Pharmacokinetics and brain uptake of a genetically engineered bifunctional fusion antibody targeting the mouse transferrin receptor. *Mol Pharm* **7**, 237-244, doi:<https://doi.org/10.1021/mp900235k> (2010).
- 688 Zhou, Q. H., Boado, R. J., Lu, J. Z., Hui, E. K. & Pardridge, W. M. Brain-penetrating IgG-iduronate 2-sulfatase fusion protein for the mouse. *Drug Metab Dispos* **40**, 329-335, doi:<https://doi.org/10.1124/dmd.111.042903> (2012).
- 689 Zhou, Q.-H. *et al.* Receptor-mediated abeta amyloid antibody targeting to Alzheimer's disease mouse brain. *Mol Pharm* **8**, 280-285, doi:<https://doi.org/10.1021/mp1003515> (2011).
- 690 Zhou, Q. H., Boado, R. J., Hui, E. K., Lu, J. Z. & Pardridge, W. M. Brain-penetrating tumor necrosis factor decoy receptor in the mouse. *Drug Metab Dispos* **39**, 71-76, doi:<https://doi.org/10.1124/dmd.110.036012> (2011).
- 691 Zhou, Q. H., Boado, R. J., Lu, J. Z., Hui, E. K. & Pardridge, W. M. Monoclonal antibody-glial-derived neurotrophic factor fusion protein penetrates the blood-brain barrier in the mouse. *Drug Metab Dispos* **38**, 566-572, doi:<https://doi.org/10.1124/dmd.109.031534> (2010).
- 692 Boado, R. J., Hui, E. K. W., Lu, J. Z., Zhou, Q. H. & Pardridge, W. M. Reversal of Lysosomal Storage in Brain of Adult MPS-I Mice with Intravenous Trojan Horse-Iduronidase Fusion Protein. *Mol Pharm* **8**, 1342-1350, doi:<https://doi.org/10.1021/mp200136x> (2011).
- 693 Thom, G. *et al.* Enhanced Delivery of Galanin Conjugates to the Brain through Bioengineering of the Anti-Transferrin Receptor Antibody OX26. *Mol Pharm* **15**, 1420-1431, doi:<https://doi.org/10.1021/acs.molpharmaceut.7b00937> (2018).
- 694 Zhou, Q. H., Boado, R. J., Lu, J. Z., Hui, E. K. & Pardridge, W. M. Re-engineering erythropoietin as an IgG fusion protein that penetrates the blood-brain barrier in the mouse. *Mol Pharm* **7**, 2148-2155, doi:<https://doi.org/10.1021/mp1001763> (2010).
- 695 Zhou, Q. H., Boado, R. J., Hui, E. K. W., Lu, J. Z. & Pardridge, W. M. Brain-Penetrating Tumor Necrosis Factor Decoy Receptor in the Mouse. *Drug Metab Dispos* **39**, 71-76, doi:<https://doi.org/10.1124/dmd.110.036012> (2011).
- 696 Sumbria, R. K., Boado, R. J. & Pardridge, W. M. Brain protection from stroke with intravenous TNF alpha decoy receptor-Trojan horse fusion protein. *J Cereb Blood Flow Metab* **32**, 1933-1938, doi:<https://doi.org/10.1038/jcbfm.2012.97> (2012).

- 697 Yang, M., Chen, J. C., Zhao, J. & Meng, M. Etanercept Attenuates Myocardial Ischemia/Reperfusion Injury by Decreasing Inflammation and Oxidative Stress. *Plos One* **9**, doi:<https://doi.org/10.1371/journal.pone.0108024> (2014).
- 698 Boado, R. J., Hui, E. K. W., Lu, J. Z., Zhou, Q. H. & Pardridge, W. M. Selective targeting of a TNFR decoy receptor pharmaceutical to the primate brain as a receptor-specific IgG fusion protein. *J Biotechnol* **146**, 84-91, doi:<https://doi.org/10.1016/j.jbiotec.2010.01.011> (2010).
- 699 Sumbria, R. K., Boado, R. J. & Pardridge, W. M. Combination stroke therapy in the mouse with blood-brain barrier penetrating IgG-GDNF and IgG-TNF decoy receptor fusion proteins. *Brain Res* **1507**, 91-96, doi:<https://doi.org/10.1016/j.brainres.2013.02.022> (2013).
- 700 Chang, R. *et al.* Blood-Brain Barrier Penetrating Biologic TNF-alpha Inhibitor for Alzheimer's Disease. *Mol Pharm* **14**, 2340-2349, doi:<https://doi.org/10.1021/acs.molpharmaceut.7b00200> (2017).
- 701 Gash, D. M. *et al.* Functional recovery in parkinsonian monkeys treated with GDNF. *Nature* **380**, 252-255, doi:<https://doi.org/10.1038/380252a0> (1996).
- 702 Kirik, D., Georgievska, B. & Bjorklund, A. Localized striatal delivery of GDNF as a treatment for Parkinson disease. *Nat Neurosci* **7**, 105-110, doi:<https://doi.org/10.1038/nn1175> (2004).
- 703 Fu, A. L. *et al.* Intravenous treatment of experimental Parkinson's disease in the mouse with an IgG-GDNF fusion protein that penetrates the blood-brain barrier. *Brain Res* **1352**, 208-213, doi:<https://doi.org/10.1016/j.brainres.2010.06.059> (2010).
- 704 Sonoda, H. *et al.* A Blood-Brain-Barrier-Penetrating Anti-human Transferrin Receptor Antibody Fusion Protein for Neuronopathic Mucopolysaccharidosis II. *Mol Ther* **26**, 1366-1374, doi:<https://doi.org/10.1016/j.ymthe.2018.02.032> (2018).
- 705 Boado, R. J., Hui, E. K., Lu, J. Z., Zhou, Q. H. & Pardridge, W. M. Reversal of lysosomal storage in brain of adult MPS-I mice with intravenous Trojan horse-iduronidase fusion protein. *Mol Pharm* **8**, 1342-1350, doi:<https://doi.org/10.1021/mp200136x> (2011).
- 706 Chang, R. *et al.* Blood-Brain Barrier Penetrating Biologic TNF- $\alpha$  Inhibitor for Alzheimer's Disease. *Mol Pharm* **14**, 2340-2349, doi:<https://doi.org/10.1021/acs.molpharmaceut.7b00200> (2017).
- 707 Sumbria, R. K. *et al.* Pharmacokinetics and brain uptake of an IgG-TNF decoy receptor fusion protein following intravenous, intraperitoneal, and subcutaneous administration in mice. *Mol Pharm* **10**, 1425-1431, doi:<https://doi.org/10.1021/mp400004a> (2013).
- 708 Zhou, Q. H. *et al.* Neuroprotection with a brain-penetrating biologic tumor necrosis factor inhibitor. *J Pharmacol Exp Ther* **339**, 618-623, doi:<https://doi.org/10.1124/jpet.111.185876> (2011).
- 709 Fu, A. *et al.* Intravenous treatment of experimental Parkinson's disease in the mouse with an IgG-GDNF fusion protein that penetrates the blood-brain barrier. *Brain Res* **1352**, 208-213 (2010).
- 710 Zhou, Q. H., Boado, R. J., Hui, E. K., Lu, J. Z. & Pardridge, W. M. Chronic dosing of mice with a transferrin receptor monoclonal antibody-glia-derived neurotrophic factor fusion protein. *Drug Metab Dispos* **39**, 1149-1154, doi:<https://doi.org/10.1124/dmd.111.038349> (2011).
- 711 Chang, R. *et al.* Brain Penetrating Bifunctional Erythropoietin-Transferrin Receptor Antibody Fusion Protein for Alzheimer's Disease. *Mol Pharm* **15**, 4963-4973, doi:<https://doi.org/10.1021/acs.molpharmaceut.8b00594> (2018).
- 712 Boado, R. J., Lu, J. Z., Hui, E. K. W. & Pardridge, W. M. Reduction in Brain Heparan

- Sulfate with Systemic Administration of an IgG Trojan Horse-Sulfamidase Fusion Protein in the Mucopolysaccharidosis Type IIIA Mouse. *Mol Pharm* **15**, 602-608, doi:<https://doi.org/10.1021/acs.molpharmaceut.7b00958> (2018).
- 713 Webster, C. I. *et al.* Enhanced delivery of IL-1 receptor antagonist to the central nervous system as a novel anti-transferrin receptor-IL-1RA fusion reverses neuropathic mechanical hypersensitivity. *Pain* **158**, 660-668, doi:<https://doi.org/10.1097/j.pain.0000000000000810> (2017).
- 714 Okuyama, T. *et al.* Iduronate-2-Sulfatase with Anti-human Transferrin Receptor Antibody for Neuropathic Mucopolysaccharidosis II: A Phase 1/2 Trial. *Mol Ther* **27**, 456-464, doi:<https://doi.org/10.1016/j.ymthe.2018.12.005> (2019).
- 715 Boado, R. J., Zhang, Y., Zhang, Y. & Pardridge, W. M. Humanization of anti-human insulin receptor antibody for drug targeting across the human blood-brain barrier. *Biotechnol Bioeng* **96**, 381-391, doi:<https://doi.org/10.1002/bit.21120> (2007).
- 716 Boado, R. J. *et al.* Genetic engineering of a lysosomal enzyme fusion protein for targeted delivery across the human blood-brain barrier. *Biotechnol Bioeng* **99**, 475-484, doi:<https://doi.org/10.1002/bit.21602> (2008).
- 717 Boado, R. J., Zhang, Y., Zhang, Y., Wang, Y. & Pardridge, W. M. GDNF fusion protein for targeted-drug delivery across the human blood-brain barrier. *Biotechnol Bioeng* **100**, 387-396, doi:<https://doi.org/10.1002/bit.21764> (2008).
- 718 Hui, E. K., Boado, R. J. & Pardridge, W. M. Tumor necrosis factor receptor-IgG fusion protein for targeted drug delivery across the human blood-brain barrier. *Mol Pharm* **6**, 1536-1543, doi:<https://doi.org/10.1021/mp900103n> (2009).
- 719 Lu, J. Z., Hui, E. K., Boado, R. J. & Pardridge, W. M. Genetic engineering of a bifunctional IgG fusion protein with iduronate-2-sulfatase. *Bioconjug Chem* **21**, 151-156, doi:<https://doi.org/10.1021/bc900382q> (2010).
- 720 Boado, R. J. & Pardridge, W. M. Genetic engineering of IgG-glucuronidase fusion proteins. *J Drug Target* **18**, 205-211, doi:<https://doi.org/10.3109/10611860903353362> (2010).
- 721 Lu, J. Z., Boado, R. J., Hui, E. K., Zhou, Q. H. & Pardridge, W. M. Expression in CHO cells and pharmacokinetics and brain uptake in the Rhesus monkey of an IgG-iduronate-2-sulfatase fusion protein. *Biotechnol Bioeng* **108**, 1954-1964, doi:<https://doi.org/10.1002/bit.23118> (2011).
- 722 Boado, R. J., Lu, J. Z., Hui, E. K., Sumbria, R. K. & Pardridge, W. M. Pharmacokinetics and brain uptake in the rhesus monkey of a fusion protein of arylsulfatase a and a monoclonal antibody against the human insulin receptor. *Biotechnol Bioeng* **110**, 1456-1465, doi:<https://doi.org/10.1002/bit.24795> (2013).
- 723 Boado, R. J., Zhang, Y., Zhang, Y., Xia, C. F. & Pardridge, W. M. Fusion antibody for Alzheimer's disease with bidirectional transport across the blood-brain barrier and abeta fibril disaggregation. *Bioconjug Chem* **18**, 447-455, doi:<https://doi.org/10.1021/bc060349x> (2007).
- 724 Boado, R. J., Hui, E. K., Lu, J. Z. & Pardridge, W. M. Glycemic control and chronic dosing of rhesus monkeys with a fusion protein of iduronidase and a monoclonal antibody against the human insulin receptor. *Drug Metab Dispos* **40**, 2021-2025, doi:<https://doi.org/10.1124/dmd.112.046375> (2012).
- 725 Boado, R. J., Lu, J. Z., Hui, E. K. & Pardridge, W. M. Insulin receptor antibody-sulfamidase fusion protein penetrates the primate blood-brain barrier and reduces glycosaminoglycans in Sanfilippo type A cells. *Mol Pharm* **11**, 2928-2934, doi:<https://doi.org/10.1021/mp500258p> (2014).

- 726 Boado, R. J., Lu, J. Z., Hui, E. K. & Pardridge, W. M. Insulin receptor antibody-sulfamidase fusion protein penetrates the primate blood-brain barrier and reduces glycosaminoglycans in Sanfilippo type A cells. *Mol. Pharm.* **11**, 2928-2934, doi:<https://doi.org/10.1021/mp500258p> (2014).
- 727 Boado, R. J., Hui, E. K., Lu, J. Z. & Pardridge, W. M. AGT-181: expression in CHO cells and pharmacokinetics, safety, and plasma iduronidase enzyme activity in Rhesus monkeys. *J Biotechnol* **144**, 135-141, doi:<https://doi.org/10.1016/j.jbiotec.2009.08.019> (2009).
- 728 Boado, R. J. & Pardridge, W. M. Brain and Organ Uptake in the Rhesus Monkey in Vivo of Recombinant Iduronidase Compared to an Insulin Receptor Antibody-Iduronidase Fusion Protein. *Mol Pharm* **14**, 1271-1277, doi:<https://doi.org/10.1021/acs.molpharmaceut.6b01166> (2017).
- 729 Pardridge, W. M., Boado, R. J., Giugliani, R. & Schmidt, M. Plasma Pharmacokinetics of Valanafusp Alpha, a Human Insulin Receptor Antibody-Iduronidase Fusion Protein, in Patients with Mucopolysaccharidosis Type I. *Biodrugs* **32**, 169-176, doi:<https://doi.org/10.1007/s40259-018-0264-7> (2018).
- 730 Giugliani, R., Nestrasil, I., Chen, S., Pardridge, W. & Rioux, P. Intravenous infusion of iduronidase-IgG and its impact on the central nervous system in children with Hurler syndrome. *Mol Genet Metab* **1**, S55-S56, doi:<https://doi.org/10.1016/j.ymgme.2016.11.121> (2017).
- 731 Giugliani, R. *et al.* Neurocognitive and somatic stabilization in pediatric patients with severe Mucopolysaccharidosis Type I after 52 weeks of intravenous brain-penetrating insulin receptor antibody-iduronidase fusion protein (valanafusp alpha): an open label phase 1-2 trial. *Orphanet J Rare Dis.* **13**, 110, doi:<https://doi.org/10.1186/s13023-018-0849-8> (2018).
- 732 Boado, R. J., Hui, E. K., Lu, J. Z. & Pardridge, W. M. IgG-enzyme fusion protein: pharmacokinetics and anti-drug antibody response in rhesus monkeys. *Bioconjug Chem* **24**, 97-104, doi:<https://doi.org/10.1021/bc3005123> (2013).
- 733 Lajoie, J. M. & Shusta, E. V. Targeting receptor-mediated transport for delivery of biologics across the blood-brain barrier. *Annu. Rev. Pharmacol. Toxicol.* **55**, 613-631, doi:<https://doi.org/10.1146/annurev-pharmtox-010814-124852> (2015).
- 734 Hultqvist, G., Syvanen, S., Fang, X. T., Lannfelt, L. & Sehlin, D. Bivalent Brain Shuttle Increases Antibody Uptake by Monovalent Binding to the Transferrin Receptor. *Theranostics* **7**, 308-318, doi:<https://doi.org/10.7150/thno.17155> (2017).
- 735 Pardridge, W. M. Drug transport across the blood-brain barrier. *J Cereb Blood Flow Metab* **32**, 1959-1972, doi:<https://doi.org/10.1038/jcbfm.2012.126> (2012).
- 736 Zuchero, Y. J. Y. *et al.* Discovery of Novel Blood-Brain Barrier Targets to Enhance Brain Uptake of Therapeutic Antibodies. *Neuron* **89**, 70-82, doi:<https://doi.org/10.1016/j.neuron.2015.11.024> (2016).
- 737 Xiao, G. & Gan, L. S. Receptor-mediated endocytosis and brain delivery of therapeutic biologics. *Int J Cell Biol* **2013**, 703545, doi:<https://doi.org/10.1155/2013/703545> (2013).
- 738 Almer, G., Mangge, H., Zimmer, A. & Prassl, R. Lipoprotein-Related and Apolipoprotein-Mediated Delivery Systems for Drug Targeting and Imaging. *Curr Med Chem* **22**, 3631-3651, doi:<https://doi.org/10.2174/0929867322666150716114625> (2015).
- 739 Johnsen, K. B., Burkhart, A., Thomsen, L. B., Andresen, T. L. & Moos, T. Targeting the transferrin receptor for brain drug delivery. *Prog Neurobiol* **181**, doi:UNSP 101665 10.1016/j.pneurobio.2019.101665 (2019).

- 740 Spencer, B. *et al.* Peripheral delivery of a CNS targeted, metallo-protease reduces abeta toxicity in a mouse model of Alzheimer's disease. *Plos One* **6**, e16575, doi:<https://doi.org/10.1371/journal.pone.0016575> (2011).
- 741 Spencer, B. J. & Verma, I. M. Targeted delivery of proteins across the blood-brain barrier. *P Natl Acad Sci USA* **104**, 7594-7599, doi:<https://doi.org/10.1073/pnas.0702170104> (2007).
- 742 Demeule, M. *et al.* High transcytosis of melanotransferrin (P97) across the blood-brain barrier. *J Neurochem* **83**, 924-933, doi:<https://doi.org/10.1046/j.1471-4159.2002.01201.x> (2002).
- 743 Thom, G. *et al.* A peptide derived from melanotransferrin delivers a protein-based interleukin 1 receptor antagonist across the BBB and ameliorates neuropathic pain in a preclinical model. *J Cereb Blood Flow Metab* **39**, 2074-2088, doi:<https://doi.org/10.1177/0271678X18772998> (2019).
- 744 Bockenhoff, A. *et al.* Comparison of Five Peptide Vectors for Improved Brain Delivery of the Lysosomal Enzyme Arylsulfatase A. *J Neurosci* **34**, 3122-3129, doi:<https://doi.org/10.1523/Jneurosci.4785-13.2014> (2014).
- 745 Song, B. W., Vinters, H. V., Wu, D. F. & Pardridge, W. M. Enhanced neuroprotective effects of basic fibroblast growth factor in regional brain ischemia after conjugation to a blood-brain barrier delivery vector. *J Pharmacol Exp Ther* **301**, 605-610, doi:<https://doi.org/10.1124/jpet.301.2.605> (2002).
- 746 Pardridge, W. M., Kang, Y. S. & Buciak, J. L. Transport of Human Recombinant Brain-Derived Neurotrophic Factor (Bdnf) through the Rat Blood-Brain-Barrier in-Vivo Using Vector-Mediated Peptide Drug-Delivery. *Pharm Res* **11**, 738-746, doi:<https://doi.org/10.1023/A:1018940732550> (1994).
- 747 Zhang, Y. & Pardridge, W. M. Blood-brain barrier targeting of BDNF improves motor function in rats with middle cerebral artery occlusion. *Brain Res* **1111**, 227-229, doi:<https://doi.org/10.1016/j.brainres.2006.07.005> (2006).
- 748 Deguchi, Y., Kurihara, A. & Pardridge, W. M. Retention of biologic activity of human epidermal growth factor following conjugation to a blood-brain barrier drug delivery vector via an extended poly(ethylene glycol) linker. *Bioconjug Chem* **10**, 32-37, doi:<https://doi.org/10.1021/bc9800522> (1999).
- 749 Wu, D. F., Song, B. W., Vinters, H. V. & Pardridge, W. M. Pharmacokinetics and brain uptake of biotinylated basic fibroblast growth factor conjugated to a blood-brain barrier drug delivery system. *J Drug Target* **10**, 239-245, doi:<https://doi.org/10.1080/10611860290022679> (2002).
- 750 Wu, D. F. & Pardridge, W. M. Pharmacokinetics and blood-brain barrier transport of an anti-transferrin receptor monoclonal antibody (OX26) in rats after chronic treatment with the antibody. *Drug Metab Dispos* **26**, 937-939, doi:PMID: 9733674 (1998).
- 751 Kang, Y. S., Bickel, U. & Pardridge, W. M. Pharmacokinetics and Saturable Blood-Brain-Barrier Transport of Biotin Bound to a Conjugate of Avidin and a Monoclonal-Antibody to the Transferrin Receptor. *Drug Metab Dispos* **22**, 99-105, doi:PMID: 8149897 (1994).
- 752 Kang, Y. S. & Pardridge, W. M. Use of Neutral Avidin Improves Pharmacokinetics and Brain Delivery of Biotin Bound to an Avidin Monoclonal-Antibody Conjugate. *J Pharmacol Exp Ther* **269**, 344-350, doi:PMID: 8169841 (1994).
- 753 Bickel, U., Yoshikawa, T., Landaw, E. M., Faull, K. F. & Pardridge, W. M. Pharmacologic effects in vivo in brain by vector-mediated peptide drug delivery. *P Natl Acad Sci USA* **90**, 2618-2622, doi:<https://doi.org/10.1073/pnas.90.7.2618> (1993).

- 754 Zhang, Y. & Pardridge, W. M. Conjugation of brain-derived neurotrophic factor to a blood-brain barrier drug targeting system enables neuroprotection in regional brain ischemia following intravenous injection of the neurotrophin. *Brain Res* **889**, 49-56, doi:[https://doi.org/10.1016/s0006-8993\(00\)03108-5](https://doi.org/10.1016/s0006-8993(00)03108-5) (2001).
- 755 Zhang, Y. & Pardridge, W. M. Neuroprotection in transient focal brain ischemia after delayed intravenous administration of brain-derived neurotrophic factor conjugated to a blood-brain barrier drug targeting system. *Stroke* **32**, 1378-1384, doi:<https://doi.org/10.1161/01.str.32.6.1378> (2001).
- 756 Wu, D. & Pardridge, W. M. Neuroprotection with noninvasive neurotrophin delivery to the brain. *P Natl Acad Sci USA* **96**, 254-259, doi:<https://doi.org/10.1073/pnas.96.1.254> (1999).
- 757 Albeck, D. S. *et al.* A non-invasive transport system for GDNF across the blood-brain barrier. *Neuroreport*. **8**, 2293-2298, doi:<https://doi.org/10.1097/00001756-199707070-00039> (1997).
- 758 Friden, P. M. *et al.* Blood-brain barrier penetration and in vivo activity of an NGF conjugate. *Science* **259**, 373-377, doi:<https://doi.org/10.1126/science.8420006> (1993).
- 759 Backman, C. *et al.* Effects of transferrin receptor antibody-NGF conjugate on young and aged septal transplants in oculo. *Exp Neurol* **132**, 1-15, doi:[https://doi.org/10.1016/0014-4886\(95\)90037-3](https://doi.org/10.1016/0014-4886(95)90037-3) (1995).
- 760 Backman, C. *et al.* Systemic administration of a nerve growth factor conjugate reverses age-related cognitive dysfunction and prevents cholinergic neuron atrophy. *J Neurosci* **16**, 5437-5442, doi:<https://doi.org/10.1523/JNEUROSCI.16-17-05437.1996> (1996).
- 761 Granholm, A. C. *et al.* NGF and anti-transferrin receptor antibody conjugate: short and long-term effects on survival of cholinergic neurons in intraocular septal transplants. *J Pharmacol Exp Ther* **268**, 448-459, doi:PMID: 8301587 (1994).
- 762 Charles, V., Mufson, E. J., Friden, P. M., Bartus, R. T. & Kordower, J. H. Atrophy of cholinergic basal forebrain neurons following excitotoxic cortical lesions is reversed by intravenous administration of an NGF conjugate. *Brain Res* **728**, 193-203, doi:[https://doi.org/10.1016/S0006-8993\(96\)00398-8](https://doi.org/10.1016/S0006-8993(96)00398-8) (1996).
- 763 Kordower, J. H. *et al.* Intravenous Administration of a Transferrin Receptor Antibody Nerve Growth-Factor Conjugate Prevents the Degeneration of Cholinergic Striatal Neurons in a Model of Huntington Disease. *P Natl Acad Sci USA* **91**, 9077-9080, doi:<https://doi.org/10.1073/pnas.91.19.9077> (1994).
- 764 Zhang, Y. & Pardridge, W. M. Delivery of beta-galactosidase to mouse brain via the blood-brain barrier transferrin receptor. *J Pharmacol Exp Ther* **313**, 1075-1081, doi:<https://doi.org/10.1124/jpet.104.082974> (2005).
- 765 Broadwell, R. D., BakerCairns, B. J., Friden, P. M., Oliver, C. & Villegas, J. C. Transcytosis of protein through the mammalian cerebral epithelium and endothelium .3. Receptor-mediated transcytosis through the blood-brain barrier of blood-borne transferrin and antibody against the transferrin receptor. *Exp Neurol* **142**, 47-65, doi:<https://doi.org/10.1006/exnr.1996.0178> (1996).
- 766 Lachowicz, J. E. *et al.* in *Poster presented at AACR Annual Meeting April*.
- 767 Lachowicz, J. E. *et al.* in *Society of neuro-oncology SNO Annual Meeting November*.
- 768 Leppert, W. & Woron, J. The role of naloxegol in the management of opioid-induced bowel dysfunction. *Ther Adv Gastroenter* **9**, 736-746, doi:<https://doi.org/10.1177/1756283x16648869> (2016).
- 769 Ji, H. J. *et al.* Neuroprotective effects of the novel polyethylene glycol-hemoglobin conjugate SB1 on experimental cerebral thromboembolism in rats. *Eur J Pharmacol*

- 566, 83-87, doi:<https://doi.org/10.1016/j.ejphar.2007.02.061> (2007).
- 770 Veronese, F. M., Caliceti, P., Schiavon, O. & Sergi, M. Polyethylene glycol-superoxide dismutase, a conjugate in search of exploitation. *Adv Drug Deliv Rev* **54**, 587-606, doi:[https://doi.org/10.1016/s0169-409x\(02\)00029-7](https://doi.org/10.1016/s0169-409x(02)00029-7) (2002).
- 771 Lejeune, M. P. G. M., Hukshorn, C. J., Saris, W. H. M. & Westerterp-Plantenga, M. S. Effect of dietary restraint during and following pegylated recombinant leptin (PEG-OB) treatment of overweight men. *Int J Obes Relat Metab Disord* **27**, 1494-1499, doi:<https://doi.org/10.1038/sj.ijo.0802431> (2003).
- 772 Hukshorn, C. J. *et al.* The effect of pegylated recombinant human leptin (PEG-OB) on weight loss and inflammatory status in obese subjects. *Int J Obes Relat Metab Disord* **26**, 504-509, doi:<https://doi.org/10.1038/sj.ijo.0801952> (2002).
- 773 Lo, K. M. *et al.* Engineering a pharmacologically superior form of leptin for the treatment of obesity. *Protein Eng Des Sel* **18**, 1-10, doi:<https://doi.org/10.1093/protein/gzh102> (2005).
- 774 Kuroiwa, T., Ting, P., Martinez, H. & Klatzo, I. The biphasic opening of the blood-brain barrier to proteins following temporary middle cerebral artery occlusion. *Acta Neuropathol.* **68**, 122-129, doi:<https://doi.org/10.1007/bf00688633> (1985).
- 775 Pitto-Barry, A. & Barry, N. P. E. Pluronic (R) block-copolymers in medicine: from chemical and biological versatility to rationalisation and clinical advances. *Polym Chem* **5**, 3291-3297, doi:<https://doi.org/10.1039/c4py00039k> (2014).
- 776 Kabanov, A. V., Batrakova, E. V. & Alakhov, V. Y. Pluronic((R)) block copolymers for overcoming drug resistance in cancer. *Adv Drug Deliv Rev* **54**, 759-779, doi:[https://doi.org/10.1016/S0169-409x\(02\)00047-9](https://doi.org/10.1016/S0169-409x(02)00047-9) (2002).
- 777 Alakhova, D. Y. & Kabanov, A. V. Pluronic and MDR Reversal: An Update. *Mol Pharm* **11**, 2566-2578, doi:<https://doi.org/10.1021/mp500298q> (2014).
- 778 Batrakova, E. V. *et al.* Mechanism of pluronic effect on P-glycoprotein efflux system in blood-brain barrier: contributions of energy depletion and membrane fluidization. *J Pharmacol Exp Ther* **299**, 483-493, doi:PMID: 11602658 (2001).
- 779 Batrakova, E. V. *et al.* Polypeptide point modifications with fatty acid and amphiphilic block copolymers for enhanced brain delivery. *Bioconjug Chem* **16**, 793-802, doi:<https://doi.org/10.1021/bc049730c> (2005).
- 780 Price, T. O. *et al.* Transport across the blood-brain barrier of pluronic leptin. *J Pharmacol Exp Ther* **333**, 253-263, doi:<https://doi.org/10.1124/jpet.109.158147> (2010).
- 781 Yi, X. *et al.* Pluronic modified leptin with increased systemic circulation, brain uptake and efficacy for treatment of obesity. *J Control Release* **191**, 34-46, doi:<https://doi.org/10.1016/j.jconrel.2014.05.044> (2014).
- 782 Yi, X. *et al.* Pluronic-modified superoxide dismutase 1 attenuates angiotensin II-induced increase in intracellular superoxide in neurons. *Free Radic Biol Med* **49**, 548-558, doi:<https://doi.org/10.1016/j.freeradbiomed.2010.04.039> (2010).
- 783 Yi, X., Batrakova, E., Banks, W. A., Vinogradov, S. & Kabanov, A. V. Protein conjugation with amphiphilic block copolymers for enhanced cellular delivery. *Bioconjug Chem* **19**, 1071-1077, doi:<https://doi.org/10.1021/bc700443k> (2008).
- 784 Banks, W. A. *et al.* Principles of strategic drug delivery to the brain (SDDB): development of anorectic and orexigenic analogs of leptin. *Physiol Behav* **105**, 145-149, doi:<https://doi.org/10.1016/j.physbeh.2011.05.024> (2011).
- 785 Tong, J., Luxenhofer, R., Yi, X. A., Jordan, R. & Kabanov, A. V. Protein Modification with Amphiphilic Block Copoly(2-oxazoline)s as a New Platform for Enhanced Cellular

- Delivery. *Mol Pharm* **7**, 984-992, doi:<https://doi.org/10.1021/mp100102p> (2010).
- 786 Mero, A. *et al.* Synthesis and characterization of poly(2-ethyl 2-oxazoline)-conjugates with proteins and drugs: Suitable alternatives to PEG-conjugates? *J Control Release* **125**, 87-95, doi:<https://doi.org/10.1016/j.jconrel.2007.10.010> (2008).
- 787 Viegas, T. X. *et al.* Polyoxazoline: Chemistry, Properties, and Applications in Drug Delivery. *Bioconjug Chem* **22**, 976-986, doi:<https://doi.org/10.1021/bc200049d> (2011).
- 788 Tong, J. *et al.* Conjugates of Superoxide Dismutase 1 with Amphiphilic Poly(2-oxazoline) Block Copolymers for Enhanced Brain Delivery: Synthesis, Characterization and Evaluation in Vitro and in Vivo. *Mol Pharm* **10**, 360-377, doi:<https://doi.org/10.1021/mp300496x> (2013).
- 789 Galstyan, A. *et al.* Blood-brain barrier permeable nano immunoconjugates induce local immune responses for glioma therapy. *Nat Commun* **10**, 3850, doi:<https://doi.org/10.1038/s41467-019-11719-3> (2019).
- 790 Jain, K. K. Nanobiotechnology-based strategies for crossing the blood-brain barrier. *Nanomedicine* **7**, 1225-1233, doi:<https://doi.org/10.2217/nnm.12.86> (2012).
- 791 Agrawal, M. *et al.* Recent advancements in the field of nanotechnology for the delivery of anti-Alzheimer drug in the brain region. *Expert Opin Drug Deliv* **15**, 589-617, doi:<https://doi.org/10.1080/17425247.2018.1471058> (2018).
- 792 Khare, S., Alexander, A. & Amit, N. Biomedical applications of nanobiotechnology for drug design, delivery and diagnostics. *Res J Pharm Technol* **7**, 915-925, doi:<http://www.indianjournals.com/ijor.aspx?target=ijor:rjpt&volume=7&issue=8&article=017> (2014).
- 793 Teleanu, D. M., Chircov, C., Grumezescu, A. M., Volceanov, A. & Teleanu, R. I. Blood-Brain Delivery Methods Using Nanotechnology. *Pharmaceutics* **10**, doi:<https://doi.org/10.3390/pharmaceutics10040269> (2018).
- 794 Jones, A. R. & Shusta, E. V. Blood-brain barrier transport of therapeutics via receptor-mediation. *Pharm Res* **24**, 1759-1771, doi:<https://doi.org/10.1007/s11095-007-9379-0> (2007).
- 795 Grabrucker, A. M. *et al.* in *The Blood Brain Barrier (BBB)* Vol. 10 (ed Ott M. Fricker G., Mahringer A.) 71-89 (2013).
- 796 Barua, S. & Mitragotri, S. Challenges associated with penetration of nanoparticles across cell and tissue barriers: A review of current status and future prospects. *Nano Today* **9**, 223-243, doi:<https://doi.org/10.1016/j.nantod.2014.04.008> (2014).
- 797 Putney, S. D. Encapsulation of proteins for improved delivery. *Curr Opin Chem Biol* **2**, 548-552, doi:[https://doi.org/10.1016/S1367-5931\(98\)80133-6](https://doi.org/10.1016/S1367-5931(98)80133-6) (1998).
- 798 Lee, H. J. *et al.* Enzyme delivery using the 30Kc19 protein and human serum albumin nanoparticles. *Biomaterials* **35**, 1696-1704, doi:<https://doi.org/10.1016/j.biomaterials.2013.11.001> (2014).
- 799 Ortac, I. *et al.* Dual-Porosity Hollow Nanoparticles for the Immunoprotection and Delivery of Nonhuman Enzymes. *Nano Lett* **14**, 3023-3032, doi:<https://doi.org/10.1021/nl404360k> (2014).
- 800 Leite, P. E., Pereira, M. R. & Granjeiro, J. M. Hazard effects of nanoparticles in central nervous system: Searching for biocompatible nanomaterials for drug delivery. *Toxicol In Vitro* **29**, 1653-1660, doi:<https://doi.org/10.1016/j.tiv.2015.06.023> (2015).
- 801 Sharma, A. K., Singh, V., Gera, R., Purohit, M. P. & Ghosh, D. Zinc Oxide Nanoparticle Induces Microglial Death by NADPH-Oxidase-Independent Reactive Oxygen Species as well as Energy Depletion. *Mol Neurobiol* **54**, 6273-6286,

- doi:<https://doi.org/10.1007/s12035-016-0133-7> (2017).
- 802 Grissa, I. *et al.* The effect of titanium dioxide nanoparticles on neuroinflammation response in rat brain. *Environ Sci Pollut Res Int* **23**, 20205-20213, doi:<https://doi.org/10.1007/s11356-016-7234-8> (2016).
- 803 Tosi, G. *et al.* Potential Use of Polymeric Nanoparticles for Drug Delivery Across the Blood-Brain Barrier. *Curr Med Chem* **20**, 2212-2225, doi:<https://doi.org/10.2174/0929867311320170006> (2013).
- 804 Patel, T., Zhou, J. B., Piepmeier, J. M. & Saltzman, W. M. Polymeric nanoparticles for drug delivery to the central nervous system. *Adv Drug Deliv Rev* **64**, 701-705, doi:<https://doi.org/10.1016/j.addr.2011.12.006> (2012).
- 805 Reddy, M. K. & Labhasetwar, V. Nanoparticle-mediated delivery of superoxide dismutase to the brain: an effective strategy to reduce ischemia-reperfusion injury. *FASEB J* **23**, 1384-1395, doi:<https://doi.org/10.1096/fj.08-116947> (2009).
- 806 Chen, H. *et al.* Nanoerythropoietin Is 10-Times More Effective Than Regular Erythropoietin in Neuroprotection in a Neonatal Rat Model of Hypoxia and Ischemia. *Stroke* **43**, 884-887, doi:<https://doi.org/10.1161/Strokeaha.111.637090> (2012).
- 807 Vilella, A. *et al.* Insight on the fate of CNS-targeted nanoparticles. Part I: Rab5-dependent cell-specific uptake and distribution. *J Control Release* **174**, 195-201, doi:<https://doi.org/10.1016/j.jconrel.2013.11.023> (2014).
- 808 Tosi, G. *et al.* Investigation on the mechanisms for Blood-Brain Barrier crossing of brain-targeted glycopeptides nanoparticles. *Nanomedicine* **6**, 423-436, doi:<https://doi.org/10.2217/nnm.11.11> (2011).
- 809 Costantino, L. *et al.* Peptide-derivatized biodegradable nanoparticles able to cross the blood-brain barrier. *J Control Release* **108**, 84-96, doi:<https://doi.org/10.1016/j.jconrel.2005.07.013> (2005).
- 810 Tosi, G. *et al.* Brain-targeted polymeric nanoparticles: in vivo evidence of different routes of administration in rodents. *Nanomedicine* **8**, 1373-1383, doi:<https://doi.org/10.2217/Nnm.12.172> (2013).
- 811 Salvalaio, M. *et al.* Targeted Polymeric Nanoparticles for Brain Delivery of High Molecular Weight Molecules in Lysosomal Storage Disorders. *Plos One* **11**, e0156452, doi:<https://doi.org/10.1371/journal.pone.0156452> (2016).
- 812 Gelperina, S. *et al.* Drug delivery to the brain using surfactant-coated poly(lactide-co-glycolide) nanoparticles: Influence of the formulation parameters. *Eur J Pharm Biopharm* **74**, 157-163, doi:<https://doi.org/10.1016/j.ejpb.2009.09.003> (2010).
- 813 Chaturvedi, M., Molino, Y., Sreedhar, B., Khrestchatisky, M. & Kaczmarek, L. Tissue inhibitor of matrix metalloproteinases-1 loaded poly(lactic-co-glycolic acid) nanoparticles for delivery across the blood-brain barrier. *Int J Nanomed* **9**, 575-588, doi:<https://doi.org/10.2147/IJN.S54750> (2014).
- 814 Kreuter, J. Influence of the surface properties on nanoparticle-mediated transport of drugs to the brain. *J Nanosci Nanotechnol* **4**, 484-488, doi:<https://doi.org/10.1166/jnn.2003.077> (2004).
- 815 Kreuter, J. Mechanism of polymeric nanoparticle-based drug transport across the blood-brain barrier (BBB). *J Microencapsul* **30**, 49-54, doi:<https://doi.org/10.3109/02652048.2012.692491> (2013).
- 816 Vaishya, R., Khurana, V., Patel, S. & Mitra, A. K. Long-term delivery of protein therapeutics. *Expert Opin Drug Deliv* **12**, 415-440, doi:<https://doi.org/10.1517/17425247.2015.961420> (2015).

- 817 van de Weert, M., Hennink, W. E. & Jiskoot, W. Protein instability in poly(lactic-co-glycolic acid) microparticles. *Pharm Res* **17**, 1159-1167, doi:<https://doi.org/10.1023/A:1026498209874> (2000).
- 818 Galliani, M. *et al.* Cross-Linked Enzyme Aggregates as Versatile Tool for Enzyme Delivery: Application to Polymeric Nanoparticles. *Bioconjug Chem* **29**, 2225-2231, doi:<https://doi.org/10.1021/acs.bioconjugchem.8b00206> (2018).
- 819 Hasadsri, L., Kreuter, J., Hattori, H., Iwasaki, T. & George, J. M. Functional Protein Delivery into Neurons Using Polymeric Nanoparticles. *J Biol Chem* **284**, 6972-6981, doi:<https://doi.org/10.1074/jbc.M805956200> (2009).
- 820 Kurakhmaeva, K. B. *et al.* Brain targeting of nerve growth factor using poly(butyl cyanoacrylate) nanoparticles. *J Drug Target* **17**, 564-574, doi:<https://doi.org/10.1080/10611860903112842> (2009).
- 821 Lin, Y. *et al.* Delivery of large molecules via poly(butyl cyanoacrylate) nanoparticles into the injured rat brain. *Nanotechnology* **23**, doi:<https://doi.org/10.1088/0957-4484/23/16/165101> (2012).
- 822 Olivier, J. C. *et al.* Indirect evidence that drug brain targeting using polysorbate 80-coated polybutylcyanoacrylate nanoparticles is related to toxicity. *Pharm Res* **16**, 1836-1842, doi:<https://doi.org/10.1023/A:1018947208597> (1999).
- 823 Kreuter, J. *et al.* Apolipoprotein-mediated transport of nanoparticle-bound drugs across the blood-brain barrier. *J Drug Target* **10**, 317-325, doi:<https://doi.org/10.1080/10611860290031877> (2002).
- 824 Wood, H. FDA approves patisiran to treat hereditary transthyretin amyloidosis. *Nat Rev Neurol* **14**, 570, doi:<https://doi.org/10.1038/s41582-018-0065-0> (2018).
- 825 Akinc, A. *et al.* Targeted delivery of RNAi therapeutics with endogenous and exogenous ligand-based mechanisms. *Mol Ther* **18**, 1357-1364, doi:<https://doi.org/10.1038/mt.2010.85> (2010).
- 826 Ren, H. & Huang, X. Polyacrylate nanoparticles: toxicity or new nanomedicine? *Eur Respir J* **36**, 218-221, doi:<https://doi.org/10.1183/09031936.00022410> (2010).
- 827 Tian, X. *et al.* LRP-1-mediated intracellular antibody delivery to the Central Nervous System. *Sci Rep* **5**, 11990, doi:<https://doi.org/10.1038/srep11990> (2015).
- 828 Deng, J. *et al.* Recombinant Tissue Plasminogen Activator-conjugated Nanoparticles Effectively Targets Thrombolysis in a Rat Model of Middle Cerebral Artery Occlusion. *Curr Med Sci* **38**, 427-435, doi:<https://doi.org/10.1007/s11596-018-1896-z> (2018).
- 829 Nieto-Marquez, A., Romero, R., Romero, A. & Valverde, J. L. Carbon nanospheres: synthesis, physicochemical properties and applications. *J Mater Chem* **21**, 1664-1672, doi:<https://doi.org/10.1039/c0jm01350a> (2011).
- 830 Chemmannur, S. V., Bhagat, P., Mirlekar, B., Paknikar, K. M. & Chattopadhyay, S. Carbon nanospheres mediated delivery of nuclear matrix protein SMAR1 to direct experimental autoimmune encephalomyelitis in mice. *Int J Nanomed* **11**, 2039-2051, doi:<https://doi.org/10.2147/IJN.S93571> (2016).
- 831 Mathai, J. *et al.* SMAR1 binds to T(C/G) repeat and inhibits tumor progression by regulating miR-371-373 cluster. *Sci Rep* **6**, 33779, doi:<https://doi.org/10.1038/srep33779> (2016).
- 832 Malonia, S. K. *et al.* Gene regulation by SMAR1: Role in cellular homeostasis and cancer. *Biochim Biophys Acta* **1815**, 1-12, doi:<https://doi.org/10.1016/j.bbcan.2010.08.003> (2011).
- 833 Agrawal, M. *et al.* Recent advancements in liposomes targeting strategies to cross

- blood-brain barrier (BBB) for the treatment of Alzheimer's disease. *J Control Release* **260**, 61-77, doi:<https://doi.org/10.1016/j.jconrel.2017.05.019> (2017).
- 834 Ramos-Cabrer, P. & Campos, F. Liposomes and nanotechnology in drug development: focus on neurological targets. *Int J Nanomed* **8**, 951-960, doi:<https://doi.org/10.2147/Ijn.S30721> (2013).
- 835 Salade, L. *et al.* Development of coated liposomes loaded with ghrelin for nose-to-brain delivery for the treatment of cachexia. *Int J Nanomed* **12**, 8531-8543, doi:<https://doi.org/10.2147/Ijn.S147650> (2017).
- 836 Daraee, H., Etemadi, A., Kouhi, M., Alimirzalu, S. & Akbarzadeh, A. Application of liposomes in medicine and drug delivery. *Artif Cells Nanomed Biotechnol* **44**, 381-391, doi:<https://doi.org/10.3109/21691401.2014.953633> (2016).
- 837 Postmes, T. J., Hukkelhoven, M., Vandenbogaard, A. E. J. M., Halders, S. G. & Coenegracht, J. Passage through the Blood-Brain-Barrier of Thyrotropin-Releasing-Hormone Encapsulated in Liposomes. *J Pharm Pharmacol* **32**, 722-724, doi:<https://doi.org/10.1111/j.2042-7158.1980.tb13051.x> (1980).
- 838 Onodera, H., Takada, G., Tada, K. & Desnick, R. J. Microautoradiographic Study on the Tissue Localization of Liposome Entrapped or Unentrapped H-3-Labeled Beta-Galactosidase Injected into Rats. *Tohoku J Exp Med* **140**, 1-13, doi:<https://doi.org/10.1620/tjem.140.1> (1983).
- 839 Imaizumi, S., Woolworth, V., Fishman, R. A. & Chan, P. H. Liposome-Entrapped Superoxide-Dismutase Reduces Cerebral Infarction in Cerebral-Ischemia in Rats. *Stroke* **21**, 1312-1317, doi:<https://doi.org/10.1161/01.Str.21.9.1312> (1990).
- 840 Chan, P. H., Longar, S. & Fishman, R. A. Protective Effects of Liposome-Entrapped Superoxide-Dismutase on Posttraumatic Brain Edema. *Ann Neurol* **21**, 540-547, doi:<https://doi.org/10.1002/ana.410210604> (1987).
- 841 Karim, R., Palazzo, C., Evrard, B. & Piel, G. Nanocarriers for the treatment of glioblastoma multiforme: Current state-of-the-art. *J Control Release* **227**, 23-37, doi:<https://doi.org/10.1016/j.jconrel.2016.02.026> (2016).
- 842 Guo, L. *et al.* TRAIL and doxorubicin combination enhances anti-glioblastoma effect based on passive tumor targeting of liposomes. *J Control Release* **154**, 93-102, doi:<https://doi.org/10.1016/j.jconrel.2011.05.008> (2011).
- 843 Xie, Y. *et al.* Transport of nerve growth factor encapsulated into liposomes across the blood-brain barrier: In vitro and in vivo studies. *J Control Release* **105**, 106-119, doi:<https://doi.org/10.1016/j.jconrel.2005.03.005> (2005).
- 844 Rotman, M. *et al.* Enhanced glutathione PEGylated liposomal brain delivery of an anti-amyloid single domain antibody fragment in a mouse model for Alzheimer's disease. *J Control Release* **203**, 40-50, doi:<https://doi.org/10.1016/j.jconrel.2015.02.012> (2015).
- 845 Joshi, S. *et al.* Cationic surface charge enhances early regional deposition of liposomes after intracarotid injection. *J Neurooncol* **120**, 489-497, doi:<https://doi.org/10.1007/s11060-014-1584-1> (2014).
- 846 Bozzuto, G. & Molinari, A. Liposomes as nanomedical devices. *Int J Nanomed* **10**, 975-999, doi:<https://doi.org/10.2147/Ijn.S68861> (2015).
- 847 Knudsen, K. B. *et al.* In vivo toxicity of cationic micelles and liposomes. *Nanomedicine* **11**, 467-477, doi:<https://doi.org/10.1016/j.nano.2014.08.004> (2015).
- 848 Yun, X. *et al.* Nanoparticles for targeted delivery of antioxidant enzymes to the brain after cerebral ischemia and reperfusion injury. *J Cereb Blood Flow Metab* **33**, 583-592, doi:<https://doi.org/10.1038/jcbfm.2012.209> (2013).

- 849 Bodratti, A. M. & Alexandridis, P. Formulation of Poloxamers for Drug Delivery. *J Funct Biomater* **9**, doi:<https://doi.org/10.3390/jfb9010011> (2018).
- 850 Meng, X. *et al.* Pluronic F127 and D-alpha-Tocopheryl Polyethylene Glycol Succinate (TPGS) Mixed Micelles for Targeting Drug Delivery across The Blood Brain Barrier. *Sci Rep* **7**, 2964, doi:<https://doi.org/10.1038/s41598-017-03123-y> (2017).
- 851 Kim, J. Y., Choi, W. I., Kim, Y. H. & Tae, G. Brain-targeted delivery of protein using chitosan- and RVG peptide-conjugated, pluronic-based nano-carrier. *Biomaterials* **34**, 1170-1178, doi:<https://doi.org/10.1016/j.biomaterials.2012.09.047> (2013).
- 852 Sezgin, Z., Yuksel, N. & Baykara, T. Preparation and characterization of polymeric micelles for solubilization of poorly soluble anticancer drugs. *Eur J Pharm Biopharm* **64**, 261-268, doi:<https://doi.org/10.1016/j.ejpb.2006.06.003> (2006).
- 853 Jaturanpinyo, M., Harada, A., Yuan, X. F. & Kataoka, K. Preparation of bionanoreactor based on core-shell structured polyion complex micelles entrapping trypsin in the core cross-linked with glutaraldehyde. *Bioconjug Chem* **15**, 344-348, doi:<https://doi.org/10.1021/bc034149m> (2004).
- 854 Harada, A. & Kataoka, K. Chain length recognition: Core-shell supramolecular assembly from oppositely charged block copolymers. *Science* **283**, 65-67, doi:<https://doi.org/10.1126/science.283.5398.65> (1999).
- 855 Batrakova, E. V. *et al.* A macrophage-nanozyme delivery system for Parkinson's disease. *Bioconjug Chem* **18**, 1498-1506, doi:<https://doi.org/10.1021/bc700184b> (2007).
- 856 Klyachko, N. L. *et al.* Cross-linked antioxidant nanozymes for improved delivery to CNS. *Nanomedicine* **8**, 119-129, doi:<https://doi.org/10.1016/j.nano.2011.05.010> (2012).
- 857 Harada, A. & Kataoka, K. Pronounced activity of enzymes through the incorporation into the core of polyion complex micelles made from charged block copolymers. *J Control Release* **72**, 85-91, doi:[https://doi.org/10.1016/S0168-3659\(01\)00264-4](https://doi.org/10.1016/S0168-3659(01)00264-4) (2001).
- 858 Manickam, D. S. *et al.* Well-defined cross-linked antioxidant nanozymes for treatment of ischemic brain injury. *J Control Release* **162**, 636-645, doi:<https://doi.org/10.1016/j.jconrel.2012.07.044> (2012).
- 859 Gaydess, A. *et al.* Visualization of exogenous delivery of nanoformulated butyrylcholinesterase to the central nervous system. *Chem-Biol Interact* **187**, 295-298, doi:<https://doi.org/10.1016/j.cbi.2010.01.005> (2010).
- 860 Chen, W. *et al.* Brain Targeting Delivery Facilitated by Ligand-Functionalized Layered Double Hydroxide Nanoparticles. *ACS Appl Mater Interfaces* **10**, 20326-20333, doi:<https://doi.org/10.1021/acsami.8b04613> (2018).
- 861 Choi, S. J. & Choy, J. H. Layered double hydroxide nanoparticles as target-specific delivery carriers: uptake mechanism and toxicity. *Nanomedicine* **6**, 803-814, doi:<https://doi.org/10.2217/nnm.11.86> (2011).
- 862 Yang, H. W. *et al.* Bioconjugation of recombinant tissue plasminogen activator to magnetic nanocarriers for targeted thrombolysis. *Int J Nanomed* **7**, 5159-5173, doi:<https://doi.org/10.2147/ij.n.S32939> (2012).
- 863 Huang, L. J. *et al.* Polyacrylic acid-coated nanoparticles loaded with recombinant tissue plasminogen activator for the treatment of mice with ischemic stroke. *Biochem Bioph Res Co* **516**, 565-570, doi:<https://doi.org/10.1016/j.bbrc.2019.06.079> (2019).
- 864 Thomsen, L. B., Thomsen, M. S. & Moos, T. Targeted drug delivery to the brain using magnetic nanoparticles. *Ther Deliv* **6**, 1145-1155, doi:<https://doi.org/10.4155/tde.15.56>

- (2015).
- 865 Ma, Y. H. *et al.* Magnetically targeted thrombolysis with recombinant tissue plasminogen activator bound to polyacrylic acid-coated nanoparticles. *Biomaterials* **30**, 3343-3351, doi:<https://doi.org/10.1016/j.biomaterials.2009.02.034> (2009).
- 866 Gao, H. Perspectives on Dual Targeting Delivery Systems for Brain Tumors. *J Neuroimmune Pharmacol* **12**, 6-16, doi:<https://doi.org/10.1007/s11481-016-9687-4> (2017).
- 867 Gao, H. Progress and perspectives on targeting nanoparticles for brain drug delivery. *Acta Pharm Sin B* **6**, 268-286, doi:<https://doi.org/10.1016/j.apsb.2016.05.013> (2016).
- 868 Ashwell, G. & Morell, A. G. The role of surface carbohydrates in the hepatic recognition and transport of circulating glycoproteins. *Adv Enzymol Relat Areas Mol Biol* **41**, 99-128, doi:<https://doi.org/10.1002/9780470122860.ch3> (1974).
- 869 Ashwell, G. & Morell, A. G. The role of surface carbohydrates in the hepatic recognition and transport of circulating glycoproteins. *Adv. Enzymol. Relat. Areas Mol. Biol.* **41**, 99-128, doi:<https://doi.org/10.1002/9780470122860.ch3> (1974).
- 870 Stockert, R. J., Morell, A. G. & Ashwell, G. Structural characteristics and regulation of the asialoglycoprotein receptor. *Targeted Diagn Ther* **4**, 41-64, doi:PMID: 1797163 (1991).
- 871 Pricer, W. E., Jr., Hudgin, R. L., Ashwell, G., Stockert, R. J. & Morell, A. G. A membrane receptor protein for asialoglycoproteins. *Methods Enzymol* **34**, 688-691, doi:[https://doi.org/10.1016/s0076-6879\(74\)34090-6](https://doi.org/10.1016/s0076-6879(74)34090-6) (1974).
- 872 Morell, A. G., Irvine, R. A., Sternlieb, I., Scheinberg, I. H. & Ashwell, G. Physical and chemical studies on ceruloplasmin. V. Metabolic studies on sialic acid-free ceruloplasmin in vivo. *J Biol Chem* **243**, 155-159, doi:PMID: 5635941 (1968).
- 873 Gross, V. *et al.* Involvement of Various Organs in the Initial Plasma-Clearance of Differently Glycosylated Rat-Liver Secretory Proteins. *Eur J Biochem* **173**, 653-659, doi:<https://doi.org/10.1111/j.1432-1033.1988.tb14048.x> (1988).
- 874 Morell, A. G., Gregoriadis, G., Scheinberg, I. H., Hickman, J. & Ashwell, G. The role of sialic acid in determining the survival of glycoproteins in the circulation. *J Biol Chem* **246**, 1461-1467, doi:PMID: 5545089 (1971).
- 875 Sola, R. J. & Griebenow, K. Effects of glycosylation on the stability of protein pharmaceuticals. *J Pharm Sci* **98**, 1223-1245, doi:<https://doi.org/10.1002/jps.21504> (2009).
- 876 Lis, H. & Sharon, N. Protein glycosylation. Structural and functional aspects. *Eur J Biochem* **218**, 1-27, doi:<https://doi.org/10.1111/j.1432-1033.1993.tb18347.x> (1993).
- 877 Vegarud, G. & Christnsen, T. B. Glycosylation of Proteins: a new method of enzyme stabilization. *Biotechnol Bioeng* **17**, 1391-1397, doi:<https://doi.org/10.1002/bit.260170918> (1975).
- 878 Vegarud, G. & Christnsen, T. B. Glycosylation of Proteins: a new method of enzyme stabilization. *Biotechnol Bioeng* **17**, 1391-1397, doi:<https://doi.org/10.1002/bit.260170918> (1975).
- 879 Nissen, C. Glycosylation of recombinant human granulocyte colony stimulating factor: implications for stability and potency. *Eur J Cancer* **30A Suppl 3**, S12-14, doi:PMID: 7535065 (1994).
- 880 Carter, C. R., Keeble, J. R. & Thorpe, R. Human serum inactivates non-glycosylated but not glycosylated granulocyte colony stimulating factor by a protease dependent mechanism: significance of carbohydrates on the glycosylated molecule. *Biologicals*

- 32**, 37-47, doi:<https://doi.org/10.1016/j.biologicals.2003.12.002> (2004).
- 881 Grinnell, B. W., Walls, J. D. & Gerlitz, B. Glycosylation of human protein C affects its secretion, processing, functional activities, and activation by thrombin. *J Biol Chem* **266**, 9778-9785, doi:PMID: 2033065 (1991).
- 882 Kim, B. M., Kim, H., Raines, R. T. & Lee, Y. Glycosylation of onconase increases its conformational stability and toxicity for cancer cells. *Biochem Bioph Res Co* **315**, 976-983, doi:<https://doi.org/10.1016/j.bbrc.2004.01.153> (2004).
- 883 Weintraub, B. D., Stannard, B. S. & Meyers, L. Glycosylation of thyroid-stimulating hormone in pituitary tumor cells: influence of high mannose oligosaccharide units on subunit aggregation, combination, and intracellular degradation. *Endocrinology* **112**, 1331-1345, doi:<https://doi.org/10.1210/endo-112-4-1331> (1983).
- 884 Sareneva, T., Cantell, K., Pyhala, L., Pirhonen, J. & Julkunen, I. Effect of carbohydrates on the pharmacokinetics of human interferon-gamma. *J Interferon Res* **13**, 267-269, doi:<https://doi.org/10.1089/jir.1993.13.267> (1993).
- 885 Raju, T. S. & Scallon, B. Fc glycans terminated with N-acetylglucosamine residues increase antibody resistance to papain. *Biotechnol Prog* **23**, 964-971, doi:<https://doi.org/10.1021/bp070118k> (2007).
- 886 Clowers, B. H., Dodds, E. D., Seipert, R. R. & Lebrilla, C. B. Site determination of protein glycosylation based on digestion with immobilized nonspecific proteases and Fourier transform ion cyclotron resonance mass spectrometry. *J Proteome Res* **6**, 4032-4040, doi:<https://doi.org/10.1021/pr070317z> (2007).
- 887 Byrne, B., Donohoe, G. G. & O'Kennedy, R. Sialic acids: carbohydrate moieties that influence the biological and physical properties of biopharmaceutical proteins and living cells. *Drug Discov Today* **12**, 319-326, doi:<https://doi.org/10.1016/j.drudis.2007.02.010> (2007).
- 888 Schlesinger, P. H. *et al.* Plasma clearance of glycoproteins with terminal mannose and N-acetylglucosamine by liver non-parenchymal cells. Studies with beta-glucuronidase, N-acetyl-beta-D-glucosaminidase, ribonuclease B and agalacto-orosomuroid. *Biochem J* **176**, 103-109, doi:<https://doi.org/10.1042/bj1760103> (1978).
- 889 Schlesinger, P. H. *et al.* The role of extra-hepatic tissues in the receptor-mediated plasma clearance of glycoproteins terminated by mannose or N-acetylglucosamine. *Biochem J* **192**, 597-606, doi:<https://doi.org/10.1042/bj1920597> (1980).
- 890 Townsend, R. & Stahl, P. Isolation and characterization of a mannose/N-acetylglucosamine/fucose-binding protein from rat liver. *Biochem J* **194**, 209-214, doi:<https://doi.org/10.1042/bj1940209> (1981).
- 891 Achord, D. T., Brot, F. E., Bell, C. E. & Sly, W. S. Human beta-glucuronidase: in vivo clearance and in vitro uptake by a glycoprotein recognition system on reticuloendothelial cells. *Cell* **15**, 269-278, doi:[https://doi.org/10.1016/0092-8674\(78\)90102-2](https://doi.org/10.1016/0092-8674(78)90102-2) (1978).
- 892 Varamini, P. *et al.* Synthesis and biological evaluation of an orally active glycosylated endomorphin-1. *J Med Chem* **55**, 5859-5867, doi:<https://doi.org/10.1021/jm300418d> (2012).
- 893 Polt, R. *et al.* Glycopeptide enkephalin analogues produce analgesia in mice: evidence for penetration of the blood-brain barrier. *P Natl Acad Sci USA* **91**, 7114-7118, doi:<https://doi.org/10.1073/pnas.91.15.7114> (1994).
- 894 Poduslo, J. F. & Curran, G. L. Increased permeability across the blood-nerve barrier of albumin glycated in vitro and in vivo from patients with diabetic polyneuropathy. *P Natl Acad Sci USA* **89**, 2218-2222, doi:<https://doi.org/10.1073/pnas.89.6.2218> (1992).

- 895 Poduslo, J. F. & Curran, G. L. Glycation Increases the Permeability of Proteins across the Blood Nerve and Blood-Brain Barriers. *Mol Brain Res* **23**, 157-162, doi:[https://doi.org/10.1016/0169-328x\(94\)90222-4](https://doi.org/10.1016/0169-328x(94)90222-4) (1994).
- 896 Hickman, S., Shapiro, L. J. & Neufeld, E. F. A recognition marker required for uptake of a lysosomal enzyme by cultured fibroblasts. *Biochem Biophys Res Commun* **57**, 55-61, doi:[https://doi.org/10.1016/s0006-291x\(74\)80356-6](https://doi.org/10.1016/s0006-291x(74)80356-6) (1974).
- 897 Ashwell, G. & Harford, J. Carbohydrate-specific receptors of the liver. *Annu Rev Biochem* **51**, 531-554, doi:<https://doi.org/10.1146/annurev.bi.51.070182.002531> (1982).
- 898 Grubb, J. H. *et al.* Chemically modified beta-glucuronidase crosses blood-brain barrier and clears neuronal storage in murine mucopolysaccharidosis VII. *Proc Natl Acad Sci USA* **105**, 2616-2621, doi:<https://doi.org/10.1073/pnas.0712147105> (2008).
- 899 Huynh, H. T., Grubb, J. H., Vogler, C. & Sly, W. S. Biochemical evidence for superior correction of neuronal storage by chemically modified enzyme in murine mucopolysaccharidosis VII. *Proc Natl Acad Sci USA* **109**, 17022-17027, doi:<https://doi.org/10.1073/pnas.1214779109> (2012).
- 900 Meng, Y., Sohar, I., Wang, L., Sleat, D. E. & Lobel, P. Systemic administration of tripeptidyl peptidase I in a mouse model of late infantile neuronal ceroid lipofuscinosis: effect of glycan modification. *Plos One* **7**, e40509, doi:<https://doi.org/10.1371/journal.pone.0040509> (2012).
- 901 Gregoriadis, G., Jain, S., Papaioannou, I. & Laing, P. Improving the therapeutic efficacy of peptides and proteins: a role for polysialic acids. *Int J Pharm* **300**, 125-130, doi:<https://doi.org/10.1016/j.ijpharm.2005.06.007> (2005).
- 902 Varki, N. M. & Varki, A. Diversity in cell surface sialic acid presentations: implications for biology and disease. *Lab. Invest.* **87**, 851-857, doi:<https://doi.org/10.1038/labinvest.3700656> (2007).
- 903 Pisal, D. S., Kosloski, M. P. & Balu-Iyer, S. V. Delivery of therapeutic proteins. *J Pharm Sci* **99**, 2557-2575, doi:<https://doi.org/10.1002/jps.22054> (2010).
- 904 Kabanov, A. V., Levashov, A. V. & Alakhov, V. Y. Lipid Modification of Proteins and Their Membrane-Transport. *Protein Eng* **3**, 39-42, doi:<https://doi.org/10.1093/protein/3.1.39> (1989).
- 905 Slepnev, V. I. *et al.* Fatty-Acid Acylated Peroxidase as a Model for the Study of Interactions of Hydrophobically-Modified Proteins with Mammalian-Cells. *Bioconjug Chem* **6**, 608-615, doi:<https://doi.org/10.1021/bc00035a016> (1995).
- 906 Chekhonin, V. P., Kabanov, A. V., Zhirkov, Y. A. & Morozov, G. V. Fatty-Acid Acylated Fab-Fragments of Antibodies to Neurospecific Proteins as Carriers for Neuroleptic Targeted Delivery in Brain. *FEBS Lett* **287**, 149-152, doi:[https://doi.org/10.1016/0014-5793\(91\)80037-4](https://doi.org/10.1016/0014-5793(91)80037-4) (1991).
- 907 Chekhonin, V. P., Ryabukhin, I. A., Zhirkov, Y. A., Kashparov, I. A. & Dmitriyeva, T. B. Transport of hydrophobized fragments of antibodies through the blood-brain barrier. *Neuroreport*. **7**, 129-132, doi:<https://doi.org/10.1097/00001756-199512290-00031> (1995).
- 908 Chekhonin, V. P., Kabanov, A. V., Zhirkov, Y. A. & Morozov, G. V. Fatty acid acylated Fab-fragments of antibodies to neurospecific proteins as carriers for neuroleptic targeted delivery in brain. *FEBS Lett* **287**, 149-152, doi:[https://doi.org/10.1016/0014-5793\(91\)80037-4](https://doi.org/10.1016/0014-5793(91)80037-4) (1991).
- 909 Bondi, M. L., Di Gesu, R. & Craparo, E. F. Lipid nanoparticles for drug targeting to the brain. *Methods Enzymol* **508**, 229-251, doi:<https://doi.org/10.1016/B978-0-12-391860->

- [4.00012-4](#) (2012).
- 910 Edmond, J. Essential polyunsaturated fatty acids and the barrier to the brain: the components of a model for transport. *J Mol Neurosci* **16**, 181-193; discussion 215-221, doi:<https://doi.org/10.1385/JMN:16:2-3:181> (2001).
- 911 Edmond, J., Higa, T. A., Korsak, R. A., Bergner, E. A. & Lee, W. N. Fatty acid transport and utilization for the developing brain. *J Neurochem* **70**, 1227-1234, doi:<https://doi.org/10.1046/j.1471-4159.1998.70031227.x> (1998).
- 912 Herve, F., Ghinea, N., D'Athis, P., Carrupt, P. A. & Scherrmann, J. M. Covalent modifications of antitetanus F(ab')<sub>2</sub> fragments with natural and synthetic polyamines and their effects on the antibody endocytosis in cultured HL60 cells. *Bioconjug Chem* **19**, 1543-1555, doi:<https://doi.org/10.1021/bc800045x> (2008).
- 913 Poduslo, J. F. *et al.* Design and chemical synthesis of a magnetic resonance contrast agent with enhanced in vitro binding, high blood-brain barrier permeability, and in vivo targeting to Alzheimer's disease amyloid plaques. *Biochemistry* **43**, 6064-6075, doi:<https://doi.org/10.1021/bi0359574> (2004).
- 914 Welfringer, F., d'Athis, P., Scherrmann, J. M. & Herve, F. Development and validation of an antigen-binding capture ELISA for native and putrescine-modified anti-tetanus F(ab')<sub>2</sub> fragments for the assessment of the cellular uptake and plasma kinetics of the antibodies. *J Immunol Methods* **307**, 82-95, doi:<https://doi.org/10.1016/j.jim.2005.09.015> (2005).
- 915 Poduslo, J. F. & Curran, G. L. Increased permeability of superoxide dismutase at the blood-nerve and blood-brain barriers with retained enzymatic activity after covalent modification with the naturally occurring polyamine, putrescine. *J Neurochem* **67**, 734-741, doi:<https://doi.org/10.1046/j.1471-4159.1996.67020734.x> (1996).
- 916 Kumagai, A. K., Eisenberg, J. B. & Pardridge, W. M. Absorptive-Mediated Endocytosis of Cationized Albumin and a Beta-Endorphin-Cationized Albumin Chimeric Peptide by Isolated Brain Capillaries - Model System of Blood-Brain-Barrier Transport. *J Biol Chem* **262**, 15214-15219, doi:PMID: 2959663 (1987).
- 917 Triguero, D., Buciak, J. B., Yang, J. & Pardridge, W. M. Blood-Brain-Barrier Transport of Cationized Immunoglobulin-G - Enhanced Delivery Compared to Native Protein. *P Natl Acad Sci USA* **86**, 4761-4765, doi:<https://doi.org/10.1073/pnas.86.12.4761> (1989).
- 918 Poduslo, J. F. *et al.* In vivo targeting of antibody fragments to the nervous system for Alzheimer's disease immunotherapy and molecular imaging of amyloid plaques. *J Neurochem* **102**, 420-433, doi:<https://doi.org/10.1111/j.1471-4159.2007.04591.x> (2007).
- 919 Poduslo, J. F. & Curran, G. L. Amyloid beta peptide as a vaccine for Alzheimer's disease involves receptor-mediated transport at the blood-brain barrier. *Neuroreport* **12**, 3197-3200, doi:<https://doi.org/10.1097/00001756-200110290-00011> (2001).
- 920 Poduslo, J. F., Curran, G. L. & Gill, J. S. Putrescine-modified nerve growth factor: Bioactivity, plasma pharmacokinetics, blood-brain/nerve barrier permeability, and nervous system biodistribution. *J Neurochem* **71**, 1651-1660, doi:<https://doi.org/10.1046/j.1471-4159.1998.71041651.x> (1998).
- 921 Wengenack, T. M., Curran, G. L. & Poduslo, J. F. Postischemic, systemic administration of polyamine-modified superoxide dismutase reduces hippocampal CA1 neurodegeneration in rat global cerebral ischemia. *Brain Res* **754**, 46-54, doi:[https://doi.org/10.1016/S0006-8993\(97\)00041-3](https://doi.org/10.1016/S0006-8993(97)00041-3) (1997).
- 922 Reinholz, M. M., Merkle, C. M. & Poduslo, J. F. Therapeutic benefits of putrescine-modified catalase in a transgenic mouse model of familial amyotrophic lateral sclerosis. *Exp Neurol* **159**, 204-216, doi:<https://doi.org/10.1006/exnr.1999.7142> (1999).

- 923 Poduslo, J. F., Whelan, S. L., Curran, G. L. & Wengenack, T. M. Therapeutic benefit of polyamine-modified catalase as a scavenger of hydrogen peroxide and nitric oxide in familial amyotrophic lateral sclerosis transgenics. *Ann Neurol* **48**, 943-947, doi:[https://doi.org/10.1002/1531-8249\(200012\)48:6<943::Aid-Ana18>3.0.Co;2-1](https://doi.org/10.1002/1531-8249(200012)48:6<943::Aid-Ana18>3.0.Co;2-1) (2000).
- 924 Reinholz, M. M., Haggard, J. J., Curran, G. L. & Poduslo, J. F. Plasma pharmacokinetics, nervous system biodistribution and biostability, and spinal cord permeability at the blood-brain barrier of putrescine-modified catalase in the adult rat. *Exp Neurol* **159**, 191-203, doi:<https://doi.org/10.1006/exnr.1999.7117> (1999).
- 925 Pardridge, W. M., Kumagai, A. K. & Eisenberg, J. B. Chimeric Peptides as a Vehicle for Peptide Pharmaceutical Delivery through the Blood-Brain-Barrier. *Biochem Bioph Res Co* **146**, 307-313, doi:[https://doi.org/10.1016/0006-291x\(87\)90726-1](https://doi.org/10.1016/0006-291x(87)90726-1) (1987).
- 926 Pegg, A. E. Recent advances in the biochemistry of polyamines in eukaryotes. *Biochem J* **234**, 249-262, doi:<https://doi.org/10.1042/bj2340249> (1986).
- 927 Adler, S. G., Wang, H., Ward, H. J., Cohen, A. H. & Border, W. A. Electrical Charge - Its Role in the Pathogenesis and Prevention of Experimental Membranous Nephropathy in the Rabbit. *J Clin Invest* **71**, 487-499, doi:<https://doi.org/10.1172/jci110793> (1983).
- 928 Huang, J. T., Mannik, M. & Gleisner, J. In situ formation of immune complexes in the choroid plexus of rats by sequential injection of a cationized antigen and unaltered antibodies. *J Neuropathol Exp Neurol* **43**, 489-499, doi:<https://doi.org/10.1097/00005072-198409000-00004> (1984).
- 929 Ward, H. J., Cohen, A. H. & Border, W. A. In situ formation of subepithelial immune complexes in the rabbit glomerulus: requirement of a cationic antigen. *Nephron* **36**, 257-264, doi:<https://doi.org/10.1159/000183165> (1984).
- 930 Nagy, Z., Peters, H. & Huttner, I. Charge-related alterations of the cerebral endothelium. *Lab. Invest.* **49**, 662-671, doi:PMID: 6656198 (1983).
- 931 Vehaskari, V. M., Chang, C. T., Stevens, J. K. & Robson, A. M. The effects of polycations on vascular permeability in the rat. A proposed role for charge sites. *J Clin Invest* **73**, 1053-1061, doi:<https://doi.org/10.1172/JCI111290> (1984).
- 932 Nisbet, R. M., Polanco, J. C., Ittner, L. M. & Gotz, J. Tau aggregation and its interplay with amyloid-beta. *Acta Neuropathol* **129**, 207-220, doi:<https://doi.org/10.1007/s00401-014-1371-2> (2015).
- 933 Tarasoff-Conway, J. M. *et al.* Clearance systems in the brain-implications for Alzheimer disease. *Nat Rev Neurol* **11**, 457-470, doi:<https://doi.org/10.1038/nrneuro.2015.119> (2015).
- 934 Binder, L. I., Guillozet-Bongaarts, A. L., Garcia-Sierra, F. & Berry, R. W. Tau, tangles, and Alzheimer's disease. *Biochim Biophys Acta* **1739**, 216-223, doi:<https://doi.org/10.1016/j.bbadis.2004.08.014> (2005).
- 935 Zlokovic, B. V. *et al.* Blood-brain barrier transport of circulating Alzheimer's amyloid beta. *Biochem Bioph Res Co* **197**, 1034-1040, doi:<https://doi.org/10.1006/bbrc.1993.2582> (1993).
- 936 Zlokovic, B. V. *et al.* Brain uptake of circulating apolipoproteins J and E complexed to Alzheimer's amyloid beta. *Biochem Bioph Res Co* **205**, 1431-1437, doi:<https://doi.org/10.1006/bbrc.1994.2825> (1994).
- 937 Zlokovic, B. V. *et al.* Glycoprotein 330/megalyn: probable role in receptor-mediated transport of apolipoprotein J alone and in a complex with Alzheimer disease amyloid beta at the blood-brain and blood-cerebrospinal fluid barriers. *P Natl Acad Sci USA* **93**,

- 4229-4234, doi:<https://doi.org/10.1073/pnas.93.9.4229> (1996).
- 938 Ghersi-Egea, J. F. *et al.* Fate of cerebrospinal fluid-borne amyloid beta-peptide: rapid clearance into blood and appreciable accumulation by cerebral arteries. *J Neurochem* **67**, 880-883, doi:<https://doi.org/10.1046/j.1471-4159.1996.67020880.x> (1996).
- 939 DeMattos, R. B. *et al.* Peripheral anti-A beta antibody alters CNS and plasma A beta clearance and decreases brain A beta burden in a mouse model of Alzheimer's disease. *Proc Natl Acad Sci USA* **98**, 8850-8855, doi:<https://doi.org/10.1073/pnas.151261398> (2001).
- 940 Bard, F. *et al.* Peripherally administered antibodies against amyloid beta-peptide enter the central nervous system and reduce pathology in a mouse model of Alzheimer disease. *Nat Med* **6**, 916-919, doi:<https://doi.org/10.1038/78682> (2000).
- 941 Bacskai, B. J. *et al.* Imaging of amyloid-beta deposits in brains of living mice permits direct observation of clearance of plaques with immunotherapy. *Nat Med* **7**, 369-372, doi:<https://doi.org/10.1038/85525> (2001).
- 942 Klyubin, I. *et al.* Amyloid beta protein immunotherapy neutralizes Abeta oligomers that disrupt synaptic plasticity in vivo. *Nat Med* **11**, 556-561, doi:<https://doi.org/10.1038/nm1234> (2005).
- 943 Castillo-Carranza, D. L. *et al.* Passive Immunization with Tau Oligomer Monoclonal Antibody Reverses Tauopathy Phenotypes without Affecting Hyperphosphorylated Neurofibrillary Tangles. *J Neurosci* **34**, 4260-4272, doi:<https://doi.org/10.1523/Jneurosci.3192-13.2014> (2014).
- 944 Dong, X. X., Wang, Y. & Qin, Z. H. Molecular mechanisms of excitotoxicity and their relevance to pathogenesis of neurodegenerative diseases. *Acta Pharmacol. Sin.* **30**, 379-387, doi:<https://doi.org/10.1038/aps.2009.24> (2009).
- 945 Gottlieb, M., Wang, Y. & Teichberg, V. I. Blood-mediated scavenging of cerebrospinal fluid glutamate. *J Neurochem* **87**, 119-126, doi:<https://doi.org/10.1046/j.1471-4159.2003.01972.x> (2003).
- 946 Boyko, M. *et al.* Pyruvate's blood glutamate scavenging activity contributes to the spectrum of its neuroprotective mechanisms in a rat model of stroke. *Eur J Neurosci* **34**, 1432-1441, doi:<https://doi.org/10.1111/j.1460-9568.2011.07864.x> (2011).
- 947 Zhang, D., Xiao, M., Wang, L. & Jia, W. Blood-based glutamate scavengers reverse traumatic brain injury-induced synaptic plasticity disruption by decreasing glutamate level in hippocampus interstitial fluid, but not cerebral spinal fluid, in vivo. *Neurotox. Res.* **35**, 360-372, doi:<https://doi.org/10.1007/s12640-018-9961-8> (2019).
- 948 Ruban, A. *et al.* Combined Treatment of an Amyotrophic Lateral Sclerosis Rat Model with Recombinant GOT1 and Oxaloacetic Acid: A Novel Neuroprotective Treatment. *Neurodegener Dis* **15**, 233-242, doi:<https://doi.org/10.1159/000382034> (2015).
- 949 Doolittle, N. D., Muldoon, L. L., Culp, A. Y. & Neuwelt, E. A. Delivery of chemotherapeutics across the blood-brain barrier: challenges and advances. *Adv Pharmacol* **71**, 203-243, doi:<https://doi.org/10.1016/bs.apha.2014.06.002> (2014).
- 950 Kroll, R. A. & Neuwelt, E. A. Outwitting the blood-brain barrier for therapeutic purposes: Osmotic opening and other means. *Neurosurgery* **42**, 1083-1099, doi:<https://doi.org/10.1097/00006123-199805000-00082> (1998).
- 951 Farrell, C. L. & Shivers, R. R. Capillary junctions of the rat are not affected by osmotic opening of the blood-brain barrier. *Acta Neuropathol* **63**, 179-189, doi:<https://doi.org/10.1007/BF00685243> (1984).
- 952 Neuwelt, E. A. *et al.* Delivery of melanoma-associated immunoglobulin monoclonal antibody and Fab fragments to normal brain utilizing osmotic blood-brain barrier

- disruption. *Cancer Res* **48**, 4725-4729 (1988).
- 953 Neuwelt, E. A., Barnett, P. A., McCormick, C. I., Frenkel, E. P. & Minna, J. D. Osmotic blood-brain barrier modification: monoclonal antibody, albumin, and methotrexate delivery to cerebrospinal fluid and brain. *Neurosurgery* **17**, 419-423, doi:<https://doi.org/10.1227/00006123-198509000-00004> (1985).
- 954 Ulapane, K. R., Kopec, B. M. & Siahaan, T. J. Improving In Vivo Brain Delivery of Monoclonal Antibody Using Novel Cyclic Peptides. *Pharmaceutics* **11**, doi:<https://doi.org/10.3390/pharmaceutics11110568> (2019).
- 955 Kopec, B. M., Kiptoo, P., Zhao, L. Q., Rosa-Molinar, E. & Siahaan, T. J. Noninvasive Brain Delivery and Efficacy of BDNF to Stimulate Neuroregeneration and Suppression of Disease Relapse in EAE Mice. *Mol Pharmaceut* **17**, 404-416, doi:<https://doi.org/10.1021/acs.molpharmaceut.9b00644> (2020).
- 956 Ulapane, K. R., Kopec, B. M. & Siahaan, T. J. In Vivo Brain Delivery and Brain Deposition of Proteins with Various Sizes. *Mol Pharmaceut* **16**, 4878-4889, doi:<https://doi.org/10.1021/acs.molpharmaceut.9b00763> (2019).
- 957 Ulapane, K. R., Kopec, B. M., Moral, M. E. G. & Siahaan, T. J. Peptides and Drug Delivery. *Adv Exp Med Biol* **1030**, 167-184, doi:[https://doi.org/10.1007/978-3-319-66095-0\\_8](https://doi.org/10.1007/978-3-319-66095-0_8) (2017).
- 958 Laksitorini, M. D. *et al.* Modulation of Intercellular Junctions by Cyclic-ADT Peptides as a Method to Reversibly Increase Blood-Brain Barrier Permeability. *J Pharm Sci* **104**, 1065-1075, doi:<https://doi.org/10.1002/jps.24309> (2015).
- 959 On, N. H., Kiptoo, P., Siahaan, T. J. & Miller, D. W. Modulation of Blood-Brain Barrier Permeability in Mice Using Synthetic E-Cadherin Peptide. *Mol Pharmaceut* **11**, 974-981, doi:<https://doi.org/10.1021/mp400624v> (2014).
- 960 Ulapane, K. R. *et al.* Improving brain delivery of biomolecules via BBB modulation in mouse and rat: Detection using MRI, NIRF, and mass spectrometry. *Nanotheranostics* **1**, 217, doi:<https://doi.org/10.7150/ntno.19158> (2017).